Lecture Notes in Physics

Springer
Berlin
Heidelberg
New York
Barcelona
Budapest
Hong Kong
London
Milan
Paris
Santa Clara
Singapores
Tokyo

The Editorial Policy for Proceedings

The series Lecture Notes in Physics reports new developments in physical research and teaching – quickly, informally, and at a high level. The proceedings to be considered for publication in this series should be limited to only a few areas of research, and these should be closely related to each other. The contributions should be of a high standard and should avoid lengthy redraftings of papers already published or about to be published elsewhere. As a whole, the proceedings should aim for a balanced presentation of the theme of the conference including a description of the techniques used and enough motivation for a broad readership. It should not be assumed that the published proceedings must reflect the conference in its entirety. (A listing or abstracts of papers presented at the meeting but not included in the proceedings could be added as an appendix.)

When applying for publication in the series Lecture Notes in Physics the volume's editor(s) should submit sufficient material to enable the series editors and their referees to make a fairly accurate evaluation (e.g. a complete list of speakers and titles of papers to be presented and abstracts). If, based on this information, the proceedings are (tentatively) accepted, the volume's editor(s), whose name(s) will appear on the title pages, should select the papers suitable for publication and have them refereed (as for a journal) when appropriate. As a rule discussions will not be accepted. The series editors and Springer-Verlag will normally not interfere with the detailed editing except in fairly obvious cases or on technical matters.

Final acceptance is expressed by the series editor in charge, in consultation with Springer-Verlag only after receiving the complete manuscript. It might help to send a copy of the authors' manuscripts in advance to the editor in charge to discuss possible revisions with him. As a general rule, the series editor will confirm his tentative acceptance if the final manuscript corresponds to the original concept discussed, if the quality of the contribution meets the requirements of the series, and if the final size of the manuscript does not greatly exceed the number of pages originally agreed upon. The manuscript should be forwarded to Springer-Verlag shortly after the meeting. In cases of extreme delay (more than six months after the conference) the series editors will check once more the timeliness of the papers. Therefore, the volume's editor(s) should establish strict deadlines, or collect the articles during the conference and have them revised on the spot. If a delay is unavoidable, one should encourage the authors to update their contributions if appropriate. The editors of proceedings are strongly advised to inform contributors about these points at an early stage.

The final manuscript should contain a table of contents and an informative introduction accessible also to readers not particularly familiar with the topic of the conference. The contributions should be in English. The volume's editor(s) should check the contributions for the correct use of language. At Springer-Verlag only the prefaces will be checked by a copy-editor for language and style. Grave linguistic or technical shortcomings may lead to the rejection of contributions by the series editors. A conference report should not exceed a total of 500 pages. Keeping the size within this bound should be achieved by a stricter selection of articles and not by imposing an upper limit to the length of the individual papers. Editors receive jointly 30 complimentary copies of their book. They are entitled to purchase further copies of their book at a reduced rate. As a rule no reprints of individual contributions can be supplied. No royalty is paid on Lecture Notes in Physics volumes. Commitment to publish is made by letter of interest rather than by signing a formal contract. Springer-Verlag secures the copyright for each volume.

The Production Process

The books are hardbound, and the publisher will select quality paper appropriate to the needs of the author(s). Publication time is about ten weeks. More than twenty years of experience guarantee authors the best possible service. To reach the goal of rapid publication at a low price the technique of photographic reproduction from a camera-ready manuscript was chosen. This process shifts the main responsibility for the technical quality considerably from the publisher to the authors. We therefore urge all authors and editors of proceedings to observe very carefully the essentials for the preparation of camera-ready manuscripts, which we will supply on request. This applies especially to the quality of figures and halftones submitted for publication. In addition, it might be useful to look at some of the volumes already published. As a special service, we offer free of charge LaTeX and TeX macro packages to format the text according to Springer-Verlag's quality requirements. We strongly recommend that you make use of this offer, since the result will be a book of considerably improved technical quality. To avoid mistakes and time-consuming correspondence during the production period the conference editors should request special instructions from the publisher well before the beginning of the conference. Manuscripts not meeting the technical standard of the series will have to be returned for improvement.

For further information please contact Springer-Verlag, Physics Editorial Department II, Tiergartenstrasse 17, D-69121 Heidelberg, Germany

Gisbert Winnewisser Guido C. Pelz (Eds.)

The Physics and Chemistry of Interstellar Molecular Clouds

Proceedings of the 2nd Cologne-Zermatt Symposium
Held at Zermatt, Switzerland, 21–24 September 1993

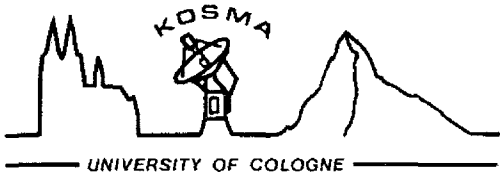

Springer

Editors

Gisbert Winnewisser
Guido C. Pelz
I. Physikalisches Institut
Universität zu Köln
Zülpicher Strasse 77
D-50937 Köln, Germany

Library of Congress Cataloging-in-Publication Data

The physics and chemistry of interstellar molecular clouds :
proceedings of the 2nd Cologne-Zermatt Symposium held at Zermatt,
Switzerland, 21-24 September 1993 / G. Winnewisser, G.C. Pelz, eds.
p. cm. -- (Lecture notes in physics ; 459)
"Lectures and posters presented at the Cologne-Zermatt Symposium
on "The Physics and Chemistry of Interstellar Molecular Clouds,"
held in the Triftbachhalle in Zermatt"--Pref.
Includes bibliographical references and index.
ISBN 3-540-60482-0 (hardcover : alk. paper)
1. Molecular clouds--Congresses. 2. Galaxies--Congresses.
3. Astrophysics--Congresses. 4. Cosmochemistry--Congresses.
I. Winnewisser, G. (Gisbert), 1936- . II. Pelz, G. C., 1965- .
III. Cologne-Zermatt Symposium on "The Physics and Chemistry of
Interstellar Molecular Clouds" (2nd : 1993 : Zermatt, Switzerland)
IV. Series.
QB791.4.P49 1995
523.1'125--dc20 95-42051
CIP

ISBN 3-540-60482-0 Springer-Verlag Berlin Heidelberg New York

Typesetting: Camera-ready by the authors
SPIN: 10514970 55/3142-543210 - Printed on acid-free paper

Preface

This volume contains the lectures and posters presented at the second Cologne-Zermatt Symposium on „The Physics and Chemistry of Interstellar Molecular Clouds" held in the Triftbachhalle in Zermatt from 20 to 24 September 1993. Almost to the day 5 years ago, 1988, the first Cologne-Zermatt meeting was held at the same location. At that time we commemorated the 600th anniversary of the University of Cologne, 20 years of the detection of interstellar NH_3 and H_2O by C.H. Townes, W.J. Welch and collaborators, 20 years of astronomical observations from the Gornergrat, and 5 years of operation of the KOSMA 3m millimeter and submillimeter wave telescope. The most recent 5 years of operation of the KOSMA telescope have proved the high transparency of the atmosphere which allows observation in all atmospheric windows accessible from the ground. With less than 1mm precipitable water content during about 20% of the winter months, Gornergrat observational conditions are comparable to those of Mauna Kea, Hawaii. The main objective of this second Cologne-Zermatt Symposium was, just as 5 years ago, to take stock of the tremendous scientific and technical developments in the field of submillimeter and far-infrared astrophysics. Although nearly two years have elapsed since the Symposium, the present volume still represents the most recent results, both in science and technology.

The topics covered by the conference reached from the galactic distribution of molecular, atomic, and ionized matter to the properties of external galaxies, the special properties of molecular clouds, fractionation, star formation and outflow regions. The conference put ample emphasis on the interplay between theoretical modelling and experimental results, as well as the intimate and necessary connection between laboratory and interstellar spectroscopy. Finally, half a day was devoted to future prospects in submillimeter and far-infrared observations and the technological developments, including those required for satellite observations. The Burgerpräsident of Zermatt, E. Aufdenblatten, welcomed the participants and gave a short account of the historical development of Zermatt. We were very fortunate to have Gerhard Herzberg as our Guest of Honour with us. At the Conference Dinner, held at the Grand Hotel Zermatterhof, G. Herzberg demonstrated vividly the importance of „Triatomic Carbon in the Lab and Space", while A. Dalgarno gave us a „Theorist's View of Interstellar Chemistry". His reflections will close this volume. In his after dinner speech „Ramblings on Interstellar Chemistry" W. Klemperer reminded us of the importance of intuition in an interdisciplinary field such as astrochemistry.

The four day meeting was attended by almost 180 participants from 16 countries, and they all can testify to its great success, due both to the excellent oral presentations and posters and the enthusiasm for the subject by all participants. They were confined to the Triftbachhalle for all four days because of torrential rainfalls, the worst

this area has had in many years. Thus the symposion will not only be remembered for its scientific quality but it will equally be recalled as the wettest conference ever, the „Water Symposium". Some participants had to leave by helicopter because the valley was blocked by mud slides for several days. Frau A. Kretschmer, the conference secretary, took care of all the organizational details with grace, efficiency and a touch of humor. All members of the I. Physikalisches Institut helped with the many organisational details, making the symposium smoothly running. The Burgergemeinde and the people of Zermatt were again generous hosts. In particular the competent staff of the Grand Hotel Zermatterhof under the perfect direction of Jean-Pierre Lanz knew how to cope with all the diverse wishes astrophysicists can come up with. To all a warm „merci vielmals".

It is a great pleasure to express our thanks to the Deutsche Forschungsgemeinschaft, whose financial support made this conference possible. In addition, we have received generous contributions from the following institutions: Internationale Stiftung Hochalpine Forschungsstationen Jungfraujoch und Gornergrat; Burgergemeinde Zermatt; Gornergrat-Bahn; Brig-Visp-Zermatt-Bahn. The Observatoire de Genève supplied the poster walls. Finally the financial contribution of the Universität zu Köln towards the publication of this volume is greatfully recognized.

Köln, August 1995

G. Winnewisser
G.C. Pelz

Contents

Galactic Molecular Cloud Distribution 1

Three New Galactic CO Surveys
P. Thaddeus, T.M. Dame, S. Digel, D. Puche 2

Molecular Clouds at the Edge of the Galaxy: Clouds of FOG
J.G.A. Wouterloot, J. Brand 13

Far-Infrared [C II] Line Survey of the Galaxy
T. Nakagawa, Y. Doi, K. Mochizuki, Y.Y. Yui, H. Okuda, M. Yui,
H. Shibai, T. Nishimura, F.L. Low 22

Molecular Gas and Star Formation Beyond the Optical Disk of the Galaxy
E.J. de Geus, S.W. Digel 30

Molecular Gas Surrounding the Galactic Center
P.T.P. Ho 33

Near-Infrared High-Resolution Imaging of the Galactic Center
A. Eckart, R. Genzel, R. Hofmann, B.J. Sams, L.E. Tacconi-Garman . 41

Properties of the OMC-2 and OMC-3 Cores in Orion
A. Castets, W.D. Langer, G. Duvert 50

Vibrationally Excited CS in Star Forming Cores - Infrared Pumping?
H. Hauschildt, R. Güsten, P. Schilke 52

Millimetre Observations of Southern Translucent Clouds
R. Gredel, E.F. van Dishoeck, J.H. Black 54

Molecular Clouds in LMC: Evaluation of Physical Parameters
by Means of MM Observations
P. Merluzzi, P. Andreani, L. Colangeli, G. Dall'Oglio, V. Mennella,
L. Pizzo, A. Rotundi 56

The 4D-Structure of a Dark Cloud, B164 Under the Influence
of a Bright Star, Azelfafage
L. Pagani, C. Breart de Boisanger 58

External Galaxies 59

Dense Molecular Gas in Ultraluminous and High Redshift Galaxies
S.J.E. Radford 60

Interstellar Molecules in the Large Magellanic Cloud
L.E.B. Johansson 68

Magnetic Fields in Molecular Clouds
R.M. Crutcher 76

Mapping Magnetic Fields in the ISM: Infrared and Sub-mm Polarimetry
A.A. Goodman 82

The Formation of Molecular Lines in Turbulent Clouds
W.H. Kegel, G. Piehler, M.A. Albrecht 86

158 Micron [CII] Imaging of NGC 891
G.J. Stacey, N. Geis, R. Genzel, F. Herrmann, M. Hires,
S.C. Madden, A. Polglitsch, C.H. Townes 90

COBE Observations of the H II Region Around IC 1848
D. Leisawitz, P.M. Mitra, M.G. Hauser 92

A Survey of the Large Magellanic Cloud in the [C II] 158 Micron Line
K. Mochizuki, T. Nakagawa, Y. Doi, Y.Y. Yui, H. Okuda, M. Yui,
H. Shibai, T. Nishimura, F.J. Low 94

Atomic Carbon Emission from Shocked and Preshocked Gas in the IC 443 Supernova Remnant
T.G. Phillips, J. Keene, E.F. van Dishoeck 96

Molecular Cloud Structure 99

Turbulence in Interstellar Clouds
E. Falgarone 100

Multiscale Structural Analysis of Perseus
W.D. Langer, R.W. Wilson, C.H. Anderson, A. Castets 112

Nonlinear Waves and Solitons in Molecular Clouds
R. Watkins, F.C. Adams, M. Fatuzzo, C. Gehman 115

The Formation, Evolution, and Disruption of Molecular Clouds: The Influence of Massive Stars
J. Bally 118

Molecular Absorption in Interstellar Clouds Observed with the Plateau de Bure Interferometer
R. Lucas, H.S. Liszt 120

Dynamical Modelling of Self-Gravitating Magnetic Clouds
Z.Y. Yue, B. Zhang, G. Winnewisser, J. Stutzki 123

Kinematics, Fragmentation, and Heating of Molecular Streamers in the Orion Ridge
J.J. Wiseman, P.T.P. Ho 125

Large-Scale Submm-CO and FIR [CII] Observations of the Rosette Molecular Complex and S140/L1204
N. Schneider, S. Madden, J. Stutzki, D. Block, G. Winnewisser 128

2-D Monte Carlo Models of Clumpy Interstellar Clouds
M. Spaans 130

The Clumpiness of Molecular Clouds
C. Kramer, T. Zimmermann, J. Stutzki, G. Winnewisser 132

Large-Scale CO-Observations of the GMCs Orion A and B Excitation Conditions and Fragmentation
C. Kramer, A. Tigges, J. Stutzki, G. Winnewisser 134

High Spectral Resolution CCS($J_N = 2_1 - 1_0$) Studies of Clumps in Cold Dark Cloud Cores
T. Velusamy, T.B.H. Kuiper, W.D. Langer, S. Levin, E.T. Olsen 136

Photodissociation and Rotational Excitation of CO and Its Isotopomers in Interstellar Clouds
S. Warin, J.J. Benayoun, Y.P. Viala 138

The Distribution of Line Wing Emission in MBM16
B. Götting, J. Stutzki 140

Molecular Observations of HH34: Does NH_3 Accurately Trace Dense Molecular Gas Near Young Stars?
C. Davis, B. Dent 142

Low-J-CO-Multiline Studies of Molecular Clouds: NGC7538
R. Röhrig, J. Stutzki, H. Ungerechts, G. Winnewisser 144

L1780: a Cometary Globule in Disguise of a High-Latitude Cloud. – CO Observations
L.V. Tóth, L. Haikala, T. Liljeström, K. Mattila 146

Influence of the Photospheric Line Spectrum on the Optical Pumping of Circumstellar CO
T. Hertenstein, T. Tsuji, W.H. Kegel 148

Clumping in M17SW
T. Jenness 150

Interpretation of CO Lines from Turbulent Molecular Clouds
G. Piehler, W.H. Kegel 152

CO Multiline Survey in the Galactic Center
J. Staguhn, J. Stutzki, G. Winnewisser 154

The Spatial Distribution of Emission from the Unidentified Infrared Bands
F.O. Clark, R. Assendorp, P. Wesselius, P. Roelfsema, D. Kester,
R.F. Shipman, T.A. Kuchar, M.P. Egan, R.L. Phelps 156

The Distribution of Gas and Dust in the ρ Oph Cloud
R. Liseau, C. Ceccarelli, Y. Fukui, D. Lorenzetti, A. Mizuno,
S. Molinari, B. Nisini, P. Saraceno, L. Spinoglio 158

Millimeter-Wave Observations of H_2CO in ρ Oph B1
M. Barsony, D.D. Sasselov, E.E. Bloemhof, L.A. Nyman 160

Photon Dominated Regions **163**

Theoretical Models of Photodissociation Regions (PDRs)
D.J. Hollenbach, A.G.G.M. Tielens 164

Chemistry in Dense Photon Dominated Regions
A. Sternberg 175

Photon-Dominated Regions: Linking Observations and Theory
D.T. Jaffe 178

Observations of $^3P_1$ to $^3P_0$ C I Emission from Molecular Clouds
and Envelopes of Evolved Stars
J. Keene 186

Carbon Monoxide Line Emission from Photon-Dominated Regions
B. Köster, H. Störzer, J. Stutzki, A. Sternberg 195

Line Emission from Spherical UV Irradiated Clumps
H. Störzer, B. Köster, J. Stutzki, A. Sternberg 197

Radiative Transfer of Continuum Photons in Hierarchical Clouds
M.P. Hobson 199

Submm Observations of Molecular Lines in the Orion Bar:
Towards a Physical Model
M.R. Hogerheijde, D.J. Jansen, E.F. van Dishoeck 201

The PDR IC 63: Observations, Physics and Chemistry
D.J. Jansen, E.F. van Dishoeck, J.H. Black, J. Keene, M. Spaans . . . 203

Star Formation in Bok Globules – A 1.3 mm Continuum Survey
R. Launhardt, T. Henning 206

Radiation-Driven Implosion of Cometary Globules
Modelling and Observations
B. Lefloch, B. Lazareff 208

CI Emission from the Outflow and PDR in S140
N.R. Minchin, D. Krause, J. Stutzki, G.J. White 210

Large-Scale Observations of [CI] $^3P_1 \rightarrow {}^3P_0$ in Photon-Dominated Regions
R. Plume, D.T. Jaffe, K. Tatematsu, J.B. Keene 212

The [C II] 158 μm Line Emission from the ρ Ophiuchi Cloud
Y.Y. Yui, T. Nakagawa, Y. Doi, H. Okuda, H. Shibai,
T. Nishimura, F.J. Low 214

Interstellar Chemistry **217**

How Stable Are the Results of Simple Model Calculations of Interstellar Chemistry?
E. Herbst 218

Interstellar Hydrides
E.F. van Dishoeck 225

CO Chemistry and Optical/FIR Structure of Interstellar Cirrus: Low-Density PDRs
R. Stark 237

Around the $HCNH^+$ Chemistry Astrophysical Implication
D. Talbi 240

About the Presence of Water in IRAS 10214+4724
M. Gerin, F. Casoli, P.J. Encrenaz, F. Combes 243

Hot Ammonia Associated with Ultracompact HII Regions
P. Hofner, E. Churchwell, S. Kurtz, R. Cesaroni, M. Walmsley 245

Structure and Chemistry of IRAS 05338-0624
J.P. McMullin, L.G. Mundy, G.A. Blake 247

Circumstellar Disks at Centimeter Wavelengths
L.G. Mundy, J.P. McMullin, A.W. Grossman, G. Sandell 249

Optical Pumping of Circumstellar SiO Masers
E. Rausch, W.H. Kegel[1], T. Tsuji 251

Observations of Interstellar CN, ^{13}CN and $C^{15}N$
R. Simon, A.H. Saleck, N. Schneider, K. Jacobs, B. Vowinkel,
G. Winnewisser 252

Physical and Chemical Variations Within the W3 Star-Forming Region
F.P. Helmich, D.J. Jansen, T. de Graauw, T.D. Groesbeck,
E.F. van Dishoeck 254

Star Formation in Molecular Clouds **257**

Chemical and Physical Gradients Along the OMC-1 Ridge
H. Ungerechts, E.A. Bergin, P.F. Goldsmith, W.M. Irvine, F.P. Schloerb,
R.L. Snell 258

Dense Cores and Star Formation: Before and After
P.J. Barnes, P.C. Myers 265

Sulfur Molecules in Low-Density Molecular Clouds
C.M. Walmsley, A. Tieftrunk, G. Pineau des Forêts, P. Schilke 268

Chemistry of the Orion Molecular Cloud Core
E.C. Sutton, R. Peng, W.C. Danchi, P.A. Jaminet, G. Sandell, A.P.G. Russell 269

The Structure of the Dense Core in the High-Latitude Cloud MCLD 126.6+24.5
A. Heithausen, U. Corneliussen 271

The W49A Molecular Cloud Core
E. Serabyn 274

Massive Star Nurseries
E. Churchwell 276

High-Resolution $C^{34}S$ Images of the W51 Region Taken with the Plateau de Bure Interferometer
K.I. Uchida, H. Wiesemeyer, R. Güsten 285

The Synthesis of Molecular Line, Neutral Carbon and Dust Continuum Observations in the Molecular Cloud G34.3 + 0.2
L.T. Little 288

Methyl Cyanide and Propyne in the Hot Molecular Core G34.3+0.15
G.H. Macdonald, R.J. Habing 291

CS $J = 2 - 1$ and HCN $J = 1 - 0$ Observations of Dense Molecular Cores in Regions of Massive Star Formation
I. Zinchenko, V. Forsström, A. Lapinov, K. Mattila 294

Analysis of Maser Proper Motion Kinematics
E.E. Bloemhof 296

H_2O and CO Emission Towards IRAS Point Sources in Regions of Star Formation
K. Fiegle, J.G.A. Wouterloot, J. Brand 298

Luminosity vs. Circumstellar Mass: An Evolutionary Diagram for YSOs
P. Saraceno, P. André, C. Ceccarelli, M. Griffin, S. Molinari, S. Russell 300

Model Envelopes of Post–AGB Stars from IR and Sub–mm Data
J. Gürtler, C. Kömpe, T. Henning 304

Distributions and Kinematics of Molecular Species Around T Tau
H.J. van Langevelde, E.F. van Dishoeck, G.A. Blake 306

Ammonia Towards High Luminous IRAS Sources
K. Martin, T. Henning, C. Kömpe, C.M. Walmsley 308

JCMT Continuum Survey of Pre-Protostellar Cores
D. Ward-Thompson, P.F. Scott, R.E. Hills, P. André 310

Comparison of the Structure of a Star-Forming and Non-Star-Forming GMC
J. Williams, E. de Geus, L. Blitz 312

Outflow-Free Class I Sources: Protostars?
R. Liseau, C. Ceccarelli, Y. Fukui, D. Lorenzetti, A. Mizuno, S. Molinari, B. Nisini, P. Saraceno, L. Spinoglio 314

Evidence for a Recombining Wind in DR21
A. Harrison, A. Russell, P. Puxley, P. Brand 316

Vorticity Generation in Bow Shocks of Low Excitation
M.D. Smith 318

Near Infrared Observations of S155. Evidence of Induced Star Formation?
L.K. Hunt, F. Lisi, M. Felli, G. Tofani 320

FIR/NIR Spectroscopy of the Galactic Center Arc Region: The Importance of Massive Star Formation for Ionization
T. Krenz, T.R. Geballe, R. Genzel, A.I. Harris, A. Krabbe, D. Lutz, A. Poglitsch 322

Molecular Outflows **325**

Multi-wavelength Study of NGC 281 A
T. Henning, K. Martin, R. Launhardt, H.-G. Reimann 326

First Tentative Detection of the Molecular Oxygen Isotopomer $^{16}O^{18}O$ in Interstellar Clouds
L. Pagani, W.D. Langer, A. Castets 329

Molecular Outflows Driven by Optical Jets
R. Padman, J. Richer 331

Jet-Driven Molecular Outflows
C.R. Masson, L. Chernin 334

$C^{17}O$ and Submillimetre Continuum Observations of M17SW
M.P. Hobson 337

Submillimetre Observations of the Mon R2 Cluster
H.E. Matthews, G.F. Mitchell, J. Giannakopoulou 340

Molecular Outflow in the Vela Molecular Ridge
M. Olberg 342

New Instrumentation **343**

Prospects for Submillimeter Observations
T.G. Phillips 344

The Submillimeter Wave Astronomy Satellite: Mission Science Objectives
G.J. Melnick, A. Dalgarno, N.R. Erickson, G.G. Fazio, P.F. Goldsmith, M. Harwit, D.J. Hollenbach, D.G. Koch, D.A. Neufeld, R. Schieder, R.L. Snell, J.R. Stauffer, P. Thaddeus, V. Tolls, G.F. Winnewisser . . . 352

The Submillimeter Wave Astronomy Satellite: Instrument Hardware
V. Tolls, G.J. Melnick, N. Erickson, P. Goldsmith, M. Harwit, R. Schieder, R.L. Snell, J.R. Stauffer 356

The James Clerk Maxwell Telescope. Developments into the 1990's
E.I. Robson 360

The Kuiper Widefield Infrared Camera (KWIC)
G.J. Stacey, T.L. Hayward, H. Latvakoski, L. Peng, G.E. Gull 362

Receiver A2 – A 210 to 280 GHz SIS Receiver for the James Clerk Maxwell Telescope
S.R. Davies, C.T. Cunningham, L.T. Little, D.N. Matheson 364

The Arcetri 40/50 GHz Receiver for the Medicina Radiotelescope
G.Tofani, M.Cetarzi, V.Natale 366

The Renewal of the POM_2 Radiotelescope
G.Duvert, A. Castets, L. Pagani, B. Fouilleux, P.Petmezakis 368

ODIN — A Swedish Submillimetre Wave Satellite for Astronomy and Aeronomy
Å. Hjalmarson 369

New Techniques for Submillimeter Precision Broadband Spectroscopy
M. Liedtke, Th. Klaus, R. Schieder, G. Winnewisser, K.M.T. Yamada, V. Wagener, M. Winnewisser, O.P. Pavlovsky, G.M. Altshuller, O.K. Anikin, A.A. Uljanov, S.P. Belov, E.N. Karyakin, A.F. Krupnov, A.P Shkaev, M.Yu. Tretyakov, N.F. Zobov 370

ARNICA, the NICMOS 3 Imaging Camera of TIRGO
F. Lisi, C. Baffa, L. Hunt, R. Stanga 373

JCMT Receivers – Present and Future
A.P.G. Russell 375

Submillimeter Bolometer Array for the CSO
N. Wang, T. Hunter, D. Benford, T.G. Phillips 376

FTS Atmospheric Transmission Measurements and Observations of Planetary Atmospheres
E. Serabyn, E.W. Weisstein, D.C. Lis 377

A Theorist's View of Interstellar Chemistry
A. Dalgarno 380

Index 383

List of Molecules 386

List of Participants 389

Three New Galactic CO Surveys

P. Thaddeus, T. M. Dame, S. Digel, and D. Puche

Harvard-Smithsonian Center for Astrophysics,
60 Garden Street, Cambridge, MA 02138

Our small millimeter-wave telescope at the Center for Astrophysics continues to be an extremely powerful instrument for the study of molecular clouds in our Galaxy and its nearest neighbors. Its linear resolution at the Galactic center, about 20 pc, is not only high by the standards of single-dish 21 cm radio astronomy, it is high by the standards of all extragalactic CO research, even that with interferometers. To match it at the distance of the Virgo Cluster, for example, would require an instrument with an aperture or baseline of nearly 2000 meters—well beyond the scale of existing facilities. Close molecular clouds in the Milky Way can be studied with our telescope at a resolution that has not yet been attained with CO in any extragalactic system.

When the telescope was constructed 20 years ago, it seemed likely that after a few large scale investigations with CO and ^{13}CO and perhaps a few other simple molecules, all requiring no more than three or four Ph. D. dissertations, the useful work of the instrument would end, and it would be time to build a larger telescope. With better and better receivers, however, the molecular phenomenology revealed by CO at our angular resolution (8.7' at the $1\rightarrow0$ line at 115 GHz) has turned out to be so rich that today after more than 20 dissertations the zeroth order experiment has yet to be completed; our study of the normal isotopic species is still very much in progress, with no end in sight. Here we will describe briefly three recent investigations with the telescope which would have been difficult or impossible with larger instruments, or which would have represented such a cost-ineffective use of a large instrument that they are not likely to have been scheduled. The questions addressed are rather interesting and fundamental ones in Galactic structure and the study of molecular clouds: How far above the Galactic plane do molecular clouds extend? How far out from the center of the Galaxy can they be found? And what is the arm-interarm contrast in molecular clouds?

Detection of a Thick Molecular Disk

Early CO surveys close to the Galactic plane by our telescopes and others showed that the molecular disk of the Milky Way is significantly thinner—by a factor of 2–3—than the disk of atomic gas determined from 21-cm observations (e.g., Bronfman et al. 1988). Between the solar circle and the peak in the molecular distribution half way to the Galactic center the full width at half maximum of the molecular disk is about 100 pc—not coincidentally about that of OB stars. Near the plane both the H I and the CO disks are approximately Gaussian with displacement z from the plane, but the H I distribution far from the plane possesses pronounced wings which extend to at least 1 kpc (Lockman 1984). This thick H I disk, which Heiles (1984) has shown is resolved into an intricate tangle of shells, arcs, and other structures, is most plausibly the result of multiple supernovae and OB winds which accelerate gas to high velocity, ejecting some well above the inner Gaussian H I disk. Our early CO surveys and those of other CO

observers were not sensitive enough to detect a CO counterpart to this thick H I disk, and one might be persuaded that such a molecular counterpart is implausible because molecular gas is fragile—readily dispersed and dissociated by the violent activity which accompanies the formation of early-type stars.

Nonetheless, it seemed to us two years ago that the distribution of molecular gas far from the plane was an interesting observational question, and a challenging one, too, because it would push our small telescope, currently equipped with an SIS receiver with a single-sideband system noise temperature of only about 65 K, to the limit of its high sensitivity, and would require extremely tight control of spectral baseline curvature and standing waves. For us the best place to start was the vicinity of the Galactic terminal velocity between longitudes of roughly 30° and 50°, a section of the Milky Way observable many hours each day from mid-latitude in the northern hemisphere. The terminal velocity in that longitude range is between 5.5 and 7.5 kpc away, distances at which the thin molecular disk is only about 1° thick. To conduct a good search for a thick counterpart therefore requires observations over only say ±4° in b—not an excessive range.

In observations during the colder months over two years we have now covered that range in three deep, well sampled strips centered at l = 30°, 40°, and 50°, each 1° wide. Observations have been done on a regular square grid in l and b spaced at slightly better than the Nyquist limit—specifically, every 3.'75, or 0.43 of a beamwidth. To obtain extremely flat baselines, fast position switching (a full period of 30 s) was employed against two OFF positions, one above the source in elevation, the other below; by adjusting the time spent on each OFF, residual switched powers were generally held below 1 K, and baseline curvature or standing waves were imperceptible or very small. The telescope is equipped with two 256-channel filterbank spectrometers with velocity resolutions at the CO line of 0.65 and 1.3 km s^{-1}, respectively; the two were used simultaneously, centered on the same frequency, but since all observed CO emission fell within the range of the higher resolution filterbank, the lower resolution one was used only to provide additional clean channels for setting the spectral baseline. A uniform rms sensitivity of 0.1 K at Δv = 1.3 km s^{-1} was achieved with typical integration times of ~3 minutes. The total number of observations in all three strips is 6800, for a total observing time of about 340 hours.

Figure 1 shows, on the left, the b,v diagram for the strip across the Galactic plane at l = 30°, with, on the right, the corresponding H I diagram. In the CO diagram the molecular gas detected in previous galactic surveys is delineated approximately by the unshaded, high intensity contours, which at high velocities (50-120 km s^{-1}) are seen to lie mainly within 1° of the plane. The shaded contours, the lowest at 2.2 σ above the instrumental noise, the highest at 22 σ, represent CO emission that is far more intense than is predicted by a single Gaussian fit to the near-plane data. This is the essential evidence for a thick molecular disk. Similar results are obtained for the two strips across the plane at 40° and 50°.

When weak emission of the kind here is observed in the vicinity of a strong extended source such as the Galactic plane, the question of antenna sidelobe contamination is crucial. We have taken pains to demonstrate that what is apparently high-z CO in

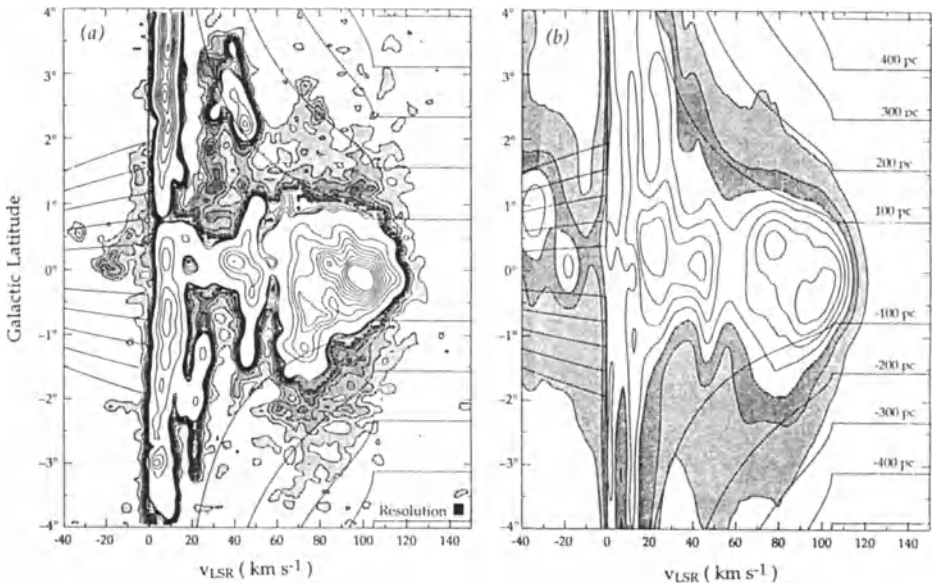

Figure 1: Evidence for a thick molecular disk: *(a)* CO latitude-velocity diagram at a Galactic longitude of 30°, with *(b)*, a comparable diagram for H I from the Weaver and Williams (1973) survey. The longitude integration is over 1° in either case. The CO emission has been smoothed to a resolution of 10' by 4 km s^{-1}; the lowest contour is at 0.02 K deg, and the contour interval is also 0.02 K deg in the shaded region, but increases by a factor of 20 in the unshaded region. Lines in both diagrams indicate displacement z from the Galactic plane, on the assumption that all emission is from the near kinematic distance.

Figure 1 and in our other longitude windows is not merely the intense, extended emission of the Galaxy caught in the sidelobes of the 1.2 m telescope. By mapping the sidelobe pattern of the antenna by means of a 115 GHz transmitter on a distant building, and by measurements of the solar continuum emission at that frequency in all directions out to angles of more than 3° from the center of the sun, we have shown that near-plane Galactic CO emission in our sidelobes is about 6 dB too low to account for the high-z emission. By refining our knowledge of the sidelobe pattern somewhat, it ought to be possible eventually to "clean" our high-z observations spectrum by spectrum of nearly all sidelobe contamination, but from what we already know about the sidelobe level that is expected to lower our estimate of the amount of thick-disk CO by at most 25%.

Figure 2 shows the number density of molecular hydrogen as a function of z, derived from our three 1° strips across the Galactic plane. For want of a better mass calibration, the density has been calculated on the assumption that $N(H_2)/W_{CO} = 2.3 \times 10^{20}$ cm^{-2} K^{-1} km^{-1} s—the value found by Strong et al. (1988) from an intercomparison of CO, H I, and diffuse Galactic γ-rays over much of the inner Galaxy—with the reservation that this is a purely tentative procedure, subject to revision if some independent method can be found to calibrate molecular mass at high z. It is worth noting that estimates of

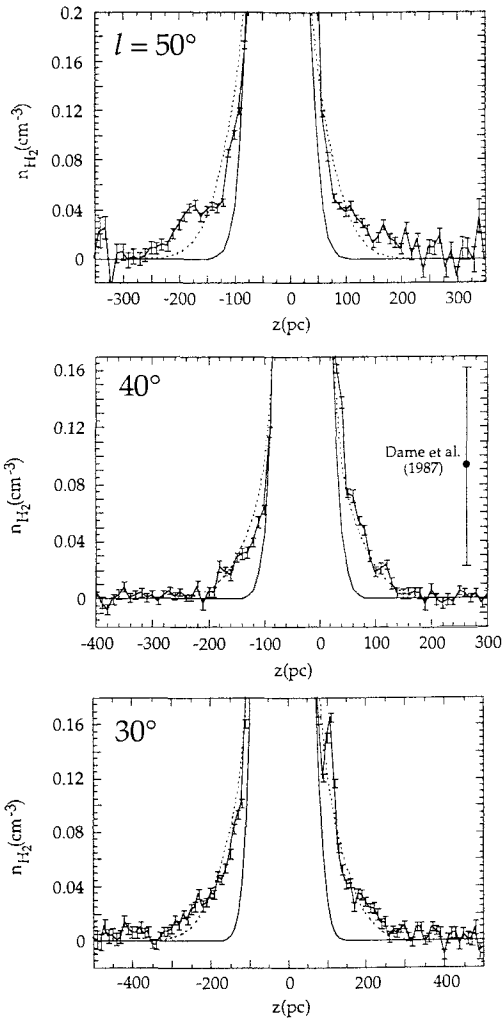

Figure 2: Molecular hydrogen number density as a function of displacement from the Galactic plane. Error bars correspond to ±1 σ; the single large error bar in the 40° plot corresponds to the only previous extensive wide-latitude CO survey of the Galaxy. (Per unit solid angle, the several in-plane surveys from which the thickness of the central CO layer was derived were at most a factor of 4 more sensitive than the survey of Dame et al. 1987).

the mass calibration that have been made in several cirrus clouds are significantly smaller than the value of Strong et al. (e.g., de Vries, Heithausen, & Thaddeus 1987; Heithausen & Thaddeus 1990).

As Figure 2 shows, the distribution of H_2 number density with z more than 100 pc from the plane is poorly approximated by a single Gaussian fit, but it is quite well described by a double Gaussian. As shown in Table 1, the thickness of the thin Gaussian component varies from 53 to 80 pc, and that of the thick component from 147 to 225 pc, but the ratio of the two is a constant 2.8 for all three windows to within the observational uncertainties. The thick molecular disk is about as thick as the thin H I disk—possibly a coincidence, but possibly not. Our data suggests that ~5% of the CO emission of the entire Galaxy (not including the very agitated material within 1 kpc of the center) lies beyond the wings of the thin Gaussian layer, for a total molecular mass of order 35 x 10^6 $M_\odot$—assuming again that the Strong et al. mass calibration is valid. Perhaps the most interesting question posed by the present findings is how to account for such a large mass of material so far from the plane—how to eject it via supernova explosions or OB winds from the dense inner molecular disk, or how to make it *in situ*.

As yet it is difficult to say whether the molecular gas we see at high-z is mainly diffusely distributed or is mainly clumped into well defined clouds, and if so whether the cloud mass spectrum is like that in the plane, where much or most of the mass is contained in the large concentrations, the giant molecular clouds. Our present view of the high-z distribution through three narrow longitude windows is not well suited to defining clouds, and it is evident that

TABLE 1

THE THIN AND THICK CO DISKS

Longitude window	FWHM of Gaussian Component		Ratio
	thin (pc)	thick (pc)	
30°	80 ± 2	225 ± 23	2.8 ± 0.3
40°	57 ± 2	162 ± 22	2.8 ± 0.4
50°	53 ± 6	147 ± 28	2.8 ± 0.6

greater areal coverage is required for the kind of cloud inventory required to ascertain the mass spectrum. With the limited data at hand however, there is already some evidence for cloud-like lumps or concentrations, and some evidence that the mass spectrum may be somewhat flatter than in the plane, with a significant amount of diffuse CO emission not resolved into clouds. Since sidelobe contamination is likely to simulate a more-or-less diffuse CO continuum, however, this evidence must be treated with considerable reserve until our survey windows are enlarged—a project to be undertaken during the upcoming observing season.

If the high-z molecular gas is material ejected from near the Galactic plane by star formation, young stars, and supernovae, one might expect to see more of such gas above the spiral arms than elsewhere. Our data to date does not allow us to say whether this is true or not, but the observations now planned should allow us to test this idea. A full description of the work to date has been submitted for publication (Dame & Thaddeus 1994).

Molecular Clouds at the Edge of the Stellar Disk and Beyond

The search for molecular clouds in the far outer Galaxy is a daunting exercise for several reasons: (i) because of the very large areas to be surveyed to cover the flare and warp of the outer Galactic disk, (ii) because clouds far beyond the solar circle may be systematically faint in CO as a result of lower metallicity or temperature (or both), and (iii) because of the lack of apparent star formation as signposts of molecular gas. The edge of the stellar disk of the Milky Way is claimed to lie at about R = 18 kpc from the Galactic center (Chromey 1978; Moffat, Fitzgerald, & Jackson 1979; Chini & Wink 1984; Schechter 1993), but well beyond to at least R = 30 kpc there is a vast region with detectable H I at 21 cm (Henderson, Jackson & Kerr 1982). The absence of stars or star formation in this cold, remote part of the Galaxy might persuade one that a search there for molecular clouds is a waste of effort or worse, but we again regarded the question as an empirical challenge, and decided to look.

Even with our very sensitive telescope and its moderately large beam, a well sampled survey of an appreciable segment of the Galactic plane—say 30° in l and a few degrees in b—would require at the required sensitivity a number of years of observation. We therefore began our survey toward the only fiducial points available, the rather shallow ripples that can be discerned in the 21 cm distribution. In the longitude range 130°–155°, 71 H I emission peaks at kinematic Galactic radii of 18-30 kpc were identified in the Maryland-Green Bank Survey (Westerhout & Wendlant 1982) and surveyed in CO in

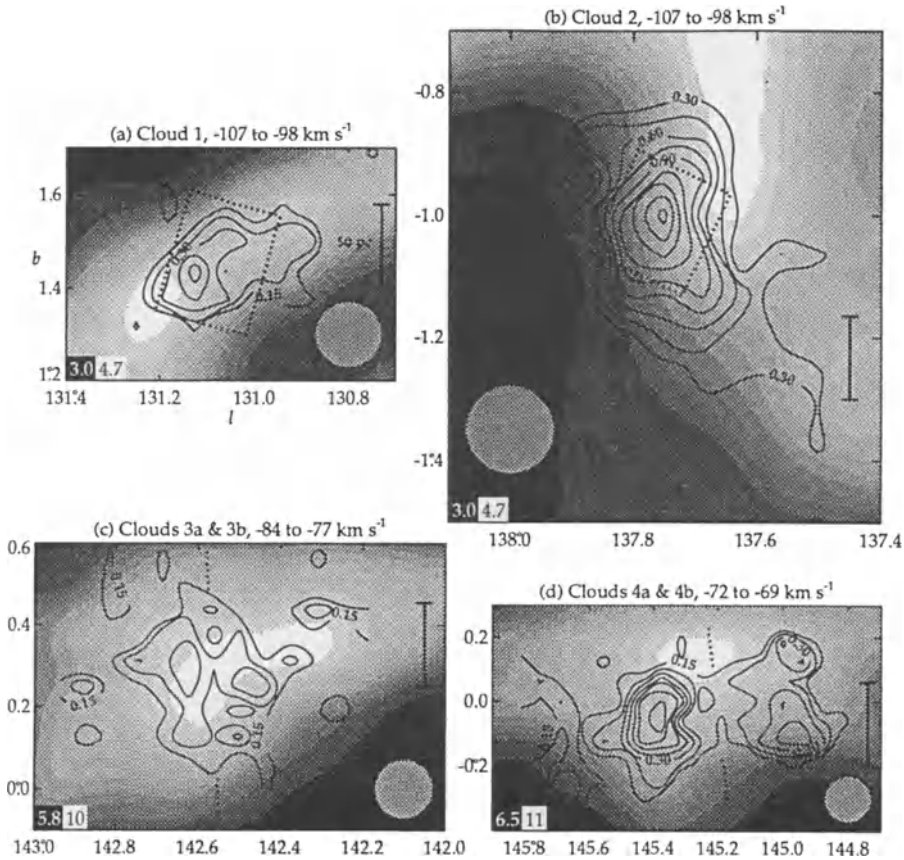

Figure 3: Contours of velocity-integrated CO emission from four of the distant molecular clouds at or beyond the optical disk of the Galaxy, overlaid on similar gray-scale representations of the H I column density from the Maryland-Green Bank survey. The CO contours are linear, the lowest contour (labeled in K km s^{-1}) at twice the contour interval.

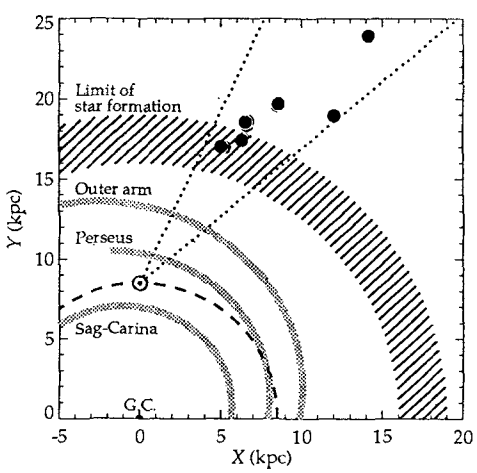

Figure 4: Location of distant molecular clouds on the Galactic plane with respect to the Sun, the solar circle, and three of the better defined outer spiral arms of the Milky Way. The cross-hatched region indicates the approximate limit of the optical disk, the straight dashed lines the longitude range of the present search.

square or rectangular fields at least 0.5° on a side. Somewhat to our surprise, CO was detected in over 10% of the fields studied, and eleven molecular clouds have now been fully mapped (again on a uniform 3'.75 grid) to high sensitivity (0.035 K per 0.65 km s^{-1} channel). Four are shown in Figure 3; the locations of all eleven clouds in projection on the Galactic plane are shown in Figure 4. It is to be emphasized that owing to the lack of other distance estimates, all distances here (and as a rule elsewhere in this paper) are of necessity kinematic: they are based on the assumption of circular Galactic rotation and a rotation curve that is flat beyond the solar circle (e.g., Merrifield 1992), with $R_\odot$ = 8.5 kpc and $V_\odot$ = 220 km s^{-1}.

Some of the properties of the extreme outer Galaxy clouds, and other inferences which can be drawn from the present data, are the following:

- The clouds at the edge of the optical disk or beyond are generally found near but not coincident with the 21-cm ripples, a typical displacement being about 40 pc.
- They have typical dimensions of 50-100 pc, comparable to that of the largest molecular complexes near the solar circle, e.g., the Orion and Taurus clouds. They also might be better described as complexes of clouds rather than clouds, since at higher resolution (observations have now been done with the NRAO 12 m and IRAM 30 m telescopes) they are found to possess a wealth of fragmentation and internal structure.
- Their overall CO linewidths are comparable to that of large local clouds.
- They are underluminous in CO with respect to those large local clouds which are copious producers of young stars (such as those in Orion), but are not greatly underluminous relative to quiescent local clouds (such as those in Taurus).
- Their masses are fairly uncertain, since the usual methods of estimating cloud mass from CO data are either poorly calibrated or are of dubious validity so far beyond the solar circle. By any reasonable estimate, however, the mass of the circumadjacent H I is an order of magnitude or more larger than that of the molecular cloud. The masses derived using the Strong et al. calibration lie between 4 x 10^3 and 4 x 10^4 $M_\odot$.
- At least one of the clouds—interestingly enough the one most remote from the Galactic center at 28 kpc if its kinematic distance is to be trusted—has been found to possess associated Hα emission and young stars.
- From the detection rate in the fairly narrow band of Galactic longitude so far studied, it is estimated that 100 or more molecular clouds comparable to those already found may lie beyond the apparent edge of the optical disk of the Galaxy.

A paper describing detection of the distant molecular clouds discussed here has been accepted by the *Astrophysical Journal*, and will appear before the proceedings of the present meeting (Digel, de Geus, & Thaddeus 1994). A *Letter* describing the detection of Hα emission associated with the most distant outer Galaxy cloud has just appeared (de Geus et al. 1993).

The Arm-Interarm Contrast in Molecular Clouds

It was evident from the earliest large-scale surveys with the 1.2 m telescope that CO molecular clouds are excellent tracers of the large scale spiral structure of the Milky

Way, and that spiral arms are especially clearly seen toward the outer part of the system, where kinematic distances are free of the twofold distance ambiguity within the solar circle. By 1980, from analysis of our first rather insensitive observations toward the Perseus arm, we succeeded in showing that the arm-interarm contrast in that direction was at least 5:1 (Cohen et al. 1980). A few years later when Grabelsky analyzed his CO survey of the Carina region obtained with our telescope's twin instrument in Chile (Grabelsky 1985; Grabelsky et al. 1987), he derived a value of at least 13:1 at the well defined tangent of the Carina arm.

During the last few years we have begun a new survey of the Perseus arm and outer Galaxy in the second quadrant, the long-term strategy being to start in the direction of specific objects of interest like the large molecular complex near the supernova Cas A, and eventually to fill in the gaps to obtain well-sampled, uniform coverage of much of the second Galactic quadrant. As part of this program we have recently resurveyed the large molecular clouds associated with the well-known H II regions W3, W4, and W5, first studied with the 1.2 m telescope by Cong as part of his Columbia dissertation (Cong 1977; Lada et al. 1978). The new observations, which cover a nearly 13° by 8° uniform, well-sampled field in l and b, reveal a great wealth of molecular detail in both the Local

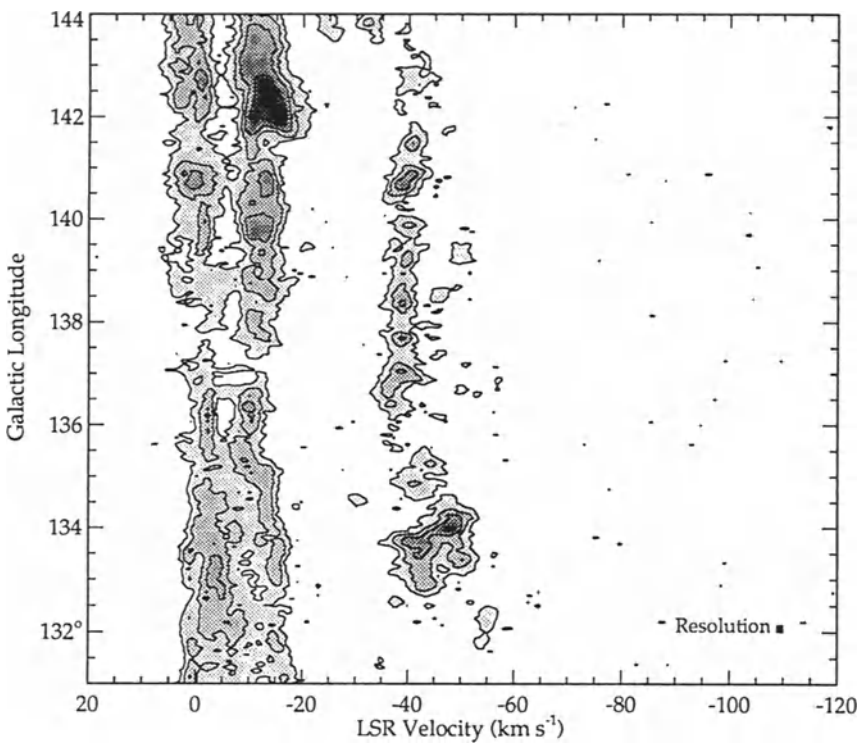

Figure 5: CO longitude-velocity diagram for the new survey of the W3-W5 region of the Galactic plane, integrated in Galactic latitude from –2° to +4°. Contours are at 0.3 (3 σ), 0.6, 1.2, 2.4, and 4.8 K deg. The map has been smoothed slightly in velocity to a resolution of 1.3 km s^{-1}.

and Perseus arms which Cong was unable to detect owing to the limited sensitivity of his observations, and they allow a much more stringent limit to be set on the arm-interarm molecular contrast toward the Perseus Arm. Here we will consider only the new information provided by the survey on the extensively debated question of how well molecular clouds define spiral arms. We are specifically interested in seeing if there is any evidence for the claimed population of "cold", ubiquitous molecular clouds which are supposed to exist both within the spiral arms of the Milky Way and between them, with a number density comparable to that of the familiar "warm" clouds found within the arms (Solomon, Sanders, & Rivolo 1985).

The very clean nature of the interarm gap is apparent in Figure 5, the longitude-velocity diagram of the new survey. The Local arm is the intense lane of CO emission mainly between 0 and –15 km s^{-1}; it stands out because it is so close, all of the Local arm clouds in this direction probably lying within 1 kpc of the sun. The Perseus Arm is the well separated lane mainly between –35 and –50 km s^{-1}, fainter because, at between 3 and 6 kpc, it is at least three times further away than nearly all of the Local arm gas. Since the distance to most of the Local arm clouds in Figure 5 is rather uncertain, and may vary by a factor of 5 or more from cloud to cloud, it makes the most sense to determine the ratio of emission in the Perseus Arm to that in the interarm gap, because the Perseus arm clouds are all at about the same distance—to say 30%. To determine the arm-interarm contrast, proper geometrical correction must of course be made for the larger area observed in the Perseus Arm. The projected areas are shown in Figure 6, where it is evident that we are observing substantial areas both in the interarm gap and in the Perseus arm—of order 1 kpc^2, an area large enough to include many of the claimed randomly-distributed interarm clouds.

The result of correcting our survey data for distance to obtain the projected mass density of molecular hydrogen per unit area on the Galactic plane is shown in Figure 7, where the data have been binned into the four indicated longitude ranges, and finally, in the bottom panel, averaged over the entire longitude range of the survey. Distances, as discussed in the section above on the clouds near the edge of the Galaxy, are kinematic, and for that reason the derived surface density of molecular gas in the Local arm (R = 8.5–10 kpc, in Fig. 7), where random radial velocities are comparable to or greater than those from Galactic rotation, is somewhat uncertain; the surface density of the more distant gas, however, is expected to be fairly insensitive to kinematic uncertainties. The important

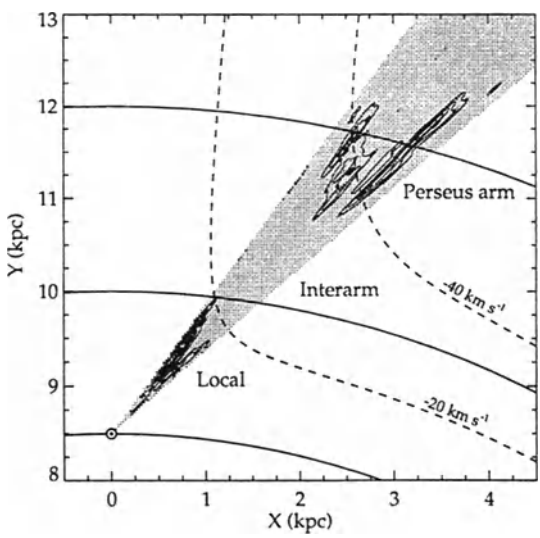

Figure 6: Region of the Galactic plane covered by the W3-W5 survey.

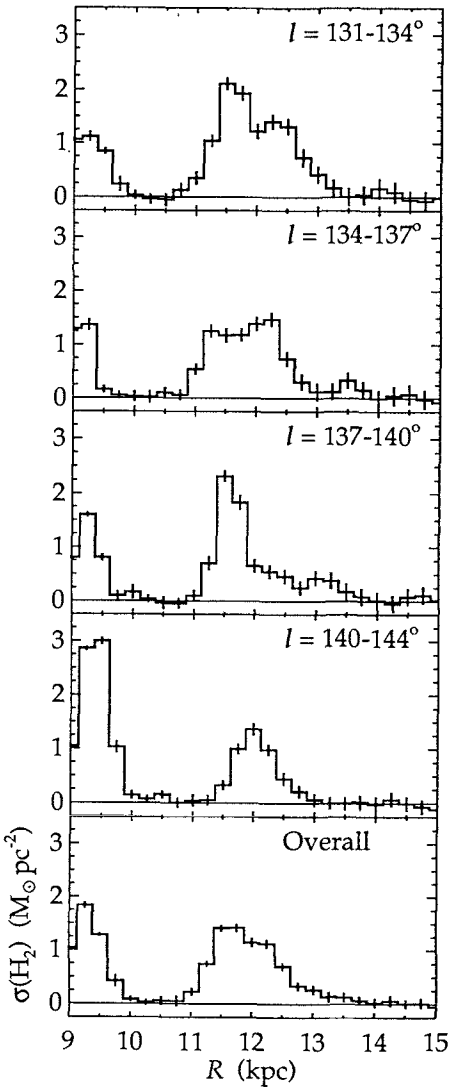

Figure 7: Total molecular (H_2) column density projected onto the Galactic plane for four longitude strips of the present survey, and (bottom) averaged over the entire survey. Error bars indicate the 3-σ uncertainties that result from instrumental noise.

quantitative conclusion to be drawn from Figure 7 is that the arm-interarm contrast—specifically, between the peak in the Perseus arm near R = 11.5 kpc and the trough in the interarm gap around 10.5 kpc—is at least 25:1. This is an apparent arm-interarm contrast significantly higher than hitherto has been set elsewhere in the Milky Way, or—as far as we are aware—in any external galaxy. Owing to streaming motions the actual arm-interarm contrast might be somewhat lower, perhaps by as much as 30%, but that still leaves the contrast extremely high—more than 18:1.

The final conclusion reached when we consider the present work in conjunction with Grabelsky's (1985) 13:1 limit near the tangent point of the Carina arm is that, *at least near the solar circle and beyond, there is no evidence whatsoever for the claimed population of interarm molecular clouds.* It is of course conceivable that interarm clouds are entirely confined to the inner Galaxy, but since the normal population extends so far beyond—as we have seen to nearly 30 kpc from the Galactic center—that would appear to be an extremely unlikely possibility.

To summarize, we have found molecular clouds in two regions of the Galaxy not covered at all—or very inadequately—by previous CO surveys: above the familiar molecular disk in the inner Galaxy, and beyond the apparent edge of the stellar disk in the outer Galaxy. Just how molecular gas is formed in (or transported to) these low density regions is a question which has not yet been addressed, but one now of some interest. Finally, in a large region of nearly 1 kpc^2 between here and the Perseus arm we find almost no trace of molecular gas, allowing a stringent limit to be set on the space density of hypothetical interarm clouds.

References

Bronfman, L., Cohen, R. S., Alvarez, H., May, J. & Thaddeus, P. 1988, ApJ, 324, 248.

Chini, R. & Wink, J. E. 1984, A&A, 139, L5.

Chromey, F. R. 1978, AJ, 83, 162.

Cohen, R. S., Cong, H.-I., Dame, T. M., & Thaddeus, P. 1980, ApJ, 239, L53.

Cong, H.-I. 1977, Ph.D. dissertation, Physics Dept., Columbia University.

Dame, T. M. et al. 1987, ApJ, 322, 706.

Dame, T. M., & Thaddeus, P. 1994, ApJ *Letters* (*submitted*).

de Geus, E. J., Vogel, S. N., Digel, S. W., & Gruendl, R. A. 1993, ApJ, 413, L97.

de Vries, H. W., Heithausen, A., & Thaddeus, P. 1987, ApJ, 319, 723.

Digel, S., de Geus, E., & Thaddeus, P. 1994, ApJ, 422, 92.

Grabelsky, D. A. 1985, Ph. D. dissertation, Astronomy Dept., Columbia University.

Grabelsky, D. A., Cohen, R. S., Bronfman, L., Thaddeus, P., & May, J. 1987, ApJ, 315, 122.

Heithausen, A., & Thaddeus, P, 1990, ApJ, 353, L49.

Henderson, A. P., Jackson, P. D., & Kerr, F. J. 1982, ApJ, 263, 116.

Heiles, C. 1984, ApJS, 55, 585.

Lada, C. J., Elmegreen, B. G., Cong, H.-I., & Thaddeus, P. 1978, ApJ, 226, L39.

Lockman, F. J. 1984, ApJ, 283, 90.

Merrifield, M. R. 1992, AJ, 103, 1552.

Moffat, A. F. J., Fitzgerald, M. P., & Jackson, P. D. 1979, A&AS, 38, 197.

Schechter, P. L. 1993, in Back to the Galaxy, ed. S. S. Holt & F. Verter (New York: AIP Press), 571.

Solomon, P. M., Sanders, D. B., & Rivolo, A. R. 1985, ApJ, 292, L19.

Strong, A. W. et al. 1988, A&A, 207, 1.

Weaver, H. & Williams, D. R. W. 1973, A&AS, 8, 1.

Westerhout, G. & Wendlandt, H.-U. 1982, A&AS, 49, 143.

Molecular Clouds at the Edge of the Galaxy: Clouds of FOG

J.G.A. Wouterloot[1], J. Brand[2]

[1]I. Physikalisches Institut, Universität zu Köln, 50937 Köln, Germany
[2]Istituto di Radioastronomia CNR, 40129 Bologna, Italy

I. Introduction

The outer Galaxy (defined as those parts of the Galaxy with $R>R_0$=8.5 kpc) in general and particularly the outermost regions ($R \gtrsim 16$ kpc; which we shall refer to as the far-outer Galaxy [FOG]) has not received the observational attention that has been dedicated to the inner Galaxy and the solar neighbourhood. Notable exceptions to this are a.o. studies of atomic hydrogen (e.g. Kulkarni et al. 1982, Henderson et al. 1982), in which the distribution and kinematic properties of HI have been analyzed out to R=20-30 kpc (kinematic distance). The reasons for this lack of attention are quite obvious: most of the molecular clouds and stars are inside $R\approx$12 kpc. Kutner & Mead (1981) were the first to specifically make a molecular survey of (a section of) the outer Galaxy, and they found relatively widespread CO emission, with kinematic distances corresponding to R up to 13 kpc. They subsequently mapped a number of these clouds in CO (Mead & Kutner 1988, hereafter MK88) and derived their masses, luminosities, and temperatures. Several other studies of individual outer Galaxy molecular clouds were carried out as well (Carpenter et al. 1990 (CSS90); Digel 1991 (Dig91); Sodroski 1991 (Sodr91)), but all of these are at $R \lesssim 14$ kpc. The objects mapped by Dig91 and MK88 are located in a region called the Outer Arm, which might either be a separate spiral arm or be connected to the Perseus arm in the second quadrant (see figure 1 of Henderson et al. 1982). Apart from the Perseus arm there are no known optical spiral arms in the outer Galaxy, with the possible exception of a collection of optical tracers 1 or 2 kpc beyond the Perseus arm, which may define a spiral arm segment (Kimeswenger & Weinberger 1989). Henderson et al. (1982) connect the Perseus arm to emission in the third quadrant, but the justification is weak.

It is however important to identify and study molecular clouds and embedded star forming regions at still larger R, in order to extend our understanding of the processes that lead to the formation of clouds and stars under physical conditions that are quite different from those found in the solar neighbourhood and in the inner Galaxy. In very general terms one could say that most things one finds in the inner Galaxy are also present in the far-outer Galaxy, but there is much less of it. To give some specific examples: The HI and H_2 gas surface and volume densities are much smaller, and their scale-heights are larger (Wouterloot et al. 1990); the star density is much smaller, there is less star formation, the interstellar radiation field (ISRF) is much weaker (Mathis et al. 1983; Bloemen 1985), there are no (known) spiral arms and fewer SNR's, so there are fewer and/or weaker external triggers for cloud- and star formation, He and metal abundances are lower (Shaver et al. 1983; Wilson & Matteucci 1992, hereafter WM92),

the FIR emissivity is smaller (Deul 1988), and the pressure of the intercloud medium is much smaller (Elmegreen 1989). This changing environment is expected to have its influence on cloud- and star formation.

This paper therefore deals with star-forming molecular clouds at the edge of the galactic - or more specifically the molecular - disk: where the edge is located depends on the tracer one uses. Atomic hydrogen has been found out to kinematic distances of 25 to 30 kpc from the center (e.g. Kulkarni et al. 1982). From CCD photometry towards l=180°, b=2.8°, Robin et al. (1992a,b) conclude that the edge of the stellar disk is between 5.5 and 6 kpc from the Sun at about 14-15 kpc from the galactic centre. Carney & Seitzer (1993) found indications for stars in one out of four fields located in the galactic warp at l=277°, b=−4.2° at R=16-17 kpc. Theoretical estimates of the location of the edge of the Galaxy depend on the value for the disk scale length and thickness at R=8.5 kpc (van der Kruit 1986). This scale length is 2.2-5.5 kpc (Robin et al. 1992b) which suggests a location of the optical edge of the Galaxy at R<21 kpc (Carney & Seitzer 1993). The scale lengths found at R>13 kpc by Wouterloot et al. (1990) are somewhat smaller: 1.5 kpc for molecular clouds and 1.9 kpc for HII regions. They found the value for the HI gas to be 4.0 kpc.
Optically visible HII regions with (spectro-) photometrically determined distances have been found out to R≈16-17 kpc (Moffat et al. 1979; Fich et al. 1989; Turbide & Moffat 1993; Brand & Blitz 1993). Wouterloot & Brand (1989; hereafter WB89) find star-forming molecular clouds out to R_{kin} ≈20 kpc (the HII region S266 has R_{kin} ≈19 kpc). The optical edge of the galactic disk is therefore located somewhere between 16 and 20 kpc from the galactic centre, and this range also defines the edge of the molecular disk. Very recently an optical HII region was found, associated with a molecular cloud at R≈28 kpc (de Geus et al. 1993, Digel et al. 1994). The ionizing star has presumably been identified and its spectrophotometric distance, although uncertain, puts it

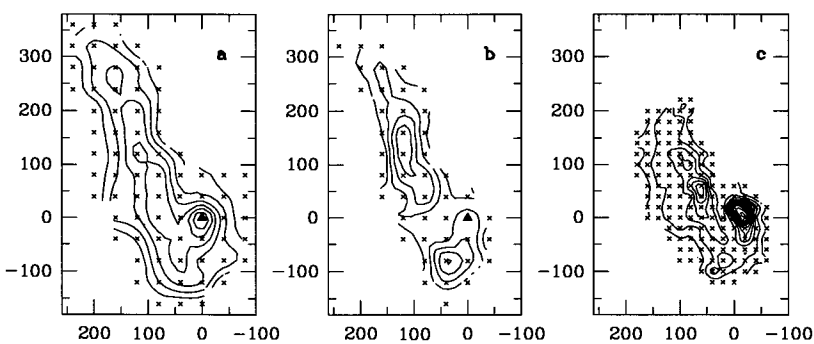

Figure 1:*Distribution of peak T_{mb} of WB1152 obtained with the SEST. a) ^{12}CO (1–0); contour levels are 1(1)K. b) ^{13}CO (1–0); 0.2(0.2)K. c) ^{12}CO(2–1); 1(1)K. The triangle indicates the position of IRAS08282−4545. Offset in arcsec in RA, Dec.*

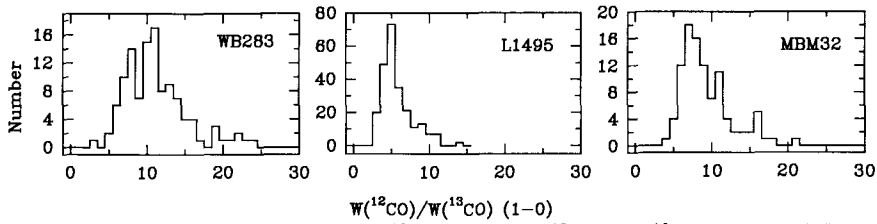

Figure 2:*Histogram of the ratio $W[^{12}CO(1\text{-}0)]/W[^{13}CO(1\text{-}0)]$ for the FOG cloud WB283, for a dark cloud in the solar neighbourhood (L1495), and for a high latitude cloud (MBM32).*

at $24.5 \lesssim R \lesssim 39$ kpc.

WB89 colour-selected IRAS sources with a FIR spectral distribution typical of star-forming regions from the Point Source Catalogue, and used them as tracers for the molecular gas. More than 1000 molecular clouds with embedded heating sources, and with R>8.5 kpc were found, of which almost 200 are at R>14 kpc. Brand & Wouterloot (1994a; hereafter BW94) mapped 27 clouds from the WB89 sample in ^{12}CO (1–0), and observed several other CO isotopes and -transitions at selected positions. The clouds in this sample have galactocentric distance $15.7<R_{kin}<20.2$ kpc (see Table 8 in BW94), with an average R of 17.3 kpc $\pm$ 1.2 kpc (1 σ); the median R is 16.8 kpc. We adopt 17 kpc as a representative value. An example of the results of the observations of one of the clouds is shown in Fig. 1.

In the present paper we analyze these data, comparing the results with those derived from similar observations of inner Galaxy clouds taken from the literature, and we try to use this to quantify differences in the various physical parameters (e.g. masses, kinetic temperature, and molecular abundances) between the inner- and far-outer Galaxy that are a result of the changing environment (see also Brand & Wouterloot 1994b for an extensive analysis).

II. Cloud Temperatures

A simple molecular cloud consists of a (dense) core, which has an approximately constant temperature, and an envelope, where the temperature increases outwards. Giant molecular clouds or -complexes (GMCs) can be thought of as a collection of cores with their envelopes, embedded in a layer of warm lower-density gas, which is part atomic, part molecular. The heating of the envelope and the inter-clump gas is dominated by the interstellar radiation field, which however in the far-outer Galaxy is probably negligible, although with the present knowledge it is not possible to make a quantitative statement. The cores are heated mostly by cosmic rays; cooling takes places through molecular line emission. For two clouds for which we have observations in up to five transitions we have used an escape probability model to derive a T_{kin} in the range 10 to 18 K, consistent with observations of inner Galaxy clouds, which show similar line

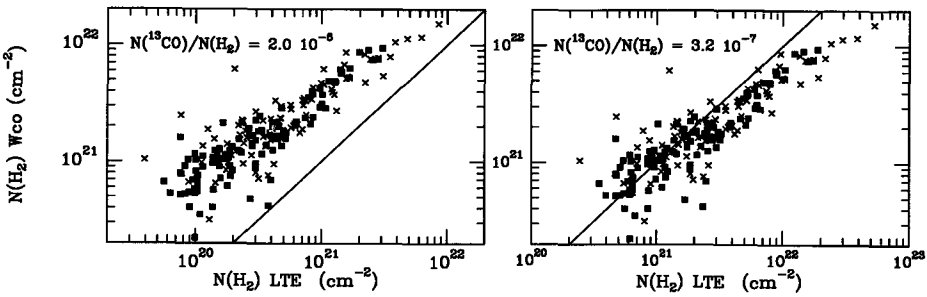

Figure 3: *Comparison of column densities of H_2 calculated via $N_{W_{CO}} = X\ W_{CO}$, with N_{lte}. The filled squares are IRAM 30-m data of the WB283 cloud and the crosses SEST data of several other FOG clouds. Left-hand panel: used local abundance ratio $N(^{13}CO)/N(H_2)$; right-hand panel: used abundance ratio at R=17 kpc, extrapolated from the gradients given by WM92. In both panels X=2.3 10^{20} $cm^{-2}(Kkms^{-1})^{-1}$, i.e. the value appropriate for local GMCs, and the drawn line is for equal column densities. When taking the abundance gradients into account $N_{W_{CO}} \approx N_{lte}$ for X in the far-outer Galaxy equal to the local value.*

ratios and from which a T_{kin} of 10 to 15 K was derived (Sanders et al. 1993). In addition we find, from a statistical analysis of measured temperatures of fore- and background clouds in WB89, that the average T_A^* does not depend on R in the range 9-16 kpc. Although the sources of cosmic rays (supernovae, pulsars) are strongly concentrated towards the central region of the disk, gamma ray observations are consistent with the existence of a cosmic ray halo (Bloemen 1989; Dogiel 1991). This might well explain the observed lack of temperature difference between inner- and outer Galaxy clouds.

III. Cloud masses

One way to determine masses from ^{12}CO data alone is to make use of the empirical fact that, at least for local GMCs, there is a constant ratio $X = [N(H_2)/\int TdV] \approx (2.3 \pm 0.3)10^{20}$ $cm^{-2}(Kkms^{-1})^{-1}$ (Strong et al. 1988). The resulting column density we shall call $N_{W_{CO}}$ ($W_{CO} \equiv \int TdV$) and the mass derived from this $M_{W_{CO}}$. For about 200 lines-of-sight towards our far-outer Galaxy clouds we have both ^{12}CO and ^{13}CO data. For one of the clouds, mapped with the 30-m IRAM telescope, we show a comparison of the observed ratio of both isotopes with that in local clouds in Fig. 2. The median values are about 10 (WB283), 5 (L1495), and 9 (MBM32). We think that the high value for the FOG is caused by the lower ^{13}CO abundance rather than a low ^{12}CO optical depth as is the case in the high latitude cloud MBM32. From these data we derive LTE-column densities (N_{lte}; mass M_{LTE}) and these are compared to $N_{W_{CO}}$ in Fig. 3. In the left-hand panel we used the local abundance ratio for $N(^{13}CO)/N(H_2)$=2.0 10^{-6} (Dickman 1978) when calculating N_{lte}, while in the right-hand panel we used the abundance ratio extrapolated to R=17 kpc (the average R of our sample), 3.2 10^{-7}, using the gradients given in WM92 for $[^{12}C]/[H]$ and $[^{12}C]/[^{13}C]$.

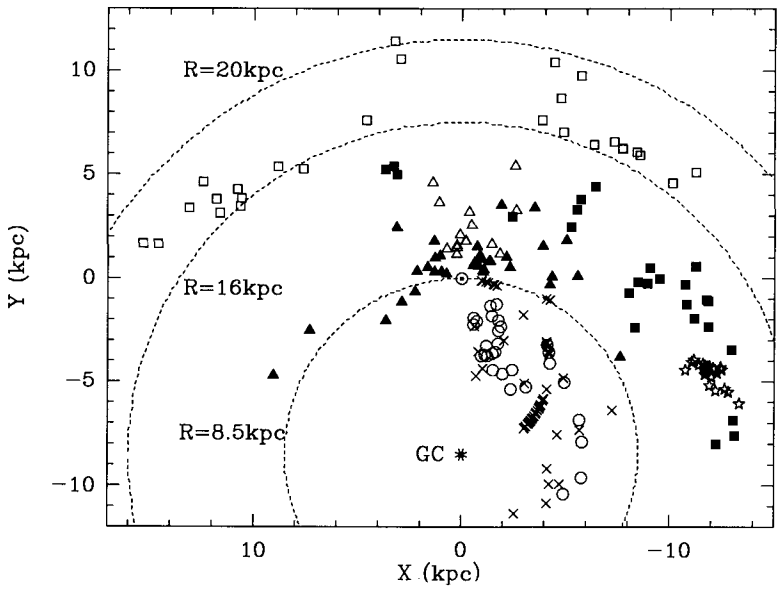

Figure 4: *Distribution of the molecular clouds in the extended data set, projected onto the galactic plane. The Sun is at (X,Y)=(0,0), and indicated by ⊙; the galactic center is at (X,Y)=(0,−8.5). Dashed circle segments indicate R=8.5, 16, and 20 kpc respectively. The individual data sets are distinguished by different symbols: BW94 (open squares), MK88 (filled squares), CSS90 (open triangles), Sodr91 (filled triangles), Dig91 (asterisks), Dame et al. 1986 (Dame86, circles), Solomon et al. 1987 (crosses).*

It is clear that when taking into account the galactic abundance gradient, both column densities are approximately equal, and the median value of X which one would derive plotting W_{CO} versus N_{lte} is 2.9 10^{20} cm^{-2}(Kkms^{-1})$^{-1}$ (with an rms deviation for *individual* positions of about 1.5 10^{20} cm^{-2}(Kkms^{-1})$^{-1}$), which is close to the assumed value of 2.3 10^{20} cm^{-2}(Kkms^{-1})$^{-1}$. This finding is in contrast to that of previous studies (e.g. MK88, Dig91, Sodr91) who all *postulate* a value of X in the outer Galaxy which is 2.5 – 4 times larger than the local value, based on a comparison of inner- and outer Galaxy cloud luminosities.

To investigate this in more detail we have combined our data set with data on outer Galaxy clouds taken from the literature (see caption of Fig. 4), making sure to scale all distances and masses to the same system, which resulted in a collection of 130 clouds with 8.5 $\lesssim$ R $\lesssim$ 20 kpc. In addition we collected data on 92 inner Galaxy clouds from the literature for which the derived parameters were also scaled with the same assumptions. The distribution projected onto the galactic plane of these clouds is shown in Fig. 4. Distinguishing between clouds at R smaller or larger than 8.5 kpc,

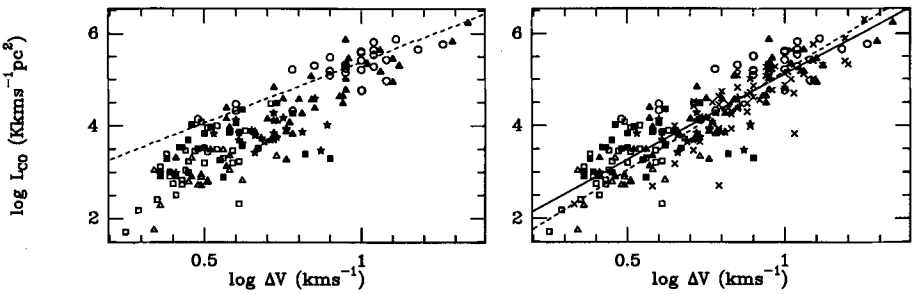

Figure 5:**a.** *Log L_{CO} versus log ΔV for all outer Galaxy clouds from the combined sample and the Dame86 inner Galaxy clouds. The dashed line is a least squares fit through these points. Symbols are as in Fig. 4.* **b.** *The same as a., but showing all inner Galaxy clouds. The drawn line is a least-squares fit through the outer Galaxy data only; the dashed line fits the inner Galaxy data.*

we show in Fig. 5 a plot of cloud luminosity L_{CO} versus linewidth. Since both quantities are independent of the beamsize, one does not expect any systematic differences between the various surveys. Taking only the Dame86 data for the inner Galaxy there seems to be a considerable difference (Fig. 5a). Dig91 concluded from similar data that the ratio X is a factor of 4 larger in the outer Galaxy, because $L_{CO} \propto M_{Wco}$, (and $\Delta V \propto \sqrt{M_{vir}}$). However least-squares fits through all inner Galaxy or all outer Galaxy data (see Fig. 5b) are essentially identical.

A comparison of Fig. 5a and 5b suggest that the conclusion of Dig91 was caused by the small number of small (i.e. low mass and low luminosity) clouds included in the inner Galaxy sample (which biases the inner Galaxy fit) and that there is no need for a sudden change of X at R_0, which confirms our conclusion based on the analysis of LTE column densities.

The distribution of cloud mass with R is shown in Fig. 6a. It is seen that in surveys of the inner Galaxy clouds of mass less than about 3 10^4 $M_\odot$ are missing, probably because of confusion. In the far-outer Galaxy there are no very massive clouds. We think that this is due to the small number of clouds in the sample. Assuming that the distribution over mass is the same for both samples and combining the data at some intermediate mass, we have binned the clouds in mass, fitted a power law to the resulting mass spectrum, and obtained $dN/dM_{Wco} \propto M_{Wco}^{-1.90\pm0.11}$. A similar excercise applied only to the outer Galaxy clouds gives a slope of -1.48 ± 0.12. These mass spectra are consistent with those found for other samples of local and inner Galaxy clouds as well as with those found for clumps within molecular clouds, and this gives important information on cloud- and clump formation scenarios. These spectra are in fact what one expects when GMCs grow via accretion and coalescence of smaller clouds (Combes 1991). If one integrates the mass function up to 10^7 $M_\odot$, the total mass of

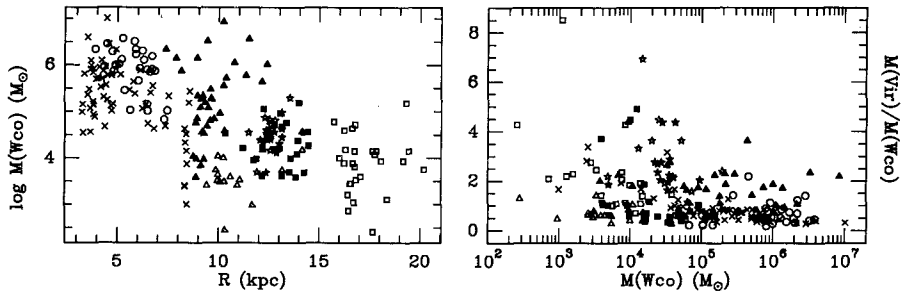

Figure 6:**a.** *Plot of M_{Wco} versus R for clouds in the combined data set.* **b.** *The ratio of virial mass and M_{Wco} as a function of the latter mass. Symbols are as in Fig. 4.*

molecular clouds in the outer Galaxy is 9.6 10^6 $M_\odot$.

The ratio of virial mass (=126 r ΔV^2) and M_{Wco} as a function of M_{Wco} is shown for the combined sample is shown in Fig. 6b. This ratio varies between 0.25 and 8.5, and the median value decreases from 1.69 for 10^2 -10^3 $M_\odot$ to 0.61 for 10^6 -10^7 $M_\odot$. Note that because of the assumption $\rho \propto r^{-2}$, the virial mass is a lower limit. The more massive clouds are situated in the inner Galaxy (see Fig. 6a), however the work of Adler & Roberts (1992) shows that clouds which seemingly are real entities, in reality may consist of clouds located along the line of sight over several kpc, and are therefore not always gravitationally bound objects.

IV. Systematic motions

The line width ΔV_{comp} of the composite spectrum (the sum of all spectra) of a molecular cloud is the result of random and systematic motions. The amount of small-scale random motion is represented by the average linewidth $<\Delta V>$ of all individual spectra, while the systematic component is characterized by the dispersion σ_{sys} around the average V_{lsr} of all detections: $\Delta V_{comp} = \sqrt{(<\Delta V>^2 + [2.35\sigma_{sys}]^2)}$.

We have compared the random- and systematic components in the 27 clouds observed by us (BW94; see Fig. 7). Most clouds have a random component which is larger than the systematic one, but four clouds have $\Delta V_{sys} > \Delta V_{rand}$. For a number of clouds we have determined the direction along which the gradient is largest in one coordinate, while being smallest in the other. Spectra were then summed in strips perpendicular to the direction of the gradient, and gauss fits were made to the sum spectra to get the velocity of the peak of the emission at each position along its direction. Interpreting this as being due to (solid body) rotation we have thus derived a.o. the angle of the rotation axis with respect to the (equatorial) coordinate system in which the observations were made, and the magnitude of the gradient, which has values between 0.018 and 0.266 $kms^{-1}pc^{-1}$. A typical value for local GMCs is $\lesssim$ 0.05 $kms^{-1}pc^{-1}$ (Blitz 1991).

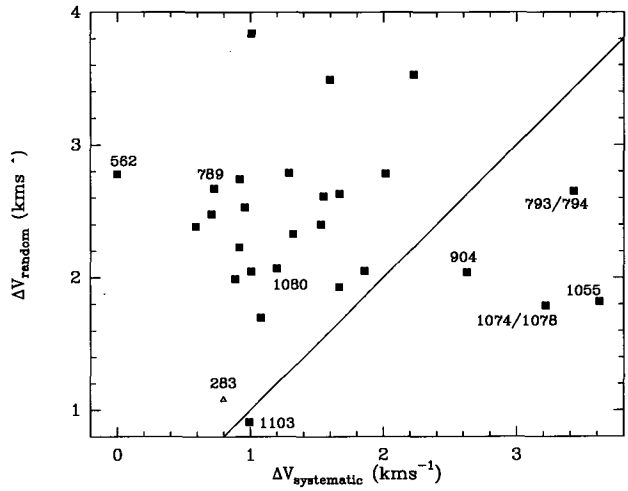

Figure 7:*Comparison of random and systematic velocity components in FOG clouds. The random component of a cloud is derived from the average of all line widths, while the systematic component is characterized by the dispersion around the average V_{lsr} of the peak of the emission. The drawn line indicates equal contributions. Some clouds are identified by their number from WB89.*

V. Conclusions

• The line ratios of different CO transitions (except $^{12}CO/^{13}CO$) in the FOG are similar to those in the inner Galaxy. Using escape probability models we derive kinetic temperatures of the clouds which are in the same range for both parts of the Galaxy.

• In the range R=9-16 kpc there is no change in the mean observed T_A^* of mapped clouds and of clouds happening to be in the line of sight towards IRAS point sources. If this T_A^* is related to the kinetic temperatures of these clouds, this would suggest that if there is a population of very cold clouds in the FOG as recently proposed by Lequeux et al. (1993), it is not detected in normal surveys or the relative number of such clouds is not depending on R.

• Assuming that the average galactic abundance gradients can be extrapolated to R=17 kpc, we derive, from LTE calculations, a median value of X=2.9 10^{20} $cm^{-2}(Kkms^{-1})^{-1}$, close to the value derived by Strong et al. (1988) for the inner Galaxy.

• Previous suggestions that X is larger in the outer Galaxy by a factor of 2.5-4 are wrong due to small number statistics.

• At least 20% of the FOG clouds show significant velocity gradients, comparable to those found in local clouds.

References

Adler D.S., Roberts W.W.: 1992 ApJ 384, 95

Blitz L.: 1991, in: Lada C.J. & Kylafis N.D. (eds), The Physics of Star Formation and Early Stellar Evolution, p. 3

Bloemen J.B.G.M.: 1985 A&A 145, 391

Bloemen J.B.G.M.: 1989 ARA&A 27, 469

Brand J., Blitz L.: 1993 A&A 275, 67

Brand J., Wouterloot J.G.A.: 1994a A&AS *in press*

Brand J., Wouterloot J.G.A.: 1994b A&A *submitted*

Carney B.W., Seitzer P.: 1993 AJ 105, 2127

Carpenter J.M., Snell R.L., Schloerb F.P.: 1990 ApJ 362, 147

Combes F.: 1991 ARA&A 29, 195

Dame T.M., Elmegreen B.G., Cohen R.S., Thaddeus P.: 1986 ApJ 305, 892

de Geus E.J., Vogel S.N., Digel S.W., Gruendl R.A.: 1993 ApJ 413, L97

Deul E.R.: 1988 Ph.D. Thesis, University of Leiden

Dickman R.L.: 1978 ApJS 37, 407

Digel S.W.: 1991 Ph.D. Thesis, Harvard University

Digel S.W., de Geus E.J., Thaddeus P.: 1994, ApJ *in press*

Dogiel V.A.: 1991 in: Bloemen J.B.G.M. (ed), I.A.U. Symp. 144, p. 175

Elmegreen B.G.: 1989 ApJ 338, 178

Fich M., Blitz L., Stark A.A.: 1989 ApJ 342, 272

Henderson A.P., Jackson P.D., Kerr F.J.: 1982 ApJ 263, 116

Kimeswenger S., Weinberger R.: 1989 A&A 209, 51

Kulkarni S.R., Blitz L., Heiles C.: 1982 ApJ 259, L63

Kutner M.L., Mead K.N.: 1981 ApJ 249, L15

Lequeux J., Allen R.J., Guilloteau S.: 1993 A&A 280, L23

Mathis J.S., Mezger P.G., Panagia N.: 1983 A&A 128, 212

Mead K.N., Kutner M.L.: 1988 ApJ 330, 399

Moffat A.F.J., FitzGerald M.P., Jackson P.D.: 1979 A&AS 38, 197

Robin A.C., Crézé M., Mohan V.: 1992a ApJ 400, L25

Robin A.C., Crézé M., Mohan V.: 1992b A&A 265, 32

Sanders D.B., Scoville N.Z., Tilanus R.P.J., Wang Z., Zhou S.: 1993 in: Holt S.S. & Verter F. (eds), Back to the Galaxy, p. 311

Shaver P., McGee R.X., Newton L.M., et al.: 1983 MNRAS 204, 53

Sodroski J.: 1991 ApJ 366, 95

Solomon P.M., Rivolo A.R., Barrett J., Yahil A.: 1987 ApJ 319, 730

Strong A.W., Bloemen J.B.G.M., Dame T.M., et al.: 1988 A&A 207, 1

Turbide L., Moffat A.F.J.: 1993 AJ 105, 1831

van der Kruit P.C.: 1986 A&A 157, 230

Wilson T.L., Matteucci F.: 1992 A&AR 4, 1

Wouterloot J.G.A., Brand J.: 1989 A&AS 80, 149 (WB89)

Wouterloot J.G.A., Brand J., Burton W.B., Kwee K.K.: 1990 A&A 230, 21

Far-Infrared [C II] Line Survey of the Galaxy

T. Nakagawa,[1] Y. Doi,[1,2] K. Mochizuki,[1,2] Y. Y. Yui,[1,2] H. Okuda,[1] M. Yui,[1,2] H. Shibai,[1] T. Nishimura,[3,4] and F. J. Low [3]

[1]The Institute of Space & Astronautical Science, Sagamihara, Kanagawa 229, Japan
[2]Department of Astronomy, The University of Tokyo, Hongo, Tokyo 113, Japan
[3]Steward Observatory, University of Arizona, Tucson, AZ 85721, USA
[4]*Present Address*: National Astronomical Observatory, Mitaka, Tokyo 181, Japan

Abstract

The first detailed map of the far-infrared [C II] 158 μm line emission from the Galactic plane was obtained using a balloon-borne telescope: *BICE*. The map covers wide areas of the Galactic plane ($255° \leq l \leq 25°$, $|b| \leq 3°$) with an effective spatial resolution of 15′. We have detected strong [C II] emission from most of the regions we observed. We also obtained a position/central-velocity map of the [C II] emission.

Some of the observed regions show an excess [C II] emission comparing to the CO emission. These regions probably corresponds to translucent photodissociation regions.

The longitude distribution of the $I_{[CII]}/I_{FIR}$ ratio shows a large dip toward the Galactic center, which suggests the suppressed formation of C^+ ions in the Galactic center region.

1 Introduction

The far-infrared [C II] line ($^2P_{3/2} \rightarrow {}^2P_{1/2}$, 157.7409 μm; Cooksy, Blake, & Saykally 1986) has been thought to be the dominant coolant of diffuse interstellar gas (e.g., Dalgarno & McCray 1972), since (1) the C^+ ion is easily excited to the first excited level $^2P_{3/2}$ by collisions with other particles, for its excitation energy from the ground level is not high ($\Delta E/k = 91$ K) and its critical density is rather low ($n_{cr} = 3 \times 10^3$ cm^{-3} for H I), and (2) the C atom is ionized to C^+ easily by general interstellar radiation field since its ionization energy (11.3 eV) is lower than that of the H atom (13.6 eV).

Large-scale [C II] emission from the Galactic plane was first detected by the pioneering works by Stacey et al. (1985) and by Shibai et al. (1991), and they have shown that the [C II] line emission is really one of the brightest lines from the Galaxy. However their observed areas were very much limited.

Recently, the Far-Infrared Absolute Spectrophotometer (*FIRAS*) on the Cosmic Background Explorer (*COBE*) carried out the first unbiased line survey in the far-infrared and obtained all-sky maps of far-infrared lines including the [C II] (Wright et al. 1991). However the spatial resolution of the *FIRAS* is too large (7° FWHM) to reveal detailed structures of the [C II] emission from the Galactic plane.

Here we present the results of the first detailed mapping observations of the far-infrared [C II] line. The observations cover wide areas ($255° \leq l \leq 25°$, $|b| \leq 3°$) with a much better resolution (15′) than that of the *FIRAS*.

2 Observation

The observations were carried out with the Balloon-borne Infrared Carbon Explorer (*BICE*), which is a customized system to observe large-scale [C II] emission (Yamashita 1991; Nakagawa 1993).

The offset, oversized optics of the *BICE* telescope reduces the instrumental background radiation, which generally limits the sensitivity of the far-infrared observations with non-cooled telescopes. The *BICE* focal plane instrument is a liquid-He cooled Fabry-Perot spectrometer incorporated with a stressed Ge:Ga photoconductor. The velocity resolution is 175 km s^{-1}, and the beam size is 12.4′.

In order to observe the diffuse [C II] emission efficiently, we have adopted a spectral scanning method instead of the conventional spatial chopping; the signal is modulated in the spectral domain by continuously sweeping the high-order Fabry-Perot etalon at 2.7 Hz in the velocity range of $\Delta v = 520$ km s^{-1}. The spatial scan was simultaneously made at a rather slow speed of 12′ s^{-1} or 18′ s^{-1}. Observed spectral profiles were corrected for atmospheric and instrumental emission profiles by assuming that the astronomical [C II] emission is negligible in the regions of $|b| \geq 3°$. Each corrected spectral profile was fit by a Lorentzian, whose height, width, and the central position were free parameters. From the height and width of the Lorentzian, we derived velocity-integrated [C II] line intensity for each spectral scan. Thus derived line intensities were then interpolated spatially into 3′ grids, and the result was smoothed to the final resolution of 15′ (FWHM).

The results presented in this paper were obtained from two balloon-flights. The northern Galactic plane ($348° \leq l \leq 25°$) was observed on 1991 June 12 during a flight from the National Scientific Balloon Facility in Texas, USA, and the southern part ($255° \leq l \leq 355°$) was observed on May 24 1992 during a flight from Alice Springs, Australia.

For the absolute flux calibration, we observed M17 in the both flights. The [C II] intensity of M17 within our beam was estimated on the basis of the published [C II] map (Matsuhara et al. 1989). The absolute calibration uncertainty is ± 30 %.

3 Results

3.1 Velocity-Integrated Line Intensity Map

Fig.1 shows the velocity-integrated [C II] line intensity map of the Galactic plane. We have detected strong [C II] emission from most of the regions we observed.

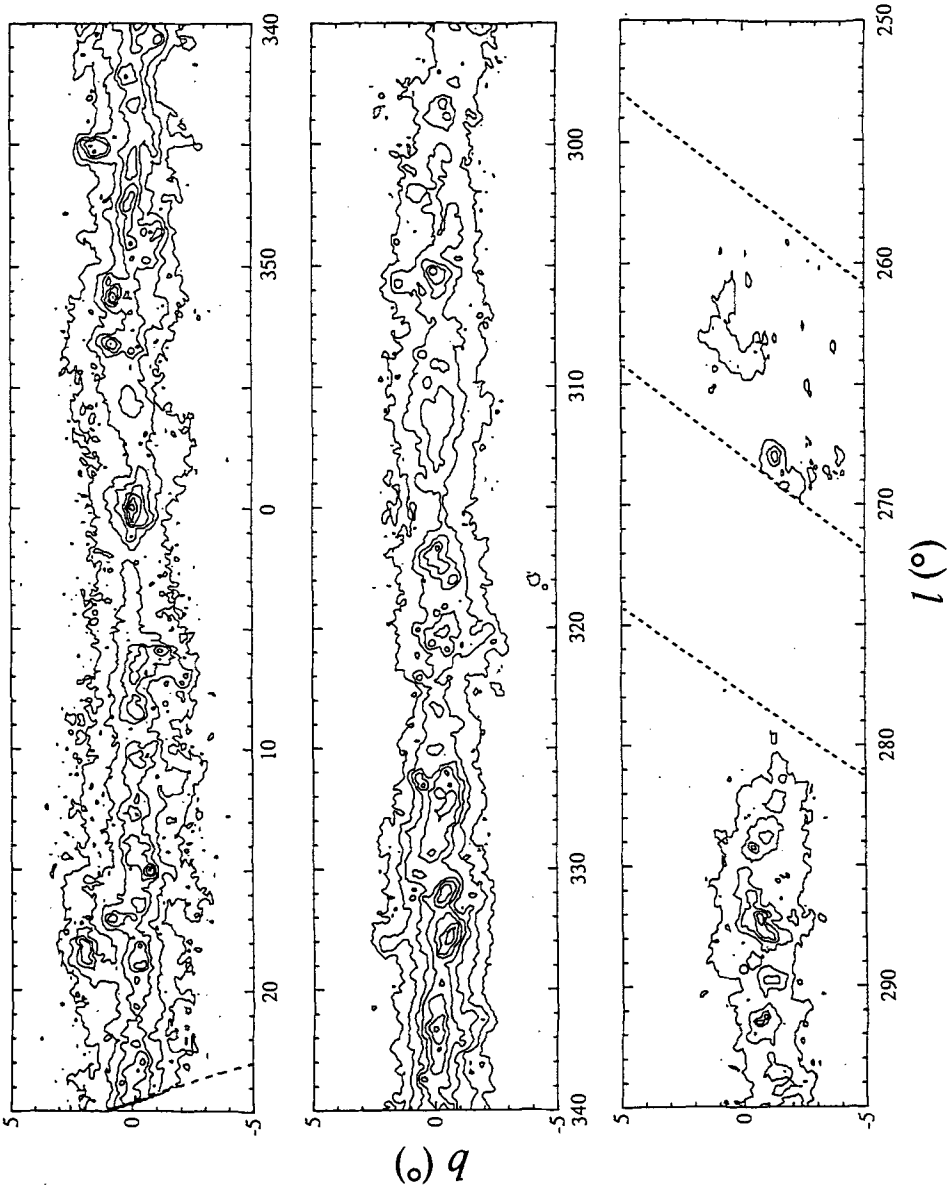

Figure 1: Velocity-integrated [CII] line intensity map. The effective spatial resolution is 15′. The contour levels are $0.2, 0.7, 1.5, 2.5, 4, 6, 9, 12 \times 10^{-4}$ erg s^{-1} cm^{-2} st^{-1} .

We can see both point sources and diffuse emission. Most of the point sources are identified as H II region/star-forming region complexes, where UV flux densities are very high. Tielens & Hollenbach (1985) defined photodissociation regions (PDRs) as the regions where far-ultraviolet (FUV) radiation dominates the heating and determines the chemical composition of gas. Around young OB stars, dense molecular clouds are irradiated by high radiation fields, and thus warm dense PDRs are formed. The point-like strong [C II] emission is attributed to these regions.

Fig.1 also shows strong diffuse [C II] emission, which is not directly associated with point sources. The scale height of this diffuse emission is similar to those of far-infrared continuum and mm CO line emission, but is much smaller than that of H I 21 cm line. These correlations suggest that the energy source of this diffuse [C II] emission is diffuse interstellar FUV radiation, which originates from these young stars.

3.2 Position/Velocity Map

As discussed above, we fit each observed line profile by a Lorentzian. From the central position of the Lorentzian, we can determine the central velocity for each spectral scan. The estimated errors of the determined velocity are very small and are less than ± 10 km s^{-1} for the lines with intensities larger than 1×10^{-4} erg s^{-1} cm^{-2} st^{-1} .

The derived central velocities are binned at each longitude weighted by their intensities.

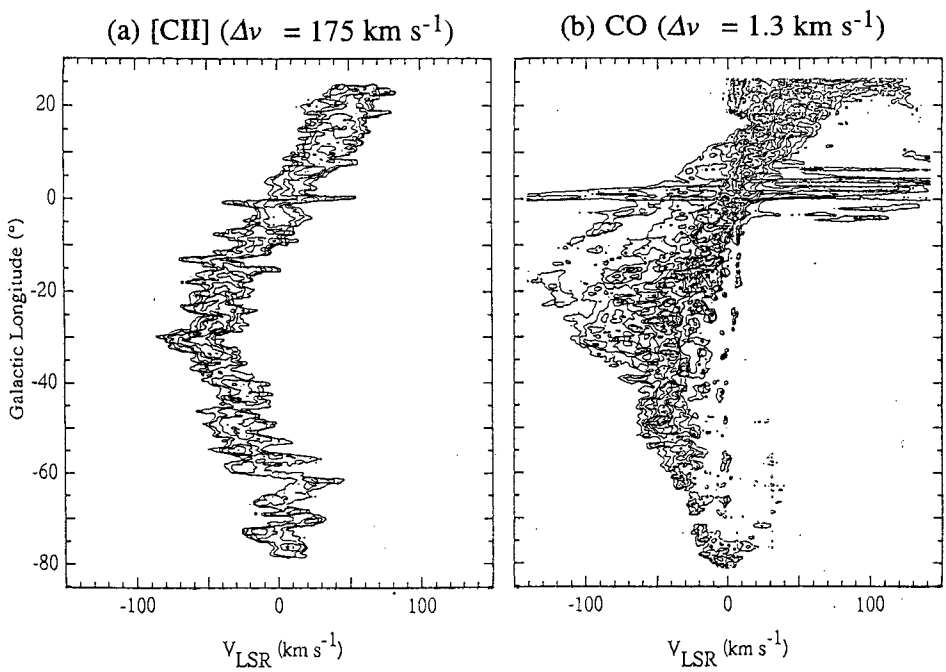

Figure 2: Position/velocity maps of the [CII] line emission (this work) and the mm CO (1-0) line (Dame et al. 1987).

Fig.2a shows the result in the form of a position/central-velocity map of the [C II] line. We can see the differential rotational pattern of the Galaxy very clearly.

For comparison, we show the position/velocity map of the CO (1-0) line emission (Dame et al. 1987) in Fig.2b. Although the instrumental resolution of the *BICE* system (Δv = 175 km s^{-1}) is much worse than that of the CO observations (Δv = 1.3 km s^{-1}; Dame et al.), the main pattern of the two diagrams are very much similar to each other. This result indicates that the spectral scanning method is very useful not only for obtaining lines intensities but also for deriving velocity patterns on a large scale.

Both Fig.2a and 2b show two velocity jumps at $l \sim 34°$ and at $l \sim 304°$, which corresponds to the tangential directions of the Galactic spiral arms. These jumps are more clearly seen in [C II] (Fig.2a) than in CO (Fig.2b). Hence we conclude that the [C II] emission traces the spiral pattern, and thus the distribution of young stars, more clearly than the CO line.

4 Discussion

4.1 Translucent Photodissociation Regions

Wolfire, Hollenbach, & Tielens (1989; hereafter WHT) modeled PDRs as a one-dimensional molecular cloud with the constant density (n) illuminated by FUV flux of G_0, which is normalized by the solar neighborhood value. They plotted $I_{[\mathrm{CII}]}/I_{\mathrm{FIR}}$ vs $I_{\mathrm{CO}}/I_{\mathrm{FIR}}$ assuming that the same PDRs produce the CO, [C II], and FIR continuum emission. Results of previous observations show a rather tight correlation in this plot. Since most of these observations are limited to star-forming region/H II region complexes, this correlation is attributed to a similar density dependence of $I_{[\mathrm{CII}]}$ and I_{CO} at high incident FUV flux (WHT).

We plotted our results in the same figure (Fig.3); our results do not show the tight correlation as active H II regions do, but show large scatter. Most of our observed points corresponds to the regions with moderate FUV flux density ($G_0 \sim 10^2$) and high density ($n \sim 10^5$ cm^{-3}). Since we observe combinations of various interstellar clouds along lines of sight, the interpretation of Fig.3 is not straightforward. For example, if only one third of the far-infrared continuum emission is attributed to PDRs, the observed points go toward upper right, and the result is consistent with that the most of the emission comes from low density ($n \sim 10^2$cm^{-3}) PDRs with moderate FUV flux ($G_0 \sim 10$). In any case, our observations are not consistent with $G_0 \sim$1 but show larger FUV fluxes ($G_0 = 10 \sim 10^2$). This result is probably attributed to the higher average FUV flux in the inner Galaxy than the solar neighborhood, since our observations are mainly for the inner Galaxy.

Active star-forming region/H II region complexes generally lie toward the lower left in Fig.3, which indicates larger G_0. This result is naturally understood since these regions are expected to be embedded in a high FLUX radiation field. Our observations,

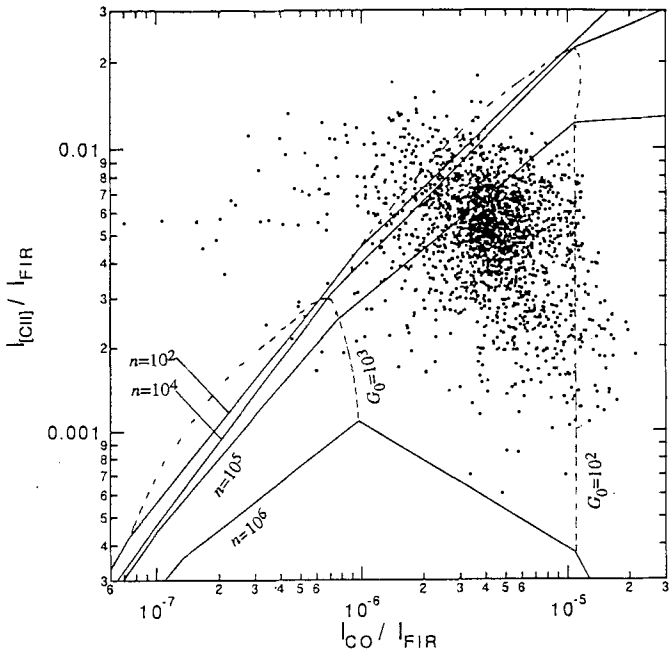

Figure 3: The ratio $I_{[CII]}/I_{FIR}$ vs the ratio I_{CO}/I_{FIR}. The [CII] data are from this work and the CO data are from Dame et al. (1987). The data are for $348° \leq l \leq 25°$. The theoretical curves are from Wolfire, Hollenbach & Tielens(1989).

however, show moderate FUV fluxes ($G_0 = 10^{3\sim3.5}$) even for the most active regions. This is due to the beam dilution effect, since we cannot spatially resolve the individual star-forming regions.

One interesting point of Fig.3 is that some data points are significantly above the theoretical lines. These points ($I_{[CII]}/I_{CO} \sim 6\times10^{-3}$, $I_{[CII]}/I_{FIR} \sim 10^{-7}-10^{-6}$) correspond to the regions where the [C II] emission is stronger or the CO emission weaker than theoretically calculated.

WHT used a semi-infinite one-dimensional slab model for their calculations. However actual clouds consist of small clumps and these clumps have finite sizes. Carbon is mostly C^+ at the surface of each clump, but becomes CO at $A_v \geq 4-6$ mag from the surface. If the size of each clump is smaller than the depth to this C^+/C/CO transition zone, the clump barely contains CO molecules. We call this type of clouds as translucent PDRs and the CO emission from these regions must be weaker than the WHT model predicts. Thus the data points above the theoretical lines in Fig.3 show the existence of this type of translucent PDRs on a large scale.

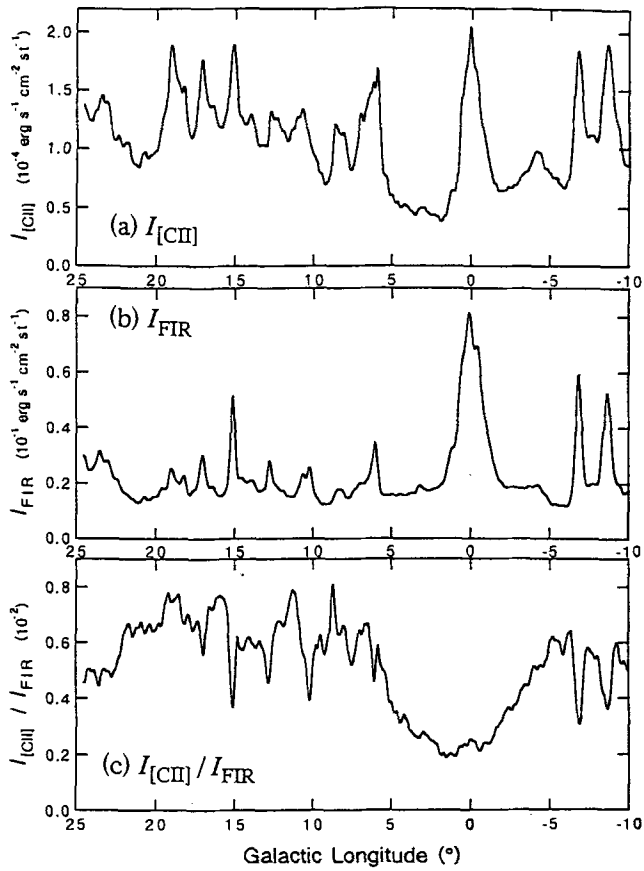

Figure 4: The longitude distribution of $I_{[CII]}$, I_{FIR}, and I_{CO}. All the data are averaged for $|b| \leq 2°$. The [CII] data are from this work, the CO data are from Dame et al. (1987), and the far-infrared continuum data are based on IRAS observations and the parameter FIR is defined by Helou, et al.(1988).

4.2 [CII] Line Deficit toward the Galactic Center

Fig.4a shows the longitude distribution of the [C II] line emission. Also shown (Fig.4b) is the longitude distribution of far-infrared continuum emission I_{FIR}. The Galactic center is a prominent peak both in the [C II] line and in far-infrared continuum. However, although the Galactic center is the dominant peak in the far-infrared continuum (Fig.4b), it is not in the [C II] line (Fig.4a). This situation is much more clearly illustrated in Fig.4c, which shows the $I_{[CII]}/I_{FIR}$ratio; the ratio is almost constant ($\sim$ 0.6%) along the Galactic disk but the ratio shows a large dip (down to 0.2%) around the Galactic center. The range of the dip is wide and covers roughly -3°< l <5°, which corresponds to 450 pc (l <0°) and to 750 pc (l > 0°).

Since the optical depth of the [C II] line toward the Galactic center was estimated to be optically not too thick (e.g., Crawford et al. 1985), this result implies that the formation of the C^+ ions is suppressed in the Galactic center.

We propose two possible mechanisms that suppress the formation of the C^+ ions.

The first mechanism is the self-shielding of molecules from photodissociation. The depth of the $C^+/C/CO$ transition zone are generally determined by dust extinction, but is determined by self-shielding of CO and H_2 molecules when $G_0/n < 10^{-2}$ (Burton, Hollenbach, & Tielens 1990). The Galactic center clouds are characterized by their pervasive higher density ($n \sim 10^4 cm^{-3}$) than typical clouds in the Galactic disk ($n \sim 10^{2.5} cm^{-3}$) (Güsten 1989). Hence G_0/n can be smaller than 10^{-2} on a large scale. If this is the case, self-shielding of molecules reduces the relative thickness of the [C II] emitting regions and also reduces the $I_{[CII]}/I_{FIR}$ ratio.

Another possible mechanism is the softness of the FUV flux in the Galactic center region. Cox & Laureijs (1989) estimated the Infrared Excess (IRE) of the Galactic center region, and showed that the diffuse component, which dominates the infrared luminosity, has much higher IREs ($\sim$30) than typical H II regions (IRE$\sim$ 10). Hence they concluded that the dominant heating source for the dust is the population of cool stars - K and M giants - comprising the Galactic nucleus. If this is the case, the ratio of the number of carbon-ionizing photons to the total photon number should be smaller in the Galactic center region, and the formation of C^+ ions is relatively suppressed.

Acknowledgements

The balloon flight operation and support was provided by the staff of the National Scientific Balloon Facility (U.S.A.). This work was supported by grants-in-aid from the Ministry of Education, Science, and Culture in Japan, and by NASA in U.S.A.

References

Burton, M. G., Hollenbach, D., & Tielens, A. G. G. M. 1990, ApJ, 365, 620

Cooksy, A. L., Blake, G. A., & Saykally, R. J. 1986, ApJ, 305, L89

Cox, P., & Laureijs, R. 1989, in IAU Symp. 136, The Center of the Galaxy, ed. M. Morris, (Dordrecht: Kluwer), 121

Crarford, M. K., Genzel, R., Townes, C. H., & Watson, D. 1985, ApJ, 291, 755

Dalgarno, A., & McCray, R. A. 1972, ARA&A, 10, 375

Dame, T. M., et al. 1987, ApJ, 322, 706

Güsten, R. 1989, in IAU Symp. 136, The Center of the Galaxy, ed. M. Morris, (Dordrecht: Kluwer), 89

Helou, G., Khan, I. R., Malek, L., & Boehmer, L. 1988, ApJS, 68, 151

Matsuhara, H., et al. 1989, ApJ, 339, L67

Nakagawa, T. 1993, in Astronomical Infrared Spectroscopy: Future Observational Directions, ed. S. Kwok (San Francisco: ASP), 373

Shibai, H. et al. 1991, ApJ, 374, 522

Stacey, G., Viscuso, P. J., Fuller, C. E., & Kurtz, N. T. 1985, ApJ, 289, 803

Tielens, A. G. G. M., & Hollenbach, D. 1985, ApJ, 291, 722

Wolfire, M. G., Hollenbach, D., & Tielens, A. G. G. M. 1989, ApJ, 344, 770 (WHT)

Wright, E. L., et al. 1991, ApJ, 381, 200

Yamashita, Y. 1991, Mast. Thesis, Univ. Tokyo

Molecular Gas and Star Formation Beyond the Optical Disk of the Galaxy

E.J. de Geus[1], and S.W. Digel[2]

[1] Caltech, Astronomy Department 105-24, Pasadena, CA 91125, U.S.A.
[2] NASA Goddard Space Flight Center, Code 662, Greenbelt, MD 20771, U.S.A.

Abstract

We report the detection of a number of molecular clouds beyond the optical disk of the Galaxy. The two most distant of these objects were found to have kinetic temperatures similar to star-forming molecular clouds in the Solar neighborhood. Hα emission was detected from the most distant cloud (R_{GC} = 28 kpc) and a B 0.5 I star identified as the most likely source of ionization. The photometric distance to the star corroborates the location of the molecular and ionized gas beyond the optical disk.

Introduction

A considerable body of evidence appears to indicate that the edge of the optical disk of the Galaxy lies between 14 and 18 kpc from the Galactic center (see de Geus *et al.* 1993 for a recent overview). Atomic gas extends out to a much greater radius, with HI traced out to at least 30 kpc from the center (e.g., Kulkarni, Blitz & Heiles 1982). Other spiral galaxies also typically have HI disks extending far beyond the optical disk. Galaxies studied by Kennicutt (1989) have sharp edges in their stellar disks correlating with a drop in the gas surface density below a critical value interpreted as the threshold for gravitational instability and thus star formation. We report here the results of a search for molecular gas associated with the atomic gas beyond the edge of the Galaxy's stellar disk.

Observations

Using the CfA 1.2-m CO telescope we searched for molecular gas near 71 HI emission peaks in the galactic longitude range 130°– 155°and at Galactic radii between 18 and 30 kpc. From this survey we found 11 molecular clouds with kinematic Galactocentric distances of 18 – 28 kpc (Digel, de Geus,& Thaddeus 1994). Higher resolution ^{12}CO, ^{13}CO, and ^{12}CO(2-1), observations of the two most distant clouds (#1 at 22 and and #2 at 28 kpc) were obtained with the NRAO 12-m, in order to measure the temperatures and column densities of the gas. Kinetic temperatures were derived from large velocity gradient models using as input the column density of CO, which was derived from the ^{12}CO and the ^{13}CO observations, and the isotopic abundance ratio. We adopted $[CO]/[^{13}CO] = 100 \pm 50$ for the extreme outer Galaxy, a factor of 2 higher than at the Solar circle (Langer & Penzias 1990). In this manner clouds 1 and 2 were found to be at 13 ± 5 K and 22 ± 7 K, respectively. These are similar to those of complexes like Taurus and Orion, star forming molecular clouds in the Solar neighborhood. Because clouds 1 and 2 are well beyond the edge of the optical disk, the high kinetic temperatures are difficult to interpret, unless local heating sources are present or the clouds cool

inefficiently. We subsequently set out to search for any heating sources near these clouds.

We observed cloud 2 (at 28 kpc) in Hα with the Maryland-Caltech Fabry-Pérot on the Palomar 60-in telescope, and discovered a faint H II region at a LSR velocity of -101 kms^{-1}. This in excellent agreement with the LSR velocity of the CO (de Geus *et al.* 1993). Furthermore, the projected proximity and the similar morphology of the bright regions of Hα and CO emission confirm that the ionized and molecular gas are closely associated. Diffuse Hα emission near -101 kms^{-1} pervades most of the field in Figure 1, and the CO contours are correlated with a narrow "shadow" over the Hα emission. The bright rim in Hα is well correlated with the edge of the molecular cloud, implying that the dense gas traps the ionizing photons. This suggests a blister-type H II region, in which the ionizing star(s) is located to the south-east of the molecular material. Assuming a distance of 21 kpc to the source, the Hα observations imply a lower limit to the Lyman continuum flux $N_{Ly} \gtrsim 7.5\ 10^{46}$ s^{-1}.

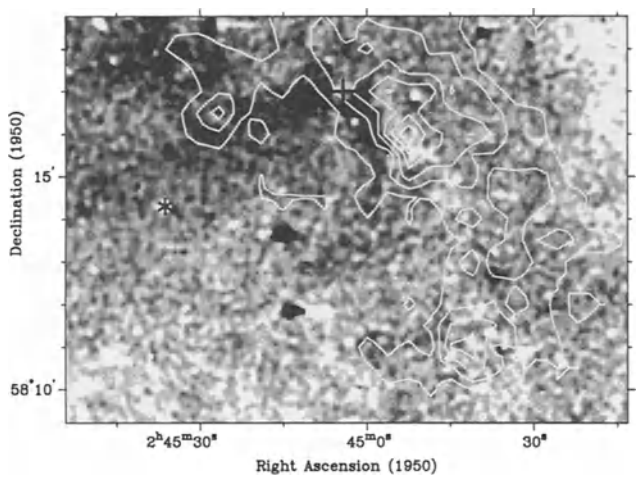

Figure 1.—Negative gray-scale image of Hα emission associated with cloud 2, obtained with the Maryland-Caltech Fabry-Pérot camera. The image was smoothed using a median filter with a smoothing radius of 5.″6, and a continuum image subtracted to remove stellar images. Compact sources in the Hα image, such as those at $\alpha \approx 2^h45^m15^s$ at $\delta \approx 58°12'$ and $58°14'$, are incompletely subtracted stellar images. Contours of CO 1–0 emission from the NRAO 12-m, integrated between -107 and -98 kms^{-1}, are overlaid (Digel *et al.* 1994). The contour levels range from 2.5 – 15 K kms^{-1}, with steps of 2.5 K kms^{-1}. The positions of the likely ionizing star (a likely early B supergiant) and an embedded IRAS source are indicated by a $*$ and a $+$, respectively. The Galactic coordinates for the center of this image are $\ell = 137.^\circ8$ and $b = -1.^\circ0$.

Discussion

Using SIMBAD we identified a possible ionizing star described by Muzzio & Rydgren

(1974, MR), who used UBV photometry to search for O–B3 stars in the outer Galaxy in fields of low apparent foreground extinction. Star 1 in their list lies a few arcminutes to the south-east of the bright rim of the H II region (Fig. 1). The UBV photometry by MR indicated that the star lies above the O5 V reddening line with a visual extinction of 3.1 mag and a distance modulus of 12.2 mag. MR also obtained a low-dispersion spectrum of this star, from which they conclude it is a late-B supergiant. MR, however, based this assignment on the presence of the Ca II K line, which, particularly at an $A_V \approx 3$ mag, is probably interstellar. This would change the derived spectral type of the star to late O or early B. Given the uncertainties in assigning a spectral type and luminosity class for early-type stars based on photometry, we may conclude that the photometry and spectroscopy are now in agreement for a late O - early B supergiant. The range of spectral types and the uncertain supergiant subclass lead to absolute magnitudes for this star from -5.9 mag for a B2 Ib star, to -7.2 mag for any O or B star with luminosity class Ia. This results in a range of distances to the Sun of 17.5 to 32.0 kpc, and Galactic radii between 24.5 and 39 kpc. *Despite the uncertainties in the derived properties of the star, we conclude that it is located beyond the edge of the optical disk of the Galaxy.*

The discovery of a massive star forming molecular cloud at 28 kpc from the Galactic center raises a number of questions and creates several opportunities for new studies. The presence of early-type stars allows a distance determination independent of velocity. We have obtained very deep photometry to search for the main-sequence component associated with the cloud; analysis is still in progress. A better constrained distance for cloud 2 will allow us to corroborate the kinematic distance, and it will extend the rotation curve of the Galaxy by a factor 1.6. The existence of this cloud and its assocated star formation raise the question whether molecular clouds occur only sporadically or if they are fairly common at large distances from the center. The molecular cloud at 28 kpc may have only been detected because it is heated by massive stars, and the presence of a substantial component of cold molecular gas cannot be ruled out. Finally, the identification of a molecular cloud and early-type stars beyond the optical disk provides an opportunity to investigate the level of chemical evolution at large distance from the center.

References

Digel, S., de Geus, E.J., & Thaddeus, P., 1994, ApJ in press.

de Geus, E.J., Vogel, S.N., Digel, S.W., and Gruendl, R.A., 1993, ApJ 413, L97.

Kennicutt, R. 1989, ApJ 344, 685.

Kulkarni, S.R., Blitz, L. & Heiles, C., 1982, ApJ 259, L63.

Langer, W.D., & Penzias, A.A. 1990, ApJ 357, 477.

Muzzio, J.C., & Rydgren, A.E., 1974, AJ 79, 864.

Molecular Gas Surrounding the Galactic Center

Paul T.P. Ho
Harvard-Smithsonian Center for Astrophysics, Cambridge, MA 02138, U.S.A.

Abstract. The Galactic Center is the nearest example of a galactic nucleus. Recent observations of the molecular gas in the vicinity of the Galactic Center suggest possible infall motions. In this paper, we review the observed morphology, kinematics, and the outstanding questions. The importance of these types of studies is obvious. As the nearest example, the details which we can study in the Galactic Center may have implications on understanding the processes which take place in more distant system.

Large Scale Structures. A great deal of progress has been made in the past decade in studying the molecular environment of the Galactic Center. Numerous surveys in a number of different molecular transitions have shown the presence of several giant molecular complexes near the Galactic nucleus (cf.Tsuboi et al. 1989; Bally et al. 1988). The most recent maps by Jackson et al. (1994), made in HCN with the FCRAO focal-plane array (Figure 1), show that the high density material are well confined to the disk (FWHM <25pc) near the Galactic Center. A dense complex of gas known as the Sgr A molecular cloud lies directly toward the Center, and is clearly delineated in high density tracers. The next complex, Sgr B2, is located some 100pc away in positive longitude. The absence of symmetry is perhaps the most striking feature of the morphology. Sgr B2 has a larger scale height as compared to Sgr A by a factor of 2. Also, the displacement from the mean disk position is quite striking, with the overall distribution undulating along the disk. In addition, there are smaller condensations in the form of filamentary structures above and below the plane. These asymmetries suggest the transient and dynamic nature of the molecular gas distribution near the Galactic Center. The effects of star formation, supernovae, as well as noncircular motions due to a stellar bar, may all influence the evolution of the nuclear gas.

In terms of kinematics, the molecular gas complexes appear to follow the Galactic rotation. This suggests that if these complexes were brought into the nuclear region through non-circular motions, they have now once again achieved quasi-equilibrium through rotational support. The nuclear GMC's are denser and warmer than the "normal" GMC's in the disk of the Galaxy. The high density suggests that self gravity may be sufficient to balance against the tidal pull of the central potential well. On the other hand, the large line widths observed for the Galactic Center clouds, typically 20 km s^{-1}, are a factor of 4–5 larger than "normal" line widths in the disk. This has led to the suggestion that tidal effects in the central gravitational potential may be responsible for the observed properties of these clouds (cf. Gusten 1989).

Hasegawa et al.(1993) recently mapped the large scale distribution of ^{13}CO emission toward Sgr B2 with the Nobeyama 45m telescope. These authors showed that a large scale cloud-cloud collision may have occured with relative motions on the order of 30 km s^{-1} over a size scale of 10pc. Such collisions may lead to a burst of star formation as is observed for this complex. Note that such activities would be hard to discern in an extragalactic nucleus because of resolution effects, but are clearly discernable in our own Galactic Center.

The University of Tokyo group also operates a 0.6m telescope at the J=2–1 CO line. The data from this survey instrument can therefore be directly compared with the J=1–0 CO results from the 1.2m CfA telescope. By mapping the spatial distribution of the J=2–1/J=1–0 ratio, Oka et al.(1993) shows the Galactocentric distribution of gas

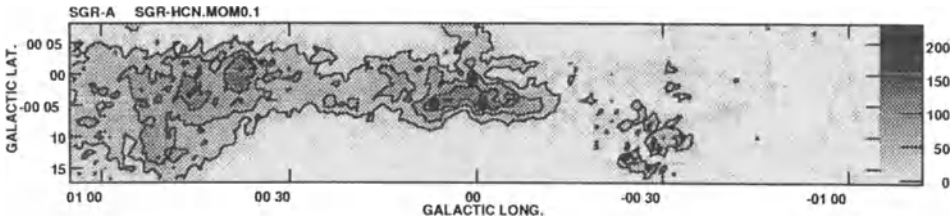

Figure 1. : The integrated HCN J=1–0 emission (*contours and greyscales*) from FCRAO (Jackson et al. 1994). Note the scale height of the emission is larger toward Sgr B2 as compared to Sgr A.

excitation. By comparing the longitude-velocity diagrams of J=2–1 CO, HI, H109α, and OH/IR stars, these authors find that the Galactic rotation curve seems to change with the age of the phenomenon. This may indicate a "phase transition" in the nuclear ISM with time.

The Inner 10pc. The close association of the Sgr A molecular complex with the nucleus, also seen in the dust continuum emission (cf. Mezger et al. 1989), suggests that this might be the gas reservoir which feeds the nuclear region. If parts of Sgr A are in fact as close to the nucleus as they are in projection, the tidal pull of the central potential well should be most evident here. If material do get pulled in, then the associated process, and the defining properties such as infall rate, the mass involved, and the morphology of the infalling gas, are all of great interest. This process at the 1–10pc scale can eventually be studied in extragalactic nuclei, given sufficient sensitivity and sub-arcsecond resolution. Note that we have not mentioned the possible presence and the potential influence of a massive black hole at the Galactic Center. At the 1–10pc scale, infall under the influence of the central potential well is important irregardless of whether or not there is a massive black hole.

The primary question then is whether the molecular gas complex is in fact at the distance of 1–10pc from the nucleus. We review here the kinematical evidence for the physical association of the gas with the Sgr A-East continuum complex. Synthesis maps in ammonia were made with the VLA (Ho et al. 1991) and the Nobeyama Array (Okumura et al. 1991). These maps show that the two molecular clouds, M-0.02-0.07 and M-0.13-0.18, parts of the Sgr A complex, lie immediately adjacent to the nonthermal supernova remnant Sgr A-East. Recently we have added to the VLA data by observing six new fields. The eleven-field mosaic synthesis in the NH_3 (3,3) line is shown in Figure 2. Morphologically, one can see that the molecular material must serve as a real boundary to the expansion of Sgr A-East on the eastern and northern sides. The edges of the continuum and molecular emission correspond very well, and the steepness in the continuum boundary suggests an edge. In contrast, on the western side, the continuum emission falls off much more gradually and there is in fact very little molecular material in that direction. The Sgr A-East remnant must be expanding relatively freely in that direction.

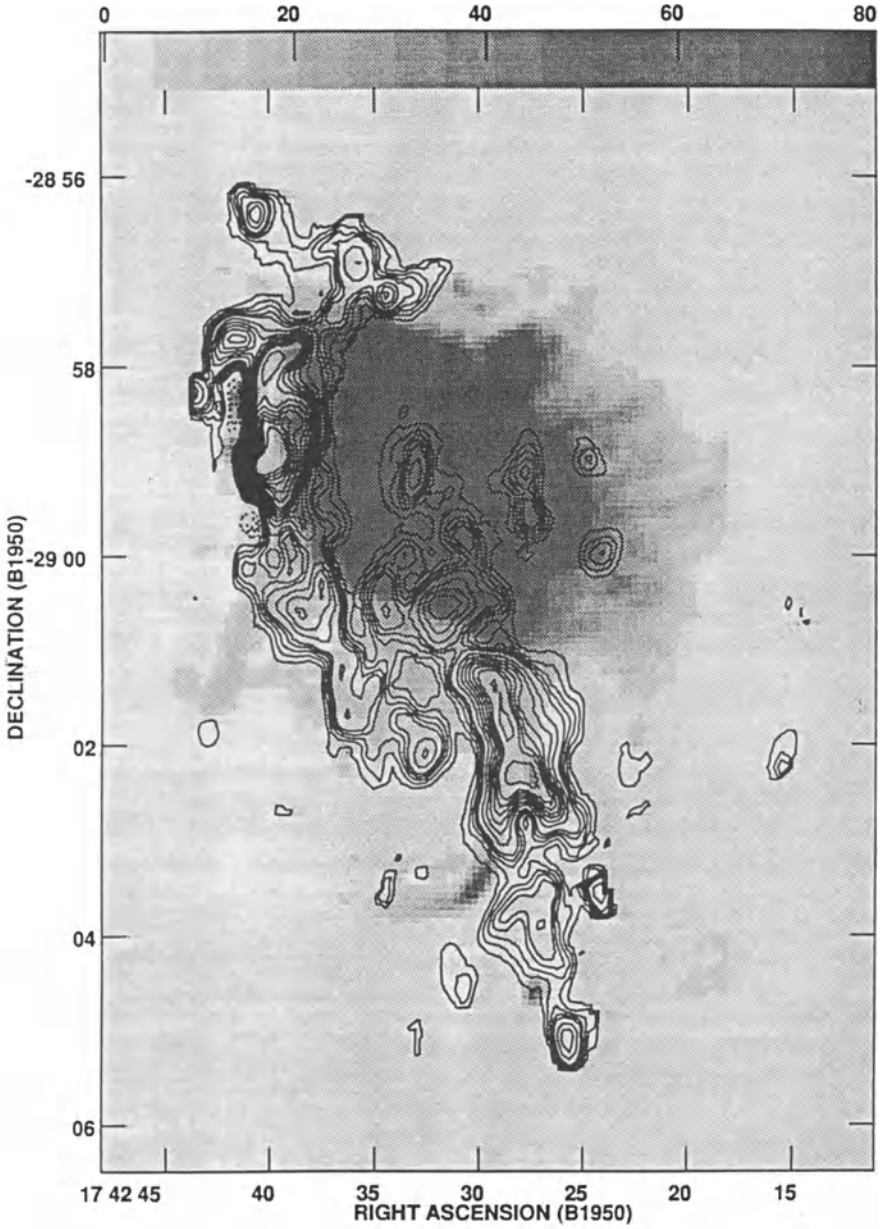

Figure 2. : The integrated NH_3 (J,K)=(3,3) emission (*contours*) from an eleven-field VLA synthesis, superposed on the 6cm radio continuum emission (*greyscale*).

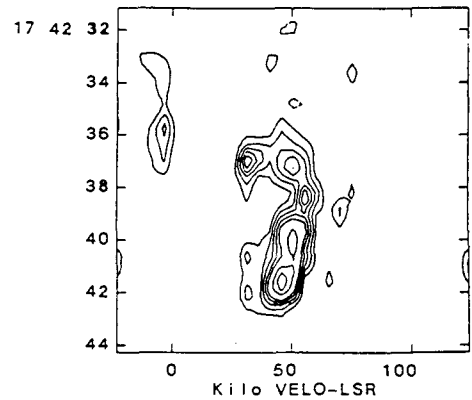

Figure 3. : A position-velocity plot of the NH_3 emission across the northern boundary of Sgr A-East. Note the classic inverted "C" pattern as is seen on the eastern boundary, which can be interpreted as radial projection of an expanding shell of gas on the near side of Sgr A-East.

In the previous five-field synthesis, there were already kinematical evidences of the impact of Sgr A-East on the gas. In position-velocity diagrams across the M-0.02-0.07 cloud on the eastern edge of Sgr A-East, one can see a change in the projected radial motions as we approach the center of Sgr A-East. The new fields to the north show the same effect (Figure 3). Gas red-shifted by about 20 km s^{-1} can be interpreted as expansion which is projected along the line of sight. The red-shifted motions suggest that SgrA-East is in front of M-0.02-0.07. The kinematical evidence when combined with the morphological evidence, suggest that these molecular clouds are in fact in physical contact with Sgr A-East. If Sgr A-East is at the Galactic Center, then these molecular clouds must lie as close to the Center as they appear in projection.

The Circumnuclear Ring. Toward the Center, Figure 2 shows that there are some NH_3 emission surrounding the central core. A much better defined and much more coherent structure has been seen before in the HCN J=1–0 transition. Using the Berkeley Hat Creek interferometer, Gusten et al. (1987) found a circumnuclear ring of emission, about 3pc in diameter, centered on the Sgr A-West and Sgr A* sources. This structure has been seen also in HCO+ with the BIMA array (Marr, Wright, and Backer 1993). Recent HCN J=3–2 data from IRAM 30m (Jackson et al. 1993), and J=3–2 and J=4–3 data from JCMT (Marshall and Lasenby 1993) further defined this circumnuclear structure (Figure 4). The interpretation is that there is a rotating ring which is tilted some 70° off the plane of the sky. The western side of the circumnuclear ring, also seen in NH_3, corresponds very well with the western ionized streamer in Sgr A-West. This suggests that the ionized streamers are features infalling from the circumnuclear ring. The kinematics of both the neutral and the ionized gas agree for some of these features, supporting this interpretation (cf. Schwarz et al. 1989, Jackson et al. 1993).

Note that the agreement between the NH_3 and the HCN is not exact by any means, and there are differences in the morphology depending on which molecule and which transition we are looking at. The missing parts of the ring structure in the NH_3 emission

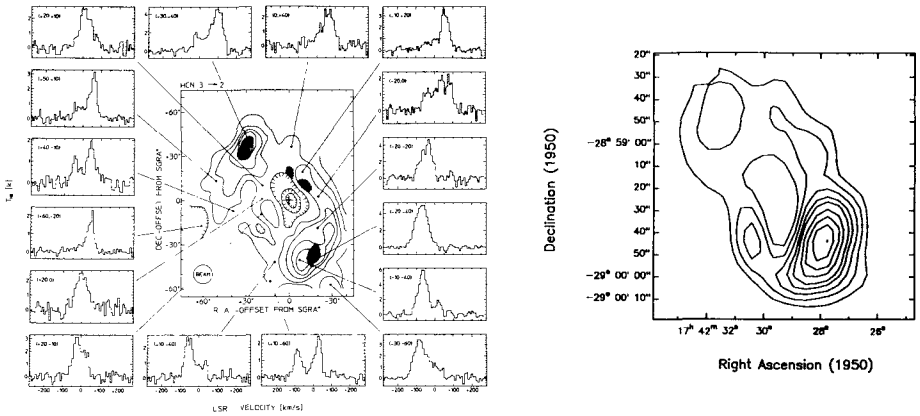

Figure 4. : *Left.* HCN J=3–2 map from IRAM 30m. *Right.* HCN J=4–3 map from JCMT. Note that the morphology changes somewhat depending on the transition.

are not due to missing short spacing information since lower resolution data from MPIfR 100m telescope show similar results. Apparently, the northern and southern portions of the circumnuclear ring are formed by high velocity material which radiate strongly in HCN and relatively faintly in NH_3. This could be a temperature effect, or an excitation problem, or even an abudance problem. Direct comparison of HCO+ to HCN by Marr et al. suggests that the HCN abundances may be enhanced in this region.

The Southern Streamer. Irregardless of the exact morphology of the circumnuclear ring, we can ask how the inner 2pc might be connected to the outer disk and nearby molecular clouds. The VLA and Nobeyama NH_3 results have shown that a finger-like streamer seems to emanate from the southern cloud M-0.13-0.08 and which terminates in the vicinity of the circumnuclear ring (Figure 2; Ho et al. 1991; Okumura et al. 1991). This feature can also be seen in the dust continuum maps (Mezger et al. 1989). The problem is that there seems to be no kinematical evidence to tie this streamer to the circumnuclear ring. Neither acceleration nor enhanced line widths are seen which might be consistent with infall. Thus we cannot rule out that this streamer is a chance projection against Sgr A-West. Nevertheless, this streamer does terminate at the position of the circumnuclear ring, which could be consistent with a scenario where the dispersion of the streamer by the central tidal forces resulted in the formation of the ring. In addition, the HCN kinematical data cannot fit the tilted rotating ring model exactly. There are extra components which can be interpreted as the termination of the southern streamer on the ring (Jackson et al. 1993).

The Eastern Streamer. Because the morphology seems to depend somewhat on the molecular transition, and because there seems to be some evidence of material coming into the nuclear region from the south, we wanted to explore the large scale connection between the inner 2pc and the outer clouds. We chose to do some large maps in the HCN lines since the circumnuclear ring was originally found in this molecule. In

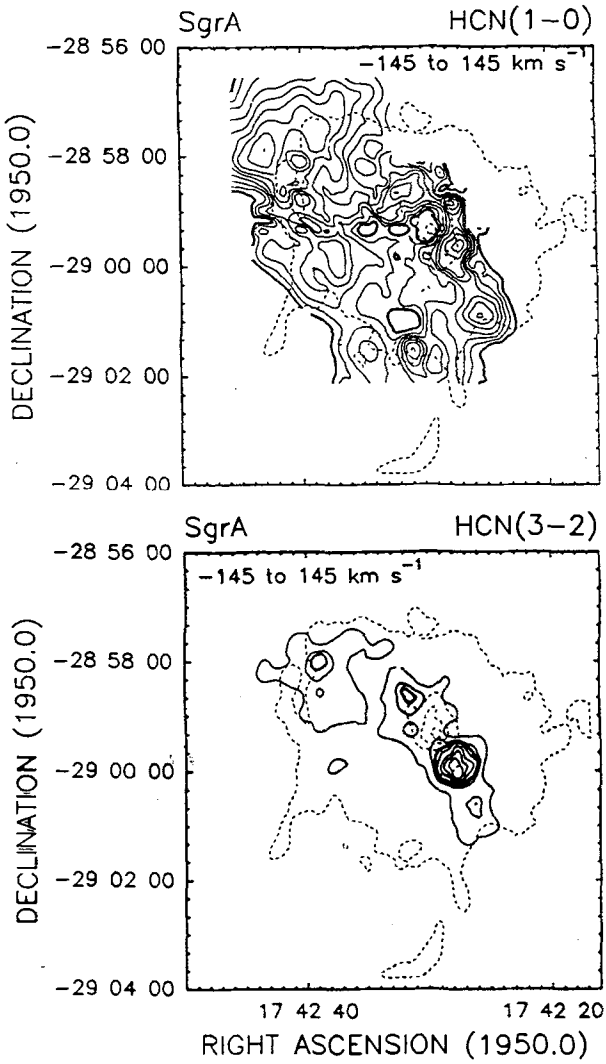

Figure 5. : *Top.* Integrated HCN J=1–0 emission as measured with the IRAM 30m telescope. Contour levels are 175 to 375 by 25K- km s^{-1}. Note that the circumnuclear ring is embedded in an extended complex. *Bottom.* Integrated HCN J=3–2 emission as measured with the CSO 10m telescope. Contour levels are 150 to 450 by 50K- km s^{-1}. Note that the J=3–2 emission does not have a ring-like appearance.

addition, it is clear that there are features which the NH_3 maps are not sensitive to. We obtained new J=1–0 data with the IRAM 30m telescope, and matched them with new J=3–2 data from the CSO 10m telescope. The achieved angular resolutions were therfore the same, about 20″. This is a factor of 2 coarser than the VLA NH_3 maps.

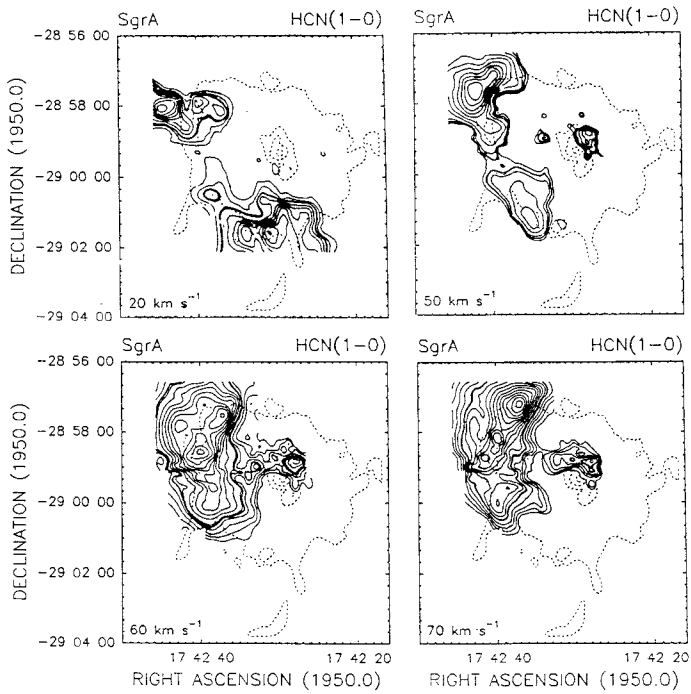

Figure 6. : The HCN J=1–0 emission at a few velocity channels. Note that at around 60 km s^{-1}, the M-0.02-0.07 cloud seems to be connected to the circumnuclear shell. This may be possibly another path by which gas flows into the nuclear region.

We find that the circumnuclear ring, observed with the interferometer, and other single-dish studies (Figure 4), is part of a much larger HCN emission complex (Figure 5). The limited primary beam response, and the small areas of the previous HCN maps, have been responsible for the isolated appearance of the circumnuclear ring. In addition, the channel maps show that the circumnuclear ring is connected to the extended material at specific velocities (Figure 6). For example, at around 60 km s^{-1}, the molecular cloud M-0.02-0.07 seems to flow toward the nuclear region. We call this the eastern streamer, and this may be another direction along which gas flows into the nuclear region. This streamer is again identified as extra gas in the nuclear region, just like the southern streamer, which do not fit into the rotating ring model. Thus, the high velocity material at >100 km s^{-1} in the circumnuclear region may be related to the M-0.02-0.07 cloud.

By comparing the J=3–2 and J=1–0 HCN emission, we see that many channels at negative velocities (between -5 and -60 km s^{-1}) are completely obscured by foreground absorption. This foreground material must be of low excitation since the absorption effects are completely absent in the J=3–2 line. These negative velocity channels turn out to be very important, because the compact high velocity material at <-100 km s^{-1}

appear to be connected to the extended emission to the northwest of Sgr A-West. This connection cannot be seen in the J=1–0 line, but can now be seen clearly in the J=3–2 line. We may therefore speculate whether the high velocity material in the circumnuclear region, at both positive and negative velocities, are directly related to the extended material outside.

Inflow to the Nucleus. In this review, we see that gas appear to come into the nuclear region from the nearby complexes at projected radial distances of 10pc. On the kiloparsec scale, the Galaxy may consist of a stellar bar (cf. Blitz et al. 1993) which helps to drive gas toward the center. Such inflows appear to be stabilized well before the 10pc scale, probably because the gravitational potential is more spherically symmetric in the core. Further more, conservation of some of the angular momentum from galactic rotation probably stabilizes against infall. Complexes like the Sgr A molecular cloud appear to be more or less stable on the large scale. Of course some amount of the gas must have become destabilized because we can see both ionized and neutral streamers which appear to be heading toward the Center. We suggest here that the destabilization may be due to the interaction between the supernovae in the nuclear region and the ambient molecular clouds. There are two supernova remnants, Sgr A-East, which lies on the western edge of M-0.02-0.07, and Sgr A-South, which lies on the eastern edge of M-0.13-0.08. Observed kinematics appear consistent with actual impacts on the molecular gas. This could have resulted in the loosening of some portions of the clouds, which are then dragged in toward the center by tidal forces. The observed finger-like streamers could be due to tidal stretching. This scenario suggests that a number of mechanisms operate in the nuclear region to bring the gas in to the Center. The mechanism which dominates at any one point depends probably on a variety of factors and depends also on the scale length under consideration. The extrapolation to external systems await better spatial resolution measurements.

References

Bally, J. et al., 1988, ApJ, 324, 223.
Blitz, L. et al., 1993, Nature, 361, 417.
Gusten, R. 1989, in *The Center of the Galaxy*, ed. M. Morris, p.89.
Gusten, R. et al., 1987, ApJ, 318, 124.
Hasegawa, T., Sato, F., Whiteoak, J.B., and Miyhawaki, R. 1993, preprint.
Ho, P.T.P. et al., 1991, Nature, 350, 309.
Jackson, J.M. et al., 1993, ApJ, 402, 173.
Jackson, J.M., Heyer, M., and Paglione, T., 1994, in preparation.
Marr, J.M., Wright, M.C.H., and Backer, D.C. 1993, ApJ, 411, 667.
Marshall, J., and Lasenby, A. 1993, in *Nuclei of Normal Galaxies: Lessons from the Galactic Center*, ed. R. Genzel, A. Harris, in press.
Mezger. P.G. et al., 1989, A&A, 209, 337.
Okumura, S.K. et al., 1991, ApJ, 378, 127.
Oka et al.1993, in *Back to the Galaxy*, ed. S.Holt, F. Verter, p.50.
Schwarz, U.L., Bregman, J.D., and van Gorkom, J.H. 1989, A&A, 215, 33.
Tsuboi, M. et al. 1989, in *The Center of the Galaxy*, ed. M. Morris, p.135.

Near-Infrared High-Resolution Imaging of the Galactic Center

A. Eckart, R. Genzel, R. Hofmann, B.J. Sams, L.E. Tacconi-Garman

Max-Planck-Institut für extraterrestrische Physik, Giessenbachstraße, Postfach 1603, 85740 Garching bei München, Germany

Abstract: We present deep 1.6 (H) and 2.2 μm (K) images of the central parsec of the Galaxy at a resolution of 0.15". We also give a brief history of high spatial resolution imaging of the Galactic Center in the near-infrared. Our recent speckle imaging results are:
Most of the flux in earlier seeing limited images comes from about 340 unresolved stellar sources with K magnitudes $\leq$14. Most of the fainter stars in the central parsec are likely to be M- rather than K-giants. The IRS 16 and 13 complexes are resolved into about 25 and 6 sources, many of which are probably luminous hot stars. We confirm the presence of a blue near infrared object (K$\approx$13) at the position of the compact radio source Sgr A*. This source either has a $\sim$0.5" east-west size or it is multiple with its western component closest to Sgr A*. The spatial centroid of the number distribution of compact sources is consistent with the position of Sgr A* but not with a position in the IRS 16 complex. The stellar surface density is very well fitted by an isothermal cluster model with a core radius of 0.15$\pm$0.05 pc. If the 2μm emitting stars sample the overall mass distribution of the stellar cluster the stellar density is a few times $10^7\,M_\odot\,pc^{-3}$. Buildup of massive stars by collisional merging of lower mass stars and collisional disruption of giant atmospheres are very probable processes in the central 0.2 pc.

1. Introduction

The structure and composition of the stellar cluster in the Galactic center has been subject of many investigations (e.g. Bailey 1980; Allen 1987) ever since the first near-infrared mapping of Becklin and Neugebauer (1968). Here we report initial results of 0.15" resolution (6.2×10^{-3}pc at 8.5 kpc) near-infrared speckle interferometry observations of the central parsec and summarize the data reduction analysis that led to the mosaics presented in Eckart et al. (1992) and Eckart et al. (1993).

2. A Brief History

Attempts to detect a source at the position of the Galactic Center in the near infrared started as early as 1945 (Stebbins and Whitford, 1947, Moroz, 1961). Due to a combination of a lack in sensitivity and a coarse sampling these initial efforts were not successful. The first detection was achieved by Becklin and Neugebauer (1968) in scans with 0.25' and 0.08' apertures at a wavelength of 2.2μm (Fig.1). These scans for the first time revealed the compact central stellar cluster. In the following years single detector maps with higher spatial resolution were obtained by a number of authors (see references listed in Tab.1).

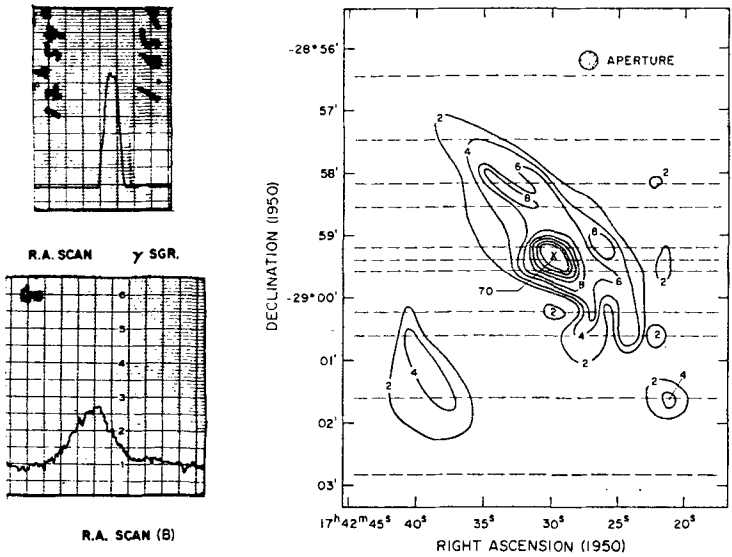

Figure 1: Left: 2.2 μm strip-chart recording in right-ascension of the unresolved star γSgr and the Galactic Center (Becklin & Neugebauer 1968) showing for the first time the presence of the central stellar bulge. Right: First contour map resulting from those strip-charts.

These maps resolved the central cluster into individual bright complexes. The introduction of near-infrared arrays allowed more efficient mapping with yet higher spatial resolution (see Tab.1). The first maps of the Galactic Center using array detectors were obtained by Forrest, Pipher and Stein (1986). These measurements started to resolve the central IRS16 complex into several sources. Lunar occultation measurements (see Tab.1) demonstrated that the brightest sources in the IRS 16 complex (IRS 16NE, 16C, 16SW and 16NW) are very compact with diameters less than 100 AU and therefore most likely individual or multiple stars but not large clusters. The two-dimensional speckle imaging (Eckart et al. 1992, Eckart et al. 1993) resulted in first diffraction limited maps (0.15" spatial resolution) of the central 20"×20" at 2.2μm and 1.6μm. These measurements resolved the central cluster including several compact complexes like IRS 1, IRS 13, and IRS 16SW complex into about 340 stars (see section 6). They also revealed for the first time a near-infrared source at the position of Sgr A* (see section 7). These results have been confirmed by repeated speckle imaging as well as first tip-tilt measurements (Close et al. 1992) at 1.6μm with a resolution of 0.3".

3. Recent Speckle Observations at the NTT

The observations were carried out using the new MPE infrared high resolution camera, SHARP (Hofmann et al. 1993), at the New Technology Telescope (NTT) of the

Table 1:

Direct Imaging Using Single Detectors
(Moroz, 1961, Astr.Zh., 38, 487.)
(Stebbins and Whitford, 1947, Ap. J., 106, 235.)
Becklin & Neugebauer, 1968, Ap. J., 151, 145.
Rieke & Low, 1973, Ap. J., 184, 415.
Balick & Brown, 1974, Ap. J., 194, 265.
Becklin & Neugebauer, 1975, Ap. J. (Letters), 200, L71.
Rieke, Telesco, & Harper, D.A., 1978, Ap. J., 220, 556.
Becklin, Gatley, & Werner, 1982, Ap. J., 258, 135.
Baily, Hough, Axon, 1984, M.N.R.A.S., 208, 661.
Gezari et al., 1985, Ap. J., 299, 1007.
Allen & Sanders, 1986, Nature, 319, 191.
Direct Imaging Using Arrays
Forrest, Pipher, & Stein, 1986, Ap. J. (Letters), 301, L49.
Rieke, Rieke, & Paul, 1989, Ap. J., 336, 752.
Tollstrup, Capps, & Becklin, 1989, A. J., 98, 204.
Simon et al. 1990, Ap. J., 360, 95.
DePoy & Sharp, 1991, A. J., 101, 1324.
Herbst et al., 1993, Ap. J. (Letters), 411, L21.
Rosa et al., 1992, Astron. Astrophys., 257, 515.
NIR Lunar Occultation Measurements of the Galactic Center
McLean et al., 1987, IR Astron. with Arrays.
Adams et al., 1988, Ap. J. (Letters), 327, L65.
Simon et al. 1990, Ap. J., 360, 95.
Simons, Hodapp, Becklin, 1990, Ap. J., 360, 106.
NIR Speckle and Adaptive Optics on the Galactic Center
Eckart et al., 1992, Nature, 355, 526.
Eckart et al., 1993, Ap. J. (Letters), 407, L77.
Close et al., 1992.

List of relevant publications dealing with high spatial resolution near-infrared continuum imaging of the Galactic Center.

European Southern Observatory (ESO) in La Silla, Chile. SHARP uses a 256×256 pixel NICMOS 3 detector array developed by Rockwell International Cooperation. A system of digital signal processors allows continuous read-out of the array as fast as 10 Hz, as well as on-line image processing for quick-look purposes. With an image scale of 0.05" per pixel the camera is used for diffraction limited imaging at H (1.6μm) and K (2.2μm) band.

Observations of the central ≈10" radius region of our Galaxy were carried out in 1991 August (mostly in K-band, see Eckart et al. 1992), 1992 March (K and initial H), 1992 August, and 1993 August (both in K and H). The very first observations in 1991 were carried out using a single 128×128 array quadrant only. In 1992 and 1993 we obtained between 30,000 and 47,000 frames of 0.3 to 1.0 second integration time for the K and H wavelength bands. The individual frames were dead pixel corrected, flat fielded, and

a simple shift-and-add (SSA) algorithm (Bates 1982, Christou 1991) was applied to seeing-selected images. In all data sets used for mapping the long-exposure seeing was between 0.6" and 1.0" FWHM.

The flux-conserving Lucy (Lucy 1974) deconvolution, followed by reconvolution with a Gaussian of the original FWHM resolution as the last step, has turned out to be the most efficient method for removing the 'dirty' SSA beam and creating a high dynamic range map (more than 7 magnitudes or a factor >630 in Fig.2) in a crowded field. A detailed description of the applied mapping algorithm is given in Eckart et al. 1994.

4. The Galactic Center Resolved

Fig.2 shows a 0.15" resolution, speckle reconstruction of K-band emission from the central parsec (23" at 8.5 kpc) of the Galaxy, obtained in March 1992 with the MPE speckle camera SHARP on the 3.5m ESO NTT (Eckart et al. 1993). It is the result of a SSA processing of about 30,000 short exposure (0.3 to 1 second integration time) frames. The data show that at least 90% of the K-band flux of the central parsec of the Galaxy comes from about 340 compact sources (Fig.3). The central IRS 16 complex is resolved into about two dozen compact sources. These are likely individual or multiple stars as lunar occultation observations set limits of about 100 AU to the sizes of its brightest members (Simon et al. 1990, Simons et al. 1990). Infrared spectroscopy has shown that a number of the bright K-band sources in Fig.2 are HeI/HI emission line stars and are probably massive and luminous blue supergiants that have formed within the last few million years (Allen, Hyland and Hillier 1990, Krabbe et al. 1991, 1993). The central cluster of blue supergiants likely provides a significant fraction of the total and Lyman continuum luminosity of Sgr A West. Becklin and Neugebauer (1968) assumed that most of the 2μm continuum emission is due to K5-giants of about 4,000 K color temperature. However, K-giants would have K>14 in the Galactic center while most of the fainter sources in the speckle image have K$\approx$11–13. Most of the late type stars in the central parsec are thus more likely M-giants (K(M3)=12.5, K(M5)=10.8) of surface temperature $\approx$3,000 K, consistent with the 2μm CO bandhead spectroscopy of the brightest late type stars by Sellgren et al. (1987) and Lebofsky, Rieke and Tokunaga (1982). In addition a number of the fainter 2μm sources may also be O/B main sequence stars (K$\approx$13).

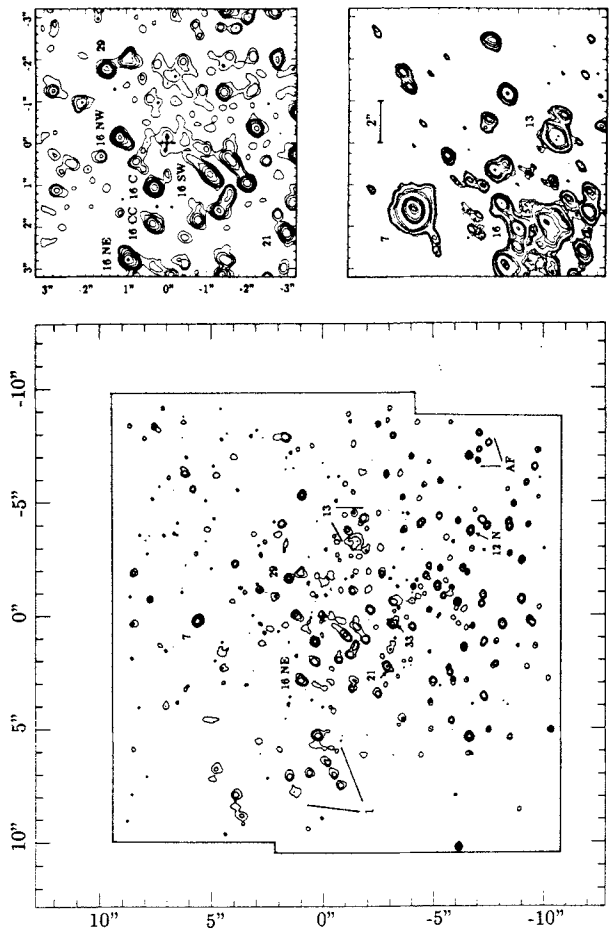

Figure 2: Left: Mosaic of K-band speckle image reconstructions of the central 20"×20" of the Galaxy at a spatial resolution of 0.15" FWHM centered on the position of the compact radio source Sgr A* (cross). Boundaries of the mosaic are indicated by solid lines. Contour levels are 14.5, 12.5, 10.5, 8.5, 6.8 magnitudes. Faint sources within a radius of 1.5" of IRS 7 may be missing. The registration of Sgr A* is described in Eckart et al.(1993). Top right: K-band contour map of the central 6.4"×6.4" of the Galactic center region centered on the position of the compact radio source Sgr A*. This most sensitive part of the image contains information of about 30,000 individual frames taken with integration times between 0.3 and 1.0 second each. The spatial resolution is 0.15" FWHM. Contour levels are 15, 14, ..., 9 magnitudes. Bottom right: Raw shift-and-add image of a representative subset of 3,000 K-band frames (March 1992). Contour levels are 0.2, 0.25, 0.3, 0.5, 0.7, 1, 3, 4, 6, 10, 30, 50, 70, 100% of the peak intensity of IRS 7 (K=6.8).

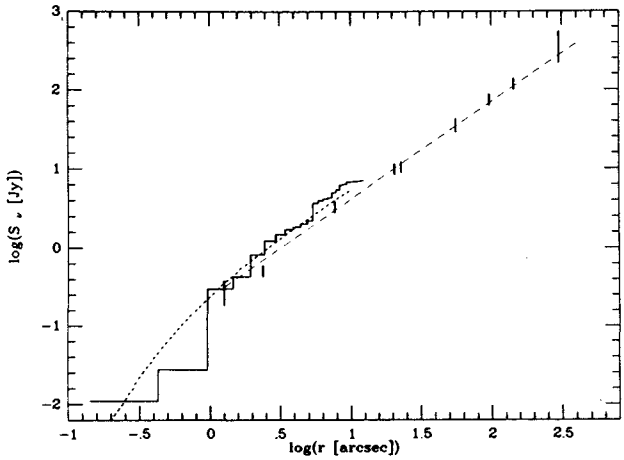

Figure 3: The observed K-band flux density S_ν contained in circular apertures centered on the position of Sgr A* for both the speckle mosaic (solid line histogram) and the 1" resolution long exposure mosaic (short dashed line). The long-dashed line shows a fit to data from Becklin & Neugebauer (1968, 1975) as summarized in Bailey (1980) and indicated by the thick vertical lines.

There is no central stellar 'cusp', and the number distribution (Fig.4) of sources with K<14 can be well described by an isothermal distribution with core radius 4 to 5" (0.15 to 0.2 pc), centered within about 0.8" (3σ) of the position of the compact radio source Sgr A* ((0,0) in Fig.2). The $r^{-1.8}$ volume density power law previously determined from the surface brightness distribution (e.g. Bailey 1980) does not fit the data inside of a few arcseconds. Varying the assumed centroid position anywhere from 1.5" SW of Sgr A* (the formal centroid) to 1" E of Sgr A*, or choosing a cutoff at K=13 instead of 14 varies the derived core radius over the range from 0.1 to 0.2 pc and the central surface density from 2 to 3.3 sources per arcsec^2. The brightest sources (K$\leq$11) perhaps have a slightly smaller core radius (0.1 pc) than the fainter sources (0.17 to 0.25 pc). With a core radius of r_o=0.15$\pm$0.05 pc and a line-of-sight central velocity dispersion σ_o=100$\pm$25 km/s (e.g. Sellgren et al. 1990) the central density of the cluster becomes $\rho_o = 9\sigma_o^2/4\pi G r_o^2 = 10^{7.7\pm0.5} M_\odot pc^{-3}$, with a core mass of $M_o(r_o) = 10^{5.7\pm0.3} M_\odot$. If the number distribution of K<14 sources in Fig.4 is the right guide, the stellar density in the central core exceeds 10^7 $M_\odot$ pc^{-3}, resulting in a high rate of stellar collisions (Eckart et al. 1993). This conclusion relies on the assumption that most of the fainter sources in Fig.2 are old K and M-giants with a spatial distribution similar to the majority of stars in the cluster. That assumption needs to be verified. However, such an environment allows the formation of the hot, massive stars via sequential buildup by collisions and mergers (Lee 1987, 1990). The stellar collision rates would be sufficient (Phinney 1989,

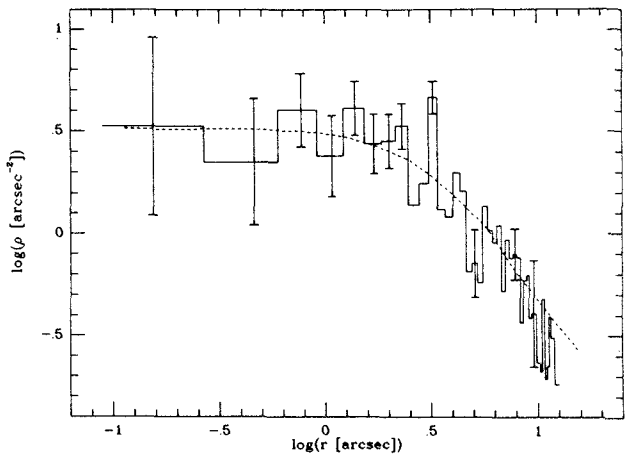

Figure 4: Surface density ρ in sources per (arcsec)^2 for all 340 stars with K<14 in 0.3" wide annuli of radius r from the radio position of Sgr A* (histogram). Representative error bars indicate the statistical ($N^{1/2}$) uncertainties. The resulting distribution is well fitted by an isothermal stellar density distribution (dashed curve) with a core radius of 3.8" (0.15 pc) and a central surface density of three sources per (arcsec)^2.

Eckart 1993) to explain the presence of about 10 to 10^2 stars with masses >10 $M_\odot$ (Lee 1987). Consistent with this hypothesis, all of the hot He I emission line stars discovered so far by Krabbe et al. (1991, 1993) are located in the dense part of the cluster at r<0.5 pc.

Alternatively the distribution of the blue stellar component in the central part of our Galaxy does not represent the distribution of the overall stellar content but outlines the region of recent massive star formation at the nucleus. In this case the core radius could be significantly larger and hence the central mass density much smaller than indicated above. However, at present there is no compelling evidence for for massive star formation activity by self-gravitating gas clouds in the central few parsecs (e.g. Jackson et al. 1993). Perhaps the amount of very dense gas in the innermost region was much greater in the past than it is now and star formation may be time dependent (e.g. Rieke and Lebofsky 1982). Further sensitive, high spatial resolution investigations of the distributions of different stellar populations in the central bulge will address this question.

5. Sagittarius A*

In agreement with the first report by Eckart et al. (1991, 1992 see also Eckart et al. 1993) there is a relatively faint (K=13 in 0.3″) source positionally coincident with Sgr A*, within the relative position uncertainty of the infrared/radio frames of about ±0.2″. The existence of a blue source near Sgr A* is confirmed by several other recent data sets (Close et al. 1992, Herbst et al. 1993). The morphology of Sgr A*(IR) is complex. The source may be multiple, or spatially extended over about 0.5″ with a total K-band magnitude of about 12.

From the absolute position of Sgr A* (R.A.=$17^h42^m29.316^s$, Dec.=$-28°59'18.38"$ [1950], Rosa et al. 1992), we derive the absolute position for the western infrared source as R.A.=$17^h42^m29.306^s$ ($\pm 0.015^s$), Dec.=$-28°59'18.45"$ ($\pm 0.2"$) [1950]. It appears to be part of a 1.5" emission ridge (P.A.$\approx -20°$). Integrating over 0.5" it has K=12$\pm$0.5 and H=13.9$\pm$0.5. With A_K=3.4 and A_H=5.4 (Rieke, Rieke and Paul 1989) it has a blue color (H-K$\approx$0.0) consistent with the Rayleigh-Jeans tail of a hot blackbody (T>7,000 K) extincted by 30 magnitudes of interstellar extinction. Its color is therefore similar to other hot sources in the field. The luminosity of the Sgr A* source then is $1\text{–}5\times10^5$ $(T_{eff}/35{,}000\ K)^3\ L_\odot$, not including possible local extinction.

The nature of Sgr A*(IR) is still uncertain, however. It may be a chance alignment, hot star in the central core of the stellar cluster that is not related to the radio source. It could also be the emission from an accretion disk associated with Sgr A*. If Sgr A* is in fact a $10^6\ M_\odot$ black hole, the relative faintness of its infrared emission in any case suggests that the hole presently accretes at a low rate ($<10^{-7}\ M_\odot$/yr), or with low radiation efficiency.

An identification of the new source as the near-infrared counterpart of Sgr A* can only be tentative at present, as spectroscopic, polarimetric and proper motion studies are required. The probability of a chance alignment in the crowded central few arcsecs is between 4% and 20%.

Acknowledgements We thank S. Drapatz, A. Harris, P. Mezger, G. Rieke, M. Rieke, and J. Lacy for helpful comments. We also thank ESO for generously supporting the observations with the SHARP camera at the NTT.

References

Adams, D.J., Becklin, E.E., Jameson, R.F., Longmore, A.J., Sandquist, A.A., Valentijn, E., 1988, Ap. J. (Letters), 327, L65.

Allen,D.A., Hyland,A.R. and Hillier,D.J., 1990, M.N.R.A.S., 244, 706.

Allen,D.A., Sanders, R.H., 1986, Nature, 319, 191.

Allen, D.A., 1987, in The Galactic Center, ed. D. Backer, AIP 155 (New York), p.1.

Bailey, M.E., 1980, M.N.R.A.S., 190, 217.

Bailey, J., Hough, J.H., Axon, D.J., 1984, M.N.R.A.S., 208, 661.

Balick, B., & Brown, R.L, 1974, Ap. J., 194, 265.

Bates, R.H.T., 1982, *Physical Reports*,**90**,203.

Becklin, E.E. and Neugebauer, G., 1968,Ap. J., 151, 145.

Becklin, E.E. and Neugebauer, G., 1975,Ap. J. (Letters), 200, L71.

Becklin, E.E., Gatley, I., Werner, M.W., 1982,Ap. J., 258, 135.

Christou,J.C., 1991, *Experimental Astr.* **2**, 27.

Close, L.M., McCarthy, D.W., Christou, J.C, Melina, F., 1992, BAAS 24, 1178.

DePoy,D.L. and Sharp,N.A., 1991, A. J., 101, 1324.

Eckart, A., Genzel, R., Krabbe, A., Hofmann, R., van der Werf, P.P., Drapatz, S., 1992, *Nature*, **335**, 526.

Eckart, A., Genzel, R., Hofmann, Sams, B.J., Tacconi-Garman, L.E., 1993, Ap. J. (Letters), 407, L77.

Eckart, A., and Duhoux, P.R.M., 1990, *Proc. of a Conference on "Astrophysics with Infrared Arrays"*, held in Tucson, Arizona, February 19, 1990, Astronomical Society of the Pacific Conference Series, Elston R.(eds.)., p.336.

Eckart, A., Genzel, R., Hofmann, Sams, B.J., Tacconi-Garman, L.E., Cruzalebes, P., 1994, Proc. on a Conference on Nuclei of Normal Galaxies held at Schloß Ringberg in June 1993, eds. R.Genzel & A.I.Harris Kluwer (Dordrecht).

Forrest,W.J., Pipher,J.L., Stein, W.A., 1986, Ap. J. (Letters), 301, L49.

Gezari, D.Y., Tresch-Fienberg, R., Fazio, G.G., Hofmann, W.F., Gatley, I., Lamb, G., Shu, P., McCreight, C., 1985, Ap. J., 299, 1007.

Gezari, D., 1992, in The Center, Bulge and Disk of the Milky Way, ed. L.Blitz (Kluwer:Dordrecht), 23.

Herbst, T.M., Beckwith, S.V.W., Shure, M., 1993, Ap. J. (Letters), 411, L21.

Hofmann, R., Blietz, M., Duhoux, P., Eckart, A., Krabbe, A. and Rotaciuc, V., 1993, in Progress in Telescope and Instrumentation Technologies, ed. M. H. Ulrich, ESO Report, 42, 617.

Jackson, J.M., Geis, N., Genzel, R., Harris, A.I., Madden, S.C., Poglitsch, A., Stacey, G.J. and Townes, C.H., 1993, Ap.J. January.

Krabbe,A., Genzel,R., Drapatz,S. and Rotaciuc,V., 1991, Ap. J. (Letters), 382, L19.

Krabbe, A., et al. 1993, in preparation.

Lee, H.M., 1987, Ap. J., 319, 771.

Lee, H.M., 1990, in Dynamics of Dense Stellar Systems, ed. D. Merritt, Cambridge Univ. Press, p.105.

Lebofsky, M.J., Rieke, G.H. and Tokunaga, A.T., 1982, Ap. J., 263, 736.

Lucy,L.B., 1974, A. J., 79, 745.

McLean, I.S., Aspin, C., Longmore, A.J., Dixon, R.I., 1987, in Infrared Astronomy with Arrays, ed. G.G. Wynn-Williams and E.E. Becklin, University of Hawaii,p. 321.

Moroz, 1961, Astr.Zh., 38, 487.

Phinney, E.S., 1989, in The Center of the Galaxy, ed. M.Morris, Kluwer (Dordrecht), p.543.

Rieke, G.H. and Lebofsky, M.J. 1982, in The Galactic Center, eds. G.R. Riegler and R.D. Blandford (New York: AIP), p.194.

Rieke,G.H., Low, F.J., 1973, Ap. J., 184, 415.

Rieke,G.H., Rieke,M.J. and Paul,A.E., 1989, Ap. J., 336, 752.

Rosa,M.R., Zinnecker,H., Moneti,A. and Melnick,J., 1992, Astron. Astrophys., 257, 515.

Sellgren, K., Hall, D.N.B., Kleinmann, S.G., and Scoville, N.Z., 1987, Ap. J., 317, 881.

Sellgren, K., McGinn, M.T., Becklin, E.E., Hall, D.,N.,B., 1990, Ap. J., 359, 112.

Simon,M., Chen,W.P., Forrest,W.J., Garnett,J.D., Longmore,A.J., Gauer,T. and Dixon,R.I., 1990, Ap. J., 360, 95.

Simons, D.A, Hodapp, K.W. and Becklin, E.E., 1990,Ap. J., 360, 106.

Stebbins, J., Whitford, A.E., 1947, Ap. J., 106, 235.

Tollestrup, E.V.,Capps,R.W. and Becklin,E.E., 1989, A. J., 98, 204.

Properties of the OMC-2 and OMC-3 Cores in Orion

A. Castets[1], W.D. Langer[2] and G. Duvert[1]

1. Laboratoire Astrophysique, Observatoire de Grenoble BP 53X 38041 Grenoble Cedex France. 2. Jet Propulsion Laboratory, Caltech, Pasadena, CA 91109 USA

Introduction

The physical conditions in dense condensations are critical input parameters for any theory of star formation. Furthermore once young stellar objects form they influence the conditions in these cores. Any theory of molecular cloud energetics or dynamics should account for these conditions. To study the relationships between physical conditions in the cores and star formation, , including the influence of age, requires a comparison of different cores, preferably in the same cloud. Orion provides one of the best sites for such studies. Orion has been the focus of several surveys but detailed analysis of the star forming regions has concentrated mainly on OMC-1. However, at least two other regions are equally important, OMC-2 and OMC-3. From our $C^{18}O$ multi-transition analysis made at 2.4 arcminutes resolution (Dutrey et al, 1993) these regions have the highest $N(H_2)$ and $n(H_2)$ peaks in our maps. 2) They are also high density cores in NH_3 maps (Batrla et al 1983, Cesaroni et al 1993). They are sites of star formation possibly in a less evolved state than OMC-1. In the Orion molecular cloud there exist other regions with comparable physical conditions, particularly to the south of OMC-1. However these southern regions have a very complex velocity field (Castets et al 1990), while the northern region shows only one velocity component along the line of sight. Here we present a preliminary analysis of the properties of these cores based on multi-transition, multi-species observations.

Observational results

$C^{18}O$ (1-0) and (2-1), $C^{32}S$ (2-1) and (5-4) and $C^{34}S$ (2-1) have been observed in September 1991 with the SEST Telescope. Because of lack of space we present here only the OMC-3 $C^{18}O$ and $C^{32}S$ (2-1) maps while we discribe briefly some features seen in the others.

OMC-2 maps

The $C^{18}O$ (2-1) map is very inhomogeneous and shows several peaks. In contrast the $C^{32}S$ map is smoother with one large central core and a second core to the NW, which is also seen in $C^{18}O$.

OMC-3 maps

In $C^{18}O$ (2-1) OMC-3 has a long narrow filament (2.5' x 1') extending NW-SE and opening to an elliptical core (2' x 1.5') in the S-E. The $C^{32}S$ (2-1) map, which is at lower resolution than the $C^{18}O$ (2-1), has a different shape (banana-like) with the peak offset (4") from the $C^{18}O$ peak. The $C^{34}S$ and $C^{32}S$ J = 2-1 integrated intensities seem to trace the same material but the $C^{34}S$ map is more inhomogeneous on small scales - probably due to its much lower opacity and therefore ability to trace deeper into the cores.

Physical properties of the cores

To determine $N(H_2)$ and $n(H_2)$ we adopted an LVG model with T_{kin} obtained from NH_3 measurements in the cores (Batrla et al. 1983; Cesaroni et al. 1993). The excitation analysis was made at the lowest resolution (55") by convolving the higher resolution maps of $C^{18}O$ (2-1) and $C^{32}S$ (5-4) to match the lower ones.

OMC-2

The $N(C^{18}O)$ map is smooth while the N(CS) map is centrally peaked. The computed peak $N(C^{18}O) = 2.8 \times 10^{15}$ cm^{-2} and, by scaling with $H_2/C^{18}O = 1.4 \times 10^{-7}$, yields $N(H_2) = 2 \times 10^{22}$ cm^{-2} ($A_v \simeq 20$ mag). The peak $N(CS) = 5 \times 10^{13}$ cm^{-2} is derived from the 2-1 and 5-4 transitions and using the results above suggests a fractional abundance $X(CS) \simeq 2.5 \times 10^{-9}$. The density peak derived from CS, $n(H_2) = 9 \times 10^5$ cm^{-3}, while the $C^{18}O$ analysis produces a much lower value 2×10^4 cm^{-3}.

OMC-3

In this source the CS and $C^{18}O$ column density maps are much smoother than those for

OMC-2. The peak in N($C^{18}O$) = 7 x 10^{15} cm^{-2}, yielding N(H_2) = 5 x 10^{22} cm^{-2} ($A_v \simeq 50$ mag), 2.5 times larger than OMC-2, but comparable to OMC-1 ($A_v > 50$ mag.). We find N(CS) = 3.5 x 10^{13} cm^{-2} yielding a fractional abundance of 7 x 10^{-10}, much smaller than that found in OMC-2 and OMC-1 (2 x 10^{-8}, Blake et al 1987). The density derived from CS is 6 x 10^5 cm^{-3} again much higher than that from C18O = 10^4 cm^{-3}.

Discussion

The large discrepancies in peak density for OMC-2 and -3 derived from $C^{32}S$ and $C^{18}O$ can be due to several factors:1) The $C^{18}O$ (2-1) intensity is not sensitive to densities above 10^4 cm^{-3} because it is readily thermalized at this density. 2) Clumpiness will affect the analysis of the CS, which is much more sensitive to high densities. 3) In the latter case the CS opacity could be much larger.

Core masses

The mass and area traced by the $C^{18}O$ molecule are: M(OMC-2) = 40 $M_\odot$for an Area = 6 (arcmin squared) and M(OMC-3) = 80 $M_\odot$, Area = 9 (arcmin squared). The OMC-2 value is in excellent agreement with the value found with the $C^{18}O$, using the POM-2 telescope (Dutrey et al 1993). This agreeement means that the OMC-2 core is not clumpy on the size of the 55" SEST maps. In both studies it seems that OMC-2 contains only one massive core. However in the OMC-3 region the mass derived here is 2 times higher than in the POM-2 survey. This result is due to the fact that the OMC-3 mapping at high resolution (22" and 55") reveals several very massive cores which were not resolved in the POM-2 beam.

Outflows and structure

It appears that OMC-2 and OMC-3 are less evolved than OMC-1, because: OMC-2 is the site of a cluster of infrared sources (Johnson et al 1990) and outflows, but not comparable to the massive outflow in OMC-1. OMC-3 has not yet been studied in the IR, but does have outflows as seen in our CS,^{13}CO and $C^{18}O$ velocity maps (not shown), also not comparable to OMC-1. We see only one outflow in OMC-2 but several in OMC-3. However the OMC-2 outflow may be more energetic (it is conspicuous in CS) than those in OMC-3. Therefore, we suggest that OMC-2 is closer in its characteristics to OMC-1 (one very energetic outflow) than is OMC-3.

References

Batrla W., Wilson T. L., Bastien P. and Ruf K. 1983, A&A, 128, 279.
Blake G. A., Sutton E. C., Masson C. R. and Phillips T. G. 1987, Ap J 315, 621.
Castets A., Duvert G., Dutrey A., Bally J., Langer W. D. and Wilson R. W. 1990, A&A, 234, 469.
Cesaroni R. and Wilson T. L. 1993, A&A., in press.
Dutrey A., Duvert G., Castets A., Langer W. D., Bally J. and Wilson R. W. 1993, A&A, 270, 468.
Johnson J. J., Gehrz R. D., Jones T. J., Hackwell J. A. and Grasdalen G. L. 1990, As. J., 100, 518.

Vibrationally Excited CS in Star Forming Cores - Infrared Pumping?

H. Hauschildt[1], R. Güsten[1], and P. Schilke[2]

[1] MPI für Radioastronomie, Auf dem Hügel 69, 53121 Bonn, Germany
[2] California Institute of Technology, 320-47, Pasadena, CA 91125, USA

1. Introduction

The recent detection of rather strong submm CS(J=10-9) emission towards galactic star forming cores (Hauschildt et al., 1993) raises the question about the underlying excitation processes. If excited by collisions only, H_2 densities $\geq 10^7 cm^{-3}$ are required. However, Carroll and Goldsmith (1981) already demonstrated that the effect of strong infrared pumping on the molecular level population is to mimic the excitation by collisions, and thus may lead to overestimate the H_2 density. One promising way to constrain the relative importance of IR pumping is by observation of $v = 1$ rotational CS transitions: at 1830 K above ground, they cannot be populated collisionally, and their intensity will directly reflect the intensity of the IR field at work.

2. Observations and Results

The observations towards in total 9 hot-core type sources were carried out with the IRAM 30m-telescope in September 1992. Three SIS receivers were operated in parallel, centered on the CS(v=1) J=2-1, 3-2 and 5-4 transitions, respectively. The measurements were performed by wobbler switching symmetrically in azimuth ±120-140".
Weak CS(3-2,v=1) emission was detected in 4 sources (Ori-KL, G34.26, W51-d and W51-e_1/e_2). The J=5-4 spectra are heavily confusion-limited, due to strong blending with unrelated features from both the signal- and the image-band. Upper limits for the CS(2-1,v=1) transitions are system noise limited.

3. Discussion

Relative intensities of v=1 rotational lines varying from source to source, require a case-by-case excitation study for each individual object, and thus make the determination of H_2 densities, with CS as a densitometer, much more complicated than it was before. While towards e.g. the G10.62–0.38 hot-core the influence of IR-pumping must be rather confined, towards other sources detailled excitation models, including the effect of the IR radiation field, have to be performed.
To exemplify the procedure, we analyse the vibrationally excited CS and $C^{34}S$ (v=0) lines of G34.26+0.15. No self-consistent solution, fitting both the vibrationally excited and the v=0 ground-state transitions, could be obtained in terms of a uniform homogeneous source model. Instead a composite model is required that incorporates:

- a **dense core** with a density profile $n(H_2) \propto r^{-\alpha}$ (calculated in a microturbulent code, allowing for radial excitation gradients), that harbors
- a compact (~ 3-5") deeply embedded **hot-core** (calculated in a LVG code, that takes into account the influence of IR emission from the embedded dust).

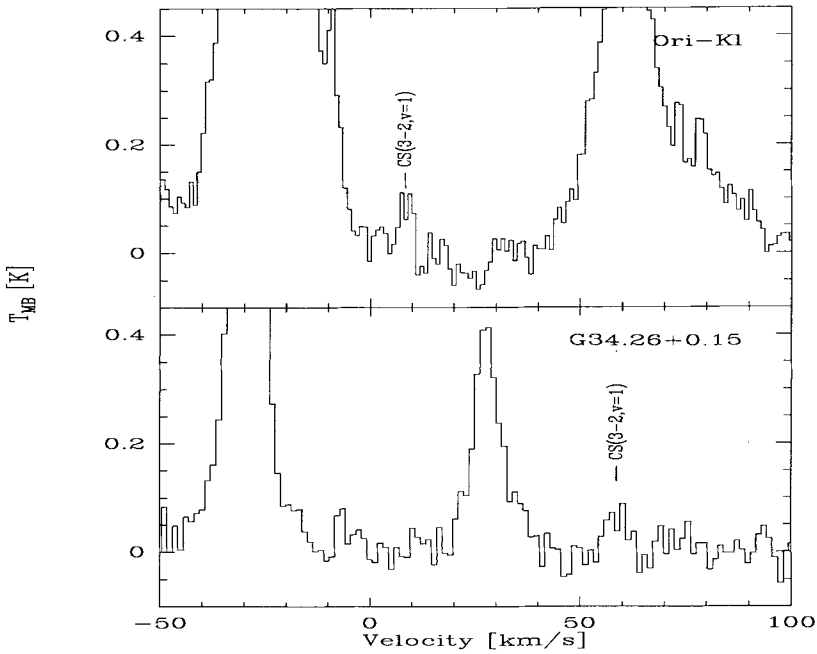

Figure 1: CS(3-2,v=1) spectra towards G34.26+0.15 and Ori-KL. Line temperatures are given on the main-beam brightness temperature scale. The angular resolution of the IRAM 30m-telescope at the frequency of the transition, ν ~146 GHz, is 17".

The hot core accounts for the vibrationally excited lines, while the surrounding gas envelope is constrained by the v=0 rotational data. The envelope morphology is well fit by $\alpha \sim 1.5$ ($R_{out} \sim 1.45$ pc, $n_{H_2}(R_{out}) \sim 5.5 \times 10^4$ cm^{-3}). The intensity of the CS(3-2,v=1) line requires a hot-core column density $N(C^{34}S) \sim 5 \times 10^{14} - 1.1 \times 10^{15}$ cm^{-2}/ km s^{-1} and a dust temperature of ~ 320 – 330 K ($T_{dust} = T_{kin}$, within 20 %). The rather low limit on the CS(5-4,v=1) brightness poses some severe constraints on the model. To keep the predicted brightness within the derived limit, a rather high opacity of the dust continuum is required ($\tau \sim 1.5$ at the frequency of the J=5-4 line), thus suppressing the line brightness ($T_{ex} - T_{dust}$ $(1-e^{-\tau})$). The equivalent H_2 column density of $N(H_2) \sim 5 \times 10^{24} - 1 \times 10^{25}$ cm^{-2} is high, but not unlikely in hot-cores (see Uchida 1993, this conference).
The detailed results of this investigation will be presented in Hauschildt et al. (1994).

References

Carrol, T.J., Goldsmith, P.F. 1981, ApJ, 245, 891
Hauschildt, H., Güsten, R., Phillips, T.G., Schilke, P., Serabyn, E., Walker, C.K. 1993, A&A, 273, L23

Millimetre Observations of Southern Translucent Clouds

R. Gredel, E.F. van Dishoeck, J.H. Black

European Southern Observatory, Casilla 19001, Santiago 19, Chile
Sterrewacht Leiden, P.O. Box 9513, NL-2300 RA Leiden, The Netherlands
Steward Observatory, University of Arizona, Tucson, AZ 85721, USA

Introduction

In a recent series of papers, we have presented optical absorption line observations of a sample of southern translucent clouds with visual extinctions in the range A_V=1–5 mag (van Dishoeck & Black 1989; Gredel, van Dishoeck & Black 1991, 1993; Gredel et al. 1992). The optical observations have resulted in column densities of CH, CH^+, CN and C_2 towards the stars, have allowed determination of the kinetic temperature, density and electron fraction of the foreground material, and have provided constraints on the kinematics through determinations of the Doppler parameter along the lines of sight. Here we present complementary millimetre line studies obtained with SEST. Observations of ^{12}CO , ^{13}CO and $C^{18}O$ $J = 1 \rightarrow 0$ were performed towards the background stars, and sensitive searches for other molecules at millimetre wavelengths have been made for a few of the best characterized clouds. The main advantage of the present work is that A_V towards the background stars is known, which allows a determination of the foreground total hydrogen column densities.

Results

The average of our measurements is T_A^* (^{12}CO) / T_A^* (^{13}CO) = 6.2 ± 5.5 but reaches values > 20 for the most diffuse clouds. A significant increase in the ^{12}CO / ^{13}CO line ratio occurs if T_A^* (^{12}CO) < 3 K. This is primarily because the ^{12}CO millimetre lines become optically thick, whereas those of ^{13}CO remain optically thin. The ^{13}CO / $C^{18}O$ antenna temperature ratios range from 7 – 25, and the lower limits from > 13 to > 35. The overall interstellar $([^{13}C] \cdot [^{16}O])/([^{12}C] \cdot [^{18}O])$ isotope ratio is in the range 5.5–8 in the solar neighborhood. Thus, isotope selective photodissociation appears to be significant in some of the clouds.

Table 1 summarized the results of our molecular line searches. A major uncertainty in the determination of column densities is the density in the cloud. The upper entry listed in Table 1 indicates the column density if the lowest density permitted by the C_2 observations is used; the second entry the result if the highest density is used, inferred from CO J=3 $\rightarrow$ 2 observations. The third entry for HD 62542 refers to $n = 2 \times 10^4$ cm^{-3}. The values for C_2, CN, and CH are from optical absorption line data. The most remarkable finding is that C_2H and C_3H_2 are not detected in any of the clouds. This is surprising since their formation is thought to be stimulated by atomic C and C^+ (Suzuki et al. 1992), which are abundant in the clouds. On the other hand, the HCO^+ ion is detected in a number of clouds, most notably towards HD 62542. Because of rapid dissociative recombination, model predictions are up to an order of magnitude smaller. A similar conclusion applies to HCN, which has been detected towards HD 62542 and HD 29647. The observed CS column densities are reasonably consistent with the model results of Drdla et al. (1989).

The resulting abundances in HD 62542 are compared with those found in the small reflection nebula IC 63 (Jansen et al. 1993; see contribution in this issue). Both clouds may be rather dense clumps of gas with stellar winds having blown away most of the surrounding more diffuse gas.

The abundances of most species are similar within an order of magnitude. Another interesting comparison is that between the cloud towards HD 29647 and the TMC–1 core, which is located only 10′ away. The abundances of most polyatomic molecules appear significantly higher in TMC–1, emphasizing again the unique nature of TMC–1 regarding complex carbon–bearing molecules.

Table 1: Molecular Abundances relative to H_2

Species	HD29647	HD62542	HD94413	HD154368	HD169454	IC 63	TMC-1
H_2	1.0	1.0	1.0	1.0	1.0	1.0	1.0
CO	≥1.3(-5)	5.0(-5)	9.2(-6)	8.3(-6)	1.1(-5)	6.0(-5)	8(-5)
	≥4.0(-6)	1.4(-5)	5.4(-6)	3.3(-6)	3.4(-6)		
^{13}CO	3.3(-6)	1.1(-6)	1.5(-6)	5.6(-7)	1.3(-6)	4.4(-7)	4(-6)
	1.3(-6)	6.5(-7)	1.1(-6)	3.3(-7)	5.6(-7)		
$C^{18}O$	4.0(-7)	2.0(-8)	9.2(-8)	...	2.5(-8)	8.0(-8)	
	2.0(-7)	1.5(-8)	7.7(-8)	...	1.3(-8)		
CH	5.0(-8)	3.8(-8)	3.4(-8)	3.0(-8)	2.8(-8)	...	2(-8)
C_2	5.7(-8)	8.0(-8)	2.7(-8)	3.2(-8)	4.4(-8)	...	...
CN	5.3(-8)	4.2(-8)	4.0(-8)	1.8(-8)	2.6(-8)	4.8(-9)	3(-8)
CS	8.7(-8)	6.5(-8)	1.3(-8)	...	3.6(-8)	1.5(-9)	3(-8)
	5.0(-9)	8.0(-9)	1.7(-9)	...	5.3(-9)		
		1.0(-9)					
C_2H	<5.0(-8)	<2.0(-8)	...	<5.0(-8)	3.4(-8):	4.0(-9)	8(-8)
	<3.3(-9)	<3.0(-9)	...	<1.4(-8)	6.3(-9):		
		<7.0(-10)					
HCN	1.7(-7)	8.0(-8)	<3.8(-8)	<6.1(-8)	<8.8(-8)	3.6(-9)	2(-9)
	8.3(-9)	1.0(-8)	<5.4(-9)	<1.0(-8)	<1.1(-8)		
		1.2(-9)					
HCO^+	3.0(-8)	2.2(-8)	1.9(-8):	1.3(-8)	8.8(-9)	3.6(-9)	2(-8)
	1.7(-9)	2.5(-9)	2.5(-9):	2.5(-9)	1.3(-9)		
		4.0(-10)					
C_3H_2	<1.0(-8)	<1.5(-8)	<6.9(-9)	...	...	...	2(-8)
	<1.7(-9)	<2.5(-9)	<1.0(-9)	...	...		
		<2.5(-10)					

References

Drdla, K., Knapp, G.R., van Dishoeck, E.F., 1989, ApJ 345, 815
Gredel, R., van Dishoeck, E.F., Black, J.H., 1991, A&A 251, 625
Gredel, R., van Dishoeck, E.F., de Vries, C.P., Black, J.H., 1992, A&A 257, 245
Gredel, R., van Dishoeck, E.F., Black, J.H., 1993, A&A 269, 477
Jansen, D.J., van Dishoeck, E.F., Black, J.H., 1993, A&A in press
Suzuki, H. et al. 1992, ApJ392, 551
van Dishoeck, E.F. Black, J.H., 1989, ApJ 340, 273

Molecular Clouds in LMC: Evaluation of Physical Parameters by Means of MM Observations

P. Merluzzi[1], P. Andreani[2], L. Colangeli[3], G. Dall'Oglio[4],
V. Mennella[3], L. Pizzo[4], A. Rotundi[1]

1 - Ist. Ing. Aerospaziale, Università Federico II, Ple. Tecchio 80, I-80125 Napoli, Italy
2 - Dip. Astronomia, Università Padova, v.lo dell'Osservatorio 5, I-35122 Padova, Italy
3 - Oss. Astr. di Capodimonte, Via Moiariello 16, I-80131 Napoli, Italy
4 - Dip. Fisica, Università di Roma, P.le A. Moro 2, I-00185 Roma, Italy

Introduction

The thermal emission by dust sitting in molecular clouds can be used to evaluate their mass content and, if the gas-to-dust mass ratio is known, the total mass of the cloud. To this aim, *mm* observations of molecular clouds are properly used together with all other available informations about the dust properties.

The observations

We have considered the 2 *mm* observations of the LMC carried out during the Antarctic summer 1990-91 with the O.A.S.I. 2.6 *m* telescope whose field of view is 5′ [1]. Two signals have been detected respectively at $5.2 \div 5.3h$ and $5.6 \div 5.8h$ in R.A. and at the declination of $-69°$. The signal between 5.6 and 5.8 *h* can be associated with the 30 Dor region and is spatially well correlated with the 100 μm scan of IRAS. In principle the radiation detected at *mm* wavelengths may be due both to thermal and non-thermal emission. A comparison between the different contributions allows us to consider the *mm* fluxes as due mainly to thermal emission coming from particles sitting in molecular clouds.

Dust mass evaluation

Thermal emission can be used to estimate the dust mass M_d [2]. The temperature of the dust in the molecular cloud can be estimated from the spectra of the source when available. The evaluation of T_d is obtained both by using the extinction efficiency Q_{ext} for different dust grains suggested by current models and by using Q_{ext} derived from laboratory measurements on cosmic analogues (see Table 1). The interstellar radiation field appropriate to LMC condition is also used. The mass values are shown in Table 2 for the two regions of sky.

Table 1
Interstellar dust: physical properties of different dust grains
(grain radius: $a \sim 0.1 \mu m$)

Dust grains	ρ_d $g\ cm^{-3}$	Q/a cm^{-1}	T_{eq} K
Astronomical Silicates [3]	3.3 [3]	$6\ 10^{-1}$ [4]	30 - 35
Graphite [3]	2.26 [3]	$5\ 10^{-1}$ [4]	35 - 40
Composite grain [5]	~ 1 [5]	5 [5]	30 - 35
Amorphous/disordered carbon [6]	1.87 [7]	~ 20 [6]	23 - 25
Amorphous carbon RM [8]	1.87 [7]	5 [8]	~ 20
Amorphous carbon MW [5]	1.87 [7]	2.6 [5]	~ 25

Table 2
Estimated dust masses (in $M_\odot$) from the signals detected at 2 *mm*.

Dust grains	Cloud 1 (C1) 5.2-5.3 *h* R.A.	Cloud 2 (C2) 5.6-5.8 *h* R.A.
Astronomical Silicates [3]	$7.1\ 10^2$ – $1.6\ 10^3$	$1.4\ 10^3$ – $3.1\ 10^4$
Graphite [3]	$5.0\ 10^2$ – $9.3\ 10^3$	$8.0\ 10^2$ – $2.0\ 10^3$
Composite grain [5]	26 – 57	51 – 112
Amorphous/disordered carbon [6]	18 – 36	35 – 71
Amorphous carbon RM [8]	91 – 170	180 – 334
Amorphous carbon MW [5]	135 – 215	266 – 494

Discussion

The dust masses of C2 are systematically larger than those of C1. This is true for every dust models; it follows directly from the fact that the first region has the higher 2 *mm* flux. In that direction IRAS has detected the highest fluxes of the LMC.
The parameter that "plays the leading rôle" in the dust mass determination is the grain opacity rather than its temperature. The latter does not vary too much for the different kinds of grain in thermal equilibrium in the ISRF of the LMC.
Because of the lack of laboratory measurements at *mm* wavelengths, these have derived by extrapolation from FIR. The computed values depend critically from the extrapolation method. Mathis and Whiffen [5] and Rouleau and Martin [8] used the same method to evaluate the amorphous carbon optical constants, obtaining similar values for the emission efficiency and for the dust masses. On the other hand, by using the composite grain, we obtain dust masses that are in agreement with those estimated using a dust grain made of amorphous/disordered carbon.
We consider the previous estimates of the total cold dust mass in the LMC [9] which are derived from IRAS data ($60 - 100\mu m$), and combine them with the masses derived from 2 *mm* observations. According to the considered model we find out quite different amount of cold dust in the source. An amount of a cold dust component which is negligible or comparable with that estimated from the $100\mu m$ observations is in agreement with the high gas-to-dust ratio at 100μ. On the contrary, the IRAS FIR measurements which evidence the presence of hotter particles do not allow to estimate the dust mass fraction for dust at $T < 20K$.

References

[1] - G. Dall'Oglio, P.A.R. Ade, P. Andreani, P. Calisse, A. Iacoangeli, L. Martinis, P. Merluzzi, L. Pizzo, L. Rossi, R Vio 1993, submitted to M.N.R.A.S.
[2] - R.H. Hildebrand 1983, *Q.Jl R. Astr.Soc.*, **24** 267.
[3] - Draine, B. T. & Lee, H. M. 1984, *Ap.J.*, **285**, 89.
[4] - Draine, B. T., 1985, *Ap.J.Supp.Ser.*, **57**, 587.
[5] - Mathis, J. S. and Whiffen, G. 1989, *Ap.J.*, **341**, 808.
[6] - Bussoletti, E., Colangeli, L., Borghesi, A., and Orofino, V. 1987, *A.&A.Supp.Ser.*, **70**, 257.
[7] - Koike, C., Hasegawa, H., and Manabè, A. 1980, *Ap.&S.S.*, **67**, 495.
[8] - F Rouleau, P.G. Martin, *Astrph.J.*, **377**, 526.
[9] - Schwering, P. 1988, *An Infrared Study of the Magellanic Clouds*, Ph.D. Thesis, University of Leiden.

The 4D-Structure of a Dark Cloud, B164 Under the Influence of a Bright Star, Azelfafage

L. Pagani [1], C. Breart de Boisanger [2]

[1] DEMIRM, URA 336 du CNRS, Observatoire de Meudon, 92190 Meudon, France
[2] Centre d'Etudes de Bruyeres-le-Chatel, Service PTN, 91680 Bruyeres- le-Chatel, France

We present the 3D image and temporal evolution of a remarkable dark cloud: B164. This large Bok globule (Bok & Cordwell 1973) possesses a seldom shared property : it rotates. The rotation curve presents a clear 'S' shape but this cloud is unique today because a third of the rotation curve is missing. Indeed all the observations show that the cloud ends up abruptly on one side suggesting that a part of the cloud is missing. Taking the present rotational axis as the original symmetry axis we can deduce some important information such as the original size and mass of the cloud and an upper limit on the time at which the perturbation took place. The rotation curve also allows to give a 3D picture of the cloud which we explore with a Monte- Carlo model : the closest solution indicates a large envelope of increasing density from 100 $cm^{-3}$to 1000 $cm^{-3}$and a relatively small core of density of the order of 5000 cm^{-3}. CO isotopomers have a relatively low abundance in this model with the ^{13}CO abundance peaking at 2 - 3 x 10^{-6} for Av = 0.5 to 1 mag. and $C^{18}O$ being one to two orders of magnitude less abundant, as a function of depth. Next, we show that if Azelfafage (HD 206672), a Be3-III star is at the same distance from us and thus only at 3 pc from the cloud, it could be the progenitor of the observed perturbation. Using a chemico- hydro-dynamical model (CHD) (Breart de Boisanger et al. 1992) we show that the most probable explanation is that the star has just arrived and that its main action is to compress the cloud via the heating of the diffuse interstellar medium and/or the increase in radiation pressure rather than by photodissociating the molecular gas. Preliminary HI data and ^{12}CO observations show some evidence that the general contraction of the molecular envelope would be due to a direct pressure of the HI halo. It would seem that under the action of the star the whole molecular cloud is moving backwards and is getting compressed against its HI halo. The HD model to describe this effect is being currently developed and also more HI observations are underway to confirm this idea.

A detailed version of this poster has been submitted to A&A.

References

Bok B.J., Cordwell C.S., 1973. In : Gordon M.A., Snyder L.E. (eds) Molecules in the Galactic Environment, Wiley, New-York, p. 53
Breart de Boisanger C., Chieze J.P., Meltz B., 1992, ApJ 401, 182

Dense Molecular Gas in Ultraluminous and High Redshift Galaxies

Simon J. E. Radford
Institut de Radio Astronomie Millimétrique, 38406 St. Martin d'Hères, France
National Radio Astronomy Observatory, Tucson, AZ 85721, USA

Abstract

Molecular gas is the raw material for star formation and hence a crucial factor in galactic evolution. Ultraluminous infrared galaxies emit the bulk of their power in the far infrared, show disturbed morphologies indicative of recent mergers, and rival QSOs in their bolometric luminosities, but are more numerous in the local universe. Although they are as rich in molecular gas as the most gas rich normal spiral galaxies, they have elevated ratios of infrared luminosity to molecular mass that suggest they are undergoing bursts of very rapid and efficient star formation. A survey of HCN($1\rightarrow0$) emission from ten ultraluminous and normal galaxies shows far infrared emission correlates better with the amount of dense, $n(\mathrm{H_2}) > 10^4\,\mathrm{cm^{-3}}$, molecular gas than with the total amount of molecular gas. The star formation efficiency appears to depend on the fraction of the molecular gas reservoir at high density.

The galaxy IRAS 10214+4724 at $z = 2.286$ is perhaps the most luminous object in the universe. Observations of its CO($6\rightarrow5$), CO($4\rightarrow3$), and CO($3\rightarrow2$) lines indicate this galaxy has as much molecular gas as the total mass of the Milky Way. The molecular gas in 10214+4724 is both warmer and denser than that in the Galaxy and the normal gas to dust ratio suggests the abundances are nearly Solar. In the Milky Way, CO($6\rightarrow5$) is only observed in regions of high-mass star formation, so its presence in 10214+4724 implies the occurance of active star formation there. A map of the CO($3\rightarrow2$) emission with $2.3''$ resolution shows a small source slightly extended EW with a deconvolved size of $(10 \times 4) \pm 4h^{-1}$ kpc. The mass of molecular gas is comparable to the dynamical mass. This extraordinary primeval galaxy appears to have most of its mass in molecular gas and to be undergoing an extreme starburst that is generating metals with close to Solar abundances.

1 Dense Molecular Gas in Ultraluminous Galaxies

Rivalling QSOs in emitted power, ultraluminous infrared galaxies ($L_{\mathrm{FIR}} > 5 \times 10^{11} h^{-2}\,\mathrm{L_\odot}$; $H_0 = 100h\,\mathrm{km\,s^{-1}\,Mpc^{-1}}$, $q_0 = 0.5$) are three times more common in the local universe ($z < 0.3$) (Sanders et al. 1988). Almost all show disturbed optical morpholgy: double nuclei, tidal bridges and tails, or other signs of mergers or interactions(Melnick & Miralbel 1990). Rich in molecular gas, they typically contain $> 5 \times 10^9 h^{-2}\,\mathrm{M_\odot}$ of $\mathrm{H_2}$(Sanders et al. 1986). Although some normal spiral galaxies are equally gas rich, e. g. NGC 3147 (Solomon & Sage 1988), ultraluminous galaxies have $L_{\mathrm{FIR}}/L_{\mathrm{CO}}$ ratios 30 times higher than do normal galaxies of the same mass (Sanders et al. 1986; Solomon & Sage 1988) What powers ultraluminous galaxies, obscured black holes in active nuclei or rapid bursts of star formation?

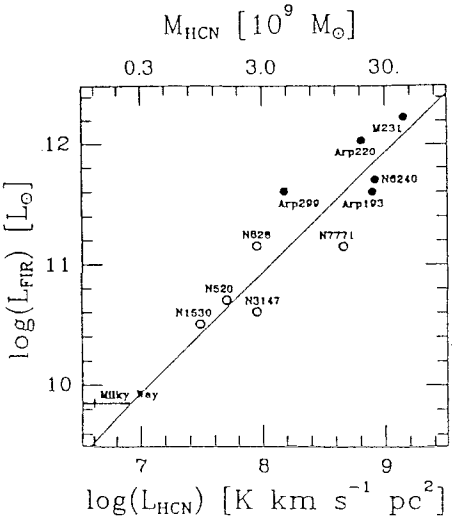

Figure 1:
For both ultraluminous (*solid circles*) and more normal (*open circles*) galaxies, FIR and HCN($1\rightarrow0$) luminosity are well correlated (Solomon, Downes, & Radford 1992a). The upper scale indicates the mass of high density molecular gas, $n(H_2) \approx 10^4\,cm^{-3}$. In this Figure, $H_0 = 75\,km\,s^{-1}\,Mpc^{-1}$.

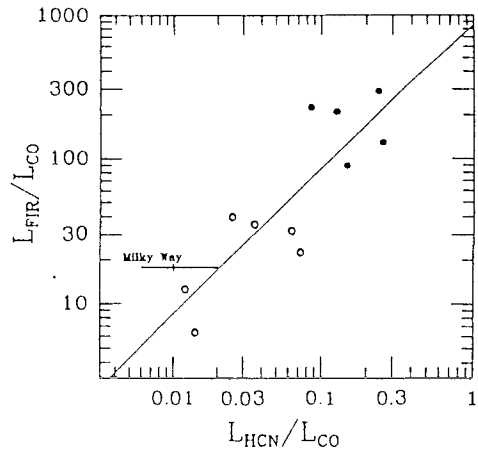

Figure 2:
The tight correlation between L_{FIR}/L_{CO} and L_{HCN}/L_{CO} suggests the star formation efficiency of galaxies depends on the fraction of available molecular gas in a dense phase (Solomon, Downes, & Radford 1992a). While L_{HCN}/L_{CO} is dimensionless, L_{FIR}/L_{CO} is measured in $L_\odot\,(K\,km\,s^{-1}\,pc^2)^{-1}$.

Molecular gas is the raw material for star formation and hence a crucial factor in galactic evolution. The CO($1\rightarrow0$) line traces gas at $n(H_2) < 10^3\,cm^{-3}$ and indicates the total H_2 mass in a galaxy. In ultraluminous galaxies, far IR radiation, emitted by dust warmed by UV radiation from O and B stars, indicates the formation rate of massive stars. The $L_{FIR}/M(H_2)$ ratio measures, then, the star formation rate per mass of gas, or the star formation efficiency. Why is this efficiency so much higher in ultraluminous galaxies than in normal gas rich spiral galaxies? Does another parameter besides the amount of fuel control star formation in galaxies? In the Milky Way most of the H_2 is in low density giant molecular cloud envelopes. Massive stars form, however, not in those envelopes, but in dense cloud cores, objects like M 17, W 51, etc. Although CO traces most of the H_2 mass, it does not necessarily trace the regions of active star formation where the gas density is more than ten times higher than average. Dense molecular gas is better indicated by the HCN($1\rightarrow0$) line, which traces gas at $n(H_2) \approx 10^4\,cm^{-3}$.

In a sample of ten galaxies surveyed with the IRAM 30 m telescope (Solomon, Downes, & Radford 1992a), ultraluminous galaxies have much stronger HCN($1\rightarrow0$) lines than normal galaxies (Figure 1). In absolute terms, Mrk 231, the most luminous galaxy in the local universe, has an HCN($1\rightarrow0$) line luminosity larger than the CO($1\rightarrow0$) luminosity of the Milky Way, while in relative terms, Mrk 231 has $L_{CO}/L_{HCN} \approx 4$ whereas $L_{CO}/L_{HCN} \approx 100$ in the Galaxy. For the whole sample, FIR luminosity correlates better with HCN($1\rightarrow0$) luminosity than with CO($1\rightarrow0$) luminosity. Over a range of 50 in L_{FIR}/L_{CO}, the range in L_{FIR}/L_{HCN} is only three. When normalized by the CO($1\rightarrow0$) luminosity, there is a very tight correlation between L_{HCN}/L_{CO} and L_{FIR}/L_{CO} (Figure 2). The L_{HCN}/L_{CO} ratio indicates the fraction of the total H_2 mass that has a density $\approx 10^4\,cm^{-3}$, i. e. that has conditions necessary for formating massive stars. In any galaxy, ultraluminous or not, the star formation efficiency, measured by L_{FIR}/L_{CO}, depends on how much of the total molecular gas is in a dense phase.

In the most luminous galaxies in the sample, Mrk 231 and Arp 220, the mass of high density gas exceeds $5 \times 10^9 h^{-2}\,M_\odot$ and accounts for roughly half the total gas reservoir. In the

Milky Way and other normal galaxies, on the other hand, only a small fraction of the gas is sufficiently dense to form high mass stars. The bulk of the molecular gas in the ultraluminous galaxies is, therefore, more similar to that in active star-forming cloud cores than that in the envelopes of GMCs. In our Galaxy, O stars form in massive cloud cores with high density gas and they will form under similar circumstances in ultraluminous galaxies as well. The large masses of high density gas implied by the strength of their HCN($1 \rightarrow 0$) lines indicate ultraluminous galaxies are extraordinary star forming environments and suggest star formation is their principal power source. These galaxies are evolving rapidly under conditions reminiscent of those when galaxies formed.

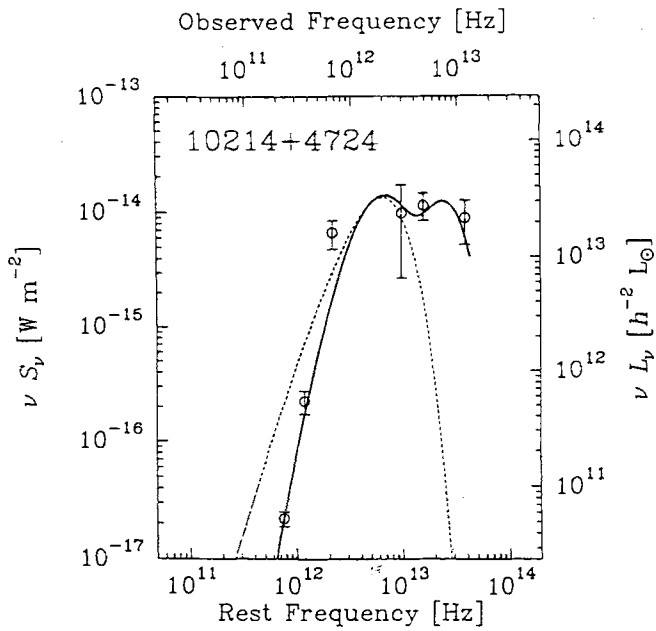

Figure 3:

FIR and submm continuum spectrum of 10214+4724. The sum of an 80 K dust spectrum and a 300 K black body (*solid curve*) fits the measurements while an 80 K black body (*dashed curve*) would produce too much long wavelength radiation (Downes et al. 1992).

2 Warm Molecular Gas in a High Redshift Galaxy

With a total luminosity near $10^{14}h^{-2}\,L_\odot$, the faint IRAS galaxy 10214+4724 at $z = 2.286$ is as luminous as the strongest QSOs and 20 times more powerful than other known ultraluminous infrared galaxies (Rowan-Robinson et al. 1991) It may be a primeval galaxy in an early evolutionary stage. Is this galaxy powered by star formation or by an active nucleus?

Submillimeter continuum emission from 10214+4724 was observed at 450 and 800 μm with the JCMT (Clements et al. 1992) and at 1.2mm with the IRAM 30 m telescope (Downes et al. 1992). The spectrum (Figure 3) shows the dust is optically thin longward of 175 μm (rest frame). For a ν^2 dust emissivity law, the dust temperature is 80 ± 10 K and the dust mass (Downes et al. 1992) is $2 \times 10^8 h^{-2}\,M_\odot$.

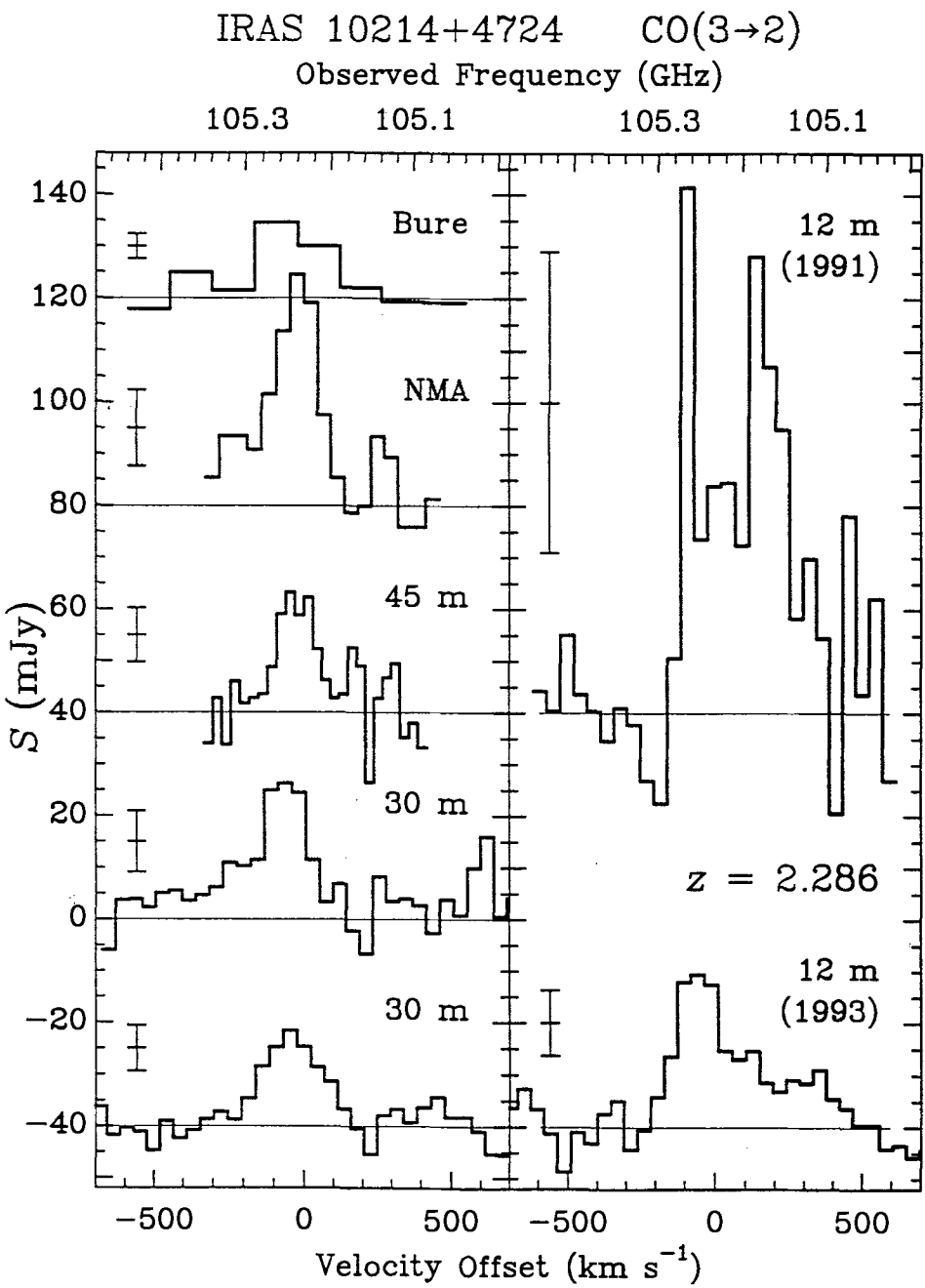

Figure 4:

Spectra of CO(3 → 2) emission at $z = 2.286$ from IRAS 10214+4724 observed with the NRAO 12 m telescope at 16 MHz resolution in 1991 (Brown & Vanden Bout 1991) and 1993, the IRAM 30 m telescope at 16 MHz resolution (upper Brown & Vanden Bout 1992b; lower Solomon, Downes, & Radford 1992b), the Nobeyama 45 m telescope at 10.5 MHz resolution (Tsuboi & Nakai 1992), the Nobeyama Millimeter Array at 32.5 MHz resolution (Kawabe et al. 1992; Sakamoto et al. 1992), and the IRAM interferometer (Bure) at 50 MHz resolution (Radford, Brown, & Vanden Bout 1993). The $\pm 1\sigma$ error bars represent the per channel uncertainty in each spectrum.

The extraordinary detection (Brown & Vanden Bout 1991) of CO($3 \rightarrow 2$) line emission from 10214+4724 indicates this galaxy has as much molecular gas as the total mass of a large spiral galaxy (Solomon, Radford, & Downes 1992). There has been, however, some uncertainty about the true line flux. While the flux measured originally with the NRAO 12 m telescope is $21 \pm 5\,\mathrm{Jy\,km\,s^{-1}}$ (Brown & Vanden Bout 1991), the weighted average of subsequent measurements with other telescopes, $4 \pm 1\,\mathrm{Jy\,km\,s^{-1}}$, is five times less (Figure 4). Furthermore, a new spectrum obtained with the NRAO 12 m telescope in 1993 June shows a component with a redshift, width, and flux consistent with the measurements from other telescopes. Although there is a positive velocity line wing in this spectrum, this might be merely a baseline swell. There remains little, if any, evidence for proposed explanations of the flux discrepancy between the original and subsequent measurements (Brown & Vanden Bout 1992b; Kawabe et al. 1992; Sakamoto et al. 1992; Tsuboi & Nakai 1992) that had invoked additional sources, not coincident with the optical and radio (cm) source.

Both CO($4 \rightarrow 3$) (Brown & Vanden Bout 1992b) and CO($6 \rightarrow 5$) (Solomon, Downes, & Radford 1992b) have been detected in 10214+4724 (Figure 5). In the Milky Way the warm dense gas required for significant excitation of CO($J = 6$) is found only in molecular cloud cores near sites of massive star formation (Jaffe et al. 1989). The measured line ratios in 10214+4724, $\mathrm{CO}(6 \rightarrow 5)/\mathrm{CO}(3 \rightarrow 2) = 0.6 \pm 0.2$ and $\mathrm{CO}(4 \rightarrow 3)/\mathrm{CO}(3 \rightarrow 2) = 0.8 \pm 0.2$, are considerably higher than overall values for the Milky Way. An LVG radiative transfer calculation shows these ratios are both consistent with $n(\mathrm{H_2}) \approx 5000\,\mathrm{cm^{-3}}$ and $T_{\mathrm{kin}} \approx 50\,\mathrm{K}$ (Solomon, Downes, & Radford 1992b). This calculation predicts $\mathrm{CO}(3 \rightarrow 2)/\mathrm{CO}(1 \rightarrow 0) = 0.9$ (this ratio is 0.24 in the Galaxy) and $M(\mathrm{H_2})/L_{\mathrm{CO}} = 4\,\mathrm{M_\odot\,(K\,km\,s^{-1}\,pc^2)^{-1}}$. Because the temperature of the Cosmic Background Radiation (CBR) should increase as $(1 + z)$, gas at $z \approx 2$ will always have $\mathrm{CO}(3 \rightarrow 2)/\mathrm{CO}(1 \rightarrow 0) > 0.5$, even if the density is quite low. The CO($3 \rightarrow 2$) line flux observed with the IRAM 30 m telescope then implies $M(\mathrm{H_2}) = 1 \times 10^{11}\,\mathrm{M_\odot}$ in 10214+4724. The gas to dust mass ratio, 500, is quite normal and suggests the metal abundance is already approximately Solar (Downes et al. 1992).

The distribution of CO in 10214+4724 has been mapped with the Nobeyama (Kawabe et al. 1992; Sakamoto et al. 1992), Owens Valley (Brown, Vanden Bout, & Wooten 1993), and IRAM (Radford, Brown, & Vanden Bout 1993) interferometers. The IRAM map (Figure 6), with 2.3″ resolution, shows a small source coincident with the Hα (Clements et al. 1993; Soifer et al. 1992) and extended 8.4 GHz continuum emission (Lawrence et al. 1992). The ratio of the intrinsic CO($3 \rightarrow 2$) brightness temperature derived from the observed line ratios and a radiative transfer calculation, 40 K, and the peak rest frame brightness temperatures measured in the channel maps, 0.7 K, indicates about 1.7% of the synthesized beam area is occupied by radiating gas. A completely filled source of equivalent luminosity would be 0.3″ in diameter. Despite this low filling factor and the large apparent size of the CO($3 \rightarrow 2$) emission region, the average surface density, $2500\,\mathrm{M_\odot\,pc^{-2}}$, is ten times higher than for Galactic giant molecular clouds (Solomon et al. 1987). In two channels $143\,\mathrm{km\,s^{-1}}$ apart, there is a predominantly E-W shift of 1.4″ between the positions of maximum emission. After deconvolving the beam, the source size in the integrated map is $(2.5'' \times 1'') \pm 1''$ [$(10 \times 4) \pm 4h^{-1}\,\mathrm{kpc}$]. This size scale is characteristic of an entire galaxy, rather than just its nucleus. The velocity gradient implied by the E-W shift suggests the molecular gas is distributed in a rotating structure and the apparent dimensions and aspect ratio further suggest this structure is mostly edge on. For an edge on system with a velocity width of $240\,\mathrm{km\,s^{-1}}$ and a characteristic dimension of $6\text{–}10h^{-1}\,\mathrm{kpc}$, the dynamical mass is $8\text{–}13 \times 10^{10}h^{-1}\,\mathrm{M_\odot}$, which is consistent with the $\mathrm{H_2}$ mass determined from the line flux.

The outstanding property of 10214+4724 is its $L_{\mathrm{FIR}}/L_{\mathrm{CO}}$ ratio, $3000\,\mathrm{L_\odot\,(K\,km\,s^{-1}\,pc^2)^{-1}}$, which is ten times greater than that of other ultraluminous galaxies. If star formation powers this galaxy, then a short starburst of primarily high mass stars in required. The energy available from nuclear burning in $10^{11}\,\mathrm{M_\odot}$ of stars indicates star formation can only maintain the luminosity of 10214+4724 for $\approx 10^7\,\mathrm{yr}$. For a burst of formation of 10 to $100\,\mathrm{M_\odot}$ stars, the necessary formation rate is $\approx 3000\,h^{-2}\,\mathrm{M_\odot\,yr^{-1}}$, about 5000 times the rate in the Milky Way. A starburst of this magnitude will rapidly enrich the interstellar medium in heavy elements.

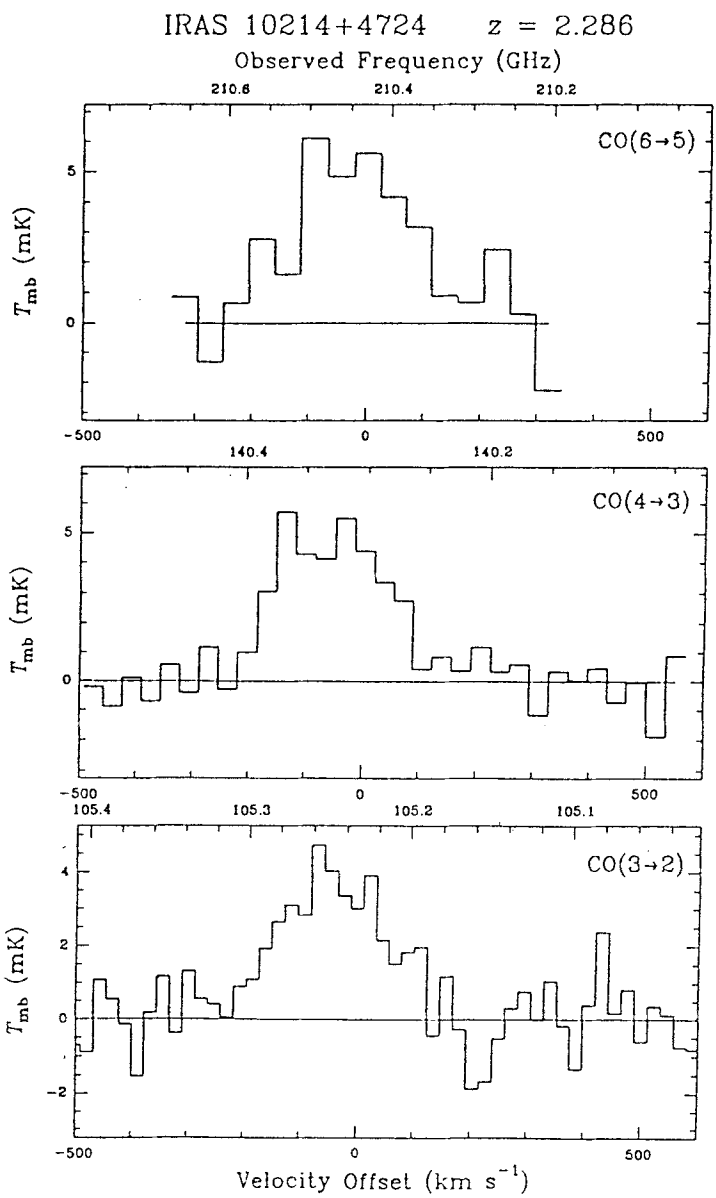

Figure 5:

Spectra of CO(6→5), CO(4→3), and CO(3→2) emission at $z = 2.286$ from 10214+4724 observed with the IRAM 30 m telescope (Brown & Vanden Bout 1992b; Solomon, Downes, & Radford 1992b).

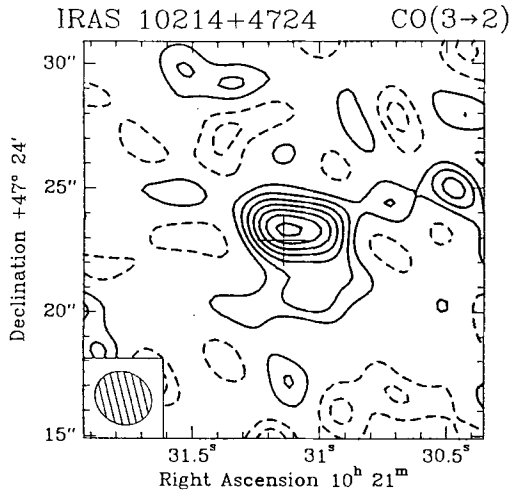

Figure 6:

IRAM interferometer map of CO(3→2) emission from 10214+4724 at $z = 2.2858$ integrated over $\pm 143\,\mathrm{km\,s^{-1}}$. Contour interval is 1 mJy (Radford, Brown, & Vanden Bout 1993).

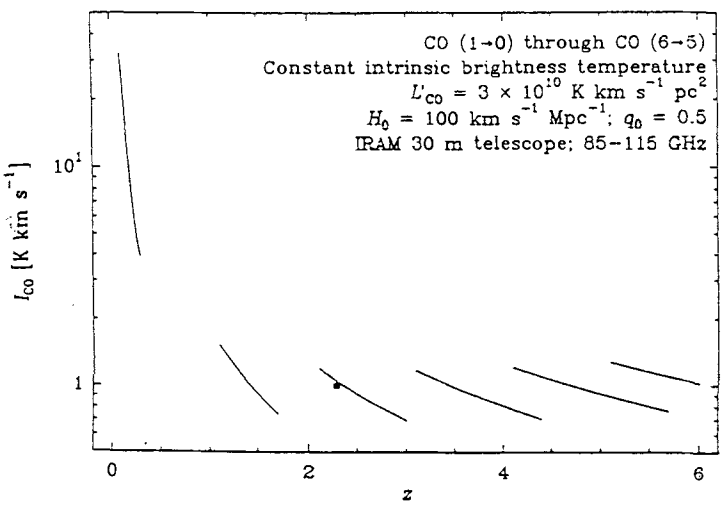

Figure 7:

Predicted intensity of CO(1→0) through CO(6→5) line emission from sources of the same luminosity but different redshifts if observed with the IRAM 30 m telescope in the 3 mm atmospheric window (85–115 GHz). The square symbol indicates the observed CO(3→2) intensity of IRAS 10214+4724. Here $q_0 = 0.5$; if $q_0 = 0.05$ the results are, similiar, although somewhat less favorable for high redshifts. This assumes the intrinsic brightness temperatures are the same for all lines. If the high J lines are not thermalized, they will be, of course, weaker. For this telescope and wavelength, there are $4.5\,\mathrm{Jy\,K^{-1}}$.

3 Further Prospects

Because of the large redshift of IRAS 10214+47624, it's possible to observe several submillimeter spectral lines from the ground that are normally impossible or at least very difficult. The $(2_{1,1} \rightarrow 2_{0,2})$ line of para water has been detected with the IRAM 30 m telescope (Encrenaz et al. 1993; Casoli et al. 1994) The $^3P_2 \rightarrow {}^3P_1$ and $^3P_1 \rightarrow {}^3P_0$ fine structure lines of neutral atomic carbon have been observed with the NRAO 12 m and IRAM 30 m telescopes (Brown & Vanden Bout 1992a). These observations remain, however, unconfirmed and controversial.

Because of the difference between angular size distance and luminosity distance (Weinberg 1972), spectral lines from high redshift objects are somewhat easier to observe than was first expected (Solomon, Radford, & Downes 1992; Solomon, Downes, & Radford 1992b). Furthermore, for observations in a particular atmospheric window, the CO rotational ladder is convenient since the redshift where a line leaves the lower edge of the band is roughly the same redshift where the next higher transition enters the upper edge of the band. Both because of the increase in the temperature of the CBR with redshift and because we have detected $CO(6 \rightarrow 5)$ emission from 10214+4724, we expect CO lines up to $J = 6$ should have roughly the same intrinsic brightness temperatures. For objects with the same luminosity as 10214+4724 but at different redshifts, the predicted CO line intensities are almost constant for any $z > 1$ (Figure 7). Current millimeter wave telescopes can detect molecular gas in objects as distant as any known in the Universe.

The observations with the 30 m and 12 m telescopes were done with Phil Solomon and Dennis Downes and the interferometery with Bob Brown and Paul Vanden Bout.

References

Brown, R. L., & Vanden Bout, P. A. 1991, AJ 102, 1956
Brown, R. L., & Vanden Bout, P. A. 1992, ApJ 397, L11
Brown, R. L., & Vanden Bout, P. A. 1992, ApJ 397, L19
Brown, R. L., Vanden Bout, P. A., & Wooten, H. A. 1993, *private communication*
Casoli, F., Gerin, M., Encrenaz, P. J., & Combes, F. 1994, A&A, submitted Clements, D. L., et al. 1992, MNRAS 256, 35P
Clements, D. L., et al. 1993, MNRAS *in press*
Downes, D., et al. 1992, ApJ 398, L25
Encrenaz, P. J., et al. 1993, A&A, 273, L19
Jaffe, D. T., et al. 1989, ApJ 344, 265
Kawabe, R., Sakamoto, K., Ishizuki, S., & Ishiguro, M. 1992, ApJ 397, L23
Lawrence, A., et al. 1992, MNRAS 260, 28
Melnick, J., & Mirabel, I. F. 1990, A&A 231, L19
Radford, S. J. E., Brown, R. L., & Vanden Bout, P. A. 1993, A&A 271, L71
Rowan-Robinson, M., et al. 1991, Nature 351, 719
Sanders, D. B., et al. 1986, ApJ 305, L45
Sanders, D. B., et al. 1988, ApJ 325, 74
Sakamoto, K., Ishizuki, S., Kawabe, R., & Ishiguro, M. 1992, ApJ 397, L27
Soifer, B. T., et al. 1992, ApJ 399, L55
Solomon, P. M., Downes, D., & Radford, S. J. E. 1992, ApJ 387, L55
Solomon, P. M., Downes, D., & Radford, S. J. E. 1992, ApJ 398, L29
Solomon, P. M., Radford, S. J. E., & Downes, D. 1992, Nature 356, 318
Solomon, P. M., Rivolo, A. R., Barrett, J., & Yahil, A. 1987, ApJ 319, 730
Solomon, P. M., & Sage, L. J. 1988, ApJ 334, 613
Tsuboi, M., & Nakai, N. 1992, PASJ 44, L241
Weinberg, S. 1972, Gravitation and Cosmology (Wiley: New York)

Interstellar Molecules in the Large Magellanic Cloud

L.E.B. Johansson
Onsala Space Observatory
Chalmers University of Technology, S-439 92 Onsala, Sweden

Abstract. The results of a mm-wave molecular line search in the Large Magellanic Cloud are presented. The observations were done with the SEST in the area of the N159 complex of HII regions. Isotopomers of CO, CS, SO, CN, HCN, HNC, HCO^+ and H_2CO have been detected. All observed isotopic intensity ratios are consistent with small optical depths provided that abundance ratios typical of the Galactic disc hold for the interstellar gas in N159. The data indicate a $^{12}C/^{13}C$ abundance ratio of 50^{+25}_{-20}. The $^{18}O/^{17}O$ abundance ratio is observed to be about a factor of 2 lower than in the Galaxy, and another factor of 2 lower than in starburst galaxies. Normalized to the CO intensity, most lines detected in N159 are weaker than observed in the Galaxy. The only exception is HCO^+, which also shows a large emission extent. Estimates of fractional abundances indicate that those of N159 typically are a factor of 10, or more, lower than in the Galaxy.

1. Introduction

In recent years the interstellar gas of the Magellanic Clouds has been extensively studied in the $^{12}CO(1\text{-}0)$ line at 115 GHz with linear resolutions ranging from about 150 pc (Cohen et al. 1988; Rubio et al. 1991; Garay et al. 1993) to 10 pc (Johansson 1991; Israel and de Graauw 1991; Israel et al. 1993; Rubio et al. 1993; Rubio, Lequeux and Boulanger 1993). The latter resolution is obtained with the Swedish-ESO Submillimetre Telescope (SEST) and is comparable to the sizes of molecular clouds or cloud complexes in the Galaxy.

Dwarf galaxies, including the Magellanic Clouds, generally show weak CO emission (see e.g. Elmegreen, Elmegreen and Morris 1980). However, CO antenna temperatures approaching those typical for Galactic molecular clouds have been observed in the LMC with the SEST (Johansson 1991; Israel et al. 1993), indicating that the weak emission observed on larger scales is rather a result of a small beamfilling than excitation or opacity effects. On the other hand, low CO abundances are expected in the Magellanic Clouds due to the relatively low abundances of heavy elements (Dufour 1984). Moreover, the low dust abundance (Koornneef 1984; Martin, Maurice and Lequeux 1989) combined with the relatively strong UV radiation enhances the photodissociation rates, which further emphasizes the expectations for low CO abundances.

To gain further information on the physical and chemical properties of the molecular clouds in the LMC, observations of a significant number of molecules and transitions with different excitation criteria are required. In this paper we present results of such a study, done with the SEST. The observations were focused on a molecular cloud in the N159 complex of HII regions in the LMC.

A more detailed discussion of these data is presented by Johansson et al. (1993).

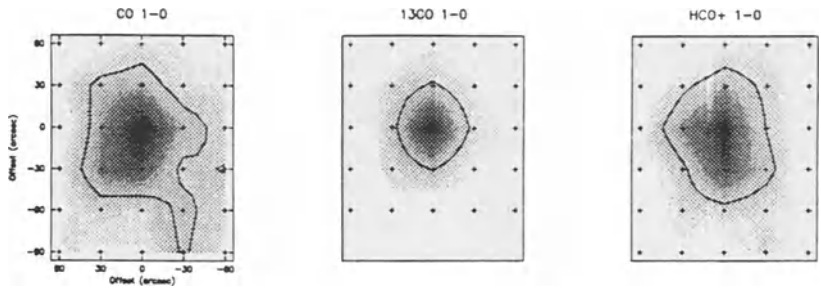

Figure 1 Greyscale maps of integrated emission in N159. The greyscales extend out to the 30% level of the peak emission in each map. Half intensity contours are also plotted.

2. Interstellar molecules detected in the N159 region

SEST observations of the CO(1-0) emission in the N159 area show three well defined cloud complexes (see e.g. Fig.1 in Johansson 1991). Two of them are most likely associated with OB star formation. Pilot surveys showed that one of the latter objects was the most promising one with respect to detection rates of molecular transitions. The final line search position, RA(1950.0)=$05^h40^m03.0^s$ and DE(1950.0)=-69°47'03", was refined by mapping in the 3 mm transitions of ^{13}CO CS, HCN, and HCO^+. Greyscale maps of the integrated emissions of ^{12}CO ^{13}CO and HCO^+ are shown in Figure 1.

Table 1 summarizes the molecular line data observed towards the N159 cloud. The intensity scale is main beam brightness temperature. The indicated uncertainties are 2σ errors defined by the noise fluctuations.

3. Line intensity ratios

In the following we will make frequent use of intensity and abundance ratios when discussing the properties of the molecular gas in the LMC. For this purpose we compare with the corresponding ratios observed in the Galaxy and in a sample of external galaxies. The galaxy sample is dominated by spirals associated with nuclear activity.

To investigate the dependence of intensity ratios on spatial resolution we have mapped a Galactic disc cloud associated with the HII region S138 in most of the 3 mm transitions detected towards N159. Table 2 gives integrated intensities normalized to those of ^{12}CO. In addition to the emissions observed in the centre positions, luminosities have also been estimated from more or less extended maps. Generally, the normalized intensities observed in the cloud centres are a factor 2-3 higher than the corresponding luminosities. The exception is HCO^+, which shows essentially the same ratio in the two cases. This is a reflection of the relatively large extent of its emission (see Figure 1).

Table 1: Detections and significant upper limits in the N159 molecular cloud (an asterisk indicates data convolved to the beam size of the lower transition)

Transition	T_{MB} [K]	v_{lsr} [km s^{-1}]	Δv [km s^{-1}]	Integrated [K km s^{-1}]
CO 1-0	6.80	238.0	7.7	56.5 ± 0.3
2-1	8.93	238.0	7.4	70.3 ± 0.6
2-1 *	7.20	238.0	7.4	56.4 ± 0.4
^{13}CO 1-0	0.80	237.6	7.8	6.80 ± 0.2
2-1	2.35	237.6	7.3	18.1 ± 0.7
2-1 *	1.33	237.6	7.4	10.5 ± 0.3
C^{18}O 1-0	0.030	237.6	6.6	0.20 ± 0.02
2-1	0.098	237.6	5.3	0.55 ± 0.15
2-1 *	0.037	238.4	4.9	0.20 ± 0.10
C^{17}O 1-0	0.010	237.7	10.2	0.19 ± 0.02
CS 2-1	0.26	237.1	6.8	1.80 ± 0.13
5-4	0.17	236.9	6.0	1.10 ± 0.30
5-4 *	0.075	237.4	6.4	0.51 ± 0.11
^{13}CS 2-1	0.010	236.3	4.0	0.041 ± 0.015
C^{34}S 2-1	0.020	237.3	4.5	0.091 ± 0.018
HCO$^+$ 1-0	0.61	237.7	7.3	4.72 ± 0.26
3-2	0.32	236.4	8.4	2.86 ± 0.40
3-2 *	0.12	236.7	9.2	1.18 ± 0.10
H^{13}CO$^+$ 1-0	0.018	237.2	5.2	0.098 ± 0.020
HCN 1-0	0.20	239.2	10.3	2.14 ± 0.17
3-2				< 1.0
3-2 *				< 0.7
H^{13}CN 1-0				< 0.08
SO 2_3-1_2				< 0.15
3_2-2_1	0.10	237.5	7.6	0.77 ± 0.10
5_5-4_4				< 0.10
6_5-5_4				< 0.5
CN 2-1 J=5/3-3/2	0.12		8.4	1.03 ± 0.06
HNC 1-0	0.12	237.3	5.4	0.72 ± 0.07
H_2CO $3_{1,2}$-$2_{1,1}$		239.3		1.00 ± 0.10

Table 2 Integrated intensity ratios, I_{CO}/I_{mol} (indicated uncertainties are 2σ total observational errors)

Transition	Centre position		Luminosity		
	S138	N159	S138	N159	CO galaxy sample
^{13}CO 1-0	5.6 ± 1.3	8.3 ± 1.3	7.3 ± 1.1	14 ± 2	13
C^{18}O 1-0	59 ± 20	283 ± 53	107 ± 21	>500	60
CS 2-1	16 ± 4	31 ± 6	37 ± 6	55 ± 16	44
HCO$^+$ 1-0	17 ± 4	12 ± 2	26 ± 5	13 ± 2	21
HCN 1-0	11 ± 3	26 ± 5	20 ± 3	82 ± 19	25
HNC 1-0	40 ± 16	78 ± 15	84 ± 17	>150	40
SO 3_2-2_1	46 ± 10	73 ± 15	130 ± 26	>150	>200

In contrast to our data for the Galaxy and the LMC, the intensities observed from the galaxy sample can not be identified with a single cloud population. However, the normalized luminosities for S138 and the intensities for the galaxy sample are quite similar (Table 2). This is in contrast to N159, where the normalized luminosities generally are lower, again with the exception of the HCO$^+$ emission.

Table 3 shows observed isotopic intensity ratios and estimates for the corresponding Galactic disc abundance ratios. The latter data are based on the following abundance ratios: $^{12}C/^{13}C \approx 50$ (Langer and Penzias 1990), $^{16}O/^{18}O = 490$ and $^{32}S/^{34}S = 22.5$ (Solar system), and $^{18}O/^{17}O = 3.2$ (Wilson and Matteucci 1992). A comparison with the Galactic disc isotopic abundance ratios listed (Column 5) indicates that the emissions of the main isotopomers in S138 are saturated, as expected. This also applies to the observed lines in the galaxy sample. In N159, on the other hand, all ratios involving main isotopomers are consistent with low optical depths provided that the Galactic disc abundance ratios can be applied. However, there are certainly reasons to question such an assumption for the interstellar gas in the LMC: a different history of stellar processed matter and a more hostile environment for the molecular species due to stronger radiation fields and less dust shielding. A higher rate of isotope-selective photodissociation is thus expected in the LMC. Another process that may alter isotopic abundance ratios is chemical fractionation.

Observations of the ^{12}CO / ^{13}CO abundance ratio reveal a radial gradient in the Galaxy - a ratio of about 25 in the centre and a factor of 2-3 higher in the solar neighbourhood (Wannier 1980; Langer and Penzias 1990, 1993). Such a trend is expected as a consequence of the stellar CNO cycle that converts ^{12}C to ^{13}C. On the other hand, CS observations of the interstellar gas throughout the Galaxy show $^{32}S/^{34}S$ abundance ratios consistent with the terrestrial value of 22.5 (Frerking, Wilson and Linke 1980). The measured stability of the sulphur ratio in the interstellar gas is further emphasized by observations of SiS isotopomers in the circumstellar gas of the carbon star IRC+10216, which also agree, to within the observational errors, with the terrestrial ratio (Kahane et al. 1988). Applying the terrestrial sulphur ratio to the interstellar

Table 3. Isotopic integrated intensity ratios (indicated uncertainties are 2σ total observational errors)

Isotopes	S138	N159	CO galaxy sample	Galactic disc abundance ratios
$^{13}CO/C^{18}O$	10 ± 4	34 ± 7	5.0	≈ 10
$C^{18}O/C^{17}O$	4.0 ± 1.6	2.0 ± 0.5	> 8	≈ 3.2
$HCO^+/H^{13}CO^+$	17 ± 5	50 ± 16	15	≈ 50
$HCN/H^{13}CN$	12 ± 3	> 22	16	≈ 50
$CS/^{13}CS$	16 ± 5	44 ± 18		≈ 50
$CS/C^{34}S$	8.5 ± 3	20 ± 5		22.5
$C^{34}S/^{13}CS$	1.9 ± 0.7	2.2 ± 0.9		≈ 2.2

gas in the LMC, we find a negligible opacity correction for the emission of the main isotopomer of CS. This suggests that the observed $^{12}CS/^{13}CS$ intensity ratio in N159 is a good measure of the corresponding abundance ratio. Although less well based, we also assume that small optical depths apply to the HCO^+ emission. While isotope-selective photodissociation is unlikely to be important for CS and HCO^+, particularly in view of their low column densities (see next Section), chemical fractionation can not be excluded. Model calculations by Langer and Graedel (1989) indicate that the ^{12}C and ^{13}C variants of HCO^+ and CS place a lower and an upper limit, respectively, to the $^{12}C/^{13}C$ abundance ratio. Using this bracketting, we find a $^{12}C/^{13}C$ abundance ratio of 50^{+25}_{-20} in N159. The indicated uncertainties are 2σ errors.

The observed $C^{18}O/ C^{17}O$ ratio in N159 is about a factor of 2 lower than in the Galaxy and another factor of 2 lower than in a small sample of starburst galaxies, observed by Sage, Mauersberger and Henkel (1991), and Henkel and Mauersberger (1993). These authors suggest an overproduction of ^{18}O in the starburst sample, due to a preference for massive stars in the initial mass function of the burst. Whether the low ratio observed in N159 is a local phenomenon or an indication of a different global intial mass function in the LMC is an open question.

4. Rotation temperatures and abundances

Rotation temperatures and the corresponding total column densities for CS, HCO^+, HCN, ^{13}CO and $C^{18}O$ have been derived from a two level analysis assuming uniform excitation (i.e. a population distribution described by a single temperature). It is further assumed that opacity corrections are insignificant as suggested in the previous Section. The results for N159 are given in Table 4, which shows rotation temperatures between 5 and 10 K. The four transitions observed in SO (see Table 1) are consistent with an upper limit of about 10 K. For ^{12}CO we find a lower limit of 14 K.

To derive fractional abundances we have estimated hydrogen column densities with the aid of the CO to H_2 conversion factor. For S138 we have used a value of 2.3×10^{20} $cm^{-2}(K\ km\ s^{-1})^{-1}$ (Strong et al. 1988) and for N159 a conversion factor 1.5 times

Table 4. Derived rotation temperatures and column densities in N159 (numbers in brackets are determined by the 2σ total errors)

Isotope	Transitions	Rotation temp. [K]	Column density [cm^{-2}]
^{13}CO	1-0 / 2-1	10.2 (8.3, 13)	6.3 (6.4, 6.4) 10^{15}
$C^{18}O$	1-0 / 2-1	6.9 (4.9, 10)	1.8 (2.2, 1.6) 10^{14}
CS	2-1 / 5-4	8.8 (8.0, 9.6)	7.9 (8.6, 7.3) 10^{12}
HCO^+	1-0 / 3-2	5.5 (5.2, 5.9)	3.5 (4.0, 3.2) 10^{12}
HCN	1-0 / 3-2	< 6.0	$> 3.5\ 10^{12}$

Table 5. Abundances relative to molecular hydrogen in S138 and N159 (numbers in brackets are assumed values)

Isotope	S138			N159		
	T_{ex} [K]	$\tau/(1-e^{-\tau})$	Fractional abundance	T_{ex} [K]	Fractional abundance	X(S138) / X(N159)
^{13}CO	(40)	1.1	$2\ 10^{-6}$	10.2	$3.2\ 10^{-7}$	6
$C^{18}O$	(20)	1.0	$1\ 10^{-7}$	6.9	$9.0\ 10^{-9}$	11
CS	(20)	3.1	$5\ 10^{-9}$	8.8	$4.0\ 10^{-10}$	12
SO	(20)	(3.0)	$3\ 10^{-9}$	(7)	$2.6\ 10^{-10}$	13
HCO^+	(20)	3.0	$9\ 10^{-10}$	5.5	$1.8\ 10^{-10}$	5
HCN	(20)	4.2	$4\ 10^{-9}$	(5)	$2.0\ 10^{-10}$	22
HNC	(20)	(3.0)	$8\ 10^{-10}$	(5)	$6.2\ 10^{-11}$	13
CN				(7)	$2.6\ 10^{-10}$	
H_2CO				(7)	$5.1\ 10^{-10}$	

higher (Johansson 1991). The latter factor is the lowest estimate reported for the LMC, but is justified in the sense that the central column of the N159 cloud probably represents one of the densest regions in the LMC. Other estimates (e.g. Cohen et al. 1988) are based on a cruder linear resolution, resulting in a higher fraction of intercloud gas in the beam. Such a component represents gas of lower molecular abundances, thus raising the conversion factor.

In Table 5 estimates of fractional abundances are given, expressed as column densities relative to those of H_2, for S138 and N159. The S138 data are corrected for opacity effects (Column 3), calculated from the observed isotopic intensity ratios and assuming Galactic disc abundance ratios. The last Column in Table 5 shows the resulting fractional abundance ratios between S138 and N159. Although individual ratios suffer from relatively large uncertainties, a general underabundance by a factor of 10 is indicated in N159. This factor scales directly with the conversion factor applied to the LMC data and should probably be considered a lower limit.

5. Physical and chemical conditions in N159

Optical and IR tracers suggest that the N159 cloud is associated with the formation of massive stars. This is supported by the relatively high HCN/HNC ratio, 3.0, observed in N159; Galactic observations indicate ratios close to unity for dark clouds while OB star forming regions generally show considerably higher ratios (se e.g. Goldsmith et al. 1981; Goldsmith and Irvine 1986).

Observations of the [CII] fine structure emission at 158 μm toward the 30 Doradus nebula provide strong indications that the physical state of the interstellar gas in the LMC is rather different from that in the Galaxy (Stacey et al. 1991): the [CII]/CO(1-0) emission ratio is a factor of 5 higher than the best fit to starburst galaxies and Galactic OB star forming regions, suggesting more extended photon-dominated regions in the LMC than in the Galaxy. The comparatively strong and extended HCO^+ emission in the LMC may be a manifestation of this.

Galactic cloud models modified to represent some of the expected conditions in the Magellanic Clouds (Millar and Herbst 1990) predict significantly higher fractional abundances than those derived from our observations. However, when the comparison is based on models that incorporate the depth-dependent effects of photon-dominated chemistry (Bel, Viala and Guidi 1986), the agreement is qualitatively better. Thus, models including photon-dominated chemistry are probably needed to explain the observed molecular abundances.

Acknowledgements

I would like to express my thanks to my collaborators in this project: J.H. Black, R. Gredel, Å. Hjalmarson and H. Olofsson.

References

Bel N., Viala Y.P., Guidi I., 1986, A&A, 160, 301

Cohen R.S., Dame T.M., Garay G., Montani J., Rubio M., Thaddeus P., 1988, ApJ 331, L95

Dufour R.J., 1984, in: van den Bergh S., de Boer K.S. (eds.) Proc. IAU Symp. 108, Structure and Evolution of the Magellanic Clouds, Riedel, Dordrecht, p.353

Elmegreen B.G., Elmegreen D.M., Morris M., 1980, ApJ 240, 455

Frerking M.A., Wilson R.W., Linke R.A., 1980, ApJ 240, 65

Garay G., Rubio M., Ramirez S., Johansson L.E.B., Thaddeus P., 1993, A&A 274, 743

Goldsmith P.F., Irvine W.M., 1986, ApJ 310, 383

Goldsmith P.F., Langer W.D., Ellder J., Irvine W.M., Kollberg E., 1981, ApJ 249, 524

Henkel C., Mauersberger R., 1993, A&A 274, 730

Israel F.P., de Graauw Th., 1991, in: Haynes R., Milne D. (eds.) Proc IAU Symp. 148, The Magellanic Clouds, Kluwer, Dordrecht, p. 45

Israel F.P., Johansson L.E.B., Lequeux J., Booth R.S., Nyman L.-Å., Crane P., Rubio M., de Graauw Th., Kutner M.L., Gredel R., Boulanger F., Garay G., Westerlund B., 1993, A&A 276, 25

Johansson L.E.B., 1991, in: Combes F., Casoli F. (eds.) Proc. IAU Symp. 146, Dynamics of Galaxies and Their Molecular Cloud Distributions, Kluwer, Dordrecht, p. 1

Johansson L.E.B., Olofsson H., Hjalmarson Å., Gredel R., Black J.H., 1993, A&A, submitted

Kahane C., Gomez-Gonzalaz J., Cernicharo J., Guelin M., 1988, A&A 190, 167

Koornneef J., 1984, in: van den Bergh S., de Boer K.S. (eds.) Proc. IAU Symp. 108, Structure and Evolution of the Magellanic Clouds, Riedel, Dordrecht, p.333

Langer W.D., Graedel T.E., 1989, ApJS 69, 241

Langer W.D., Penzias A.A., 1990, ApJ 357, 477

Langer W.D., Penzias A.A., 1993, ApJ 408, 539

Martin N., Maurice E., Lequeux J., 1989, A&A 215, 219

Millar T.J., Herbst E., 1990, MNRAS 242, 92

Rubio M., Garay G., Montani J., Thaddeus P., 1991, ApJ 368, 173

Rubio M., Lequeux J., Boulanger F., 1993, A&A 271, 9

Rubio M., Lequeux J., Boulanger F., Booth R.S., Garay G., de Graauw Th., Israel F.P., Johansson L.E.B., Kutner M.L., Nyman L.-Å., 1993, A&A 271, 1

Sage L.J., Mauersberger R., Henkel C., 1991, A&A 249, 31

Stacey G.J., Geis N., Genzel R., Lugten J.B., Poglitsch A., Sternberg A., Townes C.H., 1991, ApJ 373, 423

Strong A.W., Bloemen J.B.G.M., Dame T.M., Grenier I.A., Hermsen W., Lebrun F., Nyman L.-Å., Pollock A.M.T, Thaddeus P., 1988, A&A 207 ,1

Wannier P.G., 1980, ARA&A 18, 399

Wilson T.L., Matteucci F., 1992, A&AR 4, 1

Magnetic Fields in Molecular Clouds

R. M. Crutcher

Department of Astronomy, University of Illinois, Urbana, IL 61801 USA

Introduction

This paper is a brief review of our knowledge of magnetic fields in molecular clouds, primarily from the observational point of view. In the following five sections I discuss (1) why magnetic fields are important, (2) methods of observation, (3) observational results, (4) a case study, and (5) conclusions and possible future work.

Why are magnetic fields important?

Understanding the physics governing the structure and evolution of dense interstellar clouds is a necessary step toward understanding the fundamental astrophysical process of star formation. The importance of magnetic fields has become increasingly evident over the past decade. If typical ($M \sim 10^{3-4} M_\odot$) molecular clouds were in free-fall collapse, their lifetimes would be unrealistically short and the implied star formation rate could be much higher than observed (e.g., Zuckerman & Palmer 1974; Mouschovias 1976). For uniform spherical clouds the free-fall time scale $\tau_{ff} = (3\pi/32G\rho)^{1/2} \approx 1 \times 10^6 (n/10^3)^{-1/2}$ yr, much shorter than is consistent with observations. Moreover, free-fall velocities are not observed. Rotational support is ruled out by mapping of velocity fields in clouds. It has long been clear that thermal pressure forces alone cannot support dense, massive clouds against their self-gravity, since the Bonnor-Ebert (Jeans) critical mass is so small, $M_{BE} \approx 6(T/10)^{3/2}(10^3/n)^{1/2} M_\odot$. Supersonic hydrodynamical turbulence could in principle support larger masses, but the turbulent energy would dissipate too quickly. The time scale for the dissipation of turbulence is $\tau_{dis} \approx E/(dE/dt)$, and the rate (per unit mass) of energy dissipation of purely hydrodynamical turbulent energy is $dE/dt \approx \sigma^3/\ell$, where σ is the velocity and ℓ the length scale of the turbulence (Fleck 1981). For the dissipation of the *entire* gravitational potential energy $E = 3GM^2/5R$ of a uniform, spherical cloud, $\tau_{dis}/\tau_{ff} \approx 6(\ell/R)$. Since the turbulent length scale $\ell < R$, turbulence would dissipate on a time comparable to the free-fall time scale. Clouds that have formed stars may have additional energy sources from the new stars. But how this energy could be transformed into turbulence is unknown, and in any case this does not solve the problem for pre-star formation clouds.

Magnetic fields therefore appear to be a necessary component of the physics of dense clouds and star formation. The pressure provided by fairly weak, static magnetic fields can be sufficient to provide effective support against gravity (Mouschovias & Spitzer 1976). OH Zeeman-effect observations have detected magnetic fields of the requisite strengths (Crutcher 1988; Troland 1990; Crutcher et al. 1993). Moreover, magnetohydrodynamical (MHD) waves at sub-Alfvénic but supersonic speeds can persist an order of magnitude longer than purely hydrodynamical turbulence, providing additional support both parallel and perpendicular to the field direction. MHD waves could also explain the observed supersonic (but sub-Alfvénic) line widths generally observed in molecular clouds. Myers & Goodman (1988) have discussed the assumption that the non-thermal part of line widths could be related to MHD motions.

Fiedler & Mouschovias (1993) have given a recent discussion of theoretical modelling of the evolution of magnetically supported dense clouds, and include detailed references to earlier work. The crucial parameter governing the state of magnetically supported clouds is the ratio of the magnetic flux to the mass, Φ_B/M. A cloud might initially have a magnetically subcritical Φ_B/M and therefore be supported throughout by a static magnetic field. The evolution of a cloud in magnetohydrostatic equilibrium may be driven entirely by internal physical processes, without a requirement for external triggers of star formation processes. The magnetic field is frozen into only the ionized component of the gas; therefore, the neutral gas undergoes gravitational contraction through the ionized gas component, with the neutrals supported against free-fall collapse by collisions with the ions. The time scale for this ambipolar diffusion process is $\tau_{ad} \approx \tau_{ff}^2/\tau_{ni}$, where τ_{ni} is the neutral-ion collision time. Because of the density dependence, τ_{ad} is typically 3-4 orders of magnitude smaller in dense cores than in envelopes and exceeds τ_{ff} by at least a factor of 10 everywhere in clouds. The strength

of the magnetic field increases by typically only a factor of two in the envelope region, which remains magnetically subcritical. Ambipolar diffusion lowers Φ_B/M in the core as the mass in the core increases. The core eventually becomes magnetically supercritical and collapses, with the strength of the core magnetic field increasing approximately as $\rho^{1/2}$. Magnetically supported clouds therefore evolve on the ambipolar diffusion time scale (typically one to two orders of magnitude longer than the free-fall time scale). Finally, the magnetic field is called upon to play another crucial role in the star formation process—the transport of angular momentum from the forming protostar to the surrounding molecular cloud envelope.

It is essential for our understanding of the physics of dense clouds and of the star formation process to observe magnetic fields in molecular clouds and to test theoretical results and models of magnetically supported clouds.

Methods of Observation

The important parameter to be determined from observations is Φ_B/M, which is proportional to the observable ratio $\mid \mathbf{B} \mid$/N(H). All methods of studying magnetic fields in molecular clouds (or elsewhere in the interstellar medium) involve the detection of polarized radiation emitted from or passing through these regions. Practical observations of magnetic fields in molecular clouds are of two types which are quite different yet complementary. One type of observation involves the detection of linear polarization at optical, infrared, or millimeter wavelengths; the other type involves detection at radio wavelengths of the Zeeman effect in spectral lines. (Because of the very low electron densities in molecular clouds, Faraday rotation will be dominated by the general interstellar medium and is not useful for molecular clouds.)

Linear polarization at optical, infrared, or millimeter wavelengths arises from elongated grains with the short axes aligned with the magnetic field. The grain alignment mechanism is not understood in sufficient detail for the strength of the field to be reliably inferred, but such studies are invaluable in establishing the morphology of the field in molecular clouds. Optical and near infrared linear polarization comes from selective absorption of the radiation from embedded or background stars. Therefore, this technique is limited by the numbers of available stars and by extinction effects, especially at optical wavelengths. Near infrared (K-band) observations circumvent to some extent extinction problems, permitting studies of field direction in denser regions of the clouds. In *absorption* the angle on the sky of maximum extinction is perpendicular to the magnetic field, so the angle of maximum polarization is *parallel* to the field direction. Far infrared and millimeter wavelength linear polarization arises from thermal dust emission. Therefore, this technique samples material throughout dense cores of molecular clouds, and it does not require a grid of embedded or background sources. Since *emission* from grains is being observed, the direction of maximum emission is along the long axis of the grains and therefore *perpendicular* to the field direction.

The other type of observation involves detection at radio wavelengths of the Zeeman effect in spectral lines. Studies of the Zeeman effect in radio frequency spectral lines which originate in molecular clouds provide the only known method to directly measure magnetic field strengths in dense gas. If the region where a spectral line is formed is permeated by a field $\mathbf{B}$, the radiation is split into three separate frequencies, $\nu_0 + \nu_z$, ν_0, $\nu_0 - \nu_z$, where $\nu_z = \mid \mathbf{B} \mid Z$. The Zeeman factor Z (in Hz/μG) is 2.80 for the 1420 MHz line of H I, and it is 3.27 and 1.96 for the 1665 and 1667 MHz lines of OH, respectively. Other paramagnetic molecules such as CN, CCS, and SO (but unfortunately not CO) have values of Z approximately equal to those for H I and OH. If $\mid \mathbf{B} \mid$ is sufficiently large, the three Zeeman lines may be observed as distinct components and the magnetic field strength derived directly. Measurement of the Stokes parameters V, Q, and U for the three Zeeman components would in principle allow the orientation of the field on the sky and with respect to the line of sight to be inferred. Unfortunately, distinct separation of the Zeeman components is the case only for OH maser lines. For ν_z much less than the line width $\Delta\nu$, full information about the magnetic field cannot be obtained. As discussed by Crutcher et al. (1993), measurement of Stokes parameter V spectra gives the sign (direction) and magnitude of the field component $B_{||}$ parallel to the line of sight; $V = [dI/d\nu]\nu_z \cos\theta$, where θ is the angle between the line of sight and the magnetic field. By fitting the frequency derivative of the Stokes parameter I spectra ($dI/d\nu$) to the V spectra, $B_{||} = \nu_z \cos\theta/Z$ may be inferred. Where sensitivity considerations permit, Zeeman effect observations at adjacent positions in a cloud (either by single-antenna mapping or synthesis mapping) reveal aspects of the morphology of the

field. In principle, even when $\nu_z \ll \Delta\nu$, the Zeeman effect can provide information about the magnitude and position angle of the magnetic field in the plane of the sky. Unfortunately, for $\nu_z \ll \Delta\nu$, Q or U $\propto [d^2I/d\nu^2][\nu_z \sin\theta]^2$; since the frequency splitting ν_z is small, the squared dependence means that the resulting linearly polarized line radiation is typically an order of magnitude smaller than the circularly polarized signal, and therefore undetectable (Crutcher et al. 1993). Hence, for practical purposes, the Zeeman effect yields only $B_{||}$ when $\nu_z \ll \Delta\nu$. For a random orientation of θ among a large number of clouds, statistically one would expect that on average $B_{||} = | \mathbf{B} | /2$.

Observational Results

Examples of relevant optical polarization studies include those of the Taurus region by Moneti et al. (1984), Hsu (1984), and Heyer et al. (1987), and the survey work of Goodman et al. (1990). These studies, limited by extinction to the peripheries of the molecular clouds, generally reveal the presence of a well ordered field component. However, as Scalo (1990) notes, there are a number of stars whose polarization angle deviates significantly from the mean direction, and there may be no correlation between fine details in the cloud structure and orientation of the optical polarization. It is difficult to understand how magnetic fields can dominate the support of clouds if there is no correlation between cloud morphology and field orientation, but the optical data do not sample interior regions of clouds. Tamura et al. (1987), Sato et al. (1988), and Goodman et al. (1992) have carried out K-band polarization observations of stars behind dark clouds in Taurus and/or Ophiuchus. Fields in these clouds appear to be very uniform and aligned with the field direction in the surrounding medium. Goodman et al. (1992) stressed that the dark clouds seem to have no effect on the projected direction of the magnetic field, and suggested that it is possible that near-infrared polarization may be insensitive to the field direction in the denser interiors of dark clouds, due to a drop in polarization efficiency. If so, then even the near-infrared data may tell us little about magnetic fields in dense molecular clouds.

However, the situation for far infrared and millimeter wavelength polarized emission studies is more favorable. Hildebrand (1988) has reviewed earlier observations of far-infrared polarization, and additional results are beginning to become available (Morris et al. 1992; Hildebrand 1993). Novak et al. (1990) and Leach et al. (1991) report recent observations of millimeter wavelength polarization in the Orion BN/KL region. These studies suggest that fields in dense molecular cores are quite uniform. The far infrared and millimeter-wave polarization techniques have great promise for mapping the morphology of the $B_\perp$ component of magnetic fields in dense clouds. However, like other linear polarization studies at shorter wavelengths, these results provide at best only an order of magnitude indication of field strengths.

Zeeman splitting in maser lines of OH (Lo et al. 1975, Reid et al. 1980, Norris 1984, Baart et al. 1986, Gaume & Mutel 1988) has been observed; a typical result is $| \mathbf{B} | \sim$ a few mG. Because the Zeeman splitting $\nu_z \geq \Delta\nu$, the OH masers give the full field strength $| \mathbf{B} |$ rather than just the line-of-sight component $B_{||}$. Also, because OH masers require densities $\sim 10^{7-8}$ cm^{-3}, the OH masers allow us to explore magnetic field strengths at quite high densities. Observations have also been made of the Zeeman effect in H_2O masers (Fiebig & Güsten 1989). Unfortunately, H_2O is a non- paramagnetic molecule, so the Zeeman splitting factor Z is reduced from characteristic values for H I and OH by the ratio of the nuclear magneton to the Bohr magneton; hence, the H_2O Zeeman results are about three orders of magnitude less sensitive. However, since the production of H_2O maser lines requires densities $\sim 10^{9-10}$ cm^{-3}, detection of Stokes V signals allows measurement of $B_{||}$ at extremely high densities. Fiebig & Güsten (1989) reported $B_{||}$ values up to about 50 mG. Nedoluha & Watson (1992) have considered in detail effects in the radiative transfer of maser radiation which can affect the interpretation. They concluded that the straightforward interpretation of the V spectra would typically lead to $B_{||}$ values about 50% higher than the real values. Although caution is necessary, their detailed treatment generally supports the interpretation that magnetic field strengths are $\sim$ 10s of mG at the very high densities probed by H_2O masers. The maser results support the theoretical prediction that $| \mathbf{B} | \propto \rho^{1/2}$ in supercritical regions.

The first detection of the Zeeman effect in a spatially distributed molecular species was in the 18-cm lines of OH seen in absorption against the background radio continuum sources Orion B (NGC2024) and W22 (Crutcher & Kazès 1983). Almost all subsequent measurements of magnetic field strengths in molecular lines have utilized this same technique—detection of

the Zeeman effect in OH absorption lines. Exceptions are the detections in weak OH emission lines toward B1 (Goodman et al. 1989) and possibly toward the ρ Ophiuchi cloud (Crutcher et al. 1993). Even though it has been a decade since the first detection, today there are only *eleven* clouds for which the OH Zeeman effect has been detected!

Crutcher (1988) listed all of the single-antenna results available five years ago; see that review for detailed references. Unfortunately, the B1 detection has been the only addition to the list since that time. Crutcher divided the results into clouds physically associated with H II regions and those without massive star formation. A justification for this division is that massive star formation may take place preferentially in clouds that initially had a critical Φ_B/M ratio. All available results for clouds associated with H II regions, with $B_{||} \pm 1\sigma$ (μG) in parentheses following the source name, are: S106 (+137±17), Orion A (−125±20), W3 (+73±7), S88B (+69±5), Orion B (+38±1), and W40 (−14±3). The average of the magnitude (ignoring the direction sign) of these results is $B_{||} \approx 75$ μG. If we make the entirely unsupported assumption that $\mid \mathbf{B} \mid$ is a constant among these clouds (and that therefore the range in $B_{||}$ is due entirely to random θ from cloud to cloud), $\mid \mathbf{B} \mid \approx 150$ μG. Unfortunately, sufficient data are not available for these clouds to estimate $\mid \mathbf{B} \mid / N(H_2)$ and hence Φ_B/M.

The dark clouds (for our purposes defined as molecular clouds not associated with H II regions) with OH Zeeman detections are: the 6 km/s component toward W22 (−18±1), Cas A (+9±2), the Sagittarius-arm clouds toward W49B (+21±5), ρ Oph (+10±3), and B1 (−27±4, −19±4 with 3′ and 18′ telescope beams, respectively). Crutcher et al. (1993) also reported ten additional very sensitive (typical $\sigma_B \approx 3$ μG) OH Zeeman measurements that did not yield detections. A statistical analysis of the detection and upper limit data was carried out with the assumption that $\mid \mathbf{B} \mid / N(OH)$ was constant. This analysis indicated that $\mid \mathbf{B} \mid \approx 16$ μG toward the central regions of dark clouds sampled by the 18′ telescope beam (for which $A_V \approx 5$ magnitudes and $n(H_2) \sim 10^3$ cm^{-3}), and that the dark cloud regions were approximately magnetically critical. However, the large telescope beam sampled mainly envelope regions rather than cores. The data were found to be consistent with the hypotheses that (1) dark clouds are in approximate virial equilibrium between magnetic and gravitational energy, and (2) the supersonic line widths observed in dark clouds are consistent with MHD motions at sub-Alfvénic speeds.

It is possible to map the spatial structure of magnetic fields in molecular clouds with radio aperture-synthesis arrays, such as the VLA. Almost all of the work to date has used the 21-cm line of H I, which in general does not sample the dense molecular gas. One probable exception was the study of the core of the W3 cloud (Roberts et al. 1993). Van der Werf & Goss (1990) analyzed WSRT maps and concluded that the −38 km/s component in H I is photodissociated molecular gas surrounding the compact H II regions. Zeeman observations of this H I component may therefore measure the magnetic field in the dense molecular gas. Roberts et al. (1993) found that $B_{||}$ varied across the compact H II regions A and B from −120 μG in the northeast to +220 μG in the southwest, with a locus of $B_{||} = 0$ from southeast to northwest passing through the infrared point source IRS5. They modelled the three-dimensional magnetic field morphology as an hourglass shape (such as would occur in the contraction of a cloud with a frozen-in magnetic field) and concluded that $\mid \mathbf{B} \mid \approx 1$ mG, which would imply that Φ_B/M was approximately critical.

A Case Study

Available observational data on the mass, density, temperature, and magnetic field for the molecular cloud B1 are sufficiently complete that it has been possible to compute a detailed theoretical model specifically for this cloud (Crutcher et al. 1994). The model used fully implicit, multifluid, adaptive-grid codes that reliably followed both the early, quasistatic, ambipolar diffusion controlled phase of core formation as well as the later, dynamic contraction phase of thermally and magnetically supercritical cores (Ciolek & Mouschovias 1994). Crucial input parameters from the observations included only the observed parameters of the cloud envelope [$M \approx 600$ $M_\odot$ within $r = 2.9$ pc (Bachiller et al. 1990) with a mean magnetic field (from OH Zeeman observations) along the line of sight of $B_{||} = 16$ μG (Crutcher et al. 1993)]. The calculations first showed that these parameters could be represented very well by a model in exact magnetohydrostatic equilibrium. The evolutionary calculation then followed the ambipolar-diffusion induced formation and collapse of a supercritical protostellar core.

The central density increased from an initial value of $\sim 10^4$ cm^{-3} successively by an order of magnitude in times 13.48, 14.69, 14.83, 14.85, 14.857, and 14.858 million years. Hence, the cloud changed extremely slowly for $\tau > 10^7$ yr, with a rapid evolution of the core to a central density $\sim 10^{10}$ cm^{-3} at the end of the model computations. The exponent S of the magnetically supported cloud model in a $\rho \propto r^S$ power law description is quite different from that of an isothermal sphere, for which S=–2 (see discussion in Shu 1992); for a free-falling inside-out collapsing core, the expectation is S=–1.5. Instead, the model core had a flat density profile (S=0), although of course the radius of this core became very small as the density exceeded $\sim 10^6$ cm^{-3}. Just outside the critical core, S $\approx$ –2.5 for the evolved B1 model; this steepness was due to the collapsing core draining matter from the region just outside the core, while the envelope remained subcritical and largely unchanged. Crutcher et al. (1994) compared the calculated spatial profiles of the volume density, column density, and magnetic field strength (hence Alfvén speed, related directly to line widths) with existing observations and found excellent agreement. Hence, this first case study supported magnetic models of molecular clouds.

Conclusions and Future Work

Our conclusion is that magnetic fields are a crucial element in the physics governing the structure and evolution of molecular clouds and hence in the star formation process. The regrettably very sparse set of observations of magnetic field directions and strengths in dense clouds is consistent with theoretical models of the structure and evolution of magnetically supported clouds. Moreover, the models provide explanations for aspects of the physics of dense clouds that otherwise seem inexplicable—the agent providing support against gravitational collapse, the observed supersonic line widths, and the low angular momentum of cloud cores and of stars.

The most important factor which today limits our understanding of the evolution of clouds is the sparseness of the observations of magnetic fields in dense clouds. Future work to bring our knowledge of magnetic field strengths and morphologies in dense clouds up to the state of our knowledge of kinematics, temperature, and density structures is extremely important. What is needed are maps from Zeeman observations of the line-of-sight field strengths at a wide range of densities and spatial scales together with maps of the field directions on the plane of the sky from linear polarization observations at far-infrared and millimeter wavelengths. Although such maps will still not completely describe the magnetic field strengths and morphologies, they are the best that we can hope to achieve at this time. Together with maps of molecular lines to define density and temperature structure and the kinematics of dense clouds, the magnetic field maps can be compared in detail with theoretical models of the structure of clouds at various evolutionary states. Perhaps one day we will be at a stage similar to that for stellar structure and evolution—comparing HR diagram equivalents with relevant observations of molecular clouds!

Acknowledgement—This work has been supported by the National Science Foundation under grant AST91-16917.

References

Baart, E.E., Cohen, R.J., Davis, R.D., Norris, R.P., Rowland, P.R. 1986, MNRAS, 219, 145
Bachiller, R., Menten, K.M., del Rio-Alvarez, S. 1990, A&A, 236, 461
Ciolek, G.E., Mouschovias, T.Ch. 1994, to be published in ApJ
Crutcher, R.M., Kazès, I. 1983, A&A, 125, L23
Crutcher, R.M. 1988, in 'Molecular Clouds in the Milky Way and External Galaxies', p. 105
Crutcher, R.M., Troland, T.H., Goodman, A.A., Heiles, C., Kazès, I., Myers, P.C. 1993, ApJ, 407, 175
Crutcher, R.M., Mouschovias, T.Ch., Troland, T.H., Ciolek, G.E. 1994, to appear in June 1 ApJ
Fiebig, D, Güsten, R. 1989, A&A, 214, 333
Fiedler, R.A., Mouschovias, T.Ch. 1993, ApJ, 415, 680
Fleck, R.C. 1981, ApJ, 246, L151
Gaume, R.A., Mutel, R.L. 1987, ApJ Suppl, 65, 193
Goodman, A.A., Crutcher, R.M., Heiles, C., Myers, P.C., Troland, T.H. 1989, ApJ, 338, L61
Goodman, A.A., Bastien, P., Myers, P.C., Menard, F. 1990, ApJ, 359, 363
Goodman, A.A., Jones, T.J., Lada, E.A., Myers, P.C 1992, ApJ, 399, 108
Heyer, M.H., Vrba, F.J., Snell, R.L., Schloeb, F.P., Strom, S.E., Goldsmith, P.F., Strom, K.M. 1987, ApJ, 321, 855

Hildebrand, R.H. 1988, QJRAS, 29, 327
Hildebrand, R.H. 1993, private communication
Hsu, J.-C. 1984, University of Texas at Austin PhD thesis
Leach, R.W., Clemens, D.P., Kane, B.D., Barvainis, R. 1991, ApJ, 370, 257
Lo, K.Y., Walker, R.C., Burke, B.F., Moran, J.M., Johnston, K.J., Ewing, M.S. 1975, ApJ, 202, 650
Moneti, A., Pipher, J.L., Helfer, H.L., McMillan, R.S., Perry, M.L. 1984, ApJ, 282, 508
Morris, M., Davidson, J.A., Werner, M., Dotson, J., Figer, D.F., Hildebrand, R., Novak, G., Platt, S. 1992, ApJ, 399, L63
Mouschovias, T.Ch. 1976, ApJ, 206, 753
Mouschovias, T.Ch., Spitzer, L.H. 1976, ApJ, 210, 326
Myers, P.C., Goodman, A.A. 1988, ApJ, 329, 392
Nedoluha, G.E., Watson, W.D. 1992, ApJ, 384, 185
Norris, R.P. 1984, MNRAS, 207, 127
Novak, G., Predmore, C.R., Goldsmith, P.F. 1990, ApJ, 355, 166
Reid, M.J., Haschick, A.D., Burke, B.F., Moran, J.M., Johnston, K.J., Swenson, G.W. 1980, ApJ, 239, 89
Roberts, D.A., Crutcher, R.M., Troland, T.H., Goss, W.M. 1993, ApJ, 412, 675
Sato, S., Tamura, M., Nagata, T., Kaifu, N., Hough, J., McLean, I.S., Garden, R.P., Galey, I. 1988, MNRAS, 230, 321
Scalo, J.M. 1990, in 'Physical Processes in Fragmentation and Star Formation', p. 151
Shu, F.H. 1992, 'The Physics of Astrophysics, Vol. II, Gas Dynamics', p. 244-246
Tamura, M., Nagata, T., Sato, S., Tanaka, M. 1987, MNRAS, 224, 413
Troland, T.H. 1990, in 'Galactic and Extragalactic Magnetic Fields', p. 293
Van der Werf, P.P., Goss, W.M. 1990, A&A, 238, 296
Zuckerman, B., Palmer, P. 1974, ARA&A, 12, 279

Mapping Magnetic Fields in the ISM: Infrared and Sub-mm Polarimetry

Alyssa A. Goodman
Harvard-Smithsonian Center for Astrophysics

ABSTRACT: This paper outlines why mapping the magnetic field in the interstellar medium is useful, why established techniques for mapping the field (e.g. polarimetry of background starlight) fail in dense clouds, and why new techniques that exploit the polarized emission from grains should succeed.

Why should we care about magnetic fields in the ISM?

Magnetic fields possess the ability to modify the dynamics of gas. Even if a gas is only very lightly ionized (as is much of the dense ISM), collisions between ions and neutrals will enable the gas to feel the effect of the magnetic field to some degree. Recent measurements of the strength of the magnetic field in the ISM show it to have energy approximately equal to the gas kinetic energy inferred from observed spectral line widths, over a range of densities from ~10^0 to 10^9 cm^{-3} (see Heiles *et al.* 1993 for a review). In regions where the (self-)gravitational energy is similar to the kinetic energy the magnetic energy is then also of order the gravitational energy, and thus is significant in cloud support (Myers and Goodman 1988).

These facts support a picture where the magnetic energy in the ISM is in some sense analogous to thermal energy in an unmagnetized, neutral gas. In other words, the speed of dynamic disturbances is limited by the Alfvén speed instead of the sound speed, and the support of clouds against their own gravity is magnetic in origin, rather than thermal. The analogy is not perfect though: magnetic support is potentially less isotropic than thermal support, because a magnetic field will not directly affect the motion of gas moving along it. However, wave-like disturbances in an otherwise straight field *can* provide support in the direction parallel to the "straight" field, and a very tangled field, perhaps containing many wave modes, can provide almost isotropic support in three dimensions. So, in order to understand the mechanism(s) by which fields interact with gas in the ISM, we must quantify the structure of the magnetic field.

What's wrong with polarimetry of background starlight?

Since Davis and Greenstein (1951) first interpreted the polarization of background starlight as due to magnetically aligned dust grains in the ISM, polarimetry of background starlight has been used as a technique to map out field structure. Recently, however, it has become apparent that this technique may not be useful in measuring fields in the denser portions of the ISM. This inadequacy has come to light in attempts to use near infrared background starlight polarimetry to map out magnetic field structure in nearby "dark clouds," where the gas density is $>10^3$ cm^{-3}. It is normally assumed that most of the dust grains along the line of sight to a star behind a dark cloud are associated with the cloud, which implies that most of the polarization observed is produced *in* the dark cloud, and would trace out the field geometry associated with the cloud. However, several studies (e.g. Vrba *et al.* 1976; Wilking *et al.* 1979; Tamura *et al.* 1987, 1988; Goodman *et al.* 1992, 1994) of polarization of background starlight in dark clouds have shown: (1) no change in either the polarization *direction* or the *dispersion* of polarization directions associated (in projection)

with the cloud; and (2) no, or very little, increase in percentage polarization as a function of extinction. The data suggest that a dark cloud along the line of sight to a background star often has no effect on the polarization observed, and in turn that polarimetry of background starlight cannot reveal the field structure in dark clouds (Goodman *et al.* 1994).

In order to understand why the absence of an increase in percentage polarization with extinction means that background star polarimetry cannot reveal the field in dark clouds, consider the following. If all dust grains along a line of sight are similar, and are equally well-aligned by magnetic fields, then only the magnetic field geometry will modify the percentage of polarization observed for a given value of extinction. If the magnetic field were perfectly straight and constant along a line of sight, we would observe a polarization $p = \zeta_{max} A_V$, where A_V represents visual extinction and ζ_{max} is a constant representing the maximum possible "polarization efficiency." On a log-log plot of p vs. A_V similar to the one below, this relation would have slope unity. If the field bends, or becomes tangled, then $p < \zeta_{max} A_V$, but polarization will still increase as a function of extinction if all grains are equally well-aligned. Jones and collaborators (Jones 1989; Jones *et al.* 1992) have used random-walk style arguments to show that even in the case where the field is completely tangled, polarization will still increase as extinction increases, *as long as each grain contributes equally.* In what is likely to be a realistic situation, where magnetic energy is divided equally between a non-uniform field and a straight field, p should increase with A_V in the manner illustrated by the solid line in the figure below.

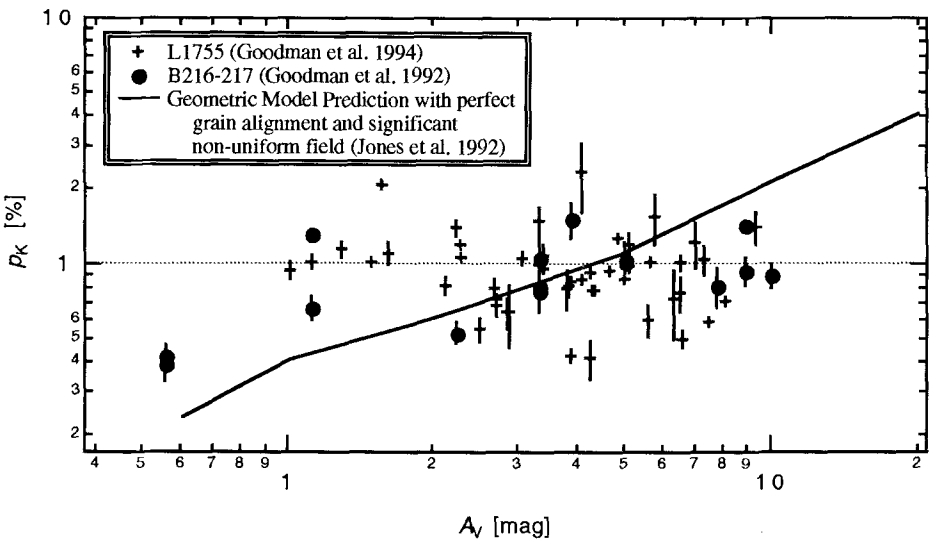

The data points in the figure above show the measured dependence of K-band polarization on extinction for the dark clouds B216-217 in Taurus and L1755 in Ophiuchus. A fit to these points gives $p_K \propto A_V^0$. In other words, polarization is observed to be independent of extinction over the range of extinctions ($0.5 < A_V < 10$ mag) associated with the dark clouds, and *the dust in the dark clouds*, which is responsible for virtually all of the extinction at $A_V > 1$ mag, is *having no perceptible effect on the observed polarization.*

Polarization maps almost never show any change in polarization direction or dispersion associated with dark clouds, and the p vs. A_V relation is flat in dark clouds. Both of these

observations can be explained if the polarization efficiency in dense clouds is greatly diminished in comparison with its value(s) in the lower density ISM. Either inefficient grain alignment or changes in grain shape, or both, can cause such variation in polarization efficiency. Dark clouds contain cold gas and dust, are very predominantly molecular, and are ideal sites for growing "big" (fat, round) grains. These properties can cause poor grain alignment, and low polarization efficiency, even if grains are aligned. The data clearly suggest that most of the polarization of background starlight observed along lines of sight through dark clouds is produced in the low density ISM between the background star and the cloud and between the cloud and the observer, and *not* in the dark cloud. The observed polarization of background starlight is weighted by the changing polarization efficiency along the line of sight. Thus, we cannot use polarimetry of background starlight to reliably trace out the field in the dense ISM.

What do we do instead?

Background starlight polarimetry relies on the concept that aligned grains extinguish light from a background star along one axis (the long axis of the grain) more than any other. The trick to measuring the magnetic field structure in the dense ISM is to forget about background stars, whose light can be polarized by dust anywhere along the long line of sight to the star. The trick is to appreciate that aligned grains *emit* polarized blackbody radiation, and that one can pick out a particular distribution of grains along the line-of-sight by observing blackbody emission at particular wavelength. As illustrated by the figure below, only grains at temperatures near that which gives a blackbody spectrum peak at the wavelength being observed will contribute significantly to measurements of the polarized *emission* from dust. Thus, even if the polarization efficiency in the dense ISM is very low, by selecting only grains associated with a particular cloud (temperature), one can probe the field structure *in that cloud.*

The figure at right shows blackbody curves for dust at temperatures between 10 and 100 K, representative of most of the neutral ISM. From the figure, it is apparent that polarized emission from dust at these temperatures is most easily observable at wavelengths between 1 mm and 10 μm. (Also noted are some representative present and future instruments capable of observing polarization at these wavelengths. Instruments not shown in the figure that will be useful in observing the polarized thermal emission from dust include the new SCUBA array for the JCMT, similar instrumentation on the CSO, and the BIMA and OVRO interferometers.)

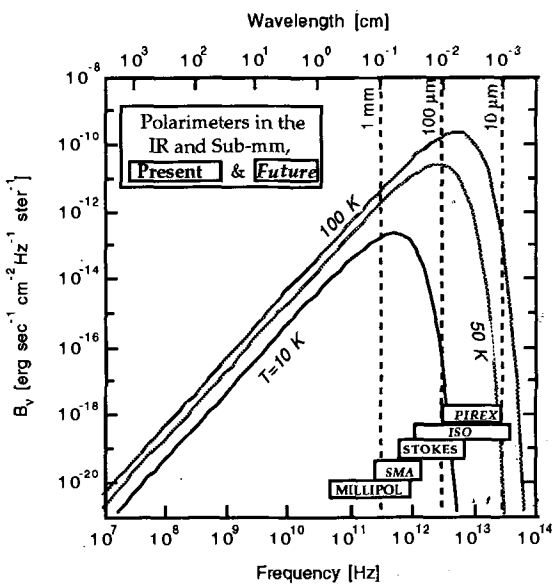

At present, the polarization of thermal emission from dust has only been observed in a handful of regions, where the dust emission is very strong at far-IR and sub-mm wavelengths. These measurements are not easily obtained, due to the opacity of the Earth's atmosphere at far-IR and sub-mm wavelengths and the low level of polarization (a few %) produced by grain alignment. What is needed now are more, high-resolution, sensitive maps of the polarization of dust emission, and a geometric model of the field with which to interpret the maps. The group led by Roger Hildebrand, at the University of Chicago, is using their multi-element far-IR polarimeter, known as STOKES, on the Kuiper Airborne Observatory to map out the field in a number of dense clouds, including the Orion Core, Sgr B2, W3, W51, and M17SW.

The M17SW measurements (Dotson 1994) are most intriguing, since polarimetry of background starlight has been measured in the same region at red optical wavelengths (Schulz *et al.* 1981) and at near-IR wavelengths (Goodman *et al.* 1994). The optical and near-IR data show a very messy, perhaps bimodal distribution of polarization position angle and are similar to each other. In stark contrast, the far-IR measurements made with STOKES show a very smooth structure in the polarization map, which is completely uncorrelated with the optical and near-IR data. In addition, the p vs. A_V relation derived from the near-IR data is as "flat" as that shown above for the cold dark clouds B216-217 and L1755. The interpretation is clear: the far-IR data is giving us information about the field associated with the dust producing the emission *in* M17SW, and the optical and near-IR data are only telling us about other regions along the line-of-sight.

Questions for the future are many. Just what dust in the ISM *is* producing the polarization of background starlight? What does this mean about the field structure inferred from maps of the polarization of background starlight? Does emission polarimetry see "all the way in" to a cloud, or is there still significant weighting by polarization efficiency? Can we untangle dust emission polarimetry maps to infer a unique field structure in three dimensions? Both an abundance of new data, much of which will need to be obtained outside the Earth's atmosphere, and new theories of field structure will be needed to sort out the answers to these questions.

References

Davis, L., Jr. and Greenstein, J.L. 1951, *ApJ*, **114**, 206.

Dotson, J. 1994, Ph. D. Thesis, University of Chicago, in preparation.

Goodman, A.A., Jones, T.J., Lada, E.A., and Myers, P.C. 1992, *Ap. J.*, **399**, 108.

_____ 1994, *Ap. J.*, in prep.

Goodman, A.A., Myers, P.C., and Jones, T.J. 1994, *Ap. J.*, in prep.

Heiles, C., Goodman, A.A., McKee, C.F. and Zweibel, E.G. 1993, in *Protostars and Planets III*, ed. E. Levy and J.I. Lunine, (Tucson: University of Arizona Press), p. 279.

Jones, T.J. 1989, *ApJ*, **346**, 728.

Jones, T.J., Klebe, D. and Dickey, J.M. 1992, *ApJ*, **389**, 602.

Myers, P.C. and Goodman, A.A. 1988, *Ap. J. (Letters)*, **326**, L27.

Schulz, A., Lenzen, R., Schmidt, T., Proetel, K. 1981, *A&A*, **95**, 94.

Vrba, F.J., Strom, S.E. and Strom, K.M. 1976, *AJ*, **81**, 958.

Tamura, M., Nagata, T., Sato, S. and Tanaka, M. 1987, *MNRAS*, **224**, 413.

Tamura, M., Yamashita, T., Sato, S., Nagata, T. and Gatley, I. 1988, *MNRAS*, **231**, 445.

Wilking, B.A., Lebofsky, M.J., Rieke, G.H. and Kemp, J.C. 1979, *AJ*, **84**, 199.

The Formation of Molecular Lines in Turbulent Clouds

W.H. Kegel[1], G. Piehler[1], M.A. Albrecht[2]
[1] Institut für Theoretische Physik der Universität Frankfurt/M.
[2] European Southern Observatory, Garching

1. Introduction

The profiles of most interstellar molecular lines are considerably wider than expected for purely thermal broadening. This indicates that within the clouds there occur large hydrodynamical velocities which, at least partly, are to be expected to be of a stochastic nature. Radiative transfer in such a turbulent medium depends on the ratio of the mean free path of the photons to the correlation length of the velocity field. This ratio varies across the profile of a given spectral line. The importance of the correlations in the velocity field increases with increasing optical depth. Qualitatively this is obvious since τ_ν is a measure for how often a photon is emitted and reabsorbed on the average, before it leaves the cloud.

2. The Generalized Transfer Equation

The classical radiative transfer equation in principle allows to account for any velocity field, if the latter is fully specified. However, if the velocity field is of a stochastic nature, classical theory allows only to treat the two limiting cases of a very small correlation length (microturbulence) and a very large one (macroturbulence). As is well-known, the equivalent width of an optically thick line differs substantially in these two limiting cases. This is a direct indication that it may be very important to account for a finite correlation length.

To deal with this problem Gail et al. (1974a,b, 1975, 1980) derived a generalized transfer equation (see also Traving 1975). For this they assumed that all higher order correlations in the velocity field may be expressed in terms of the two-point correlation function

$$f(\Delta s) = \frac{< v(s)v(s+\Delta s) >}{\sqrt{< v^2(s) >< v^2(s+\Delta s) >}} \tag{1}$$

where s is the spatial coordinate along a given line of sight. This correlation function was assumed to correspond to an exponential

$$f(\Delta s) = exp(- \mid \Delta s \mid /l) \tag{2}$$

while the distribution for the hydrodynamical velocities was assumed to be Gaussian

$$W(v)dv = \frac{1}{\sqrt{2\pi}} exp(-\frac{v^2}{2\sigma^2})\frac{dv}{\sigma} \tag{3}$$

v being the velocity component along the line of sight. With these assumptions the generalized transfer equation for the conditional intensity $q_\nu(s,u)$ reads

$$\frac{\partial q_\nu}{\partial s} = \frac{1}{l}\{-u\frac{\partial q_\nu}{\partial u} + \frac{\partial^2 q_\nu}{\partial u^2}\} - \kappa_\nu(u)[q_\nu - S_\nu] \tag{4}$$

where $u = v/\sigma$ is the normalized velocity,κ_ν the (local) absorption coefficient and S_ν the source function. The expectation value of the intensity I_ν is related to q_ν by

$$< I_\nu >= \int q_\nu(u)W(u)du \tag{5}$$

In order to solve Eq.(4) one has to specify initial conditions at $s = 0$ and boundary conditions at $u = \pm\infty$. Since the line profile vanishes for $u \to \pm\infty$, the proper boundary condition is

$$q_\nu(s,-\infty) = q_\nu(s,\infty) = I_c(\nu,s) \tag{6}$$

I_c being the local continuum intensity.

The absorption coefficient κ_ν and the source function S_ν depend in the usual manner on the occupation numbers of the upper and the lower level of the transition under consideration. Under NLTE conditions, the occupation numbers now depend on the spatial coordinate s as well as on the velocity u. The rate equation for level j reads

$$\sum_{i \neq j} \{n_i(C_{ji} + A_{ji}) - n_j(C_{ij} + A_{ij})\}$$

$$+ \sum_{i \neq j} \{(n_i B_{ji} - n_j B_{ij}) \frac{4\pi}{c} < \Phi(\nu, u) q_\nu(s, u) >\} = 0 \qquad (7)$$

with $\Phi(\nu, u)$ being the normalized profile of the local absorption coefficient, and

$$4\pi < \Phi(\nu, u) q_\nu(s, u) >= \int_0^\infty \int_\Omega \Phi(\nu, u) q_\nu(s, u) d\Omega' d\nu \qquad (8)$$

We note that Eq.(4) does not only describe the influence of correlation effects but also accounts in some approximation for the effects of partial redistribution, since we have assumed complete redistribution only over the profile of the local absorption coefficient which in the present context is given by the thermal line profile, while the broadening caused by the hydrodynamical velocities is described by the diffusion term.

In view of the facts that (4) is a partial differential equation with u as a new independent variable, compared to the classical transfer equation which is an ordinary differential equation, and that the occupation numbers have to be determined as functions of s and u, it is obvious that the numerical effort necessary to solve the radiative transfer problem selfconsistently with the rate equations is substantially larger than in the case that one accounts for the turbulent velocities only in the microturbulent limit.

3. Results for

For two reasons we have up to now performed numerical calculations for CO only. On one side CO is an abundant interstellar molecule. On the other side it has a very simple energy level diagram, and it is therefore sufficient to account for only a relatively low number of energy levels and spectral lines in order to obtain relevant results.

We started our investigation by considering only the simplest geometry, i.e. that of a plane parallel homogeneous slab (Albrecht, Kegel 1987; Kegel et al. 1993). The numerical results obtained in this case show that accounting for a finite correlation length affects

a) *the line shapes.* In particular, the selfabsorption normally occurring at low densities and large optical depths is reduced or even vanishes (depending on the values of l and σ). Thus, the theoretical profiles look more like the observed ones. It should be noted in particular that for large values of l and σ the central intensity of an optically thick line does not correspond to $B_\nu(T_{ex})$.

b) *the equivalent width.* For given occupation numbers these are smaller than in the microturbulent limit. Since the influence of the correlations depends on τ, different lines are affected differently.

c) *the occupation numhers.* These depend under NLTE conditions on the mean intensities which in turn are affected by the correlations.

d) *the intensity ratio of different lines*, since different lines are affected differently due to differences in τ and due to the effects on the occupation numbers. In particular the ratio of corresponding lines of different isotopomeres is changed.

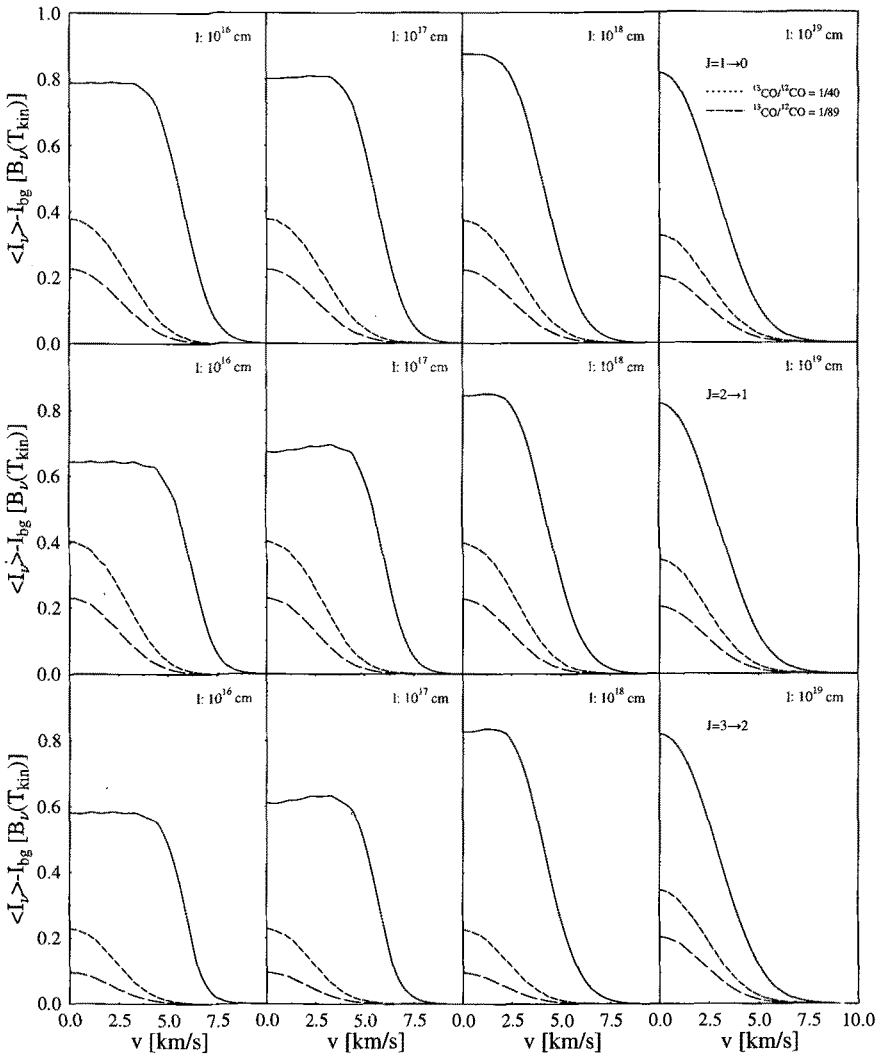

Fig.1 CO line profiles for different correlation length l. The assumed physical model corresponds to a homogenous plane parallel slab with T_{kin}=20 K, n_{H_2}=1000 cm^{-3}, n_{CO}/n_{H_2}=10^{-4}, N_{CO}=2 10^{18} cm^{-2}, σ=2.2 km/s

From these findings it becomes apparent that it is at least as important in a quantitative analysis of molecular line observations to account for a finite correlation length of the tur-

bulent velocity field as to account for NLTE effects. It therefore appears to be desirable to perform similar calculations for more realistic physical models. For this purpose we developed a numerical code for non-homogeneous spherically symmetric models. In a first step we applied this code to isothermal models in hydrostatic equilibrium. First results are given in the poster paper by Piehler and Kegel (1993).

4. Future Prospects

It appears that our numerical methods have now reached a stage that it becomes meaningful to perform extensive calculations the results of which then may be compared in some detail with observations. For this also other molecules than CO will be considered, and we shall, of course, also vary our physical models.

To account for the influence of density fluctuations in addition to that of velocity fluctuations requires to generalize the present theory. In principle this appears to be more or less straight forward. For this one has to introduce the density as an additional independent variable, by which the necessary numerical effort is again increased very much. We intend to attack this problem in the future, but it is clear from the beginning that it will be possible to treat only a very limited number of models.

References

Albrecht, M.A., Kegel, W.H. 1987, A&A, 176, 317
Gail, H.P., Hundt, E., Kegel, W.H., Schmid-Burgk, J., Traving, G. 1974a, A&A, 32, 65
Gail, H.P., Sedlmayr, E. 1974b, A&A, 36, 17
Gail, H.P., Sedlmayr, E., Traving, G. 1975, A&A, 44, 421
Gail, H.P., Sedlmayr, E., Traving, G. 1980, JQRST 23, 267
Kegel, W.H., Piehler, G., Albrecht, M.A. 1993, A&A, 270, 407
Piehler, G., Kegel, W.H. 1993, this conference
Traving, G. 1975, in Prohlems in Stellar Atmospheres and Envelopes, eds. B. Baschek, W.H. Kegel, G. Traving, Springer-Verlag

158 Micron [CII] Imaging of NGC 891

G. J. Stacey[1], N. Geis[2], R. Genzel[3], F. Herrmann[3], M. Hires[4], S.C. Madden[3], A. Polglitsch[3], and C.H. Townes[2]

[1]Department of Astronomy, Cornell University, Ithaca, NY 14853-6801, USA [2]Department of Physics, University of California, Berkeley, CA 94720, USA [3]Max-Planck-Institut fur extraterrestrische Physik, W-8046 Garching, Germany [4]Department of Astronomy, University of Massachusetts, Amherst, MA 01003 USA

To evaluate the effects of star formation activity on the interstellar medium in "starburst" galaxies, it is important to compare and contrast the ISM in starbursters with "normal" spiral galaxies such as the Milky Way. NGC 891 is a nearby (d $\sim$ 9.6 Mpc) Sb galaxy believed in many respects to resemble the Milky Way, so that it is a particularly interesting case for studies of the ISM. [CII] emission was previously detected from the nucleus of NGC 891 (Stacey et al. 1991). Here we present the first large scale mapping of NGC 891 in the [CII] line (KAO beam size: 55" = 2.6 kpc). The map was obtained with the UCB/MPE **F**ar-infrared **I**maging **F**abry-Perot **I**nterferometer (**FIFI**) (Poglitsch et al. 1991). We find:

(1) The [CII] emission extends over the entire disk of the galaxy ($\sim$ 30 kpc). The line is very bright, amounting to $\sim$ 0.3% of the total far-infrared (FIR) luminosity in the central regions (r $\sim$ 1.3 kpc) Integrated over the entire galaxy, the [CII] luminosity is $\sim 1.4 \times 10^8; L_\odot$, or $\sim$ 1% of the total FIR luminosity.

(2) The [CII] line emission largely tracks the galactic plane, but has a distinct asymmetry to the north. The [CII] emission is well correlated with the CO(1 - 0) (Garcia-Burillo et al. 1992) and the 2.8 cm radio continuum emission (Klein et al. 1984) but is *not* well correlated with the HI 21 cm line emission (Rupen (1991)). The [CII] emission is associated with the molecular and ionized interstellar medium (ISM).

(3) More than 60% of the observed [CII] emission arises from warm dense photodissociation regions (PDRs) on the far-UV exposed surfaces of giant molecular clouds (GMCs). Less than 25% of the [CII] emission arises from low density HII regions, and less than 15% arises from "standard" atomic clouds. The modest fraction in these diffuse components contrasts with our results from the Scd galaxy NGC 6946. Here, a far greater fraction ($\sim$ 65%) of the [CII] emission arises from either atomic clouds or the ionized interstellar medium (Madden et al. 1993).

(4) Over much of NGC 891, the [CII]/CO(1 - 0) line intensity ratio is $\sim$ 1000 - nearly identical to that we observe from galactic molecular clouds (Stacey et al. 1993) - suggesting that the molecular medium in NGC 891 may be constructed through a superposition of Galactic type molecular clouds. At the putative northern spiral arm, however, we observe an enhanced (by a factor $\sim$ 3) line intensity ratio consistent with enhanced far-UV fields (star formation activity) there. The KAO far-IR (120 μm) continuum (Harper 1992) is also enhanced at the spiral arm.

(5) The [CII] and CO data are combined with the 120 μm continuum map and photodissociation regions models to derive the physical conditions of the emitting clouds (cf. Wolfire et al. 1989, Stacey et al. 1991). We find that most of the molecular medium may be described by low density clouds ($n \sim 100\text{cm}^{-3}$) exposed to modest far-UV interstellar radiation fields ($\sim$ 100 times the local ISRF). At the position of the spiral arm, the [CII] intensity requires somewhat higher density clouds ($\sim$ 600 cm^{-3}). The filling factor for these sources is $\sim$ 28% and 67% respectively in our 55" beam. Assuming the [CII] source has intrinsic width $\sim$ 10" (as for the CO line emission), we require on the average 1.5 and 3.6 PDR surfaces along the line of sight respectively.

Acknowledgement This work was supported in part by NASA grant NAG2-208.

References

Garcia-Burillo, S., Guelin, M., Cernicharo, J. and Dahlem, M. 1992, A&A, 266, 21 Harper, D.A. 1992 personal communication
Klein, U., Wielebinski, R., and Beck, R. 1984 A&A 133, 19
Madden, S.C., Geis, N., Genzel, R., Herrmann, F., Jackson, J.M., Poglitsch, A., Stacey, G.J., and Townes, C.H. 1993, ApJ, 407, 579
Poglitsch, A., Beeman, J.W., Geis, Genzel, R., Haggerty, M., Haller, E.E., Rumitz, M., Stacey, G.J., and Townes, C.H. 1992, Internat. J. IR MM Waves, 12, 859.
Rupen, M.P. 1991, A.J., 102, 48
Stacey, G.J., Geis, N., Genzel, R., Lugten, J.B., Poglitsch, A., Sternberg, A., and Townes, C.H. 1991, ApJ, 373, 423
Stacey, G.J., Jaffe, D.T., Geis, N., Genzel, R., Harris, A.I., Poglitsch, A., Stutzki, J., and Townes, C.H. 1993, ApJ, 404, 219
Wolfire, M. G., Hollenbach, D. and Tielens, A.G.G.M. 1989, ApJ, 344, 770

COBE Observations of the H II Region Around IC 1848

D. Leisawitz[1], P. M. Mitra[2], and M. G. Hauser[3]

[1] NASA/Goddard Space Flight Center, Code 631, Greenbelt, MD 20771, USA
[2] General Sciences Corp., NASA/GSFC, Code 685.3, Greenbelt, MD 20771, USA
[3] NASA/Goddard Space Flight Center, Code 680, Greenbelt, MD 20771, USA

IC 1848 is a cluster of O stars situated in the Perseus arm at $(\ell, b) = (137.^\circ19, +0.^\circ92)$. Infrared photometric and spectroscopic observations of IC 1848 from the COBE DIRBE and FIRAS instruments were combined with a map of the CO $J = 1 \rightarrow 0$ emission (Leisawitz, Bash, and Thaddeus 1989) to derive physical properties of the dust and gas in the H II region and in the molecular clouds heated by the massive stars.

We analyzed Diffuse Infrared Background Experiment (DIRBE) observations of a $2^\circ \times 2^\circ$ region centered on the cluster. With its $42' \times 42'$ field of view, the DIRBE provided independent spectral energy distributions from 9 sub-regions covering the spectral range from 1.25 μm to 240 μm in 10 bands. The region around IC 1848 is a discrete and resolved DIRBE source at all wavelengths. The intensity maxima shift systematically as a function of wavelength such that at 1.25 μm a plateau of emission surrounds the cluster, whereas at 240 μm the brightest emission coincides with the two largest molecular clouds associated with the hot stars.

Dust temperatures (T_d) inferred from observations at wavelengths longward of about 60 μm are thought to apply exclusively to classical dust grains in thermal equilibrium; there should be virtually no contribution from a non-equilibrium or PAH-like grain component. We applied color corrections and subtracted local estimates of the zodiacal plus diffuse Galactic background emission at 140 μm and 240 μm, and then derived a T_d map from the resulting data assuming a dust emissivity proportional to $\nu^{1.5}$. Dust in the diffuse H II region is at about 28 K, and the temperature decreases to $T_d \sim 22\,K$ in the only molecular cloud resolved by the DIRBE, IC1848A. The true temperature at the center of that cloud is probably somewhat lower than the apparent temperature because warm dust on the illuminated back surface contributes substantially to the observed intensity.

A map of dust mass column density was derived from the T_d and 240 μm maps assuming a 240 μm absorption coefficient of 7.2 $\mathrm{cm^2\,g^{-1}}$ (Draine 1990). A single, pronounced peak in the resulting map coincides with the CO cloud IC1848A. If 2.31 kpc is adopted as the distance (Becker and Fenkart 1971), the mass of dust in the cloud is $5.7 \times 10^2\,\mathrm{M_\odot}$, and the total gas mass inferred from the CO observations is $6.6 \times 10^4\,\mathrm{M_\odot}$ (Leisawitz 1990). Independent of the distance, the average dust-to-gas mass ratio is about 0.9%. Uncertainty in this number stems primarily from the following possible sources of error: the $W(CO)/N_{H_2}$ ratio, the dust emissivity, and the infrared background intensity.

Sodroski *et al.* (1994) analyzed the global Galactic 140 μm and 240 μm emission as seen by the DIRBE and found that the molecular cloud component could be characterized by a bolometric infrared luminosity per unit H mass of $2.7 \pm 0.1\,\mathrm{L_\odot/M_\odot}$ (assuming a ν^2 emissivity law). Following an analogous procedure, and, for consistency, making the same assumption about the dust emissivity, we derived $3.2 \pm 0.2\,\mathrm{L_\odot/M_\odot}$ for IC1848A. This suggests, not surprisingly, that the CO-emitting gas analyzed by Sodroski *et al.*, namely that detected in the Goddard-Columbia CO survey (Dame *et al.* 1987), tends to be associated with massive stars; were this not the case, we would expect the Galactic molecular gas to have L/M much lower than that of the cloud heated by IC 1848.

Leisawitz and Hauser (1988) compared the bolometric infrared luminosity of the IC 1848 region with the stellar luminosity ($\sim 1.1 \times 10^6\,\mathrm{L_\odot}$) using IRAS 60 μm and 100 μm data, and found that only about half of the starlight can be accounted for in the infrared within a 40 pc radius, the molecular cloud notwithstanding. Repeating the determination of the bolometric infrared luminosity with the DIRBE 140 μm and 240 μm observations leads to a very similar result ($5.4 \times 10^5\,\mathrm{L_\odot}$), and supports the previous conclusion that the non-molecular material around IC 1848 is rather tenuous. Approximately 35% of the infrared luminosity comes from

the molecular cloud IC1848A, owing to its naturally high UV/visible opacity and the fact that it subtends a large solid angle as viewed from the stars.

A spectrum of the 7° diameter region surrounding IC 1848 from the COBE Far Infrared Absolute Spectrophotometer (FIRAS) shows strong [C II] 158 μm and weak [N II] 205 μm line emission. The ratio of line intensities, 20 ± 3, is consistent with what one would expect of a photodissociation region at the surface of a dense cloud, and inconsistent with emission from an ionization-bounded Strömgren sphere (Petuchowski and Bennett 1993).

In conclusion, the COBE DIRBE and FIRAS observations of IC 1848 support the idea that molecular clouds strongly affect the spatial brightness and spectral energy distributions of H II regions. The surfaces of these clouds, heated when they are in proximity to massive stars, are especially important; such an association of clouds with stars is common in the Galaxy.

The COBE datasets were developed by the NASA Goddard Space Flight Center under the guidance of the COBE Science Working Group. The data used in this study are publicly available and may be obtained by anonymous `ftp` from the NSSDC. This work was supported by the COBE Project.

References

Becker, W., and Fenkart, R. 1971, A&AS, 4, 241
Dame, T. M. *et al.* 1987, ApJ, 322, 706
Draine, B. T. 1990, in *The Interstellar Medium in Galaxies,* ed. H. A. Thronson, Jr. & J. M. Shuli (Dordrecht: Kluwer), p. 483
Leisawitz, D. 1990, ApJ, 359, 319
Leisawitz, D., Bash, F. N., and Thaddeus, P. 1989, ApJS, 70, 731
Leisawitz, D., and Hauser, M. G. 1988, ApJ, 332, 954
Petuchowski, S. J., and Bennett, C. L. 1993, ApJ, 405, 591
Sodroski, T. J. *et al.* 1994, ApJ, in press

A survey of the Large Magellanic Cloud in the [C II] 158 micron line

K. Mochizuki,[1,2] T. Nakagawa,[1] Y. Doi,[1,2] Y. Y. Yui,[1,2] H. Okuda,[1] M. Yui,[1,2] H. Shibai,[1] T. Nishimura,[3,4] and F. J. Low[3]

[1]The Institute of Space & Astronautical Science, Sagamihara, Kanagawa 229, Japan
[2]Department of Astronomy, The University of Tokyo, Hongo, Tokyo 113, Japan
[3]Steward Observatory, University of Arizona, Tucson, AZ 85721, USA
[4]*Present Adrress:* National Astronomical Observatory, Mitaka, Tokyo 181, Japan

We have mapped the Large Magellanic Cloud (the LMC) in the [C II] 158 μm fine-structure line with the Balloon-borne Infrared Carbon Explorer (BICE) system. The [C II] line emission was detected over most of the LMC. The [C II]/CO intensity ratio in the LMC is 23000 ($\log[I_{[CII]}/I_{CO}] = 4.4 \pm 0.3$), 18 times larger than that in the Galactic plane, 1300 ($\log[I_{[CII]}/I_{CO}] = 3.1 \pm 0.5$; Nakagawa et al. 1993).

Constituent clumps of molecular clouds, which emit [C II] and CO lines, are immersed in interstellar UV field. Each clump has a C^+ envelope irradiated by UV radiation and a CO core shielded from the radiation. Our observation implies that each clump of the molecular clouds in the LMC has a larger C^+ envelope relative to its CO core than those in our Galaxy.

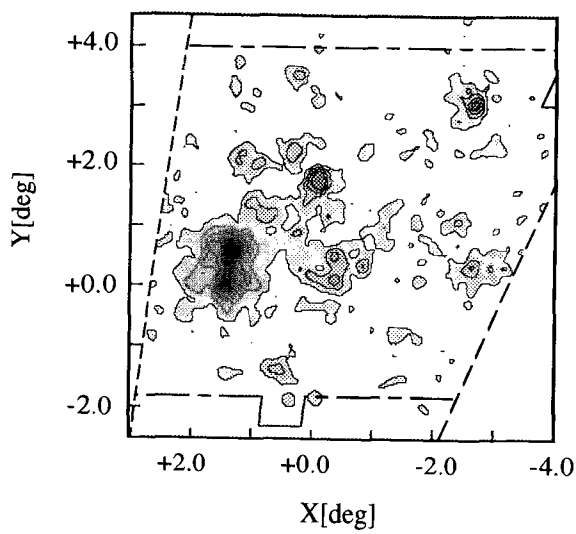

FIG. 1.-Velocity-integrated [C II] line intensity map of the LMC. The contour levels are 1, 2, 4, 6, 8, 10, and 12 $\times 10^{-5}$ ergs s^{-1} cm^{-2} ster^{-1}. Our detection limit is 1.4 $\times 10^{-5}$ ergs s^{-1} cm^{-2} ster^{-1} (3σ). The coordinate (X, Y) is defined by Isserstedt (1975). The angular resolution is 15.0'.

For typical [C II] emitting clouds, which are immersed in a relatively strong UV field, the thickness of [C II] layers is determined by the extinction of UV field by dust grains. Hence the low dust abundance in the LMC allows CO dissociating UV photons to penetrate deeper into each clump (Maloney & Black 1988), producing larger C^+ envelopes relative to CO cores in the LMC than in our Galaxy. As a result, the [C II]/CO intensity ratio is expected to be larger in the LMC than in our Galaxy.

The mean strength of interstellar UV field, which is 5 times greater in the LMC than in our Galaxy

(Lequeux 1989), might affect [C II]/CO intensity ratios. But the UV strength in general [C II] emitting regions has a range of several orders of magnitude. On the other hand, the observed difference of the [C II]/CO ratios between the two galaxies is much larger than the scatter of the ratios within each galaxy.

Therefore, we conclude that the variation of UV field strength cannot reproduce the [C II]/CO ratios observed, and that the lower dust abundance is the dominant factor to increase the ratios in the LMC.

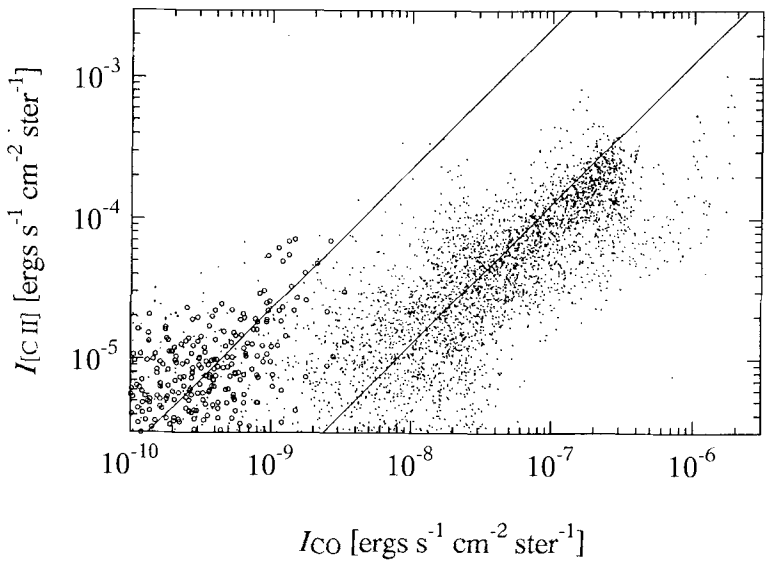

FIG. 2.-Velocity-integrated [C II] line intensity, $I_{[CII]}$, vs. that of the CO line, I_{CO}, in the LMC (open circles) and in the Galactic plane $-12° \leq l \leq 26°$ (dots). All the data are spatially resampled into 15.0' grids. Data are from: Nakagawa et al. (1993) for [C II] in the galactic plane; Cohen et al. (1988) for CO in the LMC; Dame et al. (1987) for CO in the Galactic plane.

References

Cohen, R. S., Dame, T. M., Garay, G., Montani, J., Rubio, M., & Thaddeus, P. 1988, ApJ, 331, L95

Dame, T. M., Ungerechts, H., Cohen, R. S., De Geus, E. J., Grenier, I. A., May, J., Murphy, D. C., Nyman, L.-A., & Thaddeus, P. 1987, 322, 706

Isserstedt, J. 1975, A&A, 41, 21

Lequeux, J. 1989, in Recent Developments of Magellanic Cloud Research, ed. K. S. de Boer, F. Spite, & G. Stasinska (Paris: Obs. Paris), 119

Maloney, P., & Black, J. H., 1988, ApJ, 325, 389

Nakagawa, T., Doi, Y., Mochizuki, K., Yui, Y. Y., Okuda, H., Yui, M., & Shibai, H. 1993, in AIP conference proceedings 278 (New York: American Institute of Physics), 303

Atomic Carbon Emission from Shocked and Preshocked Gas in the IC 443 Supernova Remnant

T. G. Phillips[1], Jocelyn Keene[1], and Ewine F. van Dishoeck[2]

[1]California Institute of Technology, Pasadena, CA 91125, USA

[2]Leiden Observatory, The Netherlands

Abstract

We have obtained maps of C I ($^3P_1 \rightarrow ^3 P_0$) emission at 492 GHz in the Supernova Remnant IC 443, concentrating on clump G. Broad-line shocked CI emission ($\sim$ 10 kms^{-1} FWHM) with spatial distribution similar to that of ^{12}CO is observed. Also, very interestingly, we see a narrow-line ($\sim$ 1 kms^{-1} FWHM) component of C I emission that corresponds to no observed ^{12}CO emission and its distribution is very different from that of the shocked component, apparently lying upstream from the shock front. Both wide and narrow components are also weakly visible in our ^{13}CO(2$\rightarrow$1) map. The inferred ratio of C I to CO in the shocked component is > 0.5 and in the narrow-line component is > 2, rather than the usual value of about 0.1. We speculate that this predominantly atomic region may mark the radiative precursor of the shock.

Observations

Shocks resulting from the interaction of a supernova remnant with a molecular cloud can heat and compress the gas. The resulting high temperatures and densities not only affect the chemistry, but also cause substantial excitation of the molecules. The strongest molecular lines are therefore expected to lie at submillimeter wavelengths. At the moment there is no information on the atomic carbon content of such gas. We present here a C I ($^3P_1 \rightarrow ^3 P_0$) study of one component of the shocked gas associated with the SNR IC 443, which is one of the best-studied and nearest ($D \approx 1500$ pc) examples.

We present C I and CO maps (Figs. 1 & 2) of one of the clumps, designated "G" (Huang et al. 1986), in a region which is strongly emitting in H_2 lines, indicating that the gas is presently being shocked. The ^{12}CO emission occurs mainly in a bright bar running NE to SW, presumably delineating a shockfront from material impinging on the ambient gas from the East (Fig. 2). The integrated intensity peaks are found on this bar. Here the C I and ^{13}CO emissions are also predominantly from shocked gas with line widths of $\sim$10 kms^{-1}. However, the C I distribution has a second peak to the NW (Figs. 1 & 2). At this position the peak C I temperature is very high (up to $T_R \approx 25$ K) and the line is very narrow ($\sim$ 1.5 kms^{-1}). This narrow line is also seen in ^{13}CO with a much lower intensity, but has no counterpart in ^{12}CO. Possibly this narrow, bright line marks the position of a shock radiative precursor in the preshocked gas. Although the spatial and velocity distribution of ^{13}CO and C I are similar in this object the C I integrated temperature is a factor of >5 more than the ^{13}CO(2$\rightarrow$1) throughout. This means that C I is greatly overabundant here with a C I/CO ratio > 2, compared to most molecular clouds with a typical valve of 0.1.

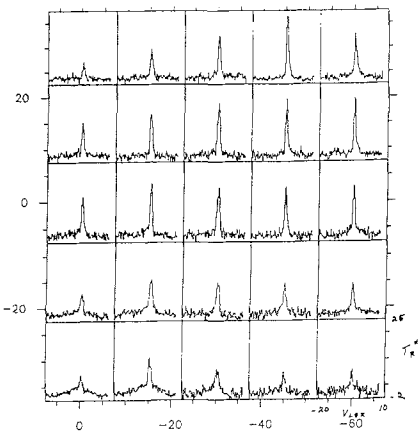

Fig. 1. C I spectral map of the IC 443 G I region. The 0,0 position is at α = 6:13:42.0, δ = +22:33:40.0 (1950).

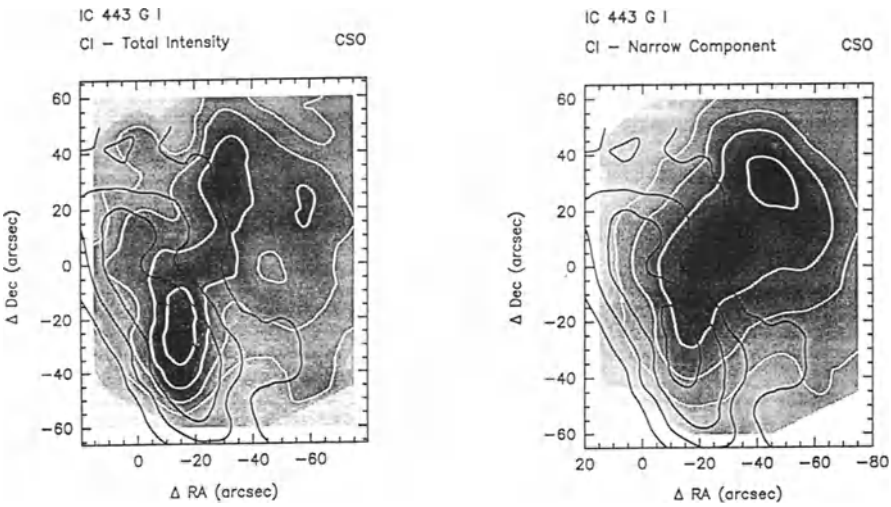

Fig. 2(left). Integrated intensity maps of G I for CO(3→2) (black contours) and for C I (gray scale and white contours). The C I distribution is partly the broad-line shocked feature and partly the newly detected warm narrow-line feature. The 0,0 position is at α = 6:13:42.0, δ = +22:33:40.0 (1950). (right). Peak intensity map of C I (gray scale and white contours) with the CO(3→2) integrated intensity contours (black). The C I peak intensity distribution is dominated by the narrow-line component.

Work at the CSO is funded by NSF contract #AST 90–15755.

References

Huang, Y.-L., Dickman, R.L., & Snell, R.L. 1986, ApJ, 302, L63

Turbulence in Interstellar Clouds

Edith Falgarone

Radioastronomie Millimétrique, Ecole Normale Supérieure, 24 rue Lhomond, 75005 Paris, France

1 - Introduction

Several comprehensive reviews have been written in the past ten years on the issue of turbulence in interstellar clouds and we suggest them as preliminary readings because they take different and complementary points of view on a difficult issue (Dickman, 1985; Scalo, 1987; Pouquet, Passot & Léorat 1990).

The understanding of interstellar turbulence proceeds at the pace of the understanding of turbulence in general, which is still one of the least understood fields in physics. Experiments in flows, in tanks and in the atmosphere, theory and numerical simulations have all contributed to refine the early Kolmogorov–Obukhov theory. In particular, the phenomenon of intermittency, (*i.e.* the uneven distribution in space and time of the dissipation rate of kinetic energy), which had been postulated quite early by Landau & Lifchitz (1959) and by Kolmogorov (1962), presently focuses many of the observational and theoretical efforts in the investigations of turbulence.

As far as interstellar clouds are concerned, one may ask whether or not the suprathermal motions observed in all clouds, with the exception of small dense cores, are turbulent, random or due to wave motions, likely magneto–hydrodynamic (MHD) waves. The question is of importance because the amount of energy in these non–thermal motions is the major support of interstellar clouds against self–gravity. Moreover, if, like in terrestrial flows, the dissipation of this energy occurs intermittently in space and time, local but significant modifications in the thermodynamics of interstellar clouds are to be expected.

2 - Is there any evidence for turbulence in the data?

2.1 - The existence of a confining pressure of kinetic origin

Many clouds and cloud substructures in molecular complexes of the Solar Neighborhood are far out of virial balance between their internal kinetic energy T and their gravitational energy W. This departure, expressed in terms of a dimensionless parameter $\alpha = 2T/\mid W \mid = 5\sigma^2 R/GM$ in which σ is the internal velocity dispersion (predominantly non–thermal) and R and M are the radius and total gas mass of a given structure, is displayed in Figure 1 as a function of H_2 gas mass as in Bertoldi & McKee (1992). The straight lines are the least square fits performed by these authors

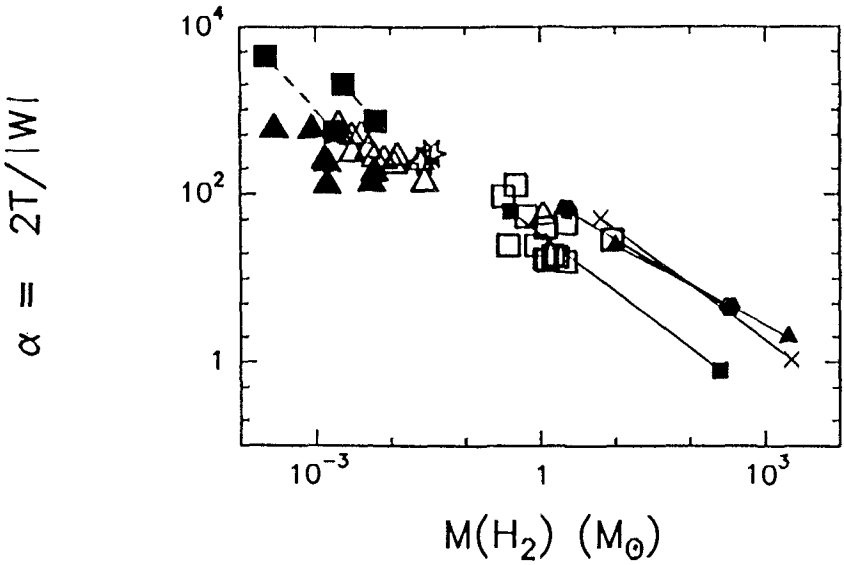

Figure 1: The virial parameter α as a function of the H_2 mass of substructures in high latitude clouds and star-forming molecular complexes. The solid lines are least square fits obtained by Bertoldi and McKee (1992) in the substructures of four molecular clouds. The symbols are described in the text.

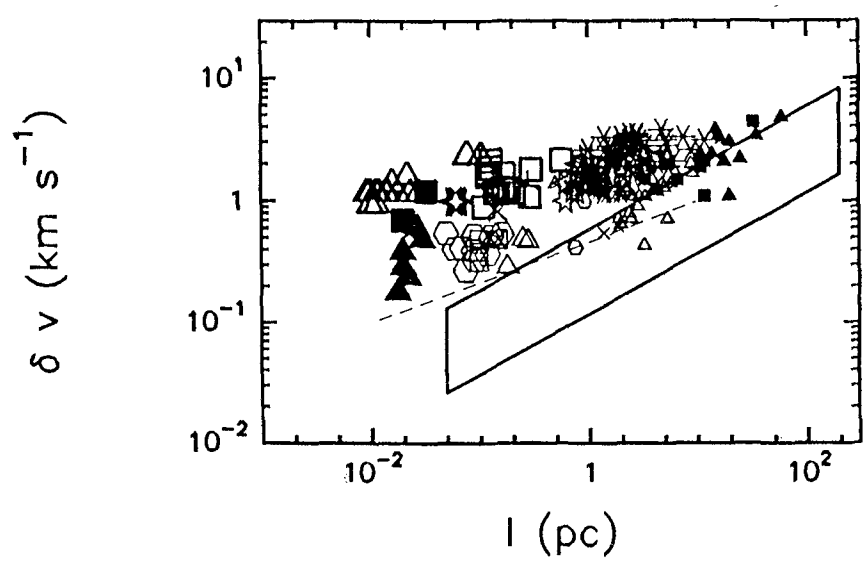

Figure 2: Non-thermal velocity dispersion versus size of an ensemble of structures drawn for a variety of data sets. The references and corresponding symbols are given

on data in Orion B (Bally et al. 1987, crosses), the ρ Ophiuchus filaments (Loren 1989a, solid squares), Cepheus OB3 (Carr 1987, solid hexagons) and the Rosette nebula (Blitz & Stark 1986, solid triangles). In these star–forming complexes, α ranges between values close to unity for the most massive substructures and values as large as $\sim 10^2$ for the least massive ones. Still larger ratios are found in high latitude clouds and cloud edges, if the gas mass M_{H_2} is correctly estimated. The data are drawn from high latitude clouds in MBM 12 or L1457/58 (Pound et al. 1990, empty squares; Zimmermann 1993, empty triangles), in Ursa Major (Falgarone & Pérault 1988, solid triangles; Falgarone et al. 1994, solid squares) and in a cloud edge (Falgarone & Phillips in preparation, stars). Substructures observed in these fields have a kinetic energy up to 2×10^3 times their gravitational energy.

The dependence $\alpha \propto M_{H_2}^{-2/3}$ can be interpreted, as proposed by Loren (1989b) and Bertoldi & McKee (1992), as the existence of a confining pressure. An average value of this pressure in the Solar Neighborhood, derived from Figure 1, is $P_e = 1.5 \times 10^{-11} (n_{H_2} / 10^3 \, \mathrm{cm}^{-3})^{4/3}$ erg cm^{-3}. This pressure is clearly not thermal because it is much larger than any thermal pressure in the interstellar medium (for HI clouds, $P_{th} \sim 5 \times 10^{-13}$ erg cm^{-3} and is still smaller in the warm neutral medium). But the observed kinetic pressure $P_{kin} = \frac{1}{3} \rho \bar{v}^2$ within molecular clouds in the Solar Neighborhood has been found to fluctuate by $\pm$ one order of magnitude about an average value, independent of scale and density, $P_{kin} \sim 4 \times 10^{-12}$ erg cm^{-3} (Falgarone, Puget & Pérault 1992) which is consistent with the idea that the pervading pressure has a kinetic origin. Moreover, measurements of the magnetic field intensity in interstellar clouds (Myers & Goodman 1988; Crutcher et al. 1993; Goodman et al. 1994) show that the magnetic pressure $P_B = B^2/8\pi \sim 10^{-11}$ erg cm^{-3} on the average in interstellar clouds (thus, of the order of the kinetic pressure given above), suggesting some equipartition between the kinetic and magnetic energy of clouds. The question of the mechanism responsible for the momentum transfer is still open: is it due to waves or to turbulence, or to a combination of both?

2.2 - The scale invariant structure

When they are not violently affected by star–formation, interstellar clouds exhibit, spatially and dynamically, an impressive self–similar structure, which may be viewed as a signature of turbulence.

In velocity space, the size–linewidth relation $\delta v \propto l^h$ between the internal velocity dispersion of a structure of size l has an exponent $h \sim 0.5$ when built on samples of large complexes defined in molecular line surveys of the Galaxy (Dame et al. 1986; Solomon et al. 1987) or dense cores in molecular clouds (Myers 1983). When combined with the observational result that the average density of all these structures is decreasing as an inverse power of the size, this scaling leads to the interpretation

that molecular clouds are in virial balance between self–gravity and internal kinetic energy. But many clouds or substructures do not follow this $l^{0.5}$ scaling. This is illustrated in Figure 2 where the data points found in the samples of Dame et al. (1986), Solomon et al. (1987) and Myers (1983) lie within the parallelogram of slope 0.5. The other points which rather follow a law $\delta v \propto l^{0.3}$ come from data sets described in Falgarone, Puget & Pérault (1992), namely Herbertz et al. (1991) for NGC1499 (small stars) and Carr (1987) for Cepheus OB3 (asterisks), while the rest of the fields are described in Falgarone and Pérault (1987). The large symbols have the same meaning as in Figure 1. Entities in virial balance between self–gravity and kinetic energy for which the confining pressure is negligible thus coexist with structures for which the flatter exponent of the size–linewidth scaling law $l \sim 0.3$ may be reminiscent of incompressible turbulence (Kolmogorov 1941), as first proposed by Larson (1981).

Another signature of the self–similar behaviour of interstellar clouds is the fractal geometry of their projected boundaries. Fractal dimensions $1.2 < D_B < 1.6$ for the boundaries are found for all the tracers of the gas (and indirectly through that of dust emission) *i.e.* in the HI emission (Wakker 1990), in the visible extinction (Beech 1987), in the 100 μm emission of the dust detected by IRAS (Bazell & Désert 1988; Scalo 1989; Dickman, Horvarth & Margulis 1990) in the CO emission in several rotational transitions (Falgarone, Phillips & Walker 1991; Zimmermann 1993). This dimension, often derived from data sets spanning four orders of magnitude in size, does not seem to have any systematic dependence with the tracer used.

This fractal dimension was brought together with the fractal dimension of the dissipative structures in turbulence (see the review of Sreenivasan 1991 and references therein) and it was proposed that the cold cloud population in the interstellar medium might have a fractal geometry with the same dimension, if somehow it traces the regions of large dissipation rate of kinetic energy in a turbulent interstellar medium (Falgarone, Phillips & Walker 1991). This would be an indirect evidence of the existence of turbulence in the interstellar medium. This complex scenario is under investigation (Minier, Falgarone & Chièze in preparation). Several other interpretations of the fractal geometry have been proposed: collisional fragmentation (Nozakura 1993), gravitational clustering and virial balance (Hetem & Lépine 1993; Pfenniger & Combes 1994). In all these models, the fractal dimension is dependent of the laws adopted to build the fractal structure.

2.3 - Correlation lengths in the velocity field

Early searches for a finite correlation length in the velocity field of molecular clouds have been described in the two first reviews quoted above. More recent searches have been similarly inconclusive (Pérault, Falgarone & Puget 1986; Kleiner & Dickman

1987; Kitamura et al. 1993). All the determinations are so close to the resolution of the observations in each case (smaller than three times the resolution) that a wise conclusion would be that a correlation length of the velocity field has never been unambiguously measured in molecular clouds.

2.4 - The shapes of lineprofiles and non–Gaussian linewings

The shapes of line profiles, when observed with the high spectral resolution available in heterodyne measurements ($\Delta\lambda/\lambda \sim 10^7$), have long been thought of as powerful probes of the nature of the velocity field in clouds. The former hypothesis of microturbulence (*i.e.* the velocity correlation length is small compared with the photon mean free path, according to the definition adopted by Leung & Liszt 1976) has been discarded as not relevant for the bulk of the molecular clouds because it easily produces self–absorbed profiles in optically thick lines, which is not a common shape in the interstellar lines. However, Leung (1978) discussed again the various regimes relevant to the line formation mechanism and showed that the parameter of importance is the ratio of systematic to turbulent velocities in the region of line formation. Very early also, Baker (1976) recognized that macroturbulence was adequate to explain all the observed attributes of the ^{12}CO and ^{13}CO profiles: the fact that the line intensity ratio is much smaller than the molecular isotopic ratio, the scarcity of flat–topped or self–absorbed profiles in ^{12}CO, the large linewidth ratio, and the fact that the emission maps in each species follow each other quite closely. These ideas were not very popular then, because they had to face the severe problem that no known mechanism was envisioned at that time to balance the rapid dissipation rate of a supersonic macroturbulence in clouds.

The issue indeed is especially difficult because turbulence generates velocity correlations at all scales. It explains why more recent attempts at computing line profiles in turbulent fields with one correlation length only are not yet satisfactory (Albrecht & Kegel 1987; Kegel, Piehler & Albrecht 1993). The results of these computations, however, clearly illustrate the fundamental role played by the value of the correlation length.

Independently of the unsolved issue of radiative transfer in a turbulent cloud, the existence of weak non–Gaussian wings found in molecular clouds line profiles has been proposed, recently, as a specific signature of the existence of turbulence, namely its property of intermittency (Falgarone & Phillips 1990). The argument was relying on the fact that linewings exhibit the same self–similar properties as linecores, but it was not a demonstration. Furthermore, several interpretations for these non–Gaussian wings exist, independent of the existence of intermittency (cloud collisions, Keto & Lattanzio 1989; non–linear steepening of waves in inhomogeneous clouds, Elmegreen 1990) and further investigations of this hypothesis were clearly needed. We give recent results in the next sections, but start with a small section on intermittency.

2.5 - What is the intermittency of a turbulent field?

As said before, its existence has been known for more than 40 years, and it is as pronounced as the Reynolds number is large. Intermittency is thought to be linked to the quasi-singularities (discontinuities, sharp fronts) of the velocity field in turbulent flows, and the fact that the turbulent activity is confined to a smaller fraction of space as its intensity increases, thus leading to an uneven distribution in space and time of regions of large vorticity or shear and dissipation. There is not yet a generally accepted physical model of intermittency (Frisch, Sulem & Nelkin 1978; Frisch 1985; She 1991; Castaing 1989; Castaing, Gagne & Hopfinger 1990), but it appears best described statistically by the non-Gaussian probability distribution functions (PDFs) of velocity increments, cross-derivatives and vorticity. The statistical behavior of the PDFs appears to be related to the existence of spatially coherent structures which, by their localization in space and their intermittent interactions may be responsible for the observed space-time intermittency (see Basdevent et al. 1981). Coherent structures can be detected only if the measurement keeps track of the spatial (or temporal) coherence of the velocity field. A pair of sensors located at a known separation (in the case of flow experiments) or the separation used in a simulation to compute increments or derivatives play this role. Wavelet analysis is also well suited for the decomposition of structures in turbulent flows (Farge 1992; Langer et al. 1993) although difficult to perform in a multidimensional case.

Intermittency has now been studied statistically in experimental flows and jets at high Reynolds numbers (Anselmet et al. 1984; Fauve 1993) and is found in numerical simulations of turbulence at high Reynolds number (see for example Vincent & Meneguzzi 1990; She & Orzsag 1991; Porter, Pouquet, & Woodward 1992, 1993, 1994). Regions of intermittent large vorticity have been visualized in turbulent flows seeded either with gas bubbles which inflate and percolate in the pressure minima of strong vortices (Douady, Couder & Brachet 1990) or with crystalline platelets which adopt a preferential orientation in regions of strong shear (Schwarz 1990).

3 - Confrontation of observed and synthetised interstellar profiles

To test the relevance of the existence of turbulence to the interstellar medium, the recent three-dimensional numerical simulations of compressible turbulence with an unprecedented resolution (512^3 grid points) of Porter, Pouquet and Woodward (1994) have been used to synthesize line profiles (Falgarone et al. 1994). The Mach number of the simulation is moderate, only 1.1 (rms) at t=0. The fluid is a perfect gas with $\gamma = 7/5$. The evolution of the flow is not forced. Energy is fed into the fluid at

t=0 and the system subsequently evolves freely under the constraint of these initial conditions. For a detailed description of the method used (PPM) see Porter, Pouquet and Woodward (1992; 1993).

These simulations shed a new light on the evolution of shocks and energy transfers between the various modes. A first short phase, during which compressional waves steepen, ends at $t \sim 0.3\tau_{ac}$ with shock formation, and a density contrast ~ 60 ($\tau_{ac} = L/c_S$ is the sound crossing time of the energy containing scale, L). Then, in the long second phase, up to $t \sim 3\tau_{ac}$, shock interactions generate vorticity and most of the kinetic energy is rapidly transferred to non compressible modes. The energy dissipation rate is thus considerably reduced. In this phase, the flow has most of the properties of incompressible turbulence: an inertial range of scales has developed with a power spectrum for the solenoidal (incompressible) part of the flow (which contains more than 90% of the whole energy) close to that predicted by Kolmogorov $E(k) \propto k^{-5/3}$ although the density contrast is still ~ 5. The PDF of vorticity in this phase has a conspicuous non-Gaussian tail, illustrative of the intermittency of the flow. At the end of this phase only a few shocks have survived. A last phase is that of the self–similar decay of turbulence.

The synthetised spectra in the optically thin approximation are simply histograms of the line of sight projection velocity. The similarity between the observed line profiles and the synthetic profiles is striking. All the diversity of the observed lineshapes is found in the simulated profiles: almost Gaussian profiles coexisting with double–peaked and asymmetric profiles. A quantitative comparison has been attempted in Falgarone et al. (1994).

This is only a first step in the analysis of the effect of turbulence on the formation of molecular lines, but it is encouraging to see that these calculations which include no radiative transfer yet and do not introduce any of the complications due to temperature, density and abundance variations naturally produce lineshapes which resemble the observed spectra. It is a powerful indication that turbulence, taken here as a most general concept, generates velocity patterns which seem to be present in the interstellar medium.

It supports the idea that the dynamics of interstellar clouds is dominated by turbulence, (likely MHD turbulence, given the intensity of the magnetic field). It is interesting to note that the presence of magnetic field does not suppress the intermittency of the velocity field, according to recent numerical simulations of MHD turbulence by Biskamp et al. (1990) and Brandeburg et al. (1994). It is therefore very likely that intermittency is present in the interstellar medium as well. The simulations of Porter et al. (1994) show that small shocks are present and MHD shock signatures such as those discussed by Draine (1980), Draine, Roberge and Dalgarno (1983), Draine and Katz (1986) and Pineau des Forêts et al. (1986) should be present in interstellar clouds, but to a lesser extent than predicted, because of the efficient transfer of energy from compressible to incompressible modes.

4 - The impact of intermittency on the microphysics of interstellar clouds

4.1 Probability distribution of the gas kinetic temperature

The zones of large vorticity and shear in turbulent flows are closely associated in space and time with those of large dissipation rate of kinetic energy and the two subsets of space where these quantities are concentrated are highly structured and intermittent as can be seen in the numerical simulations of Brachet (1990) and Vincent & Meneguzzi (1991). The dissipation of the turbulent kinetic energy via viscous processes eventually turns this energy into heat. The rate at which the gas is heated by this process in the dissipation regions, as well as its equilibrium temperature has been computed by Falgarone & Puget (1994). Details of the computation are not recalled here. The only assumption is that turbulence can be given a universal description and that all its statistical properties depend only on two parameters, the specific energy transfer rate $\epsilon = \Delta v^3/l$ and the dissipation scale $l_D = (\nu^3/\epsilon)^{0.25}$ (ν is the kinematic viscosity). We have used data obtained in flows with large Reynolds numbers (Gagne 1987) which provide measurements of the velocity increments Δv over a large range of separations l, down to only a few times the dissipation scale. The PDFs of the dissipation rates averaged over various sizes are derived from his PDFs of velocity increments and scaled to the interstellar medium turbulence via

$$l_D \sim 10\mathrm{AU}\left(\frac{n_H}{10^2\mathrm{cm}^{-3}}\right)^{-3/4}\left(\frac{T_k}{30\mathrm{K}}\right)^{3/8}$$

and $\epsilon = 10^{-2}$ cm^2 s^{-3} which are the dissipation scale (assuming that dissipation occurs via elastic H–H scattering) and energy transfer rate estimated in atomic clouds from available observations.

The local heating source of a small region of size l in which an event of amplitude Δv occurs is:

$$\Gamma_t(l) = 3.8 \times 10^{-26}\, n_H\, (l/l_D)^{-4/3}\, (\Delta v/\sigma)^2 \mathrm{erg\,cm^{-3}s^{-1}}$$

It exceeds by orders of magnitude all the other heating terms due to UV photons, coupling to dust grains, cosmic rays, estimated following Black (1987) for instance.

Thermal balance between heating and radiative cooling processes is reached because the zones of intermittency are somewhat persistent structures: they have a lifetime almost two orders of magnitude larger than their own anticipated turnover timescale $\sim \Delta v/l$ (see for example the experiment of Douady, Couder & Brachet 1991). This lifetime, $\sim 2 \times 10^6$ yr in an HI cloud, is much larger than the cooling time obtained for radiative processes, $\tau_{cool} = E/\Lambda \sim 10^4$ yr for HI at $T = 50K$, where Λ is the radiative cooling rate taken from Dalgarno and McCray (1972).

A full range of equilibrium gas kinetic temperatures is thus derived from the probability distribution of the velocity increments. Temperatures as large as $T_k = 10^4$K are found to occur with non negligible probabilities of 10^{-2} to 10^{-3} which may be interpreted as volume filling factors within the entire cloud at any time. .

Such large temperatures are unexpected given the low average kinetic energy of cold HI clouds. This result can be understood as follows: kinetic energy is fed into the small intermittent structures over timescales which largely exceed their own turnover timescale and the amount of energy accumulated during that time in these structures, dissipated locally and turned into heat, largely exceeds the average kinetic energy.

Many chemical reactions with activation barriers of several thousands Kelvins can therefore take place in regions of intermittent large dissipation rate. Time–dependent calculations of the chemical evolution of such hot regions in interstellar clouds show that, as expected, the abundances of molecules like OH, H_2O, CH^+ are enhanced there by orders of magnitude above the values in the surrounding gas (Falgarone, Le Bourlot, Pineau des Forêts & Roueff, in preparation). A fraction as small as $N_{warm}/N_{tot} \sim 0.03$ of warm gas at $T_k = 10^3$K on a line of sight is sufficient to reproduce the observed value $N(CH^+)/E_{B-V} \sim 4 \times 10^{13}$cm^{-2}mag^{-1} found by Gredel, van Dishoeck & Black (1993) in translucent clouds. The corresponding volume filling factor of warm gas depends on the geometry of the dissipation regions.

4.2 - Decoupling of large molecules and very small grains from the gas turbulent motions

Turbulent motions are associated to large local gas accelerations which are efficient at decoupling a heavy particle from the rest of the gas. Völk et al. (1980) have computed this effect in details in the case of Kolmogorov–type turbulence. A heavy particle immersed in a gas being defined by its friction time τ_f (or slowing–down time) and any turbulent eddy k by its turnover time τ_k, the eddies which are the most efficient at decoupling a particle are those of turnover time $\tau_k \sim \tau_f$: much larger eddies simply advect the gas and the particle together without acting on their relative velocity, while much smaller (and short lived) eddies act as random independent kicks on the particle and do not transfer much momentum. The shortest turnover timescales in a Kolmogorov–type turbulence are found at about 50 times the dissipation scale (at smaller scales, dissipation has already started) and $\tau_{min} \sim$ a few 10^{11}s for the values adopted for HI clouds. Therefore all the particles which have a friction time smaller than τ_{min} *i.e.* large dust grains in low density gas or very small grains and large molecules in high density gas, are not affected by Kolmogorov–type turbulence. Intermittency is responsible for the generation of events of extremely short timescales and these events, of non–negligible probability, act on the lightest particles and succeed at decoupling them from the gas motions. The results are

given in Falgarone & Puget (1994). An immediate consequence of such a process is the possibility of local variations in the small grains size distribution because small particles will coagulate faster among each other than they stick onto large particles.

5 - Prospective

In spite of decades of dedicated efforts at understanding the nature of the velocity field in interstellar clouds, the existence of turbulence, although highly probable, is not yet clearly settled.

If it exists, it will affect the transfer of line photons and this problem still deserves thorough investigation since spectral lines carry most of the information we have on the gas in interstellar clouds. Furthermore, we expect several signatures of intermittency to show up: tiny regions of hot gas embedded in cold HI clouds (indeed with a full kinetic temperature distribution), tiny regions with chemical abundances significantly different from those in the surrounding gas, local variations of the very small dust grains size distribution. These regions of large vorticity or shear are found to be grouped in the few flow experiments where they have been visualized and even if they are individually very small, their (fractal?) organization would make their ensemble detectable by many future experiments, especially in space.

References

Albrecht, M.A. & Kegel, W.H. 1987 A&A 176 317

Anselmet F., Gagne Y., Hopfinger E.J. & Antonia R.A. 1984 JFM, 140, 63

Baker, P.L. 1976 A&A 50 327

Bally, J., Langer, W.D., Stark, A.A. & Wilson, R.W.1987, ApJL, 312, L45

Basdevent C., Legras B., Sadourny P. & Beland M. 1981 *J. Atmosph. Sci.* 38 11

Bazell D. & Désert F.X. 1988 ApJ, 333, 353

Bertoldi F. & McKee C.F. 1992 ApJ, 395, 140

Beech, M. 1987 *Astrophys. Space Sci.*, 133, 193

Biskamp D., Welter H., Waltre M. 1990 *Phys. Fluids B* 2 3024

Black, J.H. 1987 in *Interstellar processes*, D.J. Hollenbach & H.A. Thronson, Dordrecht:Reidel, 731 Blitz, L. & Stark, A.A. 1986, ApJL, 300, L89

Brachet, M.E., 1990 *C. R. Acad. Sci. Paris* 311, 775

Brandeburg A., Jennings R.L., Nordlund A.K., Rieutord, M., Stein, R.F., Tuoninen, O., 1994 JFM in press

Carr, J.S. 1987 ApJ, 323, 170

Castaing, B. 1989 *J. de Physique* 50 147

Castaing, B., Gagne, Y., & Hopfinger E.J. 1990 *Physica D* 46 177

Crutcher R.M., Troland T.H., Goodman A.A., Heiles C., Kazès I. & Myers P.C. 1992 ApJ 407 175

Dalgarno, A. & McCray, R.A., 1972 ARAA, 10, 375
Dame, T.M., Elmegreen, B.G., Cohen, R.S. & Thaddeus, P. 1986 ApJ 305 892
Dickman, R.L. 1985 in *Protostars and Planets II*, D.C. Black, M. S. Matthews, eds., The University of Arizona Press
Dickman, R.L., Horvath, M.A. & Margulis, M. 1990 ApJ, 365, 586
Douady, S., Couder, Y. & Brachet, M.E. 1991, PRL, 67, 983
Draine, B.T. 1980, ApJ, 241, 1021
Draine, B.T., Roberge, W.G., & Dalgarno, A. 1983, ApJ, 264, 485
Draine, B.T. & Katz, N. 1986, ApJ, 306, 655
Draine, B.T., & McKee, C.F. 1993 ARAA 31, in press
Elmegreen, B.G. 1990 ApJL 361 L77
Falgarone, E. & Pérault M. 1987 in *Physical processes in Interstellar clouds*, G.E. Morfill & M. Scholer, Dordrecht: Kluwer, 59
Falgarone, E. & Pérault 1988 A&A 205, L1
Falgarone, E. & Phillips T.G. 1990, ApJ 359, 344
Falgarone, E., Phillips, T.G. & Walker C.K. 1991 ApJ 378 186
Falgarone, E. & Puget, J.-L. 1994, A&A, submitted
Falgarone, E., Puget, J.-L., & Pérault, M. 1992, A&A, 257, 715
Falgarone E., Lis, D.C., Phillips, T.G., Pouquet A., Porter, D.H. & Woodward, P.R. 1994 ApJ submitted
Farge M., 1992 *Ann. Rev. Fluid Mech.*, 24, 395
Fauve, S. 1993 *J. de Physique* II,3 271
Frisch, U., Sulem, P.L., & Nelkin, M. 1978 JFM, 87, 719
Frisch, U. 1985 *Physica Scripta* T9 137
Gagne, Y. 1987, Thèse d'Etat, Université de Grenoble.
Goodman, A.A., Myers, P.C., Güsten, R., & Heiles, C. 1994, in *The First Symposium on the Infrared Cirrus and Diffuse Interstellar Clouds* R. Cutri & W. Waller eds., PASP
Gredel R., van Dishoeck, E.F., & Black, J.H. 1993 A&A, 269, 477
Herbertz, R., Ungerechts, H. & Winnewisser, G. 1991 A&A, 249, 483
Hetem A., & Lépine J.R.D. 1993 A&A 270, 451
Kegel, W.H., Piehler, G., & Albrecht, M.A. 1993 A&A 270 407
Keto, E.R. & Lattanzio J.C. 1989 ApJ 355 190
Kitamura Y., Sunada Y., Hayashi M., & Hasegawa T. 1993 ApJ 413, 221
Kleiner S.C. & Dickman, R.L. 1987 ApJ 312 837
Kolmogorov, A.N. 1941 *Dokl. Akad. Nauk. SSSR* 26 115
Kolmogorov, A.N. 1962 JFM 13 82
Landau, L.D. & Lifchitz E.M. 1959 *Fluid Mechanics* (Reading: Addison–Wesley)
Langer, W.D., Wilson, R.W. & Anderson, C.H. 1993 ApJL 408 L45
Larson, R.B. 1981 MNRAS 194 809

Leung, C.M. 1978 ApJ 225 427
Leung, C.M. & Liszt H.S. 1976 ApJ 208 732
Loren, R. 1989a ApJ, 338, 902
Loren, R. 1989b ApJ, 338, 925
Myers, P.C. 1983 ApJ 270 105
Nozakura T. 1990 MNRAS, 243, 543
Myers, P.C. & Goodman A.A 1988 ApJL, 326, L27
Pérault M., Falgarone E. & Puget J.-L. 1986 A&A 157 139
Pfenniger D. & Combes F. 1994 A&A in press
Pineau des Forêts G., Flower D.R., Hartquist T.W., Dalgarno A. 1986, MNRAS, 220, 801
Porter D.H., Pouquet A., & Woodward P.R. 1992, PRL, 68, 3156
Porter D.H., Pouquet A., & Woodward P.R. 1993, *Theor. Comp. Fluid Dynamics* in press
Porter D.H., Pouquet A., & Woodward P.R. 1994, *Phys. Fluids A* in press
Pound, M.W., Bania, T.M. & Wilson, R.W. 1990 ApJ, 351 165
Pouquet, A., Passot, T. & Léorat J. 1991 in *Fragmentation of molecular clouds and Star Formation*, E. Falgarone et al. eds., Kluwer: Dordrecht
Scalo, J. M. 1987 in *Interstellar processes*, D.J. Hollenbach & H.A Thronson eds., Reidel Pub.:Dordrecht
Scalo, J.M. 1990 in *Physical Processes in Fragmentation and Star Formation* R. Capuzzo–Dolcetta et al. eds., Kluwer: Dordrecht
Schwarz, K.W. 1990 PRL, 64, 415 She, Z.-S. 1991 PRL 66 600
She, Z.-S. & Orszag, S. 1991 PRL 66 1701
Solomon, P.M., Rivolo, A.R., Barrett, J. & Yahil A. 1987 ApJ 319 730
Sreenivasan K.R. 1991 *Ann. Rev. Fluid Mech.*, 23, 539
Vincent, A. & Meneguzzi, M. 1991, JFM, 225, 1
Völk H.J., Jones F.C., Morfill G.E. & Röser S. 1980 A&A, 85, 316
Wakker, B.P.1990 PhD Thesis, University of Gronongen, The Netherlands
Wolfire, M.G., Hollenbach, D., & Tielens A.G.G.M. 1993 ApJ 402 195
Zimmermann, T. 1993, PhD Thesis, University of Köln, Germany.

Multiscale Structural Analysis of Perseus

W. D. Langer [1], R. W. Wilson [2], C. H. Anderson [3], and A. Castets [4]

1. MS 169-506, Jet Propulsion Laboratory, Caltech, Pasadena, CA 91109.
2. HOH-L239, AT&T Bell Laboratories, Holmdel, NJ 07733.
3. Box 8108, Washington University School of Medicine, St. Louis, MO 63110.
4. BP 53X, Observatoire de Grenoble, F-38041 Grenoble Cedex, France.

To study the structure and dynamics of interstellar clouds observers have mapped them on different scales and to different degrees, mainly with the isotopes of CO, CS, and 100 and 60 micron infrared dust emission. To interpret the maps one needs a method to extract structural features and determine their properties. Several approaches have been applied and discussed in the literature (c.f. Stutzki and Güsten 1990; Houlahan and Scalo 1992). Recently we suggested that multiscale Laplacian pyramid transforms (LPT) are very suitable for determining the structure of interstellar clouds (Langer, Wilson, and Anderson 1993). The best known example of the multiscale transform is the wavelet transform (c.f. Farge 1992). Multiscale transforms provide a mathematically consistent way to extract structural components and map properties from astronomical images. It has been characterized as a generalization of the Fourier Transform which is capable of representing a function in terms of spatial and frequency localization. The localized structures at different scales are easier to identify in the transformed space than in the original (x,y) space. Here we apply a multiscale transform analysis to ^{13}CO maps of the Perseus region and compare it to infrared cirrus emission.

Laplacian pyramid transforms preceded and spurred the recent interest by mathematicians in the more formalized orthogonal wavelets. One of the major difficulties with the orthogonal wavelets is that while their basis functions display shift and scale invariant properties, the coefficients in these expansions do not (Simoncelli et al. 1992). The simple variant used here is called an FSD (Filter, Subtract, and Decimate) pyramid. Starting with the original image, designated as $G_0(x,y)$, the following rules are applied recursively to create a sequence of lowpass images (or Gaussian levels) $G_n(x,y)$ and bandpass (or Laplacian levels) $L_n(x,y)$: (1) $\hat{G}_{n+1} = H*G_n$ (Filter); (2) $L_n = G_n - \hat{G}_{n+1}$ (Subtract); and, (3) $G_{n+1} =$ (Decimate) $\hat{G}_{n+1}$.

The operation $H*G_n$ convolves the image G_n with a lowpass filter H. A separable filter, $H(x,y) = h(x)h(y)$, was used here with a five tap filter for $h(x)$ having the values 1/16, 1/4, 3/8, 1/4, 1/16, which produces an approximately circularly symmetric filter in the spatial frequency domain. The Laplacian components, L_n, are computed by subtracting the low pass version from the unblurred one at each scale. This operation is equivalent to filtering with a "Mexican hat" or difference of a Gaussian-like shaped kernal. The blurred version, G_n, is then subsampled by throwing away every other pixel and row, which is traditionally called "decimation". Typically the final level N is set when the smallest dimension of the array $G_{n+1}(x,y)$ would be no smaller than eight. Mathematically, the set of values $L_n(x,y)$ for n = 0 to N plus G_{N+1}, constitute the components of an overcomplete non-orthogonal wavelet decomposition of the original image G_0. The LPT applied to the integrated intensity ^{13}CO image of the Perseus region (Figure 1a) generates a set of amplitude maps for each of the basis functions, ranging from L_0 to L_5 covering the smallest to largest scales (1' to 32'). The L_n images represent the detailed information and have equal positive and negative areas (average over the maps is zero). Examples can be seen in Langer et al. (1993).

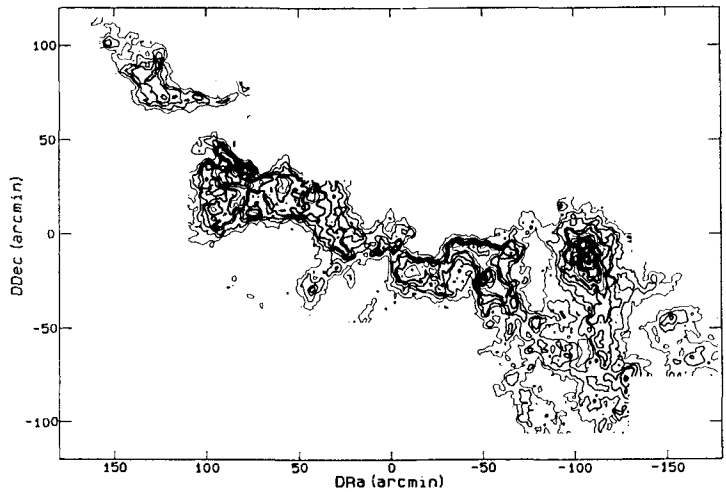

Figure 1 ^{13}CO integrated intensity map of Perseus from AT&T Bell Labs (1' map).

We have calculated the global wavelet energy spectrum, E(l) = $\int$ f(l,x,y)^{2}dA, where f(l,x,y) = amplitude of the wavelet basis function as a function of the space-scale l. This quantity is the analog of the Fourier energy spectrum and measures the distribution of intensity at different localizations. The results for Perseus are displayed in Fig. 2 along with those from 100 micron IRAS maps for the Chameleon and North Polar Cirrus (NPC) regions. Most of the power is at the largest scale-sizes, but there is a difference at small scales in the three regions. The power maps show more power at small scales in Perseus compared to Chameleon which is larger than that in the North Polar Cirrus. The more highly evolved clouds in the sense of the formation of denser, small scale structures the more power is present at small scales.

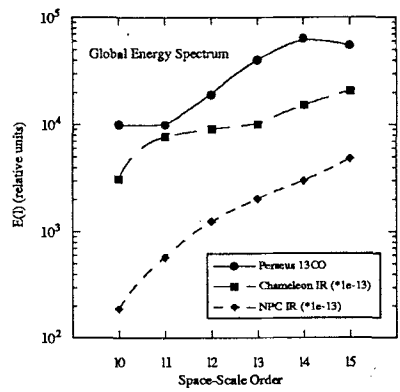

Fig. 2 Global wavelet energy spectrum: ^{13}CO - Perseus, 100μm - Chameleon & NPC

One measure of the morphology of the cloud structures is the Hausdorff (fractal) dimension (Bazell and Desert 1988, Dickman et al. 1990) of objects in the cloud, D, defined as, A$^{0.5}$ = K P$^{1/D}$, where A and P are area and perimeter, respectively. D = 4/3, characterizes the relationship expected for Kolmogorov turbulence. Filamentary structures that scale only with length have D $\approx$ 2, as would be characteristic of gas supported by magnetic fields in the radial direction. For each Laplacian image we determined P and A of the connected positive features (Langer et al. 1993). Figure 3a plots D as a function of the l value and shows significant variation with space-scale in contrast to the results of Bazell and Desert who found roughly constant average value, D $\approx$ 1.25, for the cirrus clouds. Dickman et al.'s

study of 100 micron maps of molecular regions found a similar value for D. Both groups used a contour finding technique, completely different from that used here.

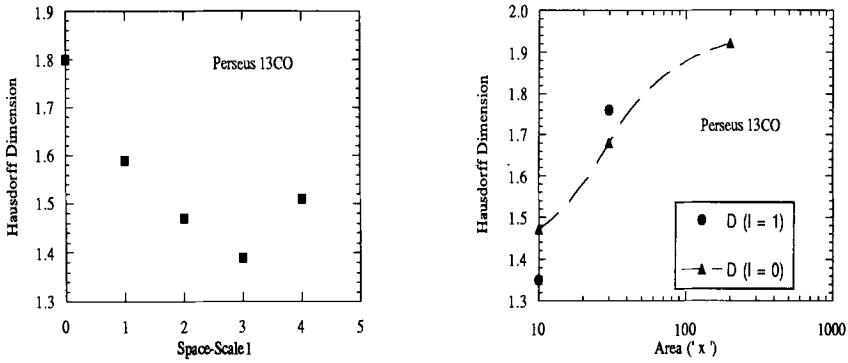

Fig. 3a) D versus space-scale l_n for all map features; b) D versus area range for l = 1.

Determining the Hausdorff dimension as a function of area (within an l map) yields somewhat different results. Figure 3b plots D for the n = 1 ($\lambda \approx 2$) image in four different area ranges. For the smallest features D $\approx$ 1.25, but it increases with area reaching a value about 2 for the largest objects in the image. As the n = 1 map corresponds to features that respond to a multiscale filter of about 2' (in at least one direction) the largest features resemble thin filamentary or web-like structures. These results suggests that the Perseus region is multi-fractal and that different forces dominate on different scales.

The research of WDL was carried out by the Jet Propulsion Laboratory, California Institute of Technology, under contract with NASA.

References

Bazell, D. and Desert, F. X. 1988, ApJ, 333, 353 .
Dickman, R. L., Horvath, M. A.,and Margulis, M. 1990, ApJ, 365, 586.
Farge, M. 1992, Ann. Rev. Fluid Mech., 24, 395.
Houlahan, P. and Scalo, J. 1992, ApJ, 393, 172.
Langer, W. D., Wilson, R. W., and Anderson, C. H. 1993, ApJ Letters, 408, L45.
Simoncelli, E. P., Freeman, W. T., Adelson, E. H., and Heeger, D. J., 1992, IEEE Trans., Info. Theory, Special Issue on Wavelets, 38, 587.
Stutzki, J. and Gusten, R. 1990, ApJ, 356, 513.

Nonlinear Waves and Solitons in Molecular Clouds

R. Watkins, F.C. Adams, M. Fatuzzo, and C. Gehman

Physics Dept., University of Michigan, Ann Arbor, MI 48109 U.S.A.

Molecular clouds are self-gravitating fluid systems and are capable of supporting a wide variety of oscillatory motions. The overall goal of this work is to understand the dynamics of volume density waves in molecular clouds and to explore the extent to which waves can explain the observed cloud structure. Our working hypothesis is that volume density wave motions can produce (at least in part) this complicated structure.

Self-gravity is an important ingredient for the existence of stationary nonlinear waves in a neutral fluid. In the absence of self-gravity, acoustic waves in fluids are known to steepen and shock. On the other hand, self-gravity provides dispersion which tends to spread out wave packets. Thus, fluids with self-gravity can, in principle, reach a balance between nonlinear steepening and gravitational dispersion. This balance leads to the possibility of nonlinear stationary waves and solitary waves, which we discuss in this contribution (see also Yueh 1981; Adams & Fatuzzo 1993; Adams, Fatuzzo, and Watkins, 1993).

We begin with the equations of motion for a molecular cloud fluid in one spatial dimension written in dimensionless form:

$$\frac{\partial \rho}{\partial t} + \frac{\partial}{\partial x}(\rho u) = 0, \tag{1}$$

$$\frac{\partial u}{\partial t} + u\frac{\partial u}{\partial x} + \frac{1}{\rho}\frac{\partial p}{\partial x} + \frac{\partial \psi}{\partial x} = 0, \tag{2}$$

$$\frac{\partial^2 \psi}{\partial x^2} = q(\rho), \tag{3}$$

where we will take the pressure of the molecular cloud fluid to have a general barotropic form, $p = p(\rho)$. In these equations we have generalized the Poisson equation by introducing a "charge density", $q(\rho)$. This generalization allows us to model a wide variety of behavior while retaining a high level of solvability.

Our interests lie in stationary waves, which correspond to traveling waves of permanent form. For these waves, the fluid fields are functions only of the quantity

$$\xi = x - v_0 t, \tag{4}$$

where v_0 is the (nondimensional) speed of the wave. Next, we introduce a new velocity variable $v = u - v_0$, which is simply the speed of the fluid relative to the speed v_0 of the wave. Using the above definitions in the continuity equation [1], we find the relation

$$\rho v = A = constant, \tag{5}$$

where the constant of integration A is the "Mach number" of the wave.

We can reduce the entire set of equations into a single nonlinear differential equation for the density ρ. This equation can be integrated once to give

$$\frac{1}{2}\rho_\xi^2 = \rho^6\left[\rho^2\frac{\partial p}{\partial \rho} - A^2\right]^{-2} f(\rho), \tag{6}$$

where $f(\rho)$ is given by

$$f(\rho) = \int^\rho d\rho \frac{q(\rho)}{\rho}\left[\frac{A^2}{\rho^2} - \frac{\partial p}{\partial \rho}\right]. \tag{7}$$

Given equation [6], we can determine the existence or non-existence of stationary waves for a particular physical system through the methods of phase plane analysis (see, e.g., Infeld & Rowlands 1990).

The simplest nontrivial example of a charge density is $q(\rho) = \rho - \rho_0$. This $q(\rho)$ puts the Poisson equation into the form used in the usual Jeans analysis, and is equivalent to subtracting out the contribution of the background fluid from the gravitational potential. In this theory we have found stationary nonlinear wave solutions, which differ in many important ways from their linear counterparts. For example, we find that there is both a minimum and a maximum wavelength for a wave with a given density contrast. For highly nonlinear waves, the allowed range of wavelengths can be extremely narrow.

These results have a relatively simple interpretation. For stationary waves, a balance must exist between dispersion, which acts to spread the wave, and nonlinear effects, which act to steepen the wave and cause it to shock. For the case at hand, the dispersion is supplied entirely by the self-gravitational interaction. For waves with $\delta\rho/\rho \gtrsim 1$, nonlinear effects will be large. To balance these large nonlinear effects, the effects of self-gravity must also be large, hence the observation that the natural length scale for nonlinear stationary waves is of order the Jeans length.

We can also derive a charge density for theories in which gravity is modeled by a Yukawa potential. The motivation for this approximation is to include the effects of a decreasing gravitational field strength while retaining the one-dimensional treatment of the problem. Here we write the Poisson equation in the generalized form

$$\frac{\partial^2 \psi}{\partial x^2} = m^2 \psi + \rho \,, \tag{8}$$

which implies an exponential fall off $\propto e^{-mx}$ in the gravitational force between point masses.

Using the stationary wave approximation, we can write equation [8] as a charge density theory by integrating the force equation and solving for ψ in terms of ρ. In this way we obtain:

$$q(\rho) = \rho + m^2 \left[E - h(\rho) - \frac{A^2}{2\rho^2} \right] . \tag{9}$$

An analysis of this theory shows that it has stationary nonlinear waves similar to those described for Jeans theory above. However, this theory also allows for special stationary waves known as solitons, or solitary waves. These solutions are stationary waves that are localized in space and approach a constant at spatial infinity.

The first obvious signature of wave motions in molecular clouds is periodic or nearly periodic structures. Several examples can be found in the existing literature (McBreen et al. 1979; Schneider & Elmegreen 1979; Shuter, Dickman,& Klatt 1987). Periodicity, however, is not enough to establish the existence of the waves discussed in this paper. Fortunately, a characteristic observable signature of these stationary waves is the relation given by the continuity equation: $\rho v = A$. If we observe a candidate wave train in a molecular cloud, then the observed line-center velocity (along the propagation direction of the wave) should vary inversely with the density.

One example of stationary wave behavior in an observed molecular cloud may be provided by the Lynds 204 complex (McCutcheon et al. 1986). This cloud is highly elongated and shows periodic structure in column density with a wavelength of $\sim 1^\circ$ ($\sim$3 pc for an assumed distance to the cloud of 160 pc). In addition, these authors find that the line of sight velocities (of CO line observations) along the filament are very well correlated with the density enhancements in the sense that the most massive parts of the filament have the smallest velocity displacement from the mean v_0. Finally, the authors derive the relation $M_j(v_j - v_0) = \textit{constant}$, where M_j and v_j are the mass and velocity of the jth segment of the filament. This relation looks suspiciously like the solution to the one dimensional continuity equation for a stationary wave.

We have also found that nonlinear stationary waves select out particular lengthscales for their wavelengths The observed wavelength should thus be a calculable function of the various physical parameters involved (wave amplitude, sound speed, magnetic field strength, etc.). Although several parameters are necessary to completely specify the preferred wavelength (or range of wavelengths), all of the parameters are physical quantities and can be determined, in principle, independently of the observations of the wavelengths.

Another observable quantity is the relative widths of the waves. The candidate wavetrains in molecular cloud regions appear as chains of "blobs" which are (more or less) lined up and regularly spaced. The aspect ratio of these blobs (at a chosen density contour) is thus a well-defined observable quantity (this aspect ratio has a value of 3 ± 1 for the sample of Schneider & Elmegreen 1979). We are currently studying stationary waves on filaments and can obtain a prediction for the relative widths of the wavetrains (Gehman et al. 1993) as a function of the physical parameters of the problem.

References

Adams, F. C., & Fatuzzo, M. 1993, *ApJ*, **403**, 142
Adams, F. C., Fatuzzo, M., & Watkins, R. 1993, *ApJ.*, in press.
Gehman, C., Adams, F. C., Fatuzzo, M., & Watkins, R. 1993, in preparation
Infeld, E., & Rowlands, G. 1990, Nonlinear Waves, Solitons, and Chaos (Cambridge: Cambridge University Press)
McBreen, B., Fazio, G. G., Stier, M., & Wright, E. L. 1979, *ApJ*, **232**, L183
McCutcheon, W. H., et. al 1986, *ApJ*, **309**, 619
Schneider, S., & Elmegreen, B. G. 1979, *ApJ*, **41**, 87
Shuter, W. L., Dickman, R. L., & Klatt, C. 1987, *ApJ*, **322**, L103
Yueh, T.Y. 1981, *Studies in Applied Mathematics*, **65**, 1

The Formation, Evolution, and Disruption of Molecular Clouds: The Influence of Massive Stars

John Bally

Center for Astrophysics and Space Astronomy, Campus Box 389, University of Colorado, Boulder, CO 80309

It is possible to combine proper motions, radial velocities, and distances near the Sun to construct a 3 dimensional picture of the distribution of nearby young stars. By making associations with clouds, one can reconstruct the recent (< 50 Myr) evolutionary history of the local ISM and investigate the origin, evolution, and destruction of molecular clouds.

Gas within about 500 pc of the Sun appears to be part of an expanding ($V_{exp} \approx 5$ kms^{-1}) network of molecular clouds (Dame et al. 1987) and HI (Lindblad 1967) associated with the local population of B and A stars known as Gould's Belt. The gas dynamics of Gould's Belt has been modeled by Olano (1982) as an expanding remnant supershell produced by a massive OB association about 30 Myrs ago. Blaauw (1991) argues that a large angular diameter (≈ 1 steradian) group of stars identified by common radial velocities and proper motions, the Cas-Tau "fossil" OB association (which is centered on the α-Persi open star cluster), may be the remnant of the massive OB association which set the supershell in motion. A half dozen giant molecular clouds and 3 or 4 OB associations younger than 15 Myr (including the Ori OB1, Per OB2, Sco-Cen, and perhaps the Lac OB1 associations) delineate the Gould's Belt/Lindblad ring system. These complexes may have condensed from the expanding supershell by gravitational instabilities (McCray and Kafatos 1987; Elmegreen 1982, 1993).

As the progenitor supershell expanded into the local ISM, it swept up over $10^6 M_\odot$ of low density gas. The evolution of supershells are influenced by a variety of physical processes once their size becomes greater than 100 pc or so. These include: [1] *Shear.* Differential rotation of the galaxy elongates the shell along the shear direction after about 10^7 yrs (Olano 1982). [2] *Blow-out.* When the shell radius becomes comparable to the thickness of the galactic gas layer, the shell expands more orthogonal to the Galactic plane than along it. Energetic shells can burst into the halo (Mac Low et al. 1989). [3] *Magnetic fields.* Magnetic fields inhibit blowout and compression in those directions where the expansion velocity is orthogonal to the field direction (Ferrier et al. 1991). [4] *Clumpy ISM.* The shell propagates fast in low density gas and slowly in high density gas. Dense clouds are overrun, overpressured, and compressed. Low density gas is swept-up in a decelerating shell. [5] *Non-coeval star formation.* The supershell is driven by the combined effects of photo-ionization and ablation, stellar winds, and supernova explosions. The energy and momentum injection rate is governed by the birth rate of massive stars (Saken & Shull - in preparation). [6] *Ablation and poisoning.* UV radiation ablates clouds trapped in the supershell, injecting plasma into the bubble which can radiatively cool the shock-heated interior, effectively "poisoning" it and forcing the shell into momentum conserving conditions. [7] *Gravitational Instabilities.* The expanding shell becomes gravitationally unstable, forming 10^5 $M_\odot$ clouds when the flow divergence from a given region becomes less than the escape velocity from the same region. For the Gould's Belt, this is expected to occur 10 to 20 Myr after the birth of the progenitor OB association (McCray & Kafatos 1987). The Gould's Belt may potentially fragment into 5 to 10 GMCs. [8] *Spiral density waves.* By increasing the mean pressure of the ISM, spiral density waves may enhance cloud formation in a shell. Conversely, the decreased ISM pressure in an inter-arm region may favor blowout and decrease cloud formation efficiency.

Gravitational fragmentation of the Gould's Belt supershell may have led to the formation of the molecular clouds now spawning the Orion, Perseus OB2, Sco-Cen, and Lacerta-1 OB associations and most local dark clouds including the Great Rift extending from Cygnus to Ophiucus. These clouds are the remnant debris of the tidally sheared and fragmented supershell produced by the Cas-Tau group. Since the age of the shell exceeds one quarter of

the z-oscillation time in the gravitational potential of the Galactic disk, dense gas ejected out of the plane is now expected to be falling back towards the Galactic plane, in agreement with the results of 21 cm all-sky HI surveys which show excess negative velocities towards high galactic latitudes. Furthermore, the lowest column density of gas (the "Lockman Hole") and dust as seen by the COBE satellite ("Baade's Hole") is found directly above and below the centroid of the Cas-Tau group and the center of the Gould's Belt expansion (towards $l = 150^o$, $b = +/- 50^o$) indicating that the parent supershell has nearly blown out of the Galactic disk. The stellar fossil record, and the distribution and velocity field of gas and dust in the Solar vicinity indicate that massive star formation has had a dominant role in the formation, evolution, and destruction of GMCs, and together with galactic dynamics, determined the kinematics, distribution, and other properties of the local ISM. Ram pressure assisted collapse may provide a more efficient cloud formation mechanism than gravitational instabilities of the Parker-Jeans type (Elmegreen 1982) or Parker-Jeans-Toomre type (Elmegreen 1989, 1991).

The Orion region provides a specific and well studied example of the interaction of OB stars with their surrounding interstellar medium. The expansion of Gould's Belt started sweeping up gas in the direction of Orion about 30 Myr ago. About 10 to 20 Myr ago, a large fragment of the supershell suffered gravitational collapse, leading to the formation of the proto-Orion cloud. By a little over 10 Myr ago, massive star formation started in the cloud near the present location of the OB1a sub-group of the Orion OB association.

The parts of the cloud nearest the luminosity centroid of the Orion OB association are dense and show signs of having been accelerated. The Oort-Spitzer rocket effect has imparted a net redshift to the molecular gas, which is seen as a velocity gradient in the Orion clouds (Maddalena et al. 1986). The projected interior of the Orion superbubble contains several dozen smaller clouds ($M_{cloud} \approx 10^3 M_\odot$) exhibiting cometary morphologies with the axes of symmetry pointing towards the center of the OB association (Bally et al. 1990). These morphological and kinematic features indicate that cloud evolution is profoundly affected by the OB association.

Orion appears to be driving a young supershell back into the debris left behind by the Gould's Belt expansion. A large 300 pc superbubble appears to be engulfing the remaining molecular clouds (Cowie et al 1979). The inner edge of the shell can be seen by Hα emission and extends from Barnard's Loop in the east to the Eridanus Loop 30^o to the west (Sivan 1974). This shell is expanding with a velocity of about 15 km s^{-1} with a substantial velocity component (at least 10 *km* s^{-1}) *towards* our line of sight (Reynolds & Ogden 1979). H I surveys show a filamentary network of clouds outside of the optical emission (Heiles 1984). Soft X-ray emission seen towards Eridanus provides evidence of hot gas in the Orion supershell interior. The elongation of this bubble towards high Galactic latitudes is naturally explained by the decrease in ambient gas density above the plane.

References

Bally, J. et al. 1991 in *Fragmentation of Molecular Clouds and Star Formation* ed E. Falgarone, F. Boulanger, and G. Duvert, p. 11
Blaauw, A. 1991 in *The Physics of Star Formation and Early Stellar Evolution* ed: C. J. Lada, and N. D. Kylafis, p. 125
Cowie, L. L., Songaila, A. and York, D. G. 1979, ApJ, 230, 469
Dame, T. M. and 8 others, ApJ, 322, 706
Elmegreen, B. G. 1982 in *Submillimeter Wave Astronomy* eds. J. E. Beckman and J. P. Phillips, p. 3
Elmegreen, B. G. 1989 ApJ, 344, 306; 1991 ApJ, 378, 139
Elmegreen, B. G. 1993 in *Protostars & Planets III* eds. E. H. Levy and J. I. Luine, p 97
Ferriere, K. M., Mac Low, M. M. and Zweibel, E. G. 1991, ApJ, 375, 239
Heiles, C. 1984, ApJSuppl., 55, 585
Lindblad, P. O. 1967 *Bull.Astron.Inst.Neth.*, 19, 34
Mac Low, M. M., McCray, R. and Norman, M. L. 1989, ApJ, 337, 141
Maddalena, R. J., Morris, M., Moscovitz, J., and Thaddeus, P. 1986 ApJ, 303, 375
McCray, R. and Kafatos, M. 1987, ApJ, 317, 190
Olano, C. A. 1982 A&A, 112, 195
Reynolds, R. J. and Ogden, P. M. 1979, ApJ, 229, 942
Sivan, J. P. 1974 A&ASuppl., 16, 163

Molecular Absorption in Interstellar Clouds Observed with the Plateau de Bure Interferometer

R. Lucas[1], H.S. Liszt[2]

[1] Institut de Radioastronomie Millimétrique,
300 rue de la Piscine, F-38406 Saint Martin d'Hères, France
[2] National Radio Astronomy Observatory,
520 Edgemont Road, Charlottesville, VA, USA 22903-2475

Measurements of millimeter wavelength lines observed in absorption provide a direct determination of the optical depths in molecular clouds. We expect that these studies should improve our understanding of the structure of molecular clouds, and of line formation mechanisms. Ideally statistics of the optical depth on numerous lines of sight (with a spatial resolution only limited by the angular size of the background source) should constrain fundamental parameters such as area and velocity filling factors. Furthermore, such optical depth measurements provide highly accurate measurements of the molecular abundances, since the molecular excitation status is well determined by the emission measurements, or even by the total abscence of emission, in which case the molecules are in equilibrium with the cosmic microwave background radiation at 2.7 K.

The use of extragalactic background sources allow the study of molecular clouds unperturbed by recent high–mass star formation and its consequences, as might be the case with galactic compact HII regions or supernova remnants. The sources have also the advantage of their very small angular size at millimeter wavelengths, thus upgrading the resolution of absorption studies to the milliarcsecond range. A search for continuum sources suitable for millimeter absorption studies has been performed by Liszt and Wilson (1993). In their survey of ~ 100 sources, they found 10 lines of sight with detectable ^{12}CO emission. Among those, only 0212+735 , 0355+508 (NRAO 150), and 2200+420 (BL Lac) present strong ^{13}CO emission and were selected as the first objects to study. BL Lac had been previously studied by Marscher et al. (1991), who observed it at the frequency of ^{12}CO(1→0) with the Owens Valley millimeter–wave interferometer, and found an optically thick absorption line, with a velocity width about equal to that seen in emission.

The ^{12}CO(1→0) line, as a tool to study molecular clouds in absorption, suffers however from severe drawbacks: it occurs in a relatively noisy region of the telluric spectrum, is very opaque, and is very sensitive to unresolved fluctuations in the foreground emission. We decided to use instead the weaker, but optically thin, ^{13}CO(1→0) line. The observations were done in January–February 1993 (Liszt and Lucas 1993). In May 1993 we took advantage of a flare of BL Lac, the flux of which increased from 2 Jy by about a factor of 2, to detect the $1 \rightarrow 0$ transitions of HCN, HCO$^+$, CN, CCH, and HNC (Lucas and Liszt 1993a). In July we measured absorption spectra of HCN and HCO$^+$in the two other sources (Lucas and Liszt 1993b). Using the Kitt Peak 12m and Pico Veleta 30m telescopes, we have mapped $1 \rightarrow 0$ and $2 \rightarrow 1$ emission lines of ^{12}CO and ^{13}CO around the continuum sources (Liszt and Lucas 1993); emission from HCO$^+$ or HCN was undetected, except for HCO$^+$ emission in front of BL Lac (Lucas and Liszt 1993a). Most of the data are displayed in Fig. 1-3.

^{13}CO was detected in all of 4 (may be 5) of the clouds seen in ^{13}CO(1→0) emission. The observed optical depths may be compared to the "apparent" optical depths one could determine with emission results alone, that is, in the traditional manner in which one assumes (i) that the ^{12}CO(1→0) radiation temperature is a measurement of its excitation temperature, since this line is saturated, and (ii) that the ^{13}CO and ^{12}CO excitation temperatures are equal. One finds a very good correlation between the true and apparent optical depths (Fig. 4). The true optical depths are in fact systematically higher by $\sim 25 - 50\%$, indicating that the ^{12}CO(1→0) excitation temperatures are higher that those of ^{13}CO, due to radiative trapping in the ^{12}CO(1→0) line. LVG analyses provide a good fit of all the available emission and absorption data, with temperatures of about 7 K, pressures in the range $3 - 5 \times 10^4$ cm^{-3} K, and *areal covering factors close to unity* for all clouds.

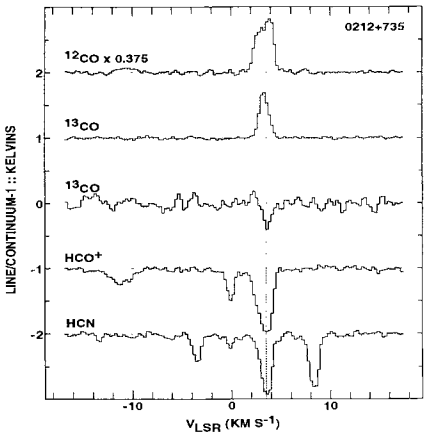

Figure 1: ^{12}CO and ^{13}CO emission, ^{13}CO, HCO^+ and HCN absorption in front of 0212+735

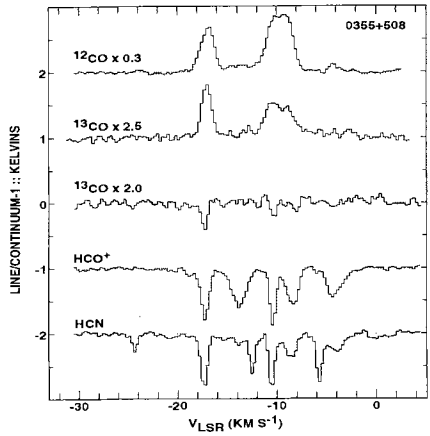

Figure 2: Same but for 0355+508 (NRAO 150)

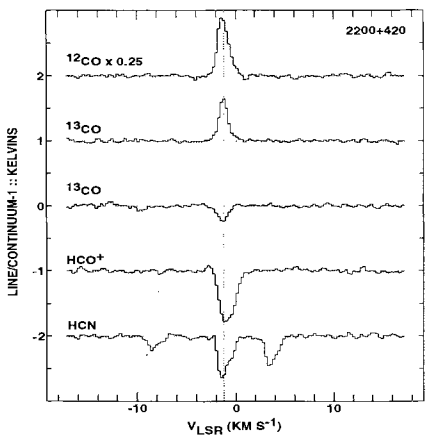

Figure 3: Same but for 2200+420 (BL Lac)

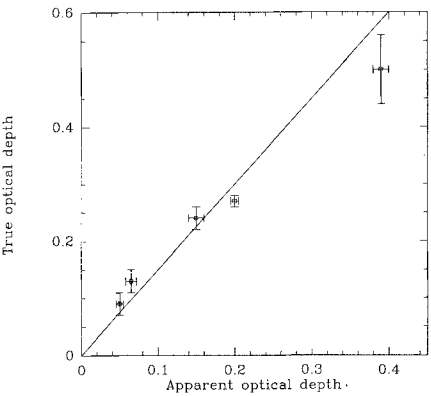

Figure 4: The ^{13}CO optical depths measured from ^{13}CO absorption versus the apparent optical depths (as deduced from ^{12}CO and ^{13}CO emission lines)

In the direction of BL Lac, the observed optical depths of the various molecules provide highly reliable total column densities, since the abscence (or weak intensity, in the case of HCO^+), of emission lines constrains the excitation temperatures to values very close to the cosmic background temperature. The relative abundances of ^{13}CO, HCO^+, HCN, CN and C_2H are typical of dark clouds such as TMC1, but N_2H^+ and HNC are deficient by factors of $3-6$.

In the directions of 0215+735 and 0355+508, the HCO^+ absorption profiles have remarkably more and/or wider lines than present in ^{13}CO: some very strong HCO^+ components are absent in the ^{13}CO emission profiles and either quite weak or absent even in ^{12}CO emission. We are able to derive reliable abundance ratios for 10 clouds detected in the three sources altogether: the $N_{^{13}CO}/N_{HCO^+}$ ratio ranges from 70 to 630, while N_{HCN}/N_{HCO^+} ranges from 0.71 to 3.1. Such variations can be easily reproduced by varying the conditions in models of dark cloud chemistry (Langer and Graedel 1989). Our observations seem to show that species like HCO^+ and HCN, observed in absorption, are the most sensitive probes for the presence of molecular gas.

References

Langer, W. D., Graedel, T. E. 1989, ApJS, 69, 241
Liszt, H. S., Wilson, R. W. 1993, ApJ, 403, 663
Liszt, H.S., Lucas, R. 1993, in preparation
Lucas, R., Liszt, H.S. 1993a, A&A 276, L33
Lucas, R., Liszt, H.S. 1993b, A&A (submitted)
Marscher, A. P., Bania, T. M., Wang, Z. 1991, ApJ, 371, L77

Dynamical Modelling of Self-Gravitating Magnetic Clouds

Z.Y.Yue[1,2], B.Zhang[1,2], G.Winnewisser[1], and J.Stutzki[1]

[1]I. Physikalisches Institut, Universität zu Köln, 50937 Köln, Germany
[2]Department of Geophysics, Beijing University, Beijing, China

1. Two-dimensional MHD modelling

The purpose of this modelling is to show that the nonlinearity of the hydrodynamic equations and self-gravity will inevitably generate the observed clumpy structure of molecular clouds. We solve the 2D MHD equations and the Poisson equation in terms of the Fourier space. The calculations of the time evolution of the density distribution from different initial states show that, as the detailed density distribution changes considerably, the fractal dimension of the density contours remains $\sim 1.4 - 1.5$ as long as the clumpy structure has been fully developed (Yue et al., 1993a,b). This insensibility of the fractal dimension to both the initial state and the evolution time is in good agreement with observations (*cf.* Zimmermann and Stutzki, 1992).

2. N-body simulation of the 3D motions of clumps in a self-gravitating magnetic cloud

We treat clumps and interclump medium separately. N bodies in our simulation only represent the clumps rather than the fluid elements. Thus, N does not have to be extremely large. By this simplification, we will be able to follow the detailed motions of the flux tubes threading the clumps in terms of the freezing-in assumption. We will also be able to study the detailed process of collisions and coalescence between clumps and the corresponding energy dissipation, the entanglements of flux tubes, and the kinetic release of some entanglements under proper conditions. The main purpose of the present simulation is to study the effect of magnetic field on the dissipation rate. The force acting on a clump is the sum of the gravitation due to other clumps, the gravitation due to the interclump medium, the magnetic tension caused by the flux tubes connected to this clump, and the magnetic pressure associated with the field strengh distribution in the interclump medium, which is connected to the density distribution of the interclump medium through a power law.

The initial velocities of the clumps are randomly oriented, with an average magnitude equal to the virial speed. The mean magnetic field is in z direction.

The entanglement situation for the case with a magnetic field such that the initial average Alfven speed is equal to the initial virial speed is shown in the following table, where N_E, N_R, and N_K are the number of entanglements which have happened, the number of kinetic release of kinks, and the number of existing kinks respectively ($N_K = N_E - N_R$), and t is the time scaled by R_0/σ_v, where R_0 is the initial radius of the cloud, and σ_v is the initial virial speed. For comparison, the corresponding numbers for another case which differs from the above one by reducing only the field strength by one half are given in parentheses in the following table.

t	0.5		1.0		1.5		2.0	
N_E	0	(12)	8	(67)	13	(137)	35	(189)
N_R	0	(0)	0	(33)	8	(91)	21	(141)
N_K	0	(12)	8	(34)	5	(46)	14	(48)

From these calculations, we obtain the following conclusions: (1) A magnetic field with an average Alfven speed close to the virial speed is able to globally support the cloud against self-gravity. (2) Such a magnetic field is also able to reduce the dissipation rate by one order of magnitude. (3) Kinetic release of entanglements is an important process because otherwise the magnetic fields would be much more irregular than observed. (4) Stronger fields are less entangled.

References

Yue,Z.Y., Zhang,B., Winnewisser,G., and Stutzki,J., 1993a, *Ann. Physik*, **2**, 9.

Yue,Z.Y., Zhang,B., Winnewisser,G., and Stutzki,J., 1993b, *Fractals*, **1**, 908.

Zimmermann,Th., and Stutzki,J., 1992, *Physica A*, **191**, 79.

KINEMATICS, FRAGMENTATION, AND HEATING OF MOLECULAR STREAMERS IN THE ORION RIDGE

J. J. Wiseman and P.T.P. Ho

Center for Astrophysics, 60 Garden St., Cambridge, MA 02138 USA

1. Observations of Filamentary Structure and Fragmentation

The extended molecular ridge of OMC-1 surrounding the Orion-KL high mass star forming core has recently been found to contain a striking pattern of long clumpy filaments which fan out to 0.5 pc from their base in Orion-KL (Martín-Pintado *et al.* 1990, Murata *et al.* 1990, Wiseman and Ho 1994). To clarify the structure and kinematics of the region over a large scale at high angular resolution (8″) and high velocity resolution (0.3 kms^{-1}), we have constructed a linear mosaic of 10 adjacent VLA fields observed in the NH_3 (1,1) and (2,2) rotation-inversion lines covering a 3′ by 8′ region encompassing the KL core. The resulting large scale image is presented in **Figure 1b**. Long streamers branch 0.5 pc to the north and northwest of the KL region at the bottom of the image. The contours represent the integrated intensity of the (1,1) transition and reveal a pattern of low mass cores spaced somewhat regularly along the filaments, possibly the result of instability and fragmentation of the filaments.
The resulting constituent cores are also of interest. The core at α = 05h32m49s, δ = -05°22′30″ contains a localized outflow (Wilson and Mauersberger 1991), evidence that these fragments may have become sites of low mass star formation.

2. Kinematics

The greyscale shades of **Figure 1b** display the first moment integral of the intensity over the (1,1) line channels and represent the velocity field of the region. The darker shades indicate higher velocity and show that the velocity of the main ridge filamentary material is about 10 kms^{-1}. The northwestern filaments are at about 8 kms^{-1} and appear to lie superimposed with the 10 kms^{-1} material in the active KL region in the southern part of the image. Fields to the south of KL show a similar bimodal velocity distribution (Wiseman and Ho 1994), suggesting the possibility that two clouds are interacting energetically (see Womack *et al.* 1991, Wang *et al.* 1993). Notably, the region of projected overlap is at the KL high mass star forming core, where such a cloud interaction could have triggered instabilities and star forming conditions. The kinematics on a small scale also show interesting gradients. The core at α = 05h32m47s, δ = -05°20′00″ has a fast gradient (30 $\mathrm{kms}^{-1}\,\mathrm{pc}^{-1}$), confirming previous evidence for core rotation in the region (Harris *et al.* 1983). Fragmenting filaments may produce unstable cores which collapse, spin up, and if they can lose their angular momentum, become sites for low mass star formation.

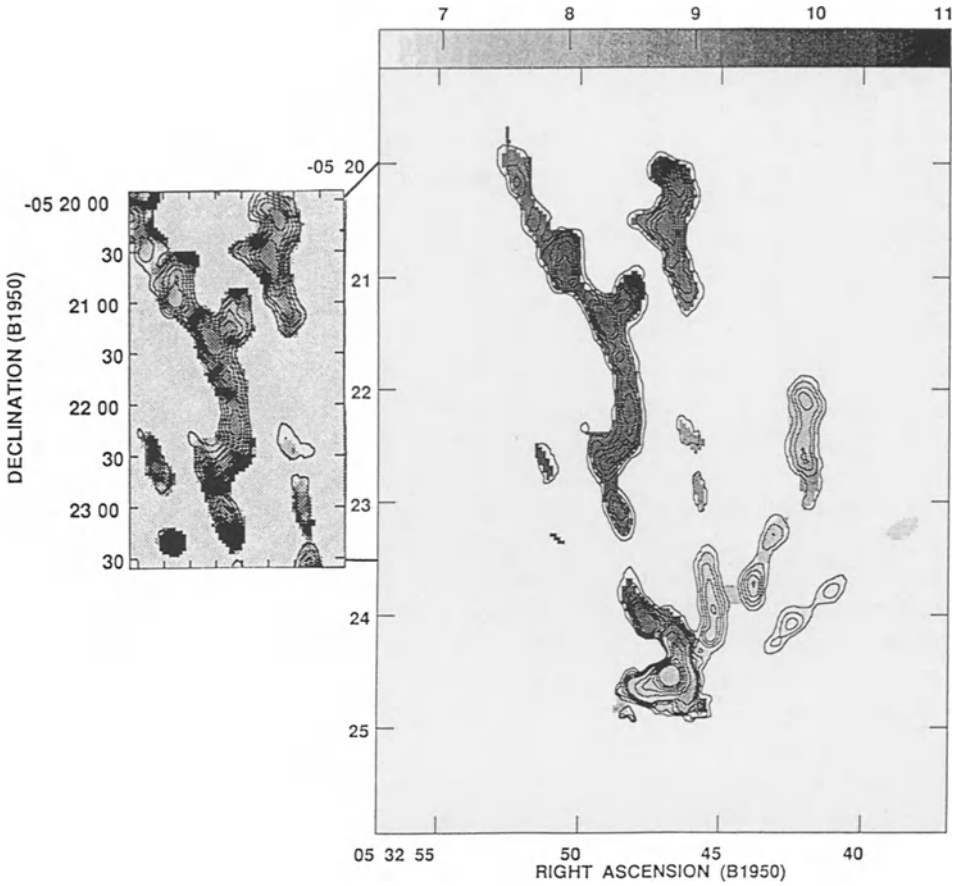

Figure 1: The OMC-1 ridge. **a, left:** The contours are the integrated NH_3 (1,1) emission for the northern filamentary region. Contour levels are 60, 120, 180, 240, 300, 600, 900, 1200, and 1500 (mJy/(8″beam))kms^{-1}. The shades are the ratio of (2,2) to (1,1) emission intensity, with darker shades representing warmer temperature. Note the edge heating toward the outflow source region to the south, and the heating between clumps along the filaments. **b, right:** The contours levels are the same as for **1a**; shades are the first moment integral of the (1,1) line representing velocity in kms^{-1}. The darker, 10 kms^{-1} main ridge filament overlaps with the western, 8 kms^{-1} filaments in the Orion-KL high mass star forming core region at the bottom of the image.

3. Heating of Clumps and Filaments

The OMC-1 filaments lie in a region of high velocity outflows emanating from young stellar objects in the Orion-KL core region, such as IRc2. Lobes of high velocity CO, shocked H_2, and an array of Herbig-Haro objects moving away from the KL core with velocities of hundreds of kilometers per second (Taylor 1984, Lane 1989) are all evidence that high velocity material is injecting energy into the surrounding environment. The shades of **Figure 1a**, created from the ratio of the NH_3 (2,2) and (1,1) transitions, represent the temperature for this part of the region of northern filaments. The darker areas are the regions with a higher ratio and correspondingly higher temperature. Two striking features are apparent here: Near the bottom of the image, facing IRc2 to the south, the core edges show strong heating effects. Similar effects have been reported in comparisons of H_2 shock emission with CS (J=1-0) maps of the filaments (Sugai *et al.* 1994, Murata 1990). H_2 emission clumps are located along the molecular filaments, avoiding the peaks of emission in the molecular cores (Sugai *et al.* 1984). The implication is that shocks from the large scale outflow may have penetrated and heated the cloud edges facing the outflow source. The other striking feature is the apparent inter-clump heating all along the ridge. These may be sheaths around the dense cores which are likely sites for turbulence and prolonged heating from the surrounding shearing outflow (Hartquist and Dyson 1993), or alternatively this effect could be the result of radiative heating from foreground O and B stars, where regions of lower density have allowed photon penetration and the production of heating gradients. Such complexities in heating, structure, and kinematics in OMC-1 reveal the rich nature and large extent of interaction between an active star forming core and its molecular environment.

References:

Harris, A., Townes, C.H., Matsakis, D. N., and Palmer, P., 1983, Ap.J., 265, L63

Lane, A. P., 1989, in *Low Mass Star Formation and Pre-Main Sequence Objects,* ESO Conference Proc. No. 33, ed. Bo Reipurth, p. 331

Martín-Pintado, J., Rodríguez-Franco, A., and Bachiller, R., 1990, Ap.J., 357, L49

Hartquist, T. W., and Dyson, J. E., 1993, Q. J. R. Astr. Soc., 34, 57

Murata, Y., Kawabe, R., Ishiguro, M., Morita, K., Kasuga, T., Takano, T., Hawegawa, T., 1990, Ap.J., 359, 125

Sugai, H., Usuda, T., Kataza, H., Tanaka, M., Inoue, M., *et al.* , 1994, Ap. J., 420, 746

Taylor, K. N, R., Storey, J. W. V., Sandell, G., Williams, P. M., and Zealey, W. J., 1984, *Nature*, 311, 236

Wang, T. Y., Wouterloot, J. G. A., and Wilson, T. L., 1994, A. A., *in press*

Wilson, T. L., and Mauersberger, T., 1991, A. A., 244, L33

Wiseman, J.J., and Ho, P. T. P., 1994, *in press*

Womack, M., Ziurys, L. M., and Sage, L. J., 1993, Ap.J., 406, L29

Large-Scale Submm-CO and FIR [CII] Observations of the Rosette Molecular Complex and S140/L1204

N. Schneider[1], S. Madden[2], J. Stutzki[1], D. Block[3], and G. Winnewisser[1]

[1] I. Physikalische Institut, Universität zu Köln, 50937 Köln, Germany
[2] MPI für extraterrestrische Physik, 8574 Garching, Germany
[3] University of the Witswatersrand, South Africa

We present extended observations of the Rosette Molecular Cloud Complex (RMC) and the S140/L1204 molecular cloud, combining [CII] 158 μm KAO observations with isotopomeric CO 3→2, 2→1 and [CI] 492 GHz KOSMA observations. The goal of this study is to investigate the large scale interaction of UV radiation and molecular clouds. We selected the RMC and S140/L1204 regions for our observations in order to cover the lower density/lower UV-intensity regime. The dispersed and clumpy morphology of the **RMC** is revealed in isotopomeric CO J=3→2 and 2→1 observations. The [CII] 158μm line shows extended emission throughout the cloud complex. Figure 1 displays the [CII] distribution (grey scale) overlayed to the intergrated CO J=3→2 intensity (contour lines). The [CII] emission is well correlated with molecular clumps traced in the submm CO lines, which we interpret to be emitted from a layer of ionized material on the surface of clumps. Additionally, the two IR-sources AFGL 961 and IRAS 06314+0427 show locally enhanced [CII] emission. Specially processed optical images show the diffuse optical emission to trace the same structure visible in CO. For a detailed comparison of the small substructures revealed in the optical, high resolution IRAM ^{13}CO J=2→1 observations were started this year. Figure 2 (top) shows the correlation of CO with the optical picture. These new data begin to resolve the small clumps, the CO contours outline the clumps visible in the optical picture. The origin of line wing emission, previously interpreted as 'interclump gas', can be attributed to several discrete velocity features. They presumable represent a blend of different cloud components accelerated by the interaction with the UV radiation or possibly influenced by embedded outflow sources. A striking correspondance between the CO and [CII] emission shows figure 2 (bottom). The peak CO emission coincidences with the position of an IRAS point source (marked as a cross), possibly indicating the presence of a young embedded star. The **S140/L1204** observations in ^{13}CO J=2→1 and ^{12}CO/^{13}CO J=3→2 exhibit the large scale structure of the molecular cloud and show that the cloud consists of three spatially and kinematicaly distinct complexes. The integrated molecular line intensity peaks at the IR-sources in the cloud core, where the ^{12}CO J=3→2 spectra exhibit broad lines, confirming the presence of an outflow source. The line wing emission is also visible in [CI] 492 GHz. The line core integrated intensity, in contrast, drops in the immediate neighbourhood of the embedded sources. The [CI] line core emission generally follows the molecular distribution. The distribution of the [CII] emission can be well matched by a clumpy cloud model, illuminated by a $1/r^2$ decreasing UV field from the single exciting star and additionally attenuated in the clumpy cloud according to Boisse's UV penetration model. This model also reproduces the large scale [CI] distribution. A [CII] emission peak in the cloud core indicates additional contribution to the carbon ionizing flux from the embedded sources.

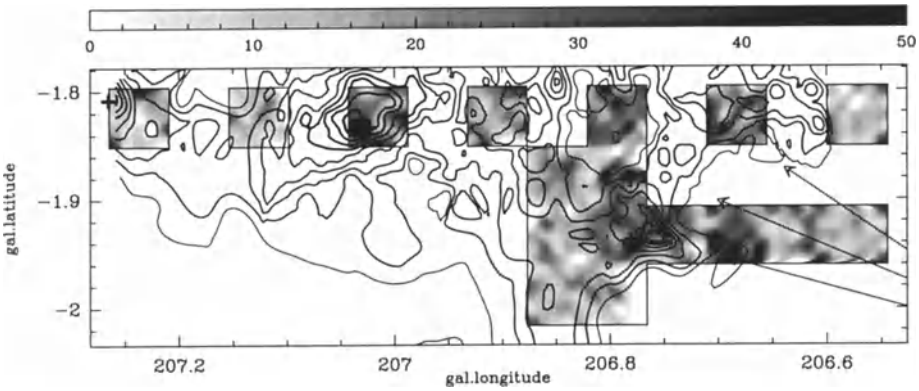

Figure 1: The Rosette Molecular Cloud complex : The integrated line intensity of the ionized carbon 158 μm fine structure line as a grey scale (in units of 10^{-5} erg s^{-1} cm^{-2} sr^{-1}) overlayed to the integrated ^{12}CO J=3→2 intensity (contours from 15 to 55 in steps of 5 K km s^{-1}.

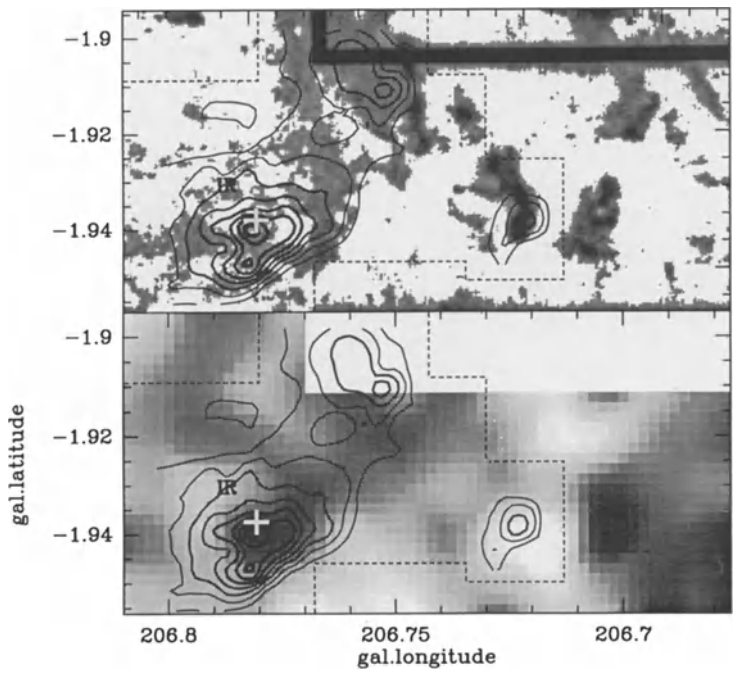

Figure 2: Small scale comparison between the high angular resolution ^{13}CO J=2→1 map (contours from 8 to 29 in steps of 3 K km s^{-1}) and the optical image (top) resp. the [CII] map (bottom). The IRAS point source IRAS 06306+0437 is marked as a cross.

2-D Monte Carlo Models of Clumpy Interstellar Clouds

Marco Spaans

Sterrewacht Leiden, P.O. Box 9513, 2300 RA Leiden, The Netherlands

Introduction and Method

Interstellar clouds are illuminated by the diffuse galactic background radiation. The dust and molecules which are ubiquitously present in the clouds attenuate part of this UV radiation leading to an increase in lifetimes of molecular species against photodissociation. So far most investigations have been based on the assumption of homogeneity. However, nowadays a large (and growing) amount of data has been gathered in different molecular lines which indicate a highly clump-like structure of interstellar clouds on different scales (Falgarone and Pérault 1988).

We have developed a two-phase model of clumpy clouds consisting of a high and low density phase (Boissé 1990). Observations (Mezger et al. 1992) seem to indicate a value of the clump-interclump density ratio of about 100. The clumpy structure is characterized by a volume filling factor F, where F is the volume of the cloud which is in the high density phase.

We use a Monte Carlo method to solve the transfer equation for the penetration of UV radiation subject to attenuation by coherent, nonconservative, anisotropic scattering from grains over the full 912-5000 Å wavelength range. We are not limited to any geometry or to any specific angular distribution of the incident radiation field. We use the grain properties of Roberge et al. (1991) and treat the H_2 and CO self-shielding in the one-line approximation. For the present investigation we have taken a slab geometry, with the radiation field incident on both sides.

Table 1: Homogeneous versus Clumpy Radiative Solutions

	F=1	F=0.5	F=0.2
A_λ	$<T>_H$	$<T>_1$	$<T>_2$
2.5	7.10×10^{-2}	1.03×10^{-1}	1.79×10^{-1}
5.0	8.96×10^{-3}	1.90×10^{-2}	5.99×10^{-2}
7.5	1.23×10^{-3}	3.79×10^{-3}	2.32×10^{-2}
10.0	1.73×10^{-4}	7.75×10^{-4}	9.41×10^{-3}
15.0	3.57×10^{-6}	3.39×10^{-5}	1.63×10^{-3}
20.0	7.42×10^{-8}	1.49×10^{-6}	2.89×10^{-4}

Results and Conclusions

Table 1 shows a comparison between clumpy and homogeneous models for λ = 1400 Å with $<T>=<I/I_0>$, the ratio between the intensity at a certain depth A_λ and the incident intensity. We furthermore show calculations of a generic model with an average density of 10^3 cm^{-3}, a volume filling factor F=25%, a clump density of 4×10^3 cm^3, a total extent of A_V=4 mag (2 pc), and illuminated by the average interstellar UV field, with I_{UV}=1, see Table 2.

The presence of clumpiness may increase the internal UV field by more than an order of magnitude at $A_V \sim 5$ with respect to the homogeneous case. The angular distribution of the incident radiation field is also important, especially in those parts of the spectrum where the radiation is scattered mainly in the forward direction. The fluctuations in measured column densities as functions of line of sight depend on the clumpiness as well as on the particular molecule. For realistic values of the filling factor this effect largely averages out as is reflected in the quantity $\sigma(N)$, which measures the scatter in column densities for various lines of sight through the cloud. The CO abundance is very sensitive to the presence of higher density gas inside the clumps for the diffuse and translucent part of the cloud. Because CO is just becoming optically thick a small shift in the transition layer with extinction due to the high density will result in a large increase in column density (van Dishoeck and Black

1988). The C^+ emission extends much further into the cloud and has a smooth underlying component, since the UV radiation may leak through the holes in the density distribution, in agreement with observations (Howe et al. 1991).

Table 2: Column Densities for Clumpy versus Homogeneous Models

Parameters and	Translucent Cloud			ζ Oph		
Species	Hom	Clumpy	$\sigma(N)[\%]$	Hom	Clumpy	Observed
n_H	1000	1000		500	500	
T_0	50	50		20	30	
F	1	0.25		1	0.6	
A_V	5.1	5.0		0.86	0.90	1.0
b	3.0	3.0		1.2	3.0	
δ_C	0.4	0.4		0.50	0.50	0.36
δ_O	0.5	0.5		0.60	0.60	
I_{UV}	1.0	1.0		4.0	4.0	
H_2	4.0(21)	4.1(21)	5.17	4.2(20)	4.5(20)	(4.2±0.3)(20)
H	1.5(20)	2.6(19)	57.3	5.3(20)	5.2(20)	(5.2±0.2)(20)
C	2.6(17)	9.6(16)	10.4	3.1(15)	2.8(15)	(3.2±0.6)(15)
C^+	7.9(17)	2.7(17)	5.82	4.5(17)	4.4(17)	(1.8±0.4)(17)
CO	3.0(17)	1.1(18)	16.5	2.0(14)	1.2(15)	(2.0±0.3)(15)
CH	5.2(14)	5.5(14)	48.0	2.1(13)	2.5(13)	(2.5±0.1)(13)
O	3.1(18)	2.2(18)	14.2	7.1(17)	6.7(17)	(4.0±0.4)(17)
OH	1.8(15)	1.0(15)	22.6	4.5(13)	4.0(13)	(4.8±0.5)(13)
H_2O	2.5(15)	7.1(14)	14.8	5.5(11)	2.9(11)	<2.2(13)

References

Boissé, P., 1990, A&A, 228, 483
Falgarone, E., Pérault, M., 1988, A&AL, 205, L1
Howe, J.E., Jaffe, D.T., Genzel, R., Stacey, G.J., 1991, ApJ, 373, 158
Mezger, P.G., Sievers, A., Zylka, R., Haslam, C.G.T., Kreysa, E., Lemke, R., 1992, A&A, 265, 743
Roberge, W.G., Jones, D., Lepp, S., Dalgarno, A., 1991, ApJ, 77, 287
van Dishoeck, E.F., Black, J.H., 1988, ApJ, 334, 771

The Clumpiness of Molecular Clouds

C. Kramer, T. Zimmermann, J. Stutzki, and G. Winnewisser
I. Physikalisches Institut, Universität zu Köln, 50937 Köln, Germany

There is ample evidence that molecular clouds exhibit structure on all scales observed down to the resolution limit. This fragmentation is best seen in velocity channel maps or position velocity maps of CO-isotopomeres like ^{13}CO. Many investigators assumed that the clouds consist of well defined basic building blocks, called clumps , and used the channel maps to identify these clumps by eye inspection. We have used two alternative, automated approaches to find clumps (Winnewisser and Herbst 1993):

The first automated algorithm (Herbertz 1992) first searches for local, clearly separable intensity maxima in the three-dimensional data cube of a cloud. If the maxima are stronger than a selected intensity and if the contrast to the neighbouring maxima is large enough, then these maxima are identified as clumps. The algorithm finds well-defined clumps but does not try to subdivide all emission into clumps. It was applied to a ^{13}CO(1→0) map of NGC1499 (Herbertz 1992) and to maps of Orion B (Kramer 1992) and L1457 (Zimmermann 1993). Lada et al. (1991) selected CS-clumps in Orion B by eye-inspection in a similar way.

The second algorithm employs an iterative least squares fitting to the peak intensity and successive substraction of Gaussian shaped clumps (Stutzki & Güsten 1990). This procedure has been applied to five clouds observed with the KOSMA 3m radiotelescope and with the IRAM 30m telescope. These clouds, namely L1457 (Zimmermann 1993), NGC1499 (Herbertz 1992), Orion B South (Kramer 1992), S140 (Johnen 1992), M17SW (Stutzki & Güsten 1990), exhibit widely different physical conditions, sizes, and masses. The clump mass range of the different sets of observations covers 3×10^{-4} $M_\odot$ to 2500 $M_\odot$. All clouds analysed show power law distributions of clump masses $dN/dM \propto M^{-\alpha}$ with the index α ranging between 1.5 and 1.7 similar to the results of other authors who identified clumps by eye inspection. The spectral index seems to be invariant to different physical parameters of clouds and seems to be a general property of molecular clouds. We discuss the distributions of clump characteristics in the different clouds.

References

Herbertz, R. 1992, Ph.D. thesis, University of Cologne
Johnen, C. 1992, Diplom thesis, University of Cologne
Kramer, C. 1992, Ph.D. thesis, University of Cologne
Kramer, C., Stutzki, J., Winnewisser, G. 1993, A&A, in preparation
Lada, E.A., Bally, J., Stark, A&A 1991, ApJ, 368, 432
Röhrig, R. 1994, Ph.D. thesis, University of Cologne, in preparation
Stutzki, J., Güsten, R. 1990, ApJ, 356, 513
Stutzki, J. 1992, to appear in Reviews of Modern Astronomy, Vol. 6
Zimmermann, T. 1993, Ph.D. thesis, University of Cologne

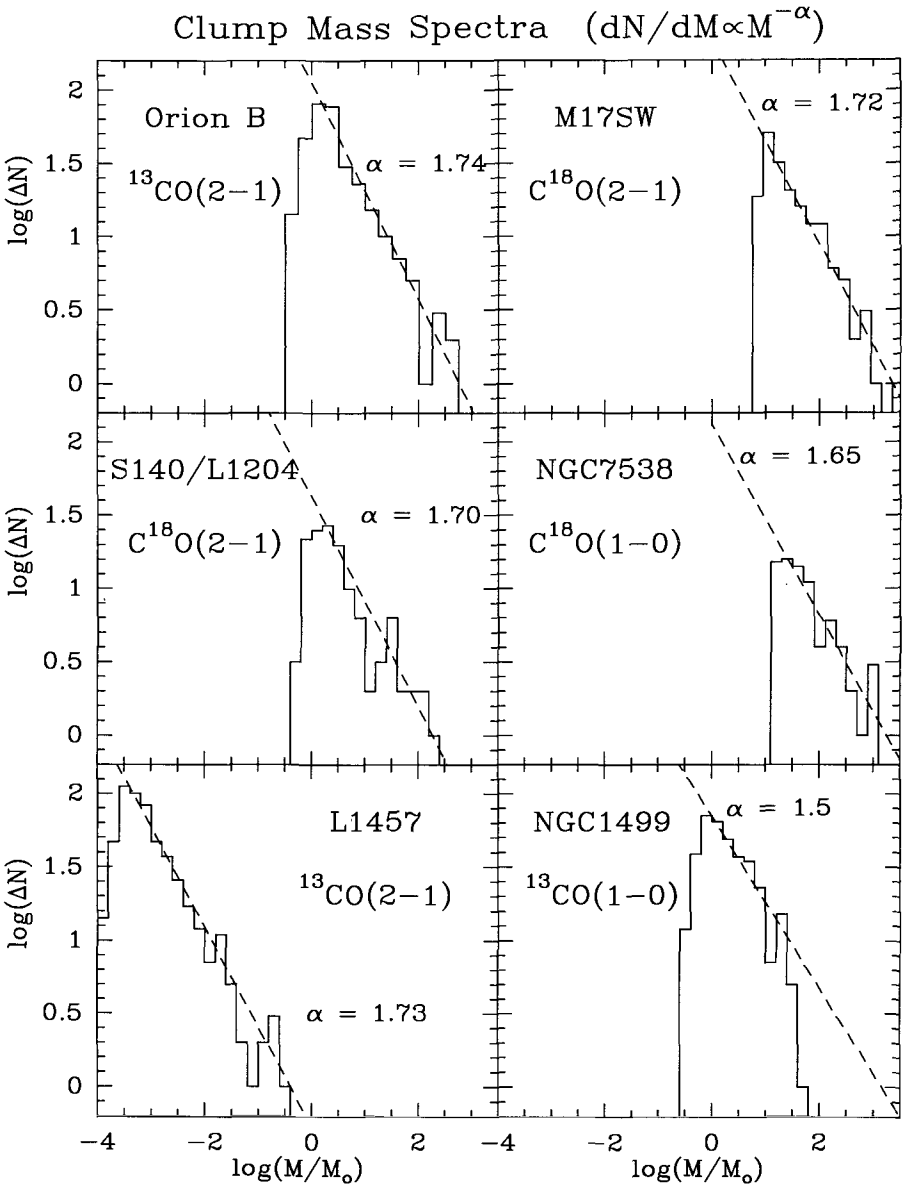

Clump mass spectra for the observed regions in the giant molecular clouds Orion B (Kramer 1992, Kramer et al. 1993), M17 SW (Stutzki & Güsten 1990), NGC7538 (Röhrig 1993), S140/L1204 (Johnen 1992) and for clouds devoid of any hints at star formation like the clouds north of NGC1499 (Herbertz 1992) and the nearby cloud L1457 (Zimmermann 1993) are shown. Despite of the different range of physical conditions, sizes, and masses covered, the mass spectra follow approximately the same power law with the index in the range of $1.50 \leq \alpha \leq 1.74$.

Large-Scale CO-Observations of the GMCs Orion A and B Excitation Conditions and Fragmentation

C. Kramer, A. Tigges, J. Stutzki, and G. Winnewisser

I. Physikalisches Institut, Universität zu Köln, 50937 Köln, Germany

The Orion-Monocerus complex of giant molecular clouds is the nearest region of ongoing, massive star formation. The analysis of the large scale structure and excitation conditions of the GMCs Orion A and B was the aim of our multiline-observations with the KOSMA 3m radiotelescope. We observed the radiation of CO and its main isotopomers in the two rotational transitions (J=3-2) and (J=2-1) with half power beamwidths of 71″ and 125″ respectively.

At nearly all positions the line ratios are contradictory with a single temperature and density model, hinting at temperature gradients within the clumps: the surfaces are heated by the stellar UV-field whereas the inner regions are shielded from this radiation. The interpretation is in accordance with theoretical models of UV-irradiated clumps (Gierens et al. 1992; Köster et al. 1993). A comparison between our CO maps and the large scale [CII] 158 μm map of Jaffe et al. (1993) reveals interesting details about the excitation and heating conditions within Orion B.

The large scale observations of the northern part of Orion A and the southern part of Orion B (see Fig. 1) reveal the fragmented structure on all scales between 0.1 pc (the resolution limit) and the extension of the observed regions (8 pc). The total mass of the surveyed region of Orion B is 3150 $M_\odot$. A major part of the total mass of Orion B, 44%, is found in the five most massive clumps with $M > 200$ $M_\odot$. These clumps are associated with the prominent star forming regions NGC2024 and NGC2023. A Gaussian decomposition algorithm (Stutzki & Güsten 1990) identifies 244 clumps. The resulting mass spectrum is well fitted by a power-law with an index of 1.74. None of the clumps found are gravitationally bound – the more massive of the well-defined clumps are closer to virial-equilibrium than the less massive clumps. Our data imply that external pressures between 10^4 and 10^6 Kcm^{-3} are needed to stabilize the clumps. The average clump density is 4×10^3 cm^{-3} which is significantly lower than the critical density of the CO(3-2) transition, indicating unresolved substructures.

References

Gierens, K., Stutzki, J., Winnewisser, G. 1992, A&A, 259, 271
Jaffe et al. 1993, in preparation
Köster, B., Störzer, H., Stutzki, J., Sternberg, A. 1993, A&A, submitted
Kramer, C. 1992, Ph.D. thesis, University of Cologne
Kramer, C., Stutzki, J., Winnewisser, G. 1993, A&A, in preparation
Lada, E.A., Bally, J., Stark, A&A 1991, ApJ, 368, 432
Stutzki, J., Güsten, R. 1990, ApJ, 356, 513

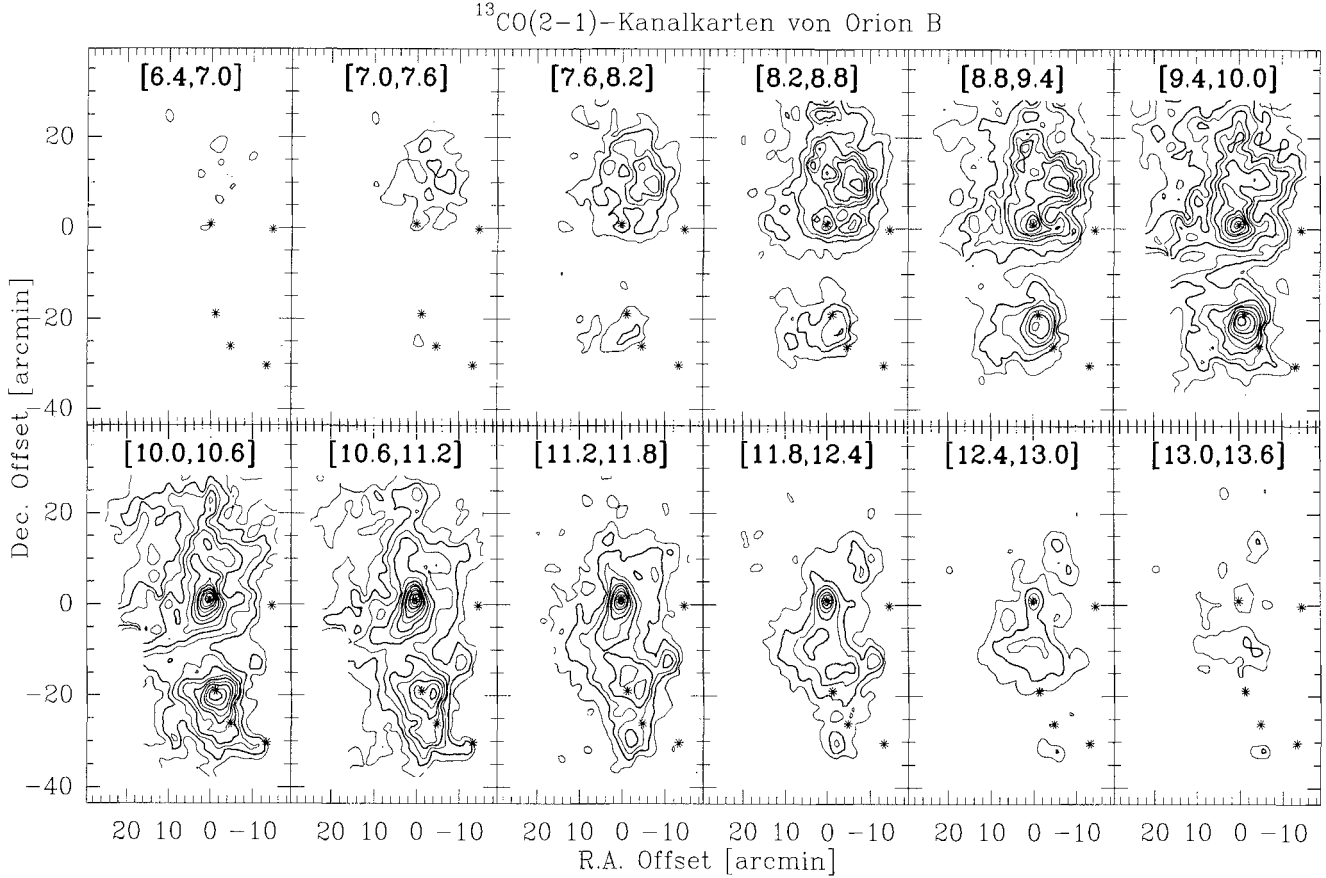

^{13}CO(2-1)-channelmaps of the southern part of the Orion B molecular cloud. The velocity interval of each channel is 0.6 kms^{-} contours are at 0.7 (=3σ) (0.7) 9.1 Kkms^{-1}.

High Spectral Resolution CCS($J_N = 2_1 - 1_0$) Studies of Clumps in Cold Dark Cloud Cores

T. Velusamy[1], T.B.H. Kuiper, W.D. Langer, S. Levin, and E.T. Olsen

Jet Propulsion Laboratory, Caltech, 4800 Oak Grove Drive, Pasadena, CA 91109

We report new observational evidence of high degree of clumpiness in dense dark clouds cores using high resolution spectra of the CCS transition ($J_N = 2_1 - 1_0$) at 22.344033 GHz made with 0.008 km s^{-1} resolution. The CCS lines are excellent tracers for investigating the velocity structure in dense cores, because they have no hyperfine structure, are heavy enough to have intrinsically narrow thermal line width (0.09 km s^{-1} at 10 K), require high density for excitation, and are probably not too opaque. Such intrinsic narrow thermal line widths afford better separation of velocity structure of individual components than lines of CO, ammonia, and most other molecular tracers. We used NASA's 70-m antenna (spatial resolution of 45 arcsec) and the HRMS two million channel Wide Band Spectrum Analyzer at Goldstone. We observed the spectra in several quiescent dark cloud cores which have the brightest emission in the CCS survey of Suzuki et al (1992), and B335 which has a protostellar core.

Fig. 1 shows some of the ultra-high resolution CCS spectra. All profiles show evidence of multiple components except L1498, which appears to have a single velocity component. L1498 is the smallest core in the sample (3.6 arcmin) and has the narrowest spectrum, $\Delta V =$ 0.15 km s^{-1}. In contrast TMC-1, L1544, L1521B & B335 profiles exhibit distinct velocity features and presence of very narrow gaussian width components. The narrowest features as indicated by the gaussian fits to TMC-1(Core-D) profile have $\Delta V = 0.15$ km s^{-1}, which we interpret as the intrinsic line-width of a typical coherent structure (clump) in the cores.

These cores are very cold, with kinetic temperatures $\sim$ 10 K (from NH_3 data of Benson & Myers, 1989) and thermal broadening for CCS is 0.09 km s^{-1}. Therefore, the nonthermal broadening (turbulence, rotation, infall and outflow, etc) in a single clump is < 0.12 km s^{-1}, which is less than the speed of sound (0.19 km s^{-1}).

We can rule out effects of shadowing and self-absorption in the CCS spectra (Velusamy et al. 1993), and the structure seen in the line profiles is most simply explained by a superposition of the emission from several quiescent clumps. The profiles in Fig. 1 show high degree of clumpiness (about 1 to 3 clumps per arcmin^2) in the cores. To gain more insight into the clumpines and velocity structure we also made CCS position-velocity (P-V) maps of some of the cores, with Nyquist sampling at every 24 arcsec. The P-V maps of Core-D in TMC-1 indicates that there may be at least 30 clumps within a 5$\times$ 6 arcmin^2 extent of this core (Velusamy et al., 1993). Several show complexity possibly due to velocity gradients (rotation) or substructure. We estimate the mass of the clumps in TMC-1 to range from 0.07 to 0.5 $M_\odot$ using the clump size and the mean density $n(H_2) \sim 4\times10^4$ cm^{-3} derived by Hirahara et al (1992). At least half of the clumps have masses less than 0.1 $M_\odot$.

We conclude that a large number of low mass (< 1 $M_\odot$) clumps make up the larger structures in dark cloud cores. We interpret these clumps to be stable or quasi-stable fragments formed by successive fragmentation.

[1]NRC Senior Research Associate on leave from Tata Institute of Fundamental Research, Bombay.

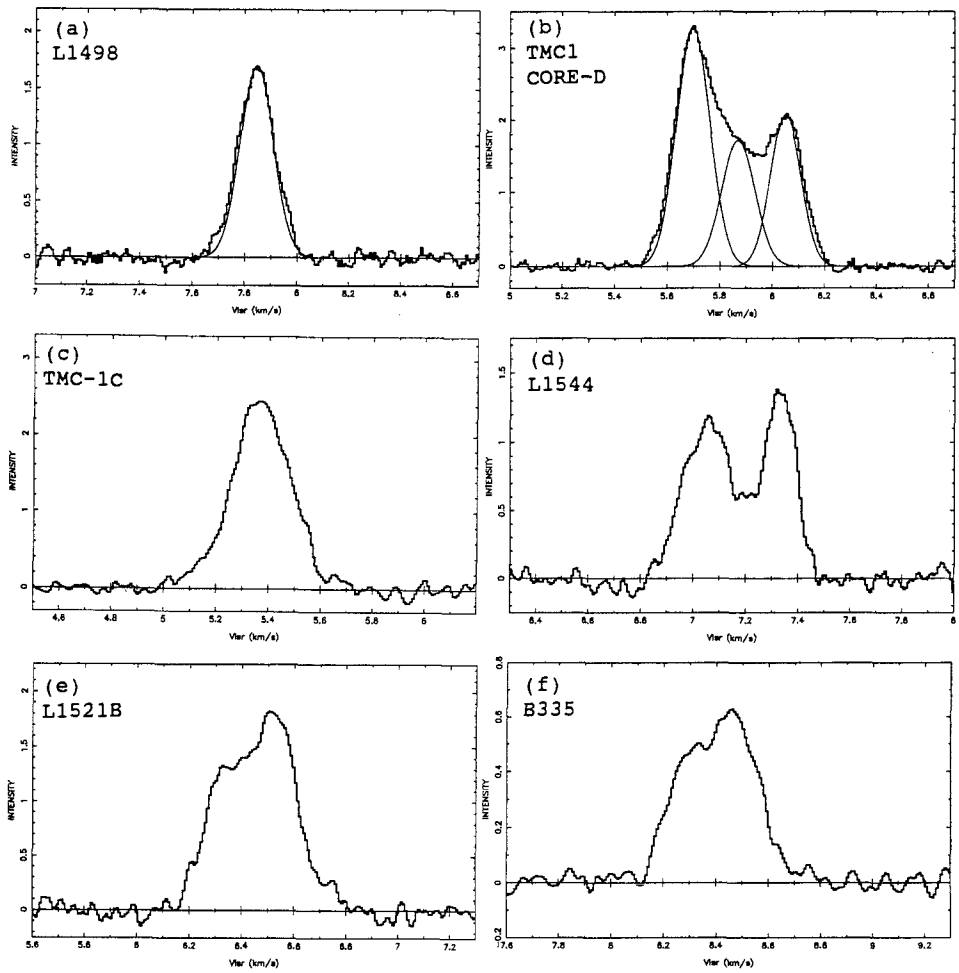

Figure 1. Ultra-high resolution CCS($J_N = 2_1 - 1_0$) spectra of dark cloud cores at 22 GHz. The velocity channel separation is 0.008 km s^{-1} and profiles have been smoothed to a resolution of 0.025 km s^{-1}. Velocity range is 1.7 km s^{-1} in each profile. The gaussian curves in (a) & (b) represent velocity components (clumps) each with intrinsic line-width of 0.15 km s^{-1}.

References

Bensen, P.J, & Myers, P.C. 1989, ApJ. Suppl. **71** , 89.
Hirahara, Y., Suzuki, H., Yamamoto, S., Kawaguchi, K., Kaifu, N., Ohishi, M., Takano, S., Ishikawa, S., & Masuda, A. 1992, ApJ **394** , 539.
Suzuki, H., Yamamoto, S., Ohishi, M., Kaifu, N., Ishikawa, S., Hirahara, Y., Takano, S., & Masuda, A. 1992, ApJ **392** , 551.
Velusamy, T., Langer, W.D., Kuiper, T.B.H., Levin, S., & Olsen, E. 1993 (in preparation)

Photodissociation and Rotational Excitation of CO and Its Isotopomers in Interstellar Clouds

S. Warin[1], J.J. Benayoun[1], Y.P. Viala[2]

[1] Observatoire de Grenoble, BP 53X, F-38041 Grenoble Cedex 9, France
[2] DEMIRM, Observatoire de Meudon et Radioastronomie, ENS, F-92195 Meudon Cedex, France

We have developed a model of an interstellar cloud that treats the chemistry among simple carbon and oxygen bearing molecules, including ^{13}C and ^{18}O isotopic compounds together with the rotational excitation of H_2, CO, ^{13}CO and $C^{18}O$. The reactions involving isotopic species include isotopic fractionation reactions and reactions obtained by duplicating those between the main isotopomers. The library of chemical reactions contains 3113 reactions among 159 species. The rotational population of the CO and its isotopomers is controlled by chemical processes (including photodissociation by UV photons which, for H_2 and CO, occurs through absorption in rotational lines, Warin et al (1993)), collisionnal processes, UV pumping through excited electronic levels (for H_2 alone), radiative processes including emission and absorption of millimeter and submillimeter lines connecting the rotational levels (for CO and its isotopes alone). The transfer problem for these lines is resolved using an escape probability formalism. At last, the model can compute the temperature of the gas together with its chemical composition. This is done by solving a thermal balance equation together with the chemical balance equations and a transfer equation for UV photons. The transfer problem is solved by assuming a plane parallel geometry.

In this study we do not solve thermal problem. We assumed a constant temperature of 50K in most models and constant density of 10^3 cm^{-3}. The visual optical depth to the mid plane of the cloud is $\tau_v = 1$. The UV external radiation field is that of Mathis et al (1983). The cosmic ray ionisation rate is $\zeta_H = 6.8 * 10^{-18} s^{-1}$. The elemental abundances and isotopic ratios are those adopted by Le Bourlot et al (1992).

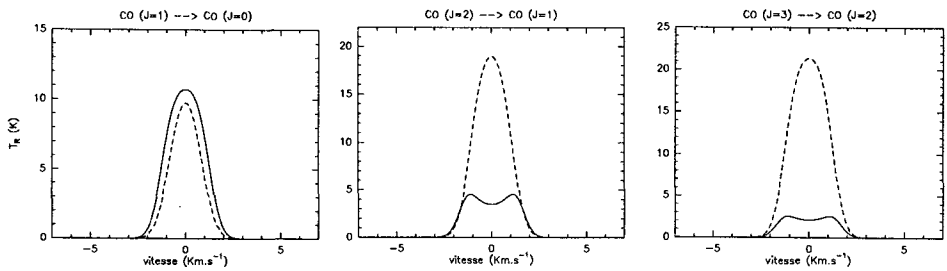

Figure 1: - *Line profiles emergent for the standard model assuming microturbulent broadening of mean velocity $v_{turb} = 1$ kms^{-1}, ^{12}CO $(J = 1 - 0)$, $(J = 2 - 1)$ and $(J = 3 - 2)$. Rayleigh-Jeans brightness temperature is plotted as a function of the velocity. The contribution from the 2.7 K background radiation has been removed. Full line : exact calculation, dashed line : LTE calculation.*

These preliminary calculations emphasize the importance of self-shielding for CO photodissociation wich result in a very selective photodissociation between the isotopes and among rotational levels : the more populated the level, the lowest its photodissociation rate. The net effect of self-shielding is to overpopulate low-lying levels and to underpopulate high levels in comparison with an LTE calculation.

The consequences on the profiles of emergent rotational lines J=1-0, 2-1, 3-2 are shown on fig. where the Rayleigh-Jeans brightness temperature is plotted as a function of velocity assuming a microturbulent broadening of the line. In the exact calculation the brightness temperature decreases as excitation increases. It is the opposite in the LTE calculation, at least up to the 4-3 transition. The most spectacular difference between the two sets of calculation is obtained for the 2-1 and 3-2 lines.

The self-shielding for the rare isotopes is much less efficient than for CO, leading to much larger photodissociation rates, of the same order for all rotational levels and with a smoother

variation with optical depth. This seems to indicate that the rare isotopes are not efficiently shielded by the main one.

Because the photodissociation is more efficient for the rare isotopomers, we expect a $^{12}CO/^{13}CO$ and $^{12}CO/C^{18}O$ ratio larger than the cosmic isotopic ratio $[^{12}C/^{13}C]$=90 and $[^{16}O/^{18}O]$=500. In the case of ^{13}CO, this effect is counterbalanced by the isotopic fractionation reaction : $^{13}C^+ + {}^{12}CO \rightleftharpoons {}^{13}CO + {}^{12}C^+$ (ΔE=-35K) which favours the transformation of ^{12}CO in ^{13}CO at low temperature, as can be seen on fig.. On the other hand, the fractionation reaction for $C^{18}O$ involves $HCO^+$and then the ratio $^{12}CO/C^{18}O$ is increased with respect to regard the cosmic ratio, by a factor of 5 towards the center of the cloud (Warin et al (1993)).

It is worth noting that these results strongly depend on the temperature, since the efficiency of isotopic fractionation for ^{13}CO increases as the temperature decreases.

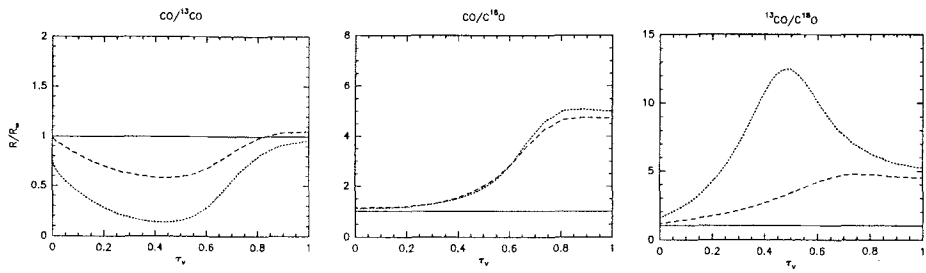

Figure 2: - *Abundance ratios of various isotopic forms of CO as function of visual optical depth (τ_v) from the edge of the cloud. R/R_∞ is the computed ratio (R) divided by the ratio that would occur in the absence of any isotopic fractionation effects (R_∞)- that is the ratio of the isotopic forms of the nuclei in the gas. The solid line represents the isotopic ratio (equal to 1). Full line : isotopic ratio equal to 1, short-dashed line : model with T = 10, long-dashed line : standard model.*

We study the influence of the geometry; for this, we choose a plane parallel geometry with : i) finite thickness and isotrope radiation flux. ii) semi-infinite thickness and isotropic radiation flux. iii) finite thickness and collimated incident radiation flux. Warin et al (1993).

Plane parallel semi-infinite geometry neglects the radiation coming from the opposite side of the cloud compared to the finite thickness situation : the consequence is that it underestimates in each point the radiation field, the difference reaches its maximum of a factor 2 at the center.

The difference is much more sensitive between an isotrope and a collimated radiation flux. The collimated flux overestimates the capacity of penetration of the radiation from the nearest two edges of the cloud to the current point. The effect on the abundances of C, C^+ and CO oversteps the order of magnitude: C^+ is strongly increased and remains dominant across the cloud. Conversely CO is strongly decreased due to an enhancement of the photodestruction rates. The effect on C is more complex. It is less abundant at the surface because it is more strongly ionized and more abundant at the center because it is more easily produced by the photodissociation of CO.

References

Le Bourlot, J., Pineau des Forêts, G., Roueff, E. and Flower, D.R. 1993 A&A 267, 233
Mathis, J.S., Mezger, P.G. and Panagia, N. 1983, A&A 128, 212
Warin, S., Benayoun, J.J. and Viala Y.P. 1993, to be published in AIP, "Physico-Chimie des Molecules et Grains dans l'espace"

The Distribution of Line Wing Emission in MBM16

B. Götting, J. Stutzki
I. Physikalisches Institut, Universität zu Köln, 50937 Köln, Germany

Complex spectral line profiles have been observed in many molecular clouds. Most spectra have a non-gaussian line shape and a line width much greater than the thermal line width. Strong line wings are observed in star forming regions with outflows. Blitz et al. (1988) first detected line wings in non-star-forming regions. These line wings are narrower and weaker than typical outflow wings in star forming regions and are thus very difficulty to observe. Subsequent observations showed these wings to be possibly a rather common phenomenon (Falgarone & Philips 1990, Vallee & Avery 1990, Magnani et al. 1990).

Several explanations have been suggested to explain these line wings: collision of two cloudlets (Keto & Lattanzio 1989), intermittency of turbulent motions (Falgarone & Philips 1990) and the steepening of magnetosonic waves in the density gradients near cloud edges (Elmegreen 1990).

Using the 3m KOSMA telescope and the 30m IRAM telescope we observed the region of the high latitude cloud MBM16, where line wings have been found before. We mapped a 400"× 120" area in the ^{12}CO(1→0), ^{12}CO(2→1) and ^{12}CO(3→2) transitions.

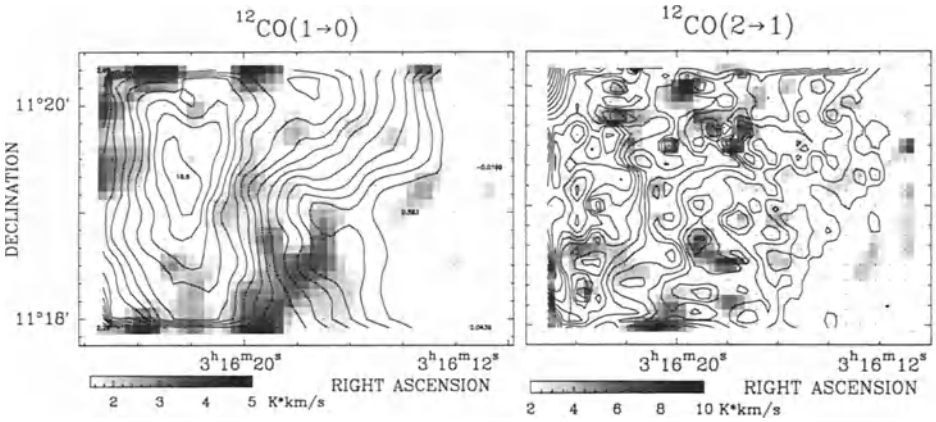

Fig.1: IRAM 30m ^{12}CO(1→0) and ^{12}CO(2→1) maps of core and wing component derived by a 2-component Gaussian fit. The wing components are marked by the grey scales, the core components by the contours: from 2 to 16 K*km/s in steps of 1 K*km/s for ^{12}CO(1→0) and from 2 to 17 K*km/s in steps of 1 K*km/s for ^{12}CO(2→1). The 1-σ level is 0.48 K*km/s for ^{12}CO(1→0) and 0.75 K*km/s for ^{12}CO(2→1).

We found the wing emission to be not smoothly distributed over the cloud. There are small patches mostly north and south of the bow shaped core of the cloud. Individual areas of wing emission are very confined (Fig.1). At a distance of 100 pc (Magnani & de Vries 1986) this corresponds to a size of 0.1 pc. The wing emission is found to be correlated with the gradient of the main component intensity (Fig.2). The regions of the highest intensity in the line core component are essentialy free from wing emission.

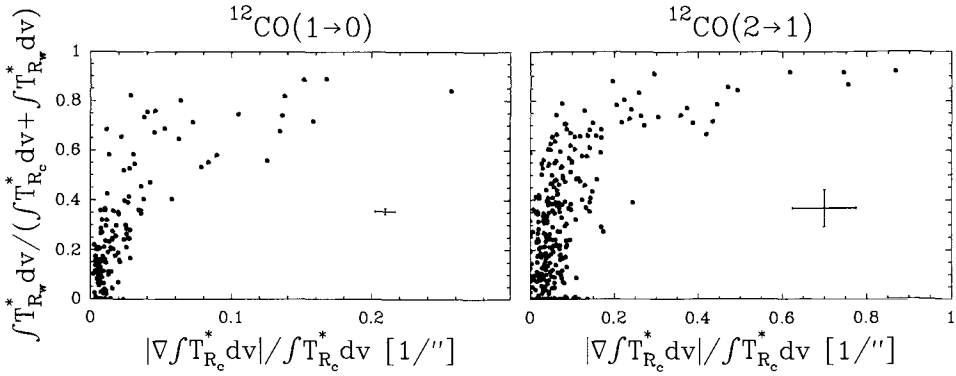

Fig.2: The integrated intensity of wing component (index w) relative to the total integrated intensity plotted against the normalized gradient of the integrated intensity of the core component (index c) for ^{12}CO(1→0) and ^{12}CO(2→1).

From a multi line analysis (Tab.1) we estimate the wing component to be warm (up to 80 K) and moderately dense (about 10^3 cm^{-3}, which is of about the same order as the values derived for the line core component emitting material), but with a ten times smaller column density than the core component material. Thus, the line wings should be arising in very small, warm and dense sheets or filaments near high density gradients of the surrounding material. These results suggest that the model of magnetosonic wave steepening may the appropiate one. The high temperature additionally indicates that the material might be heated by the interaction with the magnetosonic waves.

Tab.1: Results of Escape–Probability Radiative Transport Model: Decl.–Offset is allways 0". Index (w) means wing component, index (c) core component.

ΔR.A. ["]	log $n_{H_2(c)}$ [cm^{-3}]	log $N_{H_2(c)}$ [cm^{-2}]	$T_{k(c)}$ [K]	log $n_{H_2(w)}$ [cm^{-3}]	log $N_{H_2(w)}$ [cm^{-2}]	$T_{k(w)}$ [K]
0	1.2	16.9	40	2.5	14.5	80
-40	1.8	16.3	30	2.9	14.5	80
-80	3.0	15.8	25	3.0	14.6	80
-120	1.6	15.2	60	2.9	14.6	80
-160	2.6	15.0	60	2.6	14.8	70

References

Blitz, L., Magnani, L., Wandel, A., 1988, ApJ, 331, L127
Elmegreen, B., 1990, ApJ, 361, L77
Falgarone, E., Phillips, T.G., 1990, A&A, 359, 344
Keto, E.R., Lattanzio, J.C., 1989, ApJ, 346, 184
Magnani, L., de Vries, C.P., 1986, A&A. 168, 271
Magnani, L., Carpenter, J.M., Blitz, L., Kassim, N.E., Nath, B.B., 1990, ApJS, 73, 747
Vallee and Avery, 1990, A&A, 233, 553

Molecular Observations of HH34: Does NH_3 Accurately Trace Dense Molecular Gas Near Young Stars?

[1]Chris Davis & [2]Bill Dent

[1]Max-Planck-Institute für Astronomie, Königstuhl, D69117 Heidelberg.
[2]Joint Astronomy Centre, 660 N. A'Ohoku Place, Hilo, Hawaii 96720.

HH34 consitutes the architypal bipolar collimated jet from a young star that terminates in two optical bow shocks, HH34N and HH34S (Bührke et al. 1988). Here we discuss single-dish NH_3 (1,1) and HCO^+ J=4-3 observations of the molecular environment around HH34 and its exciting star (also in Davis & Dent 1993).

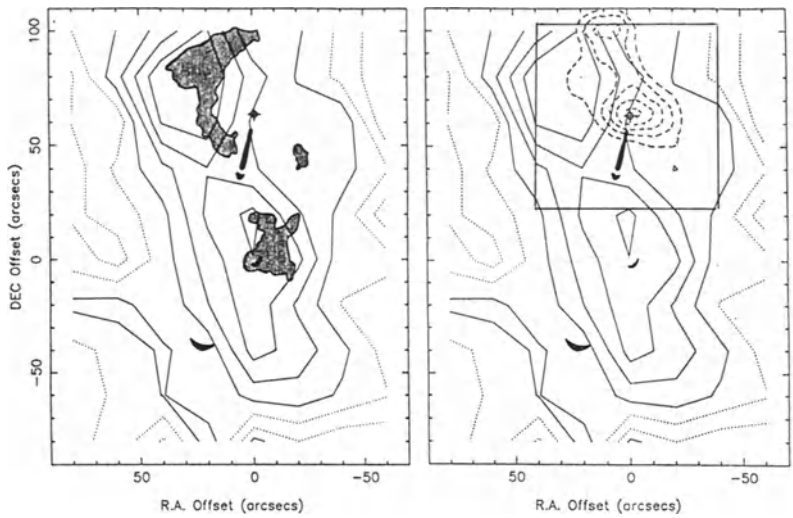

Figure 1. *a)* NH_3 (1,1) contour plot of the molecular environment in HH34. The source, jet and southern bow shock HH34S are sketched on here. The NH_3 beam measures 40". The shaded areas represent the NH_3 clumps observed by Anglada et al. (1991) with the VLA (primary beam of the VLA does not reach HH34S). **Note in this figure the close relationship between the low and high-resolution NH_3 studies, and the apparent lack of emission from the source.** *b)* The NH_3 contours from Fig.1a with (superimposed) dotted contours of HCO^+ J=4-3. The HCO^+ beam is 14"; the square shows the extent of the HCO^+ mapping. **Clearly the HCO^+ peak does not coincide with the NH_3 features, but instead peaks towards the source. The HCO^+, together with the CS observations of Cernicharo (1990) suggest a density and temperature peak associated with the source, though suprisingly this feature is not seen in NH_3.**

The observations presented in Fig.1 show a clear offset in the NH_3 peaks from the source and associated density/temperature peak traced in HCO^+ and CS (Cernicharo 1990). This is not an optical depth effect; a map of the NH_3 (1,1) optical depth peaks towards the two column density peaks, whilst the highest value suprisingly coincides with the HH34S bow shock (this latter peak coincides with clumps observed in CS, and suggests dense though unresolved clumps associated with the shock front). *It thus seems that the NH_3 is underabundant – by a factor of 10 – towards the source position.* Possible depletion mechanisms include selective fractionation of NH_3 via shocks or photodissociation, or perhaps a restriction on the gas phase formation of NH_3. The former process seems unlikely, since it requires a system that does not affect other molecules like HCO^+, CS and HCN. Additionally, low-velocity shock models predict no reduction in the NH_3 abundance, but instead favour a slight enhancement.

Shocking will also enhance NH_3 via the desorption of dust grain mantels. It is therefore likely that the observed low NH_3 column density is due to a restriction on formation, perhaps because of a reduced ionisation fraction in the molecular core associated with the source.

NH_3 peaks towards other outflows often do not coincide with the central source/density-temperature peak (see Rodriguez 1987). Instead, the NH_3 is often confined to peaks either side of the source; in many cases this structure is interpreted in terms of an NH_3 toroid. We see no evidense of a toroid in the HH34 system. However, to investigate further the possibility that the NH_3 "toroids" in other sources are related to the central star, we show here a plot of source luminosity against toroid mass. The parameters used were taken from the literature, and apply to low and high luminosity sources.

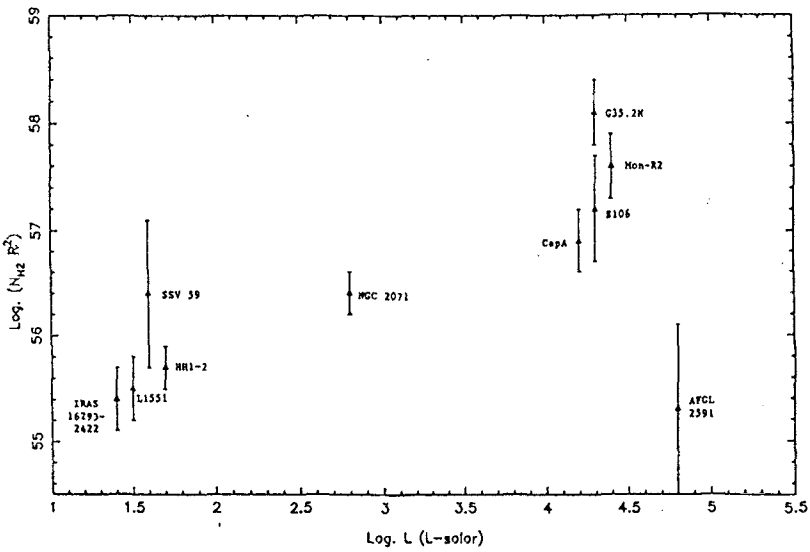

Single dish NH_3 observations are used to measure the NH_3 column density towards each source; this is then converted to a column of H_2 with $N_{NH3}/N_{H2} = 10^{-7}$. The toroid radius is simply half the distance between the two NH_3 peaks. So, although toroidal structures are not observed in all young stars, those that are seem to be related to the embedded source, and not simply random features present in the parent cloud.

Anglada, G., Estalella, R., Rodriguez, L.F., Torrelles, J.M., Canto, J. & Ho, P.T.P, 1991. In *Atoms, Ions & Molecules: New Results in Spectral Line Astrophysics*, eds Haschick & Ho, p.279.

Bührke, T., Mundt, R. & Ray, T.P., 1988. *A&A*, 200,99.

Cernicharo, J., 1990. In *Physics of Star Formation & Early Stellar Evolution*, eds Lada & Kylafis, p.287.

Davis, C.J. & Dent, W.R.F., 1993. *MNRAS*, 261,371.

Rodriguez, L.F. 1987. In *Star Forming Regions*, eds Peimbert & Jugaku, p.293.

Low-J-CO-Multiline Studies of Molecular Clouds: NGC7538

R. Röhrig[1], J. Stutzki[1], H. Ungerechts[2], G. Winnewisser[1]

[1] I. Physikalisches Institut, Universität zu Köln, 50937 Köln, Germany

[2] FCRAO, Univerity of Massachusetts, Amherst, MA. 01003

NGC 7538 is a visible HII region in the Perseus spiral arm at a distance of 2.2 kpc (Morena et al 1986), which is associated with a molecular cloud of 40 pc diameter. Werner et al. (1979) showed that the high density core of this molecular cloud is a very active star forming region. The HII region/molecular cloud interface is seen edge on, so that this is well suited to investigate sequential star formation. A remarkable range of young objects was found in this region such as several O stars, (ultra) compact HII regions, OH, H_2CO , H_2O masers (Forster *et al.* 1978, Kameya *et al.* 1989) and molecular outflows (Campbell & Thompson 1984), which are mostly associated with the infrared positions IRS 1 to 11 identified by Wynn-Williams, Becklin, and Neugebauer (1974). We have observed the three lowest transitions of the three most abundant CO isotopomeres with the KOSMA 3 m and the FCRAO 15 m radiotelescopes.

Figure 1 shows a grayscale map of the $^{12}CO(1\rightarrow0)$ integrated line intensities overlayed with the contours of the integrated $C^{18}O(1\rightarrow0)$ emission. The four most important IRS positions and the 5 mJy contour of the radio continuum emission at 21 cm (Israel *et al.* 1973) marking the HII region border are drawn as well. The optical thin $C^{18}O$ map shows a lot more structure. Especially a cavity east of the IRS position cluster becomes visible. The $C^{18}O$ emission peaks deeper in the molecular cloud near the IRS 11 position than the ^{12}CO emission. The $C^{18}O$ map was totally decomposed into 153 gaussian shaped clumps by an algorithm developed by Stutzki & Güsten (1990). The resulting mass spectrum is well fitted by a power-law with an index of 1.65. Most of the clumps show thermalized $^{12}CO(3\rightarrow2)$ emission, although the average clump density is 3.6×10^3 cm^{-3} which is a factor of 3 lower than the critical density of the $^{12}CO(3\rightarrow2)$ transition. This may be another hint to unresolved substructures.

The low rotational transitions of CO and its isotopes are often used to derive the physical parameters of molecular clouds. By comparing the observed ^{12}CO and ^{13}CO low J line intensity ratios in NGC7538 and several other molecular clouds we find that standard models like escape probability, assuming a homogeneous cloud with one single component of physical parameters for the emitting material, are leading to contradictory results. While the interisotopic ratio $^{12,13}\mathcal{R}_1 := T_{mb}(^{12}CO; 1-0)/T_{mb}(^{13}CO; 1-0)$ has values between 3 and 6 in most of the observed clouds, which implies optically thin ^{13}CO lines, the ^{13}CO line intensity ratios $^{13}\mathcal{R}_{2,1}$ and $^{13}\mathcal{R}_{3,2}$ are often not much less than one, which implies optical thick ^{13}CO lines. On the basis of homogeneous models, especially $^{13}\mathcal{R}_{3,2}$ would be expected to be significantly lower.

Molecular clouds are far away from being homogeneous spheres but consist of substructures that we call clumps. However it has been thought that single component models are still good approximations to describe the physical conditions within the individual clumps. But as one consequence of the clumpy structure, the UV radiation from neighbouring HII regions is able to heat the material on the surfaces of clumps even deep in the molecular cloud complexes. Therefore, the spectra do not reflect the emission of one homogeneous object but a superposition of radiation from heated clump surfaces and colder interior layers, which are shielded from the heating UV radiation. A new model which takes this effects into account was presented by Gierens et al. (1992). It supposes that the cloud consists of clumps with photodissociation regions on each surface incorporating temperature gradients within each clump, density gradients within each clump, chemical abundance variations, and variations of the clump volumefilling factors. The ^{13}CO transitions have Einstein A coefficients and therefore increasing optical depths increasing with J. With increasing J we see less deep into the clumps and therefore trace higher temperatures and lower densities. This could explain the high ^{13}CO intensity ratios.

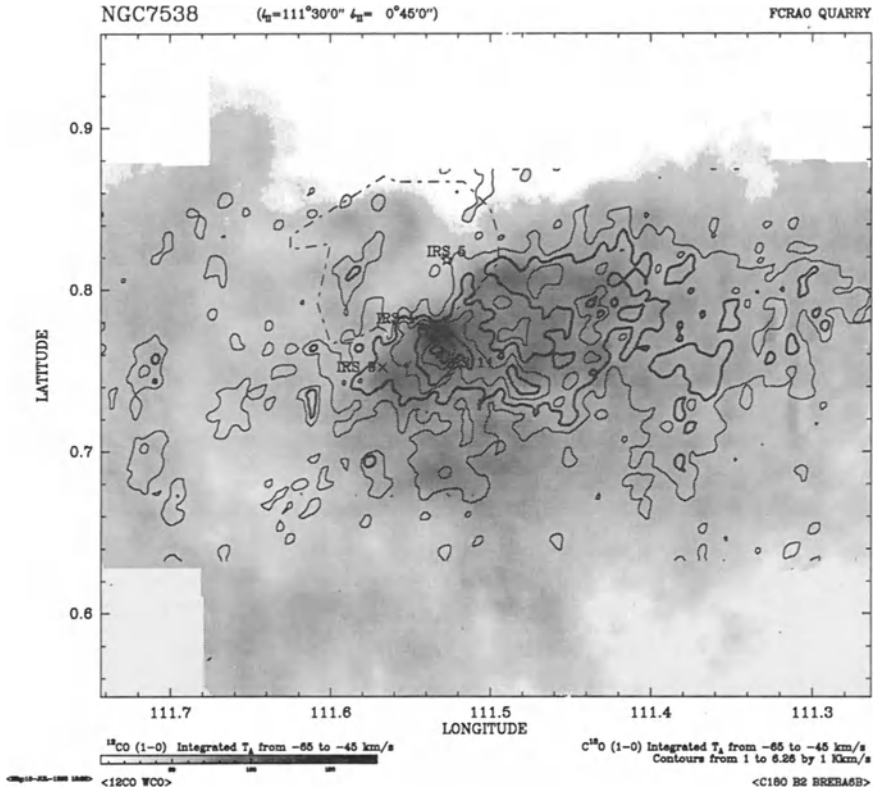

Figure 1: Integrated emission of ^{12}CO (gray) and $C^{18}O(1\rightarrow0)$ (contours).

References

Campbell, B., Thompson, R.I.: 1984, ApJ , 279, 650.
Forster, J.R., Welch, W.J., Wright, M.C.H., Baudry, A.: 1978, ApJ, 221, 137.
Gierens K., Stutzki J., Winnewisser G.: 1992, A&A, 259, 271.
Israel F.P., Habing H.J., deJong T. : 1973, A&A, 27, 143.
Kameya O., Hasegawa T.I., Hirano N., Takakubo K., Seki M. : 1989, ApJ, 339, 222.
Morena M.A.,Chavarria-K. C.: 1986, A&A, 161, 130.
Stutzki, J., Güsten, R.:1990, ApJ, 356, 513.
Werner, M.W. *et al.* : 1979, MNRAS, 188, 463.
Wynn-Williams, C.G., Becklin, E.E., Neugebauer, G.: 1974, ApJ, 187,473.

L1780: a Cometary Globule in Disguise of a High-Latitude Cloud. – CO Observations

L.V. Tóth[1,2] L. Haikala[3,2] T. Liljeström[2] and K. Mattila[2]

1. L. Eötvös University, Ludovika tér 2., H-1083 Budapest, Hungary
2. Helsinki University Observatory, P.O. Box 14, FIN-00140, Finland
3. I. Physikalisches Institut, Universität zu Köln, 50937 Köln, Germany

The L1778/L1780 cloud (Lynds 1962), hereafter referred to as L1780, is a compact HLC object with a maximum visual extinction of $4^m.6$. The angular size of L1780 is $40' \times 30'$ and it is elongated in the E-W direction. The cloud is located at $l = 359°$, $b = 36°.7$ at a distance of 110±10pc (Franco 1989). This prototypical "bright dark nebula" has a well defined boundary at its northern and western sides, and is more diffuse on the south-eastern side. A tail, pointing eastwards from the cloud, is also outlined in the optical surface brightness distribution (Mattila 1979).

CO observations and results: Large scale ^{12}CO and ^{13}CO J= 1 → 0 observations were made with the University of Cologne 3m telescope (HPBW=3'.9). The observations revealed a cometary cloud structure: a dense core asymmetrically surrounded by a diffuse outer layer. The core of L1780 was observed in ^{13}CO J= 1 → 0 using the 15-m SEST telescope (HPBW=45") and a few spectra also in C^{18}O J= 1 → 0 were obtained .

Contour maps of the ^{12}CO and ^{13}CO integrated line areas are shown superposed in Fig. 1a. The regions of maximum emission in the two isotopes are shifted by 8' with respect to each other. The region of the ^{13}CO maximum at $15^h36^m55^s$, $-7°02'$ is referred to as the core. The ^{12}CO line profiles are asymmetric: the blueshifted side shows clear excess emission, which varies depending on the position in the cloud (see Fig. 1 b, c, d). The mass of the cloud calculated from the CO observations is $20M_\odot$. The compact ^{13}CO core has a mass of $8.3M_\odot$. Both the density distribution and virial stability calculations imply that the core is in virial equilibrium.

Comparison of our CO results to previous observations: (i) optical: The N(^{13}CO) to A_V visual extinction ratio obtained for the L1780 core region agrees better with the Coalsack (Harjunpää and Mattila, 1993) than with the Taurus (Frerking et al. 1982) relation.
(ii) HI 21cm: The line profiles of the excess HI (21cm) emission found by Mattila and Sandell (1979) towards L1780 are similar to our ^{12}CO spectra (see Fig. 1.): (1) there is an assymmetry in both cases with a blue-shifted excess emission and (2) the maximum broadening of the line takes place in both cases at around $15^h37^m50^s$, $-7°$.
(iii) IRAS: The $\Delta I_{100\mu} = I_{100\mu} - 5 \times I_{60\mu}$ excess emission associated with the L1780 ^{13}CO core provides further evidence in favor of a compact, dense and cold cloud core. The distribution of the $I_{12\mu}$ and HI-excess emissions are similar. This suggests that the small particles responsible for the $I_{12\mu}$ emission may also act as an agent for the heating of the HI gas.

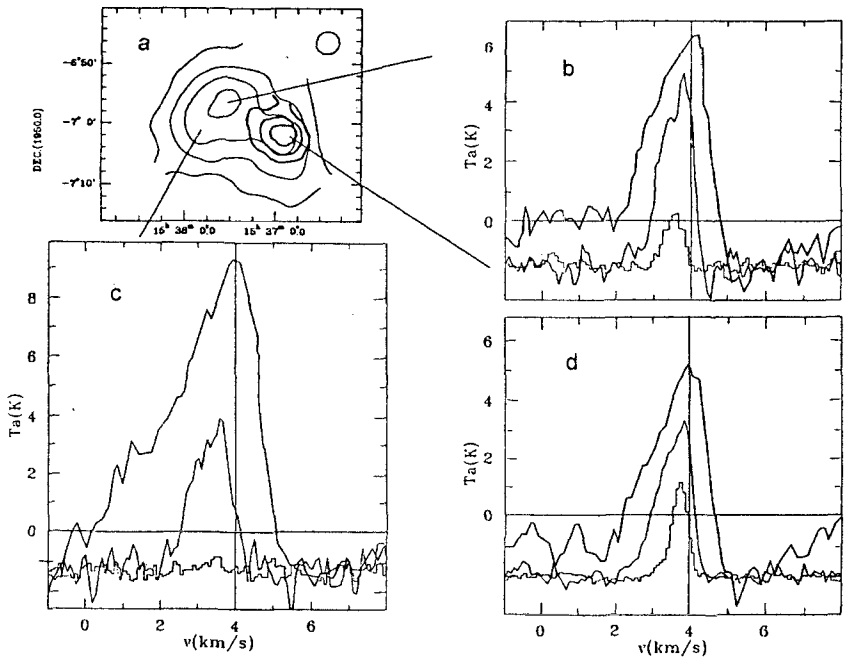

Fig. 1a: ^{12}CO and ^{13}CO (thin and thick line) integrated intensities. **b, c, d:** sample ^{13}CO, ^{12}CO and HI-excess spectra at three different positions in L1780 (HI from Mattila and Sandell 1979). Temperature scale is given for the HI spectra on the left and there is a zero point offset for the CO lines.

Large scale effects account for the observed kinematics and morphology. Judging from its position and radial velocity L1780 is associated with the HI loop (wind blown bubble shell) around the Sco-Cen-Lup association (SCL). The contribution of the closest subgroup of SCL to the energy density of the ISRF in the 912Å$\leq \lambda \leq$ 1300Å interval, at the location of L1780 has been found to be larger by a factor of 1.5 than that of the average Galactic radiation field in the Galactic plane.

We suggest that the structure and the morphology of L1780 have been influenced by two large scale environmental effects: (1) asymmetric interstellar UV radiation field and (2) a shock front caused by the high mass stars of the SCL association.

References

Lynds, B. T (1962) ApJS 7, 1
Franco, G.A.P., (1989) A&A, 223, 313.
Frerking, M.A., Langer, W.D., Wilson, R.W. (1982) ApJ, 262, 590.
Harjunpää, P.K., Mattila, K. (1993) in preparation.
Mattila, K., (1979) A&A, 78, 253.
Mattila, K., and Sandell, G., (1979) A&A, 78, 264.

Influence of the Photospheric Line Spectrum on the Optical Pumping of Circumstellar CO

T. Hertenstein[1], T. Tsuji[2], and W. H. Kegel[1]

[1] Institut für Theoretische Physik der Universität Frankfurt/M

[2] The University of Tokyo, Institute of Astronomy, Mitaka, Tokyo

CO radio lines have been detected from the cool, expanding envelopes of a large number of late-type stars. A quantitative analysis of the observed line profiles is important for the determination of the mass-loss rate. Relevant radiative transfer calculations which also account for optical pumping so far assume the spectrum of the central star to correspond to that of a blackbody (e.g. Morris 1980, Schönberg 1988). However, the photospheric infrared spectrum of late-type giants is dominated by strong absorption lines. This makes the pump process sensitive to the velocity difference between individual points in the envelope and the photosphere. A qualitative study with a VLG-code by Piehler et al. (1991) indicated a strong dependence of the emitted lines on the wind-velocity. Maser emission may occur, as was suggested by the observations of Zuckerman and Dyck (1986). We have calculated in more detail the formation of CO radio lines under the influence of pump-radiation from the photospheric line spectrum within a spherically symmetric model envelope, whose structure was adopted from Gail and Sedlmayr [1985]. The mean intensities entering the rate equations were determined using the angle dependent Sobolev approximation, while the emitted line profiles were obtained by integrating the radiative transfer equation. In the figures we compare results obtained when we account for the photospheric line spectrum (dashed lines) with those obtained when the photospheric spectrum is assumed to correspond to that of a black body (smooth lines). The calculations were performed for a central star with $Teff = 2600K$, $log(g) = 0.0$ and $\dot{M} = 3 \times 10^{-7} M_{\odot}/Y$.

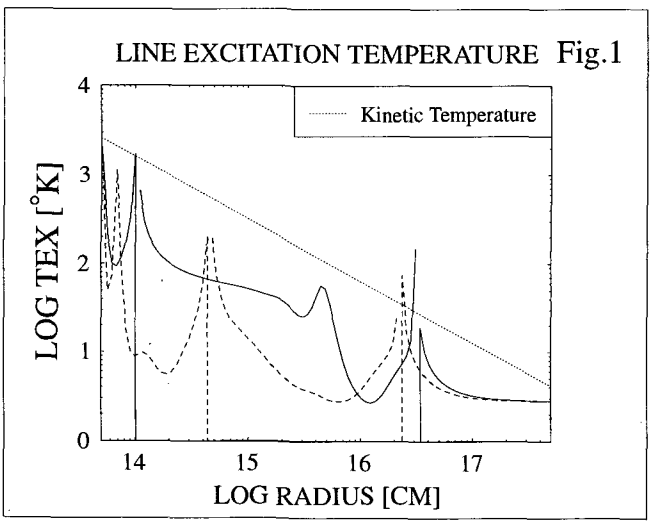

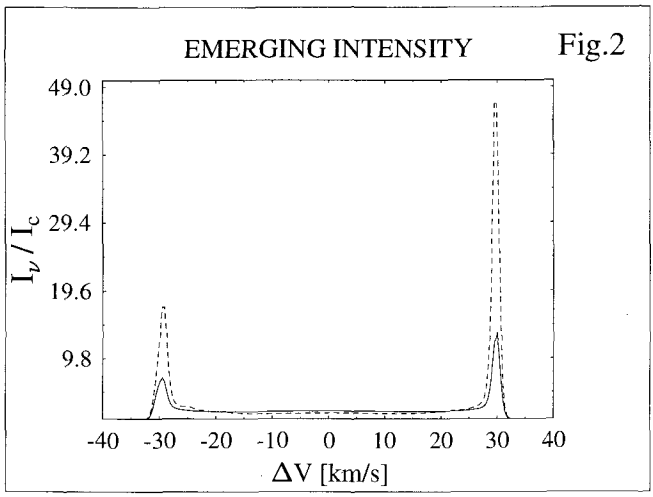

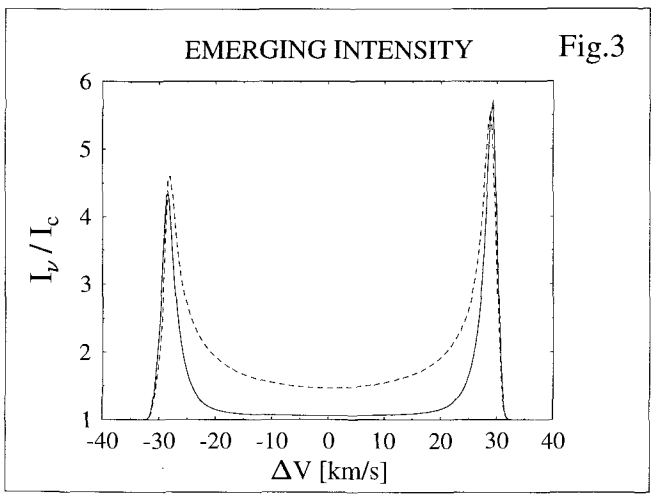

Fig.1 displays Tex for the (J=1-0)-transition (with negative values in regions between vertical lines), Fig.2 and Fig.3 show spectra for lines of sight with impact parameters of 3.2 and 100 stellar radii. Excitation structure and spectra are quite different for the two cases.

References

Morris, M.: 1980 APJ, 236, 823
Schönberg, K.: 1988 A&A, 195, 198
Piehler, G., Tsuji, T., Kegel, W.H.: 1991 A&A, 245, 580
Zuckerman, B., Dyck, H.M.: 1986 APJ, 311, 345
Gail, H.-P., Sedlmayr, E.: 1985 A&A, 148, 183

Clumping in M17SW

T. Jenness
Mullard Radio Astronomy Observatory, Cavendish Laboratory, Madingley Road, Cambridge CB3 0HE, England

M17SW has been mapped in the molecular species HCO^+, HCN and $C^{17}O$ (all with $J = 3 \rightarrow 2$) with a resolution of 15-20″ arc using the JCMT in the course of a study of cloud structure (Hobson 1992 and Hobson et al. 1994). Each of the line maps has been analyzed using `GAUSSCLUMPS`, a clump decomposition program written by Stutzki & Güsten (1990). The results, together with those from the original $C^{18}O$ $J = 2 \rightarrow 1$ data (Stutzki & Güsten 1990), have been compared in order to test the reliability and significance of this method of analysis.

The figure shows the results of the `GAUSSCLUMPS` decompositions ; for the $C^{18}O$ clumps, only the first 41 (which have a peak temperature greater than 7 K) have been plotted. In order to see best what agreement there is between species the clumps have been plotted in four separate velocity bins, with the reconstructed map plotted in the final bin; map centre is at $\alpha(1950) = 18^h\ 17^m\ 29.8^s$, $\delta(1950) = -16^o\ 14'\ 01''$ and the greyscale shows the integrated intensity due to the clumps. For the clumps to be *physically* real, one might expect them to be present in all species, although optical depths effects for HCO^+ and HCN may account for some differences. The LVG analysis described below suggests that the $C^{17}O$ and $C^{18}O$ have an optical depth, τ, of 0.2-0.5 and the HCO^+ and HCN maps, $\tau > 20$. Assuming a constant ratio for $[^{18}O]/[^{17}O]$ this would suggest that the optically thin CO clump decompositions should be compared separately from the optically thick maps.

As expected, the best agreement is found to be between the two CO isotopes. Although the $C^{17}O$ map covers a smaller area than the $C^{18}O$ map, the larger clumps do agree reasonably well in the second velocity bin. The small differences can be explained by the slightly different optical depths and beamshapes of the two maps.

The optically thick maps also have similar features but apart from the Northern Condensation the clump decomposition shows no detailed agreement between them. There is certainly no agreement between these decompositions and those of the maps of the CO isotopes despite the fact that foreground clumps detected on the optically thick HCO^+/HCN maps should still be detectable in CO. Discrepancies between the optically thick HCO^+ and HCN and the optically thin CO isotopes may partly be due to excitation and optical depth effects; alternatively there may instead be many more small-scale clumps present that remain unresolved by present day telescopes (see below).

Four lines of sight were chosen for further analysis in a range of molecules to look for temperature and density variations and to see whether the observed spectra could be accounted for by the clumps thought to be contributing to each point. LVG computer modelling of the observed spectra indicates that optically thick main line and optically thin isotope lines can not be fitted simultaneously if standard isotope abundance ratios are assumed, the main lines being consistently three times weaker than predicted (see table). This indicates that either the isotope abundances are not solar or, more likely, the clumps have not been resolved and a filling factor needs to be introduced. Wang et al. (1993) have done a similar comparison for a range of CS transitions.

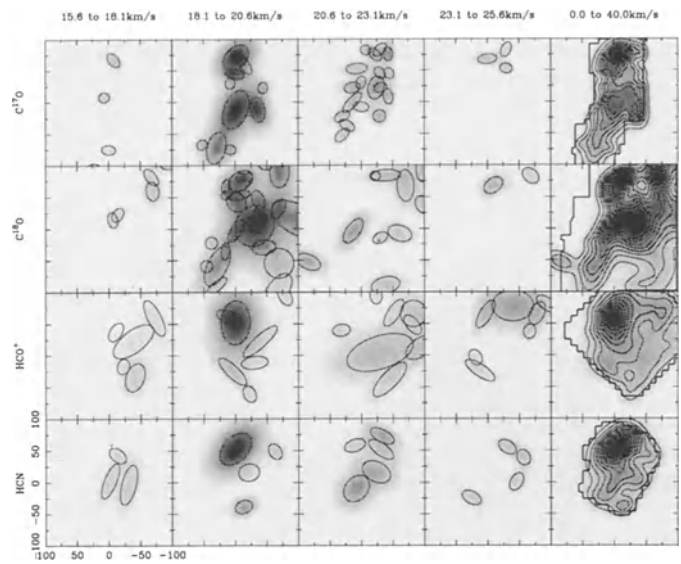

Molecule	Transition	T_A^*(K)	
		Observed	Theoretical
HCO^+	$4 \rightarrow 3$	9.0	27.8
$H^{13}CO^+$	$4 \rightarrow 3$	0.9	0.9
$HC^{18}O^+$	$4 \rightarrow 3$	0.2	0.2
HCN	$4 \rightarrow 3$	5.6	15.5
$H^{13}CN$	$4 \rightarrow 3$	0.5	0.5
$HC^{15}N$	$4 \rightarrow 3$	0.1	0.1
CS	$7 \rightarrow 6$	5.4	16.0
$C^{33}S$	$7 \rightarrow 6$	0.1	0.1
$C^{34}S$	$7 \rightarrow 6$	0.7	0.6
CO	$3 \rightarrow 2$	38.0	37.2

Observed spectral line maxima and the theoretical LVG result, for a single line of sight at $\alpha(1950) = 18^h\ 17^m\ 30.6^s$, $\delta(1950) = -16^o\ 14'\ 14''$ and $T_{kin} = 45K$ and $n_{H_2} = 5 \times 10^5 cm^{-3}$, are shown above. Standard abundances (rel. H_2) are assumed (Welch 1988) of 10^{-4} for CO, 2×10^{-8} for HCO^+, 2×10^{-8} for HCN and 3×10^{-8} for CS.

References

Hobson, M.P., 1992, MNRAS, 256, 457
Hobson, M.P., Jenness, T., Padman, R., Scott, P.F., 1994, MNRAS in press
Stutzki, J., Güsten, R., 1990, ApJ, 356, 513
Wang et al., 1993, ApJ in press
Welch, W.J., 1988, Astro. Lett. and Communications, 26, 181

Interpretation of CO Lines from Turbulent Molecular Clouds

G. Piehler and W.H. Kegel

Institut für Theoretische Physik, Johann-Wolfgang-Goethe Universität, 60054 Frankfurt, Germany

In previous papers (Albrecht & Kegel 1987, Kegel et. al. 1992 and Piehler & Kegel 1993) we investigated the formation of interstellar molecular lines in a turbulent velocity field. We used the statistical theory developed by Gail et. al. (1974, 1980). In these papers we systematically studied the effects of a finite correlation length of the stochastic velocity fluctuations at various H_2-densities, temperatures, turbulence velocities, correlation lengths and different geometries by solving the full NLTE-problem. Our main interest were the effects on line profiles, curve of growth and line widths using the CO molecule as an example. The important result of this work was that the influence of the finite correlation length is as important as NLTE-effects.

In our present investigation we concentrate more on observational values like center-to-limb variations, $^{12}CO/^{13}CO$-ratios, ratios of different rotational transitions and line profiles from higher rotational transitions. As cloud model we use an isothermal sphere in hydrostatic equilibrium assuming that the pressure is dominated by the turbulence. As molecule we selected the CO with up to 12 rotational levels.

The results can be summarised as follows:

- In most cases the well known selfabsorbtions in the line profiles disappear.
- Lines looks saturated but have not reached the LTE-Limit.
- In a sensitive range of N_{CO} the intensity ratios for $^{12}CO/^{13}CO$ are well modified for different correlation lengths.
- This is also true for intensity ratios between different transitions.
- The center-to-limb variations differ for different correlation lengths. This influences the apparent size of a cloud.
- In most cases transitions of higher rotational states are more effected because the occupation numbers of these states deviate more from LTE as the lower states.
- For a detailed analysis of observational data it seems to be necessary to include in particular higher rotational transitions to get better determined physical parameters.

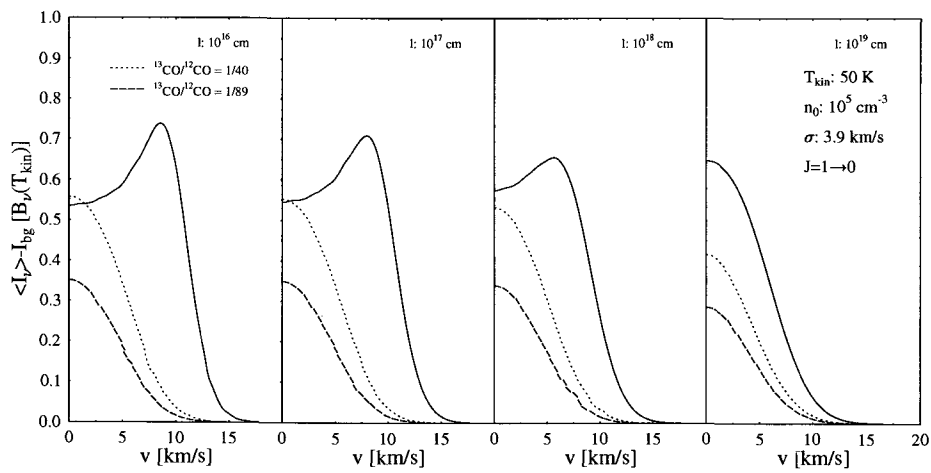

Fig 1: Line profiles for the ^{12}CO and ^{13}CO molecule for a spherical isothermal inhomogenous cloud at different correlation lengths l.

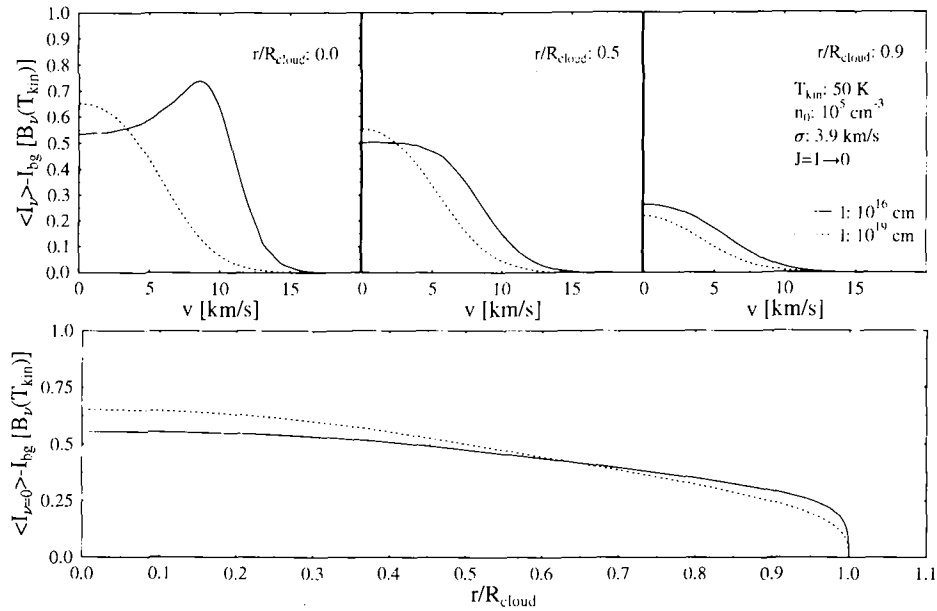

Fig 2: Center-to-limb variation of line profiles and $<I(\nu=0)>$ of the J=1→0-transition for two correlation lengths: 10^{16}cm (solid line) and 10^{19}cm (dashed line)

The numerical calculations presented in this paper were performed at the Höchstleistungsrechenzentrum Jülich (CRAY-YMP) and on the local super-computer (Fujitsu S200). This work was supported by the Bundesminister für Forschung und Technologie (BMFT) in the frame of the project No 055FM94A.

References

Albrecht, M.A., Kegel, W.H. 1987, A&A 176, 317
Gail, H. P., Hundt, E., Kegel, W. H., Schmid-Burgk, J., Traving, G. 1974, A&A 32, 65
Gail, H. P., Sedlmayr, E., Traving, G. 1980, J.Q.S.R.T 23, 267
Kegel,W.H., Piehler,G., Albrecht, M.A. 1993, A&A, 270, 407
Piehler,G., Kegel,W.H. 1993, A&A, in preparation

CO Multi-Line Survey in the Galactic Center

J. Staguhn, J. Stutzki, and G. Winnewisser

I. Physikalisches Institut, Universität zu Köln, 50937 Köln, Germany

The physical conditions in the Galactic center are quite different from those found in the Galactic Disk. Only giant, dense molecular clouds ($n_{H_2} \sim 10^4 cm^{-3}$) can survive tidal shear effects. The turbulent motions in these clouds result in linewidths in the order of 20 to 40 kms^{-1} (Bally et al., 1987, 1988). Higher gas temperatures (in the range of 50 to 100K) than dust temperatures demand direct mechanisms for the gas heating (e.g. Güsten, 1989).

A very important aspect is the interaction of these Galactic center clouds with their surrounding medium. There are good indications for interaction of the clouds with the unique features such as the thermal and nonthermal filaments and arcs (Serabyn and Güsten, 1991 ; Bally and Yusef Zadeh, 1989) It is still unknown if UV radiation from star formation regions (Genzel et al., 1990 ; Poglitsch et al., 1991) shock excitation (Bally et al. 1988) or magnetohydrodynamic ionization (Morris and Yusef-Zadeh, 1989) dominate the interaction.

Except for a few well studied regions such as the Sgr A molecular ring or the Sgr B complex, our knowledge about the Galactic center molecular clouds is based only on a very limited set of data: the large scale structure and distribution has been studied in the $^{13}CO(1\rightarrow0)$ survey by Bally et al. (1987, 1988) high densities and elevated temperatures is derived from the CS survey of Bally et al. (1987, 1988) and the NH_3 surveys of e.g. Güsten et al. (1981). Only the immediate neighbourhood of Sgr A and the Sgr B complex have been studied in other molecules (HCN, HCO^+,etc.) and even there consistent CO multiline surveys are missing. Comparison between CO studies and the more traditional way of deriving molecular cloud conditions by the mean of CS (density) and NH_3 (temperature), show large variations already for many clouds in the solar neighbourhood, presumably because the latter molecules only trace particular regions of the gas. CO, on the other hand, as a very stable and abundant molecule and at the same time, being responsible for most of the cooling of the molecular gas, is a very reliable tracer of the physical conditions in the gas. Recent improved modeling of PDR's (Gierens et al., 1992 ; Köster et al. in press.) shows CO multiline studies to be a good tracer for UV illumination of molecular clouds. Recent [CI] observations (J. Keene, priv. comm.), showing unexpected high [CI] emission for Galactic center clouds, support the result that these clouds are very different in their physical and chemical conditions.

Motivated by these reasons, we started a Galactic center observation program in the $^{12}CO(2\rightarrow1)$, $^{13}CO(2\rightarrow1)$, $^{12}CO(3\rightarrow2)$, and $^{13}CO(3\rightarrow2)$ lines at KOSMA in winter 92/93. These data have about the same angular resolution as the data from the Bell Labs 7m telescope $^{12}CO(1\rightarrow0)$, $^{13}CO(1\rightarrow0)$, and $CS(2\rightarrow1)$ survey of the Galactic center region. We started The KOSMA survey in the Sgr C complex. This region is of particular interest because it offers the chance to study the relation between the GMC's and unique features like the radio filaments in much less confused regions above the Galactic plane, as for example in Sgr A.

Despite of the difficult conditions, especially the low elevations of the Galactic Center at Gornergrat, we obtained spectra of good quality. The observations were made in the "balanced position switching" mode (BPS) which proved to be suitable for measurements at low elevations. We show an example of our first results, a comparison of a $^{12}CO(2\rightarrow1)$ and a $^{13}CO(2\rightarrow1)$ spectrum measured with the KOSMA 3m telescope.

References

Bally et al., 1987, APJ Suppl. 65, 13; 1988, APJ, 324, 223
Bally and Yusef Zadeh, 1989, APJ, 336, 173
Genzel et al., 1990, APJ, 356, 160
Gierens et al., 1992, A&A, 259, 271
Güsten, 1989, Lecture Notes in Physics, 331, 163, Springer Verlag
Köster et al. in press.
Morris and Yusef-Zadeh, 1989, APJ, 343, 703
Poglitsch et al., 1991, APJ, 374, L33
Serabyn and Güsten, 1991, A&A, 242,376

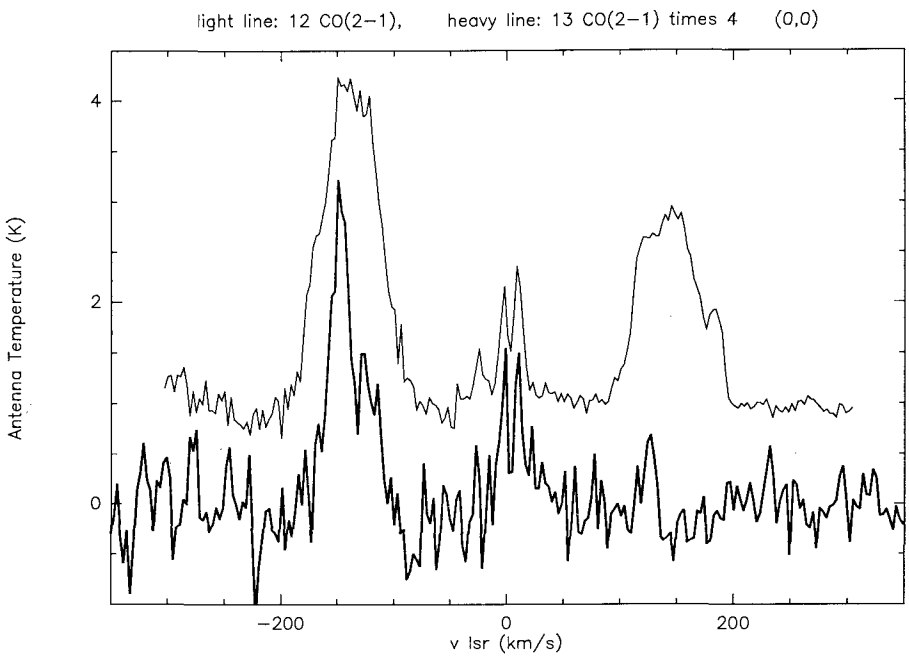

Spektrum of $^{13}CO(2\rightarrow1)$ (heavy line) and $^{12}CO(2\rightarrow1)$ (light line) at $l = 359.50766^o$ and $b = 0.12985^o$, observed with the KOSMA 3m Telescope. The ^{13}CO spectra are scaled by a factor of four. The negative velocity emission in these spectra originates in a molecular cloud near the Sgr C complex.

The Spatial Distribution of Emission from the Unidentified Infrared Bands

[1]F. O. Clark, [2]Rob Assendorp, [2]Paul Wesselius, [2] Peter Roelfsema, [2]Do Kester, [1]R. F. Shipman, [1]Thomas A. Kuchar, [1]M. P. Egan, and [1]R. L. Phelps

[1]Department of the Air Force, Phillips Laboratory, Geophysics Directorate (AFGL), 29 Randolph Road, Hanscom AFB, MA 01731-3010 and [2]Laboratory For Space Research, Postbus 800, 9700 AV Groningen, The Netherlands

Abstract. The IRAS focal plane contained a slitless spectrometer, the Low Resolution Spectrometer (LRS). Several regions in the Rosette nebula HII region are nearly unresolved in the in-scan direction, permitting extraction of LRS spectra. The spectral coverage of the LRS includes some of the unidentified infrared (UIR) bands, associated with PAHs by some authors. The extracted spectra include three clearly defined regimes: low density ionized material, of order 30 cm^{-3}, non-ionized material of the same density, and denser material with equivalent luminosity of an embedded early B star. Only the last exhibit UIR emission bands in our data.

Introduction. The objective of the current work is to model the short wavelength infrared emission from extended regions of the diffuse interstellar medium. Spectroscopy with the IRAS LRS probes the relevant emission mechanisms.The electronics of the LRS spectrometer require minimum brightness levels of a few W/m^2 on the focal plane to prevent internal electronic clamping. Therefore, we were forced to work with regions of enhanced radiation field. We have extracted spectra for several spatially large H II regions and supernova shells. New techniques developed at the Laboratory for Space Research in Groningen were used for manipulating data from the IRAS focal plane.

LRS spectra were successfully extracted from the Rosette, a large spatially resolved H II region. The ionized material in the Rosette is surrounded by an unresolved outer rim with more extended enhanced infrared emission. Much of the region surrounding the Rosette exhibits both CO and ^{13}CO emission (Blitz and Thaddeus 1980). There are four locations in which 12 and 25 micron emission peaks are precisely spatially coincident with strong CO emission (Cox, Deharveng, and Leene 1990).

Spectra. The IRAS Low Resolution Spectrometer (LRS) was of slitless design. The in-scan direction, or direction of spacecraft travel, was the IRAS LRS dispersion direction. Although the LRS was intended for use on point sources, LRS spectra may be extracted from extended objects which are unresolved in the dispersion or in-scan direction (Shipman and Clark 1994). The unresolved character of the outer rim of the Rosette was confirmed using the small IRAS edge detectors. 18 spectra LRS spectra were successfully extracted from this and other locations in the Rosette using a new Laboratory for Space Research Groningen (ROG) LRS software package.

We also extracted known spectra in the field as a check on the process. The extracted spectrum of AFGL 961 was identical to that contained in the IRAS Atlas of Low Resolution Spectra (1986) and will not be discussed further.The new spectra may be placed in three categories. 1. Four spectra from objects within the ionized region exhibit no emission shortward of about ten microns and rise steeply to the red. 2. Eight spectra exhibit a featureless continuum rising slightly to the red. 3. Three spectra exhibit the previous continuum plus three broad emission bands associated with the Unidentified Infrared Emission Bands: 7.7, 11.3, and 12.5 microns.

We focus on the three unique locations in this complex that yield spectra exhibiting the unidentified infrared bands (plus continuum). These locations are three of the four locations which Cox et al. have shown to have spatially coincident CO, ^{13}CO, and IRAS 12 and 25 micron emission (the fourth is AFGL 961). In order to have spatially coincident millimeter molecular emission and infrared emission, a local source of internal heating is required. This source would preferentially be non-ionizing but luminous, that is an early B star. The three locations yielding UIR emission have luminosity determinations by Cox et al. which have ZAMS equivalent spectral classes of B1, B1, and B2. A similar location in Cox et al. with an

equivalent spectral class of B4 does not exhibit UIR emission. Therefore, these three regions which exhibit UIR emission appear to be functionally equivalent to reflection nebulae which exhibit UIR emission.

Conclusions. IRAS LRS spectra delineate three spectral regimes in and around the Rosette. Inside of the HII region, emission is very deficient shortward of 12 microns. The neutral surrounding medium exhibits only a featureless relatively flat continuum. Only at the location of the three strongest ^{12}CO and ^{13}CO peaks is this continuum supplemented by three emission bands, associated with the suite of UIR bands. The UIR bands in the LRS spectra are clearly restricted to regions of high molecular column density with a radiation field equivalent to that of a B1 or B2 star. The UIR bands are not a general characteristic of the neutral material surrounding the Rosette in these spectra. If these spectra are characteristic of the diffuse interstellar medium, then the UIR bands are found only in regions of restricted radiation field, relatively high shielding, and large molecular abundance. Such a conclusion is not consistent with previous claims in the literature that UIR emission is a characteristic of the diffuse interstellar medium.

References

Blitz, L., and Thaddeus, P. 1980, Ap.J., 241, 676
Cox, P., Deharveng, L., Leene, A., 1990 A&A, 230, 181
IRAS Catalogs and Atlases, Atlas of Low-resolution Spectra, 1986, A&A 65, 607
Shipman, R.F. and Clark, F.O. 1994, Ap.J., February (in press)

The Distribution of Gas and Dust in the ρ Oph Cloud

R. Liseau[1], C. Ceccarelli[1], Y. Fukui[2], D. Lorenzetti[1], A. Mizuno[2], S. Molinari[1], B. Nisini[1], P. Saraceno[1], L. Spinoglio[1]

[1] IFSI – CNR, CP 27, I–000 44 Frascati (Roma), Italy

[2]Dept. of Astrophysics, Nagoya University, Chikusa-ku, Nagoya 464–01, Japan

We have mapped the ρ Oph main cloud in the J=2-1 transition of CS with the Nagoya 4m millimetre-wave telescope. The 339 positions observed in CS (2–1) cover nearly $40' \times 40'$, a region which comprises the ρ Oph main cloud. The spatial distribution of the velocity integrated intensity, viz. $\int T_A^* \, dv$, is shown in Fig. 1. The CS emission appears elliptical with dimensions $2a \times 2b \sim 47' \times 28'$, corresponding to a projected sky area 2.0 pc^2 at the distance of 150 pc, and its overall appearance is similar to that in $C^{18}O$ (2-1), also mapped onto a $2'$ grid by Wilking (1991). In CS (2-1), however, the peak at ρ Oph A appears less saturated, and also the very high density region ρ Oph B is more prominent (though not dominant) than in $C^{18}O$ (for J=1-0 data, see: Wilking & Lada 1983). From our CS data and using 1×10^{-9} for the CS abundance, we estimate the cloud mass 540 $M_\odot$ (LTE) or 1450 $M_\odot$ (NLTE).

From IRAS 60 and 100μm images we determined the distribution of the colour temperature T_{col} for a dust emissivity law $\epsilon \propto \lambda^\beta$ with $\beta = -2$ (see: Greene & Young 1989), indicating the range 18 to 35 K. For these values of T_{col}, the optical depth at 60μm was estimated, ranging from 1.4 10^{-5} to slighltly above unity at the emission maxima (max $\tau_{60} = 1.14$). To estimate the mass of the emitting dust we used the dust opacity determined by Hildebrand (1983) at 250μm, viz. $\kappa_{250} = 10$ cm^2 g^{-1}, with the λ^{-2} scaling relation mentioned above. The total mass of the dust was thus found to be $M_{\rm dust} \geq 5.5$ $M_\odot$. The derived masses for the molecular and dust constituents of the ρ Oph cloud can be used to find global and local values of the gas to dust ratio. Globally, $M_{\rm gas}/M_{\rm dust} \sim 540/5.5$ to $1450/5.5 \sim 100$ to 250, i.e. values which are comparable to those commonly quoted in the literature. Regardless the validity of these formal results in an absolute sense, any 'average' gas to dust ratio is hardly ever encountered locally, however. In Fig. 2, the pixel to pixel (190″) variation of the gas to dust ratio in the ρ Oph main cloud is shown. Displayed is the ratio of the *normalized* mass distributions (normalized by the maximum value in each image). The spatial average of this ratio is ~ 200, but the ratio exhibits fluctuations by more than three orders of magnitude on spatial scales $\lesssim 0.15$ pc. Therefore, the conclusion that the molecular gas (as traced by CS and/or $C^{18}O$) is not well coupled spatially with the dust (as seen by IRAS) seems inescapable.

References

Greene T.P., Young E.T., 1989, ApJ 339, 258

Hildebrand R.H., 1983, QJRAS 24, 267

Wilking B.A., 1991, in: Reipurth B. (ed.) Low Mass Star Formation in Southern Molecular Clouds, ESO Sci. Rep. No. 11, p. 159

Wilking B.A., Lada C.J., 1983, ApJ 274, 698

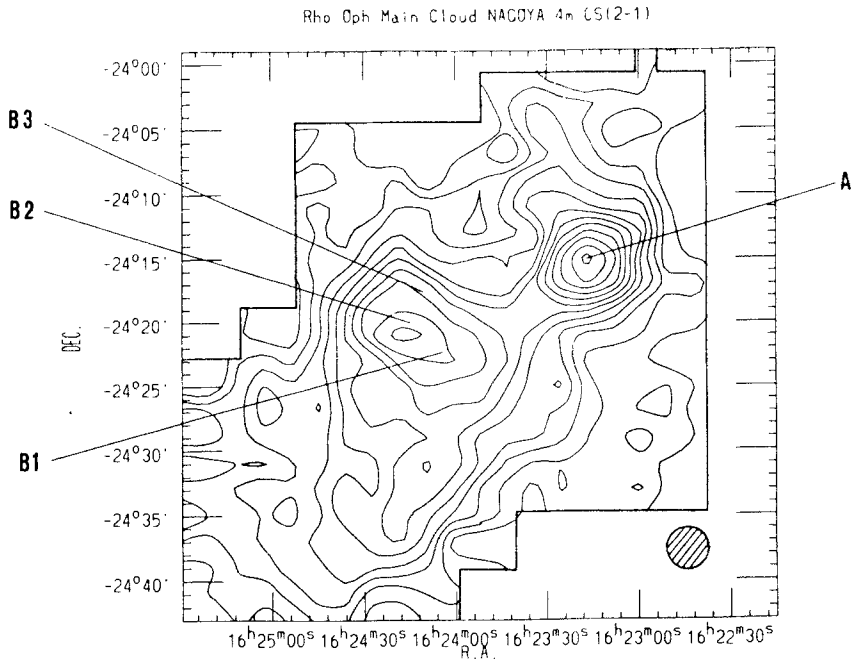

Fig. 1. The spatial distribution of the intensity of the CS (2-1) line, $\int T_A^* \, dv$ and evaluated between $v_{LSR} = +1.0$ to $+6.0$ kms^{-1}, is shown for the ρ Oph main cloud. The on a 2′ rectangular grid mapped region is outlined and the 3.2 arcmin beam of the Nagoya telescope is shown for comparison. The high density regions ρ Oph A and B are identified. The lowest displayed contour is at 0.2 K kms^{-1} and steps are in the same units.

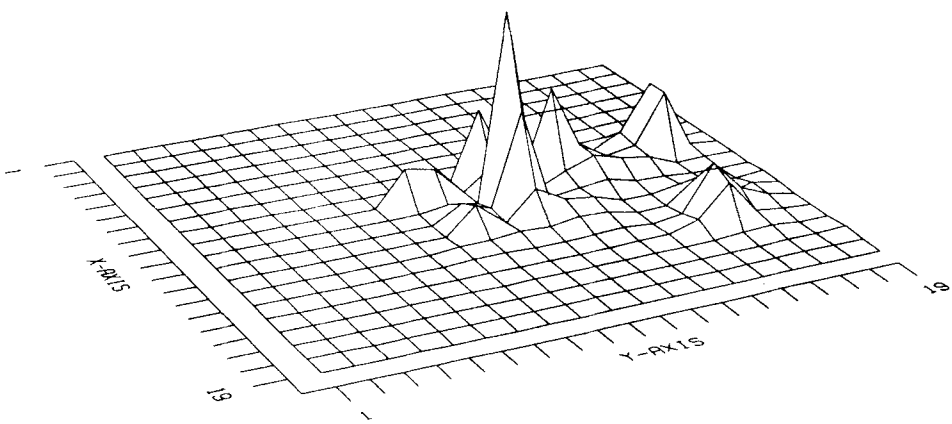

Fig. 2. The spatial distribution of the gas to dust ratio in the ρ Oph main cloud is shown on a 190″ grid, corresponding to 0.14 pc at the distance of 150 pc. Displayed is the ratio of the normalized mass distributions, i.e. $m_i/\max(m)$ for the gas (dust) mass in pixel i. Evidently, the distribution is not smooth but fluctuates wildly: the highest peak value $\gtrsim 10^3$.

Millimeter-Wave Observations of H_2CO in ρ Oph B1

M. Barsony[1,2], D.D. Sasselov[2], E.E. Bloemhof[2], and L.-A. Nyman[3]

[1] Department of Physics, University of California, Riverside, Riverside, CA 92521 USA

[2] Harvard-Smithsonian Center for Astrophysics, 60 Garden Street, Cambridge, MA 02138 USA

[3] Swedish-European Submillimeter Telescope, European Southern Observatory, La Silla, CHILE

After H_2 and CO, the most abundant molecular species in the cold, molecular clouds in which stars form are NH_3 and H_2CO. However, H_2CO has been relatively under-utilized as a probe of molecular cloud conditions simply because many of its transitions lie outside the bandpasses of millimeter receivers optimized to detect the CO transition near 115 GHz. H_2CO, however, does have a wealth of transitions spanning the cm-submm wavelength range, and with the advent of broadband, higher frequency receivers, H_2CO is being rediscovered as a valuable probe of star-forming regions.

Using H_2CO as a probe of star-forming regions has many advantages. Besides its abundance and ubiquity, H_2CO is found to be relatively homogeneous chemically, despite the striking chemical diversity found among star-forming clouds (Mangum, Wootten, & Plambeck 1993). Although the population of the energy levels of all molecules depends on both temperature and density, due to its unique geometry, certain combinations of H_2CO transitions have maximum sensitivity as tracers of either density or temperature, allowing nearly independent determinations of these two important physical quantities using just one molecular probe. Unlike linear molecules, H_2CO exhibits near-frequency coincidence of transitions originating from a wide range of excitation conditions. Finally, H_2CO comes in two flavors which do not mix: *ortho-* (H-spins parallel, S = 1) and *para-* (H spins anti-parallel, S = 0) since dipole radiation and collisions do not change spin states. The *ortho-* species is 3 times as abundant as the *para-* species, allowing for determination of optical depths.

The H_2CO J=3→2 transitions at 218 GHz and 226 GHz require much higher densities for thermalization than the more commonly observed CO J=1→0 or CS J=2→1 transitions. Therefore, H_2CO is potentially a much better density probe of the physical conditions prevalent in cold, pre-stellar cores than either CS or CO. For this reason, we decided to start a program of H_2CO observations of the unique ρ Oph B1 pre-stellar core with SEST (the Swedish-European Submillimeter Telescope).

Within the nearby (d = 140 pc) ρ Ophiuchus star-forming molecular cloud, the mass concentration known as ρ Oph B (Loren *et al.* 1980) contains $\sim$ 100 $M_\odot$ and has an extinction of $A_V > 200$ mag. The ρ Oph B core is unique in that it contains no known embedded infrared sources, is not a source of far-infrared emission, and is extremely cold (as evidenced by its DCO+ emission [Loren & Wootten 1986]). Furthermore, it is one of only a handful of sources in the Galaxy known to exhibit the 2_{12}–2_{11} 2-cm transition of H_2CO in *emission* (over an $8' \times 4'$ region). Densitites $> 10^6$ cm^{-3} are required to drive this line into emission.

The figure below shows the high-resolution VLA image of the dense gas structure viewed in the 2-cm H_2CO emission line (Wadiak *et al.* 1985). It was claimed this structure broke up into rotating clumps, but due to lack of sensitivity and higher spatial resolution this suggestion remains tentative.

We acquired a SEST 226 GHz (3_{12}–2_{11}) H_2CO line map of this same region in April of 1992 with the new 230 GHz SIS receiver developed at Harvard-Smithsonian Center for Astrophysics. As you can see, the structures of the two maps are quite dissimilar, indicating the presence of significant optical depth effects.

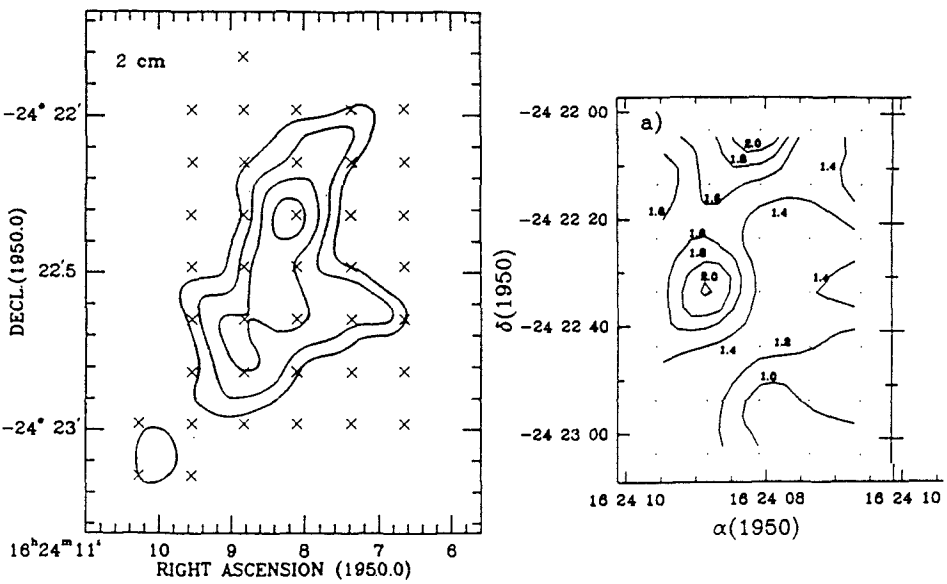

In addition to the 226 GHz map of ρ Oph B1, we also acquired a few spectra of the corresponding *para*-H_2CO (3_{03}–2_{02}) transition at 218 GHz (not shown here). For optically thin emission, we would expect the *ortho/para* line ratio to be 3:1. As you can see, the observed ratios are closer to 1:1, confirming the high optical depth of the 218 GHz *para*- line from the graph of T_R(para)/T_R(ortho) vs. log τ_{para} (taken from Sasselov & Rucinski 1990). In the same work, these authors also conclude, via their graph of T_{ex} vs. n_{H_2}, that for the observed 18K kinetic temperature of ρ Oph B1, an optically thick, or thermalized ($T_{ex} = T_{kin}$) 218 GHz *para*-H_2CO line indicates gas densities $> 10^7$ cm^{-3}!

We are in the process of acquiring and reducing further H_2CO data of this unique region in both optically thin isotopic species of the J=3→2 transition and in higher rotational transitions offering higher spatial resolution and less optical depth.

References

Mangum, J.G., Wootten, A., Plambeck, R.L. 1993, University of Texas preprint

Wadiak, E.J., Wilson, T.L., Rood, R.T. & Johnston, K.J. 1985, ApJL, 295, L43

Sasselov, D.D. & Rucinski, S.M. 1990, ApJL, 351, 578

Theoretical Models of Photodissociation Regions (PDRs)

D. J. Hollenbach and A. G. G. M. Tielens
NASA Ames Research Center, Moffett Field, CA 94035, USA

ABSTRACT

All neutral atomic gas and a large fraction of the molecular gas in the Galaxy lies in PDRs, and PDRs are the origin of most of the non-stellar infrared and the millimeter CO emission from a galaxy. On the surfaces ($A_v < 1-3$) of molecular clouds, photodissociation, grain attenuation of the FUV flux and grain photoelectric heating lead to intense emission of [CII] 158μm, [OI] 63μm, H_2 vibrotational transitions as well as IR dust continuum and PAH emission features. Deeper inside the clouds, CO rotational and [CI] 370,609μm lines are mainly produced in the PDR gas. Theoretical models compared with observations diagnose such physical parameters as the density and temperature structure, the elemental abundances, and the FUV radiation field. Applications are made to Orion, NGC 7023 and M17, to the clumpiness of molecular clouds, and to the ISM in the nuclei of infrared-luminous galaxies. Theoretical PDR models can explain the observed correlation in the CII(158μm) and CO J=1-0 emission and the correlation of the CO J=1-0 luminosity with the molecular mass. Theoretical models also suggest FUV-induced feedback mechanisms which may regulate star formation rates and the column density through giant molecular clouds. X ray PDRs may produce luminous H_2 (2μm), FeII(1.64μm), and Brackett emission in clouds near AGNs.

I. INTRODUCTION

Photon dominated regions or photodissociation regions (PDRs) include all interstellar regions where the gas is predominantly neutral and yet FUV (6eV< $h\nu$ < 13.6 eV) photons play a significant role in the heating and/or the chemistry. Most theoretical models of PDRs are one dimensional models with an FUV flux G_0 (in units of the average interstellar flux of 1.6×10^{-3} erg cm^{-2} s^{-1}, Habing 1968) incident on a neutral cloud of hydrogen nucleus density n (see Figure 1). The FUV flux can range from the

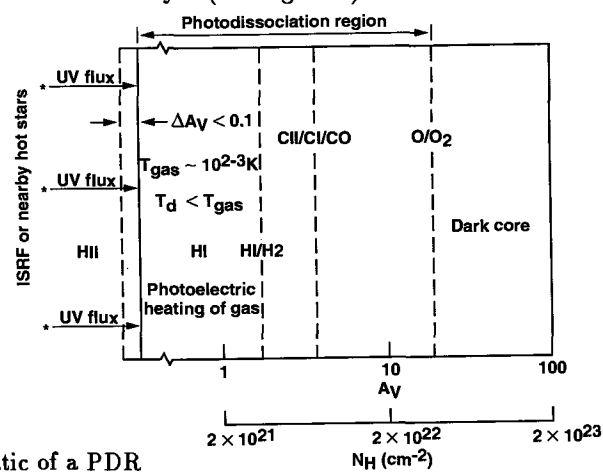

Figure 1. Schematic of a PDR

average local interstellar value, $G_0 = 1$, to $G_0 \sim 10^6$ for a PDR surrounding a compact HII region around a luminous O star ($L = 10^5$ $L_\odot$, $r = 0.1$ pc). Typically, densities range from $\sim$ 10 cm^{-3} in the diffuse interstellar medium to $\sim$ 10^7 cm^{-3} in dense clumps near newly formed O stars. Although mildly dependent on G_0, PDR models are generally characterized by a layer of photodissociated atomic hydrogen which extends to a depth $A_v \sim 2$, a layer of photoionized C^+ which extends to a depth $A_v \sim 4$ (with C and CO at deeper layers), and a layer of photodissociated atomic oxygen which extends to a depth $A_v \sim 10$. Traditionally, PDRs have been identified as being atomic gas associated with HII regions, reflection nebulae, planetary nebulae, and galactic nuclei. However, with the above definition, PDRs include material in which the hydrogen is molecular, the carbon is mostly in CO, but where FUV flux still strongly affects the chemistry of oxygen not locked in CO. Since most molecular gas in the Galaxy is found in Giant Molecular Clouds (GMCs) with $A_v \lesssim 10$, then *all of the atomic and most of the molecular gas in the Galaxy is in PDRs.*

Not only do PDRs include most of the mass of the ISM, but PDRs are also the origin of most of the IR radiation from the ISM. The incident FUV flux is absorbed primarily by grains inside a depth $A_v \sim 1$. Most of the absorbed energy is used to heat the grains and is converted to FIR continuum radiation of the cooling grains. However, typically 0.1-1% of the absorbed energy is converted to energetic ($\sim$ 1 eV) photoelectrons which are ejected from grain surfaces and heat the gas (" photoelectric heating"). Although the gas receives $10^2 - 10^3$ times less heating energy per unit volume than the grains, the gas attains higher equilibrium temperatures, $T_g > T_{gr}$, due to the much less efficient cooling of the gas (via [CII] 158 μm and [OI] 63 μm primarily) relative to the radiative grain cooling. From depths $A_v \lesssim 4$ originates much of the [CII], [OI], and [SiII] fine structure, the H_2 rotational and vibrational, and the CII recombination lines including the CI(9850Å) emission. Somewhat deeper into the PDRs comes most of the [CI] fine structure, and the CO rotational emission in galaxies. For example, the COBE 4μm–1000μm spectrum of our Milky Way Galaxy (Wright et al 1991) is dominated by PDR emission, with the exception of the [NII] and a fraction of the [CII] fine structure emission which originates in diffuse HII gas.

This review focusses on recent theoretical models of PDRs associated with molecular clouds, as opposed to diffuse or translucent clouds. Modeling of clumpy PDRs has been a particular subject of active research in recent years. Previous reviews of PDRs include Genzel et al (1989), Genzel (1991,1992), Hollenbach (1990), Jaffe & Howe (1989), Sternberg (1992), and van Dishoeck (1992). Theoretical models of diffuse and translucent clouds can be found in van Dishoeck & Black (1986) and references therein.

II. PHYSICAL PROCESSES

Theoretical models of PDRs couple treatments of chemistry, thermal balance (heating and cooling), and radiative transfer. These treatments are intimately linked because the chemistry depends on the temperature and FUV radiation fields and the temperature depends on the chemical species available for cooling. Radiative transfer is required to solve the penetration of the FUV and the cooling of the optically thick lines.

The principal difference between PDR chemistry and the chemistry of opaque molecular cores is the dominant role of FUV photodissociation and photoionization. Generally, the grains attenuate the FUV and these rates diminish with increasing depth or A_v into the cloud. Roberge et al (1991) has recently treated grain attenuation of FUV in a homogeneous medium. Boissé (1990) has developed methods for treating FUV penetration in an inhomogeneous or clumpy medium.

The photodissociation of H_2 and CO is made more complicated by the effects of self shielding. The most recent detailed treatment of the self shielding of H_2 is in Le Bourlot et al (1993); van Dishoeck & Black (1988) describe the theoretical treatment of CO self shielding. For high values of G_0/n grain attenuation results in conversion of H to H_2 and C^+ to CO at $A_v \sim 1-4$. However, when $G_0/n \lesssim 10^{-2}$ cm^3, self shielding of H_2 and CO can lead to molecular conversion at depths $A_v < 1$. G_0/n is the controlling parameter because the molecular photodissociation rate scales as $G_0 n$ while the molecular formation rate scales as n^2.

Moderately endothermic reactions or reactions with activation barriers are also important in PDR chemistry, since the PDR gas can attain temperatures $T \gtrsim 300$ K. One such key reaction is the reaction of O and H^+ ($\Delta E/k = 228$ K). In very warm gas, the reaction of O with H_2 to form OH, which is endothermic by $\Delta E/k \sim 4000$ K, becomes important. In addition, some of these same H_2 reactions with barriers proceed rapidly with vibrationally-excited H_2 (H_2^*). Large abundances of H_2^* are created in PDRs due to the FUV pumping of the molecule.

The cooling of PDRs is generally dominated by [CII] 158 μm and [OI] 63 μm cooling in the surface regions and by CO rotational cooling in the inner regions. Tielens & Hollenbach (1985a, henceforth THa) and Sternberg & Dalgarno (1989, henceforth SD) provide comprehensive treatments of the coolants, and Le Bourlot et al (1993) provide a summary of a few updated collisional rate coefficients.

FUV-excited H_2^* can be a significant source of heating if the gas densities are sufficiently large ($n \gtrsim 10^5$ cm^{-3}) to enable collisional de-excitation of the H_2^* (see Hollenbach 1988, SD, Burton et al 1990). However, the dominant PDR heating process for $A_v \lesssim 2-4$ is generally the grain photoelectric heating mechanism (Hollenbach 1988, 1989).

Following Watson (1972), d'Hendecourt & Léger (1987) recognized the importance of PAH molecules for photoelectric heating due to their higher photoelectric yields and relatively greater ability to recombine with electrons. Bakes & Tielens (1994) have constructed a detailed model of grain photoelectric heating which incorporates a realistic size distribution of particles ($\propto a^{-3.5}$) from PAH molecules (~ 3 Å) to small grains (~ 100 Å). They find that for high incident FUV fluxes as much as $\sim 50\%$ of the grain photoelectric heating comes from particles with radii between 3-15 Å (see Figure 2).

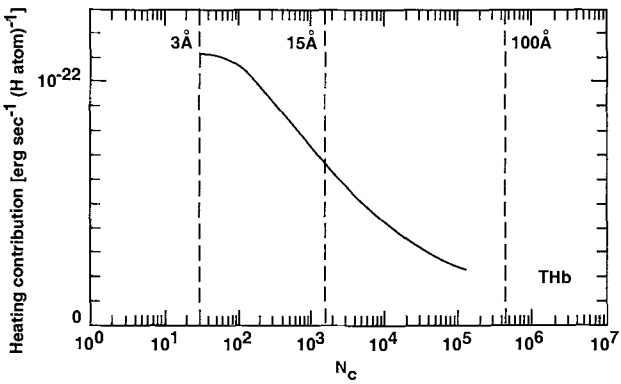

Figure 2. The heating contribution of grains of radius a, number of carbon atoms N_C for the TH standard case with $G_0 = 10^5$ and $n = 2 \times 10^5$ cm^{-3}. The area under the curve is proportional to the total heating.

III. APPLICATIONS

A. Physical Conditions in PDRs

1D homogeneous models with few free parameters fit a number of observations in regions as diverse as the dense neutral core behind the Trapezium in Orion (Tielens & Hollenbach 1985b, hereafter THb), the reflection nebula NGC7023 (Chokshi et al 1988), the Orion bar (Tielens et al 1993), and the Galactic center (Wolfire et al 1990). The parameters of the models are mainly the incident FUV flux G_0, the cloud hydrogen density n, and the gas phase abundances of the elements C, O and Si. These parameters are not totally "free", but are generally quite constrained by other observations. Figure 3 shows a typical comparison of a theoretical model with observation for the region behind Θ^1C in Orion. The theoretical model has G_0=10^5 and $n = 2 \times 10^5$ cm^{-3}. 1D

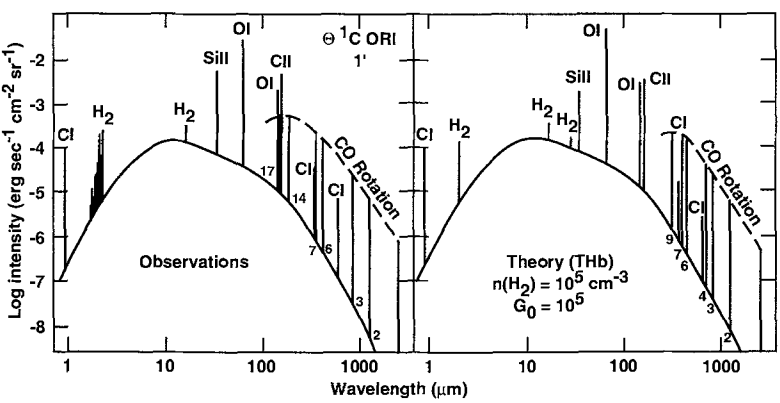

Figure 3. Observations (left) versus theory (right) of the PDR behind Θ^1C.

PDR models readily fit the observed [CII] and [CI] (if $x_C \sim 3 \times 10^{-4}$, see THb, Tielens and Hollenbach 1985c, Hollenbach, Takahashi, & Tielens 1991, hereafter HTT), [OI] 63 and 145 μm (THa, SD, HTT), [SiII] 35μm (THa, Haas et al 1986, SD, Burton et

al 1990), the H_2 2μm vibrational spectrum (Black & van Dishoeck 1987, Sternberg 1988, Sternberg & Dalgarno 1989, Burton et al 1990), the H_2 ground state rotational transitions (Burton et al 1992), the CO rotational transitions (THa, HTT, Burton et al 1990), the carbon radio (THa, Natta et al 1994) and optical (THa, Escalante et al 1991) recombination lines, and the grain FIR continuum (HTT). Typically, in PDRs near dense HII regions like Orion and M17 $G_0 \sim 10^4 - 10^5$ and $n \sim 10^5$ cm^{-3}, whereas in reflection nebulae like NGC 7023 $G_0 \sim 10^3$ and $n \sim 10^3 - 10^4$ cm^{-3}.

Homogeneous PDR models have other applications. They explain the observed correlation of [CII] to ^{12}CO J=1-0 in regions of high G_0 (Wolfire et al 1989). Recent models of Le Bourlot et al (1993), Fuente et al (1993), and Sternberg & Dalgarno (1994) include larger chemical networks and find, for example, FUV-sensitive ratios such as HNC/HCN that can be compared with observational data (e.g., Jansen et al 1993). Wannier, Andersson and coworkers (Andersson et al 1993, Wannier et al 1993, and references therein) and Roger & Dewdney (1992) focus on the HI produced in PDRs, the former group modeling HI haloes around Giant Molecular Clouds and the latter group solving the *time dependent* 1D PDR evolution initiated when an early type star "turns on" in a cloud.

B. Clumpy PDR Models

Although the 1D homogeneous models were very successful in many respects, three major shortcomings soon emerged. They could not explain the extent of [CII] and [CI] in edge-on PDRs like M17 (e.g., Keene et al 1985, Stutzki et al 1988). They underpredicted the intensities of the high J lines of CO (e.g., Graf et al 1993, Stacey et al 1993). Finally, they predict flat-topped or self-absorbed ^{12}CO J=1-0 or 2-1 profiles from molecular clouds in an ambient radiation field instead of the observed peaked profiles (e.g., Wolfire et al 1993).

Clumpy PDR models resolve these shortcomings of the homogeneous models. Stutzki et al (1988), Howe et al (1991), Meixner et al (1992, 1993) and Stacey et al (1993) showed that the observed extent of the [CII] and [CI] emission could be understood by the penetration of the incident FUV flux through a clumpy medium in which the interclump medium provided little attenuation of the flux. In M17, for example, the clump density in the models needed to be $\gtrsim 10^5$ cm^{-3} while the interclump density was $\lesssim 10^3$ cm^{-3} in order to match the extent (penetration) and observed spectra. Boissé's (1990) models of FUV penetration into clumpy media were instrumental for these studies.

A number of researchers investigated CO isotopic line strengths in clumpy media. Let us define "low J" as those transitions with J$<$ 4, "mid J" as 4$\leq$ J $\leq$ 10, and "high J" as J$>$ 10. Tauber & Goldsmith (1990) modeled low J ^{12}CO line strengths, while Gierens et al (1992) included the ^{13} CO isotope. Köster et al (1993) modeled the mid J ^{12}CO and ^{13}CO strengths and showed how clumpy medium could produce the observed strengths since more PDR "surface area" was present in the beam. Burton et al (1990) showed that dense clumps would allow self shielding of H_2 and CO *even in high FUV fields*. The self shielding brings the ^{12}CO to the warm surface region and produces strong mid and high J ^{12}CO emission. Wolfire et al (1993) showed that for GMCs

illuminated by the interstellar radiation field, the observed ^{12}CO J=1-0 line strengths cannot be produced by cosmic ray heating, but is heated by grain photoelectric heating.

The observed peaked profiles of the CO lines could also be produced in a clumpy medium, if one assigned a (macroturbulent) Gaussian velocity distribution to the clumps. Tauber & Goldsmith (1990) modeled the profiles for high values of G_0, while Wolfire et al (1993) modeled the profiles for low values of G_0 appropriate for average conditions in GMCs. To produce the observed smoothness of the profiles in nearby clouds, the clumps are numerous and very small ($\lesssim 10^{15} - 10^{16}$ cm), and these clumps are not gravitationally bound. de Boisanger & Chièze (1991) and de Boisanger et al (1992) suggest that the time dependent shadowing of the moving clumps may energize the turbulence.

C. Correlation of ^{12}CO J=1-0 with the H_2 Mass

There has been considerable discussion over the last decade concerning the correlation of the luminosity of ^{12}CO J=1-0 with the molecular mass of a cloud (e.g., Young & Scoville 1982, Solomon et al 1987). The observed ^{12}CO J=1-0 originates from FUV heated PDRs on the "surfaces" of opaque molecular clouds; Wolfire et al (1993) have applied PDR models to study this correlation. The observations indicate that there is roughly a constant column density, or A_v, through molecular clouds ($A_v \sim 7.5$, see Solomon et al 1987 or McKee 1989). In this case, the cloud's mass is proportional to its area and, if the CO line integrated intensity is relatively constant from cloud to cloud, the CO luminosity will trace area and therefore mass. (For a dissenting view that cloud densities are constant and that the mass is proportional to their volume, see Liesawitz 1990). Wolfire et al (1993) have subjected model molecular clouds to an external FUV flux G_0 and have self-consistently calculated the temperature and CO abundance as a function of position in each cloud in order to predict the ^{12}CO J=1-0 luminosity. The PDR theoretical models match the observed correlation for $G_O = 1$ and the results are insensitive to G_0 (the correlation factor changes by less than a factor of 4 for $G_0 = 0.1 - 10^3$).

D. FUV Photons, Star Formation, and the A_v of Molecular Clouds

McKee (1989) explains the observed constancy of A_v (~ 7.5) in molecular clouds with a PDR model. The basic idea derives from the assumptions that the rate of low-mass star formation is governed by ambipolar diffusion (cf., Shu, Adams and Lizano 1987) and that newly-formed stars inject energy into the cloud which supports the cloud against gravitational collapse. The ambipolar diffusion rate is set by the ionization fraction which depends on the dust shielding of the flux G_0 (i.e., the star formation rate increases as the cloud collapses and A_v increases). Equilibrium is achieved when $A_v \sim 7.5$. The external FUV flux, in controlling the ionization fraction in most of the cloud, regulates the low-mass star formation rate and the cloud column density.

Parravano (1988) proposes that a feedback mechanism exists in galaxies whereby the galaxy-wide rate of high-mass star formation is also regulated by the interaction of the FUV with the neutral gas. He notes that non-gravitationally bound neutral gas may exist in two phases (cold, $\sim$ 100 K, and warm, $\sim 10^4$ K) in a galaxy, if the ISM

pressure lies in a critical range $P_{min} < P < P_{max}$ (Field et al 1969). For pressures $P < P_{min}$ only the warm diffuse phase exists. Parravano makes two assumptions in his modeling: (i) grain photoelectric heating dominates both phases so that P_{min} monotonically increases with G_0, and (ii) molecular, star-forming clouds grow out of the cold phase (e.g., out of the coalescence of cold phase clouds). Suppose that the pressure P of the ISM is greater than P_{min} so that the cold phase exists. Molecular clouds grow, OB stars form, G_0 increases and P_{min} rises. If P_{min} exceeds P, however, the cold phase no longer exists, star formation drops, G_0 drops, and P_{min} drops. Thus, the global OB star formation rate is regulated so that $P_{min} \sim P$ in galaxies. Parravano offers some observational support of this prediction in external galaxies.

E. Formation of Molecular Clouds

Elmegreen (1991, 1993) has constructed simple analytic models of the self-shielding of H_2 in order to study the galactic conditions necessary to produce molecular clouds in the presence of an external FUV flux. He distinguishes between diffuse clouds (non-self-gravitating) and self-gravitating clouds, and shows that diffuse clouds can be molecular and that self-gravitating clouds can be atomic depending on the external pressure P_e on the cloud, G_0, the metallicity Z, and the cloud mass M. A shielding function $S \propto P_e^{13/12} M^{-1/2} Z G_0^{-1}$ determines whether a given cloud is molecular or atomic: large S implies a shielded molecular cloud. The functional form of the shielding function shows why the most massive clouds in a galaxy might be atomic, why outer Galaxy clouds with low P_e might be atomic, why large regions of galaxies can spontaneously convert to molecular form following either an interaction that triggers mass accretion or the passage of a spiral density wave (both increase P_e), and why the H_2 can convert back to H once OB stars form and G_0 rises.

F. The ISM of IR-Bright Galaxies

Wolfire et al (1990) have shown how theoretical PDR models can be compared with infrared and ^{12}CO observations to derive numerous interesting average physical parameters which describe the ISM in the central $\sim$ 1 kpc of relatively nearby, IR-bright galaxies and in the central 10 pc of our Galaxy. The required observations for this modeling procedure are the CII(158μm), OI(63μm), SiII(35μm), and ^{12}CO J=1-0 lines and the IR continuum. Typically, the beam size for these observations is of order 1', which corresponds to 1.4 kpc at a distance of 5 Mpc. The model assumes that there exist N molecular clouds in the beam, all having characteristic radius R and gas density n and illuminated by an FUV flux G_o. The above observations compared with the PDR modeling can not only determine these four parameters, but also the mass M_a of warm atomic PDR gas in the beam, the average temperature T_a of this gas, the mass M_m of molecular gas, and the average gas phase abundance of silicon x_{Si}.

Results have been obtained for M82 by Crawford et al (1985), Wolfire et al (1990), and Lord et al (1994), and for NGC 253 and NGC 3256 by Carral et al (1994). The derived average gas densities are $\sim 10^4$ cm^{-3}, and the incident FUV flux $G_0 \sim 10^3 - 10^4$ (recall these are very bright central regions with starburst activity). The atomic (CII) temperatures are $\sim 200 - 300$ K, and the mass in this component is very significant,

ranging from 2-10% of the total gas mass. The gas phase silicon abundances are high, $x_{Si} \sim 2 \times 10^{-5}$ ($\sim$ 0.5 solar), in M82 and NGC 253. This may reflect the starburst activity which results in a high rate of supernovae. The resultant high frequency of strong shock waves partially vaporizes interstellar grains and raises the *gas phase* abundances of refractories like silicon. The derived number of clouds and their sizes are surprising; there are numerous ($N \sim 10^5$) small ($R \lesssim 1$ pc) clouds present. These "clouds" are individual entities in the sense that they cannot shadow each other from the FUV flux. Nevertheless, they may be clustered together in sheets or filaments. The *average* ISM physical conditions in these galactic nuclei are similar to those in Orion and NGC 7023 (see IIIA). However, the conditions are far different from the *average* ISM conditions in the solar vicinity: the pressures, densities, and FUV fields are higher by factors of order 10^3.

G. X Ray PDRs

In much the same spirit as FUV PDR models, Maloney, Hollenbach, & Tielens (1994) model the effect of incident X rays on molecular clouds. The models include thermal balance, chemistry and radiative transfer. In these models, X rays dominate the gas heating by photoionizing atoms and molecules and depositing a significant fraction of the primary and secondary electron energy into heat. X rays also dominate much of the chemistry through the collisional dissociation and ionization of species by secondary electrons and through the photodissociation and photoionization by FUV photons produced via excitation of H and H_2 in collisions with secondaries.

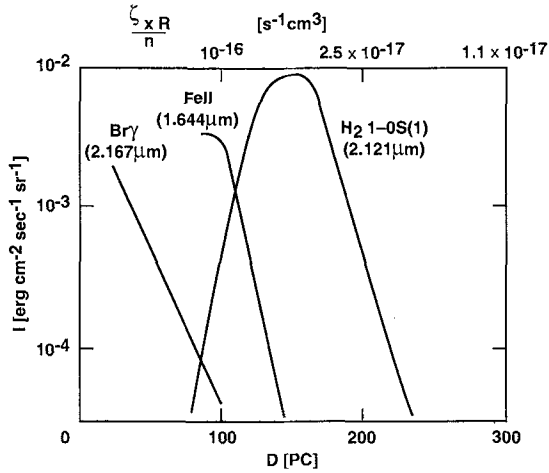

Figure 4. The H_2 1-0S(1), HII Brγ, and FeII(1.64μm) intensities from clouds of column $N = 2 \times 10^{22}$ cm^{-2} as functions of ζ_{XR}/n and D (see text).

These models can be applied to neutral gas near such X ray sources as supernova blast waves, protostars, the central stars of planetary nebulae, and the central engines of AGNs. Figure 4 shows preliminary results for the FeII(1.64 μm), HII Brγ, and H_2 1-0S(1) (2.2 μm) intensity emergent from a cloud with a hydrogen column $N = 2 \times 10^{22}$ cm^{-2} as a function of the "ionization parameter" ζ_{XR}/n, where ζ_{XR} is the total (primary

+ secondary) ionization rate per hydrogen and n is the hydrogen nucleus density. One key application of these models is to the Seyfert nucleus in NGC 1068, where H_2 and FeII emission are observed with intensity $I \sim 10^{-3}$ erg cm^{-2} s^{-1} ster^{-1} at distances $\sim$ 100 pc from the central source (Oliva & Moorwood 1990). The source is thought to be characterized by a luminosity $L_{XR} \sim 10^{44}$ erg s^{-1} in 1-100 keV X rays with a spectral index $\alpha \sim 0.7$. The horizontal axis is labelled on the top of the figure in terms of distance D from such a source, given a cloud density of 5×10^4 cm^{-3}. FeII(1.64 μm) dominates in the hot ($T \sim 5000$ K) atomic clouds located closer to the nucleus. H_2(2.2 μm) emerges from partially ($\sim$ 1%) molecular clouds somewhat further out. More distant clouds are too cold to appreciably radiate these high excitation lines ($\Delta E/k \sim 6000 - 10^4$ K above ground). Comparison of observed intensities with model predictions suggest beam filling factors of $\sim 10^{-1}$. The observed FeII line shows larger linewidths than the H_2 line, perhaps indicating that they are orbiting closer to the central source, as predicted. The H_2, FeII, and Brackett line emission are a direct consequence of the X rays emitted by the central engine, and do not require starburst activity.

IV. SUMMARY

PDRs emit much of the IR radiation (line and continuum) in galaxies. Most of the mass of the gas and dust in the Galaxy resides in PDRs and is significantly affected, either via chemistry or heating, by the FUV flux. Much of the gas is heated by the grain photoelectric heating mechanism. The spectra from PDRs is characterized by ratios $(L_{CII} + L_{OI})/L_{IR} \sim 10^{-3} - 10^{-2}$. PDRs are the origin of most of the observed CII(158μm), OI(63,145μm), SiII(35μm), CI(370,609μm), H_2 rovibrational, CO rotational, and CII recombination radiation. The spectra diagnose physical conditions such as the gas density, the clumpiness of the clouds, the FUV radiation field, and the elemental abundances. As examples, physical conditions were derived in Orion, NGC 7023, M17 and galactic nuclei. The PDR models explain the correlation of CII(158μm) emission with ^{12}CO J=1-0 emission and of ^{12}CO J=1-0 with H_2 mass. The FUV flux in PDRs may regulate low and high mass star formation in galaxies, and may regulate the column density of gravitationally-bound, star-forming molecular clouds. New models of X ray illuminated molecular clouds may explain near-IR observations of Seyfert nuclei without invoking star formation.

We would like to acknowledge that much of our research reported here was done in collaboration with M. Burton, P. Maloney, T. Takahashi, and M. Wolfire. This research was supported in part by NASA RTOP 188-44-53 and by a special NASA Theory Program which funds the Center for Star Formation Studies, a consortium of researchers from NASA Ames, UC Berkeley, and UC Santa Cruz.

References

Andersson, B-G, Wannier, P.G. 1993, ApJ, 402, 585
Bakes, E., Tielens, A. G. G. M. 1994, ApJ, in press
Black, J. H., van Dishoeck, E. F. 1987, ApJ, 322, 412
de Boisanger, C., Chieze, J. P. 1991, A&A, 241, 581

de Boisanger, C., Chieze, J. P., Meltz, B. 1992, ApJ, 401, 182
Boissé, P. 1990, A&A, 228, 483
Burton, M., Hollenbach, D., Tielens, A. G. G. M. 1990, ApJ, 365, 620
Burton, M., Hollenbach, D., Tielens, A. G. G. M. 1992, ApJ, 399, 563
Carral, P. et al 1994, ApJ, in press
Chokshi, A., Tielens, A. G. G. M., Werner, M. W., Castelaz, M. W. 1988, ApJ, 334, 803
Crawford, M. K., Genzel, R., Townes, C. H., Watson, D. M. 1985, ApJ, 291, 755
Elmegreen, B. G. 1991, in *Dynamics of Galaxies and Molecular Clouds Distribution*, ed. F. Combes and F. Casoli (Kluwer: Dordrecht), p45
Elmegreen, B. G. 1993, ApJ, 411, 170
Escalante, V., Sternberg, A., Dalgarno, A. 1991, ApJ, 375, 630
Field, G. B., Goldsmith, D. W., Habing, H. J. 1969, ApJL, 155, L149
Fuente, A., Martín-Pintado, J., Cernicharo, J., Bachiller, R. 1993, A&A, 276, 473
Genzel, R. 1991, in *The Physics of Star Formation and Early Stellar Evolution*, ed. C. Lada & N. Kylafis (Kluwer: Dordrecht), p155
Genzel, R. 1992, in *The Galactic Interstellar Medium: Saas Fe Lectures 1991*, (Springer Verlag: New York)
Genzel, R., Harris, A. I., Stutzki, J. 1989, in *Infrared Spectroscopy in Astronomy*, ed M. Kessler (ESA SP series), p115
Gierens, K., Stutzki, J., Winnewisser, G. 1992, A&A, 259, 271
Graf, U. U. et al 1993, ApJ, 405, 249
Haas, M., Hollenbach, D. J., Erickson, E. F. 1986, ApJL, 301, L57
Habing, H. J. 1968, Bull. Astr. Inst. Netherlands, 19, 421
d'Hendecourt, L., Léger, A. 1987, A&A, 180, L9
Hollenbach, D. J. 1988, Astr. Lett. and Communications, 26, 191
Hollenbach, D. J. 1989, in *IAU Symposium 135, Interstellar Dust*, ed. A. G. G. M. Tielens and L. Allamandola, (Kluwer: Dordrecht), p227
Hollenbach, D. J. 1990, in The Evolution of the Interstellar Medium, ed. L. Blitz, (ASP: San Francisco), p167
Hollenbach, D. J., Takahashi, T., Tielens, A. G. G. M. 1991, ApJ, 377, 192 (HTT)
Howe, J. E., Jaffe, D. T., Genzel, R., Stacey, G. 1991, ApJ, 373, 158
Köster, B., Störzer, H., Stutzki, J., Sternberg, A. 1993, A&A, submitted
Jaffe, D. T. and Howe, J. E. 1989, *Rev. Mex. de Astron. y Astr.*, 18, 55
Jansen, D. J., van Dishoeck, E. F., Black, J. H. 1993, A&A, in press
Keene, J., Blake, G., Phillips, T., Huggins, P., Beichman, C. 1985, ApJ, 299, 967
Le Bourlot, J., Pineau des Forets, G., Roueff, E., Flower, D. R. 1993, A&A, 267, 233
Liesawitz, D. 1990, ApJ, 359, 319
Lord, S. D. et al 1994, in preparation
Maloney, P., Hollenbach, D, Tielens, A. G. G. M. 1994, in preparation
McKee, C. F. 1989, ApJ, 345, 782
Meixner, M., Haas, M. R., Tielens, A. G. G. M., Erickson, E. F., Werner, M. 1992, ApJ, 390, 499
Meixner, M., Tielens, A. G. G. M. 1993, ApJ, 405, 216

Natta, A., Walmsley, M., Tielens, A. G. G. M. 1994, ApJ, in press
Oliva, E., Moorwood, A. F. M. 1990, ApJ, 348, L5
Parravano, A. 1988, A&A, 205, 71
Roberge, W. G., Jones, D., Lepp, S., Dalgarno, A. 1991, ApJSuppl, 77, 287
Roger, R. S., Dewdney, P. E. 1992, ApJ, 385, 536
Shu, F. H., Adams, F. C., Lizano, S. 1987, Ann. Rev. Astron. Astrophys., 25, 23
Solomon, P. M., Rivolo, A. R., Barrett, J. W., Yahil, A. 1987, ApJ 319, 730
Stacey, G. et al 1993, ApJ, 404, 219
Sternberg, A. 1988, ApJ, 322, 400
Sternberg, A. 1992, in *Astrochemistry of Cosmic Phenomena*, ed. P. D. Singh, (Kluwer: Dordrecht), p329
Sternberg, A., Dalgarno, A. 1989, ApJ, 338, 197 (SD)
Sternberg, A., Dalgarno, A. 1994, in preparation
Stutzki, J., Stacey, G., Genzel, R., Harris, A., Jaffe, D., Lugten, J. 1988, ApJ, 332, 379
Tauber, J., Goldsmith, P. 1990, ApJL, 356, L63
Tielens, A. G. G. M. et al 1993, Science, 262, 86
Tielens, A. G. G. M., Hollenbach, D. J. 1985a, ApJ, 291, 722 (THa)
Tielens, A. G. G. M., Hollenbach, D. J. 1985b, ApJ, 291, 747 (THb)
Tielens, A. G. G. M., Hollenbach, D. J. 1985c, ICARUS, 61, 40
van Dishoeck, E. F. 1992, in *Infrared Astronomy with ISO*, ed. Th. Encrenaz & M. Kessler (Nova: New York), p283
van Dishoeck, E. F., Black, J. H. 1986, ApJSuppl, 62, 109
van Dishoeck, E. F., Black, J. H. 1988, ApJ, 334, 711
Wannier, P. G. et al 1993, ApJ, 407, 163
Watson, W. D. 1972, ApJ, 176, 103
Wolfire, M. G., Hollenbach, D. J., Tielens, A. G. G. M. 1989, ApJ, 344, 770
Wolfire, M. G., Tielens, A. G. G. M., Hollenbach, D. J. 1990, ApJ, 358, 116
Wolfire, M. G., Hollenbach, D. J., Tielens, A. G. G. M. 1993, ApJ, 402, 195
Wright, E. L. et al 1991, ApJ, 381, 200
Young, J. S., Scoville, N. 1982, ApJ, 258, 476

Chemistry in Dense Photon Dominated Regions

A. Sternberg

School of Physics and Astronomy, Tel Aviv University, Israel

Molecular clouds in star-forming regions are commonly exposed to intense fluxes of far-ultraviolet (6-13.6 eV) photons emitted by external or embedded OB type stars. The stellar radiation fields control the physical and chemical structures of the outer cloud layers which are called photon-dominated regions (PDRs). These layers are often sources of intense atomic and molecular emission lines. The clumpy structure of molecular clouds allows the FUV radiation fields to penetrate to large depths (Stutzki *et al.* 1988) and in many environments the bulk of the molecular material may reside in PDRs (Stacey *et al.* 1991). A review of observational and theoretical work on interstellar photon-dominated regions is presented by Hollenbach elsewhere in this volume. Here I discuss several gas-phase chemical processes that lead to the efficient production of various molecular species in PDRs. A more detailed study is presented in Sternberg and Dalgarno (1994).

The chemical structure of PDRs depends on several cloud parameters including, in particular, the total hydrogen particle density, and the intensity of the incident FUV radiation field. In star-forming regions the hydrogen density may range from 10^3 to 10^8 cm^{-3} and the incident FUV radiation may be up to a 10^6 times more intense than the average interstellar field. The chemical structure varies with cloud depth as the FUV radiation is absorbed by atoms, molecules and dust grains. Simple one-dimensional model calculations (Tielens and Hollenbach 1985, Sternberg and Dalgarno 1989, Sternberg and Dalgarno 1994) show that several distinct zones exist in PDRs in which the gas-phase chemistry (and resulting molecular abundances) are controlled by distinct sequences of chemical reactions. The detailed chemical structure depends on the hydrogen density, the FUV intensity, the grain properties and the gas-phase elemental abundances. Below I describe several processes which may typically occur in dense clouds.

Rapid molecular photodissociation maintains an HI layer near the cloud surfaces in which most of the hydrogen is atomic and the trace elements are present in either atomic or ionic form. In clouds with hydrogen densities greater than $\sim 5 \times 10^4$ cm^{-3}) these HI layers may become hot with temperatures exceeding 10^3 K. Warm H/H_2 transition layers then exist at larger cloud depths. The chemistry in these layers is driven by several endothermic hydrogen abstraction reactions. One important example is the formation of hydroxyl by the reaction

$$O + H_2 \rightarrow OH + H \qquad (1)$$

which becomes rapid in hot gas. The OH radicals are rapidly removed by photodissociation and the reverse of (1). However, large OH abundances may nevertheless be maintained by (1) in the H/H_2 transition layer. Indeed, rotational OH line emission can contribute significantly to the gas cooling in these cloud layers. OH is a crucial intermediary in the hot gas chemistry, and reactions of the form

$$OH + X \rightarrow XO + H \qquad (2)$$

where X is any of the abundant atoms and ions (e.g. O, N, C^+, Si^+, and S^+) lead to the efficient production of XO molecules (e.g. O_2, NO, CO^+, SiO^+ and SO^+). These molecular species are removed by rapid dissociative recombination and photodissociation. However, reactions (1) and (2) are sufficiently efficient to maintain large XO densities in the H/H2 transition layers. For example, the molecular ion SO^+, which has been suggested as a unique diagnostic of dissociative shocks (Turner 1992, Neufeld and Dalgarno 1989) may also be produced in large abundance in PDRs.

At larger cloud depths a CII zone exists in which most of the carbon is present in the form of C^+ and in which the hydrogen is fully molecular (and "self-shielded"). Species such as CH^+, CH, CH_2 and CN are formed efficiently in the CII zones compared with deeper cloud layers. The carbon chemistry is initiated by radiative association

$$C^+ + H_2 \rightarrow CH_2^+ + \nu \qquad (3)$$

and the reaction

$$C^+ + H_2^* \rightarrow CH^+ + H \tag{4}$$

where H_2^* are hydrogen molecules which have been vibrationally excited by FUV fluorescence. These initiating reactions are followed by the sequence

$$CH^+ + H_2 \rightarrow CH_2^+ + H \tag{5}$$

$$CH_2^+ + H_2 \rightarrow CH_3^+ + H \tag{6}$$

$$CH_3^+ + e \rightarrow CH + H_2 \tag{7}$$

$$CH_3^+ + e \rightarrow CH_2 + H \tag{8}$$

$$CH + N \rightarrow CN + H \quad . \tag{9}$$

The CH, CH_2 and CN molecules that are produced by reactions (5) through (9) are removed by photodissociation and their abundances increase towards the inner edge of the CII zone where the radiation field is partially attenuated but where the C^+ density remains large. The production of these molecules becomes much less efficient at deeper cloud layers where the C^+ density becomes small.

An SII zone exists beyond the edge of the CII where the sulfur is present in the form of S^+ and the carbon (and hydrogen) are incorporated into molecules. Species such as SH and H_2S^+ are efficiently produced in these zones by the reactions

$$S^+ + H_2 \rightarrow H_2S^+ + \nu \tag{10}$$

$$H_2S^+ + e \rightarrow SH + H \quad . \tag{11}$$

The densities of SH and H_2S^+ increase towards the inner edge of the SII zone as the electron density and the SH photodestruction rate decreases.

Broad SI zones may also exist in PDRs in which the sulfur is primarily atomic due to effective neutralization by charge transfer reactions such as

$$S^+ + Si \rightarrow S + Si^+ \quad . \tag{12}$$

The SI zones may contain enhanced abundances of molecules such as H_2S, CS, and OCS. The molecule H_2S may be efficiently produced by reaction (12) followed by the charge transfer reaction

$$H_2S^+ + S \rightarrow H_2S + S^+ \quad . \tag{13}$$

CS is produced by reaction (11) followed by the sequence

$$SH + O \rightarrow SO + H \tag{14}$$

$$SO + C \rightarrow CS + O \quad , \tag{15}$$

and OCS may be produced by

$$S + CO \rightarrow OCS + \nu \tag{16}$$

in the SI zone. Both of these molecules are removed by photodissociation, and their abundances increase towards the inner edge of the SI zone where the radiation field is most attenuated. Reactions (12) through (16) become much less effective in the dark cloud cores where the atomic carbon abundance becomes very small and most of the sulfur is preferentially incorporated into SO_2. Thus, the CS molecule may be a tracer of FUV illuminated molecular clouds in addition to serving as a diagnostic of dense gas due to its large dipole moment. Observational evidence for enhanced CS and H_2S abundances in PDRs has recently been presented by Jansen *et al.* (1993).

In the Table below I list the molecular species that are efficiently produced in various zones in the PDRs of dense molecular clouds.

Molecules in PDRs (dense gas).

zone	molecules
HI/H_2 hot/warm	OH NO CO^+ SO^+ SiO^+ HCO^+ CH^+ CH CH_2
CII warm/cold	CH^+ CH CH_2 CN
SII cold	SH H_2S^+
SI cold	CS OCS H_2S

References

Jansen D., van Dishoeck E.F., Black J. and Keene, J. 1993 *A.A.* in press.
Neufeld, D. and Dalgarno A. 1989, *Ap.J.*, 340,869.
Stacey G.J. *et al.* 1991, *Ap.J.*, 373,423.
Sternberg A. and Dalgarno A. 1994, in preparation.
Sternberg A. and Dalgarno A. 1989, *Ap.J*, **338**,197.
Stutzki J. *et al.* 1988, *Ap.J.*, 332,379.
Tielens A.G.G.M. and Hollenbach D.J. 1985 *Ap.J.*, **291**,722.
Turner B.E. 1992, *Ap.J.Letters*, 396,L107.

Photon Dominated Regions: Linking Observations and Theory

D.T. Jaffe
Astronomy Department, University of Texas at Austin
and
Max-Planck-Institut für extraterrestrische Physik

Introduction

Photon–dominated regions (PDR's) make up a substantial fraction of the dense interstellar medium. They account for most of the atomic and molecular line emission from neutral gas. The conditions in PDR's may also have a strong effect on the stability of interstellar clouds. The beautiful [C II] data presented Nakagawa (1994, this volume) illustrate how is now possible to observe photodissociated gas over large scales in our Galaxy and to begin thinking of modeling the global distribution and physical characteristics of PDR's. We need to learn how new measurements can be combined with the well–developed theoretical models of PDR's (see Hollenbach 1994) to improve our understanding of the interstellar medium and its interaction with star formation. Large–scale studies are relevant not only to the ISM in our own Galaxy but also to other galaxies, in particular to those with starbursts. Plans for future investigations of extended PDR material with satellites and ground–based instruments make a look at this issue quite timely. We discuss here recent investigations of PDR's on scales intermediate between those discussed by Nakagawa (1994) and those of the small–scale PDR studies presented elsewhere in this volume. We concentrate on three issues: How much PDR material is there in typical dense clouds? How well do PDR models account for the observed emission? How can we use PDR tracers to evaluate the properties of clouds?

Amount of PDR Material

In his review, Hollenbach (1994) points out that most of the dense ISM is a photon–dominated region. Since the effects of UV photons become somewhat subtle beyond an $A_V \sim 2$ thick shell at the outside of each cloud, it is difficult to observe all of the PDR material. One can, however, determine the amount of material in the outer layers of the PDR where carbon is mostly atomic. Shibai et al. (1991) estimate that as much as half the dense neutral material along one Galactic line of sight has carbon in the form of C II. Stacey et al. (1991) have observed a sample of inner regions of spiral galaxies and find that typically ~25% of the line of sight gas– phase carbon is in [C II]. Jaffe et al. (1994) have mapped the NGC 2024 molecular cloud and find over a $\sim 3 \times 2$ pc region, there is more gas–phase carbon in C II than in CO. For $N(CII)/N(H+2H_2) = 3\text{–}7 \times 10^{-4}$ and $N(^{13}CO)/N(H_2) = 2 \times 10^{-6}$, the Jaffe et al. results imply that 10–20% of the dense gas mass is in the C II region. At the edge of the NGC 2024 cloud, however, the CII/CO column density ratio is much (5–10 times) higher than average. The very different column density ratio seen at the cloud edge makes the point that ensembles of small clouds or of UV illuminated clumps could have much higher mass fractions in C II dominated gas than the average for clouds like NGC 2024. This result lends further credence to the argument that dense PDR's are a major source of the [C II]

line on galaxy–wide scales (Stacey et al. 1985; Crawford et al. 1985; Shibai et al. 1991; Wright et al. 1991). Under some circumstances, however, extended low density HII regions might also be a significant source of [C II] (Stacey et al. 1985; Shibai et al. 1991). In addition, Madden et al. (1993) have argued that there are large areas of the galaxy NGC 6946 where most of the [C II] emission must come from H I clouds.

There may also be a significant amount of *neutral* carbon (C I) in dense clouds. The S 140 molecular cloud has a lower average UV field than the NGC 2024 region (10–100 times the mean interstellar field as opposed to 10^2–10^4) and a modest column density (typically, N_{H_2} $\sim 4\times10^{21}$ cm^{-2}). Plume, Jaffe, and Keene (1994) have surveyed a $\sim 10\times10$ pc region in this cloud. They find CI/CO$\sim$0.5. Since the C II and C I column densities should be roughly comparable, (CI+CII)/CO is probably of order unity.

Tests of PDR Models

Models of photon dominated regions can successfully match the emergent intensities of important cooling lines as a function of the gas density and the incident UV intensity. We usually have only a rough idea, however, of the values of these two model input parameters. A more observationally useful test of the models is to ask how well they predict the relationships between various PDR line strengths. One of the most widely observed of such relationships is that between the [C II] emission arising in the outer layers of the neutral gas and the CO J=1$\rightarrow$0 emission arising in the warm molecular layer immediately behind the [C II] region. Crawford et al. (1985) first remarked on the extraordinary correlation between the intensities in these two lines. As a number of people have pointed out, much of this correlation stems from the huge range in distances to the sources in the Crawford et al. sample and the resulting correlated variation in beam filling factor (e.g. Wolfire, Hollenbach, & Tielens 1989). There are, however, reasons to expect a relationship between I(CO J=1$\rightarrow$0) and I([C II]), even when the intensities are normalized to eliminate beam filling factor effects. If both lines arise in the outer layers of UV illuminated molecular clouds, primarily in regions with dense (n$>$1000 cm^{-3}) gas and large UV fields, G_o ($>$100 in units of the mean interstellar radiation field), the similar dependences on density and on UV intensity of the two lines should lead to a correlation of the two intensities (Wolfire et al. 1989; Stacey et al. 1991). The NGC 2024 region mapped by Jaffe et al. (1994) is an ideal place to investigate the relationship between [C II] and CO J=1$\rightarrow$0. All of the data come from a source at a constant distance, there are a large number of points observed with the same equipment and there nevertheless a wide range of excitation conditions.

Figure 1 shows the relationship between the [C II] and ^{12}CO J=1$\rightarrow$0 intensities for NGC 2024. Overall, there is little correlation between the intensities of the two lines. Different parts of the source, however, have very different distributions in the I([C II])–I(CO) plane. We have divided the source into two regions: the cloud proper (less than 10' west of the radio peak, shown as solid dots in Fig. 1), and the western edge, a region $>$ 10' west of the radio continuum peak, near the O9I star ζOri (shown as open triangles). The points representing data from the western cloud edge stretch almost horizontally across the diagram. The highest [C II]/CO intensity ratios probably result

from having resolved the photodissociated layer at the edge of the cloud. For a cloud with a density of n(H)=10^4 cm^{-3}, a column density of 3×10^{21} cm^{-2}, characteristic of the layer where the [C II] emission arises (Hollenbach et al. 1991), is reached 3×10^{17} cm into the cloud (a projected angle of 50" at the distance of NGC 2024).

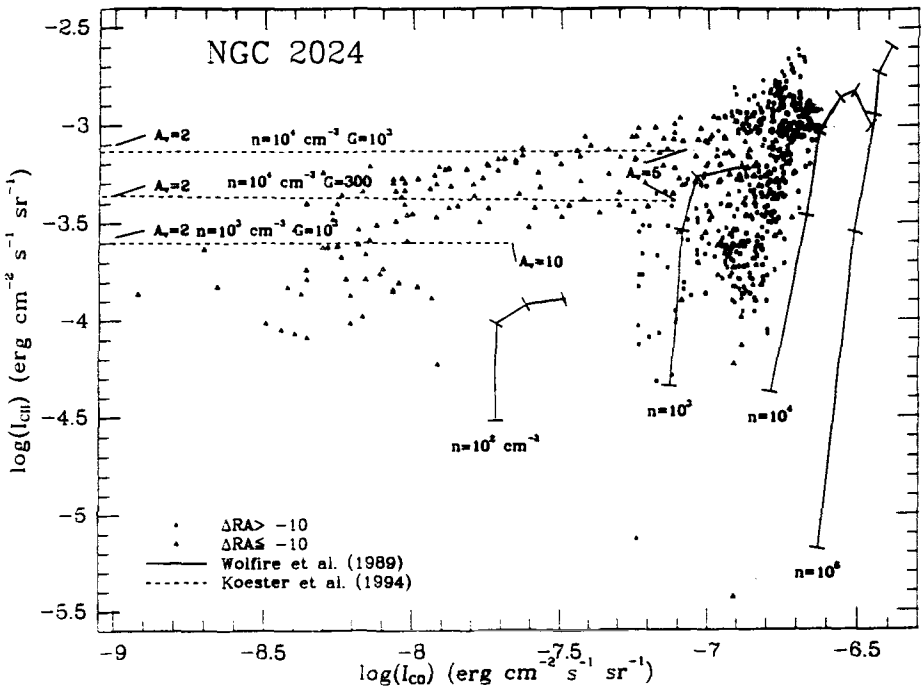

Figure 1: Comparison of [C II] 158 μm line versus ^{12}CO J=1→0 intensities for NGC 2024 (Jaffe et al. 1994). The ticks along the constant density families of Wolfire et al. models increase by factors of 10 from G_o 10 (from G_o=100 for n=10^6 cm^{-3}).

If we consider the cloud proper and western edge datasets separately, there is a significant I([C II])–I(CO) correlation. A fit to the points within the cloud yields

$$\log(I([\text{C II}])) \simeq 9.7 + [1.9\log(I(\text{CO}))] \ ,$$

while a fit to the points at the edge of the cloud yields

$$\log(I([\text{C II}])) \simeq -1.9 + [0.20\log(I(\text{CO}))] \ .$$

In both cases, the dispersion about this relation is large. Interestingly, the two relations intersect at I([C II])/I(CO)=3600 (where both intensities are expressed in the same units), close to the ratio derived by Crawford et al. (1985).

The solid lines in Fig. 1 show the PDR models of Wolfire et al. (1989) superposed on the Jaffe et al. (1994) data. Most of the points from the cloud proper lie between the groups of models calculated for n=10^3 and n=10^4 cm^{-3} within a range in far UV

flux, G_o from ~30 to 10^4. The location of the data relative to the models indicate that, in NGC 2024, variations in the strength of the UV field are more significant than variations in density. The dashed lines in Fig. 1 are based on the models of Köster et al. (1994) in which an infinite plane of finite thickness is illuminated from both sides with UV radiation. The dashed lines in Fig. 1 show how the I(CO)/I([C II]) relationship varies, for a given UV field and density, as the thickness of the slab is varied. Models with values of n and G_o close to those estimated for the western edge of NGC 2024 and thicknesses corresponding to A_V=2–5 can account for the measured strengths of the two lines in the western edge region. In addition, a comparison of the Köster et al. models with the slope of the I([C II])–I(CO) relation for the western cloud edge shows that variations in column density are responsible for the distribution of the points.

[C II] and the Interaction of OB Stars and Clouds

To the extent that [C II] emission arises in PDR's on dense clouds illuminated by external OB stars (many well–known regions, e.g. Orion A, NGC 2024, M17, and M16 fit this description), it is possible to use a tracer of Lyman continuum photons together with the [C II] line to learn about the sources of UV radiation and their characteristic distances from line emission regions. The radio continuum intensity from an ionization front depends on the number of incident Lyman continuum photons while the [C II] intensity depends on the total amount of incident UV and on the local intensity. Fig. 2 shows the ratio of [C II] to radio continuum flux intensity, $I([C\ II])/I_\nu(5GHz)$, for dense clouds as a function of the spectral type of the illuminating source and the distance to the exciting star from the cloud surface. The ratio is influenced both by the hardness and the intensity of the incident radiation. Using the radio continuum rather than far–IR continuum in the ratio makes it sensitive to stellar surface temperature and not simply to the incident far–UV flux. The value of the ratio increases initially along both axes as the radio continuum intensity drops linearly with decreasing N_L while the [C II] intensity depends only logarithmically on the far–UV luminosity, L_{UV}. At the extreme right, the ratio increases very rapidly as the stellar surface temperatures drop to the point where the Lyman continuum is on the Wien side of the stellar energy distribution and N_L drops much more rapidly than L_{UV}. The double– valued nature of the ratio as a function of distance at constant spectral type results from the sudden decrease in the [C II] intensity at the point where the UV field is insufficient to heat the gas enough to populate the C II $^2P_{3/2}$ state. Fig. 2 also shows the surface brightness of the [C II] line predicted by typical PDR models. The ratio of [C II] and radio continuum intensity is independent of the source or beam solid angle and of the distance from the observer to the source. For most well–studied sources, the position in Fig. 2 agrees well with the known spectral type of the exciting star and the source size. What then, does the diagram tell us about less well–known sources? The extended halo of W43 (Shibai et al. 1991) has the same intensity ratio as the NGC 2024 cloud. It is therefore possible in principle to explain sources like W43 as a superposition of dense PDR's. These could be ~1 pc scale O9 star regions like NGC 2024 or dense clouds ~10 pc away from early O stars. The line representing the ratio of [C II] intensity (Stacey et al. 1991) and the best guess for the thermal contribution to the radio continuum (Carlstrom and Kronberg 1991) in the nearby starburst galaxy M82 lies in between

the NGC 2024/extended W43 line and the lines representing M16 and M17 where the ionization fronts are illuminated by early O stars. The M82 result implies that the effective spectral type of the illuminating stars can only be ~O8 (Rieke 1988) if the characteristic distance of the stars from a dense molecular cloud is small (around 0.5 pc).

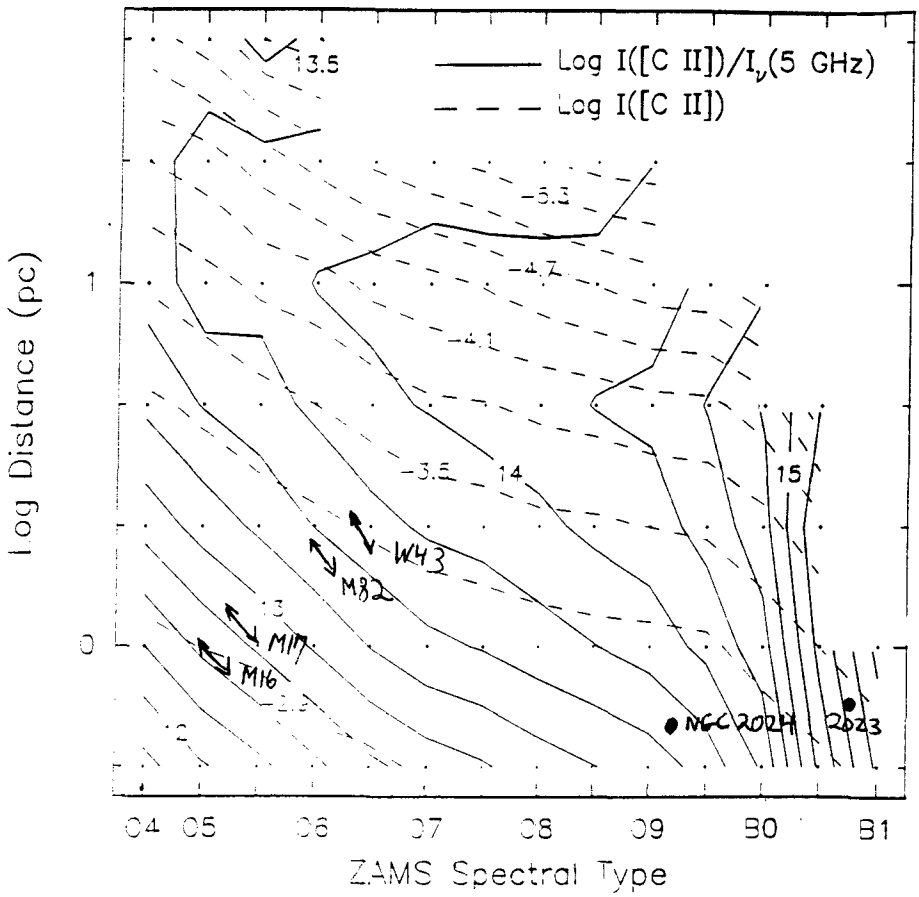

Figure 2: [C II] to radio continuum intensity ratio (Hz) and [C II] intensity vs. spectral type of the exciting star and distance to the cloud. Both quantities assume a density of $>10^4$ cm^{-3} and the [C II] intensity assumes unity filling factor.

While the [C II]/5 GHz ratio appears to be a useful quantity in our efforts to understand the relationship between PDR's and their exciting stars, there are a number of possible pitfalls. Our implicit assumption that the PDR projects the same fraction of its surface as seen from the exciting star and the observer leads to errors in placing sources in the diagram. The models assume that the regions are plane parallel which probably causes us to underestimate the [C II] intensity at a given G_o, particularly for sources with high incident far–UV fields (Orion A, for example), where the [C II] intensity is insensitive to G_o. The [C II] to radio continuum intensity ratio for Orion A lies within the parameter space shown in Fig. 2, but the [C II] intensity does not. In constructing Fig. 2, we have

assumed that all of the gas is dense which may result in an overestimate of I([C II]) for a given UV field. In the inner Galaxy and in other galaxies, the radio continuum may be largely non-thermal. Estimates of the denominator for Fig. 2 based on Brγ or Brα measurements would circumvent this problem. The assumption that all the [C II] emission arises in the PDR may not always be valid. There are good arguments for a contribution to the [C II] by extended low density H II regions, especially on large scales in the inner galaxy. What the locations of sources in Fig. 2 imply is that it is possible to explain the observed properties of inner galaxy regions with PDR material alone although an ELD H II contribution is not ruled out.

[C I] and the Internal Structure of Clouds

Plume et al. (1994) argue that PDR material is the most likely origin for the extended [C I] emission from S140 and other typical clouds with UV fields more than a few times the mean interstellar radiation field value and with modest column densities and therefore for most [C I] emission from galaxies. The intensities of the ground state fine structure lines of [C I] at 492 and 809 GHz do not vary much with physical conditions. We illustrate here how one might combine data on the 492 GHz line with observations of an optically thin CO line to derive a bulk measure of cloud structure. Let us assume that the emitting cloud is an ensemble of identical, arbitrarily shaped clumps. The carbon in the interior is primarily in the form of CO and the mean density in the interior is $n=n_{H_2(CO)}$. Ultraviolet radiation impinges on the clumps from the outside creating a layer of neutral carbon. The density in the C I layer is, $n=n_{H_2(CI)}$. We further assume that all clumps have the same (unknown) size, r_{cl}. If the [C I] emission is optically thin, the intensity of the layer is,

$$I_{CI} = \epsilon_{CI} n_{H_2(CI)} V_{CI} N_{cl} l[X(CI)],$$

where $n_{H_2(CI)}$ is the H_2 number density in the CI region, V_{CI} is the volume of the [C I] emitting region of each clump, N_{cl} is the volume density of clumps in the layer, l is the thickness of the clumpy cloud, $[X(CI)]=n_{CI}/n_{H_2(CI)}$ in the PDR, and the [C I] emissivity per particle is,

$$\epsilon_{CI} = \frac{h\nu_{CI}}{4\pi} A_{CI} \frac{n_1}{n_{tot(CI)}},$$

where ν_{CI} is the frequency of the 492 GHz transition, A_{CI} is the Einstein A coefficient for the $^3P_1 \rightarrow ^3P_0$ transition, n_1 the number density of C I in the $^3P_1$ state, and $n_{tot(CI)}$ the density of C I in all states. Similarly, for an optically thin transition of a CO isotopomer,

$$I_{CO} = \epsilon_{CO} n_{H_2(CO)} V_{CO} N_{cl} l[X(CO)],$$

where $n_{H_2(CO)}$ is the H_2 number density in the CO emission region, V_{CO} is the volume of this part of the clump, [X(CO)] is the fractional abundance within the clump of the CO isotopomer, and the optically thin CO line emissivity per particle is,

$$\epsilon_{CO} = \frac{h\nu_{CO}}{4\pi} A_{CO} \frac{n_u}{n_{tot(CO)}},$$

where n_u is the number density in the upper state of the CO transition in question. If we now assume that all clumps have both CO and CI and that the ratio of the volumes

containing the two species, V_{CO}/V_{CI}, is a constant,

$$\frac{I_{CO}}{I_{CI}} = \frac{\epsilon_{CO} n_{H_2(CO)} V_{CO} [X(CO)]}{\epsilon_{CI} n_{H_2(CI)} V_{CI} [X(CI)]}.$$

For spheres, $V_{CO}=(4\pi/3)\ r_{cl}^3$, $V_{CI}=4\pi r_{cl}^2 \Delta r$, and $V_{CO}/V_{CI}=(1/3)(r_{cl}/\Delta r)$, where Δr is the thickness of the PDR layer containing most of the CI ($V_{CO}/V_{CI}=(1/2)\ (r_{cl}/\Delta r)$ for filaments). Assuming that the clumps are spherical,

$$\frac{I_{CO}}{I_{CI}} = \frac{1}{3} \frac{\epsilon_{CO} n_{H_2(CO)} r_{cl} [X(CO)]}{\epsilon_{CI} n_{H_2(CI)} \Delta r [X(CI)]}.$$

Models of PDR's agree that C I layer on the clump surfaces has an almost constant thickness in units of column density, independent of the density of the clumps or the strength of the interstellar radiation field:

$$n_{H_2(CI)} \Delta r \sim const. = N_{H_2(CI)},$$

Similarly, the more variable column density through the molecular part of the cloud is:

$$N_{H_2(CO)} = n_{CO} r_{cl}.$$

We can now write

$$\frac{N_{H_2(CO)}}{N_{H_2(CI)}} = \frac{3 I_{CO}}{I_{CI}} \frac{\epsilon_{CI} [X(CI)]}{\epsilon_{CO} [X(CO)]}.$$

We then have, for the column density through the interior of each clump,

$$N_{H_2(CO)} = \frac{3 I_{CO}}{I_{CI}} \frac{\epsilon_{CI}}{\epsilon_{CO}} \frac{[X(CI)]}{[X(CO)]} N_{H_2(CI)}$$

and, for the total column density through each clump,

$$N_{H_2(clump)} = N_{H_2(CO)} + \eta N_{H_2(CI)} = \left(\eta + \frac{3 I_{CO}}{I_{CI}} \frac{\epsilon_{CI}}{\epsilon_{CO}} \frac{[X(CI)]}{[X(CO)]} \right) N_{H_2(CI)},$$

where η ($\sim$0.6–1) accounts for CO in the C I layer.

The method outlined above will run into problems in low column density clouds. In such clouds, the CI layer is more than a shell and the value of η becomes critical. Also, in such clouds, the abundance of CI drops. This change is offset by a corresponding drop in the CO abundance (Van Dishoeck and Black 1988), so that the ratio of [C I] and CO intensities is not so sensitive to the assumed abundances.

Measurements of the ratio of [C I] 492 GHz linestrength to the strength of an optically thin CO line therefore gives us a way to determine column density. The derived quantity is neither the total column density through the cloud as one might measure by star counts nor the column density along a line of sight as one might measure by a stellar reddening experiment. The CO/CI ratio instead determines the typical column density from where the UV strikes the surface of the cloud to the center of each shielded clump. This quantity then tells us how effectively UV radiation penetrates into a cloud with a given total column density— it is a measure of how clumpy the cloud is. It is also the

physically relevant quantity in the photoionization regulated star formation picture of McKee (1989). Here, the higher electron density in the PDR leads to long ambipolar diffusion timescales and inhibits the formation of low mass stars. Such stars can only form in regions where the electron density is at the low level determined by cosmic ray ionizations. Knowledge of the column density from the clump centers to a UV illuminated surface then tells you what fraction of the cloud has a short ambipolar diffusion timescale.

Given the number of assumptions in the above derivation, we do not expect to be able to use the line ratio as quantitative measure of the mean clump column density in all cases but rather more as a way to compare the UV permeability of different regions.

I would like to thank my many collaborators as well as E. van Dishoeck, J. Stutzki and A. Sternberg for their helpful comments. This work was supported by NASA grant NAG2-402 to the University of Texas as well as by the David and Lucile Packard Foundation and the Alexander von Humboldt Stiftung.

References:

Carlstrom, J.E. & Kronberg, P.P. 1991, ApJ, 366, 422.
Crawford, M.K., Genzel, R., Townes, C.H., & Watson, D.M. 1985, ApJ, 291, 755.
Hollenbach, D.J. 1994, this volume.
Hollenbach, D.J., Takahashi, T., & Tielens, A.G.G.M. 1991, ApJ, 377, 192.
Jaffe, D.T., Zhou, S., Howe, J.E., Herrmann, F., Madden, S.C., Poglitsch, A., van der Werf, P.P., & Stacey, G.J. 1994, ApJ, submitted.
Köster, B., Störzer, H., Stutzki, J., & Sternberg, A. 1994, A&A, submitted.
Madden, S.C., Geis, N., Genzel, R., Herrmann, F., Jackson, J.M., Poglitsch, A., Stacey, G.J., & Townes, C.H. 1993, ApJ, 407,579.
McKee, C.F. 1989, ApJ, 345, 783. Nakagawa, T. 1994, this volume.
Plume, R., Jaffe, D.T., and Keene, J. 1994, ApJL, submitted.
Rieke, G.H. 1988, Galactic and Extragalactic Star Formation, R.E. Pudritz & M. Fich eds., (Kluwer), p. 561.
Shibai, H., et al. 1991, Ap.J, 374, 522.
Stacey, G.J., Viscuso, P.J., Fuller, C.E., & Kurtz, N.T. 1985, ApJ, 289, 803.
Stacey, G.J., Geis, N., Genzel, R., Lugten, J.B., Poglitsch, A., Sternberg, A., & Townes, C.H. 1991, ApJ, 373, 423.
van Dishoeck, E.F., & Black, J.H. 1988, ApJ, 334, 771.
Wolfire, M.G., Hollenbach, D., & Tielens, A.G.G.M. 1989, ApJ, 344, 770.
Wright, E.L., et al. 1991, ApJ, 381, 200.

Observations of $^3P_1$ to $^3P_0$ C I Emission from Molecular Clouds and Envelopes of Evolved Stars

Jocelyn Keene
California Institute of Technology, Pasadena, CA 91125, USA

Abstract

The 492 GHz ground-state fine-structure transition of neutral carbon has been observed extensively with the Caltech Submillimeter Telescope since 1990. During this time we have mapped several Galactic molecular clouds, including star-forming regions, photodissociation regions, dark clouds, a shocked region, and the Galactic Center. In addition, we have detected some nearby galaxies and some evolved stars.

In large-scale maps of molecular clouds and in nearby galaxies we find that the cooling power of C I is comparable to that of CO.

1. Introduction

The ground-state fine-structure levels of atomic carbon are at energies $E(^3P_1)/k = 23.6$ K and $E(^3P_2)/k = 62.5$ K which are well suited to excitation by temperatures common in the dense interstellar medium (ISM). The two transitions, $^3P_1 \rightarrow ^3P_0$ and $^3P_2 \rightarrow ^3P_1$, are at frequencies of 492 and 809 GHz, respectively. At low temperatures carbon can be considered a three-level atom because higher energy levels are nearly inaccessible ($E/k > 10^4$ K). The ground-state fine-structure levels of atomic carbon are easily collisionally excited; $n_{crit}(^3P_1) \approx 1000$ cm^{-3} for collisions with H_2. Atomic carbon is thus an efficient coolant of moderately dense ($n > 5 \times 10^2$ cm^{-3}), cool ($15 < T < 40$ K) interstellar material.

It was recognized in about 1970 that C I could be an important coolant for interstellar clouds (Werner 1970; Penston 1970; Dalgarno & McCray 1972). Later, more detailed calculations by Langer (1976) implied that the C I emission would most likely be quite weak because of the nature of its distribution, sandwiched between the diffuse medium, where C^+ is the dominant form of gaseous carbon, and a dense molecular cloud, where CO is dominant.

Early observations of $^3P_1 \rightarrow ^3P_0$ C I emission at 492 GHz showed that it is bright and extended like CO and that the column densities are larger than had been predicted (Phillips & Huggins 1981). It was also seen that C I emission extends far into molecular clouds from photon-dominated regions (PDRs) (Keene et al. 1985; Genzel et al. 1988). The region where C I is abundant is at least 10 mag of visual extinction thick on each side of a cloud (Frerking et al. 1989).

Newer PDR models can explain the high observed column densities (van Dishoeck & Black 1988; Hollenbach et al. 1991), however they need modification to explain the spatial distribution of the emission. One promising possibility which has been discussed extensively lately, is that molecular clouds are clumpy and allow deep penetration of UV radiation to the cloud interiors. This has been discussed recently by Stutzki et al. (1988), Burton et al. (1990), and Boissé (1990). The enhancement of C I within clouds due to dynamical mixing of clumps has been discussed by Boland and deJong (1982)

and Chièze et al. (1989; 1991). Another possibility which has gained attention recently is that the presence of electrons within clouds would lead to the destruction of H_3^+ ions, to incomplete ion-molecule chemistry, and thus to a large residual abundance of C I within the shielded molecular cloud interior (Graedel et al. 1982; Pineau des Forêts et al. 1992). Thus there are currently at least two competing mechanisms to explain the wide distribution of C I emission from molecular clouds.

2. Observations

In many types of sources C I is found to be comparable to low-J ^{13}CO in line shape, line temperature, and spatial distribution. A typical peak brightness is $\int T_{MB} dV \approx 40$ K km s^{-1} which implies a column density $N(\mathrm{CI}) \approx 5 \times 10^{17} \mathrm{cm}^{-2}$ under the conservative assumption that the C I lines are optically thin. In warm gas away from embedded FIR sources the value of $N(\mathrm{CI})/N(\mathrm{CO})$ typically lies in the range 0.1 – 0.2.

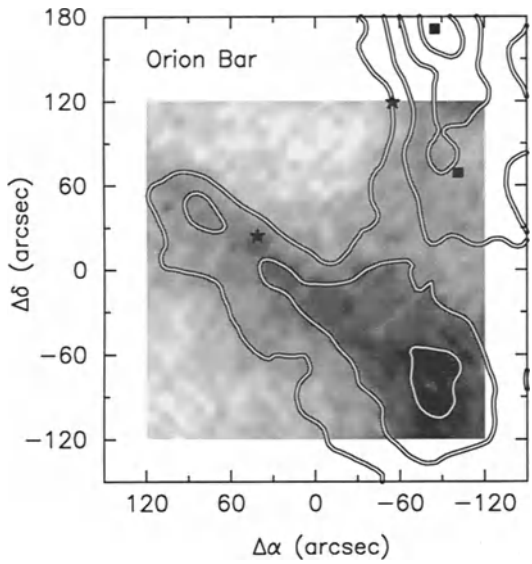

Figure 1. Orion Bar (Tauber et al. 1994). The grayscale map shows the integrated C I intensity and the contours the ^{13}CO(2→1) intensity. The squares indicate the positions of IRc 2 and FIR 4. The stars mark the position of Θ^1C (the source of ionizing radiation) and Θ^2A Ori. The resemblance of the C I and ^{13}CO emission is very close and there is no offset visible between the positions of the C I and molecular bar, though they are both shifted from the position of the ionization front.

Examples of three sources where the C I and CO maps bear a strong resemblance to each other are found in Figs. 1 – 3. These are all edge-on PDRs. The C I map of the Orion Bar (Fig. 1, grayscale; Tauber et al. 1994) looks almost identical to the ^{13}CO(2→1) map (contours). Globule A in the HII region IC 1396 (Fig. 2) is an example of a source in which the ^{13}CO(2→1) emission is very optically thick and the C I emission more closely resembles C^{18}O(2→1). In M17 (Fig. 3, left; Büttgenbach & Keene 1990) the C I emission again closely resembles the ^{13}CO(2→1) map. However, in this source the C I emission appears to be clumpy and the position of the C I clumps does not

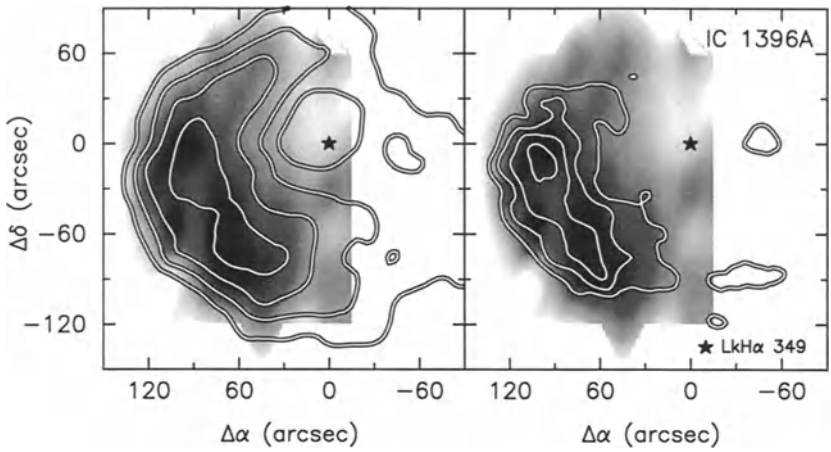

Figure 2. IC 1396A. The grayscale map in both panels shows the integrated C I intensity. The contours in the left panel are the integrated ^{13}CO(2→1) intensity and in the right panel are the integrated C^{18}O(2→1) intensity. The source of ionization is a luminous O6 star located far to the east. The star marks the position of the low-luminosity star LkHα 349 which is a source of heat but not of much ionizing radiation.

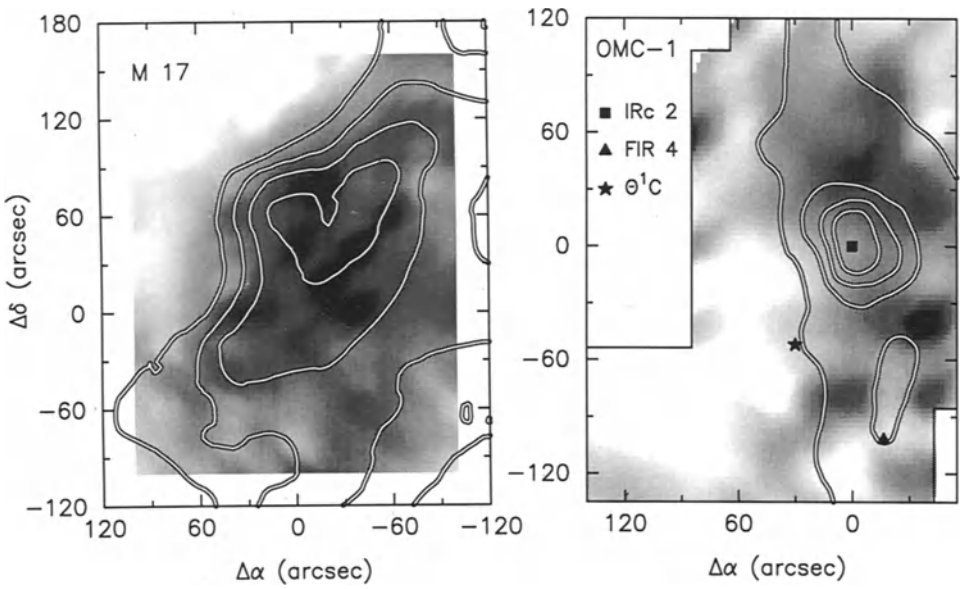

Figure 3. (left) M17 (Büttgenbach & Keene 1990). The grayscale map in each panel shows the integrated C I intensity; the contours show the integrated ^{13}CO(2→1) intensity. In M17, an edge-on H II region, the C I and ^{13}CO are very similar. (right) OMC-1 (Büttgenbach 1993). Toward OMC-1 there is a face-on H II region, M42, and the C I and molecular emission are quite different. These two C I maps are our earliest, dating from 1990, and have lower S/N than the rest in this paper.

coincide exactly with the CO peaks. This may be partly a S/N problem in the C I map or it may be real. M17 and the Orion Bar have also been mapped by White & Padman (1991). Our results are generally in satisfactory agreement with theirs.

C I appears to avoid hot dense regions. For example, Fig. 3 (right) shows a C I and ^{13}CO(2→1) map of OMC-1 (Büttgenbach 1993) which evidently has no C I emission specifically associated with either IRc 2 or FIR 4, both prominent dust continuum and molecular line peaks. FIR 4 is also included at the top of the higher S/N map shown in Fig. 1, and again there is a lack of C I emission at that position. The C I emission peaks may form an arc around Θ^1C Ori, tracing the edge of the C II region mapped by Stacey et al. (1993) and the dense H II region (Mundy et al. 1986). The relative lack of emission at the position of IRc 2 is also seen in the map of White & Padman (1991).

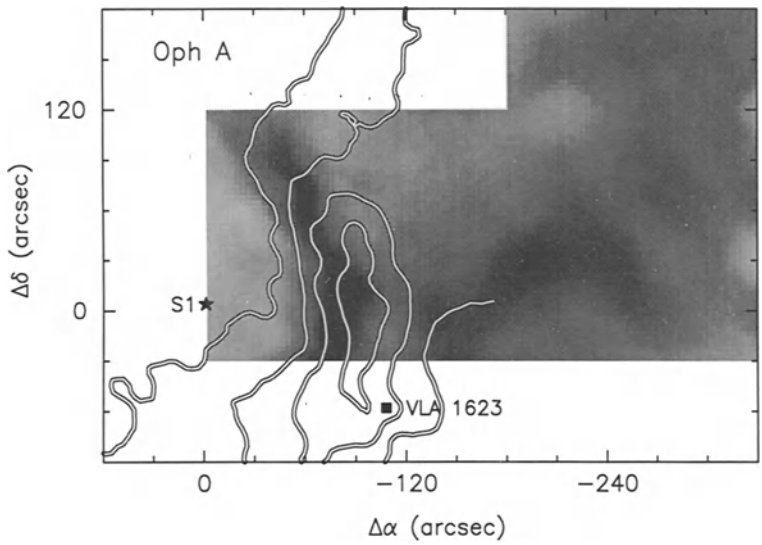

Figure 4. Oph A. The grayscale map shows the integrated C I intensity and the contours show the integrated C^{18}O(2→1) intensity. The eastern arc of strong C I emission appears to be centered on S1, a young, embedded ∼B3 star. It appears to lie midway between an arc of radio continuum emission (P. André, priv. comm.) and the dust continuum and molecular ridge shown by the C^{18}O contours. The western arc of emission is coincident with a blue outflow lobe emanating from VLA 1623 or its vicinity (André et al. 1990)

So far we have found only one example of what we might call a classical PDR region. The young ∼B3 star S1 in the Oph A region is a compact radio source (BZ 4) located in a region of carbon recombination line radiation. The C I emission forms a bright arc around this star (Fig. 4). This feature shows beautiful stratification, with the C I arc midway between the the column density arc, shown by the C^{18}O (contours in Fig. 4) and dust continuum maps (André et al. 1993) and the ionization front delineated by a radio continuum arc (André, private communication) slightly farther to the east. As this is the closest PDR we have observed, at a distance of only 160 pc, we infer that it is possible that in all sources there is some stratification in the C I abundance on small

scales. However, we also note that there is bright CI emission all over this region and that the bright rims appear to be relatively minor effects.

A survey of CO outflow regions (Walker et al. 1993) shows that $N(\mathrm{CI})/N(\mathrm{CO})$ averages about 0.2, and the ratio is generally constant from the emission line core to the line wings. This implies that the ratio of abundances is approximately the same in the outflow accelerated material as in the general cloud material. In the Oph A region, the western CI rim in Fig. 4 is coincident with a blue CO outflow lobe originating near VLA 1623 (André et al. 1990). Whether in fact, this CI rim reveals an enhancement of the CI abundance in this particular outflow remains to be investigated.

We have detected shock enhancement of CI abundance in clump G in the supernova remnant IC 443 We have mapped CI and several lines of CO (Keene et al. 1994a; van Dishoeck et al. 1993; Phillips et al. 1994, poster in these proceedings). CI is clearly visible in the hot ($\sim$ 100 K) post-shocked gas with a broad line profile (Fig. 5, left). This region has approximately equal abundances of CI and CO. Also interesting is the region of pre-shocked gas with narrow CI lines (Fig. 5, right) which has a component of warm gas ($\sim$ 30 K) where the CI abundance is a factor of 10 higher than the CO abundance. This may mark the position of a radiative precursor to the shock.

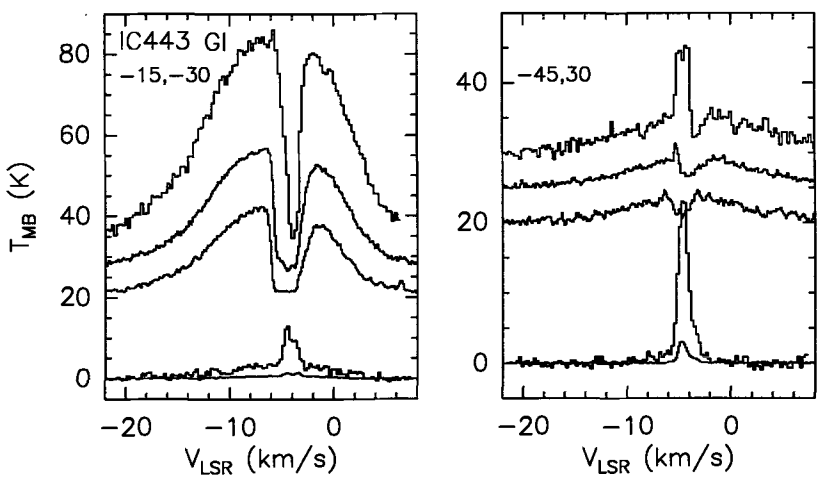

Figure 5. IC443G spectra. (left) CI and CO spectra taken at the emission peak of the post-shocked gas. (right) Spectra taken at the emission peak of the pre-shocked gas. The spectra in order from bottom to top are ^{13}CO(2→1), CI, ^{12}CO(2→1), ^{12}CO(3→2), and ^{12}CO(4→3). The ^{12}CO spectra have been displaced upwards by 20, 25, and 30 K respectively.

We have made CI strip maps of two cold (8–10 K), dark clouds: L183 (Fig. 6; Keene et al. 1994b) and TMC-1 (Schilke et al. 1994). Here CI appears optically thick with $T_R^* \approx 1.5 - 2$ K. The Rayleigh-Jeans corrected brightness temperature of CI at the eastern side of L183 (8.5 – 9.5 K) is higher than that of ^{13}CO, implying that it is more optically thick or that it arises in a warmer layer, perhaps heated by the Sco OB2 association to the SE. The implied column density is $N(\mathrm{CI}) > 10^{17}$ cm^{-2}. Unfortunately, because it is very optically thick, we are unable to tell anything about the distribution of CI deep within dark clouds.

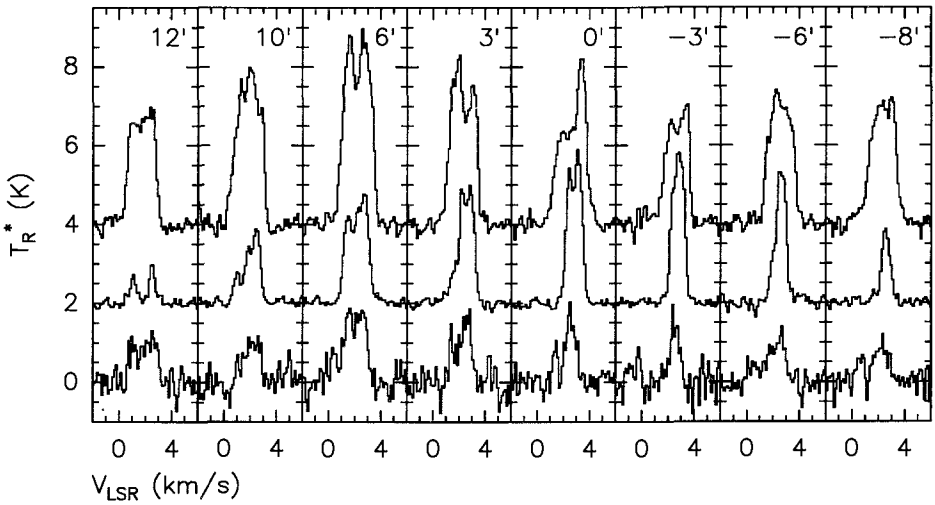

Figure 6. Scan of C I (bottom) and $^{13}CO(2\rightarrow1)$ (middle) and $^{12}CO(2\rightarrow1)$ (top) in R.A. across L183.

C I is extremely strong in Galactic center clouds. Because of its low excitation requirements it can be used to trace the circumnuclear disk to large radii (150″, 6 pc; Serabyn et al. 1994). We find that the rotational velocity of the CND is constant to as large a radius as it can be traced.

We have observed several evolved stars in the C I line (Fig 7; Keene et al. 1993; Young et al. 1994). Of these IRC +10216 seems to be a classical PDR with dissociation of CO in the envelope by the ISRF. Its spectrum is typical of a resolved shell source. Existing models can produce the right amount of C I (e.g. Cherchneff et al. 1993) but have it located at too large a radius. However, there is enough latitude to fine-tune the models to make them fit the observations. In particular, a clumpy shell may allow UV penetration from outside to produce more C I at small radii and the larger region of coexistence of CO and C I required by the observations.

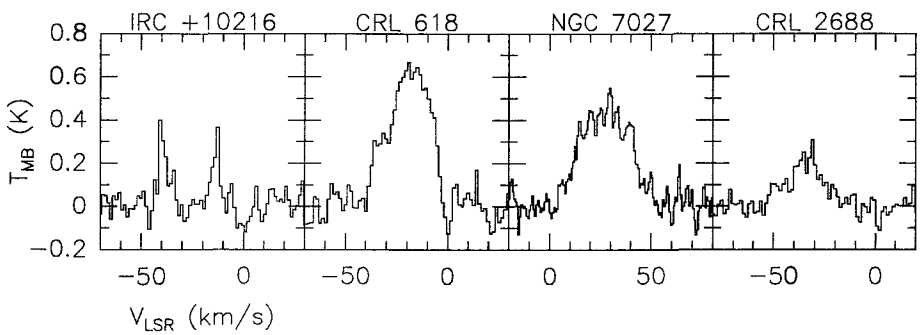

Figure 7. C I spectra of several evolved stars (Keene et al. 1993; Young et al. 1994).

Two of the other evolved stars which we have observed, CRL 618 and NGC 7027 (Young et al. 1994), are different from IRC +10216 in that the central stars in these

objects dominate the production of C I. NGC 7027 is, of course, a well-known planetary nebula with a surrounding molecular envelope and CRL 618 is a younger object which nonetheless has a central star capable of producing ionizing radiation. As a result they are quite a bit brighter in C I emission than IRC +10216. The central star in CRL 2688 is cooler than either of these two and its C I emission is considerably weaker. We do not know if CRL 2688 is a shell or filled source.

3. Measurements of Carbon Cooling

Wright et al. (1991) measured the average line intensities for the Galaxy in the millimeter to far-infrared spectral region with the COBE satellite. They found that the sum of the two C I line intensities and the sum of the five lowest CO lines (the only ones they could detect and measure) have nearly equal cooling power with the C I lines being just slightly stronger.

The effectiveness of the cooling of C I probably comes as a surprise to most people, in spite of the early predictions (Penston 1970; Werner 1970), because of models such as those of Goldsmith & Langer (1978) which showed that C I should be roughly a factor of 10 less effective than CO for cooling molecular clouds. There are several problems in comparing those early calculations with the observations. First, observations of C I showing a high abundance throughout the ISM had not yet been made, so the abundance assumed for the models was low. Second, the models were made for the shielded cloud interiors with no consideration for the influence of incident UV radiation. Third, they were made before accurate collisional cross-sections for C I with H_2 were available. Nevertheless, these calculations have not been redone in so comprehensive a fashion and are the best available, except for calculations concerning PDRs on the edges of clouds (e.g. Hollenbach et al. 1991).

The COBE observations also showed that the most important lines for cooling the whole interstellar medium lie at still higher frequencies. C II, N II and other ions and atoms that have their fine-structure transitions in the infrared to far-infrared spectral region are most important. However, these species are probably cooling a different phase of the ISM. Many of them are ions that require energetic photons in order to be created and exist only in H II regions (e.g. N II). Others have their ground-state transitions at such high frequencies they are excited only in much warmer gas than are C I or low-J CO transitions (e.g. O I). A possible exception to this rule is C II, which may be well mixed with C I and CO due to the leakage of photons with $11.3 < E < 13.6$ eV into molecular clouds and can effectively cool clouds with $T > 50$ K.

Recent calculations on the emission from low-density PDRs (Hollenbach et al. 1991) show for clouds illuminated only by the average interstellar radiation field (ISRF) that C I is exceeded in cooling efficiency solely by C II. Unfortunately, these calculations did not include the CO lines higher than (1→0). However, although the absolute intensity of the C II line is predicted to be higher than that of the C I lines, for technical reasons the C II line is extremely difficult to detect in such cold clouds, or indeed in clouds with $T < 40$ K.

Because it is still difficult to measure the upper C I line, and all of the CO lines for each object observed, we can use the ratio of the lower C I line to the CO(2→1) line intensity

as an indicator of relative cooling power. These lines are both readily observable with existing submillimeter telescopes. It is advantageous to observe a higher frequency CO line than (1→0) because the lowest frequency line in negligible in its cooling power. The value observed by COBE is $I(\mathrm{CI})/I(\mathrm{CO}(2\rightarrow1)) = 2.3$. We can use this for comparison with higher spatial resolution data with less complete spectral coverage to estimate if CI or CO is the more important coolant for molecular clouds.

In radio astronomy, the energy intensity in an emission line is commonly expressed with the unit of temperature. Unfortunately, this convenient unit hides the strong dependence on frequency that the energy intensity of an emission line actually has. The cooling power of an emission line is measured by the integral of intensity over frequency: $\int \bar{I}_\nu \, d\nu = (2k\nu^3/c^3) \int T_R^* \, dV = 10^{-15}\nu^3 \int T_R^* \, dV$ erg cm^{-2} s^{-1} sr^{-1} for ν measured in GHz, T_R^* in K, and V in km s^{-1}. This relationship makes immediately obvious the strong dependence of cooling power on line frequency which is the reason that high-frequency lines such as CI and CII lines are efficient coolants.

Large-scale maps made of S140 by Plume et al. (1994a; 1994b, poster in these proceedings) show that the efficiency of the CI cooling relative to CO increases away from the ionization front and embedded FIR sources toward the outer edges of the cloud. At the outer edges where the temperature is moderate ($T \approx 20$ K) and the average density is low ($\langle N(\mathrm{H_2}) \rangle \approx 300$ cm^{-3}, probably with large variations due to clumping) the conditions are ideal for CI to be a major coolant, and it appears to be one. Here $I(\mathrm{CI})/I(^{12}\mathrm{CO}(2\rightarrow1))$ is in the range 1.2 – 2.8. It is probable that regions such as this contribute most of the low-J CO and CI emission in the local part of the Galaxy that dominates the COBE survey.

Recent observations of CI and CO in nearby galaxies (IC342, Büttgenbach et al. 1992; M82, Schilke et al. 1993) have confirmed that CI is nearly as efficient as CO at cooling molecular clouds near galactic nuclei and we would expect the CI to become even more efficient in regions with lower densities and temperatures farther from the nuclei.

Acknowledgements

The observations reported here have been the work of many people. I would like to thank T. Büttgenbach, T. Hunter, D. Lis, T. Phillips, P. Schilke, E. Serabyn, K. Young (Caltech), E. van Dishoeck (Leiden U.), J. Tauber (ESA/ESTEC), D. Jaffe, and R. Plume (U. Texas) for their permission to reproduce their results before publication. I also thank the entire submillimeter group and the support staff at the CSO for their valuable help. I would like to thank the SAO and the SERC for support during part of this work. The CSO is funded by NSF contract # AST90–15755.

References

André, P., Martín-Pintado, J., Despois, D., & Montemerle, T 1990, A&A, 236, 180
André, P., Ward-Thompson, D., & Barsony, M. 1993, ApJ, 406, 122
Boissé, P. 1990, A&A, 228, 483
Boland, W., & deJong, T. 1982, ApJ, 261 110
Burton, M.G., Hollenbach, D.J., Tielens, A.G.G.M. 1990, ApJ, 365, 620
Büttgenbach, T.H. 1993, Thesis, California Institute of Technology

Büttgenbach, T.H., Keene, J., Phillips, T.G., & Walker, C.K. 1992, ApJ, 397, L15
Cherchneff, I., Glassgold, A.E., & Mamon, G.A. 1993, ApJ, 410, 188
Chièze, J.-P., & Pineau des Forêts, G. 1989, A&A, 221 89
Chièze, J.-P., Pineau des Forêts, G., & Herbst, E. 1991, ApJ, 373, 110
Dalgarno, A., & McCray, R.A. 1972, ARAA, 10, 375
Frerking, M.A., Keene, J., Blake, G.A., & Phillips, T.G. 1989, ApJ, 344, 311
Genzel, R., Harris, A.I., Jaffe, D.T., & Stutzki, J. 1988, ApJ, 332, 1049
Goldsmith, P.F., & Langer, W.D. 1978, ApJ, 222, 881
Graedel, T.E., Langer, W.D., & Frerking, M.A. 1982, ApJS, 48, 321
Keene, J., Blake, G.A., Phillips, T.G., Huggins, P.J., & Beichman, C.A. 1985, ApJ, 299, 967
Keene, J., Phillips, T.G., & van Dishoeck, E.F. 1994a, in preparation
Keene, J., et al. 1994b, in preparation
Keene, J., Young, K., Phillips, T.G., & Büttgenbach, T.H. 1993, ApJ, 415, L131
Hollenbach, D.J., Takahashi, T., & Tielens, A.G.G.M. 1991, ApJ, 377, 192
Langer, W.D. 1976, ApJ, 206, 699
Mundy, L.G., Scoville, N.Z., Baath, L.B., Masson, C.R., Woody, D.P. 1986, ApJ, 304, L51
Penston, M.V. 1970, ApJ, 162 771
Phillips, T.G., & Huggins, P.J. 1981, ApJ, 251, 533
Phillips, T.G., Keene, J., & van Dishoeck, E.F., 1994, these proceedings
Pineau-des-Forêts, G., Roueff, E., & Flower, D.R. 1992, MNRAS, 258, P45
Plume, R., Jaffe, D.T., & Keene, J. 1994a, ApJ, in press
Plume, R., Jaffe, D.T., Tatematsu, K. & Keene, J. 1994b, these proceedings
Schilke, P., Carlstrom, J.E., Keene, J., & Phillips, T.G. 1993, ApJ, 417, L67
Schilke, P., Keene, J., Le Bourlot, J., Pineau des Forêts, G., & Roueff, E. 1994, A&A, submitted
Serabyn, E., Keene, J., Lis, D.C., & Phillips, T.G. 1994, ApJ, 424, L95
Stacey, G.J. et al. 1993, ApJ, 404, 219
Stutzki, J., Stacey, G.J., Genzel, R., Harris, A.I., Jaffe, D.T., Lugten, J.B. 1988, ApJ, 332, 379
Tauber, J.A., Lis, D.C., Keene, J., Schilke, P., and Büttgenbach, T.H. 1994, in preparation
van Dishoeck, E.F., & Black, J.H. 1988, ApJ, 334, 771
van Dishoeck, E.F., Jansen, D.J., & Phillips, T.G. 1993, A&A, 279, 541
Walker, C.K., Narayanan, G., Büttgenbach, T.H., Carlstrom, J.E., Keene, J., & Phillips, T.G. 1993, ApJ, 415, 672
Werner, M.W. 1970, ApLett, 6, 81
White, G.J., & Padman, R. 1991, Nat, 354, 511
Wright, E.L., et al. 1991, ApJ, 381, 200
Young, K. et al. 1994, in preparation

Carbon Monoxide Line Emission from Photon-Dominated Regions

B. Köster[1], H. Störzer[1], J. Stutzki[1] and A. Sternberg[2]

[1]I. Physikalisches Institut, Universität zu Köln, 50937 Köln, Germany
[2]School of Physics and Astronomy, Tel Aviv University, Ramat Aviv, Israel

We present a theoretical study of ^{12}CO and ^{13}CO rotational line emission and [CI], [CII] fine structure emission from photon dominated regions (PDRs, see also Köster et al. 1994). We incorporate the effects of clumpy cloud structure by computing the physical structures of plane-parallel PDRs with finite thickness which are illuminated by UV-radiation fields from either one or both sides.
We examine the influence of the gas density (n_0(H) = 10^4cm^{-3} to 10^7cm^{-3}), the UV intensity (χ = 10^3 to 10^6 times the intensity of the average interstellar UV field), the cloud thickness (measured in units of the visual extinction A_V, $2 \leq A_V \leq 10$) and the doppler width (1 kms^{-1} and 3 kms^{-1}) on the emergent CO line center brightness temperatures. We explicitly include the effects of the ^{13}C chemistry on the line intensities.
We use accurate solutions of the radiative transfer equation for the UV continuum radiation which is scattered and absorbed by dust grains (Roberge et al. 1991) to compute the FUV heating and photochemical rates.

The main results of our investigations are:
a) The high brightness temperatures in the mid- and high-J ^{12}CO lines can be explained by the emission from high density ($n_0 = 10^6$cm^{-3} or $n_0 = 10^7$cm^{-3}) clumps in agreement with the calculations of Burton et al. (1990) . In our models, the brightness temperatures attained in the high-J lines are enhanced due to irradiation on both sides of finite thickness clouds. Thus, somewhat lower densities than in their model are sufficient to explain the actual line brightness temperatures observed in star-forming regions. (Fig.1a)

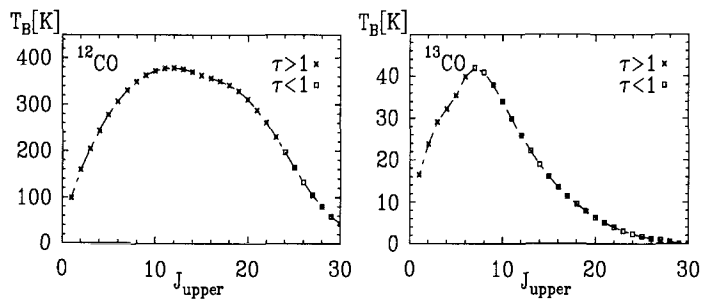

Fig.1: Brightness temperatures of ^{12}CO (a) and ^{13}CO (b) for a plane parallel layer illuminated from both sides with A_V=10, n_0(H)=10^7cm^{-3}, χ=10^5 and doppler width 1kms^{-1}.

b) The high brightness temperatures in the mid-J ^{13}CO lines observed by Graf et al. (1993) can be explained assuming that the emission originates from clumps or filaments which are illuminated from both sides and at least a few clumps overlapping along the line of sight. (Fig.1b)

c) To explain typical low-J ^{12}CO and ^{13}CO brightness temperatures and line ratios observed from more extended cloud regions (e.g. Castets et al. 1990) within the framework of a clumpy, UV penetrated cloud szenario, we need clump densities of close to $n_0 = 10^5 cm^{-3}$, i.e. substantially larger than typically derived from simple excitation arguments for the clumps in those regions (compare Gierens et al. 1992). (Fig.2b)

d) Mainly due to the more efficient photodissociation of ^{13}CO, the abundance of neutral atomic ^{13}C can get enhanced relative to ^{12}C, resulting in an inter-isotopic line intensity ratio which is a factor up to 3 larger than the assumed abundance ratio, although the lines stay optically thin. A similar enhancement of the $^{12}CII/^{13}CII$ line ratio occurs if the ^{12}CII line gets optically thick and the ^{13}CII is still optically thin, implying we can see the second, hot part of the slab in the ^{13}CII line. (Fig.2a)

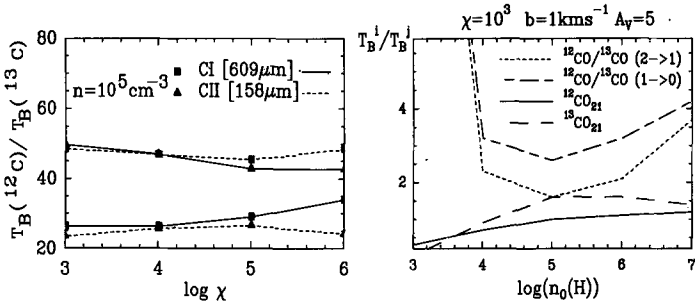

Fig.2: Line-center brightness temperature ratios of CI and CII (Fig.2a) and of ^{12}CO and ^{13}CO. (21 means J=2→1/J=1→0, Fig.2b)

References

Burton M.G., Hollenbach D., Tielens A.G.G.M., 1990, ApJ 365, 620
Castets A., Duvert G., Dutrey A., Bally J., Langer W.D., Wilson R.W., 1990, A&A 234, 469
Gierens K.M., Stutzki J., Winnewisser G., 1992, A&A 259, 271
Graf U.U., Eckart A., Genzel R., Harris A.I., Poglitsch A., Russell A.P.G., Stutzki J., 1993, ApJ 405, 249
Köster B., Störzer H., Stutzki J., Sternberg A., 1994, A&A, in press
Roberge W.G., Jones D., Lepp S., Dalgarno A., 1991, ApJS 77, 287
Sternberg A., Dalgarno A., 1989, ApJ 338, 197
Tielens A.G.G.M., Hollenbach D., 1985, ApJ 291, 722

Line Emission from Spherical UV Irradiated Clumps

H. Störzer[1], B. Köster[1], J. Stutzki[1], and A. Sternberg[2]

[1] I. Physikalisches Institut, Universität zu Köln, 50937 Köln, Germany

[2] School of Physics and Astronomy, Tel Aviv University

The clumpy structure of molecular clouds has been observed directly by high resolution observations of molecules such as $C^{18}O$ $J = 2 \rightarrow 1$ or ^{13}CO $J = 1 \rightarrow 0$, $J = 2 \rightarrow 1$ or indirectly, eg. by the observations of the large spatial extent of the [CII] 158μm fine structure line emission in photon dominated regions (PDR) (see the recent review by Stutzki, 1993).

Standard PDR models up to now assume plane-parallel semi-infinite slab geometry, what is obviously not appropriate for the observed complex structure of molecular clouds. A more sophisticated geometry, likely more realistic to model small scale structures, is that of spherical clumps.

In the following we present a model in which the physical structure and the CII, CI and OI fine structure and $^{12}CO/^{13}CO$ low-J rotational line emission of a single, UV illuminated, spherical clump is calculated.

Models for photon dominated regions have been presented for a plane-parallel semi-infinite (cf. Sternberg & Dalgarno 1989; Tielens & Hollenbach 1985) or a plane-parallel finite slab (Köster et al. 1994). In the case of spherical clumps, the depth dependence of the mean intensity in the UV range and in the submm-mm range is different than in the plane-parallel case. This results in a different temperature and chemical structure in the PDR which forms at the surface of the clump. Spherical clumps have also a defined mass, i.e. the size and number of discret clumps can be estimated if the total mass and surface area of a given molecular cloud is known. In a hydrostatic spherical configuration the density must increase in radial direction. We choose a simple power law of the form $n(r) = n_0(r/R)^{-\alpha}$. R is here the radius of the clump, n_0 is the hydrogen particle density at the clump surface, the parameter α is here assumed as $\alpha = 1.5$. The UV radiation field χ (here $10 \leq \chi \leq 1000$) is given in terms of the mean-interstellar UV field, the abundances are given by cosmic abundances. Once the temperature and density structure is determined the resulting line intensities are calculated by solving the proper NLTE rate equations and radiative transfer equation for spherical geometry (see Gierens et al. 1992 for details).

The differences in the temperature und density structure between plane-parallel and spherical models are not very drastic. The differences in the temperature are at maximum 20-30 %, the principal structure of the CII/CI/CO transition layer is not changed. In the case of the spherical models, the intensities for optically thin lines, such as the [CII] 158μm fine structure line or the ^{13}CO low-J rotational lines, can be enhanced due to limb brightning effects.

The $^{12}C/^{13}C$ fine structure line intensities are relatively insensitive against χ. The OI fine structure lines are very weak due to the relatively small temperatures in the PDR region for $\chi \leq 1000$. The ^{12}CO low-J intensity ratios range from 0.8 to 1.2 (for 10^5 cm$^{-3} \leq n(H) \leq 10^6$ cm^{-3}). The computed interisotopic $^{12}CO/^{13}CO$ line ratios for the low-J transitions range from nearly 1 ($\chi = 10$, R = 0.032 pc) to about 4 ($\chi = 1000$, R = $1.3 \cdot 10^{-3}$ pc). We need hydrogen particle densities $n(H)$ which are larger than $4 \cdot 10^5$ cm^{-3} to get ^{12}CO low-J line center brightness temperatures larger than 25 K.

In Fig. 1 we give an example for the dependence of the [CII] 158μm fine structure line emission as function of χ and the clump radius R. Smaller clump radius results in larger limb brightning, i.e. it shifts the line center brightness temperatures to larger values. Larger χ implies larger extension of the CII region, it also implies larger temperatures inside this region. Therefore, the brightness temperature increases drastically with χ.

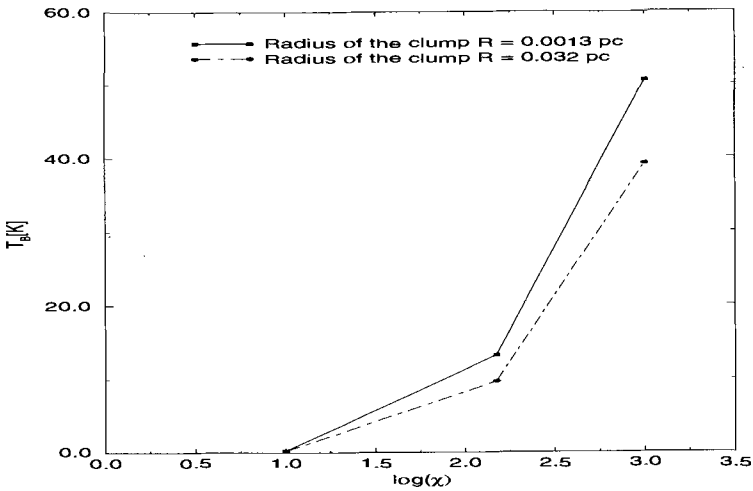

[CII] 158μm fine structure line emission for a model with $n_0(H) = 10^5$ cm^{-3}, $\alpha = 1.5$.

References

Gierens, K., Stutzki, J., Winnewisser, G. 1992, A&A 259, 271
Köster, B., Störzer, H., Stutzki, J., Sternberg, A. 1993, A&A submitted
Sternberg, A., Dalgarno, A. 1989, ApJ. 338, 197
Stutzki, J. 1993, in "Reviews in Modern Astronomy 6" p. 209, Ed. G. Klare
Tielens, A.G.G.M., Hollenbach, D. 1985, ApJ 291, 722

Radiative Transfer of Continuum Photons in Hierarchical Clouds

M.P. Hobson
Mullard Radio Astronomy Observatory, Cavendish Laboratory, Madingley Road, Cambridge CB3 0HE, England

Observations of molecular cloud complexes show them to have extremely complicated internal structure, with density fluctuations in the form of clumps, sheets and filaments present on all observed scales, i.e. these clouds exhibit a hierarchical structure. Observations of particular clouds over a wide range in spatial resolution further indicate that the structure on very different spatial scales is surprisingly similar, and suggest a self-similar hierarchy; such clouds are often described as fractal.

Following on from Boissé's (1990) 2-phase clump/interclump model, we describe a cloud complex as consisting of N mixed phases, with extinction coefficients k_n and dust grain albedos ω_n (assuming isotropic scattering), each of which has a volume filling factor of p_n. We further assume that these parameters are time-independent, and that the distribution of the phases is statistically homogeneous and isotropic.

We then model the transfer of UV continuum photon from one phase to another by an N-state Markov process; this is defined by a set of transition coefficients μ_{mn}, such that the probability of moving from phase m to phase n in the next path length ds is given by μ_{mn}ds for $m \neq n$. If we further assume $\mu_{mn} = 0$ for $|m - n| > 1$ (although not required by the subsequent analysis), then photons can only pass into phases with are adjacent in the sequence. By choosing $k_1 > k_2 \ldots > k_N$, this model then describes a *hierarchical* cloud.

To illustrate the model we consider an N-phase plane-parallel slab extending from $z = 0$ to $z = L$, illuminated at $z = 0$ by normally incident photons. Let $I_n(z, \theta)$ be the average over points lying in phase n of the specific intensity at a depth z making an angle θ with the normal to the slab, and let $\mathbf{I}(z, \theta)$ be the N-component column vector with the $I_n(z, \theta)$ as its components. Similarly, define $\mathbf{J}(z)$ as the mean intensity vector (i.e. averaged over angle). Under the Markov process assumption, we then find

$$\cos\theta \frac{\partial \mathbf{I}(z,\theta)}{\partial z} = -(\mathcal{K} - \mathcal{M})\mathbf{I}(z,\theta) + \mathcal{W}\mathcal{K}\mathbf{J}(z),$$

where $\mathcal{K} = \mathrm{diag}(k_1, k_2, \ldots, k_N)$, $\mathcal{W} = \mathrm{diag}(\omega_1, \omega_2, \ldots, \omega_N)$, and $\mathcal{M}$ is the matrix of transition coefficients μ_{mn} (with the definition $\mu_{nn} = -\sum_{m=1}^{N} \mu_{mn}$ for $m \neq n$). Solving the above equation, we find the mean intensity of unscattered radiation to be given by

$$\mathbf{J}^{(0)}(z) = J^{(\mathrm{in})} \exp[-(\mathcal{K} - \mathcal{M})z]\mathbf{1},$$

and the total mean intensity of both scattered and unscattered radiation by

$$\mathbf{J}(z) = \mathbf{J}^{(0)}(z) + \frac{1}{2}\int_0^L E_1[(\mathcal{K} - \mathcal{M})|z - z'|]\mathcal{W}\mathcal{K}\mathbf{J}(z')\mathrm{d}z',$$

where $J^{(\mathrm{in})}$ is the incident intensity, $\mathbf{1}$ is the coluimn vector with all components equal to unity and $E_1(x)$ is the first-order exponential integral function.

We now discuss three simple examples of cloud structure: a 2-phase clump/interclump model; a 3-phase hierarchical model where the clumps contain sub-clumps (model I); and a 3-phase hierarchical model where the clumps are surrounded by extended envelopes (model II). The volume filling factors and average path lengths in each phase are given in Table 1. We investigate a series of slabs with gradually increasing density contrasts between the phases, but with a constant average opacity $\langle\tau\rangle = 10$ and with $(k_1 - k_2) = 10(k_2 - k_3)$; note that an average clump opacity $\langle\tau_c\rangle = k_c\langle l_c\rangle = 0.4$ corresponds to an homogeneous medium, and $\omega_n = 0.5$ for all phases. The results shown in Figs 1(a) and 1(b) indicate that, in the same way as the 2-phase model predicts greater UV penetration into the cloud than the homogeneous approximation, the 3-phase hierarchical structure enhances this effect still further.

	p_1	p_2	p_3	$\langle l_1 \rangle$	$\langle l_2 \rangle$	$\langle l_3 \rangle$
2-Phases	0.10	0.90	-	$0.04L$	$0.36L$	-
3-Phases (I)	0.01	0.09	0.90	$0.02L$	$0.03L$	$0.36L$
3-Phases (II)	0.10	0.40	0.50	$0.04L$	$0.10L$	$0.33L$

Table 1: Model Geometries

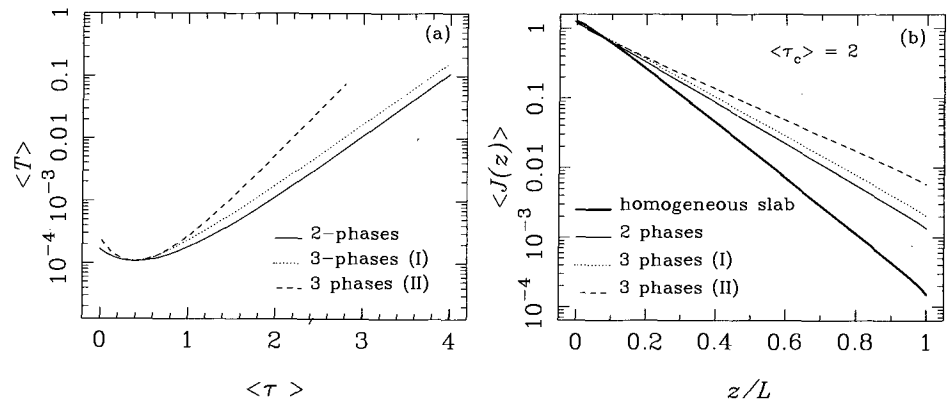

(a) Variation with average clump opacity $\langle \tau_c \rangle$ of the slab transmission coefficient for each model.

(b) Variation with depth z/L into the slab of the mean intensity of radiation for each model for the case $\langle \tau_c \rangle = 2$. The solution for the homogeneous slab with the same total optical depth, $\langle \tau \rangle = 10$, is also shown.

References

Boissé P., 1990, A&A, 228, 483

Hobson M.P., Scheuer P.A.G., 1993, MNRAS, 264, 145

Submm Observations of Molecular Lines in the Orion Bar: Towards a Physical Model

M.R. Hogerheijde, D.J. Jansen, and E.F. van Dishoeck
Sterrewacht Leiden, P.O. Box 9513, 2300 RA Leiden, The Netherlands

The Orion Bar is the ionization front connecting the H II region of the Orion Nebula with the surrounding molecular cloud, 2′ south of the Trapezium Stars. Previous observations by Hayashi et al. (1985), Parmar et al. (1991), Graf et al. (1990), Tielens et al. (1993) and Tauber et al. (1994) have shown that the intense ultraviolet radiation of these hot, young stars has created a Photon Dominated Region here, which is seen edge–on. Layers of enhanced rotational and vibrational emission of H_2 and molecular rotational emission lie 15″ and 30″ outside the ionization front respectively. This edge–on geometry provides an opportunity to study the influence of the ultraviolet radiation on the physical and chemical conditions with increasing depth into the molecular cloud.

To derive the physical and chemical structure of the Orion Bar, 53 rotational transitions of 18 molecules were observed with the JCMT, CSO and IRAM 30m (sub–)millimeter telescopes at five positions 30″ apart on a strip across the Bar. The positions are coincident in projection with the H II region ($\Delta\alpha = -20''$), the ionization front ($\Delta\alpha = 0''$; $\alpha_{1950} = 5^h32^m52.7^s$, $\delta_{1950} = -5°27'00''$), the peak of the molecular rotational emission ($\Delta\alpha = 20''$), and at increasing depth into the molecular cloud ($\Delta\alpha = 40''$ and $60''$). Derived intensities are corrected for beam efficiency and beam dilution. The contribution of a second velocity component, apparently unrelated to the Bar, has been subtracted. In addition, a $100'' \times 100''$ region centered on the Bar was mapped in the H_2CO $2_{12} \rightarrow 1_{11}$ and HCO^+ $3 \rightarrow 2$ transitions. It is found that all lines peak in intensity at the same position: $\Delta\alpha = 15''$ with respect to the ionization front.

Using an excitation code which approximates the radiative transfer with a mean escape probability, an excitation analysis of the observed transitions of $C^{18}O$, CS, HCO^+ and H_2CO has been performed. Depending on the critical density of the transitions involved, H_2 number densities ranging between 10^4 cm^{-3} and a few times 10^6 cm^{-3} were found. A kinetic temperature of 85 ± 30 K is inferred. There are no significant systematic variations in these parameters across the Bar.

Since no single density model fits the data, a two component model was constructed, with a small fraction of the total molecular column density comprised in high density clumps and the remaining part residing in a lower density interclump medium. By applying the same excitation code and taking optical depth effects into account where necessary, it was found that the observations are well fit by a clump–density of $1^{+3.0}_{-0.7}\,10^6$ cm^{-3} and an interclump–density of $3^{+2.0}_{-2.2}\,10^4$ cm^{-3}, with $\sim$ 10% of all material in the clumps. This corresponds to a 0.3% clump volume filling factor. In addition, at positions away from the emission peak the $C^{18}O$ $J = 2 \rightarrow 1$ transition is found to show a contribution of the background Orion Molecular Cloud of density $\sim 10^3$ cm^{-3} and temperature $\sim$ 20 K.

Due to the absence of variations in density or temperature across the Bar, the intensity peak corresponds to a peak in molecular column density. If the Orion Bar is the place where the PDR curves around the surrounding molecular cloud, changing from a face–on to an edge–on orientation and back, the increased length of the line–of–sight through the PDR explains this column density enhancement. We propose that the expanding H II region around the Trapezium Stars, lying at the front of the OMC, has created a 'bowl–shaped' cavity in the molecular cloud, compressing the molecular material at the edge to a density of a few $\times 10^4$ cm^{-3}. The ultraviolet radiation has created a PDR in this layer. The Orion Bar might be the place where we happen to look along one side of this 'bowl'. The extended spatial distribution of C I 609 μm (Tauber et al. 1994) precludes the possibility that the increase in column density is caused by an increase in the clump volume filling factor as proposed by Parmar et al. (1991).

MRH gratefully acknowledges the J.C. Kapteyn fund for travel support.

References

Graf, U.U., et al. 1990, ApJ 358, L49
Hayashi, M., Hasegawa, T., Gatley, I., Garden, R., Kaifu, N. 1985, MNRAS 215, 31P

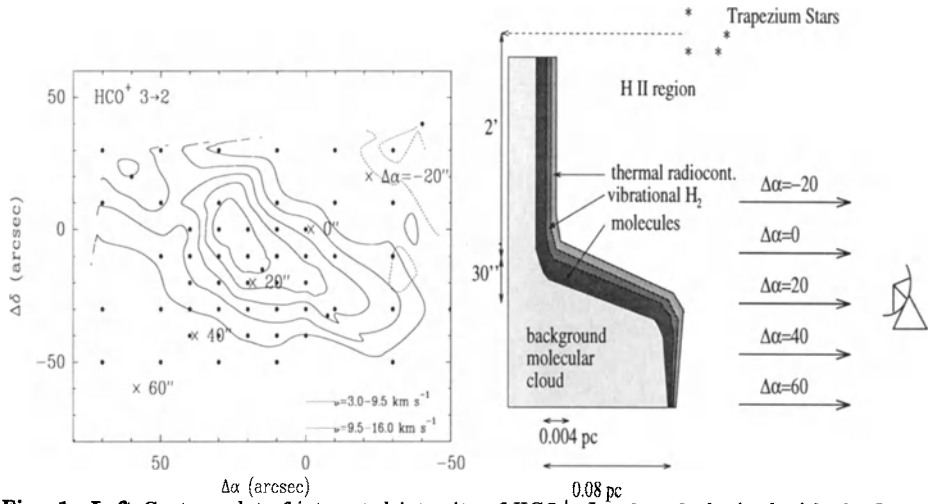

Fig. 1. Left Contour plot of integrated intensity of HCO^+ $J = 3 \rightarrow 2$ obtained with the JCMT, uncorrected for telescope efficiencies. Levels start at 10 $Kkms^{-1}$ increasing with 5 $Kkms^{-1}$. The dashed contours to the upper right correspond to a background cloud. Crosses indicate our five positions. Offsets are with respect to $\alpha_{1950} = 5^h32^m52.7^s$ and $\delta_{1950} = -5°27'00''$. **Right** Schematic view of our model for the geometry of the Orion Bar. The emission peak is caused by the increased length of the line-of-sight through the PDR as it curves around the OMC

Parmar, P.S., Lacy, J.H., Achtermann, J.M. 1991, ApJ 372, L25
Stacey, G.J. et al.1993, ApJ 404, 219
Tauber, J.A., Tielens, A.G.G.M., Meixner, M., Goldsmith, P.F. 1994, ApJ 422, 136
Tielens, A.G.G.M., et al. 1993, Science 262, 86

The PDR IC 63: Observations, Physics and Chemistry

D.J. Jansen[1], E.F. van Dishoeck[1], J.H. Black[2], J. Keene[3], M. Spaans[1]

[1] Leiden Observatory, P.O Box 9513, 2300 RA Leiden, The Netherlands
[2] Steward Observatory, University of Arizona, Tucson, AZ 85721, USA
[3] California Institute of Technology, Pasadena, CA 91125, USA

We present observations and physical and chemical models of the reflection/emission nebula IC 63. This cloud is located close to the nearby (230 pc) B0.5p star γ Cas and is an excellent example of an edge-on photon-dominated region (PDR). The (projected) distance between the star and the cloud is 1.3 pc. The resulting UV-flux is approximately 650 times the mean galactic radiation field as given by Draine.

The source has been mapped in ^{12}CO 2 $\rightarrow$ 1 and 3 $\rightarrow$ 2 (Fig. 1), ^{13}CO 2 $\rightarrow$ 1 and CS 2 $\rightarrow$ 1 and shows a small molecular cloud less than $1' \times 2'$ in extent, which coincides with the brightest optical nebulosity and IRAS 100μm emission. Various other molecules have been observed at the peak position through their rotational transitions, in order to probe the physical parameters and to derive abundances (See Table 1). The source has also been observed in C I (609 μm, CSO) and C II (158 μm, KAO, using the heterodyne receiver of Betz & Boreiko). The C II line is strong and extremely narrow with $\Delta V \approx 1$ km s^{-1}; in contrast, the C I line is surprisingly weak.

From the observed line ratios we find that the cloud is warm, $T \approx 50$ K, and dense, $n(\mathrm{H_2}) \approx 5 \times 10^4$ cm^{-3}. On the basis of these physical conditions, column densities have been derived from the observed line strengths, using statistical equilibrium calculations (Jansen et al., 1993). The electron abundance may be as high as $n(\mathrm{e})/n(\mathrm{H_2}) = 5 \times 10^{-5}$, based on the strength of the C II line.

Chemical models have been constructed to explain the low abundances. These models include a full treatment of the H_2 and CO photodissociation, including self-shielding and shielding by dust and other species (Van Dishoeck & Black, 1986, 1988). The radiation field used is the measured spectrum of γ Cas (Code & Meade, 1979), corrected for interstellar extinction. The present models assume steady state chemistry, which may be justified by the rapid photo-rates in a PDR like IC 63.

Our one-dimensional models include 1311 reactions among 199 species. These models treat the radiation field coming into the cloud from one side, and calculate the column density as seen from the other side. Since this geometry is clearly not correct, we also constructed two-dimensional models, using the actual geometry from the CO maps and a restricted chemical network, with only 165 reactions among 41 species, to speed up the calculations. These results are in good agreement with the one-dimensional models.

Table 1 lists the calculated column densities from several model runs. Model 1 is the best fitting model; results from this model are plotted in Figure 2 as functions of the extinction into the cloud. Most of the observed low abundances can be explained by the enhanced photodissociation rates. The carbon abundance appears to be well constrained from the C I, C II and CO observations : about 10 % of the solar carbon abundance is in the gas phase.

The only remaining problem seems to be H_2S, which has a surprisingly large observed abundance in IC 63, which none of our models can explain. It may be that some important reactions have not yet been included in our network, particularly those involving grain chemistry.

Table 1. Model calculations

Model	1	2	3	4	5[c]	Observed
$n(H_2)(cm^{-3})$	7×10^4	3×10^4	7×10^4	7×10^4	7×10^4	...
$\zeta(s^{-1})$	5.0×10^{-17}	5.0×10^{-17}	1.0×10^{-17}	5.0×10^{-17}	5.0×10^{-17}	...
δC	0.10	0.10	0.10	0.20	0.10	...
A_V (mag)	6.54	6.72	6.54	6.54	6.7[a]	6.7[b]
H_2	5.0×10^{21} [a]	5.0×10^{21} [a]	5.0×10^{21} [a]	5.0×10^{21} [a]	4.8×10^{21}	5.0×10^{21} [b]
H	3.9×10^{20}	6.8×10^{20}	3.9×10^{20}	4.0×10^{20}	7.1×10^{20}	$\lesssim 6.0 \times 10^{20}$
C	3.3×10^{16}	3.2×10^{16}	3.3×10^{16}	7.0×10^{16}	1.2×10^{17}	4.0×10^{16}
C^+	1.5×10^{17}	1.7×10^{17}	1.5×10^{17}	2.7×10^{16}	1.6×10^{17}	1.4×10^{17}
CO	3.0×10^{17}	3.0×10^{17}	3.0×10^{17}	6.3×10^{17}	2.1×10^{17}	$\gtrsim 1.3 \times 10^{17}$
^{13}CO	4.8×10^{15}	4.7×10^{15}	4.7×10^{15}	9.9×10^{15}	...	3.9×10^{15}
$C^{18}O$	3.8×10^{14}	4.0×10^{14}	3.0×10^{14}	7.5×10^{14}	...	5.0×10^{14}
CS	6.7×10^{12}	5.0×10^{12}	9.0×10^{12}	1.4×10^{13}	...	6.5×10^{12}
CN	2.1×10^{13}	1.8×10^{13}	2.1×10^{13}	5.0×10^{13}	...	2.5×10^{13}
HCN	3.3×10^{12}	3.5×10^{12}	2.1×10^{12}	3.1×10^{12}	...	7.0×10^{12}
HCO^+	7.1×10^{12}	1.4×10^{13}	1.7×10^{12}	1.2×10^{13}	7.1×10^{12}	6.0×10^{12}
H_2CO	2.3×10^{12}	2.2×10^{12}	1.9×10^{12}	3.0×10^{12}	3.2×10^{11}	3.0×10^{12}
C_2H	5.8×10^{13}	4.5×10^{13}	5.8×10^{13}	1.0×10^{14}	...	2.0×10^{13}
N_2H^+	3.3×10^{11}	7.0×10^{11}	6.0×10^{10}	2.2×10^{11}	...	2.2×10^{11}
H_2S	1.2×10^{09}	1.8×10^{09}	3.8×10^{08}	1.2×10^{09}	...	7.3×10^{12}

Gas phase fractions : O : 0.40, N : 0.15, S = 0.003, Metals : 0.0005; $\chi = 650$; $T = 50$ K.
[a] : This value was fixed to set the total size of the cloud. [b] : $N(H_2)$ and A_V derived from the density and size of the nebula. [c] : Two–dimensional model.

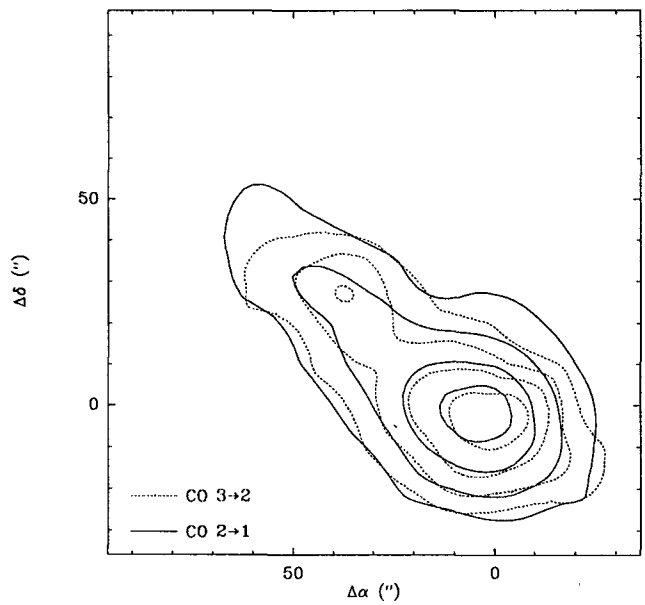

Figure 1 : Maps of the integrated intensity of CO 2 → 1 (solid) and CO 3 → 2 (dashed) of IC 63. Contours are 30, 50, 70 and 90 % of the maximum.

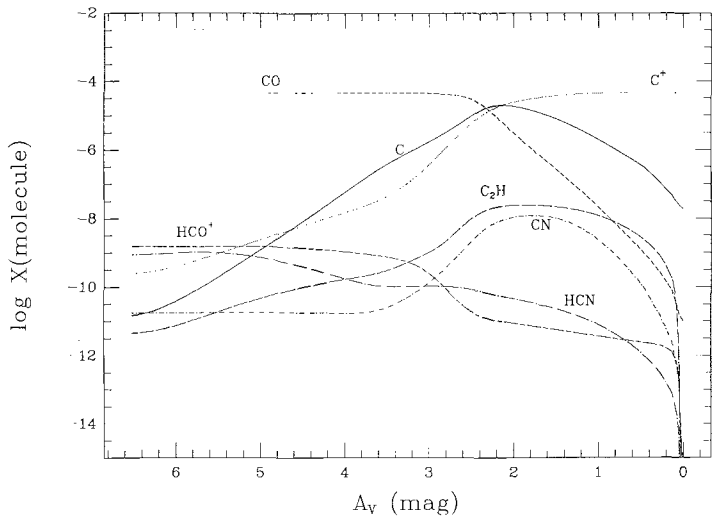

Figure 2 : Molecular densities of some important species as functions of the visual extinction. γ Cas is located to the (far) right.

References

Code, A.D., Meade, M.R., 1979, ApJS 39, 195
Jansen, D.J., Van Dishoeck, E.F., Black, J.H., 1993, A&A, in press
Van Dishoeck, E.F., Black, J.H., 1986, ApJS, 62, 109
Van Dishoeck, E.F., Black, J.H., 1988, ApJ, 334, 771

Star Formation in Bok Globules – A 1.3 mm Continuum Survey

R. Launhardt, Th. Henning

Max Planck Society, Research Group "Dust in Star-forming Regions",
Schillergäßchen 2-3, D-07745 Jena, Germany

Abstract: We present the first results of an 1.3 mm continuum survey of Bok globules which was conducted with the 30-m MRT (IRAM) and the 15-m SEST during 1992 and 1993. We detected 17 sources in a sample of 57 globules in which 7 of 13 globules with molecular outflows were detected. This leads to a total detection rate of 30% and 54% for the outflow sources. from our studies, we identified very good candidates for globules with star formation in different phases. 3 of the strongest sources are good candidates for YSOs with massive circumstellar disks.

Introduction: Bok globules are small, opaque, and isolated nearby molecular clouds. Their cores are excellent locations to study the star formation process in detail because usually they have a quite simple structure. Many globule cores are associated with very cold far-infrared sources (Clemens & Barvainis 1988,"CB"). 14 globules in a sample of 41 globules are associated with molecular outflows (Yun and Clemens 1992) indicating current star formation. Henning et al. (1994) found dense CS cores in 20 globules with spectroscopic evidence for a protostellar collapse in 5 cores.
To search for protostellar cores and circumstellar structures of young stellar objects, we have performed an 1.3 mm continuum survey. For our survey, we selected all outflow sources and those with similar IRAS colours, the strongest non-outflow IRAS sources, and 10 small, opaque, and isolated globules without IRAS sources from the CB catalogue.

Observations: The survey has been performed during three observing runs between December 1992 and March 1993 using the IRAM 30-m MRT and the 15-m SEST.
The IRAM facility bolometer system and the 7-channel MPIfR bolometer array were used at the MRT (beam size 12″) during December 1992 and March 1993 and the SEST facility bolometer (beam size 23″) was used during March 1993 for the photometry of 57 globules. In all cases, we followed the standard chopping-beam switching procedure with beam separations of 60″ at the MRT and 70″ at the SEST, respectively.

Results: We observed a total of 57 globules dividing into 47 IRAS point sources and 10 globules without IRAS point sources. 13 of the globules with IRAS sources are associated with molecular outflows. The average detection limit (3σ) was 36 mJy/12″beam for the MRT data and 75 mJy/23″beam for the SEST data. We detected 17 sources dividing into 16 globules with associated IRAS point sources in which 7 objects are outflow sources and one globule without an IRAS source. This leads to a detection rate of 30% for the whole sample and 54% for the outflow sources. Note that these detection rates are not representative for the whole CB catalogue (248 globules) because globules with ongoing star formation were preferred by our selection criteria.
Based on simple statistics, a relatively small number of globules are in a star formation phase at any instant; most globules either do not form stars at all, will undergo this process in the future, or contain embedded evolved low-mass stars.
By an analysis of the broad-band energy distributions, we found two clearly separated groups of globule sources. The sources of the first (smaller) group are very young embedded low-mass stars often connected with outflows and circumstellar dust structures. 14 of the detected sources belong to this group. The second group may encompass different stages of star formation, the earliest phases of the cloud collapse as well as embedded stars in the post-outflow stage.
By an analysis of the mm flux - luminosity ratio (see Terebey et al. 1993), we found CB 54, CB 68, and CB 230 to be very good candidates for YSOs Os with massive circumstellar disks. CB 17 and CB 155-2 are group 2 sources. By comparison with our CS observations, we found CB 17 to be a good candidate for a real protostellar core. The only detected globule without an associated IRAS point source is CB 246. The source is connected with an extended, dense CS core. CB 3 has an unusual large distance for a Bok globule and is not disussed here.

Bok globules - 1.3 mm survey - positive detections:

Source name	$RA_{(1950)}$ [h m s]	$DEC_{(1950)}$ [° ' '']	S_{1300} [$mJy/beam$]	beam ['']	Tel./yr
CB 3	00 25 56.8	56 25 32	610 ± 30	12	MRT 93
CB 6	00 46 34.3	50 28 25	46 ± 5	12	MRT 93
CB 17	04 00 30.8	56 47 59	74 ± 12	12	MRT 92
CB 34	05 44 02.8	20 59 07	99 ± 9	23	SEST 93
CB 52	06 46 25.3	-16 50 38	36 ± 9	23	SEST 93
CB 54	07 02 06.0	-16 18 47	519 ± 11	23	SEST 93
CB 58-2	07 16 09.1	-23 36 11	39 ± 9	23	SEST 93
CB 68	16 54 27.2	-16 04 48	272 ± 15	23	SEST 93
CB 145	18 29 37.2	-09 11 40	43 ± 9	23	SEST 93
CB 155-2	18 44 41.5	-04 35 14	58 ± 21	23	SEST 93
CB 205	19 43 21.7	27 43 37	67 ± 9	12	MRT 92
CB 224	20 35 33.9	63 43 08	58 ± 10	12	MRT 92
CB 230	21 16 54.4	68 04 52	361 ± 17	12	MRT 93
CB 232	21 35 14.4	43 07 05	35 ± 11	12	MRT 92
CB 243	23 22 52.9	63 20 04	70 ± 8	12	MRT 92
CB 244	23 23 48.8	74 01 08	103 ± 12	12	MRT 92
CB 246	23 54 12.0	58 17 47	37 ± 12	12	MRT 92

Summary: We have performed an 1.3 mm continuum survey of 57 Bok globule cores to search for protostellar cores and circumstellar structures of young stellar objects. 17 globules could be detected (detection rate 30%) in which 7 of the strongest sources have molecular outflows. From our study, we identified very good candidates for globules with star formation in different phases ranging from early protostellar cores to YSOs with massive circumstellar disks.

References

Clemens, D. P., Barvainis,R., 1988, Ap.J.Suppl. **68**, 257 (CB)
Hennig, Th., Launhardt, R., 1994 (in preparation)
Yun, J. L., Clemens,D.P., 1992, ApJ **385**, L21
Terebey, S., Chandler, C. J., André, P., 1993, ApJ **414**, 759

Radiation-Driven Implosion of Cometary Globules Modelling and Observations

B. Lefloch [1], B. Lazareff [2]

[1] Observatoire de Grenoble, 414 rue de la piscine, 38041, St-Martin d'Heres, France
[2] IRAM, 300 rue de la piscine, 38041, St-Martin d'Heres, France

Cometary Globules (CGs) are small isolated clouds (size of a few tenths of pc) consisting in a dense core prolongated by a long tail, surrounded by a bright rim, and commonly found in the vicinity of OB associations in HII regions. In the pioneering work by Reipurth (1983), they have been shown to be active sites of star formation, although usually not gravitationally bound. The physical properties as well as the star formation taking place in CGs are strongly dependent on the mechanism of formation and evolution, which is not yet fully established, although recent observations with high angular resolution seem to favor the so-called Radiation-Driven Implosion model (RDI) (Duvert et al., 1990) .

In order to fill the present gap between theory and observations, in particular the need for a clear evolutionnary model of CGs and direct observational predictions we have numerically studied the evolution of a globule illuminated by a planar Ly-c photon flux (Lefloch and Lazareff, 1993). For most of the situations of astrophysical interest, RDI is a two-stage process :
a) collapse phase (fig. 1a): it occurs over a short time-scale ($\approx 10^5$ yr). Maximum compression, possibly leading to star formation, occurs in the early stages of the collapse. After maximum compression, the globule undergoes a few expansions and re-compressions. This pre-cometary phase lasts $\simeq 10\%$ of the cloud's lifetime. This stage is spectroscopically characterized by a double component emission line; for an optically thin transition, in a velocity-position diagram, this 2^{nd} component is revealed by the presence of 2 wings (fig. 1b).
b) cometary phase (fig.2a): the globule is in a quasi-hydrostatic equilibrium. There is no remarkable spectroscopic signature (fig. 2b). The lifetime of this stage is of the order of a few 10^5 yr to a few My.

Our model reproduces the optical morphology of cometary globules, invoking only one physical mechanism: *photoionisation*, and using only one free parameter: *the degree of evolution*. It also accounts for the numerous bright rim globules observed at the boundary of HII regions. The results of our modelling have been confronted to millimetric observations of a globule located in the HII region IC1805, which, according to its morphology, seems to be still in the pre-cometary stage. In agreement with our model, we found:
a) a core-halo density structure in the head of the globule, oriented towards the source of the ionising flux.
b) a velocity gradient in the tail.
c) a double component kinematic structure; the second component is the signature of gas compressed by shock.
Applying our model to a few observed isolated globules in the cometary stage, it appears that *they are supported predominantly by magnetic field and not by turbulence*, unlike what is usually observed in molecular clouds (Myers and Goodman, 1988). Besides, the strength of the magnetic field that we derive ($B \approx 10^2 \mu G$) seems to follows Heiles' empirical law (1993).

Upper panel : density-velocity maps of a photoionised globule at the beginning of the collapse phase and in the cometary regime. The density map is in grey scale and the velocity field is traced by black arrows. (scale in pc).
lower panel : velocity-position cuts along the globule's axis, at the beginning of the collapse and in the cometary regime (see upper figures). These maps are calculated for an optically thin molecular line, the cloud having an inclination angle of 30° with respect to the plane of sky.

References

Duvert, G., Cernicharo, J., Bachiller, R.,Gómez-González, J., 1990, A&A, 233, 190
Heiles, C., Goodman, A., McKee, C., Zweibel, E., 1993,
in Protostars and Planets, vol. III
Lefloch, B., Lazareff, B., 1993, in prep.
Myers, P.C., Goodman, A.A., 1988, ApJ, 329, 392
Reipurth, B., 1983, A&A, 117, 183

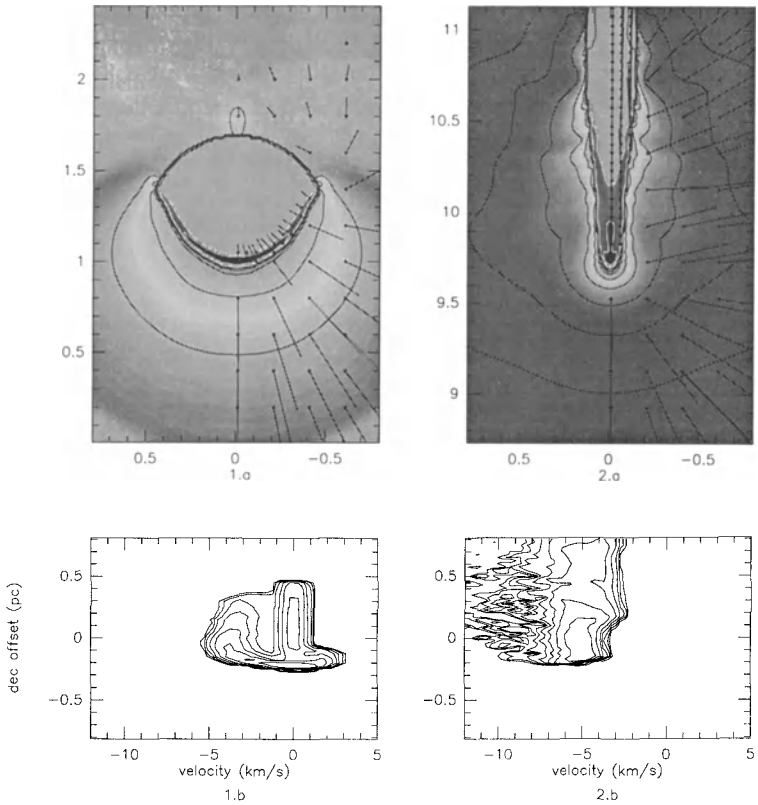
2
1.5
1
0.5
0.5
0
−0.5
1.a
11
10.5
10
9.5
9
0.5
0
−0.5
2.a
dec offset (pc)
0.5
0
−0.5
−10
−5
0
5
velocity (km/s)
1.b
0.5
0
−0.5
−10
−5
0
5
velocity (km/s)
2.b

CI Emission from the Outflow and PDR in S140

Nigel R. Minchin[1], Dirk Krause[2], Juergen Stutzki[2] and Glenn J. White[1]

[1] Department of Physics, Queen Mary and Westfield College, University of London, Mile End Road, London E1 3NS, U.K.

[2] Physikalisches Institut, Universität zu Köln, 50937 Köln, Germany

The L1204 molecular cloud lies to the northeast of the S140 HII region, produced by the nearby B0 star HD 211880. This molecular cloud is one of the best examples of an edge-illuminated PDR (e.g. Blair *et al.* 1978). Only 70-80 arcsec northeast of the PDR is an embedded cluster of three infrared sources (e.g. Beichman *et al.* 1979) which lie at the centre of a high-velocity molecular outflow (e.g. Snell *et al.* 1984). The outflow axis is along the southeast-northwest direction, parallel to the PDR. Minchin, White & Padman (1993) have recently compared single velocity channel atomic carbon (CI) $^3P_1 \rightarrow ^3P_0$ observations of White & Padman (1991) to various ^{12}CO and ^{13}CO emission line maps. The CI emission is mainly confined to a clumpy, elongated ridge-like feature adjacent to the edge of the molecular cloud and coincident with a similar feature seen in ^{12}CO emission. There is a second region of intense CI emission, located inside a ring of CS emission that surrounds the embedded infrared sources. They conclude that this CI emission may be produced by the outflow or embedded sources.

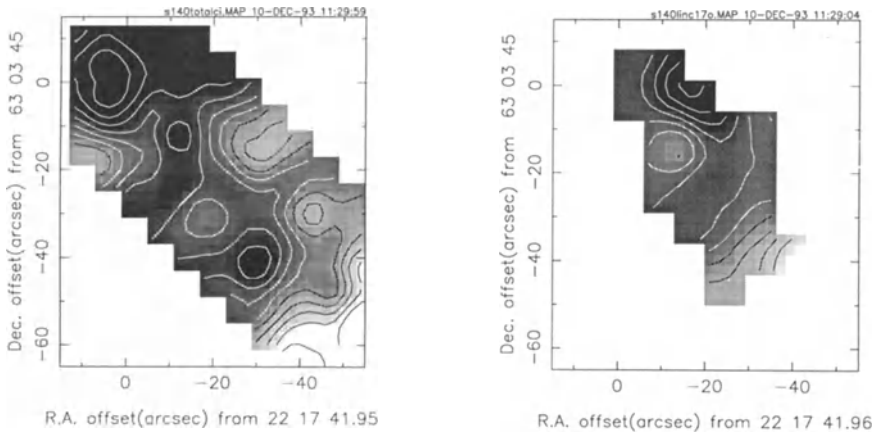

Figure: Total integrated intensity maps for the CI $^3P_1 \rightarrow ^3P_0$ and $C^{17}O$ J = 3→2 lines between -14 and 2 km s^{-1}

We have mapped the CI $^3P_1 \rightarrow ^3P_0$ (492.1607 GHz) and $C^{17}O$ J = 3→2 (337.0611 GHz) line emission from L1204/S140 at high angular resolution (10 and 14 arcsec FWHM beamsize respectively) using the JCMT. The advantage of mapping $C^{17}O$ emission is that, unlike ^{12}CO, ^{13}CO and $C^{18}O$, the line stays optically thin even in the densest core regions and is therefore the most accurate high-resolution tracer of CO morphology.

Both the CI and $C^{17}O$ integrated intensity maps show a similar morphology (Figures 1 and 2). The emission peak lies towards the molecular outflow source, and there is an arc of emission extending from the peak towards the south. The CI and $C^{17}O$ arcs are offset, with the CI arc offset to the northeast by ~10 arcsec. The CI arc feature is observed in blue and redshifted emission, whilst the $C^{17}O$ feature is only observed in blueshifted emission. This implies the CI emission traces the inner edge of the blueshifted molecular outflow wall (traced by the $C^{17}O$ emission).

CI is highly-abundant towards the molecular outflow source, $N(\mathrm{CI})/N(\mathrm{CO}) = 0.28$. A similar abundance is found for blue wing and core velocity intervals (0.24–0.25), but for the red wing the abundance is remarkably high, $N(\mathrm{CI})/N(\mathrm{CO}) = 1.36$. There is no net enhancement of the blue wing material relative to the ambient cloud material (signified by $\epsilon = 1.0$) which shows that, although the abundance of CI relative to CO is high, it is not over-abundant relative to the ambient cloud material. For the red wing the value of $\epsilon = 5.5$ confirms that not only is the abundance of CI to CO extremely high, but it is highly over-abundant relative to the ambient material.

These observations can be compared with recent modelling by Hollenbach & McKee (1989). They are consistent with a model for the outflow region in which the CI emission is produced by the effect of shocks on the chemical and physical processes at the interface between the stellar wind and the blueshifted outflow cavity wall.

The PDR is observed in CI emission as a clumpy, narrow ($\sim$0.1–0.15pc) feature, adjacent to the south-western edge of the molecular cloud. CI emission from the PDR is observed within a relatively narrow velocity range, -10 to -6 km s^{-1}. There is a localised peak in emission at offset position (-28,-42), which we have designated PDRc1 (PDR clump 1). PDRc1 is a more prominent emission feature than the outflow peak over the velocity range -9 to -7 km s^{-1}. The abundance of CI is high, $N(\mathrm{CI})/N(\mathrm{CO}) = 0.29$ at the position of PDRc1. The observed column density ($9.7\pm0.8\times10^{17}$ cm^{-2}) and emergent intensity ($8.7\pm0.7\times10^{-6}$ erg cm^{-2} s^{-1} sr^{-1}) towards PDRc1 are in close agreement with recent modelling of low-density PDRs (Hollenbach, Takahashi & Tielens 1991).

A full presentation and discussion of the data set can be found in Minchin *et al.* (1994).

References

Beichman C. A., Becklin E. E., Wynn-Williams C. G., 1979, ApJ Lett 232, L47
Blair G. N., Evans N. J., Vanden Bout P. A, Peters W. L., 1978, ApJ 219, 896
Hollenbach D. J., McKee C. F., 1989, ApJ 342, 306
Hollenbach D. J., Takahashi T., Tielens A. G. G. M., 1991, ApJ 377, 192
Minchin N. R., White G. J., Padman R., 1993, A&A, 277, 595
Minchin N. R., Krause D., Stutzki J. White G. J., 1994, A&A, in preparation
Snell R. L., Scoville N. Z., Sanders D. B., Erickson N. R., 1984, ApJ 284, 176
White G. J., Padman R., 1991, Nat 354, 511

Large Scale Observations of [CI] $^3P_1 \rightarrow {}^3P_0$ in Photon-Dominated Regions

R. Plume[1], D.T. Jaffe[1], K. Tatematsu[1], J.B. Keene[2]

1. Dept. of Astronomy, University of Texas, RLM 15.308, Austin, TX 78712
2. Dept. of Physics, Caltech, 320-47, Pasadena, CA 91125

Introduction

Observations of Wright et al. (1991) and Büttgenbach et al. (1992), have shown that the $^3P_1 \rightarrow {}^3P_0$ emission of neutral carbon ([CI]) is bright over large scales in galaxies (i.e. $I_{CI}/I_{CO2\rightarrow1} = 1.5$ in inner 100pc of IC 342; 2.3 over large scales in the Milky Way). These Galactic-scale observations imply that [CI] emission must arise from extended regions in molecular clouds. However, studies of [CI] in molecular clouds have been limited to small areas (Phillips & Huggins 1981; Keene et al. 1985; White & Padman 1991) and, therefore, we have little knowledge of the abundance and distribution of [CI] over extended regions in molecular clouds. [CI] observations require sensitive receivers at high, dry sites. Unfortunately, telescopes with the required location and instrumentation are large, resulting in small beamsizes at 492 GHz (e.g. the 10.4m CSO has $\theta = 15''$). To allow us to quickly map extended regions of molecular clouds ($30' \times 30'$) we have built a "Gaussian Focal Reducer" (GFR) for the Caltech Submillimeter Observatory (CSO). The GFR reduces the effective aperture of the CSO from 10.4m to 60cm resulting in a $3'$ beam on the sky. The instrument is described in detail by Plume et al. (1994).

Observations

Line	ν GHz	T_{rms} K	Source Name and Map Size(')
[CI]$^3P_1 \rightarrow {}^3P_0$	492.16	0.2	CepA(20×25), NGC2024(40×60), S140(30×30),W3(35×30)
^{13}COJ=2→1	220.39	0.1	CepA(30×30),NGC2024(28×40),S140(26×34),W3(36×32)
C^{18}OJ=2→1	219.56	0.1	CepA(16×16),S140(20×28),W3(34×22)

The observations were made in 1993 February, March and June at the Caltech Submillimeter Observatory.

Results

Inspecting Figures 1 and 2 it is apparent that neutral carbon is very extended and resembles the ^{13}CO morphology. The [CI], ^{13}CO, and C^{18}O lineshapes are also similar, implying that the emission arises from closely related regions within the molecular clouds. Typical column densities are: N(CI) $\sim 10^{17}$ cm^{-2} and N(^{13}CO) $\sim 6 \times 10^{15}$ cm^{-2}. Given the detailed agreement of the [CI] morphology and lineshapes with that of ^{13}CO and C^{18}O, it appears that neutral carbon in photon dominated regions (PDRs) on the surfaces of molecular clumps can explain the observed emission. Comparison of our observed [CI] column densities with PDR models yields $N_{obs}/N_{model} \sim 0.6$ - 1.3 (van Dishoeck and Black 1988) or ~ 0.3 - 1 (Hollenbach, Takahashi and Tielens 1991).

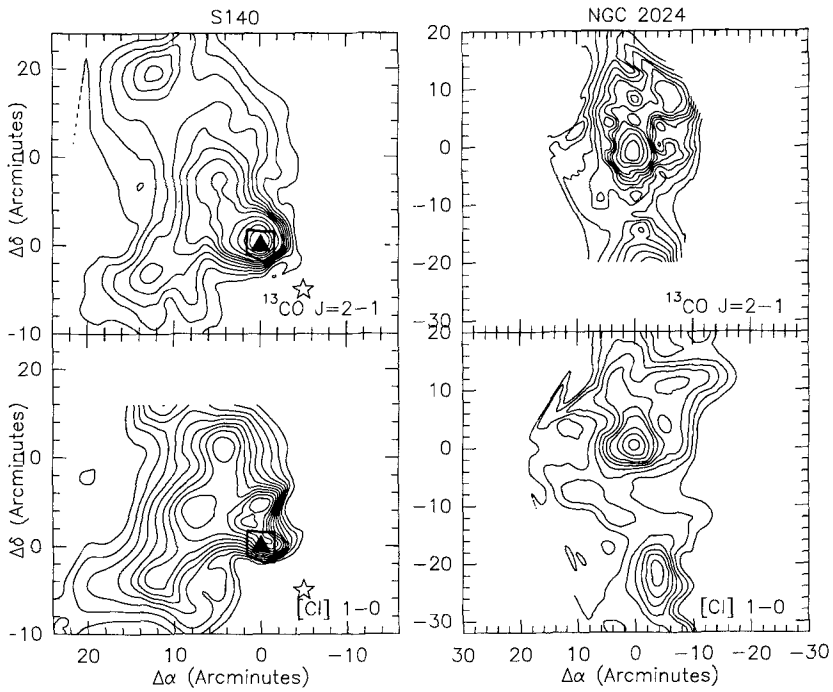

Figure 1 - (top) ^{13}CO J=2→1 integrated intensity in S140. Contour levels are 2.5 to 20 km s^{-1} in steps of 2.5 km s^{-1} and 25 to 40 km s^{-1} in steps of 5 km s^{-1}. The star denotes the position of the ionizing star HD 211880 and the triangle shows the position of IRS1. The small box delineates the area previously mapped in [CI]. **(bottom)** [CI] $^3P_1 \rightarrow ^3P_0$ integrated intensity in S140. Contour levels are 3 to 13 km s^{-1} in steps of 1 km s^{-1}. **Figure 2 - (top)** ^{13}CO J=2→1 integrated intensity in NGC 2024. Contour levels are 10 to 50 km s^{-1} in steps of 5 km s^{-1} and 60 to 80 km s^{-1} in steps of 10 km s^{-1}. **(bottom)** [CI] $^3P_1 \rightarrow ^3P_0$ integrated intensity in NGC 2024. Contour levels are 5 to 20 km s^{-1} in steps of 2.5 km s^{-1} and 25 to 35 km s^{-1} in steps of 5 km s^{-1}.

References

Büttgenbach, T.H., Keene, J., Phillips, T.G., and Walker, C.K. 1992, ApJ, 397, L15.
Hollenbach, D.J., Takahashi, T., & Tielens, A.G.G.M. 1991, ApJ, 377, 192.
Keene, J., et al. 1981, Ap. J., 251, 533.
Plume, R., Jaffe, D.T., Phillips, T.G., and Wesley, G. 1994, in prep.
van Dishoeck, E.F., and Black, J.H. 1988, ApJ, 334, 771.
White, G.J., and Padman, R. 1991, Nature, 354, 511.
Wright, E. L., et.al. 1991, ApJ, 381, 200.

The [C II] 158 μm Line Emission from the ρ Ophiuchi Cloud

Y. Y. Yui,[1,2] T. Nakagawa,[1] Y. Doi,[1,2] H. Okuda,[1] H. Shibai,[1] T. Nishimura,[3,4] and F. J. Low [3]

[1] The Institute of Space and Astronautical Science, Yoshinodai 3-1-1, Sagamihara, Kanagawa 229, Japan

[2] Dept. of Astronomy, The University of Tokyo, Bunkyo-ku, Tokyo 113, Japan

[3] Steward Observatory, The University of Arizona, Tucson, AZ 85721, USA

[4] National Astronomical Observatory, Osawa 2-21-1, Mitaka, Tokyo 181, Japan

A detailed map of the [C II] 158 μm line emission from the ρ Ophiuchi dark cloud has been obtained using the Balloon-borne Infrared Carbon Explorer (*BICE*; Nakagawa et al. 1993). The spatial resolution is 15' (FWHM), and the detection limit is 1.5×10^{-5} ergs s^{-1} cm^{-2} $ster^{-1}$ (3 σ).

Fig.1 shows the results. The [C II] emission is extended throughout the cloud (8 pc $\times$ 6 pc), indicating that UV radiation in the cloud is not localized but is ubiquitously distributed. The spatial distribution of the [C II] emission (Fig.1) is similar to that of IRAS 100 μm continuum (Fig.2), but is different from those of the CO line (Fig.3) and radio continuum (Fig.4).

The peak of the [C II] emission corresponds to the position of the highly reddened B2 V star HD147889. Since there is no O-type star in the observing area and this star is of the earliest type in the central region, HD147889 is the dominant exciting source of the [C II] emission from the central region. Although HD147889 is the primary source of C-ionizing photons ($h\nu$ >11.3 eV), the star dose not produce many H-ionizing photons ($h\nu$ >13.6 eV), and we cannot see extensive H II regions around it (Fig.4). Hence, HD147889 is a clear example of a B-type star exciting a [C II] region without an extensive H II regions.

The peak of the CO line is shifted 0°.3 toward the east from the [C II] line peak or the position of HD147889. Since HD147889 resides at the edge of the molecular cloud core, we suppose that the star illuminates the core region from one side and this configuration yields the shift of peaks in [C II] and the 100 μm continuum.

The observed [C II] emission scale length from the HD147889 into the east cloud core is 0.6 pc. If the gas in the cloud core is homogeneous ($n = 10^4$ cm^{-3}; Wilking and Lada 1983), UV radiation from the star is attenuated at only 0.1 pc from the star. Hence the core region cannot be homogeneous and must be highly clumpy to allow UV radiation to penetrate the cloud and form an extended C^+ region.

Fig.4 shows a spherical H II region around the B1 III star σSco. The south-west extension of the [C II] emission is associated with this H II region. However, the [C II] emission is shifted from the radio continuum peak toward the west by 0°.2. The emission is supposed to be arise from a neutral cloud illuminated by UV radiation from the σ Sco. The fact that no CO line emission is detected in this region indicates that the interstellar gas around σSco is almost completely photodissociated.

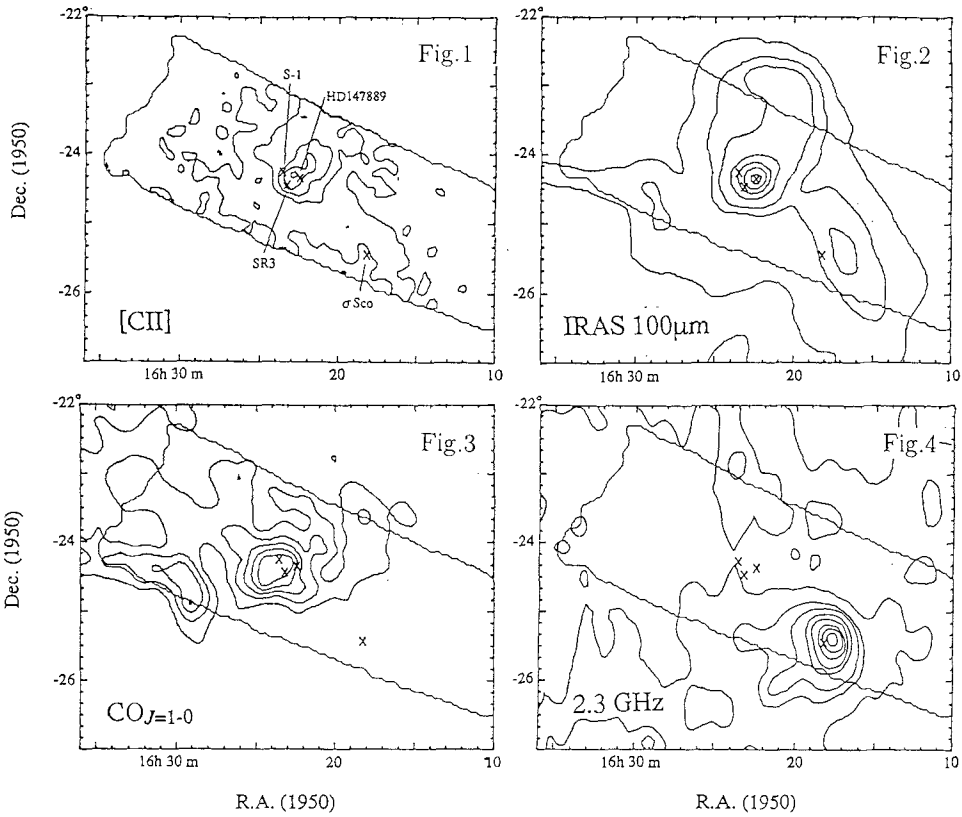

Fig.1. The [C II] line intensity map. The contour levels are 2, 4, 6, 8, and 10×10^{-5} ergs s^{-1} cm^{-2} $ster^{-1}$ (Yui et al. 1993). Crosses indicate the positions of accociated B-type stars.

Fig.2. The IRAS 100 μm continuum map corrected for zodiacal emissivity (de Geus and Burton 1991).

Fig.3. The velocity integrated CO line (1-0) antenna temperature map (de Geus, Bronfman and Thaddeus 1990).

Fig.4. The 2.3 GHz radio continuum map (Baart, de Jager and Mountfort 1980).

References

Baart, E. E., de Jager, G., Mountfort, P. I. 1980, A&A, 92, 156
de Geus, E. J., Bronfman, L., Thaddeus, P. 1990, A&A, 231, 137
de Geus, E. J., Burton, W. B. 1991, A&A, 246, 559
Nakagawa, T. 1993, in Astronomical Infrared Spectroscopy: Future Observational Directions, ed. S. Kwok (San Francisco: ASP), 373
Wilking, B. A., Lada, C. J. 1983, ApJ, 274, 698
Yui, Y. Y., Nakagawa, T., Doi, Y., Okuda, H., Shibai, H., Nishimura, T., Low, F. J. 1993, ApJ, 419, L37

How Stable are the Results of Simple Model Calculations of Interstellar Chemistry?

Eric Herbst
Departments of Physics and Astronomy, The Ohio State University,
Columbus, Ohio 43210, USA

I. Introduction

Despite their simplicity, homogeneous chemical models of the cores of dense interstellar clouds ($n = 2n(H_2) + n(H) \geq 10^4 cm^{-3}$; $A_v \geq 10$ mag) suffer from severe astronomical and chemical uncertainties which strongly affect predicted molecular abundances. In this paper, we emphasize several sources of uncertainty in the course of a discussion of recent chemical models.

Gas-phase chemical models are constructed by incorporating chemical reactions into coupled chemical kinetic equations of the form

$$\frac{dn(i)}{dt} = \sum_j \sum_l k_{jl} n(j) n(l) - \sum_m k_{im} n(i) n(m) \qquad (1)$$

where i, j, l, and m represent specific species, and the k represent rate coefficients. Photodestruction via external photons is not normally considered although secondary photons generated by cosmic rays play some role in the chemistry (Lepp & Dalgarno 1988; Gredel et al. 1989). Reaction networks are dominated by ion-molecule reactions since these processes proceed rapidly at low temperatures (Smith 1992). Specific pathways for the production of organic molecules have been discussed by Herbst & Leung (1989,1990). Solution of the coupled differential equations proceeds from given initial concentrations assumed to be atomic in nature or to resemble diffuse cloud abundances in a fractional sense.

Twenty years ago, when serious modelling began, the solution of coupled differential equations was not practical and steady-state solutions were obtained by setting the assorted derivatives dn(i)/dt equal to zero. Steady-state models can reproduce the abundances of many small gas phase species (Herbst & Klemperer 1973; Gerin et al. 1992). It is not easy to see, however, how steady state can be achieved in dense interstellar clouds because of the long time necessary (10^7 yr). A variety of dynamical processes occur more rapidly; in particular, the sticking ("adsorption") of molecules to the surfaces of classical dust particles occurs on a time scale of $\approx 3 \times 10^5$ yr for a cloud with $n = 10^4$ cm^{-3} (Herbst 1993). At a characteristic grain temperature of 10 K, evaporation is inefficient except for the light species H, He, and H_2. In the absence of non-thermal desorption, no heavier species will remain in the gas phase of quiescent sources much longer than 10^6 yr. In addition, it has been found that the calculated abundances of organic molecules are much too small at steady state to explain observed values in molecule-rich dark clouds and giant molecular clouds (Herbst & Leung 1989). Large organic molecule abundances can be produced at so-called "early time" ($10^4 - 10^{5.5}$ yr) before grain adsorption becomes a serious problem (Herbst & Leung 1989). This conclusion rests on chosen elemental abundances in the gas. Large organic molecule concentrations are not produced at early time unless the gaseous abundances of heavy elements (Na, Mg, Fe, S, Si) are substantially reduced below cosmic values. With such "low metal" abundances (Graedel, Langer, & Frerking 1982), large organic molecular abundances can also be achieved at steady state (if adsorption is neglected) as long as the C/O elemental ratio is greater than unity, contrary to standard practice (Langer & Graedel 1989; Herbst & Leung 1986). Despite these qualifications, the early-time hypothesis has gained wide spread acceptance.

II. Gas-Grain Models and Processes

Gas phase models do not yield information on condensed phase abundances. We have recently added grain chemistry (Millar & Williams 1993) to our hitherto pristine gas phase models (Hasegawa, Herbst, & Leung 1992; Hasegawa & Herbst 1993a,b; Caselli, Hasegawa, & Herbst

1993, 1994). Some of our most recent model calculations divide dust particles, assumed to be spherical, into three phases: a refractory core of radius 0.1μ, a mantle of material atop this core, and a surface layer of material atop the mantle. Rapid chemical processes between diffusive species occur only on the surface so that if reactive molecules are buried underneath the surface by adsorption, they will become inert. In previous ("two-phase") models of the grain chemistry, no distinction was made between the mantle and the surface, despite the build up of significant mantles. Consequently, condensed phase abundances of unsaturated (hydrogen-poor) molecules remain low at all cloud stages since hydrogenation via reaction with adsorbed H atoms is rapid. In the three-phase approach, the condensed phase abundances of unsaturated species can be considerably higher, especially in mature clouds ($t \approx 10^6 - 10^7$ yr). Non-thermal desorption mechanisms do not return much material to the gas at these ages in our gas-grain models. Utilizing additional non-thermal desorption mechanisms (Hartquist & Williams 1991), other modellers (Willacy & Williams 1993) have obtained somewhat higher abundances of selected gas phase species for mature clouds.

We have recently applied both two-phase and three-phase gas-grain models to the specific problem of condensed-phase CO (Caselli et al. 1994) which is observed to be quite abundant in cold sources (Whittet & Duley 1991). Our models that employ "low metal" gaseous elemental abundances to describe the initial gaseous material fail to produce enough condensed phase CO by two orders of magnitude because of rapid surface hydrogenation at all cloud ages of CO into methanol, even with our three-phase assumption. Models with "high metal" abundances achieve the desired level of condensed phase CO due principally to the catalytic reduction of surface H atoms via adsorbed sulphur (Tielens & Hagen 1982). The gas phase abundances of organic molecules predicted for early time, however, become far too low. It is best to choose so-called "depleted high metal" elemental abundances, in which "low metal" abundances are used to describe the gas at $t = 0$ while the extra abundances of heavy elements are placed on grain mantles and surfaces. With such elemental abundances, calculated gas phase concentrations of organic molecules remain high at early time while large condensed phase abundances of CO exist for all times after 10^4 yr.

Another focus of our gas-grain chemical models is the study of the chemical diversity in different hot core-type regions. Following Brown, Charnley, & Millar (1988), and Charnley, Tielens, & Millar (1992), we (Caselli et al. 1993) consider a scenario in which thermal evaporation from grain mantles at the current high (100-200 K) temperature follows a previous phase of isothermal collapse during which gas and grain chemistry occur. The thermal evaporation is followed by purely gas phase chemistry. We have found that the chemical evolution of dust mantles during the isothermal collapse phase is very sensitive to the temperature chosen. In particular, we have shown that the large chemical differences between the Hot Core ($T = 200$ K, $n \geq 10^7 cm^{-3}$) and the Compact Ridge ($T = 100$ K, $n \geq 10^6 cm^{-3}$) sources in Orion can be accounted for in the following manner. During its previous low temperature collapse phase, the Compact Ridge maintained a grain temperature of 20 K, at which temperature CO produced in the gas was able to reside on dust particles long enough to be partially converted into methanol. Subsequent evaporation of the methanol resulted in the large observed abundance of this species and the efficient gas phase production of methyl formate from methanol. On the other hand, the Hot Core possessed a grain temperature of 40 K during its collapse phase. At this rather high temperature, CO could not stick to dust particles long enough for hydrogenation to methanol to be important. Surface hydrogenation of nitrogen-containing species was quite efficient, however, leading to the large observed abundances of saturated organo-nitrogen species such as C_2H_5CN in the gas phase.

The uncertainties in grain chemistry render all gas-grain models somewhat suspect, and we have embarked on a program to understand grain processes in more detail. We are currently investigating mechanisms for non-thermal desorption of CO off bare grain cores, assumed to be silica, and ice mantles, using state-of-the-art classical and quantum mechanical procedures (Guan, Muckerman, & Uzer 1990). The CO can be treated by up to five degrees of freedom (vibration, adsorption, libration, and 2 translations) while the bulk material can be treated via use of an equivalent Langevin chain of up to 50 atoms (Adelman 1979). At present, our investigation (Galloway & Herbst 1994a,b) has revealed that desorption is possible only if large amounts of energy are put into the CO vibrational bond, such as might occur via the exothermic association reaction between C and O atoms occurring on grain surfaces or via absorption of a visible or ultra-violet photon.

III. Astronomical Uncertainties

Ion-molecule models depend on cosmic ray ionization as a source of ions. The rate of cosmic ray ionization ζ_0 used for galactic clouds need not apply for clouds in external galaxies. We (Farquhar, Millar, & Herbst 1994) have recently run a series of gas phase models in which ζ was varied from zero to values many orders of magnitude above ζ_0. A fixed gas density n = $2 \times 10^4 cm^{-3}$ and temperature T = 10 K were utilized along with the standard "low metal" elemental abunandances. For $\zeta \ll \zeta_0$, cosmic ray-induced ionization is quite weak, but some ion-molecule chmistry occurs based on the chemi-ionization reaction

$$CH + O \longrightarrow HCO^+ + e^-. \tag{2}$$

The CH radical itself can be formed via neutral-neutral reactions such as

$$C + H_2 \longrightarrow CH_2 + h\nu \tag{3}$$

$$CH_2 + O \longrightarrow CH + CO. \tag{4}$$

Some organic molecules can achieve reasonable abundances.

For $\zeta \gg \zeta_0$, (a "cosmic ray dominated region"?), secondary photons induced from the electrons generated by cosmic ray bombardment (Prasad & Tarafdar 1983) deplete polyatomic molecules efficiently at all times. The result is that the majority of polyatomic molecules achieve their highest abundance at early time for $\zeta \approx \zeta_0$ with both lower and higher values of ζ leading to reduced abundances. The effect is a gradual one.

The dependence of chemical results on elemental abundances can be dramatic if $\zeta > \zeta_0$. Pineau des Forêts, Roueff, & Flower (1992) and Le Bourlot et al. (1993) have found that for ζ somewhat higher than ζ_0, *two* steady-state solutions exist for the gas-phase chemistry at a variety of temperatures and densities ($10^3 cm^{-3} \leq n \leq 10^5 cm^{-3}; 10K \leq T \leq 40K$) depending on the elemental abundances chosen for sulphur. The effect is noticeable at standard densities ($10^4 cm^{-3} - 10^5 cm^{-3}$) for a relatively high gaseous sulphur abundance; i.e., a depletion of only 10. The two chemical phases differ according to ionization fraction (roughly 10^{-6} vs 10^{-7}), C/CO abundance ratio (roughly 10^{-1} vs 10^{-3}), and other chemical signatures. The high C phase results can be used as an alternative to the normal PDR (photon-dominated region) explanation for the observed large abundance of C in dense interstellar clouds (Schilke et al. 1994). Use of our larger chemical network pushes the two-phase region of parameter space to significantly lower densities. In the context of time-dependent models, it has been shown that one solution can be perturbed into the other by suitable density and temperature changes. Moreover, initial atomic abundances lead to the high ionization phase at steady state whereas initial molecular abundances lead to the low ionization phase. Use of the more standard atomic + H_2 abundances appear in preliminary investigations to lead to no solution at steady state, suggesting the possibility of chaos.

IV. Chemical Uncertainties

The rate coefficient for exothermic processes follows the Arrhenius formula

$$k = A(T) exp(-E_a/T) \tag{5}$$

where A(T) is the weakly temperature-dependent "pre-exponential factor", which depends on the nature of the long-range attractive force, and E_a is the activation energy, which is related to the height of the short-range potential barrier (Gardiner 1972). Until recently, it has been believed that for neutral-neutral reactions: (i), A $\leq 10^{-11} cm^3 s^{-1}$ and (ii), $E_a \geq$ 2000 K even for most reactions involving one radical, or particularly reactive species with an odd number of electrons (Smith 1988). With these parameters, the rates of most neutral-neutral gas phase reactions at very low temperature cannot compete with the rates of ion-molecule processes, for which E_a = 0 K and $10^{-9} \leq A \leq 10^{-7} cm^3 s^{-1}$ (Clary 1988). Consequently, although neutral-neutral reactions play a role in current chemical models (Herbst & Leung 1990), the gas phase processes are dominated by ion-molecule reactions.

Reactions involving the radical CN have recently been studied at low temperatures (Sims et al. 1993a,b; Rowe, Canosa, & Sims 1993). The new results show surprisingly that the CN radical reacts rapidly with a variety of neutral species ($E_a = 0$) and that the rates generally increase as temperature decreases. Some examples of low temperature rate coefficients are: k(25K) = $4.35 \times 10^{-10} cm^3 s^{-1}$ for CN + C_2H_4; k(25K) = $4.60 \times 10^{-10} cm^3 s^{-1}$ for CN + C_2H_2. These values are large enough to be quite important in interstellar cloud models. Two caveats must be mentioned, however: (i), no products have been measured for these reactions, and (ii), the size and temperature-dependence of the rates are so far devoid of theoretical rationalization.

Even more astonishing are newly-measured large rates at room temperature involving the C atom, which is very abundant in astronomical models at early time. Unlike other atoms, C appears to react rapidly (k[300K] $\geq 2 \times 10^{-10} cm^3 s^{-1}$) with all unsaturated hydrocarbons (Husain 1993; Haider & Husain 1993). Once more, products have not been studied. The general trend that the rate coefficient increases as the hydrocarbon increases in size is understandable if the reaction rates are determined solely by dispersion at long range (Clary 1993), but the absolute magnitude of the rates and the apparent lack of activation energy barriers are surprising. It is also unclear whether the rates are still large at very low temperatures; conflicting theoretical views on the subject have been expressed (Clary 1993; Graff 1989) depending on the nature of the long-range forces.

Despite the considerable uncertainty attending the new results, we have used them in a revised gas phase model of quiescent dense interstellar clouds (Herbst et al. 1994). Two large reaction networks were utilized - the Herbst/Leung network and the updated UMIST network (Herbst & Leung 1989; Farquhar & Millar 1993). We have used the CN and C results as examples for a much wider class of possibly rapid neutral-neutral reactions, some of which have previously appeared in our models but at significantly slower rates. We have been forced to guess the reaction products in all cases; in this exercise we have been guided both by chemical reasonableness and electron spin conservation, the latter a somewhat uncertain guide. The products of the C atom-hydrocarbon reactions are most often presumed to follow a carbon insertion mechanism; viz.,

$$C + C_2H_2 \longrightarrow C_3H + H \tag{6}$$

in which a more complex hydrocarbon with one fewer H atom is synthesized.

Bettens & Brown (1992) have previously shown that if reactions between O atoms and radicals are rapid, then the synthetic power of gas phase models is sharply curtailed. Based on this study, the reactions of which are included in our expanded model, we had thought that the inclusion of neutral-neutral reactions would not change the principal results of our models. At early time, the abundances of both C and O atoms are large, and the synthetic power of the former would presumably counteract the destructive power of the latter.

The model results obtained are quite surprising. We find that most organic molecules have their peak early-time abundances reduced sharply, often by several orders of magnitude. The drastic diminution is sufficient to vitiate considerably the previously close agreement between early-time results and observation in the so-called "standard" but admittedly fecund source TMC-1. For example, the newly calculated early-time (10^5 yr) fractional abundances of CN, C_3H, C_4H, HC_3N, and HC_5N with respect to n/2 (n[H_2]) in the Herbst/Leung model are $7 \times 10^{-10}, 2 \times 10^{-9}, 7 \times 10^{-10}, 6 \times 10^{-11}$, and 3×10^{-10} respectively, whereas the analogous results for the UMIST model are $5 \times 10^{-10}, 2 \times 10^{-9}, 9 \times 10^{-10}, 6 \times 10^{-11}$, and 7×10^{-10} respectively. Somewhat higher abundances can be achieved in the UMIST model if various times are utilized. In TMC-1, the observed fractional abundances are $3 \times 10^{-8}, 5 \times 10^{-10}, 2 \times 10^{-8}, 6 \times 10^{-9}$, and 3×10^{-9} respectively. Of these species, only C_3H is predicted to have a peak abundance larger than what is detected. In other sources, our revised results for the cyanopolyynes do not appear to be as far from reality. In the extended ridge in Orion, the fractional abundances of HC_3N and HC_5N are 4×10^{-10} and 6×10^{-11} respectively whereas they are 2×10^{-10} and 9×10^{-11} in L134N (Irvine, Goldsmith, & Hjalmarson 1987). The calculated abundance of HC_3N is less than that of HC_5N in both models only because it was assumed that the former molecule could be depleted by reaction with copious C. If the same assumption is made for HC_5N, the predicted peak abundance of this species would be diminished considerably.

The strong diminution in peak abundances is caused by several types of reactions, the most

unexpected and possibly the most important of which are the rapid C atom-hydrocarbon reactions. These reactions tend to destroy hydrocarbons rapidly at early time, when there is a large abundance of C. The strong reduction in the abundances of the smaller hydrocarbons means that the synthetic pathways for more complex molecule formation do not become more efficient. In addition, once complex molecules are formed, they are depleted more rapidly by reaction with C. A critical reaction, and one that should be investigated experimentally at low temperature and theoretically, is the C + C_2H_2 reaction, which must proceed via an attractive potential surface of triplet multiplicity, or via curve crossing into the deep potential well of singlet C_3H_2. The C + C_2H_2 reaction serves to convert acetylene into the radical C_3H which, although it contains more carbon atoms than acetylene, is probably reactive with both C and O atoms, although neither process has been studied in the laboratory or theoretically. These processes convert C_3H into CO:

$$C_3H + O \longrightarrow CO + C_2H, etc. \quad (7)$$

$$C_3H + C \longrightarrow C_4 + H \quad (8)$$

$$C_4 + O \longrightarrow CO + C_3, etc. \quad (9)$$

V. Conclusions

Gas-phase and gas-grain chemical models of dense interstellar clouds continue to play important roles in understanding and interpreting chemical and physical phenomena in clouds and in predicting abundances for molecular species. It is surprising, however, that twenty years after astrochemistry became an important field of research, there are still so many uncertainties that afflict the models. Some of these uncertainties are astronomical in nature, but there are large chemical uncertainties as well. Although it is generally appreciated that our knowledge of dust chemistry is plagued by uncertainty, it is also the case that our understanding of gas phase chemistry is nowhere near complete. Work on dissociative recombination reactions between polyatomic positive molecular ions and electrons, the final step in the ion-molecule synthesis of neutral molecules, has still not developed to the stage where the products of even the simplest reactions are totally understood. The efficiency of radiative association reactions between most ions and neutral molecules is still not determined. In all this uncertainty, it was not appreciated that neutral-neutral reactions presented a problem. Now even this relatively secure area of chemistry appears to be poorly understood, at least as regards reactions involving a radical or an atom.

With the large scale inclusion of rapid neutral-neutral reactions and a reasonable if not definitive choice of products, the synthetic power of gas phase chemical models is strongly reduced. The reactions involving C atoms play a crucial role in causing the dramatic effect. At this stage, it is not clear that the room temperature measurements of C reactions pertain to low temperature clouds. Much work remains in understanding these and other neutral-neutral reactions and their products at low temperatures, and in understanding the sensitivity of the model results to specific rates and products. If our model revisions are mainly correct, however, the "early-time" model fails to predict the large organic abundances seen in TMC-1. But TMC-1 may well be a uniquely fertile source for organic molecules, with its own unique chemistry. The question remains whether the models, as currently revised, are still useful for other sources that show reduced complex molecule abundances. As regards TMC-1, we note that our latest gas-grain models (Hasegawa & Herbst 1993a,b) fail to produce large abundances of complex molecules on grain surfaces. Nor are there enough photons available to power a photon-initiated condensed phase or gas phase chemistry. So the chemistry of TMC-1, if unique, remains a mystery. There is the possibility that the discrepancy in this source arises from our assumption of one phase with unchanging physical conditions. It would be interesting to determine how the new neutral-neutral reactions and rates affect the two-phase mixing model of Chièze, Pineau des Forêts, & Herbst (1991) or the hydrodynamic collapse models of Prasad, Heere, & Tarafdar (1991) and others.

Perhaps we have reached a stage in astrochemistry where we should question the correctness of laboratory results which worsen agreement with observation. There is precedence for this bold assertion in the H_3^+ + HD controversy, where the claim that this reaction, crucial to interstellar deuterium fractionation, does not proceed in the laboratory at low temperature

(Gerlich 1993a) has been withdrawn (Gerlich 1993b). Even if astrochemistry has not achieved sufficient maturity to resist "challenging" chemical results, the subject has motivated many of the newly reported laboratory measurements and has stimulated a possibly fundamental change in the basic paradigm of chemical kinetics.

Acknowledgments:

I would like to acknowledge the support of the National Science Foundation (USA) for my research program in astrochemistry.

References

Adelman, S. A. 1979, J. Chem. Phys., 71, 4471
Bettens, R. P. A., Brown, R. D. 1992, MNRAS, 258, 347
Brown, P. D., Charnley, S. B., Millar, T. J. 1988, MNRAS, 231, 409
Caselli, P., Hasegawa, T. I., Herbst, E. 1993, ApJ, 408, 548
Caselli, P., Hasegawa, T. I., Herbst, E. 1994, ApJ, 421, 000
Charnley, S. B., Tielens, A. G. G. M., Millar, T. J. 1992, ApJ, 399, L71
Chièze, J.-P., Pineau des Forêts, G., Herbst, E. 1991, ApJ, 373, 110
Clary, D. C. 1988, in Rate Coefficients in Astrochemistry, ed. T. J. Millar & D. A. Williams (Dordrecht: Kluwer), p. 1
Clary, D. C. 1993, J. Chem. Soc. Far. Trans., 89, 2165
Farquhar, P. R. A., Millar, T. J. 1993, CCP7 Newsletter No. 18, 6
Farquhar, P. R. A., Millar, T. J., Herbst, E. 1994, MNRAS, submitted
Galloway, E. T., Herbst, E. 1994a, Surf. Sci., in preparation
Galloway, E. T., Herbst, E. 1994b, ApJ, in preparation
Gardiner, Jr., W. C. 1972, Rates and Mechanisms of Chemical Reactions (Menlo Park: Benjamin)
Gerin, M., Viala, Y., Pauzat, F., Ellinger, Y. 1992, A&A, 266, 463
Gerlich, D. 1993a, J. Chem. Soc. Far. Trans., 89, 2167
Gerlich, D. 1993b, J. Chem. Soc. Far. Trans., 89, 2168
Graedel, T. E., Langer, W. D., Frerking, M. A. 1982, ApJS, 48, 321
Graff, M. M. 1989, ApJ, 339, 239
Gredel, R., Lepp, S., Dalgarno, A., Herbst, E. 1989, ApJ, 347, 289
Guan, Y., Muckerman, J. T., Uzer, T. 1990, J. Chem. Phys., 93, 4383
Haider, N., Husain, D. 1993, J. Photochem. Photobiol., A70, 119
Hartquist, T. W., Williams, D. A. 1991, MNRAS, 247, 343
Hasegawa, T. I., Herbst, E., Leung, C. M. 1992, ApJS, 82, 167
Hasegawa, T. I., Herbst, E. 1993a, MNRAS, 261, 83
Hasegawa, T. I., Herbst, E. 1993b, MNRAS, 263, 589
Herbst, E. 1993, in Dust and Chemistry in Astronomy, ed. T. J. Millar & D. A. Williams (Bristol: IOP), p. 183
Herbst, E., Klemperer, W. 1973, ApJ, 185, 505
Herbst, E., Lee, H.-H., Howe, D. A., Millar, T. J. 1994, MNRAS, submitted
Herbst, E., Leung, C. M. 1986, MNRAS, 222, 689
Herbst, E., Leung, C. M. 1989, ApJS, 69, 271
Herbst, E., Leung, C. M. 1990, A&A, 233, 177
Husain, D. 1993, J. Chem. Soc. Far. Trans., 89, 2164
Irvine, W. M., Goldsmith, P., Hjalmarson, Å. 1987, in Interstellar Processes, ed. D. J. Hollenbach & H. A. Thronson, Jr. (Dordrecht: Reidel), p. 561
Langer, W. D., Graedel, T. E. 1989, ApJS, 69, 241
Le Bourlot, J., Pineau des Forêts, G., Roueff, E., Schilke, P. 1993, ApJ, in press
Lepp, S., Dalgarno, A. 1988, ApJ, 324,553
Millar, T. J., Williams, D. A. (eds.) 1993, Dust and Chemistry in Astronomy (Bristol: IOP)
Pineau des Forêts, G., Roueff, E., Flower, D. R. 1992, MNRAS, 258, 45p
Prasad, S. S., Heere, K. R., Tarafdar, S. P. 1991, ApJ, 373, 123
Prasad, S. S., Tarafdar, S. P. 1983, ApJ, 267, 603
Rowe, B. R., Canosa, A., Sims, I. R. 1993, J. Chem. Soc. Far. Trans., 89, 2193
Schilke, P., Carlstrom, J. E., Keene, J., Phillips, T. G. 1994, ApJ, in press
Sims, I. R., Queffelec, J.-L., Travers, D., Rowe, B. R., Herbert, L. B., Karthaüser, J., Smith, I. W. M. 1993a, Chem. Phys. Lett., 211, 461
Sims, I. R., Queffelec, J.-L., Defrance, A., Rebrion-Rowe, C., Travers, D., Rowe, B. R.,

Smith, I. W. M. 1993b, J. Chem. Phys., submitted
Smith, D. 1992, Chem. Rev., 92, 1473
Smith, I. W. M. 1988, in Rate Coefficients in Astrochemistry, ed. T. J. Millar & D. A. Williams (Dordercht: Kluwer), p. 103
Tielens, A. G. G. M., Hagen, W. 1982, A&A, 114, 245
Whittet, D. C. B., Duley, W. W. 1991, A&AR, 2, 167
Willacy, K., Williams, D. A. 1993, MNRAS, 260, 635

Interstellar Hydrides

Ewine F. van Dishoeck
Sterrewacht Leiden, P.O. Box 9513, 2300 RA Leiden, The Netherlands

1. Introduction

Ever since the detection of interstellar CH and CH^+ around 1940 (Swings & Rosenfeld 1937; Adams 1941; Douglas & Herzberg 1941), hydrides have been considered to be the building blocks of the interstellar chemistry networks. Owing to the development of radio and microwave astronomy in the 1960's, the opening up of the ultraviolet window in the 1970's, and the availability of new facilities at infrared and submillimeter wavelengths in the 1980's, several new hydride molecules have been detected in interstellar clouds. The total list now numbers more than ten species, not including isotopic varieties. In this paper, an overview of the latest observational developments is given and the implications for the chemistry in both diffuse and dense interstellar clouds are discussed.

2. Hydride Chemistry

Because hydrogen is so much more abundant than any other element, hydride molecules (i.e., molecules containing at most one heavy atom besides hydrogen) are the first species to be formed in the chemistry networks. This holds not only for the ion–molecule chemistry, but also for grain surface chemistry and high–temperature (shock) chemistry. Since the reactions controlling the chemistries are very different in the three cases, the relative hydride abundances may serve as sensitive diagnostics of the type of chemistry.

In the *ion–molecule chemistry*, the formation of hydrides is initiated by either of the reactions (Solomon & Klemperer 1972; Dalgarno & Black 1976; Watson 1976)

$$X + H_3^+ \rightarrow XH^+ + H_2, \text{ or}$$

$$X^+ + H_2 \rightarrow XH^+ + H,$$

which are usually rapid if the processes are exoergic. Otherwise slower radiative association reactions such as

$$X^+ + H_2 \rightarrow XH_2^+ + h\nu$$

can lead to molecular bonds. These initial steps are followed by a series of hydrogen abstraction reactions to form XH_n^+, which are fast at low T as long as the reactions are exoergic:

$$XH_{n-1}^+ + H_2 \rightarrow XH_n^+ + H.$$

At each stage, dissociative recombination with electrons produces neutral hydrides

$$XH_n^+ + e \rightarrow XH_{n-1} + H \text{ or } XH_{n-2} + H_2 \text{ or } \ldots,$$

where the branching ratio between the products is not well known, except for H_3O^+ (Herd et al. 1990). In diffuse and translucent clouds, photodissociation of neutral hydrides is usually very rapid and results in smaller, less saturated molecules. Thus, ion–molecule chemistry is expected to produce significant amounts of unsaturated and ionized hydrides at the edges of clouds. Deeper inside, the more saturated hydrides become important, but the unsaturated hydrides remain comparable.

In contrast, *grain–surface chemistry* is thought to lead mostly to saturated hydrides through the reactions (Tielens & Allamandola 1987)

$$g - X + H \rightarrow g - XH$$

$$g - XH + H \rightarrow \ldots \rightarrow g - XH_s.$$

The saturated hydride XH_s can be released back into the gas phase by a variety of processes, including cosmic–ray induced desorption, grain–grain collisions or thermal evaporation at sufficiently high temperatures. If the time scale since injection into the gas phase is sufficiently short or if the supply of saturated molecules from the grains occurs continuously, relatively few unsaturated hydrides are expected. At later times, the ion–molecule reactions and photodissociation processes drive the chemistry back to unsaturated species.

High–temperature chemistry, such as that occurring in shocks or in the warmest parts of dense photon–dominated regions, also proceeds rapidly towards saturated hydrides through the reactions

$$X + H_2 \rightleftarrows XH + H$$

$$XH_{s-1} + H_2 \rightleftarrows XH_s + H.$$

However, if atomic hydrogen is abundant and the temperature sufficiently high, the backward reactions can be rapid as well. This leads to a mixture of unsaturated and saturated hydrides, making it more difficult to distinguish this chemistry from the other chemistries. Photodissociation of XH_s has the same effect.

3. Diffuse and Translucent Clouds

In diffuse and translucent clouds, hydrides can be observed by their electronic absorptions at visible and ultraviolet wavelengths superposed on the spectra of bright background stars. The species detected to date are H_2, HD, CH, CH^+, $^{13}CH^+$, OH and most recently NH. The list of hydrides searched for but not detected is significantly longer and includes interesting cases such as OH^+, H_2O, H_2O^+, MgH, SiH^+ and SH (see van Dishoeck & Black 1988 for a summary). Stringent upper limits can be as useful as detections for constraining the chemistry. In the following, the individual chemistries will be discussed in more detail (see also Crutcher & Watson 1985; van Dishoeck & Black 1988; van Dishoeck 1992; Wagenblast & Williams 1993 for reviews).

3.1. Hydrogen chemistry

H_2 was detected by Carruthers (1970) through its absorption lines in the Lyman & Werner systems at $\lambda < 1100$ Å, and was widely observed in diffuse clouds by the Copernicus satellite (e.g. Spitzer & Jenkins 1975). It is well established that significant amounts of H_2 can be maintained in diffuse clouds only through grain–surface chemistry (Hollenbach et al. 1971), since gas–phase processes are negligibly slow. HD has also been detected in the ultraviolet in some of the thicker diffuse clouds with a typical column density ratio $HD/H_2 \approx 10^{-6} - 10^{-5}$. The fact that this ratio is close to the overall deuterium abundance $[D]/[H] \approx 1.5 \times 10^{-5}$ implies that there must be a more rapid formation channel for HD, since the less abundant HD is much more rapidly destroyed by photodissociation than the self–shielding H_2 molecule. The gas–phase reaction $D^+ + H_2 \rightarrow H^+ + HD$, which goes preferentially to HD at low T, is the most likely route. Thus, while H_2 is the strongest case for efficient grain surface formation of molecules, HD provides clear evidence for rapid ion–molecule chemistry.

3.2. Carbon chemistry

Both CH and CH^+ can be observed by optical absorption lines in the 3800–4300 Å region. The inferred abundances $CH/H_2 \approx 5 \times 10^{-8}$ can be well reproduced by the ion–molecule reactions scheme, provided that the $C^+ + H_2$ radiative association reaction has a rate coefficient of about 5×10^{-16} cm^3 s^{-1}. Recent theoretical (Smith 1989) and experimental (Gerlich & Horning 1992) estimates are consistent with this value within a factor of 2. In contrast, the CH^+ abundances predicted by ion–molecule reactions in a cold cloud fall short by orders of magnitude compared with observations. Shocks have been proposed as the site for the CH^+ production because the reaction $C^+ + H_2 \rightarrow CH^+ + H$ is endoergic by about 0.4 eV (Elitzur & Watson 1978; Draine & Katz 1986). In recent years, the shock model has fallen out of favor, since observations fail to show the predicted velocity difference between CH^+ and CH or CN in most clouds (Lambert & Danks 1986; Crawford 1989; Hawkins & Craig 1991). Also, the CH^+ column density continues to increase in translucent clouds with A_V up to 3 mag (Gredel et al. 1993). Formation of CH^+ in turbulent boundary layers forms an attractive alternative scenario (Duley et al. 1992; Gredel et al. 1993; Falgarone, this volume), but will be difficult to test quantitatively. It is possible that such chemistry may also contribute to some extent (e.g. of order 30%) to the formation of CH, OH, and other hydrides.

The relative contributions of the various processes may be distinguishable on the basis of the line profiles. High spectral resolution ($\lambda/\Delta\lambda \approx 10^6$) observations have so far been possible only toward the brightest sources, but the limited data show significant differences in the profiles of CH and CH^+ (Lambert et al. 1990) (see Figure 1). The CH^+ profile is much wider than that of CH, but even the CH line shows an underlying broad component, suggesting that some of the CH arises in the same gas as CH^+.

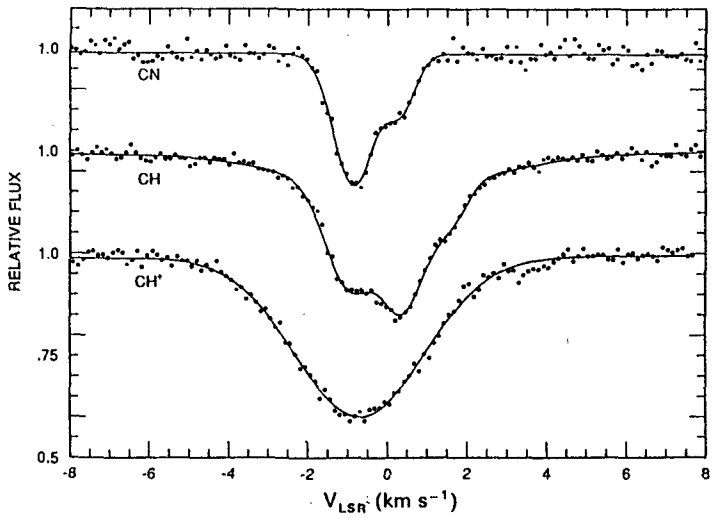

Figure 1. High resolution profiles of the interstellar CH^+ 4232 Å, CH 4300 Å and CN 3874 Å lines toward ζ Ophiuchi (from: Lambert et al. 1990).

3.3. Oxygen chemistry

Just like CH, OH is thought to be readily produced by the ion–molecule reaction scheme, provided that the cosmic ray ionization rate is of order $\zeta \approx 5 \times 10^{-17}$ s^{-1}. OH can be observed in absorption in the ultraviolet at 1220 and 3000 Å. No high resolution OH absorption line profiles yet exist, but observations of the 18 cm transition in emission in translucent clouds reveal only a narrow component (Magnani & Siskind 1990). Deeper searches for H_2O, OH^+ and H_2O^+ in these clouds are warranted.

3.4. Nitrogen chemistry

Interstellar NH was detected recently by Meyer & Roth (1991) with an abundance of about 10^{-9}. In contrast with CH and OH, NH is not rapidly formed by ion–molecule reactions since the reaction $N + H_3^+$ does not proceed and since little N^+ is available for reaction with H_2. Because the observed abundance is larger than that predicted by ion–molecule chemistry, grain surface production of NH_3 followed by photodissociation has been proposed as an alternative scheme (Wagenblast et al. 1993). Deeper searches for NH_2 in translucent clouds will be valuable to test this scenario, since it should be an important intermediary species in the chain. Shock production of NH does not appear to be efficient (Heck et al. 1993).

The abundance of NH is at least one order of magnitude less than that of CH and OH. This provides additional evidence that grain surface chemistry is not dominant for the latter two species, since comparable amounts of carbon–, oxygen– and nitrogen hydrides would be expected in that case (Crutcher & Watson 1976).

3.5. Other chemistries

The upper limits on hydrides involving other elements imply abundances with respect to H_2 of less than 10^{-9}. In analogy with the carbon chemistry, the reactions of Si^+ and S^+ with H_2 are endoergic so that no rapid ion–molecule reactions occur at low T. The non–detection of SH^+ suggests that magnetohydrodynamic shocks are not an important formation site for sulfur hydrides, although the uncertainties in the models are large (Millar & Hobbs 1988). Stringent limits on the abundances of NaH and MgH indicate that metal hydrides are not readily formed in the diffuse gas by any of the processes (Czarny et al. 1987).

In summary, the observations of the simplest diatomic hydrides in diffuse and translucent clouds show that the different chemistries contribute in different amounts to the various species. For some molecules (e.g. H_2, and perhaps NH), grain surface chemistry dominates, whereas for other cases (e.g. HD, CH and OH), ion–molecule reactions are more important. These conclusions should be kept in mind when considering the chemistry of these and more complex molecules in dense clouds.

4. Dense Clouds

4.1. Hydrogen chemistry

Because dense clouds are opaque at ultraviolet wavelengths, H_2 can only be observed via its infrared vibration–rotation and pure rotation lines. Lines in the (v', v'')=(1,0) band have been observed in emission in reflection nebulae and shocks, but those observations refer to only a small part of the cloud which is either exposed to intense ultraviolet radiation or is at an elevated temperature. The bulk of the cold H_2 can only be observed in absorption against bright infrared sources. Previous searches for H_2 at 2μm toward NGC 2024 IRS2 (Black & Willner 1984) and NGC 2264 (Black et al. 1990) have been unsuccessful. However, with the new generation of cryogenic echelle spectrometers more sensitive searches are possible, and, very excitingly, a detection of the (1,0) S(0) line has just been reported by Lacy et al. (1994) toward NGC 2024 IRS2 (see Figure 2). This detection is very important, because it allows an accurate determination of the CO/H_2 abundance in a cold dense cloud for the first time, and also of the abundances of other species along the line of sight.

Observations of the pure rotational lines of H_2 at 17 and 28 μm are possible from high mountain tops (Parmar et al. 1991) or spacecraft such as the *Infrared Space Observatory* (ISO), but most lines will be in emission from gas at $T > 100$ K. ISO will also be able to observe the lowest rotational J=1–0 line of HD at 112 μm. In dense clouds, most of the deuterium is expected to be in the form of HD so that the HD/H_2 ratio should give a direct measure of the overall deuterium abundance.

In dense clouds, a small amount of H_2 can also be formed in the icy mantles of the grains from recombining H atoms produced by photolysis of solid H_2O and other ices containing hydrogen. A tentative detection of solid H_2 has recently been claimed by

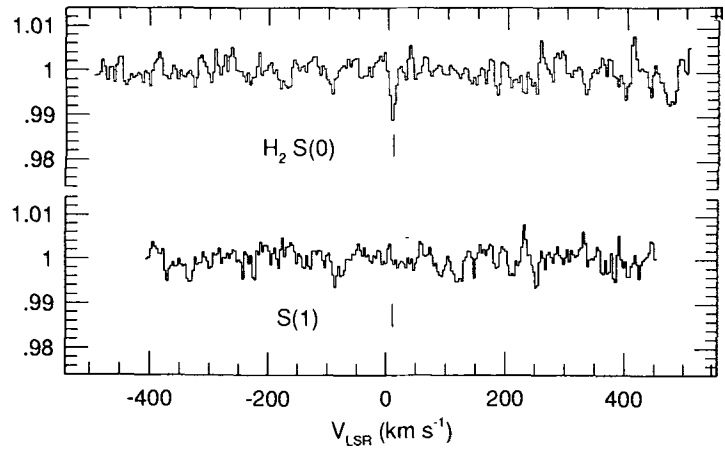

Figure 2. Detection of the H_2 (1,0) S(0) line in absorption toward NGC 2024 IRS 2 (from: Lacy et al. 1994).

Sandford et al. (1993). Its abundance is a factor of three larger than that of solid CO.

The H_3^+ ion plays a pivotal role in the ion–molecule chemistry, but does not have allowed rotational transitions and can therefore only be observed through its vibration–rotation lines at near–infrared wavelengths (Oka 1981). No detections of interstellar H_3^+ have yet been reported, with upper limits on its abundance of about $10^{-9} - 10^{-8}$ (Geballe & Oka 1989; Black et al. 1990). Identification of this ion at about this abundance level would greatly strengthen the foundation of the ion–molecule network.

In contrast with H_3^+, H_2D^+ does have a small dipole moment, resulting in allowed rotational transitions. The most stringent limits on the lowest ortho–H_2D^+ line at 372 GHz have been obtained by van Dishoeck et al. (1992). Together with detections of the HCO^+ and N_2H^+ ions in the same clouds, the upper limits suggest H_3^+ abundances in the range $10^{-11} - 10^{-9}$ (see also Pagani et al. 1992). A tentative identification of the lowest para–H_2D^+ transition at 1370 GHz in absorption toward Orion IRc2 has recently been reported by Boreiko & Betz (1993). If confirmed, it indicates that H_2D^+ is apparently present in the lower density envelope with an abundance of $\sim 3 \times 10^{-11}$. It is not seen in the warmer, denser hot core. Sensitive searches for the corresponding H_3^+ toward IRc2 are warranted.

4.2. Carbon chemistry

The CH molecule can be seen in dense clouds through its λ-doubling transition at 9 cm and its lowest rotational line at 149 μm (Stacey et al. 1987). Most of the observed emission probably arises from the cloud envelope, where ion–molecule chemistry dominates.

A tentative detection of lines in the higher $4_{04} - 3_{13}$ transition of the CH_2 radical at

70 GHz has been reported by Hollis et al. (1989), but further confirmation through observations of other lines is needed. Searches for the lowest transition of CH_2 at 127.7 μm must await suitable spacecraft.

The CH_3 molecule is symmetric and does not have allowed rotational transitions so that observations will only be possible through the vibration–rotation lines at infrared wavelengths. Such searches should be feasible with ground–based facilities and with the ISO satellite.

The CH_4 molecule can also only be observed through its infrared vibration–rotation transitions. Absorption lines at 7.6 μm of gas–phase CH_4 have been detected by Lacy et al. (1991) for at least one line of sight. The deduced abundance of $\sim 10^{-7}$, together with the possible observation of solid CH_4 in the same cloud, strongly argues in favor of grain surface chemistry, although a significant gas–phase origin cannot be excluded. Detection of CH_2, CH_3 and their ions, or of deuterated species such as CH_3D, would provide better constraints on the relative importance of gas–phase versus ion–molecule chemistry.

4.3. Oxygen chemistry

The OH radical has been observed for more than 30 years through its λ–doubling transition at 18 cm (Weinreb et al. 1963), and more recently through its far–infrared lines at 119, 84 and 163 μm (e.g. Storey et al. 1981; Melnick et al. 1987; Betz & Boreiko 1989). The derived abundances of $\sim 10^{-8} - 10^{-7}$ are consistent with ion–molecule chemistry, but do not exclude contributions from other types of chemistry.

H_2O is clearly a crucial molecule in the oxygen chemistry. Gas–phase water has been detected through its highly–excited (maser) transitions at 22 GHz (Cheung et al. 1969), 183 GHz (e.g. Cernicharo et al. 1990), and 380 GHz (e.g. Waters et al. 1980) and recently also at higher frequencies (Menten et al. 1990; Melnick et al. 1993). However, it is very difficult to derive reliable H_2O abundances from these observations. The lower–lying rotational transitions all occur at submillimeter wavelengths and must await spacecraft such as SWAS, ODIN, ISO and FIRST. The molecule can also be observed through its vibration–rotation lines at infrared wavelengths, and a tentative detection of the ν_3 band at 2.7 μm toward Orion–BN has been reported by Knacke & Larson (1991) corresponding to a H_2O abundance of 10^{-6}. The ISO satellite will be able to observe all three vibration–rotation bands in absorption, but unfortunately only at low spectral resolution ($\lambda/\Delta\lambda \approx 2000$). A high resolution infrared spectrometer in space would be very valuable. Solid H_2O is widely observed in dense clouds through its infrared bands with a typical abundance of 10^{-5} or more (Whittet 1993).

Lines of isotopic species of H_2O are less affected by the atmosphere. Observations of the $3_{13} - 2_{20}$ line of para–$H_2^{18}O$ at 203.4 GHz by Jacq et al. (1988) suggest gas–phase H_2O abundances of order $10^{-6} - 10^{-5}$ in hot–core type regions. Searches for the o–$H_2^{18}O$ ground–state line at 547.7 GHz using the KAO indicate abundances $< 10^{-6}$ in more quiescent clouds (Wannier et al. 1991). Very important is the recent identification of the $H_2^{18}O$ 547.7 GHz line in absorption toward SgrB2 by Zmuidzinas et al. (1994, this

conference). The implied H_2O abundance in the low-density envelope is of order 10^{-7}.

Deuterated water, HDO, has also been seen in hot-core type regions through its excited rotational transitions (Plambeck & Wright 1987; Jacq et al. 1990), and more recently through its lowest rotational $1_{01} - 0_{00}$ transition at 464.9 GHz (Schulz et al. 1991). The derived abundances $HDO/H_2O \approx 0.0003$–0.0006 indicate significant fractionation, even in warm regions. This has been interpreted in terms of evaporation of dust grain mantles (Brown & Millar 1989; Walmsley & Schilke 1993).

Finally, indirect information on the H_2O abundance can be obtained from observations of the protonated molecule, H_3O^+. Recent observations of lines at 364, 396 and 308 GHz by Phillips et al. (1992) have resulted in the definite detection of the ion in a few warm star-forming regions, after tentative identifications in the spectroscopically-confused sources Orion IRc2 and SgrB2 had been made by Wootten et al. (1986, 1991). The inferred H_3O^+ abundances of $\sim 10^{-9}$, together with the estimated H_2O abundances in the same regions, suggest some injection of H_2O from the grains into the gas-phase.

In summary, the observations of H_2O and its related species suggest that ion-molecule chemistry by itself may not be sufficient to reproduce the inferred abundances in warm clouds and hot cores. Moreover, the measured abundances of solid H_2O appear too large to be produced by simple freezing out of H_2O produced in the gas phase at low temperatures. It is therefore likely that significant amounts of H_2O are formed on the surfaces of grains and are released back into the gas phase if the cloud is sufficiently warm.

An important consideration in deriving gas-phase abundances of H_2O —and in fact of all hydrides— is their excitation. Because hydrides have widely-spaced rotational energy level structures and large Einstein A coefficients, many of the far-infrared and submillimeter transitions have high critical densities ($n > 10^6$ cm^{-3} for optically thin lines) and can effectively be excited by far-infrared radiation from warm dust (e.g. Scoville 1984). The importance of including radiative excitation has already been demonstrated for OH by Black & van Dishoeck (1987), Melnick et al. (1987) and Offer & van Dishoeck (1992) and for H_3O^+ by Phillips et al. (1992).

For densities below the critical density, most of the population is in the ground state level(s). As a result, the lowest rotational transitions are subthermally excited and have large optical depths. If the far-infrared radiation is sufficiently strong ($T_{rad} > T_{ex}$), these lines will occur in absorption rather than emission. On the other hand, higher excitation lines can be pumped by far-infrared radiation and will therefore occur more readily in emission. The intensity ratio of excited lines with respect to ground state lines thus depends strongly on density and column density, as well as the geometry and structure of the cloud. Under many circumstances, the higher excited lines can be stronger than the lowest lines, except in the most dense, warm regions such as hot core type regions. This effect might explain why the red-shifted 752 GHz line in the z=2.3 galaxy F10214 +4724 is more readily detected than the ground-state 557 GHz line (Encrenaz et al. 1993; Gerin et al., this volume). The most unambiguous determination of H_2O abundances will be through observations of optically thin lines in absorption, such as demonstrated for $H_2^{18}O$ toward SgrB2 (Zmuidzinas et al. 1994).

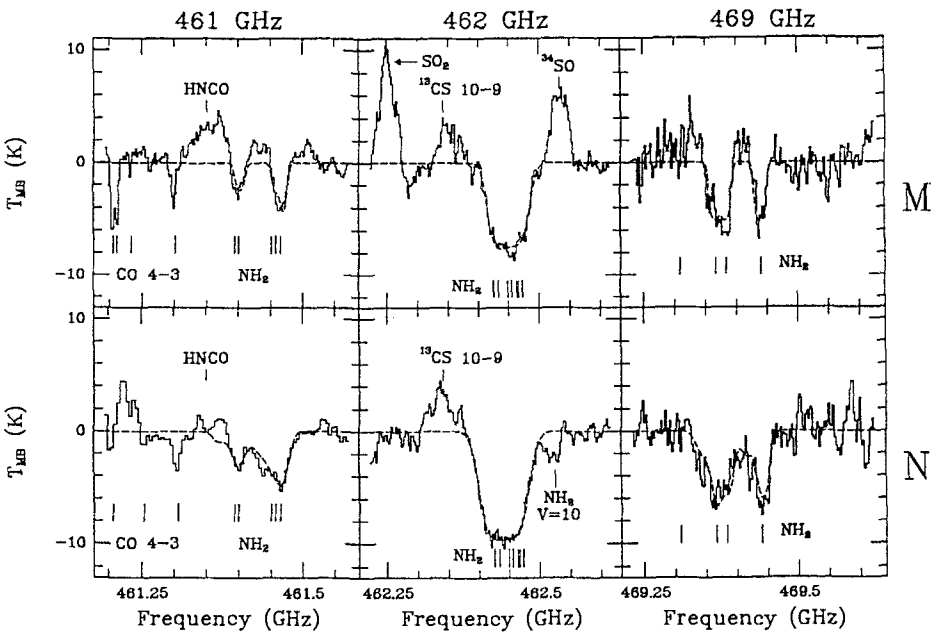

Figure 3. Spectra of NH_2 at 461, 462 and 469 GHz toward SgrB2(M) (top) and SgrB2(N) (bottom). The dashed lines are the hyperfine fits to the NH_2 lines (from: van Dishoeck et al. 1993).

4.4. Nitrogen chemistry

Ammonia was the first polyatomic molecule detected in interstellar space through its inversion transitions at radio wavelengths (Cheung et al. 1968). The lowest pure rotational transition at 572.5 GHz has been seen by Keene et al. (1983) in Orion. The NH_3 molecule is ubiquitous in dark clouds with an abundance of typically $10^{-8} - 10^{-7}$. In hot cores, the abundance may be substantially higher, $10^{-6} - 10^{-5}$ (Genzel et al. 1982).

Further constraints on the nitrogen chemistry have come from the recent detection of the NH_2 radical by van Dishoeck et al. (1993). Five features containing 15 hyperfine components of the lowest $1_{10} - 1_{01}$ transition of para-NH_2 have been seen in absorption toward SgrB2 (see Figure 3). The inferred NH_2 abundance in the low density envelope is $(1 - 3) \times 10^{-8}$ with $NH_2/NH_3 \approx 0.5$–0.75. No NH_2 emission was seen from the hot cores SgrB2(M) and (N), implying $NH_2/NH_3 < 10^{-3}$ in those regions.

The low temperature gas-phase nitrogen chemistry is notoriously complex (see §3.4). If the $N^+ + H_2$ reaction proceeds sufficiently rapid at low temperatures (Le Bourlot 1991), the observed NH_2 and NH_3 abundances in the low density envelope can be explained by ion-molecule chemistry. However, the high abundance of NH_3 in hot cores can only

be produced if grain surface formation of NH_3 (but not NH_2) is involved. Recall that some additional formation process, perhaps grain surface formation of NH_3 followed by photodissociation, is also necessary to explain the observed NH in diffuse clouds. The high abundances of NH_2D provide further support for this scenario (Turner 1990). On the other hand, solid NH_3 has not yet been firmly identified in dense clouds (Smith et al. 1989). The situation for SgrB2 is further confused by the fact that highly-excited NH_3 with $T_{rot} > 600$ K has been observed in absorption, suggesting that energetic events such as shocks play a role (Wilson 1993, private communication). To what extent they affect the NH_2 abundance is not yet clear.

4.5. Other chemistries

The H_2S molecule can be observed from the ground through its lowest $1_{10} - 1_{01}$ transition at 168.8 GHz (Thaddeus et al. 1972) and its higher $2_{20} - 2_{11}$ line at 216.7 GHz. Its abundance is typically $\sim 10^{-9}$ in dark clouds (Minh et al. 1989) and $\sim 10^{-7}$ or higher in warm star-forming cores (Minh et al. 1990, 1991). Very surprising are the relatively large abundances of H_2S observed in photon-dominated regions such as IC 63 and the Orion Bar (Jansen et al. 1994, this volume). Because sulfur hydrides are difficult to form by gas-phase reactions, grain surface chemistry is usually invoked to explain the abundances, but alternative schemes need to be explored.

The lowest $1 \rightarrow 0$ transition of HCl at 625.9 GHz has been observed in emission in Orion by Blake et al. (1985) and recently in absorption toward SgrB2 by Zmuidzinas et al. (1994). The inferred abundances of $\sim 10^{-9} - 10^{-8}$ are consistent with ion-molecule chemistry, and suggests only modest depletions of chlorine.

Searches for other hydrides such as MgH, SH^+, NaH, CaH and PH_3 have been pursued for some time, but no detections have yet been reported (Ziurys et al. 1993; Turner 1991).

5. Conclusions

The observations of hydrides in diffuse and dense clouds demonstrate that different chemical processes contribute in different amounts to their formation: for some radicals in diffuse clouds (e.g. CH, OH), standard ion-molecule gas-phase chemistry probably dominates, whereas for other species in dense clouds (e.g. CH_4) grain surface formation is more important. In general, a large ratio of unsaturated to saturated hydrides suggests that ion-molecule chemistry may be dominant, whereas a small ratio indicates significant grain-surface chemistry. Of course, the two chemistries are not independent, since the molecules that are formed on the grain surfaces and are returned to the gas phase will affect the ion-molecule chemistry. The time scale since injection and whether the process occurs continuously or intermittently are important parameters. The presence of ions also generally implies some gas-phase processes, although the precise formation of CH^+ in diffuse clouds is still not understood, whereas H_3O^+ in dense clouds may at least partly result from protonation of H_2O released from the grains. The diagnostics of shock chemistry are still uncertain; large line widths and high exci-

tation temperatures are probably the clearest indicators. In general, high signal/noise, high resolution line profiles (also at optical wavelengths) may provide important clues to the chemistry.

New hydrides continue to be discovered at infrared and submillimeter wavelengths, as witnessed by recent identifications of H_2, CH_4, H_3O^+, NH_2 and possibly H_2D^+. Because of excitation effects, the lowest pure rotational transitions may be more difficult to detect in emission than thought previously. Searches for such lines in absorption against bright submillimeter continuum sources may be more fruitful, as demonstrated for the case of SgrB2. Future ground–based observations, together with new spacecraft such as SWAS, ODIN, ISO and FIRST in the submillimeter and infrared, and the refurbished HST in the ultraviolet, will undoubtedly provide further insight into these most basic aspects of interstellar chemistry.

This review benefitted considerably from discussions and collaborations with J.H. Black, G.A. Blake, D.J. Jansen, J. Keene, J. Lacy, T.G. Phillips, P. Schilke and M. Walmsley. The author is especially grateful to J. Lacy for permission to reproduce Figure 2. Support from the Netherlands Organization for Scientific Research (NWO) is gratefully acknowledged.

References

Adams, W.S. 1941, ApJ, 93, 11.
Betz, A.L., Boreiko, R.T. 1989, ApJ, 346, 101.
Black, J.H., Willner, S.P. 1984, ApJ, 279, 673.
Black, J.H., van Dishoeck, E.F. 1987, in *Masers, Molecules and Mass Outflows in Star Forming Regions*, ed. A.D. Haschick (Cambridge, MIT Press), p. 43.
Black, J.H., van Dishoeck, E.F., Willner, S.P., Woods, R.C. 1990, ApJ, 358, 459.
Blake, G.A., Keene, J., Phillips, T.G. 1985, ApJ, 295, 501.
Boreiko, R., Betz, A. 1993, ApJ, 405, L39.
Brown, P.D., Millar, T.J. 1989, MNRAS, 237, 661.
Carruthers, G.R. 1970, ApJ, 161, L81.
Cernicharo, J., Thum, C., Hein, H., John, D., Garcia, P., Mattioco, F. 1990, A&A, 231, L15.
Cheung, A.C., Rank, D.M., Townes, C.H., Thornton, D.D., Welch, W.J. 1968, Phys. Rev. Lett., 21, 1701.
Cheung, A.C., Rank, D.M., Townes, C.H., Thornton, D.D., Welch, W.J. 1969, Nature, 221, 626.
Crawford, I.A. 1989, MNRAS, 241, 575.
Crutcher, R.M., Watson, W.D. 1976, ApJ, 209, 778.
Crutcher, R.M., Watson, W.D. 1985, in *Molecular Astrophysics*, eds. G.H.F. Diercksen, W.F. Huebner and P.W. Langhoff, NATO ASI Series **157** (Reidel, Dordrecht), p. 255.
Czarny, J., Felenbok, P., Roueff, E. 1987, A&A, 188, 155.
Dalgarno, A., Black, J.H. 1976, Rep. Prog. Phys., 39, 573.
Douglas, A.E., Herzberg, G. 1941, ApJ, 94, 381.
Draine, B.T., Katz, N.S. 1986, ApJ, 306, 655; 310, 392.
Duley, W.W., Hartquist, T.W., Sternberg, A., Wagenblast, R., Williams, D.A. 1992, MNRAS, 255, 463.
Elitzur, M., Watson, W.D. 1978, ApJ, 222, L141.
Encrenaz, P.J., Combes, F., Casoli, F., Gerin, M., Pagani, L. 1993, A&A, 273, L19.
Genzel, R., Downes, D., Ho, P.T.P., Bieging, J. 1982, ApJ, 259, L103.
Geballe, T.R., Oka, T. 1989, ApJ, 342, 855.
Gerlich, D., Horning, S. 1992, Chem. Rev., 92, .1509.
Gredel, R., van Dishoeck, E.F., Black, J.H. 1993, A&A 269, 477.
Hawkins, I., Craig, N. 1991, ApJ 375, 642.
Heck, E.L., Flower, D.R., Le Bourlot, J., Pineau des Forêts, G., Roueff, E. 1993, MNRAS, 262, 795.
Herd, C.R., Adams, N.G., Smith, D. 1990, ApJ, 349, 388.
Hollenbach, D.J., Werner, M.W., Salpeter, E.E. 1971, ApJ, 163, 165.

Hollis, J.M., Jewell, P.R., Lovas, F.J. 1989, ApJ, 346, 794.
Jacq, T., Jewell, P.R., Henkel, C., Walmsley, C.M., Baudry, A. 1988, A&A, 199, L5.
Jacq, T., Walmsley, C.M., Henkel, C., Baudry, A., Mauersberger, R., Jewell, P.R. 1990, A&A, 228, 447.
Jansen, D.J., van Dishoeck, E.F., Black, J.H. 1994, A&A, 282, 605.
Keene, J., Blake, G.A., Phillips, T.G. 1983, ApJ, 271, L27.
Knacke, R.F., Larson, H.P. 1991, ApJ, 367, 162.
Lacy, J.H., Carr, J.S., Evans, N.J., Baas, F., Achtermann, J.M. 1991, ApJ, 376, 556.
Lacy, J.H., Knacke, R., Geballe, T.R., Tokunaga, A.T. 1994, ApJ Letters, in press.
Lambert, D.L., Danks, A.C. 1986, ApJ, 303, 401.
Lambert, D.L., Sheffer, Y., Crane, P. 1990, ApJ, 359, L19.
Le Bourlot, J. 1991, A&A, 242, 235.
Magnani, L., Siskind, L. 1990, ApJ, 359, 355.
Melnick, G.J., Genzel, R., Lugten, J.B. 1987, ApJ, 321, 530.
Melnick, G.J., Menten, K.M., Phillips, T.G., Hunter, T. 1993, ApJ, 416, L37.
Menten, K.M., Melnick, G.J., Phillips, T.G. 1990, ApJ, 350, 41.
Meyer, D.M., Roth, K. 1991, ApJ, 376, L49.
Millar, T.J., Hobbs, L. 1988, MNRAS, 231, 953.
Minh, Y.C., Irvine, W.M., Ziurys, L.M. 1989, ApJ, 345, L63.
Minh, Y.C., Ziurys, L.M., Irvine, W.M., McGonagle, D. 1990, ApJ, 360, 136.
Minh, Y.C., Ziurys, L.M., Irvine, W.M., McGonagle, D. 1991, ApJ, 366, 192.
Offer, A., van Dishoeck, E.F. 1992, MNRAS, 257, 377.
Oka, T. 1981, Phil. Trans. Roy. Soc. Lon. A, 303, 543.
Pagani, L., Salez, M., Wannier, P.G. 1992, A&A, 258, 472; 479.
Parmar, P.S., Lacy, J.H., Achtermann, J.M. 1991, ApJ, 372, L25.
Phillips, T.G., van Dishoeck, E.F., Keene, J. 1992, ApJ, 399, 533.
Plambeck, R.L., Wright, M.C.H. 1987, ApJ, 317, L101.
Sandford, S.A., Allamandola, L.J., Geballe, T.R. 1993, Science, 262, 400.
Schulz, U., Güsten, R., Serabyn, E., Walmsley, C.M. 1991, A&A, 246, L55.
Scoville, N.Z. 1984, in *Galactic and Extragalactic Infrared Spectroscopy*, eds. M.F. Kessler and J.P. Phillips (Reidel, Dordrecht), p. 167.
Smith, I.W.M. 1989, ApJ, 347, 282.
Smith, R.G., Sellgren, K, Tokunaga, A.T. 1989, ApJ, 344, 413.
Solomon, P.M., Klemperer, W. 1972, ApJ, 178, 389.
Spitzer, L., Jenkins, E.B. 1975, ARAA, 13, 133.
Stacey, G.J., Lugten, J.B., Genzel, R. 1987, ApJ, 313, 859.
Storey, J.W.V., Watson, D.M., Townes, C.H. 1981, ApJ, 244, L27.
Swings, P. & Rosenfeld, L. 1937, ApJ, 86, 483.
Thaddeus, P., Kutner, M.L., Penzias, A.A., Wilson, R.W., Jefferts, K.B. 1972, ApJ, 176, L73.
Tielens, A.G.G.M., Allamandola, L.J. 1987, in *Interstellar Processes*, eds. D. Hollenbach and H.A. Thronson (Reidel, Dordrecht), p. 397.
Turner, B.E. 1990, ApJ, 362, L29.
Turner, B.E. 1991, ApJ, 376, 573.
van Dishoeck, E.F. 1992, in *The Astrochemistry of Cosmic Phenomena*, IAU Symposium 150, ed. P.D. Singh (Kluwer, Dordrecht), p. 143.
van Dishoeck, E.F., Black, E.F. 1988, in *Rate Coefficients in Astrochemistry*, eds. T.J. MIllar, D.A. Williams (Kluwer, Dordrecht), p. 209.
van Dishoeck, E.F., Phillips, T.G., Keene, J., Blake, G.A. 1992, A&A, 261, L13.
van Dishoeck, E.F., Jansen, D.J., Schilke, P., Phillips, T.G. 1993, ApJ, 416, L83.
Wagenblast, R., Williams, D.A. 1993, in *Dust and Chemistry in Astronomy*, eds. T.J. Millar, D.A. Williams (IOP, Bristol), p. 171.
Wagenblast, R., Williams, D.A., Millar, T.J., Nejad, L.A.M. 1993, MNRAS, 260, 420.
Walmsley, C.M., Schilke, P. 1993, in *Dust and Chemistry in Astronomy*, eds. T.J. Millar, D.A. Williams (IOP, Bristol), p. 37.
Wannier, P.G., Pagani, L., Kuiper, T.B.H., Frerking, M.A., Gulkis, S. 1991, ApJ, 377, 171.
Waters, J.W. et al. 1980, ApJ, 377, 171.
Watson, W.D. 1976, Rev. Mod. Phys., 48, 513.
Weinreb, S., Barrett, A.H., Meeks, M.L., Henry, J.C. 1963, Nature, 200, 829.
Whittet, D. 1993, in *Dust and Chemistry in Astronomy*, eds. T.J. Millar, D.A. Williams (IOP, Bristol), p. 9.
Wootten, A., Boulanger, F., Bogey, M., Combes, F., Encrenaz, P.J., Gerin, M., Ziurys, L. 1986, A&A, 166, L15.
Wootten, A., Mangum, J.G., Turner, B. et al. 1991, ApJ, 380, L79.
Ziurys, L.M., Barclay, W.L., Anderson, M.A. 1993, ApJ, 402, L21.
Zmuidzinas, J., Blake, G.A., Carlstrom, J., Keene, J., Miller, D., Ugras, N.G. 1994, in preparation.

CO chemistry and optical/FIR structure of interstellar cirrus: low density PDRs

Ronald Stark

Sterrewacht Leiden, P.O. Box 9513, NL–2300 RA Leiden, The Netherlands

In order to get insight in the physics and chemistry of interstellar cirrus clouds we have studied a series of five isolated and small ($\sim 1^{\square}$) cirrus clouds at high galactic ($b < -25°$) and ecliptic ($\beta < -40°$) latitudes. Deep UBRI Schmidt plates were taken with the ESO 1m Schmidt telescope and digitized with the Leiden Astroscan measuring machine. We calibrated the images through sky-brightness measurements which were made simultaneously during the plate exposures. Together with deep IRAS co-added (using 2nd generation tools) images we studied the dust in these clouds. Deep ^{12}CO and ^{13}CO ($J = 1 \rightarrow 0$) observations from these clouds have been obtained with the SEST 15m telescope. The results of this study are described in detail elsewhere (Stark, 1993 PhD Thesis; 1994 in preparation). In this paper we briefly discuss some important results of two of these clouds.

The observed ^{12}CO/^{13}CO $J = 1 \rightarrow 0$ intensity ratio in these cirrus clouds ($A_V \simeq 0.5 - 1.5$ mag) varies considerably within the individual clouds as well as between the clouds, and reaches values between 3 and 60. Such values are in agreement with values found in giant molecular clouds and diffuse clouds. This large variation is due to a change in the ^{12}CO $J = 1 \rightarrow 0$ line from optically thick to optically thin and/or to two ^{13}CO selective processes: the carbon–ion exchange reaction and photodissociation. These processes are very sensitive to small variations in physical parameters like total density and column density, and radiation field (e.g. van Dishoeck and Black 1988 ApJ 334, 771). We find good agreement between the structure seen on high resolution optical (and FIR) images, revealing the dust in the clouds by its diffusely reflected (FIR: emitted-) radiation, and the CO emission. Figure 1a and 1b show the velocity integrated ^{12}CO emission of two clouds, and Fig. 2a and 2b show their optical surface brightness. We clearly see that if the dust has a filamentary structure (Fig. 2a) the ^{12}CO is also distributed smoothly (Fig. 1a); whereas if the optical images show clumps embedded in the diffuse cirrus (Fig. 2b), we see that the the ^{12}CO emission also has a clumpy structure (Fig. 1b). In the latter case ^{13}CO emission becomes significant. This can be explained if the filaments are optically thin to the radiation field, causing a rapid photodissociation of the ^{13}CO. While ^{12}CO can become stable against photodissociation through self–shielding, ^{13}CO has a too low abundance for that and cannot benefit from mutual shielding by ^{12}CO. Only space density enhancements cause local radiation twilight zones in which ^{13}CO is able to survive the radiation field.

Fig. 1a *Map of the* $^{12}CO(J = 1 \rightarrow 0)$ *integrated antenna temperature* $\int T_A^* dv$ *of the cloud G228–29. The lowest contour is at 0.5 K km* s^{-1} *and increases with steps of 0.5 K km* s^{-1}*. Centre RA, Dec (B1950):* $05^h26^m05.5^s, -24°54'30''$

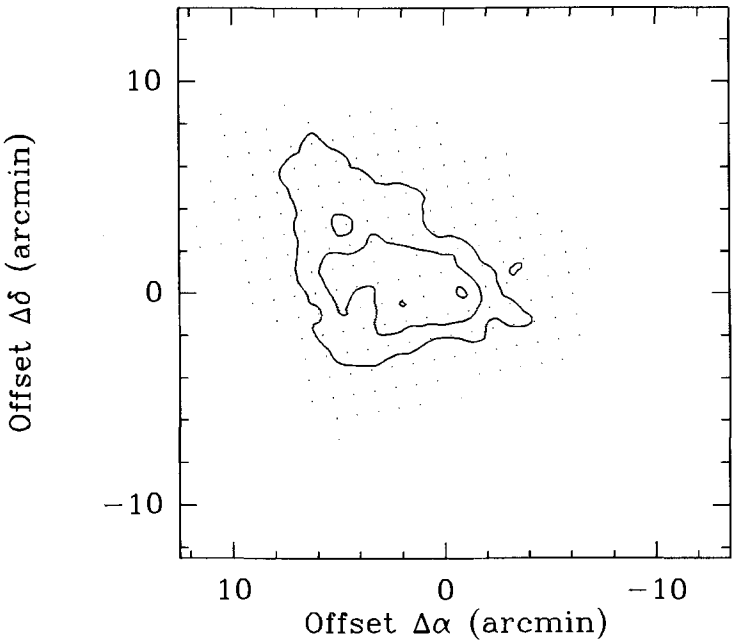

Fig. 1b *Same as Fig. 1a, but now for the cloud G310–45. Centre RA, Dec (B1950):* $23^h44^m54.4^s, -72°00'57''$ *The beamsize of the SEST is given in the lower right corner for comparison*

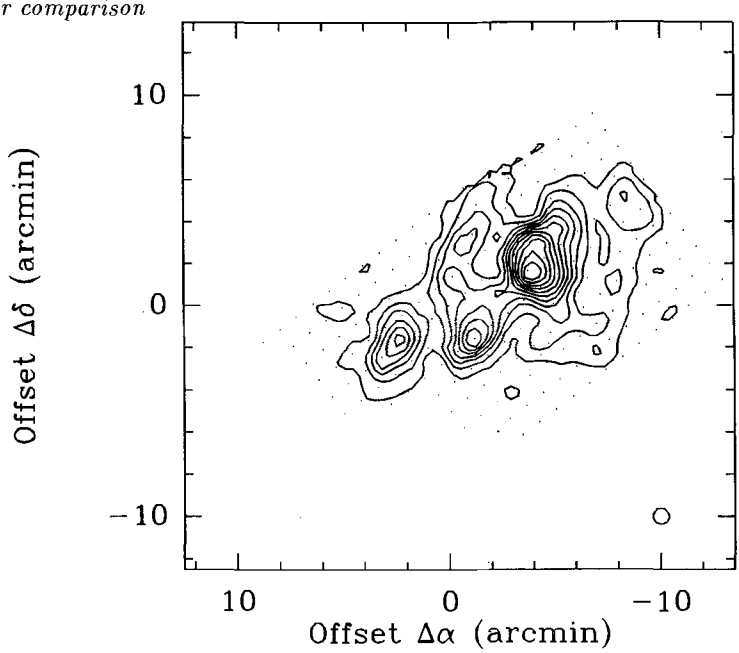

Fig. 2a *Digitized optical blue surface brightness map of the cloud G228–29 at an angular resolution of* $22'' \times 22''$. *All except the brightest stars with* $m_B < 10$ *mag have been removed. Lighter gey scales correspond to higher brightnesses. The plate limit is at 27 mag arcsec*$^{-2}$. *The maximum surface brightness of the cloud is 25.5 mag arcsec*$^{-2}$

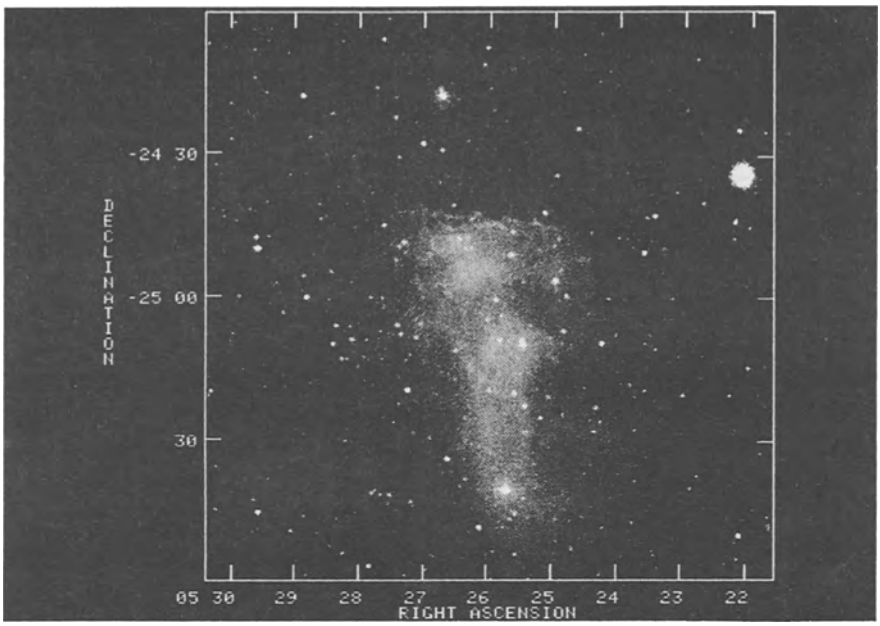

Fig. 2b *Same as Fig. 2a, but now for the cloud G310–45. The maximum surface brightness of the cloud is 25.9 mag arcsec*$^{-2}$

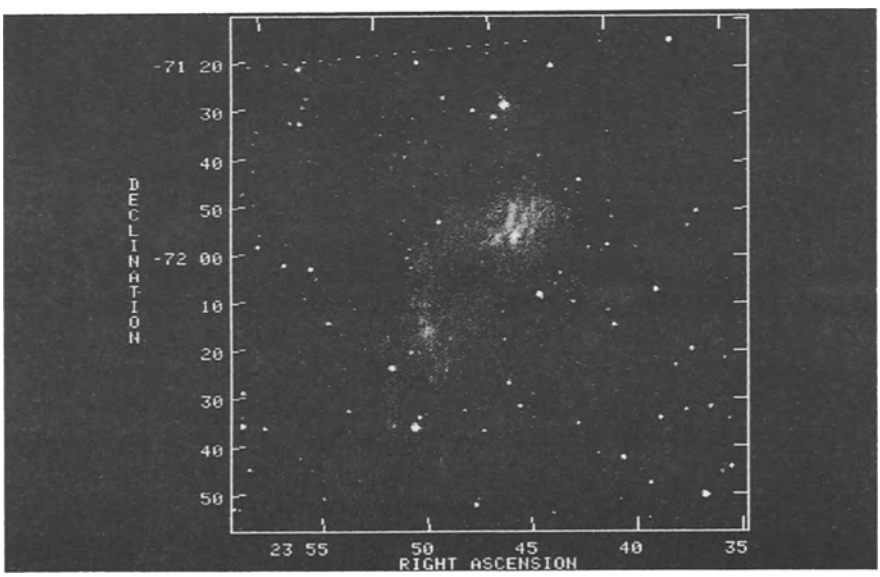

Around the $HCNH^+$ Chemistry Astrophysical Implication

D. Talbi
Lab Radioastronomie, ENS 24 rue Lhomond, 75005 Paris

Among the unanswered question, is the puzzling abundance ratio HNC/HCN that has been observed varying from one source to another. In dark cold clouds (as TMC-1) HNC/HCN=1.55 (W.M. Irvine and F.P. Schloerb 1984). In OMC-1, a region of hight mass star formation, this same abundance ratio changes drastically from 1/80 in the immediate vicinity of Orion-KL to values in the range of 1/5 for adjacent ridge positions (P. Schilke et all 1992). All these observations reveal a variation of the HCN/HNC abundance ratio with temperature. Besides, it should be emphasized that such abundances ratios are completely out of proportion with what is known on earth where HNC is a fleeting rarity much less stable than its HCN isomer. Among the reactions invoqued in the model of formation of HCN and HNC the determining ones are considered to be :

$$
\begin{aligned}
C^+ + NH_3 &\longrightarrow \begin{cases} HCNH^+ + H & (a1) \\ CNH_2^+ + H & (a2) \end{cases} \\
HCNH^+ + e^- &\longrightarrow \begin{cases} HCN + H & (b1) \\ HNC + H & (b2) \end{cases} \\
CNH_2 + + e^- &\longrightarrow HNC + H \quad (b3) \\
N^+ + CH_3 &\longrightarrow HCNH^+ + H \quad (c) \\
HNC + O &\longrightarrow NH + CO \quad (d1) \\
HNC + H &\longrightarrow HCN + H \quad (d2)
\end{aligned}
$$

To satisfy astrophysical constraints and best reproduce the observed abundances the astrochemical models show that : The high abundance ratio HNC/HCN in cold dark clouds can be obtained when:

- the branching ratio for reactions b1 and b2 is equal to unity
- reaction d1 and d2 are made inefficient in the destruction of HNC because of the presence of activation energy barriers.
- reaction a2 is as important as a1 and thus leads to an additional and independent production of HNC via b3 electronic recombination.

On the other hand the high abundance ratio HCN/HNC in hot clouds is favoured when:

- isomerization of CNH_2^+ to $HCNH^+$ is easly achieved, decreasing the HNC abundance (low probability for reaction b3 to take place).
- reactions d1 and d2 are efficient, i.e when the temperature is high enough to overcome the energy barriers.

All these assumptions, if very appealing, have never been confirmed in laboratory because of the extreme difficulties encountered in the experimental work. Another alernative is computational chemistry. In this paper we are presenting preliminary results of a quantum chemical ab initio study of reaction a1,b1 and b2.

Study of the $C^+ + NH_3$ Process

The potential energy surface for this reaction is reported Fig 1. It has been calculated at the MP2/6-31G(d,p) level using Gaussian 90. The reaction path considered is for C^+

approaching NH_3 along its C_{3v} axis. In this case, the potential energy surface reveals the possible formation of a stable CNH_3^+ complex which can dissociate to CNH_2^+ + H by going through a transition structure (Fig 1.) approximatively 50 Kcal/mol above it. CNH_2^+ is a planar molecule of C_{2v} symmetry, which can isomerize to the $HCNH^+$ linear form. However this isomerization has to go through a transition state (Fig 1.) approximatively 20 Kcal/mol above the CNH_2^+ stable molecule. At this point of the study, some conclusions can be drawn : The $C^+ + NH_3$ reaction being exothermic, $HCNH^+$ is the most likely product to be formed. However, because of the shape of the reaction path, CNH_3^+ and CNH_2^+ could be stabilized by vibrational relaxation, reducing the production of $HCNH^+$. It should be remembered that the results reported here have been obtained at a level of theory which allows only semi-quantitaive results. More sophisticated treatments (MCSCF-CI) are currently in progress for quantitative final conclusions. Collisional calculations are also planned to evaluate the proportions of $HCNH^+$ and CNH_2^+ which are produced by the $C^+ + NH_3$ collision. These calculations are crucial because they will confirm (or infirm) a possible path (a2) for the CNH_2^+ formation and then for HNC through reaction b3.

Study of the $HCNH^+ + e^-$ Process

Dissociative recombination involves capture of an electron by the positive ion to form the neutral molecule in an excited electronic state. If this state is repulsive (noted D hereafter), then dissociation takes place directly. If this state is not repulsive, for example a Rydberg bound state (noted R) recombination may give in the first time, an electronic energy greater than the ionization energy; then either autoionization takes place, or the state can relax to lower energy states of dissociative character (the D state) leading to fragmentation through what is called an indirect process (Dalgarno et al. 1975). Efficiency of these processes depends on the existence of at least one repulsive state and its position with respect to bound excited and ionized states. For that reason we have calculated the potential energy surfaces for the ionic,the lowest two Rydberg and the dissociative states of HCNH along the nuclear coordinates NH (reaction b1) and CH (reaction b2) describing the dissociations to HCN + H and HNC + H respectively. For a first approach, these potential energy surfaces have been calculated at an MCSCF level especially designed for comparing dissociation b1 and b2. The theoretical approach that will be detailed in a comming paper (D.TALBI and Y. Ellinger to be submited) is an even-handed treatment of the positif ion and the excited neutral molecule in its Rydberg states and dissociating channel. These surfaces can be visualized Fig 2 where the dissociation of $HCNH^+$ to HCN + H can be followed on the left side of the figure and the dissociation to HNC + H on the right side of the same figure. From these surfaces it appears that the crossing between the dissociative states and both the ionic and Rydberg states are close to the minima in all cases and at the same height, for both reactions b1 and b2. The consequence is that, at the electronic level, the dissociations of the ($HCNH^+ + e^-$) resulting complex, to HCN + H and HNC + H are equivalent, in agreement with the astrophysical hypotheses. However, nuclear effects have also to be taken into account and are in progress through collisionnal calculations.

Conclusion

At this point of the study, we have been able to confirm some of the astrophysical hypotheses presented above. However, before drawing any conclusion, other determining processes such as b3, c, d1 and d2, have to be studied. This is our project.

References

W.M. Irvine and F.P. Schloerb, ApJ, 282, 516-521 (1984)
P.Schilke, C.M. Walmsley, G.Pineau des Forets, E. Roueff, D.R. Flower and S. Guilloteau (1992) A&A, 256, 595-612 (1992)
A. Dalgarno, F. Masnou-Seeuws, and R.W.P. McWhirter "Atomic and molecular processes in Astrophysics" (Swiss Society of Astronomy and Astrophysics, Saas-Fee 5th advanced course) (1975)
D. Talbi and Y. Ellinger, to be submitted

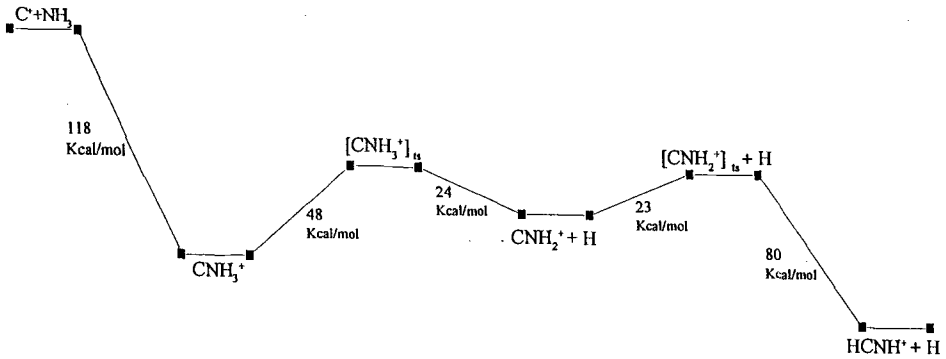

Fig. 1: Potential energy surface of the $C^+ + NH_3$ reaction.

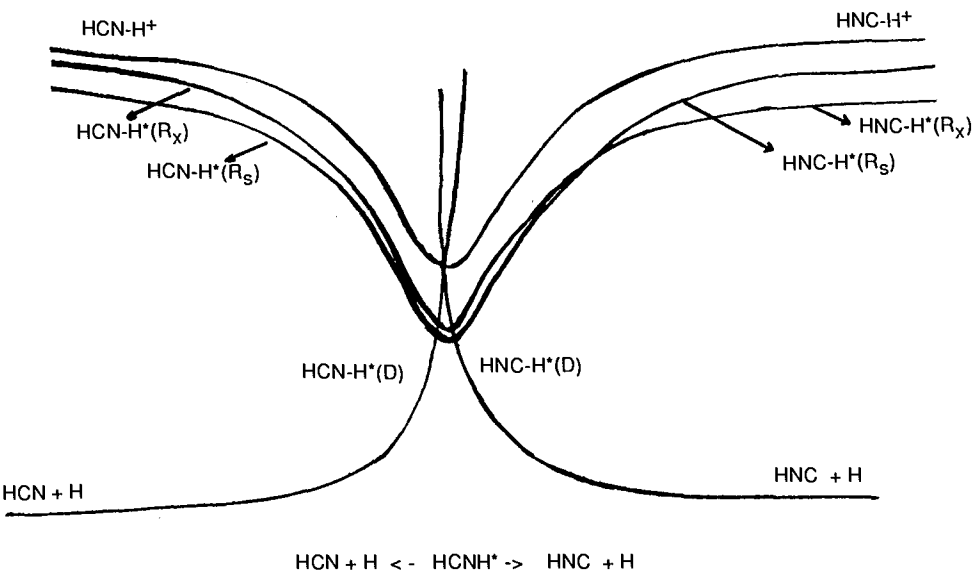

Fig. 2: Potential energy surface for the $HCNH^+$ dissociations to HCH + H and HNC + H

About the Presence of Water in IRAS 10214+4724

M. Gerin[1,2], F. Casoli[1,2], P.J. Encrenaz [2,1] & F. Combes[2,1]

[1] Radioastronomie millimétrique, Laboratoire de Physique de l'E.N.S.,
24 Rue Lhomond, 75231 Paris cedex 05, France. UA 336 du CNRS.
[2] DEMIRM, Observatoire de Paris, Section de Meudon,
92195 Meudon cedex, France. UA 336 du CNRS.

The distant galaxy IRAS 10214+4724 at a redshift of 2.286 has a huge infrared luminosity, $10^{14}h^{-2}$ $L_\odot$ ($h = H_0/100kms^{-1}Mpc^{-1}$, $q_0 = 0.5$)(Rowan-Robinson et al. 1991) and a high dust temperature of 80 K (Downes et al 1991). Rotational lines of CO were detected showing that the exceptionnally high infrared luminosity is associated with a very large mass of molecular gas, more than 10^{11} $M_\odot$ (Brown & Vanden Bout 1991, Solomon et al. 1992). This quite unexpected detection is both due to the very large content of molecular gas and to the unusual physical conditions reigning at large scale. We have thus searched for the submillimeter rotational lines of water redshifted at millimeter frequencies, where the sky transparency is good and the receivers are more sensitive. Using the IRAM 30m telescope at Pico Veleta, we have observed the following lines :
$1_{10} \rightarrow 1_{01}$ at 556.936 GHz redshifted to 169.487 GHz,
$2_{11} \rightarrow 2_{02}$ at 752.033 GHz redshifted to 228.860 GHz,
$4_{14} \rightarrow 3_{21}$ at 380.197 GHz redshifted to 115.702 GHz.
More complete reports on these observations are given in Encrenaz et al. (1993) and in Casoli et al. (1994).

Fig 1 presents both the raw and the smoothed spectrum of the $2_{11} - 2_{02}$ line obtained in three observing sessions (November 1992, January & May 1993). The line shows up as a feature centered on the galaxy redshift and whose profile looks like the CO(3-2) profile. The two other lines remained undetected as shown on Fig 2.

Assuming that the $2_{11} - 2_{02}$ line is saturated, and given a kinetic temperature of 100 K for the gas, its expected brightness temperature is 83K and the redshifted one is 25 K. Thus, we have derived an upper limit of the filling factor of the water vapour source in the 12" beam, which is about 1.4 10^{-4}. Doing this calculation with the same excitation temperature (100 K) for the CO(6-5) line, which has similar rest frequency and upper energy level as the water line, leads to a higher filling factor of about 2.2 10^{-4}. Moreover, the filling factor of the CO(3-2) source in the 2.3" beam of the IRAM interferometer is estimated to be about 1.7% if the intrinsic brightness temperature of the CO(3-2) line is 40K (Radford et al. 1993). Thus the H_2O emitting cores cover an area smaller than the CO emitting cores, but which remains nevertheless surprinsingly high for a whole galaxy : the deduced filling factor of 1.4 10^{-4} can be achieved by placing a 0.14" diameter source (0.55 kpc) in the center of 12" beam.

The sensitivity of the present observations is not good enough to detect the other lines. With the same characteristics as the 752 GHz line, and observed with a beam of 15 ", the peak expected brightness temperature of the 557 GHz line is 2.3 mK, and its expected area is 0.4 $Kkms^{-1}$. These numbers are at most comparable to our 3σ upper limit of $\int T_{mb}dV \leq 0.9$ $Kkms^{-1}$ and to the r.m.s. noise level of the spectrum shown in Fig 2, $\sigma = 1.6$ mK.

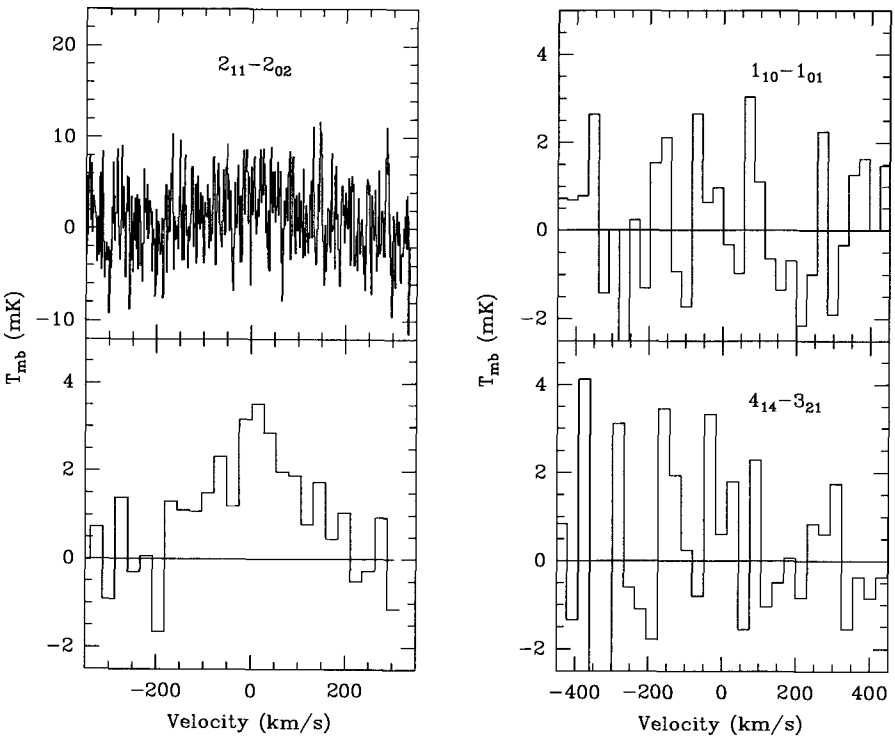

Fig. 1 Top left : Raw spectrum of the $2_{11} - 2_{02}$ para line of H_2O at 752.03 GHz redshifted to 228.86 GHz with a linear baseline removed. The frequency resolution is 1 MHz, the total integration time is 32 hours, the system temperature is 845 K (main beam scale). Bottom left : the same spectrum smoothed to a resolution of 20 MHz (26.2 kms^{-1}), the r.m.s. noise is $\sigma = 0.8$mK.

Fig. 2 Top right : Final spectrum of the $1_{10} - 1_{01}$ ortho line of water with a resolution of 16 MHz (28.3 kms^{-1}). The integration time is 19 hours with a system temperature of 1000 K. $\sigma = 1.6$mK. Bottom right : Final spectrum of the $4_{14} - 3_{21}$ ortho line of water with a resolution of 12 MHz (31.1 kms^{-1}). The integration time is 18 hours with a system temperature of 840 K. $\sigma = 1.8$mK.

References

Brown R.L., Vanden Bout P.A. : 1991, AJ 102, 1956.
Casoli F., Gerin M., Encrenaz P.J., Combes F. : 1994, A&A submitted.
Downes D., Radford S., Greve A. et al. : 1992, ApJ 398, L25.
Encrenaz P.J., Combes F., Casoli F., Gerin M., Pagani L., Horellou C., Gac G. : 1993, A&A 273, L19.
Lawrence A., Rowan-Robinson M., Oliver S. etal. : 1993, MNRAS 260, 28.
Radford S., Brown R.L., Vanden Bout P.A. : 1993, A&A 271, L71.
Rowan-Robinson M., Broadhurst T. , Lawrence A. et al. : 1991, Nature 351, 719.
Solomon P., Downes D. , Radford S. : 1992, ApJ 377, 171.

Hot Ammonia Associated with Ultracompact HII Regions

P. Hofner[1], E. Churchwell[1], S. Kurtz[2], R. Cesaroni[3], and M. Walmsley[4]

[1]Astronomy Dept., Univ. of Wisconsin, 475 N. Charter Str., Madison, WI, U.S.A.
[2]Instituto de Astronomia, UNAM, Apdo. Postal 70-264, 04510 Mexico, D. F., Mexico
[3]Osservatorio Astrofisico di Arcetri, Largo E. Fermi 5, I-50125 Firenze, Italy
[4]Max-Planck-Institut für Radioastronomie, Auf dem Hügel 69, 53 Bonn 1, Germany

Recent single dish molecular line surveys have shown that Ultracompact HII regions are associated with hot, dense molecular gas. Here we present results of VLA D-, C- and B-array observations in the $NH_3(4,4)$ and (5,5) lines for two sources of our sample. For a more detailed discussion we refer the reader to Cesaroni et al. 1993 (A&A, subm.) and Hofner et al. 1993 (Ap.J., subm.).

G29.96-0.02 is an UC HII region with a cometary morphology at a distance of 7.4 kpc. We detect hot ammonia located about 0.08 pc in front of the leading arc of the ionized gas. The derived average properties of the molecular clump are: $T_K = 90\,K$, $N_{NH_3} = 1.6 \times 10^{18}\,cm^{-2}$, $M_{vir} = 138\,M_\odot$, $n_{H_2} = 1.3 \times 10^7\,cm^{-3}$, $X_{NH_3} = 1.4 \times 10^{-6}$. Due to the high densities present in the molecular clump we expect gas and dust to be in equilibrium; based on this assumption we derive a luminosity of $\approx 2 \times 10^5\,L_\odot$.

Figure 1

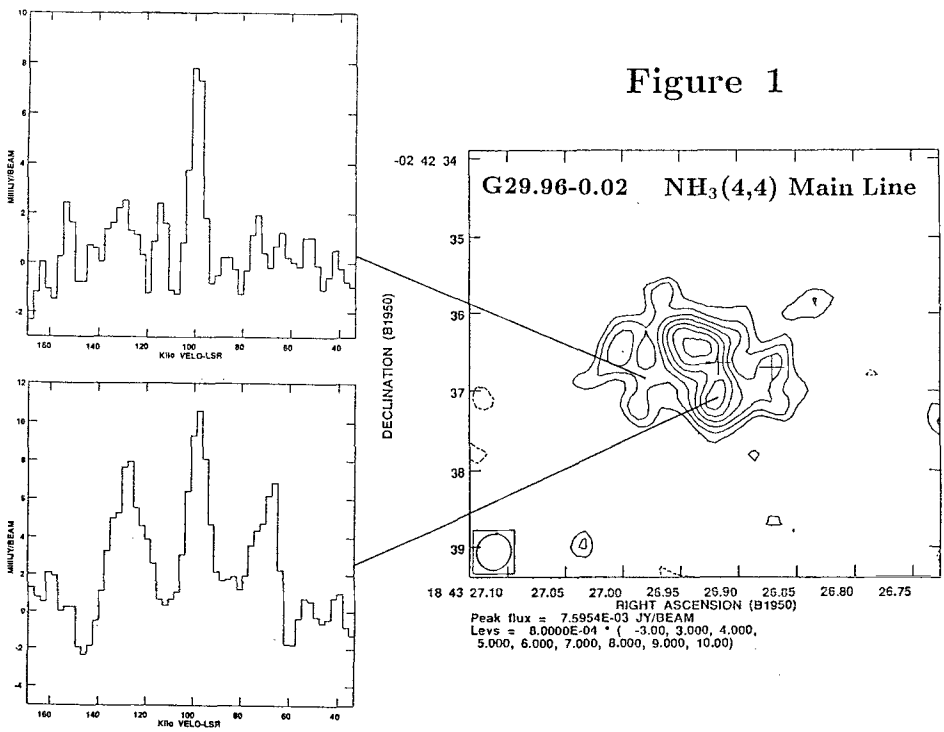

Figure 1 shows a contour map of the $NH_3(4,4)$ line emission obtained with the VLA in B-configuration. The molecular clump consists of two dense condensations of high optical depth which are embedded in an extended envelope of lower optical depth. The crosses mark the location of water maser emission. We detect a velocity gradient of about 5 km/s in the east-west direction across the clump, possibly indicating rotation.

G9.62+0.19 is a complex of HII regions consisting of two extended and several compact components. An absorption profile of the 21 cm HI line obtained with the VLA in CnB configuration toward this source shows that absorption occurs between -5 and $+55$ km/s. This excludes both near and far kinematic distances. The observed velocities of several molecular lines around 4 km/s are consistent with a location in the expanding 3 kpc arm; i.e. a distance of 5.7 kpc. Thermal ammonia is detected to the NW of the bright HII region A (Figure 2, dashed contours). The average properties of the clump are: $T_K = 50\,K$, $N_{NH_3} = 1.6 \times 10^{18}\,cm^{-2}$, $M_{vir} = 164\,M_\odot$, $n_{H_2} = 1.2 \times 10^7\,cm^{-3}$, $X_{NH_3} = 1.0 \times 10^{-6}$, $L = 1.8 \times 10^4\,L_\odot$.

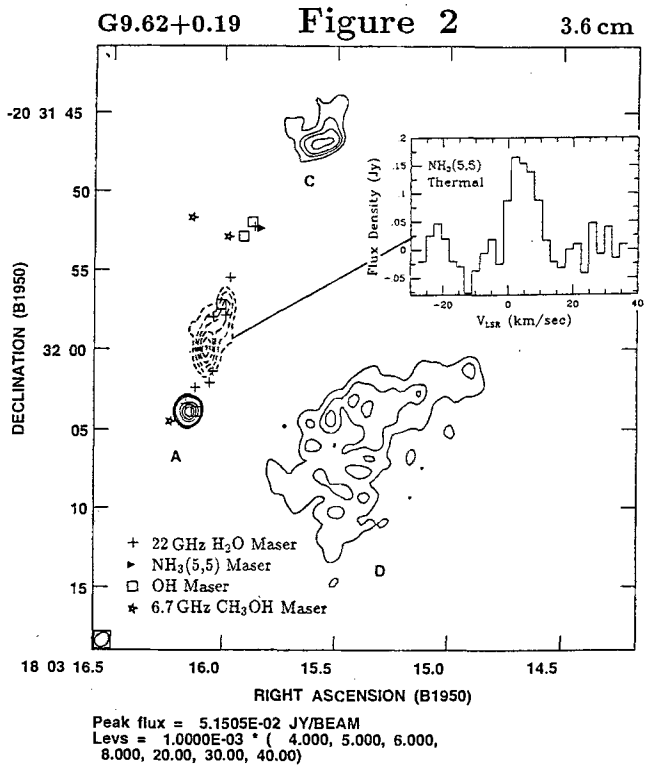

In Figure 2 we show a 3.6 cm radio continuum map from Kurtz et al. 1993 (Ap.J., in press). We also show on this map the location of maser emission from several molecules taken from the literature. There is a conspicuous alignment of UC HII regions, hot, dense ammonia and maser emission of several molecules. Possibly a shock wave originating from the more evolved HII regions to the west has compressed pre-existing molecular clumps and induced star formation along a linear front.

Structure and Chemistry of IRAS 05338-0624

J.P. McMullin[1], L.G. Mundy[1], and G.A. Blake[2]

1. Department of Astronomy, University of Maryland, College Park, MD 20742

2. Division of Geological and Planetary Sciences, California Institute of Technology 170-25, Pasadena, CA 91125

The evolution of the chemistry and molecular abundances in star forming gas is not well understood (e.g. van Dishoeck *et al.* 1993). Thus far, single dish surveys and interferometric studies of selected molecules have yielded indications of the comings and goings of molecules in the circumstellar environment, but not a complete or systematic picture. The identification of chemical "signposts" which mark different stages of development are beginning to be made (e.g., McMullin *et al.* 1994, McMullin, Mundy, & Blake 1993; Goldsmith *et al.* 1992; Blake *et al.* 1987). Ideally, we would like to construct a chemical-evolutionary sequence, based on observed sources, which would help to identify the underlying physical and chemical processes which shape the appearance of gas associated with and participating in the formation of a young stellar object (YSO).

We present a single dish study of the λ=1 and 2 mm molecular emission from the IRAS 05338-0624 region (e.g. Walker, Adams, and Lada 1990, Takaba *et al.* 1986), as part of an analysis of the structure and chemistry in this source. The following results characterize the large scale structure, excitation, and broad patterns of abundances.

Properties of IRAS 05338-0624

Quantity	Value
Assumed Gas Temperature[a]	42 K
Characteristic Size	60″(0.13 pc)
Characteristic Density[b]	2×10^5 cm^{-3}
Peak Continuum Flux λ=1.25mm[a]	2.05 Jy
Integrated Flux λ=1.25mm[a]	2.67 Jy
Peak N(H_2) from continuum flux[c]	8.3 (1.7)$\times 10^{22}$ cm^{-2}
Mass from continuum flux[c]	10.2 (2.0) $M_\odot$
Total Virial Mass	55 $M_\odot$
Peak CS Column Density[b]	5.6×10^{13} cm^{-2}
Peak HCN Column Density[d]	3.2×10^{13} cm^{-2}
Peak CH_3OH Column Density	7.6×10^{13} cm^{-2}
Peak SiO Column Density	$<2.3 \times 10^{11}$ cm^{-2}
Peak SO Column Density	6.7×10^{12} cm^{-2}
Peak DCN Column Density	7.0×10^{11} cm^{-2}
Peak CO Column Density[e]	1.2×10^{18} cm^{-2}

[a] Based on Walker *et al.*1990.
[b] Derived from LVG model; inferred from $C^{34}S$.
[c] First value based on λ^{-2} emissivity; value in parenthesis is based on λ^{-1}. Both assume C_{250}=10 gcm^{-2}.
[d] Inferred from $H^{13}CN$; assumes $^{12}C/^{13}C = 60$.
[e] Inferred from $C^{18}O$; assumes $^{16}O/^{18}O = 489$.

Molecular Fractional Abundances[a]

Molecule	Fractional Abundance					
	TMC-1[b]	IRAS 16293-2422[b]	Serpens NW Cond.[c,d]	IRAS 05338-0624[c]	Orion-S[e]	Orion-KL Hot Core[b]
CO	8(-5)	1(-4)	3(-5)	1.4(-5)	-	1(-4)
CS	1(-8)	1(-9)	6.7(-10)	6.7(-10)	>3(-10)	>1(-8)
SiO	<2(-12)	1(-10)	3.3(-11)	<2.8(-12)	<5(-12)	-
CH_3OH	2(-9)	2(-9)	3.7(-9)	9.2(-10)	1(-9)	(0.1-1)(-6)
HCN	1(-8)	7(-10)	>9.2(-11)	3.9(-10)	-	2(-7)
SO	5(-9)	2(-9)	-	8.1(-11)	-	<2(-8)
Luminosity	-	30 $L_\odot$	60 $L_\odot$	225 $L_\odot$	8.5(3) $L_\odot$	(2-10)(4) $L_\odot$

[a] Numbers in parenthesis are the exponents for the abundances.

[b] Taken from van Dishoeck *et al.* 1992 & Blake *et al.* 1993.

[c] Abundances listed are derived from N_{H_2} based on a λ^{-2} emissivity. Multiply by a factor of 5 to obtain abundances based on a λ^{-1} emissivity.

[d] Taken from McMullin *et al.* 1993.

[e] Taken from McMullin, Mundy, and Blake 1993.

Conclusions

- From the derived properties, this region is an intermediate mass star forming molecular core whose appearance is dominated by the energetics from the most luminous, deeply embedded YSO, IRAS 05338-0624.
- Maps of outflow sensitive species (SO,CH_3OH) indicate a shocked region 15" west of IRAS 05338-0624. Spectra taken at the 15" west position show pronounced wing emission, with a larger V_{LSR} than the center position and an enhanced FWHM; SiO emission, believed to trace strong shock fronts, is found *only* at the western position. If this is tracing an outflow associated with IRAS 05338-0624, it is oriented perpendicular to the large scale CO outflow seen in previous observations.
- A comparison of the derived molecular fractional abundances with quiescent and star forming regions indicates a greater similarity between quiescent/chemically youthful regions such as TMC-1, Orion-S, and the Serpens NW condensation than with more processed star forming regions such as Orion-KL.
- The derived abundances for some common tracer molecules (CS and HCN) indicates depletions of greater than a factor of 25 compared to quiescent (TMC-1) and evolved star forming gas (Orion-KL). These abundances are similar, however, to other 'young' star forming regions and are consistent with the earliest stages of star formation being marked by molecules freezing onto grain surfaces.

References

Blake,G.A.,van Dishoeck,E.F.,Jansen,D.J.,Groesbeck,T.,&Mundy,L.G. 1993 ApJ accepted
Blake, G.A., Sutton, E.C., Masson, C.R., & Phillips, T.G. 1987 ApJ 315 621
Goldsmith, P. F., Margulis, M., Snell, R. L., & Fukui, Y. 1992 ApJ 385 522
McMullin,J.P., Mundy, L.G., and Blake, G.A. 1993 ApJ 405 599
McMullin,J.P.,Mundy,L.G.,Wilking,B.A.,Hezel,T.,and Blake,G.A. 1993 ApJ in press
Takaba,H.*et al.* 1986 A&A 166, 276
van Dishoeck,E.F.,Blake,G.A.,Draine,B.T.,& Lunine,J.I. 1992 Protostars and Planets III Levy, E.H.,Lunin
Matthews,M.S. Tucson University of Arizona Press 163-241
Walker, C.K., Adams, F.C., and Lada, C.J. 1990 ApJ 349 515

Circumstellar Disks at Centimeter Wavelengths

L.G. Mundy[1], J.P. McMullin[1], and A.W. Grossman[1] and G. Sandell[2]
1. Astronomy Dept., Univ. of Maryland, College Park, MD, USA
2. Joint Astronomy Center, Hilo, HI, USA

Centimeter wavelengths can provide unique information about circumstellar dust distributions due to the low dust opacities at these wavelengths and the high spatial resolution ($\sim 0.3''$) possible with instruments such as the VLA. Unfortunately, dust emission at these wavelengths is very weak. Calculations of interstellar dust properties (c.f. Draine 1990) generally find that the emissivity, $\epsilon \propto \nu^{\beta}$, should show a β=2 spectral dependence; hence centimeter (hereafter cm) wavelength emission is expected to be 10^4 to 10^5 times weaker than the peak emission in the far-infrared. However, recent millimeter and submillimeter wavelength observations of circumstellar environments have found that the emissivity often decreases less steeply (ν^0 to $\nu^{1.5}$; Beckwith and Sargent 1991; Weintraub, Sandell, and Duncan 1989). If $\epsilon \propto \nu^1$ extends to cm wavelengths, emission from dust around T Tauri stars and deeply embedded pre-main sequence objects should be detectable at λ=1.3 cm. We present results of a search for cm wavelength dust emission from five embedded young stellar objects (YSO's), three T Tauri stars, and the YSO GG Tau N.

Data Acquisition:

Candidate T Tauri stars were drawn from the list of Beckwith *et al.* (1990); candidate embedded sources were drawn from Wilking *et al.* (1989a) and included NGC 1333 IRAS 4 from Sandell *et al.* (1991). The data were acquired during September 1991, and January and March of 1992. The λ=3.6 cm observations were made in the A and B arrays of the VLA yielding resolutions of $0.5''$ to $1''$. λ=2.0 cm data were obtained in the B array resulting in $\sim 0.4''$ resolution, and λ=1.3 cm data are from the B and C arrays with $\sim 0.6''$ resolution. Due to time constraints, only seven fields were observed yielding a total of nine sources: RY Tau, GG Tau, GG Tau N, DL Tau, NGC1333 IRAS 4A, NGC1333 IRAS 4B, IRAS 05338-0624, IRAS 05375-0731, and S68 FIRS1.

T Tauri Star Results and Discussion:

Emission was detected from only one of the T Tauri stars, RY Tau (330 μmJy at λ=3.6 cm); it is presently unclear if this emission arises from ionized gas or dust. GG Tau N was detected at λ=3.6, 2.0, and 1.3 cm and the emission is consistent with originating from ionized gas or possibly non-thermal processes.

The 3σ upper limits to the cm wavelength fluxes for DL Tau (<78 μJy at λ=3.6 cm) and GG Tau (<270 μJy at λ=1.3 cm) can be used to constrain the properties of the circumstellar dust. These upper limits are in conflict with the fluxes predicted by extrapolating the disk models of Beckwith and Sargent (1991), as shown for GG Tau and DL Tau in Figure 1 (solid line). This discrepancy is mainly due to the extrapolation of their shallow emissivity law (β=0.78 for GG Tau and -0.11 for DL Tau). The cm data require that β, as measured from millimeter to cm wavelengths, is greater than 0.8 for DL Tau and greater than 1.6 for GG Tau. There are two approaches to reconciling the data and model. A single steep emissivity law can be fitted to all data; the cm data require $\beta \sim 2$ and significantly misfit the submillimeter data (Figure 1 - dotted line). Alternatively, the dust emissivity can be modeled as a two part power law with β changing value at some wavelength, as is suggested for dust in the ISM (Hildebrand 1983). Assuming that β=2 at long wavelengths, the GG Tau data indicate that the value of β changes around λ=2 mm (Figure 1 - dashed line). This change occurs at an order of magnitude greater wavelength than that proposed for interstellar dust (2 mm versus 250 μm) and may reflect grain growth in the circumstellar environment.

Embedded Objects Results and Discussion:

Emission was detected from all of the embedded YSO's; in three of the five, this emission arises from ionized gas, probably associated with stellar winds. In two cases, NGC 1333 IRAS 4A and 4B, dust emission is present. NGC 1333 IRAS 4A and 4B are deeply embedded YSO's in the NGC 1333 molecular cloud (Sandell *et al.* 1991). Emission from IRAS 4A, the stronger of the two sources at submillimeter wavelengths, was detected at λ=6.0, 3.6, 2.0, and 1.3 cm. The spectral index of the λ=3.6 to 1.3 cm emission is 2.4$\pm$0.15. The λ=6.0 cm

emission falls significantly above an extrapolation of this fit; the spectral index of the λ=6.0 and 3.6 cm emission alone is 1.3. If the λ=6.0 emission is assumed to arise entirely from ionized gas and the ionized gas has a $\nu^{1.3}$ spectral dependence, only 38% of the λ=1.3 cm flux arises from this component. Thermal dust emission is then the dominant contributor to the flux at λ=1.3 cm.

Further details of this work are presented in Mundy *et al.* (1993).

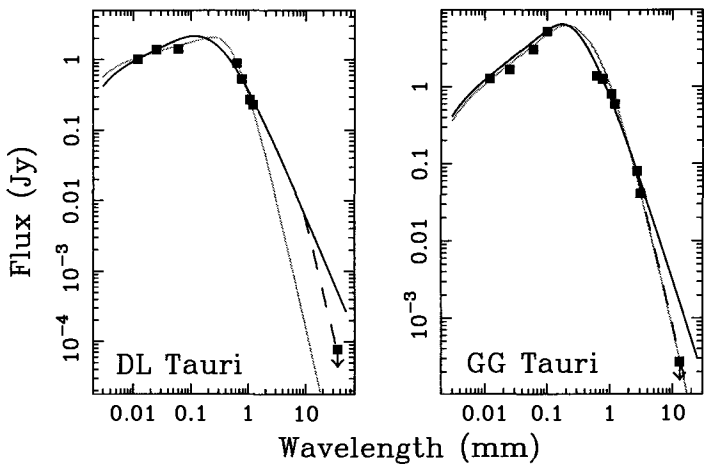

Figure 1: Spectral Energy Distribution for DL Tau and GG Tau. The filled squares are published fluxes (see Beckwith and Sargent 1991); the squares with down-arrows are 3σ upper limits. The lines are model fits as explained in the text.

References

Beckwith, S.V.W., Sargent, A.I., Chini, R.S., and Gusten, R. 1990, AJ, 99, 924
Beckwith, S.V.W. and Sargent, A.I. 1991, ApJ, 381, 250
Draine, B. T. 1990, "The Interstellar Medium in Galaxies", ed. H. A. Thronson and J. M. Shull, 483, Kluwer, Dordrecht
Mundy, L.G., McMullin, J.P., Grossman, A.W., and Sandell, G 1993, Icarus, in press
Sandell *et al.*, ApJ, 376, L17
Weintraub, D.A., Sandell, G., & Duncan, W.D. 1989, ApJ, 340, L69
Wilking, B.A., Mundy, L.G., Blackwell, J.H., and Howe, J.E. 1989, ApJ, 345, 257

Optical Pumping of Circumstellar SiO Masers

E. Rausch[1], W. H. Kegel[1], and T. Tsuji[2]

[1] Institut für Theoretische Physik der Universität Frankfurt/M

[2] The University of Tokyo, Institute of Astronomy, Mitaka, Tokyo

We investigate the influence of the photospheric line spectrum on the optical pumping of circumstellar SiO molecules. As pump radiation we consider in particular the (synthetic) line spectrum of an M-star atmosphere ($T_{eff} = 3000K$). Figure 1 shows a part of the synthetic spectrum we used. The vertical line marks the transition $v = 0 - 1$, $J = 0 - 1$ for ^{28}SiO. In the spectral range of the pump lines (8μ and 4μ) the photospheric spectrum is crowded with deep absorption lines. As a consequence the pump intensities in different lines may differ substantially. Furthermore, the pump intensity in a given line depends sensitively on the velocity difference between envelope and photosphere. Figure 2 shows the correlation between Δv_r and I_ν/B_ν for the three isotopomeres ^{28}SiO, ^{29}SiO and ^{30}SiO. I_ν is the intensity of the photospheric spectrum in the frequency of the pumpline $v = 1 - 0$, $J = 1 - 2$ seen in the coordinate system of the moving envelope.

We performed numerical calculations (LVG-code) in order to find out under which physical conditions inversion occurs. We have shown that optical pumping causes maser emission without the need of collisions. Our findings differ substantially from the results of similar calculations assuming the spectrum of the pump radiation to correspond to that of a black body. The regions of inversion in parameter space (SiO/H_2; n_{H_2}; $\mathrm{d}v_r/\mathrm{dr}$) for the different isotopomeres are distinct from each other due to the frequency differences in the pump lines. The regions also depend sensitively on the velocity difference between the photosphere and the emitting volume element.

Figure 1

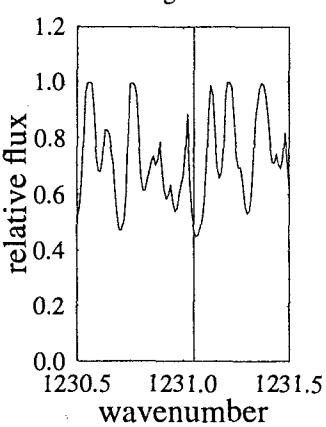

Figure 2

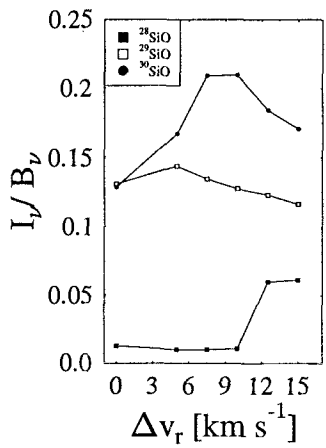

Observations of Interstellar CN, ^{13}CN and C^{15}N

R. Simon, A.H. Saleck, N. Schneider, K. Jacobs, B. Vowinkel and G. Winnewisser
I. Physikalisches Institut, Universität zu Köln, 50937 Köln, Germany

Observations of the CN radical and its isotopomeres are an important tool to study interstellar radical chemistry and abundances. The dipole moment of 1.45 Debye implies gas densities of $n_{H_2} \sim 10^5 - 10^6 cm^{-3}$ necessary for populating the N = 2 rotational level. Its relatively high abundance (CN/CO $\sim 10^{-4}$) makes CN observable in a variety of interstellar Molecular Clouds. Thus CN is a good molecular probe for dense gas at moderate kinetic temperatures ($\sim$ 40K) and, deduced from timedependent chemical models (e.g. Herbst 1986), young interstellar chemistry. As emphasized by Langer (1992), the ^{12}CN/^{13}CN ratio is sensitive to the photodestruction rate and the kinetic temperature at the observed position. Because several fine structure transition exhibiting hyperfine splitting are observed simultaneously, optical depths can be determined without uncertainties in calibration. In many cases the emission peaks of CN and other reactive species are shifted from those of closed shell molecules confirming the scenario of a significant depletion of radicals in the vicinity of hot and dense gas.

A 98 point map (2′ grid) obtained with the KOSMA 3m telescope in the two strongest fine structure transitions of CN N= 2 → 1 reveals a strong intensity maximum at the position (1′, 2′) relative to IRc–2. Based on an in depth estimate of the molecule's rotational, spin doubling and magnetic hfs constants, frequencies and relative intensities for the first three rotational transitions of C^{15}N have been predicted for the first time at our institute. The strongest feature of C^{15}N N= 2 → 1 has subsequently been detected with the KOSMA telescope at the position of peak CN intensity in Orion A (Saleck et al. 1993).

In September 1993 small maps in the transitions N= 1 → 0 and N= 2 → 1 of CN were performed in Orion A and B with the IRAM 30m telescope. The maps served as finding charts for peak CN emission at high angular resolution and show a significant decrease of CN intensity towards IRc–2 and several maxima shifted to the north–east and south. The preliminary map of CN N= 2 → 1 in Orion B (NGC 2024) shows a good correlation of molecular and dust continuum emission at the same angular resolution of 12″ (Mezger et al. 1988). At almost every position in the maps, the relative intensities of the hyperfine lines indicate high optical depths and high CN column densities.

Based on the CN maps, 4 single positions of peak CN intensity and high optical depth in Orion A and B were selected for a search for the rarer isotopomeres. The C^{15}N N= 2 → 1 detection and the calculated frequencies could be confirmed along with the first detection of C^{15}N N= 1 → 0 and ^{13}CN N= 2 → 1 . The relative intensities of the lines indicate optically thin emission (see **Fig. 1** and **Fig. 2**).

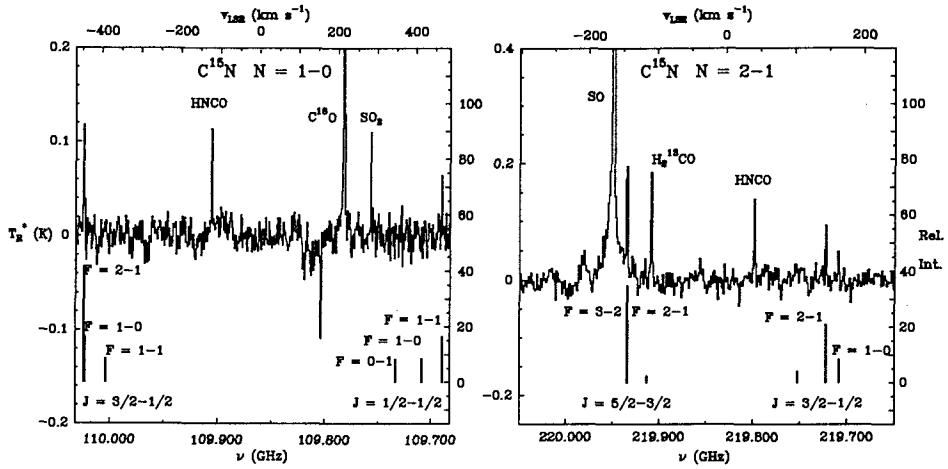

Figure 1: Spectra of $C^{15}N$ N= 1 → 0 and N= 2 → 1 towards the position (24″, 72″) relative to IRc–2 together with the theoretical hyperfine pattern. The strongest transitions are labelled by the appropriate quantum numbers.

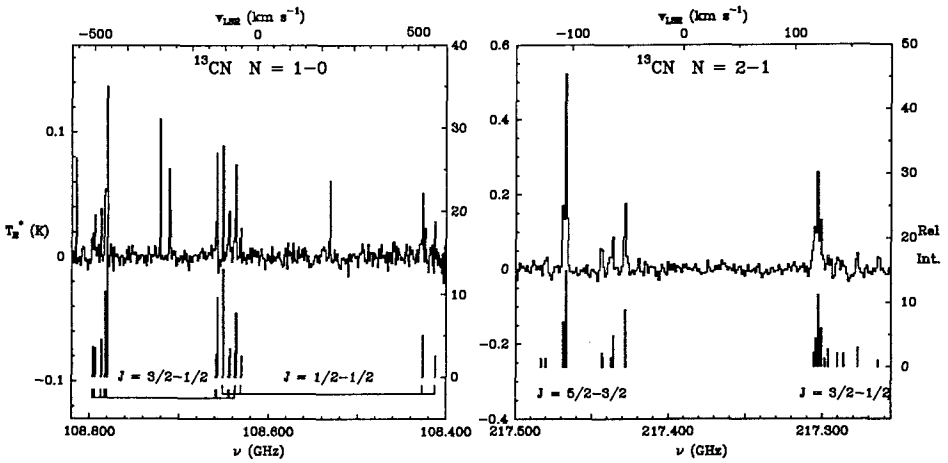

Figure 2: Same as Figure 1 for ^{13}CN N= 1 → 0 and N= 2 → 1

References

Herbst E., 1986, ApJ 310, 378
Langer W.D., 1992, IAU Symp. No. 150, 193;
Mezger P.G., Chini R., Kreysa E., Wink J.E., Salter C.J., 1988, A&A 191, 44
Saleck A., Simon R., Schneider N., Winnewisser G., 1993, ApJ 414, L133

Physical and chemical variations within the W3 star–forming region

F.P. Helmich[1], D.J. Jansen[1], Th. de Graauw[2], T.D. Groesbeck[3], E.F. van Dishoeck[1]

[1] Leiden Observatory, P.O.-Box 9513, 2300 RA Leiden, The Netherlands
[2] SRON Laboratory Groningen, P.O.-Box 800, 9700 AV Groningen, The Netherlands
[3] Division of Physics, Mathematics & Astronomy, 405-70, California Institute of Technology, Pasadena, CA 91125

The W3 region consists of a giant molecular cloud with numerous H II regions and luminous infrared sources. In its core, millimeter continuum observations (Richardson et al. 1989) have shown the existence of two dense clumps of about 2000 $M_\odot$ associated with the luminous infrared sources IRS4 and IRS5. Of comparable mass is the source W3(H_2O) located at the place of the water masers about 16′ south of the core. The three sources each have a total luminosity of $(1-2) \times 10^5\, L_\odot$ and are assumed to be places of high mass star formation. All three sources originate from the same parent cloud with comparable initial conditions. Differences in chemical constituency should therefore reflect different stages in their evolution.

We used the 15–m James Clerk Maxwell Telescope (JCMT) on Mauna Kea (Hawaii) to perform an unbiased survey in the 345 GHz window (15″ beam) and parts of the 230 GHz window (20″ beam) in order to constrain the physical conditions and abundances for the three sources IRS4, IRS5 and W3(H_2O). To date, about 15 GHz has been covered in each of the windows. Numerous molecular lines have been detected, ranging from those of simple species like CN and HCO^+ to complex molecules like CH_3OH (methanol) and CH_3OCH_3 (dimethyl ether). The initial results for three molecules, SO_2, H_2CO and CH_3OH, will appear in Helmich et al. (1994). These molecules behave very differently in the three sources: CH_3OH is strong in W3(H_2O), moderate toward IRS4 and weak toward IRS5, whereas SO_2 is strong toward IRS5 and W3(H_2O), but weak toward IRS4. Thus, there appear to be significant chemical and/or physical differences between the three sources.

To constrain the physical conditions and column densities, rotation diagrams have been made and statistical equilibrium calculations have been performed. The first method is most easily applied when many lines are measured of the same molecule (as for SO_2 and CH_3OH), but assumes that the lines are optically thin and that the populations are in LTE. The latter method is better in principle, but depends on sometimes poorly known collisional rates. For H_2CO the collisional rates are well–known, but not for SO_2 and CH_3OH.

It is found from the SO_2 and CH_3OH rotation diagrams the rotation temperatures are high, $T_{\rm rot} \approx 100-200$K, toward IRS5 and W3($H_2O$), but low, $T_{\rm rot} \approx 50$K, toward IRS4. The statistical equilibrium calculations for the H_2CO indicate kinetic temperatures $T \approx 220$ K toward W3(H_2O), $T \approx 100$ K toward IRS5 and $T \approx 55$ K toward IRS4. The derived densities are 3×10^6, 10^6 and 10^6 cm^{-3}, respectively. For all three sources, $N_{\rm ortho}/N_{\rm para}$ is close to three.

The interpretation of the results is as follows. Of the three regions W3 IRS4 appears to be the most evolved one. The radio continuum map of Colley (1980) of this region (W3C) has the same morphology as the blister-like H II regions, with an age of about 10^5 yr. This time scale since star formation is long enough for the chemistry to reset to the dark cloud values, which could account for the low abundances of complex molecules and for the smaller line widths in W3 IRS4 compared with IRS5 and W3(H_2O).

The high obscuration toward W3(H_2O) indicates that this object is still very young, as is also evidenced by the presence of H_2O masers. The richness in molecular lines and the high temperature of the gas imply a remarkable evolution compared with the quiescent cloud. W3(H_2O) appears to be an object like the Orion hot core, in which processed molecules such as CH_3OH have evaporated from the grains (Blake et al. 1987; Charnley et al. 1993; Caselli et al. 1993). The gas-phase CH_3OH abundance toward W3(H_2O) is at least an order of magnitude larger than toward IRS4 and IRS5.

Toward IRS5 the gas–phase CH_3OH and H_2CO abundances are low, in spite of the high total column density. However, Allamandola et al. (1992) have detected solid CH_3OH toward IRS5 and derived a methanol–ice abundance more than four orders of magnitude larger than our gas-phase results. Thus, most of the processed material appears to be still sitting on the grains, and IRS5 is probably younger than W3(H_2O). Radio continuum observations show that IRS5 has only very recently become hot enough to produce ionizing photons. Since the H_2CO data indicate a temperature of about 100 K we could be witnessing the birth of a hot core–like region, where processed molecules will shortly come of the grains: we speculate that IRS5 will look like W3(H_2O) within the next 10^4 yr.

The high abundance of SO_2 around IRS5 is reminiscent of that found in the Orion plateau, and probably results from shock chemistry and shock destruction of refractory grain cores in a high density environment. The shocks most likely arise when the strong outflow from IRS5 impacts the surrounding material. Mitchell et al. (1992) deduce from their near infrared CO absorption lines that the outflowing CO-gas has a rotational temperature of 200–270 K, similar to our value for SO_2. If all of the SO_2 originates in the outflow, its abundance is comparable to that for the Orion Plateau region.

References

Allamandola, L.J., Sandford, S.A., Tielens, A.G.G.M., and Herbst, T.M. 1992, ApJ 399, 134.

Blake, G.A., Sutton, E.C., and Masson, C.R., and Phillips, T.G. 1987, ApJ 315, 621.

Caselli, P., Hasegawa, T.I., and Herbst, E. 1993, ApJ 408, 548.

Charnley, S.B., Tielens, A.G.G.M., and Millar, T.J. 1993, Ap.J. 399, L71.

Colley, D. 1980, MNRAS 193, 495.

Helmich, F.P., Jansen, D.J., De Graauw, Th., Groesbeck, T.D., and van Dishoeck, E.F. 1994, A&A in press.

Mitchell, G.F., Hasegawa, T.I., and Schella, J. 1992, ApJ 386, 604.

Richardson, K.J., Sandell, G., White, G.J., Duncan W.D., and Krisciunas, K. 1989, A&A 221, 95.

Chemical and Physical Gradients along the OMC-1 Ridge

H. Ungerechts[1], E.A. Bergin, P.F. Goldsmith[2], W.M. Irvine, F.P. Schloerb, and R.L. Snell

FCRAO, 619 LGRC, University of Massachusetts, Amherst MA 01003, USA
current addresses: [1]CfA MS72, 60 Garden Street, Cambridge MA 02138, USA
[2]NAIC, Space Sciences Bldg., Cornell University, Ithaca NY 14853, USA

When we study molecular clouds we have to rely on maps of rare species like CO, because the main constituent, H_2, can only be observed in diffuse clouds against background stars and in small regions with unusually high temperatures. The correlation of CO with other tracers of total column density is fairly well established both in cold dark clouds on the scale of several arc minutes and for GMCs on a galactic scale. On the other hand, in many clouds molecules tracing higher density show significantly different distributions, sometimes because their excitation depends in different ways on temperature and density, but often because their abundances vary. We also need to know the chemical composition of molecular clouds because it strongly influences their evolution: for example, the abundance of rare species can determine the cooling rate and thus the gas temperature. For these reasons we have undertaken a survey of the distribution of 21 chemical and isotopic molecular species along the central Orion molecular ridge in 29 rotational transitions with 33 resolved lines including HfS components.

Recent Studies of the OMC-1 Ridge

The Orion A Molecular Cloud has a mass of $10^5 M_\odot$ (Maddalena et al. 1986) and is 450 pc from the sun. The most prominent feature among many filaments and shells seen in CO and CS survey maps is a ridge forming an $\int$ sign extended north-south over $\approx 1^\circ$ (e.g., Bally et al. 1987, Dutrey et al. 1991). This $\int$-filament includes the prominent molecular emission peaks OMC-2 and OMC-1; the latter lies behind the Orion Nebula M42 and the Trapezium stars, and contains the massive star forming region around the BN star and the KL nebula. The whole $\int$ has been surveyed in CS and ^{13}CO $J = 1 \rightarrow 0$ using the Nobeyama 45 m telescope (Tatematsu et al. 1993). Along the $\int$ the CS data reveal 52 cloud cores with average size 0.14 pc and density $10^{5.2}$ cm^{-3}. Line intensities are particularly high near the center of the $\int$ filament behind the H II-region M42, from about 6′ north to 6′ south of KL. While many molecules have their maximum emission near KL, for some species the lines are stronger a few arc minutes north or south.

For simplicity we will refer to this central dozen arc minute stretch of the $\int$ filament as the OMC-1 ridge. In a very broad sense all molecules follow the ridge seen in CO and CS, but each species has its own idiosyncratic modifications of the general pattern. All maps show spatial structure on scales as small as a few pixels or beam widths. The definition and identification of "clumps" or "cores" is therefore difficult to achieve consistently for more than a single molecular species. For the present discussion we distinguish six regions along the OMC-1 ridge, each of which is heavily fragmented. These regions are from North to South: i) the radical-ion region $\approx 3.5'$ north of KL; ii) the quiescent ridge ≈ 1–$2'$ north of KL; iii) the BN/KL region; iv) OMC-1-1.5′S near the second FIR peak and outflow; v) the molecular bar near the brightest part of the optical bar in M42; and vi) the junction of ridge and molecular bar 4′ south of KL.

One of the strongest abundance variations known along the OMC-1 ridge is the ratio of the isomers [HCN]/[HNC], which is about 10 times larger toward KL than elsewhere (Goldsmith et al. 1986, Schilke et al. 1992). Similarly, the fractional abundance of CH_3OH relative to H_2 toward KL and OMC-1-1.5′S is $\approx 10^{-6}$–10^{-7}, but only 10^{-8} in the ridge (Menten et al. 1988). The central area around KL forms a very bright bull's eye of $\approx 1'$ in many molecular maps; details are discussed by Sutton et al. (1993) in these proceedings. Abundance increases toward KL are believed to be the effects of young massive stars on the cloud: any energy input will raise temperatures and help overcome activation barriers and/or evaporate molecules from grain surfaces.

Maps of HC_3N emission with the IRAM 30 m telescope (Rodriguez-Franco et al. 1992) show many clumps as well as thin (15–25″) filaments. Derived densities are close to $10^5\,cm^{-3}$, and the HC_3N abundance is about 10^{-9} except in the KL hot core, where it is 30× higher, and in the molecular bar, where it decreases by an order of magnitude. The Effelsberg NH_3 maps (Batrla et al. 1983) have recently been extended (Cesaroni and Wilson 1993); they are particularly important because they give direct temperature estimates for the dense gas in the ridge: 15–24 K in regions i) and ii), 28 K in region vi), but up to $\approx$ 80 K toward KL and OMC-1-1.5′S. New VLA mosaic maps of NH_3 along the OMC-1 ridge are presented in another contribution at this conference (Wiseman and Ho 1993). Two other symmetric tops can serve as thermometers for the dense ridge. CH_3CCH gives $\approx$ 50 K toward KL and $\approx$ 30–40 K in the ridge (Churchwell and Hollis 1983, Wang et al. 1993). Results from CH_3CN toward KL are about a factor of 2 higher; it probably samples regions of higher density that are closer to embedded energy sources than does CH_3CCH (Churchwell and Hollis 1983).

The OMC-1 radical-ion region, about 2.5′–5′ north of KL, was recognized by its particularly strong lines of CN, C_2H, N_2H^+, and HCO^+ (Turner and Thaddeus 1977, Snyder et al. 1977, Tucker and Kutner 1978). The strong CN lines may in part be explainable by low excitation temperatures, but the abundances of SO, HCO^+, and HCS^+ are enhanced by factors of 5–50 (Greaves and White 1992). Observations with the VLA (NH_3: Harris et al. 1983, H_2CO: Wilson and Johnston 1989) reveal clumps with scale sizes $\approx$ 20″, temperature $\approx$ 20 K, and high densities, 10^6–$10^7\,cm^{-3}$. South of the radical-ion region the ridge stretches down to the neighborhood of KL, and appears to be mostly quiescent. Many interferometric studies show small-scale clumping, particularly several sub-arc minute filaments; densities again are 10^6–$10^7\,cm^{-3}$ (e.g. Nobeyama, NH_3: Murata et al. 1990; OVRO, CS: Mundy et al. 1986, 1988).

In maps of the FIR continuum and many molecular lines, a second peak is located about 1.5′ south of KL (Keene et al. 1982). High velocity wings in lines of thermal SiO (Ziurys and Friberg 1987) and CO $J = 7 \rightarrow 6$ (Schmid-Burgk et al. 1989), as well as FIR photometry (Jaffe et al. 1984) suggest an embedded young star. More complete references and a detailed discussion of interferometric observations are presented by McMullin et al. (1993): 3.1 mm continuum emission is seen toward a young stellar object where the dust temperature is $\approx$ 65 K; molecular abundances are close to values typical for the ridge, except toward the continuum source where they appear reduced.

Farther south and east, the molecular bar is a structure $\approx$ 5′ long that is not aligned with the ridge but closely related to a bright bar in the H II-region (e.g., Schloerb and Loren 1982). In single dish maps, CO and CS mm lines are only moderately strong near Θ^2 Ori, where the optical bar is most visible, and stronger where the molecular bar merges into the ridge. The molecular bar and its relation to the ionization front have now been investigated with radio interferometers as well as mm and submm observations (Hogerheijde et al. 1993, Tauber et al. 1994).

All interferometric maps as well as indirect evidence from many single dish observations show that the molecular ridge is clumpy. Emission from warm molecular gas, e.g. in CO $J = 7 \rightarrow 6$, as well as from fine structure lines of C II, is extended throughout the OMC-1 ridge (see the review by Genzel and Stutzki 1989, also Howe et al. 1993). Radiation from the foreground Trapezium stars can probably reach deep into the cloud and form warm layers and photodissociation regions on the high density clumps.

The FCRAO Chemistry Survey

For our observations we used the 15 element focal plane array receiver on the FCRAO 14m telescope. The telescope was stepped to obtain fully sampled maps with pixels on the sky spaced every $\approx$ 25″. We mapped an area 12 pixels in right ascension by 30 pixels in declination. We are working on a detailed analysis following several more conventional routes, but we regard as a distinctive strength of this project the chance to search systematically for relations between the many molecules and transitions by looking at **all** data simultaneously. We employ methods of multivariate analysis to identify regions of similar line intensities—and therefore presumably similar physical conditions—as well as to find a classification of the molecular species according to common features of their distributions. A full description of principal component analysis is beyond the scope of this report, but the method

has been widely used in astronomy following the classical paper by Deeming (1964) and is fully discussed in many books on advanced statistical analysis (e.g. Kendall, Stuart, and Ort 1983; Krzanowski 1988). Our main result is that a surprisingly small number of principal components, 3 to 6, is sufficient to represent the major features in 33 different maps.

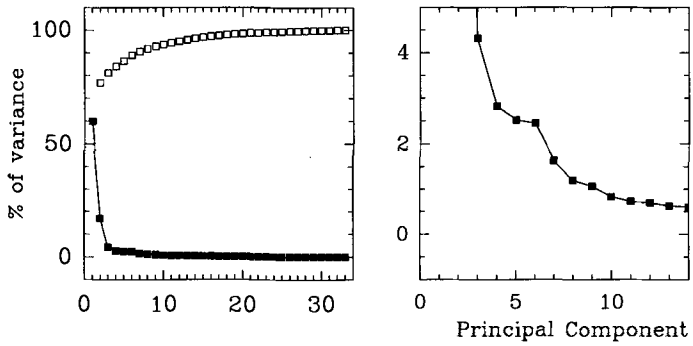

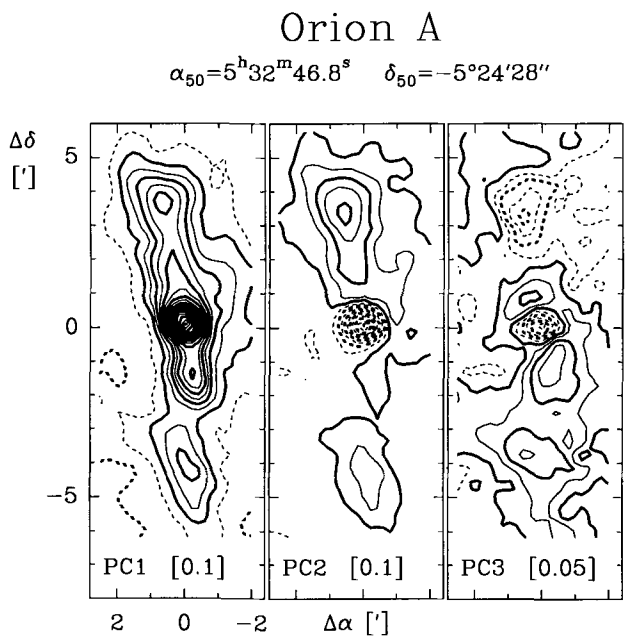

Figure 1: Principal components of the distribution of molecules in OMC-1. Top: percentage contributed by each principal component to the total variance in the data (filled squares); cumulative percentage (open squares). Bottom: distribution of principal components 1, 2, and 3; numbers in [ ] give the contour spacing.

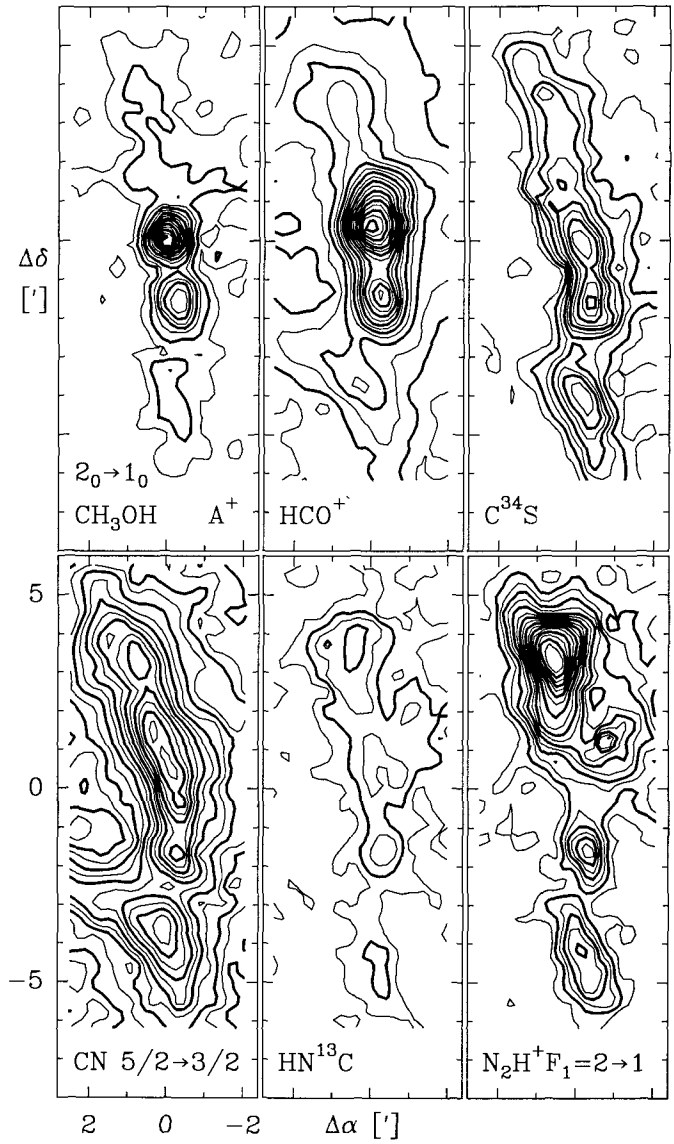

Figure 2: Maps of selected molecular line emission intensities. These six examples are representative of the different distribution classes we found: CH_3OH—strongly peaked toward KL and OMC-1-1.5′S and weak elsewhere; HCO^+—strong throughout with pronounced maxima at KL and OMC-1-1.5′S; $C^{34}S$—extended with moderate enhancement at KL and OMC-1-1.5′S; CN—widely extended emission, nearly flat along the ridge; $HN^{13}C$ and N_2H^+—weak toward KL and particularly strong in the northern radical region.

In a Principal Component (PC) analysis we regard our data as 360 points, one for each pixel, in 33 dimensional space, one dimension for each of our variates, the line intensities. Before submitting these data to PC analysis, they are standardized, i.e. mean-centered and normalized. We then determine a rotational transformation to a new coordinate system so that its first axis, the first PC, is along the direction of maximal variance of the data, the second axis along the maximal variance in the remaining subspace orthogonal to the first PC, and so on for the higher PCs. The first PC accounts for about 60%, the second for 18%, and the third for 4% of the total variance in the data (Fig. 1, top). All 33 line intensities have a positive projection onto the first principal component, which thus is a weighted mean of all line intensities. It is therefore not surprising that the first Eigenmap, i.e. a contour plot of the projections of our data onto the first PC, looks like an idealized map of "the" Orion ridge (left map in Fig. 1, bottom). The higher order PCs describe successive approximations to the variation of the observed maps from the average molecular distribution represented by PC1. Negative values of PC2 reflect the strong enhancement of many molecules around Orion-KL, positive values of PC2 are found in the radical-ion region as well as in the southern bar (center map in Fig. 1, bottom). PC3 differentiates between the properties of the northern and southern regions.

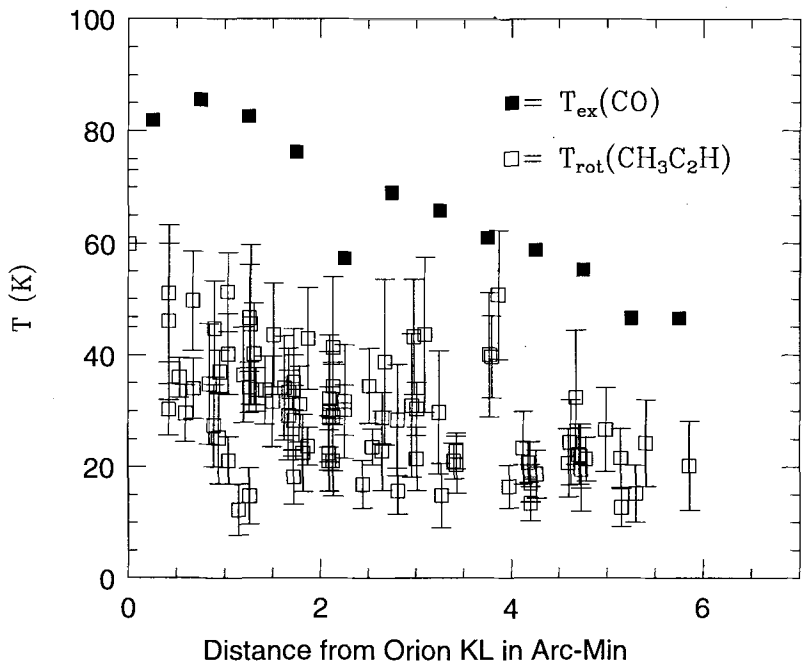

Figure 3: T_{ex}(CO) and $T_{rot}(CH_3CCH)$ as a function of distance from KL. Values for T_{ex}(CO) are averages over bins 0.5′ wide that include points north and south of KL.

Several molecules in our survey allow us to derive physical parameters, especially when we combine them with observations of higher and lower transitions using other instruments. In particular, we have two temperature tracers: the peak intensity of optically thick ^{12}CO gives a direct estimate of the temperature in a surface layer of the cloud; the CH_3CCH lines are optically thin and predominantly trace gas of higher density in the interior. As transitions between the K-ladders of the symmetric top propyne are dominated by collisions, the relative intensities of the three lines we observed, $J = 6 \rightarrow 5$, $K = 0, 1, 2$, can serve as a thermometer for the dense gas (Churchwell and Hollis 1983, Askne et al. 1984). We find that T_{ex}(CO) is larger than $T_{rot}(CH_3CCH)$ by a factor of about two throughout the region mapped (Bergin,

Goldsmith, Snell, and Ungerechts 1993). While there is considerable point-to-point variation in both temperatures, both tend to decrease with distance from Orion KL (Fig. 3). Velocities and line widths of CH_3CCH are very similar to those of HC_3N, confirming that the CH_3CCH emission is mostly from dense gas. Our data thus strengthen the generally accepted view that most of the molecular gas along the Orion ridge is heated from the outside, i.e. from the foreground, with much energy input concentrated near KL.

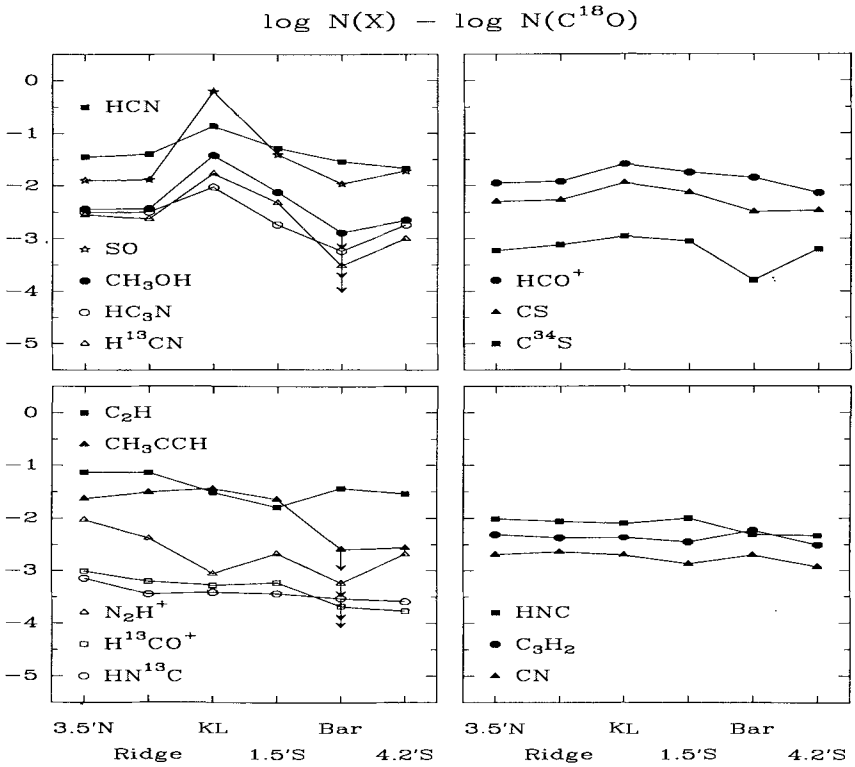

Figure 4: LTE column densities relative to $N(^{12}C^{18}O)$ toward six selected positions: i) the radical-ion region 3.5'N; ii) the quiescent ridge; iii) the BN/KL region; iv) OMC-1-1.5'S; v) the molecular bar; and vi) the junction of ridge and bar 4.2'S. Arrows indicate upper limits.

As a first step toward understanding which of the variations in the molecular distributions correspond to differences in chemical abundances, we used the observed temperatures to calculate LTE column densities for selected species at six positions representative of the six regions mentioned above. The variations of LTE column densities relative to $C^{18}O$ (Fig. 4) fall into distinct groups which correspond to the classes of line intensity distributions (Fig. 2). The LTE abundances of some species like CN, HNC, and C_3H_2 are nearly constant. For other molecules, including HCN, SO, CH_3OH, and HC_3N, the abundances are strongly enhanced toward KL. Next there are several species with a north-south gradient, showing an increase in abundance toward the northern radical region, e.g. N_2H^+ and C_2H, or a decrease in the south, e.g. CH_3CCH. Finally, some abundances are particularly low at the molecular bar position, e.g. those of HC_3N, $H^{13}CN$, $C^{34}S$, and N_2H^+.

References

Askne, J., Höglund, B., Hjalmarson, Å., and Irvine, W.M. 1984, A&A, 130, 311.
Bally, J., Langer, W.D., Stark, A.A., and Wilson, R.W. 1987, ApJ, 312, L45.
Batrla, W., Wilson, T.L., Bastien, P., and Ruf, K. 1983, A&A, 128, 279.

Bergin, E.A., Goldsmith, P.F., Snell, R.L., and Ungerechts H. 1993, in prep. for ApJ.
BN = Becklin, E.E., and Neugebauer, G. 1967, ApJ, 147, 799.
Cesaroni, R., and Wilson, T.L. 1993, submitted to A&A.
Churchwell, E., and Hollis, J.M. 1983, ApJ, 272, 591.
Deeming, T.J. 1964, MNRAS, 127, 493.
Dutrey, A., et al. 1991, A&A, 247, L9.
Genzel, R., and Stutzki, J. 1989, ARA&A, 27, 41.
Goldsmith, P.F., Irvine, W.M., Hjalmarson, Å., and Elldér, J. 1986, ApJ, 310, 383.
Greaves, J.S., and White, G.J. 1992, MNRAS, 259, 457.
Harris, A., Townes, C.H., Matsakis, D.N., and Palmer, P. 1983, ApJ, 265, L63.
Hogerheijde, M., Jansen, D., and van Dishoeck, E. 1993, this symposium, Zermatt.
Howe, J.E., et al. 1993, ApJ, 410, 179.
Jaffe, D.T., Davidson, J.A., Dragovan, M., and Hildebrand, R.H. 1984, ApJ, 284, 637.
Keene, J., Hildebrand, R.H., and Whitcomb, S.E. 1982, ApJ, 252, L11.
Kendall, M., Stuart, A., and Ort, J.K. 1983: *"The advanced theory of statistics"* (London: Charles Griffin & Company).
KL = Kleinmann, D.E., and Low, F.J. 1967, ApJ, 149, L1.
Krzanowski, W.J. 1988: *"Principles of Multivariate Analysis"*, (Oxford: Clarendon Press).
Maddalena, R.J., Morris, M., Moscowitz, J., and Thaddeus, P. 1986, ApJ, 303, 375.
McMullin, J.P., Mundy, L.G., and Blake, G.A. 1993, ApJ, 405, 599.
Menten, K.M., Walmsley, C.M., Henkel, C., and Wilson, T.L. 1988, A&A, 198, 253.
Mundy, L.G., et al. 1986, ApJ, 304, L51.
Mundy, L.G., et al. 1988, ApJ, 325, 382.
Murata, Y., et al. 1990, ApJ, 359, 125.
Rodriguez-Franco, A., et al. 1992, A&A, 264, 592.
Schilke, P., et al. 1992, A&A, 256, 595.
Schloerb, F.P., and Loren, R.B. 1982, in: *"Symposium on the Orion Nebula to Honor Henry Draper"*, Eds. Glassgold, A.E., Huggins, P.J., and Schucking, E.L., Annals of the New York Academy of Sciences, Vol. 395, p. 32.
Schmid-Burgk, J., et al. 1989, A&A, 215, 150.
Sutton, E.C., et al. 1993 this symposium, Zermatt.
Snyder, L.E., Watson, W.D., and Hollis, J.M. 1977, ApJ, 212, 79.
Tatematsu, K., et al. 1993, ApJ, 404, 643.
Tauber, J.A., Tielens, A.G.G.M., Meixner, M., and Goldsmith, P.F. 1994, to appear in ApJ.
Tucker, K.D., and Kutner, M.L., 1978, ApJ, 222, 859.
Turner, B.E., and Thaddeus, P., 1977, ApJ, 211, 755.
Wang, T.Y., Wouterloot, J.G.A., and Wilson, T.L. 1993, A&A, 277, 205.
Wilson, T.L., and Johnston, K.J. 1989, ApJ, 340, 894.
Wiseman, J.J., and Ho, P.T.P. 1993, this symposium, Zermatt.
Ziurys, L.M., and Friberg, P. 1987, ApJ, 314, L49.

DENSE CORES AND STAR FORMATION: BEFORE AND AFTER

Peter J. Barnes & Philip C. Myers, Harvard-Smithsonian Center for Astrophysics
Mark Heyer, Five College Radio Astronomy Observatory

1. Intermediate-Mass Star Formation Programme

One of the longstanding problems of star formation is understanding the origin of the IMF. To make progress with this problem we must understand first the role of the star-forming environment in determining the mass and number of stars formed. Since the most immediate precursors to stars are dense cores, understanding the initial conditions in gas giving rise to stars means analysing the properties of dense cores. For example, the shapes of cores, the relation between cores' size and linewidth as traced by various molecular species, and the different distributions of these species within a cloud gives important information on the star-forming process (*e.g.* Myers *et al.* 1991; Caselli & Myers 1994; Ungerechts *et al.* 1994). The best systematic work so far is for low-mass star formation (Myers, Linke, & Benson 1983, hereafter MLB; Benson & Myers 1989); we want to extend this to higher luminosities and masses. Intermediate-mass star-forming regions are more common and less disturbed than high-mass SFRs, so they are better candidates for systematic study and give better statistics.

We are using four main tracers: $C^{18}O$, HCO^+ or CS, NH_3, and HC_3N (with occasional ^{13}CO data). We selected a few known regions forming medium-mass stars that have associated dark clouds: IC 5146 (the Cocoon Nebula), NGC 7023, S140, and NGC 1579 (Lk Hα 101). This is because it is important to obtain data on a large sample of cores without embedded IRAS sources nearby (so-called "starless" cores) as well as cores with stars, in order to compare the properties of cores both before and after stars have formed. In this way we hope to ascertain which physical conditions *govern* star formation and which are simply a *consequence* of star formation.

2. IC 5146 Mapping Strategy

The Cocoon Nebula IC 5146 (also known as S125) is an excellent intermediate-mass region to study since it contains an optical cluster whose most massive stars are early-B at one end of an otherwise dark collection of molecular clouds, LDN 1010–55. This structure of a prominent cluster at the end of an elongated quiescent dark cloud with associated IRAS sources is similar to that of the complexes in Orion A, Ophiuchus, and Corona Australis. Our data collection for this region is the most complete so far of our selected sources.

Lada *et al.* (1994) and Dobashi *et al.* (1992) have conducted complete, sensitive surveys in ^{12}CO, ^{13}CO and CS of the L1010–55 cloud complex using the Bell Labs 7m and Nagoya 4m telescopes. Lada *et al.* have also recently performed a very sensitive SQIID-IR survey of the clouds. We have, utilising these lower-resolution surveys, zoomed in on the dense gas of the complex by conducting arcminute-resolution, Nyquist-sampled surveys in $C^{18}O$ and HCO^+ of all the cores revealed in the Lada and Dobashi surveys, using the new QUARRY receiver on the FCRAO 14m (Fig. 1). This 3mm receiver is a 15-element focal-plane array which allows very efficient mapping of large areas of sky in various molecular transitions. Using the NRAO 12m, we have also obtained spectra of ^{13}CO J=1→0 and $C^{18}O$ J=2→1 at the peak positions of each core. This has enabled us to derive column densities and excitation temperatures for the emitting gas. In addition, we have surveyed peak positions and begun to map the same cores in ammonia (24 GHz) and cyanoacetylene (36 GHz) at the Haystack 37m, in order to compare the properties of the thermally-dominated gas with the material traced by these other molecules. Further spectroscopy of HCO^+, $H^{13}CO^+$, and DCO^+ is scheduled at the NRAO 12m for the winter of 1993-94.

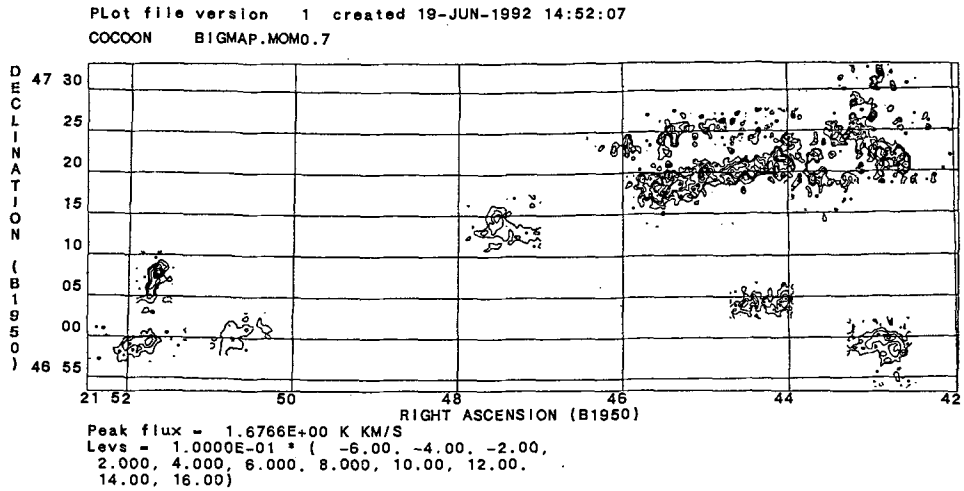

Figure 1: Our QUARRY map of integrated emission in the $C^{18}O$ J=1→0 line for the entire IC 5146/L1010–55 complex in Cygnus. The cluster and HII region S125 lie between the three cores to the east, while the dark clouds containing the non-cluster cores extend to the west.

3. Summary of Results So Far

Our QUARRY maps have revealed the existence of ~20 distinct condensations in the dense gas at this resolution, of which 12 are starless (Fig. 1). The distribution of the emission follows very closely that in the earlier surveys, after allowing for the different resolutions. Highlights of our results include:

1. Core masses are ~10–100 $M_\odot$. This compares with a similar range from the low-mass core survey of MLB, who surveyed in a similar fashion 90 dense cores, most of which are in the Taurus-Perseus or Ophiuchus clouds.

2. All cores have similar densities of a few × 10^3 cm^{-3}, compared to a somewhat higher average around 10^4 cm^{-3} from MLB. This may be attributable to beam dilution effects since the Cocoon complex is at a distance of ~900 pc, about three times greater than the typical distances to the MLB sample.

3. Cores close to the optical cluster are significantly hotter than the cores far from the cluster, and the hottest cores are also the densest. This verifies MLB's finding that the hottest sources are usually associated with optically visible nebulosity. One core has a very high T_{ex} ~ 50 K, to our knowledge second only to the temperature of the core associated with IRc2 in Orion A.

4. The non-cluster cores have a very uniform excitation temperature, T_{ex} ~ 8–9 K, again similar to the dark cores of MLB.

5. For the cluster cores, there is evidence that the cooler ones are externally heated, while the warmer ones are internally heated.

6. There is some evidence that HCO^+ and $C^{18}O$ both show a drop in ΔV as T_R^* rises, showing that the outer parts of a dense core are not as well correlated in velocity as the inner parts. This has important consequences for the density structure and pressure support of dense cores.

7. The $C^{18}O$ correlates well with IR extinction as revealed in the Lada *et al.* study.

8. Bright HCO^+ emission correlates well with positions of embedded IRAS point sources.

9. The brightest emission from NH_3 and especially HC_3N correlates well with the location of starless dense cores.

10. The HCO^+ and HC_3N (NH_3 to a lesser extent) therefore appear *anticorrelated* — see Fig. 2.

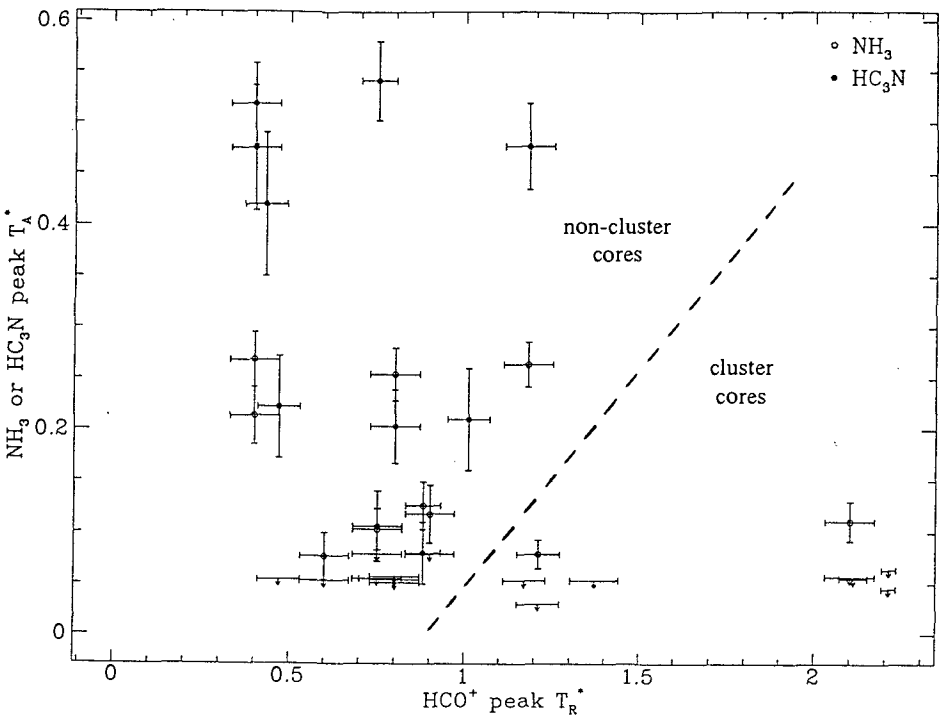

Figure 2: Comparison between peak temperatures of Cocoon cores in different tracers.

4. Conclusions

Dense cores begin to have an "identity" of their own when sufficient "fluff" (lower-density material) collects, since evidence suggests that lower-density molecular gas in a large cloud is generally quite flocculent. In forming a core, the gas adjusts itself to be isothermal and have a lower & lower velocity dispersion. Before stars form, cores are thus quiescent and cold, with abundant HC_3N and moderate amounts of NH_3 and HCO^+. As more stars form and the molecular gas gets heated by the most massive among them, more HCO^+ is produced and most NH_3 and all the HC_3N is destroyed. The data suggest that the HCO^+/HC_3N ratio is a possible evolutionary indicator — see Fig. 2. Other parameters, such as density, seem not to be much affected by star formation.

To our knowledge, the anticorrelation between HCO^+ and HC_3N is the first *systematic* chemical effect which might be attributable to core evolution.

References

Benson, P.J., & Myers, P.C. 1989, *ApJS*, **71**, 89.
Caselli, P., & Myers, P.C. 1994, in preparation.
Dobashi, K., Yonekura, Y., Mizuno, A., & Fukui, Y. 1992, *AJ*, **104**, 1525.
Lada, E.A., Lada, C.J., Clemens, D., & Bally, J. 1994, this volume.
Myers, P.C., Fuller, G.A., Goodman, A.A., & Benson, P.J. 1991, *ApJ*, **376**, 561.
Myers, P.C., Linke, R.A., & Benson, P.J. 1983, *ApJ*, **264**, 517 (MLB).
Ungerechts, H., *et al.* 1994, this volume.

Sulfur Molecules in Low-Density Molecular Clouds

C.M. Walmsley[1], A. Tieftrunk[1], G. Pineau des Forêts[2], P. Schilke[3].

[1] Max Planck Institut für Radioastronomie, Postfach 2024, D-53010 Bonn, Germany
[2] DAEC, Observatoire de Paris, F-92195 Meudon , France
[3] California Institute of Technology, MS 320-47, Pasadena, CA 91125, U.S.A

Molecular absorption lines offer considerable opportunities for testing current models of interstellar chemistry. In contrast to studies of emission line regions, one examines a relatively average sample of molecular cloud material which has been "selected" by being projected along the line of sight to a background radio source. Observations of emission lines on the other hand as a rule are sensitive to the highest density structures which fill a reasonable fraction of the beam. One thus has reason to expect absorption line regions in general to sample lower density more extended molecular cloud material than, say, that observed in well studied dark clouds such as TMC1 and L183. It is thus interesting to observe the molecular abundance distribution in regions such as the low density "spiral arm clouds" observed in absorption along the line of sight towards W49 and SgrB2 and compare the results with those derived for nearby emission line regions such as TMC1 and L183.

In a recent study, we have detected absorption lines from SO , H_2S and NH_3 in the low density molecular clouds along the lines of sight to the galactic sources SgrB2 and W49 . These results are interesting in that these are the first sulfur-bearing molecules apart from CS to be observed in absorption line clouds. Combining our results with those of previous authors (Nyman and Millar 1989, Greaves et al. 1992), we can thus make tests of the predictions of models of sulfur chemistry in low density regions. Observing the less abundant SO isotopomer allows us to check for high optical depth in the main species as well as allowing an estimate of $^{34}S/^{32}S$ in the galactic center. One sees that in ^{32}SO, we detect the -40 and -45 $km\,s^{-1}$ 3 kpc arm features as well as the strong absorption line at 60-70 $km\,s^{-1}$ characteristic of SgrB2. There is also absorption present at 0 $km\,s^{-1}$ as seen in several other species. From our data, we derive an abundance ratio $[^{32}SO]/[^{34}SO]$ of 39 ± 12 towards SgrB2(M) and 19 ± 4 towards SgrB2(N). The former value is high relative to other measurements towards the galactic center (Wannier 1980) but it needs confirmation.

We conclude from our observations that the -40,-45 $km\,s^{-1}$ clouds towards SgrB2 (as well as the 40 $km\,s^{-1}$ absorption feature towards W49) are cold (less than 20 K) and have an abundance distribution in many respects similar to that of nearby dust clouds. The 0 and 65 $km\,s^{-1}$ features referred to above in contrast have temperatures well above 50 K and probably have a more complex history. It is noteworthy however that in the cold absorption line clouds, we find that SO and NH_3 are more than an order of magnitude *less* abundant than in TMC1 and L183. Although our column density estimates have uncertainties of the order of a factor 3, the "underabundance" of SO and NH_3 is more than an order of magnitude and appears significant.

We have tried to test our understanding of the chemistry by comparison with steady state models (see Pineau des Forêts et al. 1993). From this, one finds that CS tends to be relatively more abundant at cloud borders than SO and NH_3. This is because the CS abundance is linked to that of atomic and once ionized carbon. Since these species are relatively abundant at cloud edges, the [CS]/[SO] abundance ratio also increases in regions of modest extinction. When we compare with the models however, we find that we have great difficulty in explaining the observed H_2S abundance. We have considered a number of possibile explanations of this discrepancy and conclude that either one of the reaction rates used in the model is considerably in error or H_2S is being formed on grain surfaces.

References

Greaves J.S., Glenn J.W., Ohishi M., Hasegawa T., Sunada K. 1992 A&A 260, 381
Nyman L.A., Millar T.J. 1989 A&A 222, 231
Pineau des Forêts G., Roueff E., Schilke P., Flower D.R. 1993 *Monthly Notices Roy. Astron. Soc.*, **262**, 915.
Wannier P.G. 1980 *Ann. Rev. Astron. Astrophys.*, **18**, 399.

Chemistry of the Orion Molecular Cloud Core

E. C. Sutton[1], R. Peng[1], W. C. Danchi[2], P. A. Jaminet[3], G. Sandell[4], and A. P. G. Russell[5]

[1]University of Illinois, 1002 W. Green St., Urbana, IL 61801 USA
[2]Space Sciences Laboratory, University of California, Berkeley, CA 94720 USA
[3]Smithsonian Astrophysical Observatory, 60 Garden St., Cambridge, MA 02138 USA
[4]Joint Astronomy Centre, 660 N. A'ohoku Place, Univ. Park, Hilo, HI 96720 USA
[5]Royal Observatory, Blackford Hill, Edinburgh EH93HJ, United Kingdom

We present here preliminary results from a set of molecular line surveys obtained towards several positions in the core of OMC-1. The purpose of this work is to study variations in both chemistry and excitation on small spatial scales in this complex region. As with previous spectral survey work (e.g. Sutton *et al.* 1985; Blake *et al.* 1986), measuring multiple transitions for each molecular species allows us to develop a reasonably accurate picture of excitation and molecular abundances. In this work we have obtained such information with better spatial resolution than previously possible. Still higher resolution may be obtained using millimeter-wave interferometers, although with few exceptions (c.f. Wilner *et al.* 1994) interferometric work has been confined to individual transitions, thereby leaving the issues of excitation and abundance heavily entangled.

This work takes advantage of the high spatial resolution available with the James Clerk Maxwell Telescope (JCMT) at submillimeter frequencies. We have surveyed molecular line emission between 334 and 343 GHz from five positions in the Orion molecular cloud core, with a spatial resolution of 14 arcsec. Four of our five survey beams were centered near IRc2. One was centered on IRc2 (the "hot core" position), one was centered 10 arcsec southwest of IRc2 (the "compact ridge" position), and two were centered on either side of IRc2 along the direction of the high velocity outflow (the "blueshifted" and "redshifted plateau" positions). The remaining beam was centered on a peak in the molecular and dust emission roughly 24 arcsec northeast of IRc2 (the "extended ridge").

The simplest spectrum was obtained towards the extended ridge, a region thought to be representative of the extended ambient molecular cloud. Emission at this position is characterized by narrow linewidths, approximately 3 km/s, and a relatively low density of lines, approximately 50 identified lines in a 9 GHz span. The spectrum from that position is dominated by emission from CH_3OH and CN, with the bulk of the emission line flux being due to those species plus CS and SO. The extended ridge is characterized by low excitation temperatures, of order 50 K.

The spectra towards the hot core and compact ridge positions are remarkably complex and crowded. These spectra are near the confusion limit for lines with integrated intensities of order 1 K km/s. Emission from the hot core and compact ridge is dominated by lines of SO, CS, SiO, OCS, SO_2, H_2CS, HC_3N, HCOOH, and CH_3OH. A few strong features remain unidentified, although at present we do not have accurate transition frequencies for at least one important molecular species: the E symmetry form of methyl formate. Excitation analysis indicates physical temperatures in excess of 200 K with densities of order 10^7 cm^{-3}. The chemistry of these regions indicates an oxygen- and nitrogen-rich environment.

The plateau positions yield spectra of intermediate complexity. Lineshapes in this region are quite complex and vary rapidly from position to position, indicating that a great deal of structure remains unresolved. Excitation in these regions is also quite high.

We have obtained estimates of excitation and abundance for approximately 25 species in each of the five beam positions. In some cases (e.g. SO_2 and CH_3OH) these are based on a large number of transitions and represent rather accurate measuements. For other species only a small number of transitions were measured, and our estimates of abundance are somewhat dependent on what we assume for the excitation of those species.

One of the most interesting questions about the chemistry of the Orion core is how is it possible to produce the high abundances of methanol and chemically related species observed in the compact ridge (Caselli *et al.* 1993). We have estimated abundances of methanol, methyl formate, and dimethyl ether in both the hot core and the compact ridge and conclude that

column densities for these species are enhanced by about a factor of three in the compact ridge. Fractional abundances depend in addition on the (difficult to estimate) molecular hydrogen column densities along these directions. It appears that recent chemical models incorporating grain mantle evaporation are able to explain such differences.

Overall, the observations reveal remarkable small scale variations in spectra taken towards the core of the Orion molecular cloud. These differences appear to be due to both small scale variations in molecular excitation and significant changes in chemical abundances.

The James Clerk Maxwell Telescope is operated by the Royal Observatory Edinburgh on behalf of the Science and Engineering Research Council of the United Kingdom, the Netherlands Organization for Scientific Research, and the National Research Council of Canada. This work has been supported by the National Science Foundation under grants AST-8818327, AST-9196077, and AST-9117740.

References

Blake, G. A., Sutton, E. C., Masson, C. R., & Phillips, T. G. 1986, ApJSuppl, 60, 357
Caselli, P., Hasegawa, T. I., and Herbst, E. 1993, ApJ, submitted
Sutton, E. C., Blake, G. A., Masson, C. R., & Phillips, T. G. 1985, ApJSuppl, 58, 341
Wilner, D. J., Wright, M. C. H., and Plambeck, R. L. 1994, ApJ, in press

The Structure of the Dense Core in the High-Latitude Cloud MCLD 126.6+24.5

Andreas Heithausen and Uwe Corneliussen
I. Physikalisches Institut, Universität zu Köln, 50937 Köln, Germany

One of the puzzles of high-latitude molecular clouds (HLCs) is the existence of quite a number of dense cores or condensation inside these clouds. HLCs are generally found to be gravitationally unbound systems (Magnani et al 1985; Heithausen & Thaddeus 1990) and so the question is whether the same is true for their dense cores. Are these cores

- gravitational stable?
- pressure bound?
- or shock confined?

To study this question we have started multi-transition CO and NH_3 observations of a number of dense cores with the KOSMA 3 m telescope, the IRAM 30 m telescope and the MPIfR 100 m telescope.

In this paper we concentrate on one dense core, MCLD 126.6+24.5 , located on the border of the Polaris Flare (Heithausen & Thaddeus 1990). This core has an extent of 0.1 pc as seen in the KOSMA $^{13}CO(3\rightarrow2)$ transition (see Fig. 1) and shows structure on scales below 0.02 pc (Boden & Heithausen 1993). One of the remarkable features of this core is a quite narrow transition region from atomic to molecular gas unresolved even with the 40″ resolution of the ammonia map.

To study the size of this transition region we have observed the edge of the core with high angular resolution using the IRAM 30 m telescope. At the border of the core the $^{12}CO(2\rightarrow1)$ line drops from a 2 K line inside the core to below detection limit (0.2 K) within one beamsize. The rise in the ^{13}CO and $C^{18}O$ intensity occurs at about the same position in the cloud. We find that the transition region is only 15″ wide, corresponding to 1500 AU at an adopted distance of 100 pc.

The ratio of the $C^{18}O$ $(2\rightarrow1)$ to $(1\rightarrow0)$ transitions increases towards the outer edge of the cloud (see Fig. 2). This increasing ratio might be caused by an increase of the kinetic temperature or an increase of the volume density or a combination of both effects. Being caused solely by increasing temperature the excitation of the CO molecule would indicate an increase from 15 K to above 30 K. There is little indication for such an increase based on the observations of ^{13}CO and ^{12}CO transitions.

To study the temperature profile of this cloud we have conducted high signal-to-noise observations of the ammonia (1,1) and (2,2) lines. At none of the three positions observed the (2,2) line could be detected. We therefore can only derive upper limits for the kinetic temperature of 15 K. Also we found no indication for a variation of the kinetic temperature throughout the cloud.

We therefore interpret the increasing ratio of the two lowest $C^{18}O$ transitions as being caused by increasing density, thus being an indication for a shock running through the cloud, which stabilizes the dense core.

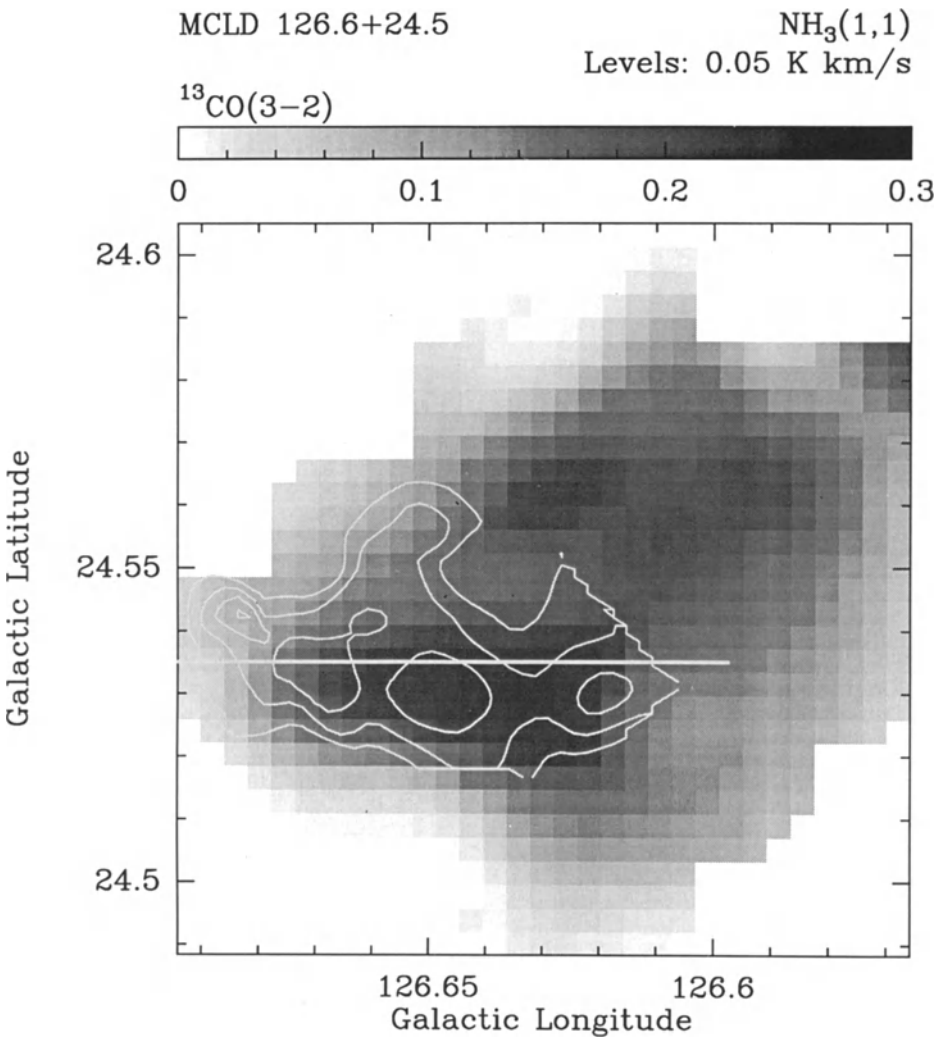

Fig. 1: Integrated $^{13}CO(3\text{-}2)$ intensity map of MCLD 126.6+24.5 overlaid with $NH_3(1,1)$ contours. Levels are indicated at the top of the figure. The white line indicates the cut through the border of the cloud discussed in this paper.

Summarizing our results we find that the transition region from atomic to molecular gas is less than 15″ or 1500 AU wide in the dense core in MCLD 126.6+24.5. The $C^{18}O$ 2→1/1→0 ratio increases from 0.6 to above 1.0 towards the edge. From this follows that as the temperature is most likely constant at $\leq$ 15K the density must rise towards the edge of MCLD 126.6+24.5 For a kinetic temperature T_{kin} = 15K it rises from 2000cm^{-3} inside the core to 6500cm^{-3} at the border, or for T_{kin} = 10K from 4000cm^{-3} to 16000cm^{-3}. One process that might create this inverse density profile is a shock front coming from the giant HI loop, the North Celestial Pole Loop (Meyerdierks et al. 1991).

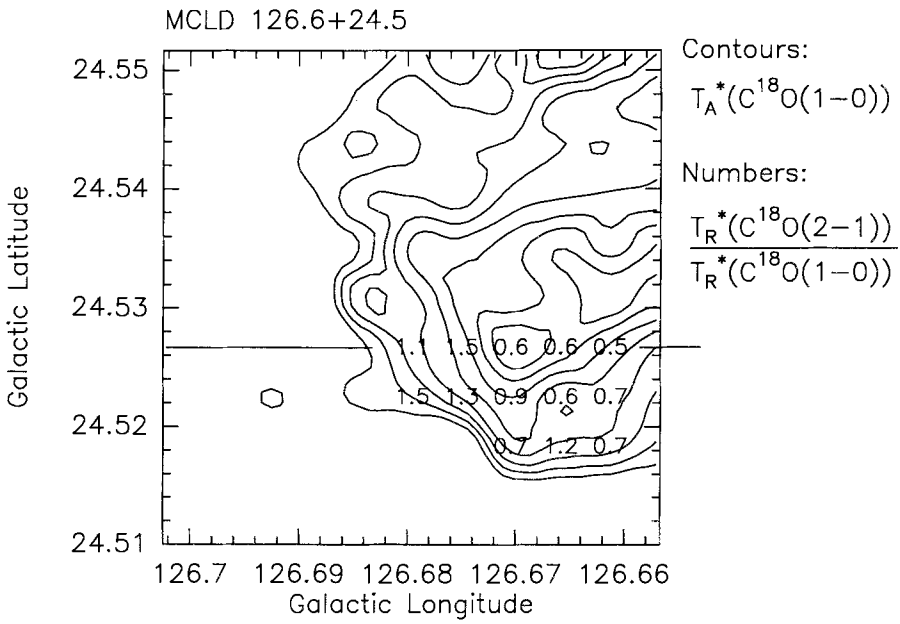

Fig. 2: The transition region from atomic to molecular gas in MCLD 126.6+24.5. Shown is the peak temperature of the $C^{18}O(1\rightarrow0)$ transition as obtained from gaussian fits to the IRAM 30 m data; contours are every 0.1 K km s^{-1} starting at 0.1 K km s^{-1}. Superimposed are the numbers indicating the ratio of the $C^{18}O$ (2→1) to (1→0) transitions.

References

Boden, K.-P., Heithausen, A., 1993, A & A 268, 255
Heithausen, A., Thaddeus, P., 1990, ApJL 353, L49
Magnani, L., Blitz, L., Mundy, L., 1985 ApJ 295, 402
Meyerdierks, H., Heithausen, A., Reif, K., 1991 A & A 245, 247

The W49A Molecular Cloud Core

E. Serabyn
California Institute of Technology 320-47, Pasadena, CA 91125, USA

W49A is one of the most massive and luminous star forming regions in our Galaxy (Welch *et al.* 1987). Furthermore, as revealed by the dense cluster of compact HII regions located near the molecular cloud core, W49A contains a rather sizable collection of massive O stars (Dreher *et al.* 1984). Given this indicator of prolific high-mass star formation, and also the suggestive arrangement of its compact HII regions on the plane of the sky (Welch *et al.* 1987), it is natural that this source has generated great interest. In seeking to explain the star formation in W49A, and more specifically, the O star formation in its most luminous cloud subcomponent, W49N, three competing models have arisen, which are briefly compared here.

Historically, the earliest models for W49N were based on a 'two-cloud collision' scenario. The reason for this was the simple fact that two velocity components, different by about 8 kms^{-1}, were observed in single dish spectra toward the cloud core (Mufson & Liszt 1977). However, as the low-J CO lines used for the early observations of W49A can be quite optically thick toward a massive cloud core, it was suggested that self-absorption in the outer cloud layers could also lead to CO line profiles with a double-humped appearance (Phillips *et al.* 1981), allowing for ambiguity in interpretation. It is possible to resolve this ambiguity with measurements of lines of rare isotopes, which are very likely optically thin, or with measurements of lines which require high densities or temperatures to excite, and so which arise preferentially in the dense cloud core, rather than the envelope. As recent measurements of a number of lines of both types still show a double-humped profile consistent with two velocity components (Miyawaki *et al.* 1986; Jaffe *et al.* 1987; Serabyn *et al.* 1993), abundant observational support for the presence of two clouds near W49A exists. However, the resolution of the W49N core into several cloud fragments (Serabyn *et al.* 1993) adds the further complication of having to distinguish inter-clump motions from possible cloud-cloud velocity shifts.

Alternatively, based on higher resolution interferometric measurements, which show spectra toward the compact HII regions with a redshifted (with respect to the systemic velocity) absorption feature, W49A was proposed to be a single very massive molecular cloud undergoing self-similar collapse (Welch *et al.* 1987). Redshifted absorption features are expected to accompany cloud collapse, because the gas between us and the collapse center must be moving away from us. However, this type of redshift pattern can be arranged in other ways, again leading to ambiguity. For example, as proposed by Keto *et al.* (1991), fragmentation of the cloud core could lead to several independent collapse centers, each showing a similar redshifted self-absorption signature. In addition, if two clouds were to converge upon each other with a velocity component along our line of sight, the nearer cloud would absorb against centrally or interstitially located HII regions at its inherently redshifted velocity. As the case of W49A has proven, it is not easy to observationally distinguish between these possibilities.

The three listed models are however not mutually exclusive. In particular, a collision between two clouds will likely lead to shock compression of the clouds' surface layers,

and so to the possible collapse of some fraction of the cloud(s). Thus, as star formation necessarily entails the collapse of some part of a molecular cloud, and as several newly formed O stars are indeed present in the core of the molecular cloud, all of the models agree in attempting to account for star formation with a collapse scenario. Where the models primarily differ is in seeking to account for the mode, and the initiation mechanism of cloud collapse. Simply put, what triggered the cloud collapse? Did the entire cloud collapse spontaneously, did the cloud fragment into multiple collapsing centers, or was the cloud externally compressed by a collision?

Primarily because of the great distance to W49A, the answers to these questions remain uncertain. The presence of a compact cluster of bright (and short-lived) O stars suggests that star formation in this cloud has proceeded in a synchronized fashion (Dreher *et al.* 1984; Miyawaki *et al.* 1986), and a cloud collision provides a ready trigger mechanism. W49A's presence in a spiral arm further suggests (Serabyn *et al.* 1993) that the collision could be a case of a cloud-cloud collision resulting from orbit crowding in a spiral arm, implying that W49A would be a good candidate for the classic mechanism of induced star formation in Galactic spiral arms.

One of the largest remaining areas of uncertainty is the actual scale of the collapse motions in W49A, as most recent observations, and especially the absorption observations, have tended to focus on the region near the bright HII regions. Absorption studies, while having the capability of measuring the gas falling toward the HII regions along our line of sight, have the disadvantage of sampling only a small fraction of the gas volume, making it difficult to derive a full three dimensional picture of the cloud. Gas outside of the lines of sight to the embedded HII regions can only be studied in emission, and, as the lateral extent of the molecular material in W49A is at least several times larger than the region of the compact HII regions, this gas should show a corresponding kinematic signature if the entire cloud is collapsing. This implies a need for further observations of a complementary nature: high angular resolution studies to resolve motions around the individual HII regions, and somewhat lower resolution observations of a wider spatial area, to define the larger-scale internal cloud motions.

This work was supported by NSF grant AST90-15755.

References

Dreher, J.W., Johnston, K.J., Welch, W.J., & Walker, R.C. 1984, ApJ, 283, 632
Jaffe, D.T., Harris, A.I., & Genzel, R. 1987, ApJ, 316, 231
Keto, E.R., Lattanzio, J.C., & Monaghan, J.J. 1991, ApJ, 383, 639
Miyawaki, R., Hayashi, M., & Hasegawa, T. 1986, ApJ, 305, 353
Mufson, S.L., & Liszt, H.S. 1977, ApJ, 212, 664
Phillips, T.G., Knapp, G.R., Huggins, P.J., Werner, M.W., Wannier, P.G., Neugebauer, G., & Ennis, D. 1981, ApJ, 245, 512
Serabyn, E., Güsten, R., & Schulz, A. 1993, ApJ, 413, 571
Welch, W.J., Dreher, J.W., Jackson, J.M., Terebey, S., & Vogel, S.N. 1987, Science, 238, 1550

MASSIVE STAR NURSERIES

Ed Churchwell
University of Wisconsin
Astronomy Department
475 N. Charter St.
Madison, WI 53706
USA

I.Introduction

The formation process of massive O and B stars is arguably the least understood of all stars. The major observational and theoretical emphasis has been concentrated on low mass star formation during the past decade for a varitey of reasons, among which are: it is a more tractable problem than massive star formation and it is well matched with advances in instrumentation and evolution of theoretical ideas. Molecular cloud cores that give rise to low mass stars have been isolated and intensely studied, providing evidence for the existence and properties of accretion disks, accretion rates, momentum shedding via HH-type jets and molecular outflows, etc. A corresponding advance in our understanding of massive stars has not occurred, although some progress has been made. Due to space limitations, this review will not be a general review of the subject, but instead will reflect some of my own particular interests although I will try to bias the topics covered to those where significant progress has been made. I will of necessity omit some interesting recent results of several groups, but many of these are discussed in posters and other reviews at this meeting.

For a broad general review of newly formed massive stars see Churchwell (1990; 1991; 1993). Here, I will concentrate mostly on new results that have not been extensively discussed previously. In particular, I will discuss: 1) a possible technique to detect the hot, wind-shocked inner cavity within UC HII regions which, at the same time, may also solve a problem with the origin of the disk component of the Fe XXV 6.7 kev line; 2) the variations of density and temperature within a particular cometary UC HII region and consider implications for heating and cooling processes within the nebula; 3) high velocity molecular outflows associated with newly formed (or forming) massive stars; and 4) recent high spatial resolution observations of hot, dense molecular cloudlets associated with UC HII regions and their possible relationship to the next generation of star formation.

II. Central, Hot, Wind-Shocked Cavities

A stellar wind supported bow shock model for cometary and core/halo UC HII regions has been suggested by Wood and Churchwell (1989), Van Buren *et al*. (1990), Mac Low *et al.* (1991), and Churchwell (1990, 1991) to explain the large number, morphologies, relative motions of ionized and molecular gas, the presence and distribution of OH and H_2O masers, and other observed properties of UC HII regions. A schematic of a wind-supported bow shock is shown in Figure 1. Here, we are interested in the possibility of confirming the presence of a hot, low density, wind-shocked cavity inside the observed UC HII region. A plasma with $T_e \geq 10^7$ K and $n_e \leq 10^2$ cm^{-3} would provide the internal pressure to prevent the cavity from "filling in" on sound

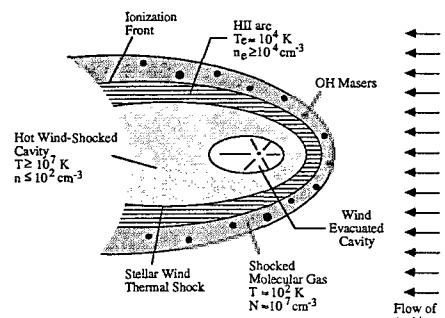

Figure 1. Schematic of a wind-supported bow shock assosciated with an O star moving supersonically through a molecular cloud. The rest frame is that of the star. See Churchwell (1991) for further discussion.

crossing time scales (a few thousand years) due to flows from the dense HII shell. Such conditions could be provided by the fast stellar winds from O and B stars.

Yamauchi and Koyama (1993) have reported extended Fe XXV 6.7 keV line emission from the galactic ridge and the galactic bulge. The integrated luminosity in the Fe XXV 6.7 keV line from the galactic ridge was measured to be $6.5\pm1.3 \times 10^{36}$ ergs s^{-1} with a scale height of only 100±20 pc. The luminosity in this emission line component accounts for ~7% of that in the 2-10 keV band and it is consistent with gas temperatures in the range $3\text{-}10\times10^{7}$ K. The confinement of gas this hot to such a thin layer in the galactic disk is very difficult to understand. It is also interesting that the scale height of the Fe line emission is about equal to that of O stars from the galactic plane (see Wood and Churchwell 1989; White, Becker, and Helfand 1991; Helfand *et al.* 1992).

Alternatively, a major fraction of the Fe line emission from the galactic ridge may be produced in the hot, wind-shocked central cavities of UC HII regions. Because opacity depends on frequency as ν^{-3}, 6.7 keV photons are not significantly attenuated by the surrounding molecular cloud or hydrogen along the line of sight. In the following, I will estimate the luminosity in the 6.7 keV line from a single UC HII region in two ways and show that the total 6.7 keV luminosity of all UC HII regions combined could produce a major fraction, if not all, of the galactic ridge emission. From Mewe *et al.* (1985), we find that the 6.7 keV line is a blend of 3 Fe transitions, which together have a cooling rate of 5.8×10^{-25} erg cm^3 s^{-1} at a temperature of 6.3×10^{7} K; this represents about 3% of the total cooling rate. Thus, the luminosity in the line is $L_{6.7}(\text{erg s}^{-1})$ $=5.8\times10^{-25}$ $EM_V(cm^{-3})$ where EM_V is the volume emission measure. From high resolution radio images, we estimate an average hot core radius of $\sim4\times10^{17}$ cm and an average density of ~100 cm^{-3}, resulting in an $EM_V\sim2.7\times10^{57}$ cm^{-3} and $L_{6.7}\sim2\times10^{33}$ erg s^{-1} per UC HII region or a total luminosity of the disk from ~2000 nebulae of $\sim3\times10^{36}$erg s^{-1}. Within the accuracy of this estimate, this is equivalent to the observed disk luminosity in the 6.7 keV line. A second, independent, method of estimating the 6.7 keV luminosity is to examine the properties of O star winds. Using data tabulated by Leitherer and Lamers (1993) for main sequence O stars, we can estimate wind luminosities $L_w = (1/2)\dot{M}_w v_w^2$ where $\dot{M}_w$ is the stellar mass loss rate and v_w is the wind terminal velocity. For ZAMS stars hotter than O8, typical values are $v_w \approx 2500$ km s^{-1} and $\dot{M}_w \approx$ 10^{-6} solar masses per year, resulting in $L_W\sim2\times10^{36}$ erg s^{-1}. We empirically estimate that ~5% of L_W goes into heating the cavity to temperatures of several keV from measured X-ray fluxes of the UC HII regions W3B and G25.40 with the IPC aboard the Einstein satellite. About 3% of this is radiated in the 6.7 keV line. Thus we find that $L_{6.7}\sim3\times10^{33}$ erg s^{-1} per UC HII region, which is essentially the same as we found from the emission measure of the hot cavity.

A theoretical spectrum at X-ray energies is shown in Figure 2 for the UC HII region W3B. This spectrum was calculated using software provided by the ASCA satellite facility assuming a 40,000 s integration time, a source temperature equivalent to 5 keV, a 1-10 keV X-ray flux of 8.5×10^{-11} erg cm^{-2} s^{-1} (based on the spectral type of the ionizing star and its expected average wind strength) attenuated by a H column density of 6×10^{23} cm^{-2}. The dominant features in this spectrum is the 6.7 keV line, an

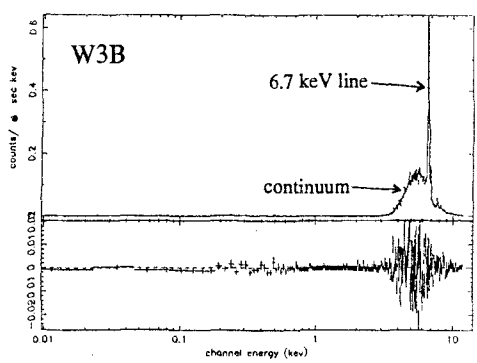

Figure 2. Simulated X-ray spectrum of W3B for a 40,000 s observation with the ASCA satellite. The source is attenuated by 6×10^{23} cm^{-2} H-atoms and has a temperature of 5 keV. The statistical noise (source + background) is shown in the lower panel.

underlying 3-10 keV continuum, and several weaker Fe lines between 7-10 keV. If the model assumptions are correct, the 6.7 keV line should be relatively easy to detect from single UC HII regions by the ASCA satellite with its much smaller beam and higher sensitivity than previous X-ray telescopes.

In Figure 3, we show the distribution of 6.7 keV ridge emission ($b \leq 2^o$) measured by Yamauchi and Koyama (1993) with the Ginga satellite. The solid curve is their fit to the Ginga data. We estimate the Fe line flux from UC HII regions (indicated by a diamond in Fig. 3) at $l=27^o$ in a $1^o \times 2^o$ field of view by assuming that about 2/3 of all UC HII regions (i.e. O8 and hotter ionizing stars) have winds strong enough to contribute to the 6.7 keV line; each has a luminosity of 1.6×10^{33} erg s^{-1} in the 6.7 keV line; and, they are uniformly distributed in a ring between 4 to 7 kpc from the galactic center. We find an Fe line flux of ~1.8 photons s^{-1} $beam^{-1}$ (see the diamond at $l=27^o$ in Fig. 3), compared to a measured value of ~2 photons s^{-1} $beam^{-1}$. This gives strong support to the hypothesis that UC HII regions may produce a large fraction (if not all) of the Fe line flux observed by Ginga to be narrowly confined to the galactic disk. It also would provide an important new tool to study hot central cavities of UC HII regions which has so far only been inferred from indirect evidence but never observed directly.

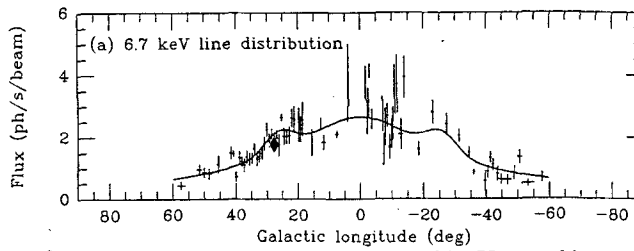

Figure 3. The 6.7 keV ridge emission measured by Yamauchi and Koyama (1993). The solid curve is their fit to the data. The diamond at $\ell=27^o$ is our estimate of the Fe line emission from all UC HII regions ionized by O8 stars or hotter along this line of sight.

III. Heating and Cooling in UC HII Regions

In this section, I will summarize the results of a detailed analysis of the distribution of temperature (T_e), density (n_e), and radial velocity of H^+ in the cometary UC HII region G29.96-0.02 by Afflerbach *et al.* (1994; hereafter ACHK94). This is of interest because together, these properties have important implications for local heating and cooling processes in the nebula and provide data required to distinguish between proposed morphological models. Previous studies of this nebula include an analysis of high resolution (0.5") H76α observations by Wood and Churchwell (1991; hereafter WC91) and a theoretical bow shock model for the nebula constrained by the data of WC91 by Van Buren and Mac Low (1992).

ACHK94 used high spatial resolution observations of H110α, H76α, H66α, and H42α lines toward G29.96-0.02 to obtain directly the distribution of radial velocity and line width (FWHM) in the nebula. The distributions of T_e and n_e were obtained by requiring that a nonLTE model reproduce the line-to-continuum ratios of all lines convolved to a given spatial resolution. The nonLTE model included electron impact broadening and stimulated emission as well as the departure of the b_n coefficients from unity. Although conclusions from this study are still preliminary, the results are interesting because they appear to require modifications of the standard heating and cooling mechanisms usually considered in the energy budget of HII regions.

I will first briefly summarize the multi-line results of ACHK 94 and then discuss how they relate to the heating and cooling processes in the nebula. The distribution of line velocities and line widths basically confirm the results of WC91 and support the bow shock model as shown by Van Buren and Mac Low (1992). The distribution of n_e is about what one would expect for a bow shock. The densities are highest along the leading edge of the parabolic ionized arc with typical

values n_e~$6x10^4$ cm^{-3} (averaged over a 1.7" HPBW), and they fall off to values of ~10^4 cm^{-3} at a distance of ~0.25 pc behind the arc. These values are also consistent with the brightness distributions of the free-free continuum emission observed at all 4 wavelengths.

The most interesting result of this study is the temperature distribution in G29.96-0.02. It was found that the minimum temperature in the entire nebula is T_e~6500±400 K at the apex of the ionized arc with a rapid increase to 8000±800 K 0.25-0.30 pc (7" - 8") behind the arc in the tail of the cometary structure (see Figure 4). The derived temperature gradient appears to be significant. I will assume that this is the case and discuss its implications, although independent observational confirmation is clearly required. Given that the apex of the ionized arc has the highest density, one would expect the hottest region of the nebula to be at the apex because the high densities here will collisionally quench many of the main cooling lines; also, this region receives the full brunt of shock heating from the stellar wind terminal shock in addition to the maximum photoionization heating rate due to its proximity to the ionizing star. Thus, it is surprising to find that the lowest temperature in the nebula lies at the apex.

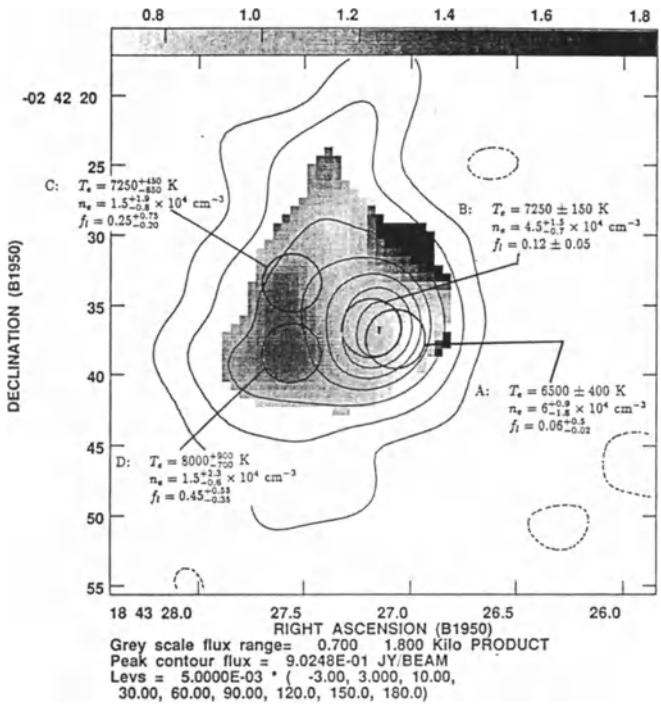

Figure 4. The 6 cm continuum contours (HPBW=4.2") toward G29.96-0.02 with the integrated H110α line-to-continuum ratio superimposed in gray scale. The nonLTE results for T_e and n_e are shown at locations A-D. f_l is the line of sight filling factor.

What could produce such an inverted temperature structure? Obviously a very efficient cooling mechanism is required in the region of the apex because there is no way to avoid a large heating rate in this region. A possible way to achieve this is to feed cold dust grains from the ambient molecular cloud into the ionized arc. As the UC HII region plunges through the molecular cloud core, the cold ambient grains are likely to pass through the neutral bow shock and enter the ionized arc. This will be especially true at the apex where the surface of the I-front is perpendicular to the direction of motion. At a relative speed of 10 km s^{-1}, it will require 3-5x10^3 yr for a grain to travel across the ionized arc using the dimensions found by WC89. Near the apex, the flux of ionizing photons from the star is ~10^{14} cm^{-2} s^{-1}, and the average time between photon impacts with a grain of size 0.05 μm is ~10^{-4} s. The grains will be slowly destroyed as they move closer to the central star, but may play an important role in the temperature structure in the region where they survive. Although the photoelectric effect may contribute to heating in this environment, cooling due to collisions of protons and electrons with much cooler grains and absorption of UV

photons by grains rather than atoms is likely to dominate in this high density environment because of the high radiative efficiency of grains. In the bow shock model, there is a continuous supply of cold dust grains from the ambient molecular cloud as long as the star remains in the molecular cloud. To determine if this hypothesis has any merit, a realistic model should be developed that includes a continuous influx of cold grains into the HII region.

IV. Molecular Outflows Associated with Massive Star Formation

The study of the early stages of massive star formation is complicated by the fact that massive stars have much shorter pre-main sequence (PMS) time scales than low mass stars. Consequently, they spend their entire PMS lifetime and a significant fraction of their main sequence lifetime embedded in the molecular cloud out of which they formed. If high mass stars form according to the scenario proposed by Shu *et al.* (1987), then an accretion disk will be created and accretion of matter through the disk will be accompanied by bipolar molecular outflows. Thus, identification of high-mass stars in an active accretion phase is to identify those with bipolar molecular outflows.

An important recent discovery is that several newly formed or forming massive stars are at the center of massive, luminous molecular outflows (Lada 1985; Harvey and Forveille 1988; Cesaroni *et al.* 1991; Garden and Carlstrom 1992; and Fukui *et al.* 1993). This is an important result for several reasons. One, it links massive star formation with that of low mass stars. A conclusion Lada (1985) had already arrived at based on the association of massive PMS stars with high velocity H_2O maser components and broad infrared hydrogen recombination lines. Two, it may indicate that the ionizing stars of UC HII regions are still accreting matter and thus are PMS objects. However, continuing accretion by OB stars that have produced a detectable HII region and have strong ionized winds would be a fundamental departure from the commonly held notion that such stars have already shut off accretion and settled onto the main sequence. This could still be true if the molecular outflows are no longer being driven but are relics of an earlier accretion phase or the outflows originate from a low-mass star close to the central star of the HII region. Three, it indicates that even during their formation process, massive stars inject large amounts of mechanical energy and momentum into the surrounding molecular cloud. The outflows may contribute substantially to the turbulent motions that help support molecular clouds. Harvey and Forveille (1988) derived a mechanical luminosity of 1600 $L_\odot$ for the outflow associated with G5.89-0.39; this is the most luminous molecular outflow yet detected. Do the outflows scale with luminosity of the star? Perhaps, but not enough is known about them to answer this question at present.

A fundamental question raised by the presence of large, massive, molecular outflows apparently from newly formed O stars is their relationship to the very fast, ionized winds from the star. Essentially all luminous O stars have fast, ionized, radiatively driven winds whose mass loss rates are proportional to the stellar luminosity to the ~1.6 power (Abbott *et al.* 1980; Garmany and Conti 1984; Abbott 1985). Thus, the more luminous the star the stronger its wind is expected to be. It is not known, however, whether the winds are isotropic, confined to an equatorial disk, flow preferentially out the poles, or have fast polar winds and slower but denser equatorial outflows. The geometry of the wind will be enormously important in determining if they play an important role in shaping the morphologies of the HII regions and if they could possibly be the driving force behind the molecular outflows found further from the star. Shu, Adams, and Lizano (1987) have estimated that the momenta carried by the winds of low-mass YSOs are insufficient to account for the cold molecular outflows by more than an order of magnitude. In G5.89-0.39 this also seems to the case. However, Margulis and Snell (1989) have suggested that high velocity CO outflows could arise from molecular gas entrained in a high velocity neutral (HI) stellar wind; this remains to be demonstrated. For young massive stars, it appears likely, though not proven, that the outflows are produced as part of the accretion process and occur prior to the establishment of the steady ionized stellar wind. In this case, the primary energy source would be gravitational rather than radiative.

Recently, Aitken *et al.* (1993) found evidence for toroidal magnetic fields that are parallel with inferred disks associated with massive YSOs. They give a good discussion of the possible

relationships between accretion disks, IR polarization, and molecular outflows associated with massive YSOs. They also summarize the various models that have been proposed for molecular outflows and conclude that their data do not support the model of Pudritz and Norman (1983, 1986). Aitken *et al.* (1993) also argue on general grounds that the driving force for the outflows must originate close enough to the central star that gravity can supply the required energy for the flow.

Keto, Ho, and co-workers have found evidence for accretion and spin-up with decreasing distance to the central star of G10.6-0.4 (Ho, Haschick 1986; Keto, Ho, Reid 1987; Keto, Ho, Haschick 1988; and others). Wilner (1993), Welch *et al.* (1987), and Rudolph *et al.* (1990) have also found evidence for accretion in G5.89, W49, and W51, respectively, from redshifted HCO^+ seen in absorption against the radio continuum. In these sources, we have direct observational evidence for infall close to the central source and outflow of molecular gas on larger scale sizes.

In an attempt to determine what fraction of UC HII regions have associated high velocity (HV) molecular gas, Shepherd and Churchwell (1994) have begun a sensitive, single dish CO survey to detect weak, broad, line wings toward about 100 UC HII regions. Preliminary results from the first phase of this study indicate that 47% of the observed sample have line wings of full width at zero intensity (FW) >50 km s^{-1} and >80% of the sample have FW >25 km s^{-1}. Since these data were obtained with a HPBW of ~60", we do not know if the HV CO gas originates at the UC HII region, nor the morphology of the gas motions (i.e. infall, bipolar outflow, rotation, etc.). If the HV CO gas turns out to be outflows from the UC HII regions, this would rule out relic outflows since only a few percent of newly formed embedded stars are expected to have detectable relic outflows at any given time. A histogram is shown in Figure 5 of the distribution of line wing FWs so far available. Apparently, most HV CO has FWs of ~40-50 km s^{-1}, but a few have FWs as large as 250 km s^{-1}. We expect the distribution in Fig. 5 to become better defined in the coming year because we hope to increase the sample by at least a factor of three.

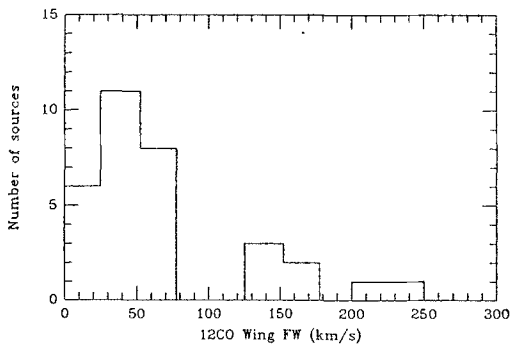

Figure 5. The number of UC HII regions versus ^{12}CO line widths (FW=full width at zero intensity;Shepherd and Churchwell 1994).

In conclusion, the discovery of molecular outflows from UC HII regions presents a powerful way to identify and study the early phases of massive star formation. However, the extent and variety of high resolution data are too sparse to answer many of the most interesting questions, but this is rapidly changing (see review by Sargent and Welch 1993).

V. The Next Generation

Is there evidence for the next generation of stars in the vicinity of UC HII regions? Can we recognize and study the properties of the regions where the next surge of star formation is likely to occur? In the following, I will argue that the answer to both questions is yes.

Plume, Jaffe, and Evans (1992) find that 58% of 179 massive star formation regions have nearby dense molecular gas from which the next generation of stars could form. The masses of the dense molecular clumps mapped by Harju, Walmsley, and Wouterloot (1993) in the Orion and Cepheus clouds indicate that they are massive enough to provide the raw material for further massive star formation.

A series of single dish molecular line studies by Churchwell, Walmsley, and Cesaroni (1990); Cesaroni *et al.* (1991); Churchwell, Walmsley, and Wood (1992); and Cesaroni, Walmsley, and Churchwell (1992) has demonstrated that hot (T_k > 50 K), dense (>10^5 cm^{-3}), molecular clumps are associated with UC HII regions. The excitation analysis of the four lowest inversion

transitions of ammonia toward ~15 UC HII regions by Cesaroni, Walmsley, and Churchwell (1992), in particular, has revealed two nebulae (G10.47 and G31.41) toward which NH_3 optical depths in the (4,4) and (5,5) lines are >100, column densities are ~$4x10^{19}$ cm^{-2}, and relative abundance is ~10^{-5}.

In an attempt to resolve the hot, dense, NH_3 emission regions and to determine their spatial relationships to the HII regions, Cesaroni *et al.* (1994) and Hofner *et al.* (1994) have obtained VLA images in the NH_3 (4,4; and 5,5) lines toward several UC HII regions. They found that the high excitation NH_3 emission originates from very small, optically thick clumps with kinetic temperatures of 50-200 K, average densities ~10^7 cm^{-3}, NH_3 column densities of ~$2x10^{18}$ to ~10^{19} cm^{-2}, cloud virial masses of ~140 to 285 $M_\odot$, and sizes ~0.1 pc. The high densities require that the gas and dust be essentially in temperature equilibrium; thus, the dust emission from these clumps should peak in the range 15-60 μm. The luminosities of the dense, molecular clumps lie in the range $2x10^4$ to $4x10^6$ $L_\odot$; these are too large to reasonably expect an outside heat source to provide. These clumps can intercept only a small fraction of the UC HII luminosity. It, therefore, appears almost unavoidable that the clumps are heated from internal sources, which we suspect are embedded protostars that are not yet emitting enough UV photons to produce a detectable HII region. Strong support for this interpretation is provided by recent high resolution VLA observations of water masers (Hofner *et al.* 1994) toward all the nebulae where high density NH_3 clumps have been imaged. Hofner *et al.* (1994) found that the H_2O masers are located in the NH_3 clumps, not around the edge of the UC HII region as we initially expected. The spatial correlation of H_2O masers with NH_3 clumps is striking, a typical example of which is shown in Figure 6. We strongly suggest that cloudlets of compact NH_3 (4,4) or (5,5) emission accompanied by coincident H_2O masers are the sites of the next generation of star formation. Further, they should also be bright at wavelengths of 15-60 μm as compact, warm clumps that are not generally coincident with the UC HII region or with hot main sequence stars.

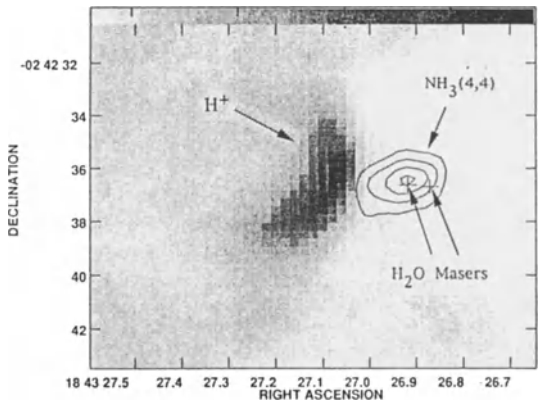

Figure 6. The 1.3 cm continuum (gray scale), the NH_3 (4,4) thermal clump, and the H_2O maser components toward G29.96+0.19.

I conclude by showing two figures from Hofner *et al.* (1994) which they argue is a spectacular example of successive star formation. In Figure 7a, we show Figure 1 from Hofner *et al.* (1994) which is a VLA C/B hybrid configuration, 6 cm, continuum image of the G9.62+0.19 HII region complex. In this figure, one sees very clearly 4 HII regions designated A-D, with size decreasing and continuum brightness systematically increasing from A to D. The area imaged in Figure 7b is indicated by the box enclosing regions B-E; the synthesized beam is indicated at the lower left of the figure. Figure 7b is Figure 6 of Hofner *et al.* (1994). Most striking in this image is the thin line of masers and the hot ammonia clump lying between the UC HII regions C and D. Not shown here is a very compact continuum source indicated by E in Fig. 7a at the position of the only known NH_3 (5,5) maser (filled triangle) in the galaxy. Hofner *et al.* (1994) argue that current star formation is occuring along this string of masers and hot, dense NH_3 clumps lying between the UC HII regions C and D. They speculate that this structure, based on its thin ($\lesssim$ 0.2 pc in projection), linear (~0.6 pc long) morphology which lies just to the east of and almost parallel to

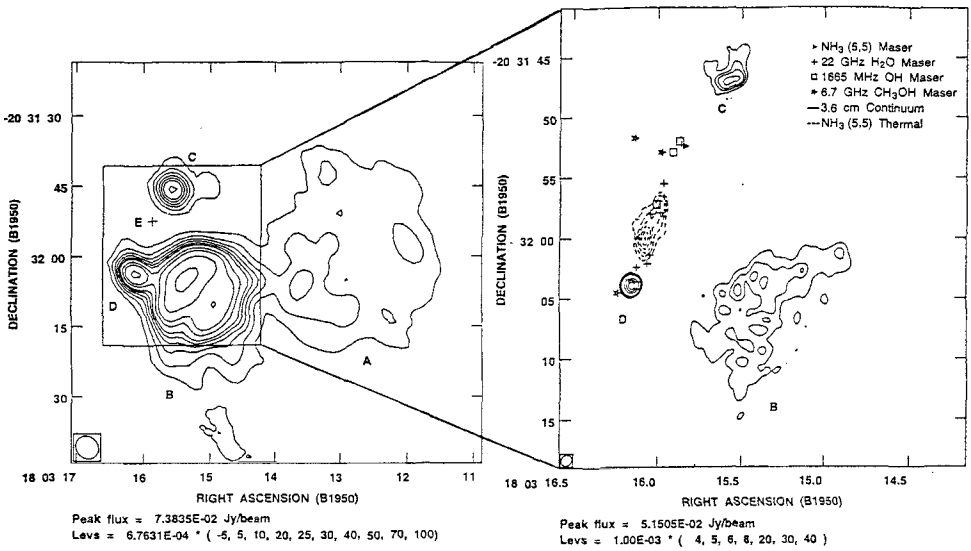

Figure 7a. A VLA 6 cm continuum image of G9.62+0.19. The HPBW is indicated at lower left. 7b. A VLA 3.6 cm continuum image with the thermal NH_3 (5,5) emission, H_2O masers, OH masers, CH_3OH masers, and the NH_3 (5,5) maser shown to scale. From Hofner *et al.* (1994).

HII region B, may be the result of shock compression ahead of the cometary HII region B. Further study will be required to confirm or disprove this.

Acknowledgements

I wish to thank all my coworkers and colleagues who have contributed to the work reported in this review with ideas, figures, and comments on the manuscript; in particular, I wish to thank Peter Hofner, Stan Kurtz, Deborah Shepherd, Andrew Afflerbach, Riccardo Cesaroni, and Malcolm Walmsley (with whom I have enjoyed collaboration for more than 20 years).

References

Abbott, D. C. 1985, in *Radio Stars*, eds. R. M. Hjellming and D. M. Gibson, Reidel Pub. Co., Dordrecht, p. 61.

Abbott, D. C., Bieging, J. H., Churchwell, E., Cassinelli, J. P. 1980, Ap. J., **238**, 196.

Afflerbach, A., Churhcwell, E., Hofner, P., Kurtz, S. 1994, in preparation (ACHK94).

Aitken, D. K., Wright, C. M., Smith, C. H., Roche, P. F. 1993, MNRAS, **262**, 456.

Cesaroni, R., Churchwell, E., Hofner, P., Walmsley, C. M., Kurtz, S. 1994, Ast. Ap., submitted.

Cesaroni, R., Walmsley, C. M., Kömpe, C., Churchwell, E. 1991, Ast. Ap., **252**, 278.

Cesaroni, R., Walmsley, C. M., Churchwell, E. 1992, Ast. Ap., **256**, 618.

Churchwell, E. 1990, Ast. Ap. Rev., **2**, 79.

Churchwell, E. 1991, in *The Physics of Star Formation and Early Stellar Evolution*, eds. C. J. Lada and N. D. Kylafis, Kluwer Acad. Pub., Dordrecht, p. 221.

Churchwell, E. 19993, in *Massive Stars: Their Lives in the Interstellar Medium*, eds. J. P. Cassinelli and E. B. Churchwell, A. S. P. Conf. Series, **35**, 35.

Churchwell, E., Walmsley, C. M., Cesaroni, R. 1990, Ast. Ap. Suppl., **83**, 119.

Churchwell, E., Walmsley, C. M., Wood, D. O. S. 1992, Ast. Ap., **253**, 541.

Fukui, Y., Iwata, T., Mizuno, A., Bally, J., Lane, A. P. 1993, in *Protostars and Planets III*, eds. E. H. Levy and J. I. Lunine, p. 603.

Garden, R. P., Carlstrom, J. E. 1992, Ap. J., **392**, 602.
Garmany, C. D., Conti, P. S. 1984, Ap. J., **284**, 705.
Harju, J., Walmsley, C. M., Wouterloot, J. G. A. 1993, Ast. Ap. Suppl., **98**, 51.
Harvey, P. M., Forveille, T. 1988, Ast. Ap., **197**, L19.
Helfand, D. J., Zoonematkermani, S., Becker, R. H., White, R. L. 1992, Ap. J. Suppl., **80**, 211.
Ho, P. T. P., Haschick, A. D. 1986, Ap. J., **304**, 501.
Hofner, P., Kurtz, S., Churchwell, E., Walmsley, C. M., Cesaroni, R. 1994, Ap. J., submitted.
Keto, E. R., Ho, P. T. P., Reid, M. J. 1987, Ap. J., **323**, L117.
Keto, E. R., Ho, P. T. P., Haschick, A. D. 1988, Ap. J., **324**, 920.
Lada, C. J. 1985, Ann. Rev. Ast. Ap., **23**, 267.
Leitherer, C., Lamers, H. G. L. M. 1993, Ast. Ap., -------?
Mac Low, M.-M., Van Buren, D., Wood, D. O. S., Churchwell, E. 1991, Ap. J., **369**, 395.
Margulis, M., Snell, R. L. 1989, Ap. J., **343**, 779.
Plume, R., Jaffe, D. T., Evans, N. J. II 1992, Ap. J. Suppl., **78**, 505.
Pudritz, R. E., Norman, C. A. 1983, Ap. J., **274**, 677.
Pudritz, R. E., Norman, C. A. 1986, Ap. J., **301**, 571.
Rudolph, A., Welch, W. J., Palmer, P., Dubrulle, B. 1990, Ap. J., **363**, 528.
Sargent, A. I., Welch, W. J. 1993, Ann. Rev. Ast. Ap., **31**, 297.
Shepherd, D. S., Churchwell, E. 1994, in preparation.
Shu, F. H., Adams, F. C., Lizano, S. 1987, Ann. Rev. Ast. Ap., **25**, 23.
Van Buren, D., Mac Low, M.-M. 1992, Ap. J., **394**, 534.
Van Buren, D., Mac Low, M.-M., Wood, D. O. S., Churchwell, E. 1990, Ap. J., **353**, 570.
Wood, D. O. S., Churchwell, E. 1989, Ap. J. Suppl., **69**, 831.
Welch, W. J., Dreher, J. W., Jackson, J. M., Tereby, S., Vogel, S. N. 1987, Science, **238**, 1550.
White, R. L., Becker, R. H., Helfand, D. J. 1991, Ap. J., **371**, 148.
Wilner, D. 1993, Ph. D. Thesis, University of Calif. Berkeley.
Wood, D. O. S., Churchwell, E. 1989, Ap. J. Suppl., **69**, 831 (WC89).
Wood, D. O. S., Churchwell, E. 1991, Ap. J., **372**, 199 (WC91).
Yamauchi, S., Koyama, K. 1993, Ap. J., **404**, 620.

High-Resolution $C^{34}S$ Images of the W51 Region Taken with the Plateau de Bure Interferometer

Keven I. Uchida, Helmut Wiesemeyer, and Rolf Güsten

Max-Planck-Institut für Radioastronomie, Postfach 2024,
53010 Bonn, Germany

1. Introduction

We present the results of a high resolution (3″ beam) $C^{34}S$ J=2-1 (3.1 mm) study of the W51 star forming region performed with the Plateau de Bure interferometer. We utilize this optically-thin isotope of CS to probe the physical properties of the high density molecular condensations and to better detail their distribution with respect to the numerous H II regions, maser and IR sources contained within the region.

2. Observational Parameters and Analysis

Three fields, centered on the W51d, W51e, and W51f subregions, were observed between 22 Oct 1991 and 01 Jan 1992 with the BC configuration of the Plateau de Bure interferometer (see, for example, Sievers *et al.* 1991 for the large-scale morphology). The correlator setup used provided a velocity resolution of 0.495 km $\cdot$ s^{-1}. The continuum was recorded simultaneously with a separate 500 MHz broadband backend. The synthesized beam is 3.″6 x 1.″8 in size and has a position angle of 22° in all three fields; the primary beam has a FWHM of 55″.

Clump parameters, including FWHM sizes, velocities, and FWHM velocity widths, were determined with a 2-D Gaussian deconvolution program. Total clump masses ($H+H_2$), based on the observed $C^{34}S$ line intensities, were determined with a CS excitation code (with LVG assumption) and those based on the observed dust continuum fluxes were determined with the relations developed by Mezger *et al.* (1986). The detailed results will be presented in Uchida, Wiesemeyer & Güsten (1994).

3. Results

3.1 The W51d Subregion

Figure 1 is a greyscale image of $C^{34}S$ line emission, at 63.2 km $\cdot$ s^{-1}, toward the W51d subregion. Superposed on the grayscale are contours of the 3.1 mm continuum. Some of the H_2O masers in the region are denoted by the circles. The square marks the location of the 20 μm IR source observed by Genzel *et al.* (1982) and the cross marks the position of the prominent compact H II region referred to as W51d.

As shown in an earlier molecular study (HCO^+, $H^{13}CN$, and SO) done by Rudolf *et al.* (1990), the bulk of the millimeter continuum emission is coincident with the W51d H II region, while the molecular emission is clearly offset toward the south. The new observations, however, resolve what was previously seen as a single elongated molecular clump, aligned in an east-west orientation, into two spatially- and velocity-distinct subclumps. Based on the observed $C^{34}S$ line intensities, we determine total masses of 1 x 10^4 $M_\odot$ and 9 x 10^2 $M_\odot$ (for the eastern and western clumps, respectively) which are an order of magnitude larger than their corresponding virial masses. This large discrepancy is likely due to the CS abundance value used — for lack of a value which is more appropriate for the hot and dense molecular cores observed here, we utilized the abundance value of 3 x 10^{-9} measured in quiesent clouds (Blake *et al.* 1987). The implied densities of the eastern and western clumps are 3 x 10^9 cm^{-3} and 7 x 10^7 cm^{-3}, respectively, very high even when considering the uncertainty in the CS abundance ratio.

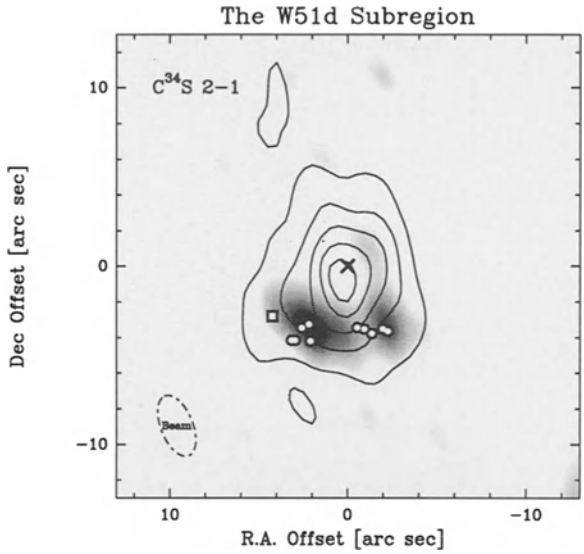

Figure 1: The W51d subregion. The 63.2 km $\cdot$ s^{-1} line emission is displayed in grayscale and the 3.1 mm continuum in contours. Contour levels 0.12 to 0.92 by 0.2 Jy/beam. Map center is at α = 19:21:22.25, δ = 14:25:16.

3.2 The W51e Subregion

Figure 2 displays in grayscale the $C^{34}S$ line emission, integrated between 50.0 and 63.6 km $\cdot$ s^{-1}, toward the W51e region. Superposed on the grayscale image are contours of the 3.1 mm continuum. The compact H II regions W51e2 and W51e1 (as seen at 1.3 and 3.6 cm) are identified by the crosses and some of the H_2O and OH masers in the region are indicated by the circles.

Figure 2 shows that both the 3.1 mm continuum emission and the molecular emission peak locally at about 2″ northeast of the compact H II region W51e1 — no appreciable emission is detected from the H II region itself at this wavelength. We conclude that thermal dust emission dominates the 3.1 mm continuum measured toward this subregion. Based on the observed continuum flux, we determine a total mass of 3 x 10^3 $M_\odot$ for the clump near W51e1. Like those in the W51d region, the derived density of the W51e1 clump is high, about 6 x 10^8 cm^{-3}. Indeed, such high densities lend support to the assertion that these clumps are protostellar condensations.

3.3 The W51f Subregion

We report the first detection of weak 3.1 mm continuum (50 mJy/beam) and line emission toward the W51f subregion (α = 19:21:28.72, δ = 14:23:56). The continuum emission observed here is also attributed to dust, since there is no evidence at longer wavelengths of an associated H II region. Based on the observed dust continuum flux, we determine a total mass of 1 x 10^3 $M_\odot$ within the W51f subregion. The total mass, based on the $C^{34}S$ line intensity, is in rough agreement with this determination.

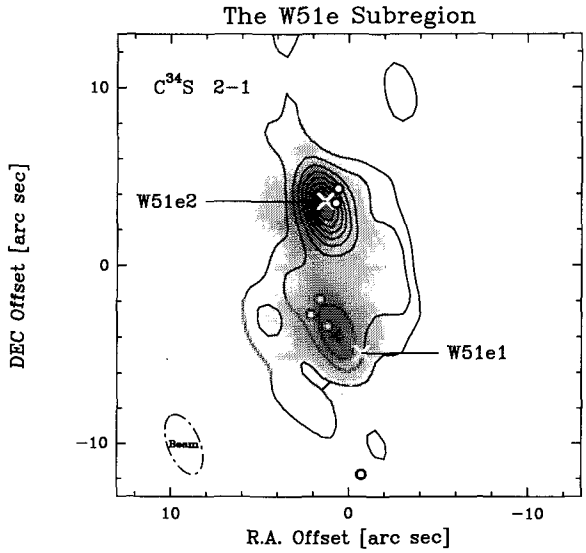

Figure 2: The W51e subregion. The integrated (50.0 to 63.6 km·s^{-1}) $C^{34}S$ emission is displayed in greyscale and the 3.1 mm continuum in contours. Contour levels = 0.2 to 2.0 by 0.1 Jy/beam. Map center is at α = 19:21:26.17, δ = 14:24:38

References

Blake, G.A., Sutton, E.C., Masson, C.R., & Phillips, T.G. 1987, ApJ, 315, 612
Genzel, R., Becklin, E.E., Wynn-Williams, C.G., Moran, J.M., Reid, M.J., Jaffee, D.T., & Downes, D. 1982, ApJ, 225, 527
Mezger P.G., Chini, R., Kreysa, E., & Gemünd, H.-P. 1986, A&A 160, 324
Rudolf, A., Welch, W., Palmer, P., & Dubrulle, B. 1990, ApJ, 363, 528.
Sievers, A.W., Mezger, P.G., Gordon, M.A., Kreysa, E., Haslam, C.G.T., & Lemke, R. 1991, A&A, 251, 231
Uchida, K.I., Wiesemeyer, H., & Güsten, R. 1994, in preparation

The Synthesis of Molecular Line, Neutral Carbon and Dust Continuum Observations in the Molecular Cloud G34.3 + 0.2

L.T. Little

Electronic Eng. Laboratory, Univ. of Kent, Canterbury, Kent CT2 7NT, U.K.

1. Introduction

Molecular cloud cores often show a strong central density concentration, retaining their structural shape over a wide range of scale; sometimes they are highly fragmented. We have determined the structure of the molecular cloud G34.3 + 0.2, as a good example of the former category. Observing G34.3 in several transitions of a single molecule, using the James Clerk Maxwell and Nobeyama 45m telescopes, we model the radiation as accurately as possible in terms of the molecular hydrogen density, temperature and species abundance producing it. Results from different molecules are then compared with each other, and with expectations derived from dust continuum observations and the virial theorem, in an attempt to deduce a self-consistent model. Apparent inconsistencies are likely to provide insight into time-dependent chemistry, uv penetration into cloud cores, and molecular accretion onto and re-evaporation from dust grains.

2. The Structure of G34.3 + 0.2

2.1 Virial mass

G34.3 has a mass of a few thousand $M_\odot$ and lies at a distance of 3.1 kpc. Observed in dust emission at 800 μm, it is the second brightest molecular cloud in the sky, behind Orion. We have mapped G34.3 in the NH_3 inversion lines with telescopes of resolution varying from 140 arcsec to 1.3 arcsec (Heaton et al, 1985; Heaton, Little and Bishop, 1989). It appears on all scales as a single dominant component. Application of the virial theorem to the line widths and dimensions derived from the NH_3 observations yields a density which varies as $r^{-2.1}$ in the range 0.02 pc $< r <$ 1 pc.

2.2 HCO+ Excitation Analysis

Over a period of several years we have mapped G34.3 in the molecular transitions J=1-0 HCO+, J=1-0 $H^{13}CO+$, J=4-3 HCO+ and J=3-2 $H^{13}CO+$, with further observations for J=4-3 $H^{13}CO+$ and J=3-2 HCO+ (Heaton et al, 1993). The maps were made with angular resolutions in the range 16–20 arcsec. Their general roundness justifies the assumption of spherical symmetry in modelling the emission, which has been achieved using a multi-level radiative transfer program employing the Stenholm-Rybicki core saturation approximation.

Power law variation for molecular hydrogen density (as $r^{-1.9}$), kinetic temperature ($r^{-0.4}$) and relative abundance ($r^{0.8}$ or r^0) was assumed to hold from r = 0.008 pc to r = 1.5 pc, which represents the outer boundary of the cloud. The density scaling, abundance scaling and systematic collapse velocity were varied to determine the best fitting power law model. The most important observational parameters that can reasonably be modelled are the peak temperatures of the lines observed towards the source centre, and the angular diameters of the emission from different lines. The principal general defect of the power law model was that the steep rise in density towards the core of the source led to a ratio for J=4-3 to 3-2 HCO+ peak brightness temperature which was too high, and a corresponding J=4-3 HCO+ angular diameter which was too small.

Rather better fits could be produced by introducing cut-offs. The molecular hydrogen density and molecular abundance were set to be constant within a common fixed radius. Details of the best fitting model are given in Table 1.

Table 1. Models derived from CO and HCO+ observations (r in pc)

	CO model	HCO + model
Outer radius (pc)	3.25	1.5
H2 density (cm^{-3})	$4.7 \times 10^3\ r^{-1.9}$ ($r > 0.15$pc)	$7 \times 10^3\ r^{-2.1}$ ($r > 0.1$pc)
	1.7×10^5 ($r < 0.15$pc)	8.8×10^5 ($r < 0.1$pc)
Kinetic temp (K)	$19\ r^{-0.4}$	$32\ r^{-0.4}$
Turbulent vel. ($km\,s^{-1}$)	4.0	5.0
Systematic vel. ($km\,s^{-1}$)	-1.75	-1.5
Abundance	7.5×10^{-6} [^{13}CO]	1.2×10^{-9} [HCO+]
	5.0×10^{-7} [$C^{18}O$]	0.6×10^{-10} [$H^{13}CO+$]

The model fits to the spectra are quite good (excluding the J=1-0 HCO+ transition which is strongly affected by low excitation temperature foreground absorption). The model diameters are still smaller than those observed. One possible explanation is that the actual density distribution is somewhat clumpy and dispersed, so that a particular transition is excited in several regions which lie over a wider area than predicted by the simple model.

The agreement between the virial and HCO+ derived densities is good for $r > 0.1$ pc. The outer region of the cloud is in near-virial equilibrium with a high turbulent component of velocity $\Delta v \sim 5\ km\,s^{-1}$ and a slow collapse ($v_{sys} \sim -1.5\ km\,s^{-1}$).

2.3 Dust continuum emission

We also mapped the 800 μm and 450 μm dust continuum emission in G34.3 with 15 and 8 arc sec resolution respectively (Strong–Jones et al., 1991). Attempts were made to fit a simple power law model to the data. The dust temperature was taken to be the same as the kinetic temperature used for the HCO+ modelling. Assuming a constant dust emissivity and gas/dust mass ratio ($= 100$) a gas density variation as r^{-2} cannot explain the 450 μm flux density distribution. A core–halo distribution is required.

If the emissivity is scaled so that the dust– and HCO+ –derived densities are equal in the outer region ($r > 0.2$ pc) of the cloud, its value agrees better with that suggested by Rowan–Robinson (1986) than with that of Hildebrand (1983).

Both the dust– and HCO+ –derived densities require a marked flattening in their radial variation at smaller radii. Although the radii at which the flattening becomes apparent differ for the two densities (0.1 pc for HCO+ –derived, 0.2 pc for dust–derived), uncertainties in the modelling mean that the differences may not be significant.

2.4 CO modelling

The modelling was further extended to include observations of CO isotopes, in particular J = 1-0, 2-1, 3-2 and 6-5 ^{13}CO and J = 2-1 $C^{18}O$ (Little, Gibb et al., in preparation). The best fitting CO model is compared with that for HCO+ in Table 1. It was necessary to extend the radius of the cloud from 1.5 to 3.25 pc, when CO self absorption could be well accounted for. The most significant difference between the HCO+ and CO models is that the temperatures for CO are only 60 % of those required for HCO+. This result suggests that the assumption of a single temperature and density at a specific radius is incorrect (ie. may support clumping, with the denser clumps, to which HCO+ is more sensitive than CO, being hotter). The CO model gives a good fit to all CO observations, both for line shapes and diameters.

2.5 CI modelling

We recently acquired E-W and N-S strip scans across G34.3 in the 492 GHz CI line. Using the same model for the density and dynamics which works for CO, we find we can fit the key parameters line intensity, diameter, and presence of an absorption dip, if [CI] $\propto r^{0.9}$, implying [CI]/[CO] $\propto r^{0.9}$ (Little, Gibb et al., in preparation). A flatter distribution (putting too much CI in the cloud centre) destroys the absorption; a steeper one leads to absorption at all positive velocities. A distribution with a sharp cut-off at a fixed radius does not match the source diameter while simultaneously producing the appropriate absorption dip. The modelling is sensitive to CI at radii > 0.24 pc. It suggests that [CI] varies from ~ 0.4, at the outer perimeter of the cloud, to 0.04 at $r \sim 0.24$ pc where $A_v \sim 55$, measured into the cloud

from the perimeter. This absolute determination of [CI]/[CO] at high A_v should be useful in formulating chemical theories.

3. Conclusion

G34.3 + 0.2 contains a compact expanding core evident in NH_3 and submillimetre dust emission, and an outer envelope responsible for the emission in all the other lines. The outer envelope is near virial equilibrium but is slowly collapsing onto the core. The density of the outer envelope falls off as r^{-2} beyond a radius of 0.1 – 0.2 pc. Combining dust and line observations in the envelope, we determine the dust emissivity, favouring the grain model of Rowan-Robinson. We also show that [CI]/[CO] varies as $r^{0.9}$ into $r \sim 0.2$ pc where $A_v \sim 55$.

References

Heaton, B.D., Matthews, N., Little, L.T. and Dent, W.R.F., 1985. Mon. Not. R. Astron. Soc. **217**, 485.
Heaton, B.D., Little, L.T. and Bishop, I.S., 1989. Astron. Astrophys. **213**, 148.
Heaton, B.D., Little, L.T., Yamashita, T., Davies, S.R., Cunningham, C.T. and Monteiro, T.S., 1993. A & A **278**, 238.
Hildebrand, R.H., 1983. Q. J. R. Astron. Soc. **24**, 267.
Rowan-Robinson, M., 1986. Mon. Not. R. Astron. Soc. **219**, 737.
Strong–Jones, F.S., Heaton, B.D. and Little, L.T., 1991. A & A **251**, 263.

Methyl Cyanide and Propyne in the Hot Molecular Core G34.3+0.15

G.H. Macdonald and R.J. Habing

University of Kent, Canterbury, U.K.

The ultracompact HII region G34.3+0.15 and its associated hot molecular cloud core lie 3.1kpc from the Sun. High resolution radio continuum maps show that the HII complex comprises two ultracompact ($\sim$ 0.3″) and one compact region (Reid & Ho 1985). The latter has the prototypical "cometary" morphology, with a compact "head" $\sim$ 4″ in size and a 20″ "tail" trailing to the west (Wood & Churchwell 1989). This HII region may have acquired its unusual shape either by relative motion between the young star and the parent cloud (Reid & Ho 1985) or be due to the HII region undergoing a champagne phase expansion from the cloud (Garay et al. 1986). We have made high resolution observations of line emission from the symmetric top molecules propyne (CH_3C_2H) and methyl cyanide (CH_3CN) in the hot molecular cloud core of G34.3+0.15 in an attempt to determine its morphology and temperature structure and to investigate its chemical evolution and detailed relationship with the cometary HII region.

Symmetric top molecules provide excellent temperature probes of molecular clouds. Rotational energy is a function of both J and K quantum numbers, and for electric dipole transitions with selection rules $\Delta J = \pm 1$, $\Delta K = 0$, centrifugal distortion causes the energy gap between J levels to fall as K number increases. This has the effect of splitting spectral lines for a given J transition into several K components representing a wide range of excitation. The line brightness ratio between K components is therefore a strong function of temperature and can be accurately measured independently of calibration problems since all the K lines may be observed simultaneously within a given receiver band. CH_3CN and CH_3C_2H have widely different electric dipole moment, μ (3.9 and 0.78 Debye respectively). Since radiation rate $\alpha\ \mu^2$, a higher temperature is required to excite the higher μ molecule. Propyne is therefore a good thermometer for warm gas ($<$ 100K) and methyl cyanide for hot gas ($>$ 100K).

Excitation temperature can be determined from observations of molecular line emission by two methods: the standard "rotation diagram" method which is not strictly valid since the assumption of LTE conditions is almost certainly incorrect in hot cores, and statistical equilibrium (SE) modelling using the LVG approximation. We have used both methods and compared the results.

The 341.7GHz J = 20-19 transition of CH_3C_2H has been observed with the JCMT. Since the source was unresolved with the 12″ beam, all spectra were averaged to give a good detection of the K = 0...3 lines, but the spectrum is contaminated by strong lines of SO, CH_3OH and HCS^+. SE modelling gives T = 40K, $n(H_2) = 10^6$ cm^{-3}, corresponding to warm gas in an extended halo around the central hot core. The JCMT has also been used to map the 349.4GHz J = 19-18 and 331.0GHz J = 18-17 lines of CH_3CN with $\sim$ 12″ resolution. The molecular cloud was again unresolved and co-adding spectra allowed detection of the K = 0.....7 components. SE modelling yielded temperatures of T = 315 $\pm$15K and 200 $\pm$25K respectively for the two transitions, and the same density, $n(H_2) > 10^7$ cm^{-3}, for each. Rotation diagram analysis of our data, together with lower excitation J = 12-11 and J = 6-5 data from IRAM (Churchwell et al. 1992) and J = 6-5 data from Onsala (Bergman & Hjalmarson 1989) gives excellent agreement in temperature measurement with the SE modelling results and confirms the trend that high J lines probe hotter, denser gas within the cloud core.

In an attempt to resolve the structure of the hot core, observations were made of the 110.3GHz J = 6-5 emission of CH_3CN with the Nobeyama Millimeter Array (NMA). Maps with 4″ resolution show a weak halo extended $\sim$ 10″ NW-SE with a strong unresolved core (Figure 1). Differences in the extended structure in different K components reflects temperature variations but the relatively poor signal to noise ratio does not allow accurate temperature measurement by SE modelling. The extended emission closely matches the 450 μm dust

continuum emission (Strong-Jones et al. 1991). Position-velocity plots reveal a N-S velocity gradient of $\sim$ 200 km s^{-1} pc^{-1}, in the same sense but intermediate between the $\sim$ 1000 km s^{-1} pc^{-1} gradient seen in recombination lines (Garay et al. 1986) and $\sim$ 100 km s^{-1} pc^{-1} in NH_3(3,3) emission (Heaton et al. 1989). The velocity gradient is consistent with rotation about the axis of symmetry of the cometary HII region.

Perhaps the most interesting and exciting new result comes from a comparison of the NMA CH_3CN map and the VLA NH_3(3,3) map (Heaton et al. 1989). The peak NH_3 emission is offset slightly to the north of the axis of symmetry of the cometary HII region and is coincident with the peak of the 450 μm dust emission. Peak CH_3CN emission is found to be displaced 2" NW of the NH_3 peak, an offset much greater than the positional error of either map (Figure 1). Could this morphology arise through a combination of chemical evolution and the relative motion of the young star and the ambient medium? NH_3 molecules form by gas phase reactions during the initial cold accretion of a molecular cloud and freeze out on to dust grains. Subsequent heating of the dust by a newly formed star returns the ammonia to the gas phase where further chemical processing occurs (Charnley et al. 1992). We have computed the time-dependent abundances of NH_3 and CH_3CN using a comparable code to Charnley et al. for 173 species linked by 1801 reactions using initial abundances constrained by hot core observations and standard dark cloud values (e.g. Herbst et al. 1989). For T $\sim$ 300K, n(H_2) $\sim$ 2x10^7 cm^{-3}, we find that the NH_3 abundance falls rapidly by $\sim$ 3 orders of magnitude at an age $\sim$ 10^5 years as the CH_3CN abundance steadily rises. This suggests a scenario in which the NH_3 molecules are evaporated from grains by local heating by a young star embedded in the cometary HII region, swept along by gas flow parallel to the bow shock at the head of the cometary HII region and chemically processed to provide peak CH_3CN abundance $\sim$ 10^5 years later. The 0.04pc displacement of NH_3 and CH_3CN corresponds to a dynamical time $\sim$ 4x10^4 years for a relative velocity between the young star and ambient medium of $\sim$ 1 km s^{-1}. The cometary morphology has been modelled with a wind bow shock by van Buren et al.(1990) and MacLow et al.(1991) assuming a relative wind velocity of 10 km s^{-1}. Our model is supported by three observational features arising from the present study:

(i) the coincidence of peak NH_3 emission with 450 μm emission from warm dust;

(ii) the relative displacement of NH_3 and CH_3CN peak emission corresponds to the direction of laminar gas flow around the cometary HII region;

(iii) the commensurate values for the dynamical time for gas flow around the bow shock between the NH_3 and CH_3CN peak positions and the chemical evolutionary time for significant conversion between these two species.

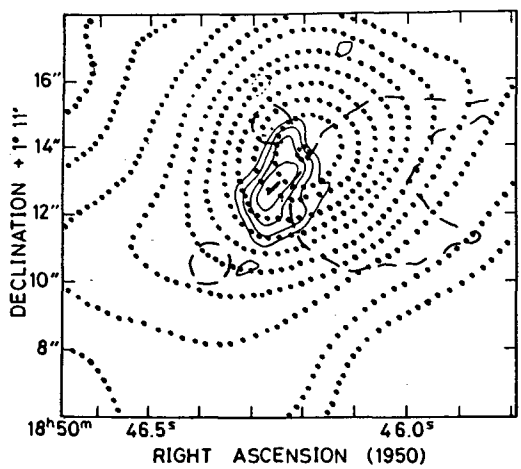

Figure 1

References

Bergman,P.,Hjalmarson,Å. 1989 in *The Physics and Chemistry of Interstellar Molecular Clouds*, ed G. Winnewisser & J.T. Armstrong (Springer-Verlag),p124
Charnley, S. B., Tielens, A. G. G. M., Millar, T. J. 1992, ApJ, 399, L71
Churchwell, E., Walmsley, C. M., Wood, D. O. S. 1992, A&A, 253, 541
Garay, G., Rodriguez, L.F., van Gorkom, J. H. 1986, ApJ, 309, 553
Heaton, B. D., Little, L. T., Bishop, I. S. 1989, A&A, 213, 148
Herbst, E., Millar, T. J., Wlodek, S., Bohme, D. K. 1989, A&A, 222, 205
MacLow, M. -M., van Buren, D., Wood, D. O. S., Churchwell, E. 1991, ApJ, 369, 395
Reid, M. J., Ho, P. T. P. 1985, ApJ, 288, L17
Strong-Jones, F. S., Heaton, B. D., Little, L. T. 1991, A&A, 251, 263
van Buren, D., MacLow, M. -M., Wood, D. O. S., Churchwell, E. 1990, ApJ, 353, 507
Wood, D. O. S., Churchwell, E. 1989, ApJ Suppl Ser, 69, 831

CS $J = 2 - 1$ and HCN $J = 1 - 0$ Observations of Dense Molecular Cores in Regions of Massive Star Formation

I. Zinchenko[1], V. Forsström[2], A. Lapinov[1] and K. Mattila[2]

[1]Institute of Applied Physics of the Russian Academy of Sciences, Uljanov st. 46, 603600 Nizhny Novgorod, Russia

[2]Helsinki University Observatory, Tähtitorninmäki, P.O.Box 14, SF-00014 University of Helsinki, Finland

In this report we present the results of our $J = 2 - 1$ CS and $C^{34}S$ observations of eleven dense cores. In addition, two cores have been partly mapped in the $J = 1 - 0$ HCN line in order to investigate the reasons for the differences between the CS and ammonia maps. We have used the LVG and Monte Carlo radiative transfer modelling to retrieve the physical parameters from our data. In some cases observations of other CS transitions are available. In particular, a comparison with the results of the recent $J = 7 - 6$ CS survey of star forming regions by Plume et al. (1992) is used to improve our estimates for the physical parameters of some sources.

The observations were carried out in 1992–1993 with the 13.7-m radio telescope in Metsähovi[1]. The targets for the observations were selected primarily from the list of dense molecular clouds associated with Sharpless H II regions studied earlier in the $J = 1 - 0$ HCN, $H^{13}CN$, HCO^+ and $H^{13}CO^+$ lines by Burov et al. (1988), Zinchenko et al. (1990) and Pirogov et al. (1993). All clouds chosen from this sample (S68, S88B, S153, S159, S184, S199 and S255) contain bright FIR sources (> 500 Jy at 100 μm) and represent sites of massive star formation except S68 (Serpens Molecular Core) where probably only low and intermediate mass stars are born. Besides, we included in the list the cloud S76E which also contains a powerful infrared source and demonstrates strong maser activity. Finally, we observed also the cloud G 35.2–0.74 (both the S and N components) which is a well-known star-forming region with a strong H_2O maser source. S140 was observed mainly for calibration purposes.

The main results of this study are the following:

1. We observed 11 dense molecular cores associated (with perhaps one exception) with regions of massive star formation in the $J = 2 - 1$ CS and $C^{34}S$ lines and mapped 6 of them in the line of the main isotope. Two cores (S152/153 and S159) have been partly mapped in the HCN $J = 1 - 0$ line.

2. In several clouds where the comparison with NH_3 is possible we found that the CS emitting regions were 2.5–5 times more extended than the ammonia regions mapped by Harju et al. (1993) in Effelsberg with a similar beam width. The CS lines are 1.5–2 times broader. The HCN distributions are closer to the CS than NH_3 distributions.

3. We derived the apparent optical depths of the $C^{34}S$ lines and the CS and $C^{34}S$ column densities, $N_L(CS)$ and $N_L(C^{34}S)$, using the LVG approximation (Table 1). The $C^{34}S$ optical depths were estimated from the peak intensity ratios (τ_p) and from the ratios of the line areas (τ_a). The LTE and LVG results for $N_L(C^{34}S)$ are close to each other. The Monte Carlo simulation yields similar results. There is a correlation between the apparent optical depth and the ratio of the CS and $C^{34}S$ column densities. This ratio decreases with increasing optical depth. Apparently, it indicates that the CS column densities are strongly underestimated. The possible physical reasons for this are the small scale clumpiness in the cores and/or the shielding effect by a low density envelope. However, the data on the HCN hfs ratios do not support the hypothesis of a scattering envelope.

4. The core masses derived from the $C^{34}S$ column densities are close to the virial masses for most sources. The mean hydrogen number densities along the line of sight found from these data are rather low, $n \sim 10^3 - 10^4$ cm^{-3}. The densities determined from

[1]Operated by the Metsähovi Radio Research Station, Helsinki University of Technology

Table 1

Source	T_{kin}	log n	$C^{34}S$				CS	
			τ_p	τ_a	log N_L^{LTE}	log N_L^{LVG}	log N_L^{LVG}(CS)	$\frac{N_L(CS)}{N_L(C^{34}S)}$
	(K)	(cm^{-3})			(cm^{-2})	(cm^{-2})	(cm^{-2})	
S68	20[a]	4.8[a]	0.11(02)	0.19(02)	12.83(08)	12.81(08)	13.97(08)	14.5(4.0)
S76E	20[a]	5.5[a]	0.36(04)	0.64(06)	13.12(03)	12.93(03)	13.62(02)	4.9(0.4)
G35.2S	50[a]	5.0[a]	0.09(01)	0.10(01)	13.16(06)	12.93(08)	14.22(03)	19.5(4.2)
G35.2N	30[a]	5.5[a]	1.20(43)	0.33(06)	12.51(07)	12.24(15)	13.06(07)	6.6(2.8)
			0.39(06)	0.31(03)	12.90(05)	12.63(06)	13.46(03)	6.8(1.0)
S88B	50[a]	5.0[a]	<0.2		<12.5	<12.0	13.17(08)	>15
S140	30[a]	5.8[a]	0.13(01)	0.13(01)	13.07(03)	12.79(03)	14.04(01)	17.8(1.2)
S153	30[a]	5.3[a]	0.25(03)	0.54(07)	13.03(06)	12.77(06)	13.46(02)	4.9(0.6)
S159	80[a]	4.3[a]	0.13(02)	0.02(01)	12.25(06)	12.34(15)	13.74(01)	25.1(7.0)
S184	20[a]	5.0[a]	<0.16		<12.5	<12.2	13.58(01)	>24
S199	40[a]	5.2[a]	0.18(02)	0.74(12)	13.02(05)	12.75(06)	13.39(02)	4.4(0.7)
S255	65[a]	6.0[a]	0.22(02)	0.34(02)	13.08(04)	12.96(05)	13.78(01)	6.6(0.7)

[a]adopted value

the comparison with the CS $J = 7 - 6$ data are 2–3 orders of magnitude higher. This probably implies strong density inhomogeneities in the sources.

5. There are correlations between source size and CS line width, source size and density similar to those found earlier for CO and NH_3 sources as well as for HCN and HCO^+ emitting cores. The absolute values of the velocity dispersion and density as found from CS are somewhat higher than in the CO and NH_3 cores of the same size.

References

Burov, A.B., Kislyakov, A.G., Krasil'nikov, A.A., et al., 1988, SvA Lett. 14, 209
Harju, J., Walmsley, C.M., Wouterloot, J.G.A., 1993, A&AS 98, 51
Pirogov, L.E., Lapinov, A.V., Shul'ga, V.M., Zinchenko, I.I., 1993, in preparation
Plume, R., Jaffe, D.T., Evans, N.J. II, 1992, ApJS 78, 505
Zinchenko, I.I., et al. 1990, SvA 34, 458

Analysis of Maser Proper Motion Kinematics

E. E. Bloemhof

Harvard-Smithsonian Center for Astrophysics, Cambridge, MA 02138 USA

The first measurement of proper motions in an interstellar OH maser source, W3(OH) (Bloemhof, Reid, and Moran 1992), has provided an impetus to seek new analytic methods that can distinguish among competing kinematic models. The key ambiguity in interpreting maser proper motions is that those motions are only known internally, with respect to a single bright and spatially compact maser spot that serves as the phase reference for synthesis mapping at each epoch. The vast difference in surface brightness between maser spots and the HII regions with which they are associated precludes directly determining the overall absolute motion of masers through their environment.

The traditional working model applied to H_2O maser sources has been a spherically-symmetric, constant-velocity outflow (Moran, Reid, and Gwinn 1992). An alternative picture that is suggested by the morphology of the HII region in W3(OH) is a quasi-parabolic cometary bow-shock flow (Van Buren et al. 1990). These two models are examined in some detail by Bloemhof, Reid, and Moran (1992). It is found that the spherical expansion model can be made to work only by imposing an ad-hoc constraint that confines the OH masers to a narrow range of radial positions directly in front of the source. This constraint then assures the narrow range of radial velocities that is one of the kinematic signatures of the OH masers in W3(OH).

It is argued by Bloemhof (1993) that a natural way to distinguish between these competing models is to consider their implications for the quantities directly measured by maser proper motion experiments: the internal velocity dispersions of the masers. These are generalized to form the velocity variance-covariance matrix (VVCM), which is then diagonalized to determine principal axes. One of these would be the cometary axis in the case of a bow-shock flow. In the plane of the sky, the cometary axis for W3(OH) is found to lie at position angle 29°, as shown by the solid lines in Figure 1. The velocity variance eigenvalue corresponding to this (major) axis is substantially larger than the eigenvalue for the minor axis.

The distinctly elliptical nature of the velocity distribution is compatible with the bow-shock model, but not with a spherically symmetric expansion. In the bow-shock model, the existence of an axis with much greater velocity dispersion is easily understood, and the dispersion in radial velocities no longer stands out as unusually small: it is comparable to the dispersion along the minor axis in the plane of the sky. Furthermore, the cometary axis is in general agreement with the flow direction suggested by the trailing contours of radio continuum maps of the HII region. The deviation may be accounted for by the lack of maser spots to sample the velocity field in the southeast part of the source, owing to the known lack of dense molecular material there. When a reasonable correction is applied for this incomplete spatial coverage, the cometary axis is the dashed line at position angle 58°, in striking agreement with the axis suggested by the radio continuum morphology.

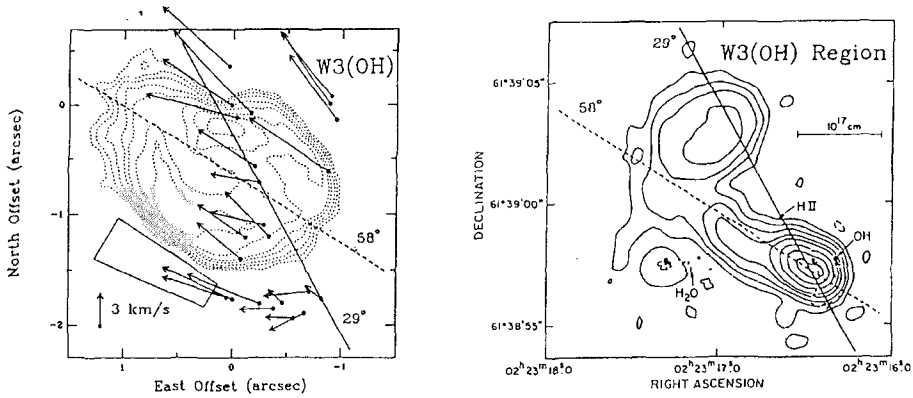

Figure 1 At left are the OH masers in W3(OH) (spots) and their proper motions (arrows) superposed on a 15 GHz radio continuum map of the ultracompact HII region (dashed contours...from C. R. Masson, private communication). The choice of reference feature motion assumed here results in a cometary bow-shock appearance to the velocity field. The cometary axis predicted by VVCM diagonalization is shown as a solid line. When the lack of uniform spatial coverage is taken into account (because, roughly speaking, masers are "missing" from the quadrilateral region drawn on the left figure), the dashed line is the resulting corrected cometary axis.

The spatial distribution of the OH masers has its principal axis at position angle 0°, and the velocity distribution in a spherical expansion would be expected to inherit this principal axis. An estimate of the level of significance at which the internal velocity dispersions are inconsistent with a spherical expansion model may be obtained from a Monte Carlo analysis of the error bars on the VVCM principal axes, taking the experimental errors on the proper motions as inputs. The velocity principal axis (PA = 29° ± 6°) deviates almost 5 σ from the position principal axis (PA = 0°). The lack of masers over the eastern half of the roughly circular HII region has no effect on this discrepancy: in other words, there is no need for a correction for spatial coverage to test the spherical expansion model.

The VVCM analysis summarized here is not a model fitting procedure, since there are no free parameters. The properties of the velocity dispersions are quite objectively known. Further refinements to the technique, including possible objective ways to handle spatial coverage corrections, are under study.

References

Bloemhof, E.E. 1993, ApJ, 406, L75
Bloemhof, E.E., Reid, M.J., & Moran, J.M. 1992, ApJ, 397, 500
Moran, J.M., Reid, M.J., and Gwinn, C.R. 1992, in *Lecture Notes in Physics* **412**, *Astrophysical Masers*, eds. A.W. Clegg and G.E. Nedoluha (New York: Springer-Verlag), 244
Van Buren, D., Mac Low, M., Wood, D.O.S., & Churchwell, E. 1990, ApJ, 353, 570

H_2O and CO Emission towards IRAS Point Sources in Regions of Star Formation

K. Fiegle[1], J.G.A. Wouterloot[1], J. Brand[2]

[1]I. Physikalisches Institut, Universität zu Köln, 50937 Köln, Germany
[2]Istituto di Radioastronomia CNR, 40129 Bologna, Italy

H_2O masers are good indicators for the presence of star formation in molecular clouds. Wouterloot & Walmsley (1986) showed that all H_2O maser sources in regions of star formation are associated with IRAS point sources with specific colours, so that the IRAS Point Source Catalogue can be used to select maser candidates.

We have searched for 22 GHz H_2O maser emission using the 100-m radiotelescope in Effelsberg and the 32-m radiotelescope in Medicina, Italy. The total sample of sources consists of 1390 objects, selected according to their IRAS colour indices. Spectra and line parameters are given in Wouterloot et al. (1993). The H_2O data are compared with results of observations of ^{12}CO(1-0) (and of ^{12}CO(2-1) and ^{12}CO(3-2) in some cases) towards a large fraction of these sources, made with the 30-m IRAM, 15-m SEST or 3-m KOSMA telescopes (Wouterloot & Brand 1989, Wouterloot et al. 1993).

All sources detected in H_2O (162), and the majority of sources not detected in H_2O were observed in CO, so that we could derive kinematic distances for these sources. Using these, FIR luminosities were obtained from the IRAS fluxes. In addition we calculated the H_2O luminosities assuming an isotropic distribution of the maser emission. The main results are the following (an extensive analysis is given by Fiegle et al. (1994)).

- The H_2O maser detection rate increases with FIR luminosity: below $log(L_{FIR}/L_\odot)$=3.5, less than 10% of the sources show maser emission, whereas towards most of the sources above $log(L_{FIR}/L_\odot)$=4.5 H_2O is detected.

- The distribution of differences between the CO and H_2O velocities is a Gaussian with a FWHM of about 11 km/s. The mean velocity difference is zero. Contrary to suggestions by Palagi et al. (1993), the velocity of the peak H_2O emission is not at a preferred location within the velocity interval where emission is detected.

- The average CO linewidth is larger (about 5.0 kms^{-1}) for those sources detected in H_2O, than for sources which were not detected (about 2.7 kms^{-1}). This effect is independent of their FIR luminosity. However the nondetected sources still have larger linewidths than the quiescent gas not related to the IRAS sources (1.9 kms^{-1}).

- There exists an upper limit for the H_2O maser luminosity at a given FIR luminosity. This upper limit is proportional to the FIR luminosity: $log(L_{H_2O})$=$log(L_{FIR}/L_\odot)$−7.4.

- In IRAS colour-colour plots (see Fig.1), sources can be distinguished according to their CO linewidths and FIR luminosity. High L_{FIR} sources with maser emission are bluer than low luminosity sources. Sources with small Δv seldom show maser emission, even if they have the correct colours. Similar effects are seen when considering the T_A^* of the CO emission.

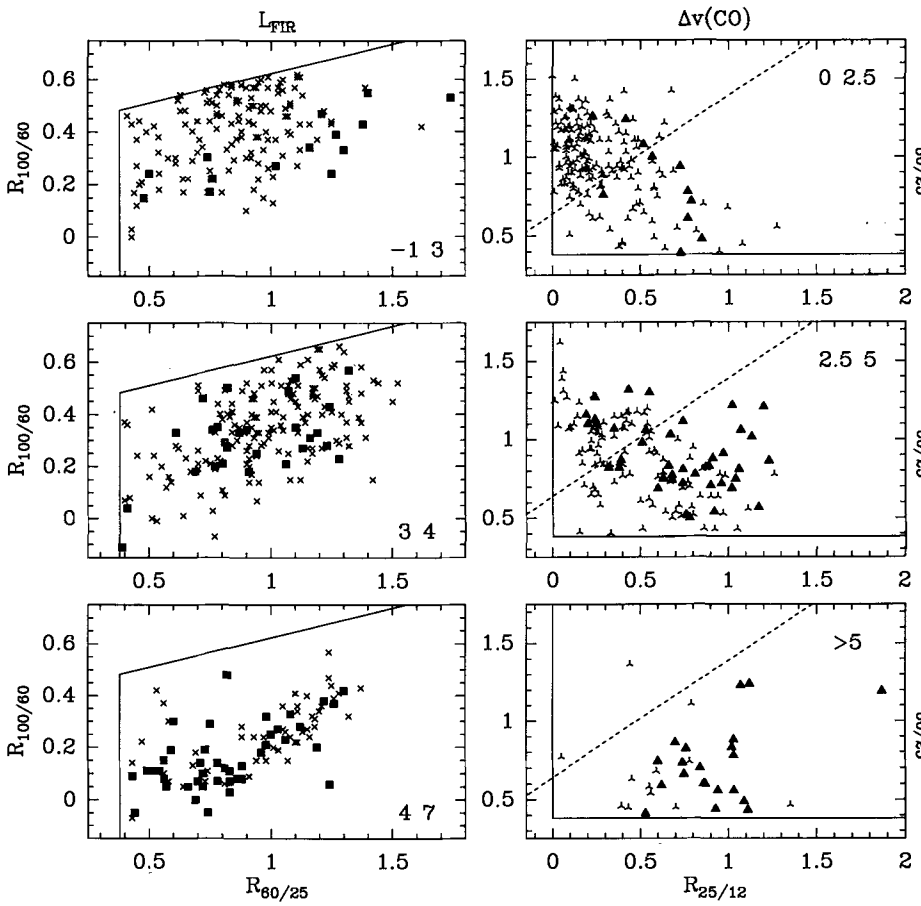

IRAS colour-colour plots for sources observed in H_2O at Effelsberg and detected in CO at IRAM. Filled symbols are sources with H_2O maser emission. The drawn lines indicate the source selection criteria (see Wouterloot & Brand 1989). $R_{60/25}$ is log(F(60μ)/F(25μ)), etc. **left:** *$R_{100/60}$ versus $R_{60/25}$ for three ranges in $log(L_{FIR}/L_\odot)$.* **right:** *$R_{60/25}$ versus $R_{25/12}$ for three ranges in $\Delta v(CO)$. Sources with maser emission are preferentially found below the dashed line.*

References

Fiegle K., Wouterloot J.G.A., Brand J., Winnewisser G.: 1994, A&A *in preparation*
Palagi F., Cesaroni R., Comoretto G., Felli M., Natale V.: 1993, A&A *in press*
Wouterloot J.G.A., Brand J.: 1989 A&AS 80, 149
Wouterloot J.G.A., Brand J., Fiegle K.: 1993 A&AS 98, 589
Wouterloot J.G.A., Walmsley C.M.: 1986 A&A 168, 237

Luminosity vs. Circumstellar Mass: An Evolutionary Diagram for YSOs

P.Saraceno[1], P.André[2], C.Ceccarelli[1,5], M.Griffin[3], S.Molinari[1], S.Russell[4]

[1]Istituto di Fisica dello Spazio Interplanetario - CNR, Frascati, Italy
[2]Centre d'Etudes de Saclay, France
[3]Queen Mary and Westfield College, London, UK
[4]School of Cosmic Physics, Dublin, Ireland
[5]Nasa Ames Research Center, Moffett Field, U.S.A.

We present a systematic study of the millimeter continuum emission of a broad sample of embedded young stellar objects (YSOs) with and without known outflow activity in nearby molecular clouds. Part of the purpose of this work is the selection of a sample of protostellar candidates for further observations with the Infrared Space Observatory (ISO) spectrometers. Our sample includes all known Class 0 objects recently identified by André et al. (1993) (7 sources), as well as 27 low-luminosity ($L \leq 10^3 L_\odot$) Class I infrared sources associated with a dense molecular core. For the Class I objects whose $60\mu m$ IRAS flux exceeds 20 Jy (the detection limit for ISO spectrometers), the sample is complete in the following molecular clouds: NGC 1333, Perseus, Taurus, L1641, Orion, Chamaeleon (I, II and III), ρ Ophiuchi and Corona Australis (no source matching the selection criteria was found in Lupus). These objects are listed in Table I, along with 17 other sources not all satisfying the luminosity criterion. Table I lists the measured 1.3 mm fluxes and the source type: CLO (Class 0), and OF or NOF Class I sources. The division between OF and NOF Class I sources is based on the apparent dynamical time-scale τ_D of the associated mass loss activity (if any): *Outflow* (OF) sources if $\tau_D \geq 10^4 yrs$, and *Non-Outflow* (NOF) sources otherwise. Figure 1 presents the **Luminosity** *vs* **1.3 mm flux** plot for our sample. In this plot, the measured 1.3 mm peak fluxes have been scaled to a single distance of 160 pc using a power law exponent of 0.7, which is appropriate for extended protostellar envelopes (cf. Terebey et al. 1993).

Discussion

Table 1 and Figure 1 suggest the following considerations:

a) All Class I OF sources lie close to a correlation line between the luminosity and the 1.3 mm continuum flux, which spans more than four orders of magnitude. The HH exciting sources (Reipurth et al. 1993) lie on the same line, showing that they cannot be distinguished from Class I OF sources on the basis of millimeter continuum fluxes alone.

b) The Class 0 objects lie to the right hand side of the Class I OF sources line in Fig. 1: They are definitely underluminous compared with Class I objects of similar mm flux, in agreement with their definition (André et al. 1993).

c) The Class I NOF sources tend to be low luminosity ($L_{bol} < 100\ L_\odot$) objects and have on average consistently lower millimeter fluxes compared with OF sources of similar luminosities (i.e., in Fig. 1, they lie on the left hand side of OF sources), which confirms the finding of Cabrit & André (1991) on a broader sample. Ceccarelli et al. (1993) have shown that, at least in the ρ Ophiuchi region, dust temperature and/or emissivity effects cannot explain the difference in mm flux between the two types of sources. Therefore, we conclude that **NOF sources have definitely less circumstellar material than OF sources.** There is no clear correlation between the bolometric luminosity and the millimeter

flux for the Class I NOF sources. In a similar plot, Classical T Tauri stars would tend to occupy the same region as NOF Class I sources, showing that these two types of objects have comparable values of the (peak) mm continuum flux.

The Outflow Line: One of the most interesting features of Fig. 1 is the striking correlation between L_{bol} and $F_{1.3mm}$ among Class I OF objects. This result was also found by Reipurth et al. (1993) on a different, but related, sample consisting of HH exciting sources. The correlation spans four orders of magnitude in luminosity, from single low-luminosity objects, of 1 $M_{\odot}$ or less, to clusters of bright, massive stars. The stellar mass, by analogy with the HR diagram, may be the parameter that determines the location of an object on this line. The observed correlation is consistent with the idea that more massive clumps tend to produce more massive stars with more massive envelopes. If the objects on the Outflow Line are in the main accretion phase and draw a large part of their luminosity (for $L_{bol} \lesssim 10^3 L_{\odot}$) from accretion, then Figure 1 suggests that $L_{acc} \propto M_{env}^2$. Therefore, we would have $L_{acc} \propto \dot{M}_{acc} M_{\star}/R_{\star} \propto M_{env}^2$ (this result depends in part on the adopted extent of the 1.3 mm emission and on its scaling with distance). Since $M_{\star}/R_{\star}$ cannot explain the factor 1000 spanned by L_{acc} (or ~ 30 by M_{env}), the correlation also suggests that the accretion rate may depend on other factors than just the temperature of the cloud (Shu 1977), such as the amount of circumstellar matter.

An Evolutionary Scheme for embedded YSOs: In Figure 1, the circumstellar mass (and the average extinction) decreases from right to left: in an evolutionary scheme, this is also indicating the arrow of time (e.g., Adams 1990) since an accreting object is expected to decrease its circumstellar mass during the course of its evolution. In this picture, the youngest objects in Figure 1 are the Class 0 sources. Since all of them are exciting molecular outflows, this implies that the mass outflow phenomenon appears at the very beginning of the accretion phase, and that protostars exhibiting only infall must be very rare, or even non existent, objects. As time proceeds, the circumstellar mass around Class 0 sources presumably decreases and their luminosity increases roughly proportionally with the mass of the core, and they will reach the Class I Outflow Line.

The low luminosities of the Class 0 objects identified so far suggest that they are low mass objects, or, in our scenario, the progenitors of the T Tauri stars. In this case, where are the progenitors of the future Ae/Be stars? In Fig. 1, they should lie above the known Class 0 sources and on the right of the outflow line, but this appears to be an "empty zone" of the diagram. It is possible that this "empty zone" is a statistical effect resulting from rapid evolution of the most massive objects toward the outflow line, and further observations may discover such objects.

Finally, if the millimeter flux of Class I objects comes from both a disk and a spherical envelope while that of optically visible PMS stars comes primarily from a disk (in agreement with the fact that Class I sources are spatially extended at 1.3 mm while PMS stars are pointlike; cf. André & Montmerle 1994), the similarity in peak millimeter flux between Class I objects and more evolved PMS stars of comparable luminosities suggests, that the circumstellar material entirely condenses into disk when the object evolves from Class I to PMS star (see also Ohashi et al. 1991).

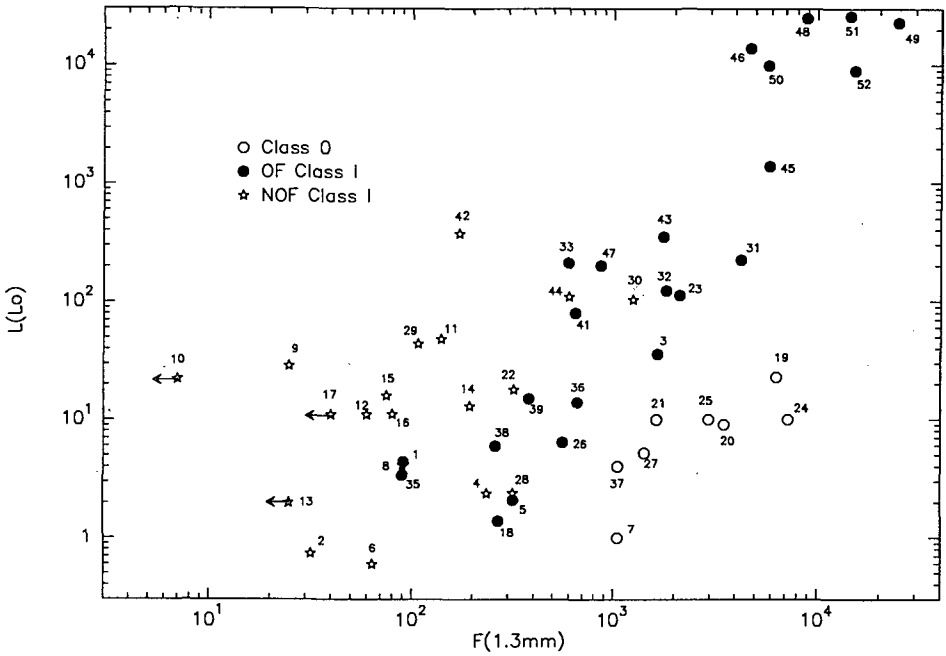

Figure 1

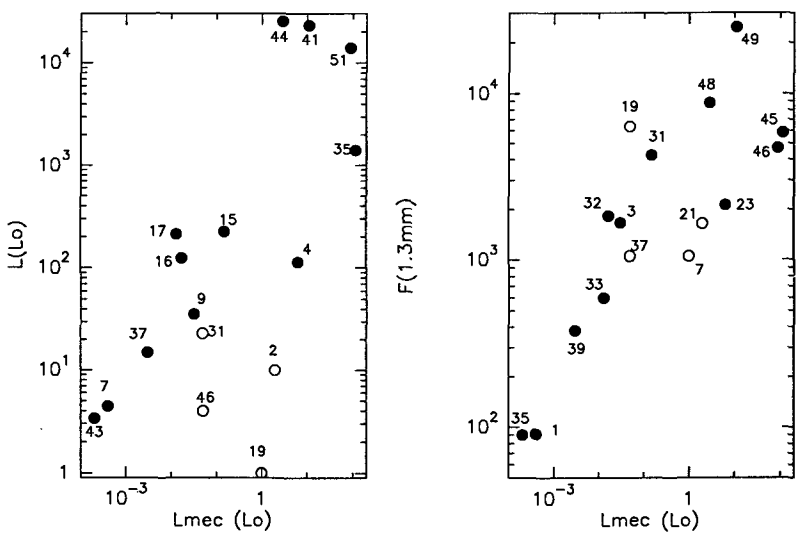

Figure 2

Link with the Outflow Mechanical Luminosity: A relationship between bolometric luminosity and outflow mechanical luminosity has been well established in the past (e.g., Levreault, 1988); this relationship is shown in Figure 2 for some of the objects of our sample. Again, we find a different distribution among the Class I OF sources and the Class 0 sources - the correlation holds only for the OF Class I sources and not for the Class 0 sources, which appear to be more efficient at driving their outflows.

However as shown in Figure 3, the 1.3 mm flux (i.e. the amount of circumstellar mass) is well correlated with the outflow mechanical luminosity, including for the Class 0 objects. This suggests that, unless outflows are powered by a different mechanism in Class 0 and Class I sources, the outflow driving mechanism is more closely related to the amount of circumstellar material (as traced by $F_{1.3mm}$) than to some stellar characteristics (such as L_{bol}). This, in turn, suggests that the circumstellar envelopes/disks themselves play a direct role in accelerating the flows (see also Cabrit & André 1991).

References

Adams, F.C. 1990, ApJ 363, 578.
André, P., Montmerle, T. 1994, ApJ January.
André, P., Montmerle, T., Feigelson, E.D., Steppe, H. 1990, A&A 240, 321.
André, P., Ward-Thompson, D., Barsony, M. 1993, ApJ 406, 122.
Cabrit, S., André, P. 1991, ApJ 379, L25.
Ceccarelli, C., André, P., Griffin, M.J., Saraceno, P., Molinari, S., Russell, S. 1993 *Il Nuovo Cimento* in press.
Chini, R., Henning, Th., Pfau, W. 1991, A&A 247, 157.
Gürtler, J., Henning, Th., Krügel, E., Chini, R. 1991, A&A 252, 801.
Levreault, R.M. 1988, ApJ 330, 897.
Mezger, P.G., Chini, R., Kreysa, E., Wink, J.E., Salter, C.J. 1988, A&A 191, 44.
Ohashi, N., Kawabe, R., Hayashi, M., Ishiguro, M. 1991, AJ 102, 2054.
Reipurth, B., Chini, R., Krügel, E., Kreysa, E., Sievers, A. 1993, A&A 273, 221.
Sandell, G., Aspin, C., Duncan, W.D., Russell, A.P.G., Robson, E.I. 1991, ApJ 376, L17.
Shu, F. 1977, ApJ 214, 488.
Terebey, S., Chandler, C.J., André, P. 1993, ApJ 414, 759.
Walker, C.K., Adams, F.C., Lada, C.J. 1990, ApJ 349, 515.

Model Envelopes of Post–AGB Stars from IR and Sub–mm Data

J. Gürtler[1], C. Kömpe[1], and Th. Henning[2]

[1]Astrophysikalisches Institut und Universitäts–Sternwarte, Schillergäßchen 2, D–07745 Jena, Germany

[2]MPG–AG "Staub in Sternentstehungsgebieten", Schillergäßchen 3, D–07745 Jena, Germany

Introduction: The transition phase from asymptotic giant branch (AGB) stars to planetary nebulae is one of the most interesting among the late stages of stellar evolution and characterized by a high mass loss rate. AGB stars evolve on a very short time scale (several thousand years) via the OH/IR stage (a dense dust shell hides the star) towards proto–planetary (a visible star surrounded by a cold dust/gas shell) and finally to planetary nebulae. Observable constraints of a possible model of post–AGB stars include the mass loss rate and the structure and composition of the gas/dust shells built up around them.

Data: We have carried out continuum measurements at 1.3 mm towards 4 infrared sources (IRAS 10215–5916, 16342–3814, 17150–3224, 19500–1709) that are considered post–AGB stars, using the bolometer system at the Swedish–ESO Submillimeter Telescope (SEST) on Cerro La Silla, Chile. Low resolution (LRS) IRAS spectra exist for all four objects. In addition, IR fluxes in the range from 1 to 8 μm were taken from the literature (Gezari et al. 1993).

Model: To analyze our data, we use a radiative transfer code that has been adapted from a program originally developed to model the environment of compact HII regions (see Chini et al. 1986). In the model, we assume that a dust envelope of spherical symmetry is centred on an evolved star. The main input parameters are the optical constants (n, k) of the dust material and the size distribution of the dust grains, the extent of and the density distribution in the dust shell, and the luminosity and effective temperature of the star. In accordance with the spectral type and/or the presence of the 10 μmsilicate feature, we assume the dust to consist of either silicate or carbon. The optical constants for the dust grains are taken from Draine (1985).

The program allows us to derive a consistent set of physical parameters for the central star ($T_{\rm eff}$, luminosity), the envelope (extent, density, temperature distribution) and the distance of the star from our model fit.

Results: Table 1 summerizes the model parameters derived for IRAS 10215−5916, 16342−3814, 17150−32214, and 19500−1709

The observed spectral energy distributions are satisfactorily reproduced if the dust model is chosen in accordance with the chemical type of the star. The only exception is the data point at 1.3 mm. The models predict a 1.3–mm flux that is lower than the observed one by a factor of 5 and more. The problem is generally encountered with model fits of the thermal emission from dust–enshrouded stellar sources (Chini et al. 1986, Gürtler et al. 1991).

One possible reason for this deviation could be the assumed opacity law in the infrared. Whereas the optical constants from Draine (1985), used in our model, imply an opacity law $\propto \lambda^{-2}$, several investigators (e.g. Ossenkopf & Henning 1991) argue in favour of a λ^{-1} law as more appropriate for the interstellar dust in dense regions. The optical data from Blanco et al. (1991) and Rouleau & Martin (1991) do not yet provide a definite solution.

Extended envelopes containing very cold dust may provide an alternative explanation for the high 1.3–mm fluxes. In fact, the observed spectral energy distributions may be readily reproduced. Primarily due to their large sizes, these outer envelopes are rather massive (up to several solar masses). Since the mass estimates are sensitive to the exact dimensions and density distribution, final numbers cannot be given and no decision can be made yet in favor of one of the alternatives.

Table 1: Model Parameters

IRAS		10215−5916	16342−3814	17150−3224	19500−1709
Star:	$T_{\rm eff}$ [K]	5000	35000	25000	8000
	L [$L_\odot$]	$4.5\ 10^4$	$1.3\ 10^4$	$1.9\ 10^3$	$2.6\ 10^3$
	d [pc]	2000	3000	1000	1500
Envelope:	$r_{\rm i}$ [cm]	$1.5\ 10^{15}$	$2\ 10^{17}$	$5.0\ 10^{15}$	$3.5\ 10^{16}$
	$r_{\rm o}$ [cm]	$1.5\ 10^{17}$	$3.13\ 10^{17}$	$6\ 10^{16}$	$7.8\ 10^{16}$
	$n_{\rm d}$ [cm^{-3}]	$2.5\ 10^{22}\ r^{-1}$	$2.5\ 10^{22}\ r^{-1}$	$3.0\ 10^{22}\ r^{-1}$	$5\ 10^4$
	$M_{\rm d}$ [$M_\odot$]	2.9	7.6	0.57	$7.6\ 10^{-2}$
	$T_{\rm max}$ [K]	134	112	285	170
	$T_{\rm min}$ [K]	61	33	49	58
Dust Type:		Silicate	Carbon	Silicate	Carbon

Acknowledgement: JG and CK acknowledge financal support from the German Bundesministerium für Forschung und Technologie (Förderkennzeichen 05 2JN13A).

References

Blanco, A., Fonti, S., Rizzo, F., 1991, Infrared Physics, 31, 167
Chini, R., Krügel, E., Kreysa, E., 1986, A&A, 167, 315
Draine, B.T., 1985, ApJS, 57, 587
Gezari, D.Y., Schmitz, M., Pitts, P.S., Mead, J.M., 1993, Catalog of Infrared Observations, NASA RP−1294
Gürtler, J., Henning, Th., Krügel, E., Chini, R., 1991, A&A , 252, 801
Ossenkopf, V. and Henning, Th., 1991, in: Physics and Composition of Interstellar Matter, Krełowski, J., Papaj, J. (eds.), Inst. Astr. Nicolaus Copernicus Univ. Toruń, p. 199
Rouleau, F., Martin, P.G., 1991, ApJ, 377, 526

Distributions and Kinematics of Molecular Species around T Tau

H.J. van Langevelde[1], E.F. van Dishoeck[1], G.A. Blake[2]

1. Sterrewacht Leiden, Postbus 9513, 2300 RA Leiden, the Netherlands
2. Div. of Geol. and Plan. Sci., CalTech 170–25, Pasadena, CA 91125, U.S.A.

Circumstellar material on small ($\lesssim$ 2000 AU) scales around T Tau has been inferred from infrared and submillimeter continuum observations of the dust as well as interferometric CO observations (Weintraub et al. 1989, Beckwith & Sargent 1991). This material, possibly a proto–planetary disk, encompasses both T Tau and its infrared companion, which is separated by 100 AU.

We report single dish and interferometer observations of several molecular species to study the chemical and physical structure of this circumbinary gas. Fig. 1*a* shows the HCO^+ J=1→0 emission in the direction of T Tau, obtained with the OVRO interferometer in a $7'' \times 7''$ beam. For comparison the spectrum of HCO^+ J=1→0 in a $25''$ beam, observed with the IRAM 30m dish, is shown in Fig. 1*b*. It is clear from these spectra that a narrow extended ($\gtrsim$ 6000 AU) component at $\approx$ 8.3 km s^{-1} is resolved out by the interferometer. A compact object remains for which the HCO^+ J=1→0 profile is quite asymmetric and peaks at $\approx$ 7.2 km s^{-1}. The same compact object is also detectable in HCO^+ J=3→2 (Fig. 1*c*) and J=4→3 (Fig. 1*d*) profiles obtained with the JCMT in $19''$ and $14''$ beams respectively. The blue side of these spectra closely resembles the OVRO spectra of the J=1→0 transition. The J=3→2 line still shows some of the narrow emission from the background cloud.

The compact object is identified with a circumbinary disk ($\approx$1000 AU size) or the inner part of an accretion envelope around the young stars. From the maps it appears that the highest velocities arise closest to the position of T Tau, consistent with either interpretation. The higher excitation HCO^+ lines indicate that warm T $\gtrsim$30 K and dense $\gtrsim 10^6$ cm^{-3} material is present.

The most satisfying interpretation for the striking dip at 8.5 km s^{-1} in Fig. 1*a* is absorption by colder foreground HCO^+. This explains why the higher excitation lines are more symmetric (Fig. 1*c* and *d*), since the excited levels are much less populated in the lower–density envelope. The IRAM J=1→0 profile (Fig. 1*b*) does not show the absorption, because it occurs only in front of the compact object covering a small fraction of the beam. Also, emission from the background cloud fills in the absorption.

Because the absorption is red–shifted with respect to T Tau this implies that material is falling onto the circumbinary material. The accretion rate is estimated to be $\approx 2 \times 10^{-7}$ $M_\odot yr^{-1}$ or larger. This is the first evidence that some infall from the surrounding envelope is continuing in the later phases of stellar evolution. Accretion through the disk in more evolved young stellar objects is often suggested to explain FU Orionis–type phenomena (Hartmann et al. 1993). In this respect it is interesting to note that a flare was recently observed for T Tau S, the IR companion (Ghez et al. 1991).

The shapes of the ^{13}CO and $C^{18}O$ J=1→0 transitions (Fig. 1*e*, *f*) can be readily understood in this picture by recalling that CO has a very small dipole moment. Thus the absorption coefficients of CO isotopes are factors of 1000 smaller than that of HCO^+. ^{13}CO, however, is 200–1000 times more abundant than HCO^+, so that some ^{13}CO absorption likely occurs. However, for $C^{18}O$ negligible absorption is expected, consistent with Fig. 1*f*.

Fig. 1*g* shows the IRAM CS J=2→1 line in the direction of T Tauri. Compared with the HCO^+ we notice that the disk component in this line is weak. This is confirmed by OVRO images in the CS J=2→1 line (not shown), which hardly show any compact emission. Also the higher excitation lines, such as the J=5→4 show little CS in the dense and warm environment close to the stars.

From the $C^{18}O$ J=1→0 interferometer spectrum a H_2 column density can be estimated, which is used to calculate a fractional abundance of HCO^+ of 10^{-9} in the circumbinary material. This is only slightly lower than that found in the surrounding Taurus cloud. In contrast, CS

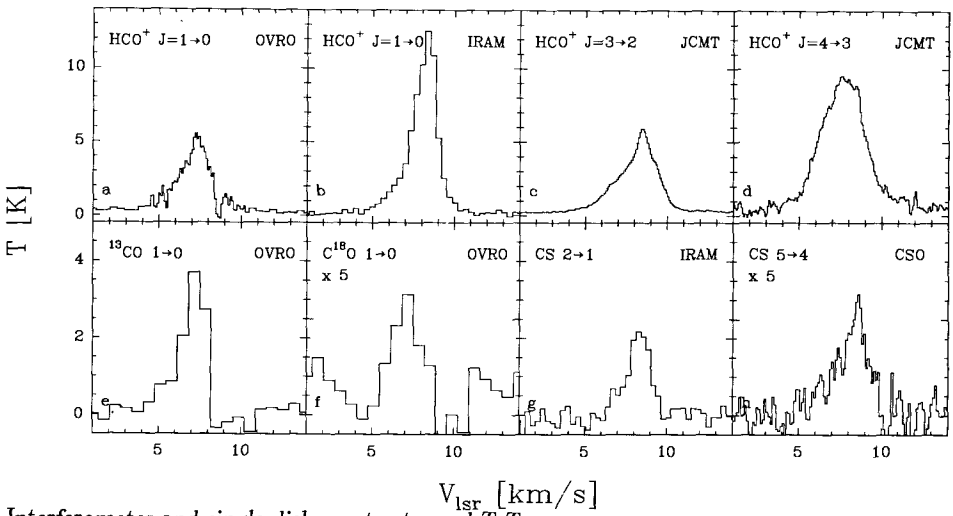

Interferometer and single dish spectra toward T Tau

is about 20 times less abundant in the circumbinary material than in the surrounding cloud. A similar result was found for HL Tau, for which Blake et al. (1992) argue that the polar molecule CS is depleted onto grains in the dense circumstellar disk. Indeed, such behavior is not expected for HCO^+, because it is an ion formed rapidly by the reaction of H_3^+ with CO.

References

Beckwith S.V.W., Sargent A.I., 1991, ApJ 381 250
Blake, G.A., van Dishoeck, E.F., Sargent, A., 1992, ApJL 391, L99.
Ghez A.M., et al. 1991, AJ 102 2066
Hartmann L., Kenyon S., Hartigan P., 1993, in *Protostars & Planets III*, eds. E.H. Levy and J.I. Lunine (Univ. of Arizona Press), p. 497
Weintraub, D.A., Masson, C.R., Zuckerman, B. 1989, ApJ, 344, 915.

Ammonia Towards High Luminous IRAS Sources

K. Martin[1], Th. Henning[1], C. Kömpe[2], and C.M. Walmsley[3]

[1]MPG–AG "Staub in Sternentstehungsgebieten",
Schillergäßchen 3, D–07745 Jena, Germany
[2]Astrophysikalisches Institut und Universitäts–Sternwarte,
Schillergäßchen 2, D–07745 Jena, Germany
[3]Max–Planck–Institut für Radioastronomie,
Auf dem Hügel 69, D–53121 Bonn, Germany

Introduction: It is well known by now that stars form within molecular cloud cores condensing from the molecular gas. However, many of the details of the star forming process are still poorly understood. One way to make progress in this field is from the statistical analysis of survey data. Massive young stars are revealed by the infrared emission of their dust shells, and were thus detected by the IRAS satellite as point sources. It is therefore not surprising that the IRAS Point Source Catalog (PSC) provides numerous young stellar objects that have been used in various NH_3 surveys (e.g. Churchwell et al. 1990, Wouterloot et al. 1988, Harju et al. 1991).

The source catalog: Of particular interest is a list of "hot core" objects that are characterized by their high flux densities at 100 μm. The source list has been obtained by searching the IRAS–PSC for objects having a 100 μm flux higher than 500 Jy and that are located in the R.A. and DEC. range from 0 to 12 h and $-30°$ to $90°$, respectively. Excluding those objects that are associated with galaxies, a total of 67 objects were found. A complete list of these sources can be found in Henning et al. (1992). The amount of observational data for these objects has been growing steadily during the last years: Snell et al. (1988, 1990) have searched 51 of these objects for bipolar outflows; Carpenter et al. (1990) have studied the physical properties of the molecular clouds associated with 21 objects; Henning et al. (1992) have searched all 67 objects for H_2O maser emission; and Carpenter et al. (1993) have imaged in the J, H and K bands and mapped in the CS(J=2–1) transition 20 objects.

Observations: We have carried out a survey of all 67 objects in the NH_3 (1,1) and (2,2) lines using the Effelsberg 100–m telescope during 3 runs in the period from December 1991 to July 1993. All objects have been observed in reasonably good weather conditions, and many have been observed several times in order to improve the data quality. Two of the sources, IRAS 06058+2138 and 06061+2151 , have been completely mapped in additional observing runs.

Results: We have used our NH_3 data, IRAS data and additional data from the literature to do a statistical analysis of our 67 sources. First of all, we present some statistical information relating the detection of NH_3 emission to the presence of H_2O masers and/or outflows:

- NH_3 (1,1) emission was detected towards 31 sources and NH_3 (2,2) emission towards 23 sources
- 20 sources detected in NH_3 (1,1) are associated with H_2O maser emission
- 18 sources detected in NH_3 (1,1) are associated with bipolar outflows
- 14 sources detected in NH_3 (1,1) are associated with both, H_2O maser emission and a bipolar outflow

In addition, we have looked for correlations of the physical parameters derived from our data:

1.–The gas densities in our sources should be high enough for the gas and dust to be sufficiently coupled so that their temperatures can be expected to be the same. However, we find that the gas temperature is systematically lower than the dust "colour" temperature. A possible explanation is that the IR radiation is emitted deeper in the clump and thus by hotter material than the NH_3 emission or that there is considerable emission from very small grains.

2.–One would expect that the embedded star(s) are the main heating source of the gas located in the vicinity of the IRAS sources. Assuming that our source sample contains similar objects with embedded stars that have similar physical properties, it is rather natural to think that the gas temperature should increase with the infrared luminosity; we do indeed find such a tendency in our data.

3.–The embedded star(s) could also be a possible source for turbulent motion of the gas in their immediate neighbourhood. The width of molecular lines is thought to originate from turbulence and should therefore increase with infrared luminosity. However, this relationship

is not confirmed by our data. There are two possible explanations: (1) the error of the measured NH_3 linewidths is too large, and (2) the luminosity range is too small to show the expected effect.

4.–Using the NH_3 column density and the optical depth at 100 μm as a measure for the amount of gas and dust, respectively, one would expect that these two parameters should correlate. However, our data do not show a clear correlation. This might be due to the relatively large error of the NH_3 column density and the relatively small number of data points.

Acknowledgement: CK acknowledges financal support from the German Bundesministerium für Forschung und Technologie (Förderkennzeichen 05 2JN13A).

References

Carpenter, J.M., Snell, R.L., Schloerb, F.P., 1990, ApJ , 362, 147
Carpenter, J.M., Snell, R.L., Schloerb, F.P., Skrutskie, M.F., 1993, ApJ, 407, 657
Churchwell, E., Cesaroni, R., Walmsley, C.M., 1990, A&AS, 83, 119
Harju, J., Walmsley, C.M., Wouterloot, J.G.A., 1991, A&A 245, 643
Henning, Th., Cesaroni, R., Walmsley, C.M., Pfau, W., 1992, A&AS, 93, 525
Snell, R.L., Huang, Y.–L., Dickmann, R.L., Claussen, M.J., 1988, ApJ, 345, 257
Snell, R.L., Dickman, R.L., Huang, Y.–L., 1990, ApJ, 352, 139
Wouterloot, J.G.A., Brand, J., Henkel, C., 1988, A&A, 191, 232

JCMT Continuum Survey of Pre-Protostellar Cores

D. Ward-Thompson[1], P. F. Scott[2], R. E. Hills[2] and P. André[3]

[1]Royal Observatory, Blackford Hill, Edinburgh, UK
[2]Cambridge University, Cavendish Laboratory, Madingley Road, Cambridge, UK
[3]Service d'Astrophysique, Centre d'Études de Saclay, Gif-sur-Yvette, France

Abstract

Results are presented of a JCMT submillimetre continuum survey of Myers cores which have no known infra-red (near-IR or IRAS) associations – the so-called starless cores. In all cases no more than one clump in each of the cores was detected in the continuum. Some of the clumps were mapped in the continuum, to demonstrate that they are true emission peaks. The clumps have insufficient bolometric luminosities to be consistent with the earliest phase of accreting protostars predicted by the standard model. The lifetimes of the clumps derived from statistical considerations are shown to be too long for the cores to be undergoing free-fall collapse, but are consistent with ambipolar diffusion timescales. They are therefore hypothesised to be pre-protostellar in nature.

Introduction

Current theories of star formation predict that stars form within molecular clouds, where density inhomogeneities lead to the formation of dense cores. Hydrostatic equilibrium is possible for a given core provided a certain critical mass is not exceeded. Once this condition is no longer satisfied, inside-out collapse sets in, with the innermost part of the core collapsing first, and collapsing material accretes onto a central object, known as a protostar.

The aim of this project was to try to observe the earliest phase of pre-protostellar cores in which collapse has not yet set in. This project has had long-term status on JCMT over the last three semesters, and the goals of the project include trying to examine in detail molecular cores which do not contain young stellar objects, to determine their physical characteristics, and to compare them with model predictions.

The sample

An extensive survey of cold cores in molecular clouds was carried out by Myers and co-workers (Benson & Myers 1983), and roughly half of the 90 or so cores were found to have associated IRAS sources (Beichman et al. 1986). Of these IRAS sources, about a third are associated with visible T Tauri stars, but the remaining two-thirds have no optical counterpart and are thus believed to be either T Tauri stars still deeply embedded in their parent cloud, or else younger objects. Therefore it was hypothesised that the cores without IRAS sources were at a still earlier evolutionary stage, and these were selected as the target sample. Around 20 cores which do not contain IRAS sources were studied.

Results

The cores do not have distinct edges, but merge into the more diffuse material of the molecular clouds in which they are embedded. However the fwhm's of the cores are <0.05pc, and the mass contained within this volume is of order 1-3$M_\odot$. The peak densities of the cores are calculated to be around 10^6 cm^{-3}, but with temperatures in the region of only 10-20K. Since the cores were not detected by IRAS we can place upper limits on their luminosities of $<1L_\odot$ for L1689B and $<0.25L_\odot$ for L183. These luminosities and temperatures, along with the derived lifetimes, are inconsistent with cores containing accreting protostars. They are therefore hypothesised to be the precursors of star formation, and pre-protostellar in nature (Ward-Thompson et al. 1994).

For the first time a size difference was found between the starless cores and the cores with IRAS sources: the continuum clumps in the centres of starless cores are all less centrally peaked and more diffuse than the equivalent continuum clumps previously found in Myers cores with IRAS sources. Nevertheless, the starless cores are more centrally condensed than a constant-density sphere. The lifetimes of the clumps derived from statistical considerations are shown to be too long for the cores to be undergoing free-fall collapse, but are consistent

with ambipolar diffusion timescales. All of the clumps were found to have masses close to their virial masses.

However, **none** of the mapped clumps shows the steep, $\rho(r) \propto r^{-2}$, power-law radial density profile predicted by the Standard Model. All have profiles which flatten out near their centres. They are, however, consistent with the predictions of a more recent theory of magnetic support of cores during ambipolar diffusion (Crutcher 1993).

References

Beichman, C. et al. 1986, ApJ 307, 337
Benson, P., & Myers, P. 1983, ApJ 266, 309
Crutcher, R. 1993, this volume
Ward-Thompson, D. et al. 1994, MNRAS in press

Comparison of the Structure of a Star-Forming and Non-Star-Forming GMC

Jonathan Williams[1], Eugène de Geus[2], and Leo Blitz[2]

[1]Astronomy Department, University of California at Berkeley, USA
[2]Astronomy Department, University of Maryland, USA

Molecular clouds are far from homogeneous. At high resolution they break up into a number of discrete, dense, "clumps". These clumps make up the overwhelming majority of the mass of the cloud, and are the sites of star formation. Thus, a clear understanding of the nature of the clumpy medium in a cloud can be expected to shed light on the issues of cloud formation and evolution, and the conditions that lead to star formation.

A number of studies have been made of individual clouds (see Blitz, 1993 and references therein). We present here a detailed, unbiased comparison of two clouds: the Rosette molecular cloud (RMC) and the Maddalena & Thaddeus (1985) molecular cloud (MMC). Both clouds have masses in excess of $10^5 M_\odot$, but their star formation histories are very different: the RMC is actively forming OB stars, evidenced in the optical by its famous nebula and also in the infrared (Cox *et al*, 1991), but the integrated IRAS 100μm flux of the MMC is $5000 L_\odot$, implying an upper limit to the star formation efficiency of only 0.1%. All other GMCs of this mass that have been studied show abundant signs of star formation, and so it is reasonable to presume that the MMC will also, eventually, form stars. In this case, the MMC may be considered a very "young" GMC, and the comparison with the RMC will reveal how cloud internal structure evolves towards star formation. Whatever the eventual fate of the MMC, because it is not currently forming stars, and the RMC is, we can compare how cloud structure differs in these two environments.

^{13}CO(1–0) maps of each cloud have been made at very nearly the same linear resolution; of paramount importance for ensuring a fair comparison. We have developed an automated clump finding algorithm (Williams etal, 1994) to permit a comparative analysis of the data. The algorithm works in very much the same way as the eye analyzes the clumpy content of a contour map; searching first for peaks in the data, and then following them down to lower intensities. The advantages of automation are speed, repeatability and reliability for large data sets, and uniformity between different data sets. The mapped area for each cloud was approximately the same. 83 clumps are found in the RMC and 78 in the MMC. For each clump, we can immediately deduce the peak temperature, integrated temperature (proportional to mass assuming optical thinness), area (implying size, ΔR), and velocity dispersion, σ_v. The latter two combine to give the virial mass $M_{vir} = 3\Delta R \sigma_v^2 / G$. We have plotted various combinations of these clump properties in the accompanying figure. There are clear relations between clump peak temperatures, sizes, linewidths, virial parameter $\alpha = M/M_{vir}$, and mass, the first three first noted by Larson (1980), the latter by Bertoldi & McKee (1991). Least squares fits for each cloud are indicated on the plots, and are strikingly similar between the two clouds. We note that, although not plotted in the limited amount of space here, the mass spectrum of clumps in both clouds is also very similar, consistent with the seemingly ubiquitous $dN/dM \propto M^{-1.5}$ that has been observed in every other cloud studied to date, (and contrary to the initial report of Williams & Blitz, 1993). However, despite these *collective similarities*, there are real *individual differences* between clumps of the same mass in each cloud: clumps in the star forming RMC are smaller (and hence more dense), possess a smaller linewidth, have greater peak temperatures, and are more bound. These differences can not all be simultaneously resolved by assuming that the distances to the clouds are in error. Finally, the four most massive clumps in the RMC are virialized, $\alpha \geq 1$, and are all sites of strong infrared emission, presumably due to protostars (Cox *et al*, 1991). There are no clumps in the MMC that have $\alpha > 0.5$. We conclude that the boundedness of a clump may be an evolutionary indicator of (high mass) star formation. These results are published in more detail in Williams *et al*, 1994).

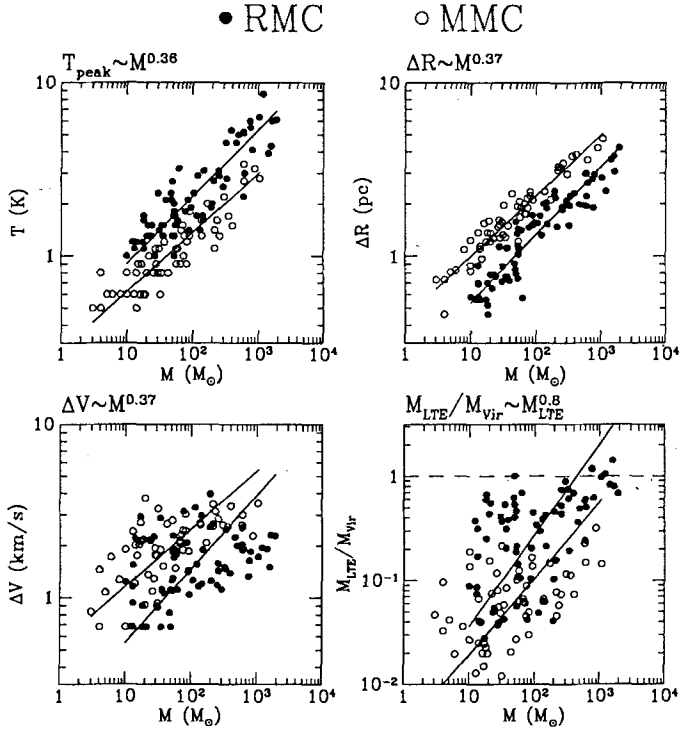

If the MMC is truly at an earlier evolutionary state than the RMC, then these observations challenge theories of cloud formation and evolution to explain how scaling relations between clump properties arise, and how they are preserved as the clumps become denser, hotter, more bound, and ultimately star forming.

References

Bertoldi, F. and McKee, C.F., 1991, Ap. J., ,, 3.95, 140.
Blitz, L., 1993, in *Protostars and Planets III*, Levy and Lunine, eds., University of Arizona Press:Tucson, p.125.
Cox, P., Deharveng, L. and Leene, A., 1991, A&A, 230, 171.
Larson, R., 1981, M.N.R.A.S., ,, 1.94, 809.
Maddalena, R. and Thaddeus, P., 1985, Ap. J., ,, 2.94, 231.
Williams, J.P. and Blitz, L., 1993, Ap. J. (Letters), ,, 4.05, L75.
Williams, J.P., de Geus, E.J., and Blitz, L., 1994, Ap. J., *in press.,*

Outflow-Free Class I sources: Protostars?

R. Liseau[1], C. Ceccarelli[1], Y. Fukui[2], D. Lorenzetti[1], A. Mizuno[2], S. Molinari[1], B. Nisini[1], P. Saraceno[1], L. Spinoglio[1]

[1] IFSI – CNR, CP 27, I–000 44 Frascati (Roma), Italy

[2]Dept. of Astrophysics, Nagoya University, Chikusa-ku, Nagoya 464–01, Japan

Stellar mass loss occurs during all known stages of early stellar evolution. For the identification of mass infall onto a protostellar low mass core the source spectrum should, however, ideally be free from contaminating emission from outflowing gas. With this in mind, we have selected Class I sources of low to intermediate luminosity in the solar neighbourhood which were known not to be associated with mass outflows or whose outflow status has been unclear (Table 1). One may assume that these Class I sources have either not (yet?) developed a strong outflow or that they are presently in an quiescent, outflow-intermittent, state.

To the extent that the Class I sources are protostellar objects, they should still possess a relatively massive envelope of gas and dust, from which they are currently accreting material onto the central, growing core. Their status as Class I sources testifies to the very existence of circumstellar material, but leaves the *envelope to core mass ratio* essentially unquantified.

CO (3-2) observations with the KOSMA telescope have confirmed the absence of strong outflows towards a number of these objects. We searched the sources for associated dense cores in CS (2-1) with the Nagoya telescope, which gave only in a few cases positive results. Derived column densities assume LTE and a unique value of the CS abundance (1×10^{-9}) has been used to estimate A_V.

Almost half of the objects have been observed in the 1300μm continuum with the SEST and only a few objects are reasonably strong emitters. From IRAS data, the dust equilibrium temperatures, T_{col}, and dust optical depths at 60μm, τ_{60}, towards the Class I sources were estimated from which it became evident that τ_{60} is much smaller than unity in all cases but one (which is uncertain). For the value of the grain opacity given by Hildebrand (1983, QJRAS 24, 267) and a scaling relation of the form λ^{-2} we determined then the values of the dust masses emitting at 60 and 1300μm, respectively, towards the Class I sources presented in the table. As also noted in previous studies, there is in general no correlation between these mass estimates.

From the available data we find that among the 28 originally selected Class I sources two objects (NGC 1333 IRAS 1 and L 1641 05338-0647) may seriously be considered as outflow-free protostellar candidate sources and as such, clearly, deserve further study. The selection process of these objects demonstrates also clearly that multi-frequency mapping observations, at both high and low spatial and spectral resolution, are essential in order to gain a better understanding of the outflow-free Class I sources.

TABLE 1: Spectral line and continuum observations of outflow-free Class 1 sources

Source	D (pc)	L ($L_\odot$)	CS(2-1) T_A^* (K)	v_{LSR} (km s^{-1})	Δv (km s^{-1})	$\int T_A^* dv$ (K km s^{-1})	T_K (K)	Ref. (T_K)	N(CS) (10^{13}cm^{-2})	A_V (mag)	T_{col} (K)	$\tau_{60\mu m}$	$M_{dust}^{60\mu m}$ ($M_\odot beam^{-1}$) (210″)	$M_{dust}^{1.3mm}$ ($M_\odot beam^{-1}$) (20″)
IRAS 1[a]	350	20	0.6	7.8	2.53	1.6	15	(1)	2.43	12.2	32	8.3×10^{-3}	2.9×10^{-3}	8.3×10^{-2}
04365+2535	140	1.9	0.5	6.2	0.98	0.6	8	(2)	0.80	3.9	27	9.7×10^{-3}	7.8×10^{-4}	1.8×10^{-3}
04368+2557	140	0.9	0.4:	6.2:	0.83:	0.3:	11	(2)	0.42:	2.1:	44	1.5×10^{-4}	1.2×10^{-5}	1.4×10^{-3}
05155+0707	500	45	0.3	−1.3	2.06	0.8	10	(0)	1.1	5.4	33	2.3×10^{-3}	2.4×10^{-3}	...
05332−0637	500	6.7	<0.36	-	-	-	22	(3)	<0.2	<2	52	2.1×10^{-5}	2.1×10^{-5}	...
05335−0645	500	2.7	<0.33	-	-	-	27	(3)	<0.2	<2	52	8.3×10^{-5}	8.6×10^{-5}	2.2×10^{-3}
05338−0647	500	122	0.8	8.9	2.90	2.6	22	(4)	4.8	24	37	2.5×10^{-3}	2.5×10^{-3}	3.7×10^{-2}
05342−0639[b]	500	58	0.3:	7.3	0.99	0.3:	20	(0)	0.52:	2.6:	48	1.4×10^{-4}	1.5×10^{-4}	...
05345−0643	500	21	<0.39	-	-	-	20	(3)	<0.2	<2	57	1.8×10^{-5}	1.9×10^{-5}	...
05367−0712	500	15	<0.42	-	-	-	20	(0)	<0.2	<2	>36	$<2.7\times10^{-4}$	2.8×10^{-4}	...
05381−0921	500	1.9	<0.42	-	-	-	20	(0)	<0.2	<2	49	5.1×10^{-5}	5.3×10^{-5}	...
05389−0756	500	15	<0.51	-	-	-	15	(5)	<0.2	<2	36	4.6×10^{-4}	4.8×10^{-4}	...
05445+0016	500	533	0.8	9.9	1.23	1.2	20	(0)	2.1	10.5	31:	1.2×10^{-1} :	1.2×10^{-1} :	...
MLY 22	800	180	<0.43	-	-	-	10	(0)	<0.2	<2	41	1.0×10^{-3}	2.7×10^{-3}	...
MLY 25[c]	800	110	0.4	7.4	2.36	0.7	10	(0)	0.96	4.8	33	3.8×10^{-3}	1.0×10^{-2}	3.6×10^{-2}
WL 12	150	4.4	0.5	4.0	1.54	0.9	15	(0)	1.4	6.8	-	-	...	...
WL 22	150	16.7	0.6	3.9	1.60	1.1	15	(0)	1.7	8.4	39	4.4×10^{-3}	4.7×10^{-4}	1.5×10^{-4}
WL 16	150	12.3	0.5	4.3	2.02	1.1	15	(0)	1.7	8.4	-	-	...	...
EL 29	150	18.5	0.6	4.0	2.14	1.4	15	(0)	2.1	10.6	36	6.5×10^{-6}	6.9×10^{-5}	9.2×10^{-4}
IRS 37	150	9.7	1.0	3.7	1.86	1.9	15	(0)	2.9	14.4	34	3.6×10^{-3}	3.8×10^{-3}	4.2×10^{-4}
IRS 43	150	6.2	0.5	4.0	2.05	1.1	15	(0)	1.7	8.4	-	-	...	...
IRS 54	150	10.5	0.5	3.9	1.28	0.6	15	(0)	0.9	4.6	26	3.0×10^{-2}	3.2×10^{-3}	$<3.9\times10^{-4}$
21046+5110	800	330	<0.26	-	-	-	4	(6)	<0.2	<2	37	3.6×10^{-3}	9.6×10^{-3}	...
21106+4712	350	4.7	<0.24	-	-	-	10	(2)	<0.2	<2	34	7.1×10^{-4}	3.6×10^{-4}	...
21526+5728	750	180	<0.28	-	-	-	3	(6)	<0.2	<2	32	7.2×10^{-3}	1.7×10^{-2}	...
22451+6154	730	370	0.63	−9.8	1.32	0.6	18	(5)	1.2	5.8	42	1.4×10^{-3}	3.2×10^{-3}	6.8×10^{-3}
22512+6201	730	3.8	<0.31	-	-	-	22	(7)	<0.2	<2	<64	$>1.9\times10^{-5}$	$>4.3\times10^{-5}$	...
22517+6215	730	39	0.3:	−9.0	2.:	0.6:	19	(5)	1.0:	5.1:	34	8.8×10^{-4}	1.9×10^{-3}	...

NOTES:
[a] the luminosity is based on recent NIR-and submm-data;
[b] suspected outflow (Morgan, Schloerb, Snell, 1991, ApJ 376, 618);
[c] *HH 124 exciting source (Walsh, Ogura, Reipurth, 1992, MNRAS 257, 110); blue and red wings in CO(3-2) spectrum (this paper).*

REFERENCES TO T_K:
(0) - assumed; (1) - Knee, Cameron, Liseau, 1990, A&A 231,419; (2) - Benson, Myers, 1989, ApJS 71, 89; (3) - Chen, Fukui, Yang, 1992, ApJ 398, 544; (4) - Bally, Langer, Stark, Wilson, 1987, ApJ 312, L45 and this work; (5) - Harju, Walmsley, Wouterloot, 1992, A&A 98, 51; (6) - Wilking, Mundy, Blackwell, Howe, 1989, ApJ 345, 257; (7) - Wouterloot, Walmsley, Henkel, 1988, A&A 203, 367

Evidence for a recombining wind in DR21

Andrew Harrison[1], Adrian Russell[2], Phil Puxley[2], Peter Brand[1]

1. Institute of Astronomy, Univeristy of Edinburgh, Edinburgh, Scotland
2. Royal Observatory, Blackford Hill, Edinburgh, Scotland

DR21 is one of the most powerful outflow sources in the Galaxy with a large HII region at the centre, Fig. 1 (bottom). There are two molecular clouds along the line of sight to DR21, at -3kms^{-1} and +8kms^{-1}. The ionised gas is sharply bounded to the west by a dense N-S ridge of molecular gas. Russell et.al.(1992) detected a 21cm HI jet which is capable of driving the molecular outflow in a momentum-conserving interaction. Russell et.al. proposed that the HI was formed by the recombination of an ionized wind. If this picture is correct then the ionized material should have sufficient momentum to drive the atomic jet.

We have made a single slit observation in $Br\gamma$ along the outflow axis to search for broad wings predicted by the model of Russell et.al. Fig. 2 shows the $Br\gamma$ line at the region around IRS1 , The FWHM of around 40kms^{-1} is constant along the slit and is larger than expected for a typical HII region. A preliminary analysis indicates that there is sufficient momentum in the ionized material to drive the atomic, and hence the molecular, outflow in agreement with the model of Russell et.al.

We have also made 11 deep integrations in DR21 in both CI (492 GHz) and $^{13}CO(3-2)$, to search for high velocity wings and to see if carbon was enhanced in the shocked outflow. Figure 1 (top) shows carbon emission as expected from the quiescent PDR (produced by UV photons from the HII region). Figure 1 (middle) shows carbon on IRS1. High velocity wings upto 20kms^{-1} are clearly visible.

We have found no extremely high velocity ($> 30 kms^{-1}$) emission even where H_2 spectra indicate 100kms^{-1} shocks. The ^{13}CO/CI column density ratio does not vary, within a factor of 2, across the outflow for the cloud at -$3 kms^{-1}$. ^{13}CO/CI varies by a factor > 10 in the cloud at +8 kms^{-1}, with the column density of neutral carbon remaining fairly constant across the outflow. Because there are two clouds along the line of sight to DR21 care must be taken when establishing the limits of red-shifted wing emission in carbon and comparing this directly with CO because the cloud at +8kms^{-1} appears to be almost a pure PDR in places in that it is bright in C but is faint in CO (Fig 3).

References

Russell,A.P.G.,Bally, J.,Padman, R., and Hills,R.E. 1992, Ap.J., 387,219

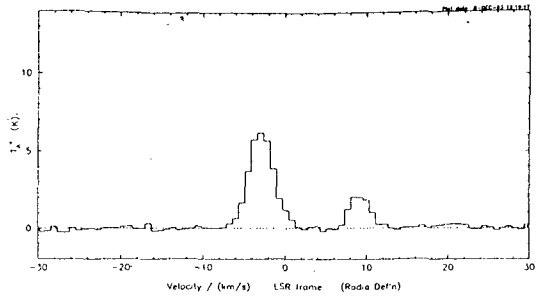

Figure 1 (top): Neutral carbon in a region purely excited by UV photons

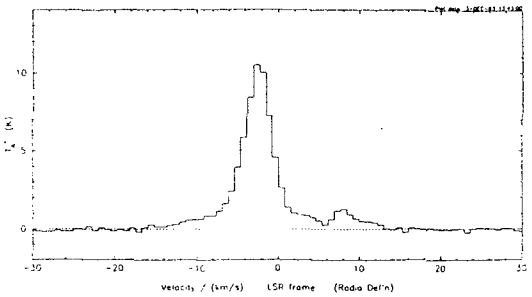

Figure 1 (middle): Neutral carbon in the outflow

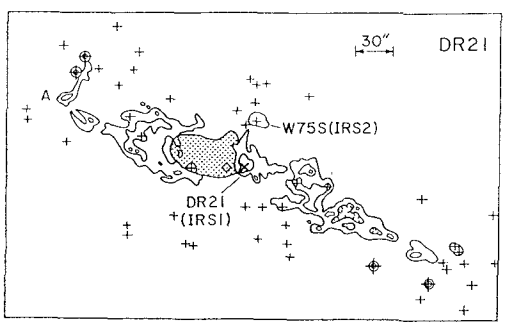

Figure 1 (bottom): Schematic outline of the H_2 emission (contours) from DR21. The dot-shaded area shows the HII region

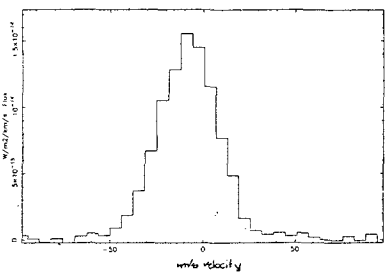

Figure 2: Brγ on IRS1.

Figure 3: A comparison of C and CO showing the cloud at $+8 kms^{-1}$ which appears to be almost a pure PDR.

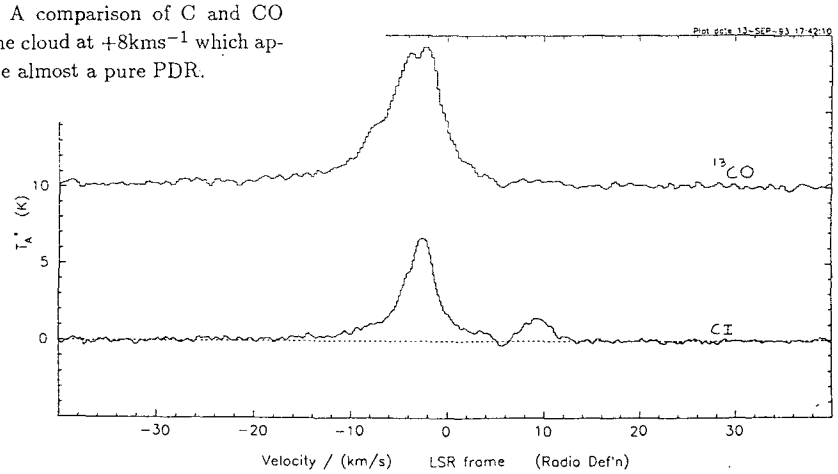

Vorticity generation in bow shocks of low excitation

Michael D. Smith

Max-Planck-Institute für Astronomie, Königstuhl, D-69117 Heidelberg.

Bow shocks are formed when clouds are disrupted by stellar outflows. A young stellar outflow may be responsible for several distinct bows, which are then designated as Herbig-Haro (HH) objects. These are radiative shocks from which we hope to learn about the physics of interstellar fluids. A comparison of emission line properties with simple theory has proved possible although the bows are often of lower excitation than would be expected from their proper motions or their spectroscopically-inferred speeds. Could this be due to the vorticity created by a curved shock front? The rapid dissipation of the vorticity through supersonic turbulence is proposed here. I show that sufficient energy is indeed available to greatly boost the high-density and low-excitation emission lines.

A quite successful model for bow shocks interprets the shock front as a mosaic of planar shocks, arranged into the chosen geometric surface. This provides a close likeness for both atomic (Hartigan et al 1987) and molecular (Smith 1991,1993) emission line properties. The model fails to explain objects with particularly low excitation (e.g. HH47A, Hartigan et al 1990) or objects with anomolous velocity dispersion differences between lines (HH2A, Böhm & Solf 1992).

Vorticity is created at a bow shock. The radiative post-shock flow is thin and hence has a strong supersonic shear. The vorticity is, in origin, caused by the obstacle in the flow which may be a jet impact, bullet or cloud. The boundary layer between the obstacle and the flow will be assumed here to be extremely thin (although it could also be unstable and turbulent and contribute to the gas heating). The decreased pressure at the flanks of the bow tends to laminarise the flow. However, turbulence seems unavoidable, being ignited by thermal and fluid instabilities, as well as upstream inhomogenieties. The turbulence is supersonic and so rapidly dissipates into heat via shocks. These weaker shocks add mainly to the strength of the low-excitation lines.

Detailed signatures of this turbulent mixing layer are difficult to extract. Displacement downstream should be observed, perhaps forming a wake or tail in cases where large-scale eddies are efficiently convected. For example, this may reproduce the long-tailed H_2 emission from the OMC-1 HH objects (Allen & Burton 1993). But can this downstream energy conversion match that of the bow shock? The total vorticity energy is estimated here. I restrict the presentation to that of a paraboloidal front with cylindrical coordinates: $z/L = (r/L)^2/2$. I take $\tan\alpha = dz/dr$ and integrate between the bow apex ($\alpha = 0$) and the tail ($\alpha = \alpha_o$, inversely related to the Mach angle or the lowest normal shock speed to significantly excite the specific energy levels of interest). The power radiated by the bow itself is $eP\int(\cos^2\alpha)rdr$, assuming a fraction e of the normal shock energy to be dissipated and $P = \pi\rho_o v_o^3 L^2$. Here $v_o\cos\alpha$ has replaced the normal component of the bow speed, v_o. Integration yields $P_b = eP\ln(\sec\alpha_o)$ with e close to unity (see below).

After complete mixing, the wake is taken to be a stream of uniform speed $\tilde{v}$. The thrust of the wake, $\dot{M}\tilde{v} = (\tilde{v}P/4\tau^2 v_o^2)(1-\tau^2)^2$ is equated here to the total post-bow thrust tangential to the bow front: $I = (2P/v_o)\int(\sin\alpha)rdr$, where $\sin\alpha$ is the tangential component of the flow speed behind the bow. This integrates to

$$I = P/(4v_o\tau^2)\left[1 + 4\tau^2\ln\tau - \tau^4\right]$$

where $\tau = \tan(\pi/4 - \alpha_o/2)$. The result is a total power dissipation a factor $P_t/P_b = \dot{M}(v_o^2 - \tilde{v}^2)/(2P_b)$ higher than that of the bow shock alone. This is rewritten as

$$\frac{P_t}{P_b} = \frac{(\tau^4 - 2\tau^2 + 1)\left[1 - \left(\frac{1+4\tau^2\ln\tau-\tau^4}{1-2\tau^2+\tau^4}\right)^2\right]}{8e\tau^2\ln(\cos\alpha_o)}.$$

I obtain $eP_t/P_b = 1.05$, 1.07 & 1.07 for $\alpha_o = 60°$, 70° and 80°. Thus it appears that at least 7% of the energy is liberated downstream of the bow surface via turbulent shocks. For an axisymmetric bow with $z \propto r^3$, 20% is reached for $\alpha_o = 80°$. A value of e is found on assuming the bow shock to be isothermal with a hydrodynamic compression factor. This yields $e \sim 1 - 1/(4\ln(M_o))$, where $M_o = v_o/c_o$ is the bow Mach number, on integrating from the apex to the Mach angle $\alpha_o = 1/M_o$. For $M_o = 10$, $e = 0.89$. Hence a paraboloid will liberate $\sim 20\%$ of the energy via supersonic turbulence.

The question then is: is 20% enough to alter the emission line strengths? A simple calculation for the commonly observed red [*SII*] lines of HH objects suggests that the vorticity generation is sufficient to account for the existing discrepancies, since the predicted [*SII*] emission is $\sim$ 0.6% and $\sim$ 3% of the total radiated emission of 100 $\mathrm{kms}^{-1}$and 20 kms^{-1}planar shocks. Hence the extra weak-shock component should at least double the [*SII*] emission line strength in this case.

In molecular shocks, the vorticity is even more significant to the far-infrared lines of [*CI*] and [*OI*] at 145μm. These lines are predicted to be extremely weak from the HH object bow surface (Smith 1991) but could be amplified by factors of 10-100 by the dissipation of the bow-generated vorticity. The turbulent eddies may be directly responsible for the observed fine-scale structure and non-uniform velocity distributions in HH objects. An extended report of this research is in preparation.

References

Allen, D.A. & Burton, M.G., 1993. Nature, 363, 54.
Böhm, K.H. & Solf, J., 1992. AJ, 104, 1193.
Hartigan, P., Raymond, J.C. & Meaburn, J. 1990. ApJ, 362, 624.
Hartigan, P., Raymond, J.C. & Hartmann 1987. ApJ, 316, 323.
Smith, M.D., 1991. MNRAS, 253, 175.
Smith, M.D., 1993. MNRAS, in press.

Near infrared observations of S155 Evidence of induced star formation?

L.K. Hunt[1], F. Lisi[2], M. Felli[2], G. Tofani[2]

[1] CAISMI-CNR, L. Fermi 5, I-50125 Firenze, Italy

[2] Osservatorio Astrofisico di Arcetri, L. Fermi 5, I-50125 Firenze, Italy

The region of sky which includes the northwestern edge of the Cepheus molecular cloud (Sargent 1979), the extended HII region S155, and the OB association Cepheus OB3 has been the subject of several studies because of a possible site of sequential star formation. The study of the OB association, which has a younger subgroup near the cloud, gives a good estimate of distance, kinematic age and expansion time scale (Blaauw et al. 1959, Garrison 1970, Garmany 1973). Radio continuum aperture synthesis observations (Felli et al. 1978) have shown that the main source of ionization of the S155 HII region, which forms a bright rim at the northern edge of the molecular cloud, is the O7 starHD 217086, a member of the OB association. The same star is the energy source of the Cepheus B clump which is the hottest core in the molecular cloud (Felli et al. 1978).

Recent measurements of molecular lines (Minchin et al. 1992), combined with IRAS maps, have shown that Cepheus B is composed of clumps encompassed by the bright rim of S155. A hotspot, observed in the CO (J=3-2) emission line, roughly coincides with an unresolved radio continuum component of the map and with a far infrared peak (Evans et al. 1981). Data are all consistent with the hypothesis of a compact HII region ionized by an embedded B1-B0.5 star. Optical and near infrared photometry (Moreno-Corral et al. 1993) has shown that the area including the interface between the molecular cloud and the extended HII region is the site of a stars cluster younger than the Cepheus OB3 association.

In order to investigate the possible existence of embedded objects of even more recent formation in the area of Cepheus B-S155 interface, we have observed the region of the compact radio continuum source with the new near infrared camera ARNICA (Lisi et al 1993) and the TIRGO telescope. The instrument is equipped with the NICMOS 3 detector array (256x256 pixels) and it operates in the broad band JHK filters with a scale of 1" per pixel. The observations were performed in two nights (Dec 24 and 26, 1992) and the 4′x4′ field was centered at the position of the unresolved radio continuum source.

Each image was obtained by coadding twenty frames, for a total integration time of 300s. The same time was spent in the integration of nearby sky frames. Sky exposures were shifted relative to the source position to an approximately empty region and taken at different non-overlapping positions. The sky frames are combined with a stack median filter and a clipping algorithm to remove most field stars, and used for the flat field corrections. A preliminary mosaic of the area was also derived from four offset images in the K-filter. The mosaic covers an area of roughly 8′x8′.

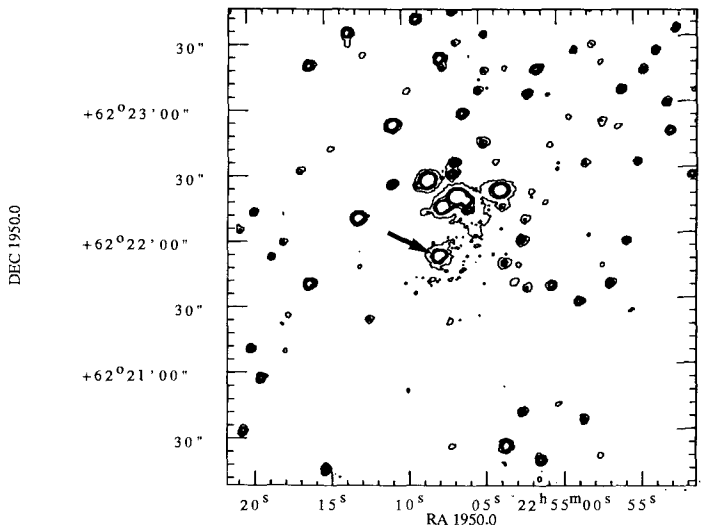

Figure 1. K-band image of CepheusB-S155 region. The arrow indicates the position of the radio component and CO peak

Standard stars were observed in the same nights, centered at different positions across the array, for photometric calibration. Images have been analyzed with the IRAF package. For each frame accurate positions were derived by a comparison with a HSTGSC optical image and star catalogues. The reduction procedure for stellar photometry is still in progress.

The preliminary analysis of the observations shows more than 150 IR sources in the JHK images (the K filter is shown in Fig. 1). Sources are not equally distributed across the area: the major density (60%) is found in the northwestern region, at the outer side of the radio continuum ridge. In the direction of the molecular cloud the number of objects decreases drastically (only 7% are in the southeast quadrant of the images).

From the astrometry, we can compare the position of the compact radiosource and of the CO (J=3-2) peak with our image . They are located south of the cluster of bright objects at the center of the frame. The radio source coincides with one of the stellar objects, which is surrounded by a faint diffuse IR emission.

References

Blaauw, A., Hiltner, W.A., Johnson, H.L. 1959, ApJ, 130, 69
Evans, N.J., Becklin, E.E., Beichman, C., Gatley, I., Hildebrand, R.H., Keene, J., Slovak, M.H., Werner, M.W., Withcomb, S.E. 1981, ApJ, 244, 115
Felli, M., Tofani, G., Harten, R.H., Panagia, N. 1978, A&A, 69, 199
Garmany, C.D. 1973, AstronJ, 78, 185
Garrison, R.F. 1970, AstronJ, 75, 1001
Lisi, F., Baffa, C., Hunt, L.K. 1993, SPIE Proc. Vol.191,6 (A.M. Fowler ed.) in press
Moreno-Corral, M.A., Chavarria-K, C., deLara, E., Wagner, S. 1993, A&A, 273, 619
Minchin, N.R., Ward-Thompson, D., White, G.J. 1992, A&A, 265, 733
Sargent, A., 1979, ApJ, 233, 163

FIR/NIR Spectroscopy of the Galactic Center Arc Region: The Importance of Massive Star Formation for Ionization

T. Krenz[1], T.R. Geballe[2], R. Genzel[1], A.I. Harris[1], A. Krabbe[1], D. Lutz[1], A. Poglitsch[1]

[1] Max–Planck–Institut für extraterrestrische Physik, Garching, FRG

[2] United Kingdom Infrared Telescope, JAC, Hilo, Hawaii

A detailed knowledge of the nucleus of our own Milky Way is of great importance for understanding galactic nuclei in general, which still is one of the most outstanding astronomical problems. Prerequisite is a detailed knowledge of the energetics and therefore of the basic heating and ionization mechanisms. The most probable processes include photoionization by recently formed OB stars, MHD shocks and relativistic particles.

Here we present evidence for recent massive star formation in the Galactic Center. We have undertaken a multiwavelength study of the "Pistol–Sickle" region, which is located ≈15' northeast of SgrA*. It is defined by two prominent radio continuum features: "The Sickle" (G0.18–0.04) and "The Pistol" (G0.15–0.05). We have obtained high resolution imaging spectroscopy of the Quintuplet, a cluster of bright IR sources 20" north of the "Pistol" using the MPE near–infrared Fabry–Perot imaging spectrometer FAST at the 4.2m William–Herschel–Telescope and subsequently observed the most interesting objects with the cooled grating spectrometer CGS4 at the United Kingdom Infrared Telescope.

In order to trace the distribution and the dynamics of the highly ionized gas we have mapped the "Pistol–Sickle" region in the [OIII]$\lambda\lambda$ 88.4μm and 51.8μm transition with the MPE–UCB far–infrared Fabry–Perot imaging spectrometer FIFI on board the NASA Kuiper Airborne Observatory (KAO). The 88μm line very closely follows the CS emission (Serabyn & Güsten 1990) and the thermal radio continuum (Yusef-Zadeh 1986), which is almost perpendicular to the straight nonthermal filaments (Fig.1).

From the [OIII] intensity ratio I(52μm)/I(88μm) we derive a density of the [OIII] emitting medium of ≈150 cm^{-3}. The column density is $N_{[OIII]} \approx 6 \times 10^{17}$ cm^{-2}.

This is much higher than the upper limit of $N_{[OIII]} = 10^{14.5}$ cm^{-2} predicted by standard shock models (Shull & McKee 1979). Therefore MHD shocks can be ruled out as the main excitation source of the [OIII].

Relativistic particles streaming along the nonthermal filaments can be ruled out for morphological reasons. As this mechanism can only work where the oxygen encounters the relativistic particles, it can not account for the observed ionization between the filaments and in the southern part of the cloud.

UV flux from hot young stars can explain the ionization. We have observed two stars in the Quintuplet showing strong HeI 2.058μm emission lines and a shallow P-Cygni absorbtion feature. Their spectra closely resemble those of the He stars recently found in the central cluster. These objects are young (10^5–10^6years) blue supergiants (Najarro et al. 1993), and their presence is clear evidence for recent massive star formation in the Galactic Center. The particular meaning of this detection is that it is now possible to identify UV luminous stars in the Galactic Center, where main–sequence OB stars

cannot be seen directly due to the high extinction ($A_V = 30$mag).
Combining the observed number and predicted properties of the He stars with a standard IMF (Scalo 1986) leads to the number of associated main-sequence OB stars. The UV flux from the $\approx$100 O stars associated with the newly found He stars can account for the amount of ionized gas in the "Pistol-Sickle" region.

References

Najarro et al. A&A, in press.
Scalo, J.M., Fundamentals of Cosmic Physics, 11, 3, 1986
Serabyn, E., Güsten, R., A&A 242, 376 (1991)
Shull, J.M., McKee, C.F., ApJ 227, 131 (1979)
Yusef-Zadeh, F., Ph.D. Thesis, Columbia University, 1986

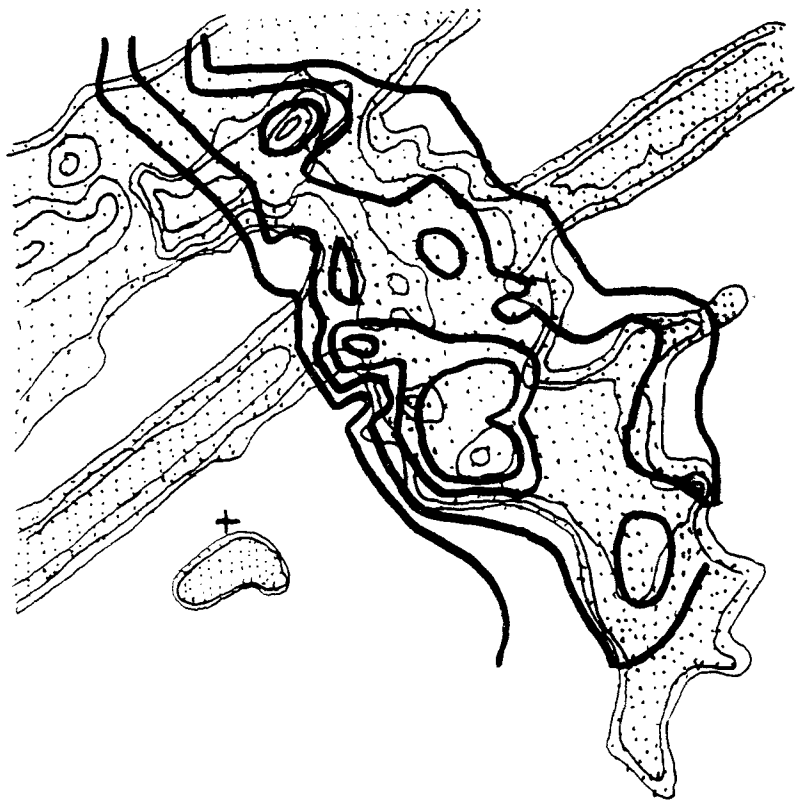

Fig.1: Map of the velocity integrated [OIII] 88μm line in the "Pistol-Sickle" region. The contour interval is 7.5×10^{-4} erg cm^{-2} sr^{-1} s^{-1}. The superimposed dotted area and the thin contours represent the 6cm radio continuum (Yusef-Zadeh 1986). The nonthermal filaments extend from the lower left to the upper right. The cross marks the position of the Quintuplet cluster.

Multi-Wavelength Study of NGC 281 A

Th. Henning[1], K. Martin[1], R. Launhardt[1], H.-G. Reimann[2]

[1] Max Planck Society, Research Group "Dust in Star-forming Regions",
Schillergäßchen 2-3, D-07745 Jena, Germany
[2] Astrophysical Institute and University Observatory,
Schillergäßchen 2, D-07745 Jena, Germany

Abstract: We present the first results of a multi-wavelength study of the molecular cloud NGC 281 A and the associated compact and young optical star cluster NGC 281 (AS 179). This complex seems to be a very promising candidate for externally triggered star formation. NGC 281 shares many properties with the Orion θ^1 OB-BN/KL system the main difference being a larger separation between the cluster centroid and the new site of star formation as well as lower mass and luminosity of the molecular cloud and the infrared cluster, respectively.

Introduction: NGC 281 (S 184) is an emission region located in the Perseus arm which is excited by a very young and compact cluster of OB stars whose brightest member is the multiple system HD 5005. In the immediate environment of HD 5005 the peanut-shaped molecular cloud NGC 281 A is located (Leisawitz et al. 1989). Observations of ^{12}CO(1→0) by Elmegreen and Lada (1978) show two molecular cloud fragments which appear to be separated by a channel of ionized gas at the southern edge of the HII region. An H_2O maser, generally considered to be an indicator of massive star formation, exists at the projected ionization boundary on the surface of the western cloud fragment (Elmegreen & Lada 1978, Henning et al. 1992). The maser is associated with the IRAS point source 00494+5617. From a NIR camera survey, Carpenter et al. (1993) found a star cluster toward this IRAS source.

The NGC 281 region is particularly well suited to offer valuable clues to the nature of the interaction between young star clusters and their adjacent molecular clouds:

1. NGC 281 is at a relatively high galactic latitude (-6° 24').
2. It is easy to analyze because the source of Lyman-continuum radiation is still a compact cluster and the spatial arrangement of interstellar matter with respect to the cluster as well as to the CO cloud structure appears to be simple.

Results: We made a multi-wavelength study of the complex in order to characterize the structure of the molecular cloud and observed the ^{12}CO(2→1), ^{13}CO(2→1), and ^{12}CO(3→2) transitions with the KOSMA 3-m Gornergrat telescope. The region around the southern part of NGC 281 was completely mapped in all three transitions.

In the ^{12}CO(3→2) transition, the eastern fragment shows some dense clumps along the ionization-dissociation front. A comparison of IRAS maps with the ^{12}CO(3→2) images reveals an association of warm clumps with IRAS sources. The western fragment shows a compact structure in all three measured transitions and contains a dense molecular cloud core. This core is associated with the IRAS source 00494+5617 and the H_2O maser. Both cloud fragments contain altogether 22 IRAS point sources which mostly share the properties of young stellar objects. They have bolometric luminosities between 150 and 8800 $L_\odot$. The ^{12}CO measurements led to a mass of about $1.7 \cdot 10^4$ $M_\odot$ for the eastern fragment and $2.4 \cdot 10^4$ $M_\odot$ for the western fragment. We found that the maxima of the 60 and 100 μm HIRES maps correspond to the maxima of the ^{12}CO(3→2) emission (see Fig. 1). From the coincidence of the CO peaks with the positions of the most luminous IRAS point sources, we conclude that the molecular gas is heated by these embedded young stellar objects.

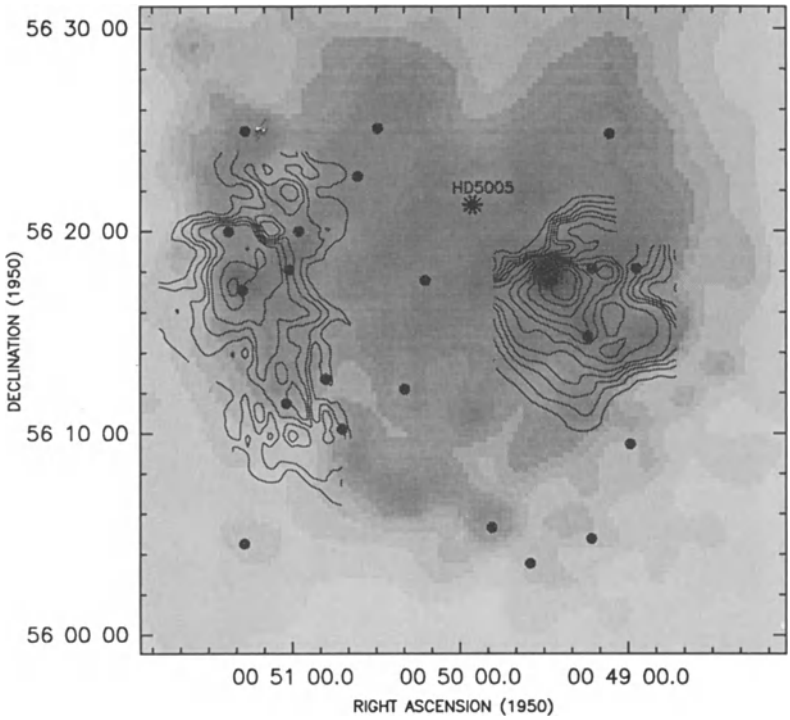

Fig. 1: 60μm (gray-scale image) and $^{12}CO(3\rightarrow2)$ emission (contour lines) together with the IRAS point sources indicated by dots

NH_3 observations were made with the Effelsberg 100-m telescope. We mapped the central part of the western cloud fragment and found that the IRAS source 00494+5617 is embedded in a dense NH_3 clump. The clump size is of the order of the beam size (40"). For the mass of this clump we estimate 500 $M_\odot$ assuming a $N(NH_3)/N(H_2)$ ratio of 10^{-8}. Such a central core of the western fragment was also found in the $CS(2\rightarrow1)$ observations by Carpenter et al. (1993).

Both molecular cloud fragments were mapped at 1.3 mm with the MPIfR 7-channel bolometer system at the IRAM 30-m Pico Veleta telescope. We clearly detected emission centered at the positions of the two luminous IRAS sources 00494+5617 and 00512+5617. However, the western clump is much more prominent compared with the eastern fragment. From the energy distribution, there is evidence that this clump contains an unresolved very dense and compact component of about 45 K temperature and a diameter of about 5000 AU or 2-3". A spherically symmetric radiative transfer model for the western fragment resulted in an estimate for the visual extinction of 160 mag. In this respect, it is quite remarkable that Carpenter et al. (1993) did not find NIR sources in the centre of the western fragment which points to high extinction even in the NIR wavelength region.

Photoelectric photometry in the uvby system for the members of the optical star cluster with the 90-cm telecope at the Großschwabhausen observing station of the Jena University Observatory led to a new and more accurate determination of the distance to the cluster. We

found a value of 3.5kpc which is definitely larger than the value previously adopted (2.2kpc). Furthermore, we obtained O6 III as the photometric spectral type for the central star HD 5005.

Summary: The NGC 281 A complex seems to be an example for externally triggered star formation. Ionization/shock fronts from a first generation of high-mass stars initiate the formation of a new generation of stars in the molecular cloud. During this process the cloud gets successively disrupted. Kinematic evidence for a shock passage through the western molecular cloud fragment was found by Elmegreen & Moran (1979). A more detailed study by Henning et al. (1994) shows that NGC 281 A shares many properties with the Orion θ^1 OB-BN/KL system the main difference being a larger separation between the centroid of the optical star cluster and the new site of star formation as well as lower mass and luminosity of the molecular cloud and the infrared cluster.

References

Carpenter, J.M., Snell, R.L., Schloerb, F.P., Skrutskie, M.F. 1993, ApJ, 407, 657
Elmegreen, B.G., Lada, C.J. 1978, ApJ, 219, 467
Elmegreen, B.G., Moran, J.M. 1979, ApJ, 227, L93
Henning, Th., Cesaroni, R., Walmsley, M., Pfau, W. 1992, A&AS, 93, 525
Henning, Th., Martin, K., Reimann, H.-G., Launhardt, R., Leisawitz, D., Zinnecker, H. 1994, in preparation
Leisawitz, D., Bash, F.N., Thaddeus, P. 1989, ApJSS, 70, 731

First Tentative Detection of the Molecular Oxygen Isotopomer $^{16}O^{18}O$ in Interstellar Clouds

L. Pagani [1], W.D. Langer [2], A. Castets [3]

[1] DEMIRM, URA 336 du CNRS, Observatoire de Meudon, 92190 Meudon, France
[2] MS 169-506, Jet Propulsion Laboratory, Pasadena, CA 91109, USA
[3] Observatoire de Grenoble, B.P. 53X, 38041 Grenoble Cedex, France

We report (Pagani et al. 1993) the first tentative detection of molecular oxygen in interstellar clouds by observation of the 234 GHz (N,J) = (2,1) - (0,1) line of the isotopomer $^{16}O^{18}O$ towards L134N (Fig. 1). The line has a peak intensity of 18 $\pm$ 6 mK and an integrated intensity of 5.3 $\pm$ 1.8 mK km s^{-1}. Two other lines are present within the ^{12}CO linewidth which are probably unidentified lines, but could arise from other weaker clumps. We also detected a feature in NGC 7538 (Fig. 2) in our first observing run with a peak intensity of 10.0 $\pm$ 2.2 mK and an integrated intensity of 13 $\pm$ 2 mK km s^{-1}. However, we could not confirm this detection during our last observing session and, although we checked that this is not a telluric line, we believe that this line is suspicious. The ratio of $^{16}O^{18}O/C^{18}O$ in L134N is 0.8 if we restrict the $C^{18}O$ column density to the $^{16}O^{18}O$ linewidth and 0.4 using the entire $C^{18}O$ line. The corresponding O_2/CO ratio (0.2 to 0.4) implies that the fractional abundance of gaseous oxygen is about (4-8) x 10-5, in agreement with gas phase chemical models. We also observed two other cold dark clouds (B5 and TMC 2) but without success; our upper limits for these sources are significantly below those reported previously but above our tentative detection in L134N.

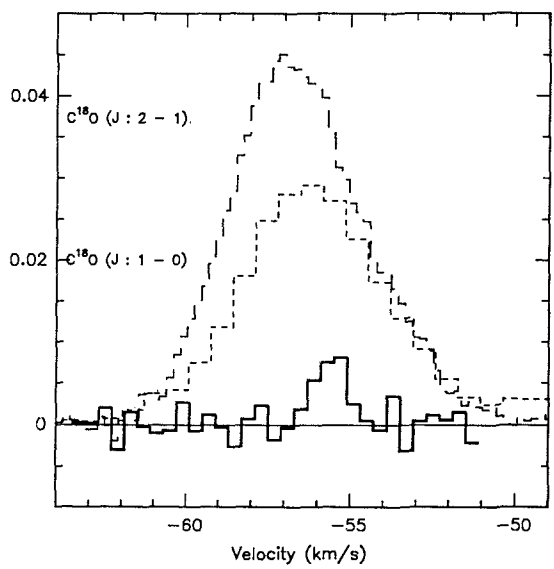

Fig. 1: L134N ^{12}CO and $C^{18}O$ (J : 1 - 0) and $^{16}O^{18}O$ (N,J) (2,1) - (0,1) lines. Horizontal axis is the LSR Velocity (km s-1) and vertical axis is the corrected radiation temperature Tr* as defined by Kutner & Ulich 1981. The $C^{18}O$ line has been divided by 30 and the ^{12}CO line by 60

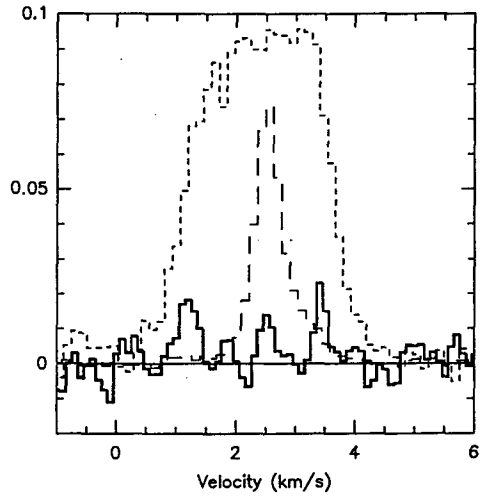

Fig. 2: NGC 7538 $C^{18}O$ (J : 1 - 0), (J : 2 - 1) and $^{16}C^{18}O$ (N,J) (2,1) - (0,1) lines. Same characteristics as in Fig.1

References

Pagani L., Langer W.D., Castets A., 1993, A&A 274, L13

Molecular Outflows Driven by Optical Jets

Rachael Padman and John Richer
Mullard Radio Astronomy Observatory, Cavendish Laboratory, Madingley Road, Cambridge CB3 0HE, England

Introduction

Examples of highly-collimated, high-velocity molecular outflow from young stellar objects are accumulating rapidly. Probably for reasons of sensitivity, the best known of these, such as the unipolar outflow from NGC 2024 FIR 5 (Richer *et al.*, 1991), occur in regions of high mass star formation, but the collimation phenomenon is not restricted to those objects with high-mass high-luminosity driving sources. L1448 (Bachiller *et al.* 1990) and VLA 1623.4-2418 (André *et al.*, 1992) are low-mass objects which also exhibit collimated molecular outflows. The outflow in L1262, another example observed recently at the JCMT, and shown below (Fig. 1), originates from a $0.3 L_{\odot}$ object, one of the lowest luminosity embedded sources found in the IRAS Point Source Catalog.

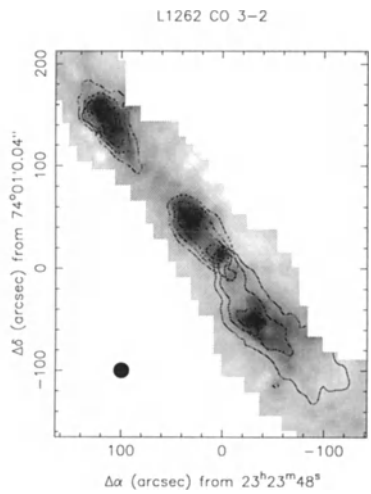

Figure 1: The molecular outflow in L 1262. Solid contours show blue-shifted CO(3→2) emission, dashed contours are red-shifted emission; both are overlaid on a greyscale of the peak temperature in the CO line.

Many more evolved, low luminosity, pre-main sequence stars have very highly collimated "optical" jets, which can be observed in such species as Hα and optical emission lines characteristic of weak shocks. It is natural to ask whether the two types of outflow are related in some way.

'The momentum problem'

The high degree of collimation seen in the very highest velocity molecular gas, and indeed, the very existence of molecular gas with velocities comparable to that of the optical jet — a few hundred kms^{-1}— strongly suggest a causal association. Intuitively, it seems that the optical jet, however *it* is itself excited, may be entraining the molecular material in the ambient cloud, and accelerating it to high velocities (see Masson & Chernin, 1993, for a review of the

case favouring this viewpoint). This then eliminates the requirement for a second mechanism independent from that driving the optical jet and allows us to dispense with the somewhat artificial "two-wind" models sometimes put forward to explain the coexistence in some sources of both optical and molecular outflow.

Unfortunately, one major objection seems to scupper this idea. A straightforward comparison of the present day momentum in the molecular outflow with the momentum *flux* in the optical jet makes it clear that the jet *cannot* have been responsible for the outflow *if* the duration of the interaction is assumed to be limited to the outflow dynamical timescale, R/V (where R is the maximum extent of the molecular outflow and V is the maximum observed velocity). There is however a body of evidence that suggests that this assumption is incorrect.

Two statistical studies in particular make this clear. Parker *et al.* (1991) used the JCMT to map a sample of 12 sources from a complete sample of embedded IRAS sources associated with Lynds dark clouds of opacity class VI. These sources have a very high probability of being proto-T-Tauri stars, which are known to have birthline ages of about 2×10^5 years. The clear detection of CO outflow in 9 sources thus gives a *statistical* lifetime of 1.5×10^5 years, which for the sources in the sample is approximately a factor of 10 higher than their dynamical timescales.

The second study, following a similar logic, compares the frequency of outflows with that of *visible* T-Tauri stars. Fukui *et al.* (1993) mapped a large area of L 1641 in CO(1→0), using the Nagoya 4-m telescope. Because of their larger beam, the dynamical timescales derived for their sources are somewhat larger than for the sample of Parker *et al.* (larger sizes and lower maximum velocities are measured for most sources), but the statistical lifetime, using the visible T-Tauri star ages as a yardstick, is again of the order of 10^5 years. So these two studies both show that the molecular outflow survives for much longer than its dynamical timescale.

Why is the dynamical timescale so much less than the source age? Either R increases much more slowly than the speed of the material in the outflow, or else the speed of the outflow is greatly overestimated. We favour the former possibility, and in support of this conclusion note that this is accepted as the norm in discussions of extragalactic double radio sources. In that case a supersonic, but light, jet (one that is less dense than the ambient medium), produces a classic two-shock structure in a momentum-conserving interaction at the jet/IGM interface. The speed of advance of this bowshock is given by:

$$v_{\rm bs} = \frac{v_{\rm j}}{1+\sqrt{\rho_{\rm amb}/\rho_{\rm j}}},$$

where $\rho_{\rm amb}$ and $\rho_{\rm j}$ are the ambient and jet densities respectively, and $v_{\rm j}$ is the jet velocity. The ages of these sources also are thus many times greater than their dynamical timescales.

Richer *et al.* (1992) used this idea to model the NGC 2024 molecular outflow, assuming an underlying and unseen "optical" jet (of really quite reasonable parameters) propagating in a cloud whose density profile was established from observations of CS and $C^{18}O(2\rightarrow1)$. Depending on the exact details of the model, the bowshock takes between 40 and 60 000 years to reach its present position, although the present-day dynamical timescale is only 6000 years. The key point is to recognize that although visible "optical" jets are, without doubt, denser than the ISM through which they propagate, this need not apply to *hidden* jets — in fact one of the reasons they are *not* visible optically is that in this case the surrounding cloud has much higher column and volume density.

Evidence for interactions

As noted, there are very few sources where an optical jet can be observed interacting with a molecular outflow. One such is RNO 43, for which CO mapping at the JCMT shows a dense parabolic shell surrounding the bowshock at the end of optical jet. The outflow in RNO 43 lies almost in the plane of the sky, so that only transverse velocities are observed. The highest velocity red and blue-shifted emission is observed to be concentrated exactly at the head of the Hα jet, while away from the jet head the expansion velocity slowly decreases as the shell radius increases (Padman & Richer, 1994). Bence, Richer & Padman (in prep.) interpret this

as the lateral component of the expansion occurring when ambient cloud material is heated in a shock interaction with a supersonic jet, as modelled using SPH techniques by Chernin *et al.*(1994). We note however that the source ages predicted by the SPH modelling are at present too low, and that it may be necessary to invoke a spatially and/or temporally varying jet in order to reproduce the observations more accurately.

References

André, Ph., Martin-Pintado, J., Despois, D., Montmerle, T. 1990. *A & A* 236 180.
Bachiller, R., et al. 1990. *A & A*, 231, 174.
Chernin, L., Masson, C.R., Gouvia Dal Pino, E.M., Benz, W., 1994. *Ap.J.* (in press)
Fukui, Y., Iwata, T., Mizuno, A., Bally, J., Lane, A.P., 1993. p603 in *Protostars & Planets III*, ed. E.H. Levy & J.I. Lunine, Univ. Arizona press, Tucson.
Masson, C.R., Chernin, L.M., 1993. *Ap.J.*, 414, 230.
Padman, R., Richer, J.S., 1994. *Kinematics and Dynamics of Diffuse Astrophysical Media*, ed. J.E. Dyson (in press)
Parker, N.D., Padman, R., Scott, P.F., 1991. *MNRAS* 252, 442.
Richer, J.S., Hills, R.E., Padman, R., 1992. *MNRAS* 254, 525.

Jet-Driven Molecular Outflows

C. R. Masson[1] and L. Chernin[2]

[1] Center for Astrophysics, 60 Garden Street, Cambridge, MA 02138, USA
[2] Astronomy Department, University of California, Berkeley, CA 94720, USA

Outflow Models

Although molecular outflows from young stars were discovered more than a decade ago, it is only recently that quantitative models describing their properties have begun to emerge. It is generally accepted that the flows are swept up from the ambient clouds by a wind or jet, but there has been some dispute about the mechanism and type of wind. The types of models discussed in the literature can broadly be divided into two classes (fig. 1): "wind" models driven by a poorly collimated wind from the star, and "jet" models driven by a highly collimated jet. Although many young stars are observed to have jets, the wind models have traditionally been favored because it was thought that the jets were too weak to drive the flows (e.g. Mundt et al. 1987). However, recent analysis (Padman 1994) shows that jets are strong enough to drive the flows. The discussion below shows that wind models also have difficulties in matching the observed characteristics of the flows.

The wind models divide into two classes, *pressure-driven*, and *momentum-driven*. In the pressure-driven type, a fast wind is supposed to shock inside the lobe, creating a high temperature gas which pushes the ambient medium outward at the surface of the lobe. In the momentum-driven type, the shock is supposed to be highly radiative, dissipating the energy, so that only the momentum remains to drive the swept-up ambient medium. The pressure-driven type can easily be ruled out, since it cannot give rise to bipolar flows. As noted by Meyers-Rice & Lada (1991), the pressure exerts a force normal to the surface of the lobe and should result in velocities in all directions in each lobe, in contradiction to observations, which show most velocities directed along the axis. This result can also be seen by considering conservation of momentum in each lobe. If one part of the lobe moves outward, away from the star, other parts must move in the opposite direction to conserve momentum (Masson & Chernin 1993).

Static pressure in the ambient medium could, in principle, oppose the pressure in the lobes, but this type of model is unable to produce the observed supersonic flows, which require shocks with very large overpressure (~ 1000). It is implausible that the ambient cloud could have such a large pressure gradient that it is in equilibrium with the inside of the lobe over most of the lobe surface, but out of equilibrium by a factor of 1000 in other parts.

Momentum-driven winds suffer from the problem that they have too much mass at the ends of the lobes. Since the momentum vector of the wind from the star is directed radially outward, the swept-up ambient material must also be pushed radially outward, sweeping up a large mass along the axis. As shown by Masson & Chernin (1992), this type of model will produce very unrealistic results, with too much mass both at extreme velocities and at the ends of the lobes.

Figure 1. (a). Wind model for a molecular outflow where the lobs are driven by a wide-angle wind from the central star. (b) Jet model, where the lobes are driven by a highly collimated jet.

It has therefore been concluded by several authors that molecular outflows must be driven by jets (Masson & Chernin 1992, 1993; Raga & Cabrit 1993; Stahler 1993). Here again, there are two types of model (DeYoung 1986). In the first, the interaction between the jet and the ambient medium is dominated by entrainment along the sides of the jet. This "steady-state" mode is dominant at low Mach numbers. It has the property that the jet is progressively weakened as its momentum is coupled to the ambient medium. After some distance, the jet becomes subsonic and rapidly disrupts. The survival distance increases rapidly with Mach number.

The second type is "prompt" entrainment, dominant in high Mach number jets, where the interaction occurs in a bow shock at the head of the jet. The resulting high pressure gas pushes the ambient medium away from the jet into a swept-up shroud, with a low density "cocoon" surrounding the jet and isolating it from the ambient medium, inhibiting the steady-state entrainment.

Model Results

We have modeled the properties of jet driven flows in two ways. First, we calculated simple analytic models which reproduced many of the properties of molecular flows, such as spatially compact extremely high velocity (EHV) regions, which we identify with bow shocks (Masson & Chernin 1993). In our numerical modelling shown in figure 2 (Chernin et al. 1994), we were able to reproduce the characteristics of EHV "bullet" features like those seen in sources such as L1448 (Bachiller et al. 1991). The dense clump of EHV material ("bullet") is produced right at the head of the bow shock, where strong cooling permits the shocked material to condense. In our model, the density was limited by a low-temperature limit of 10,000K, but in practice the density would probably be limited by magnetic fields. Although these models give a good account of the local, short-term interaction between the jet and the ambient medium, the long term development is still problematic. A straight, continuous jet would propagate to the length of a typical outflow in about 1000 years, but outflows are known to be much older, and to contain more momentum than a jet could supply in that short time. Secondly, the outflow produced by such a jet would be much narrower than typically observed. The solution to these problems is that the jet probably varies over its life, either in velocity (Raga & Cabrit 1993) or in angle (Masson & Chernin 1993) or both. So far, only simple models have been made of flows produced by such variable jets.

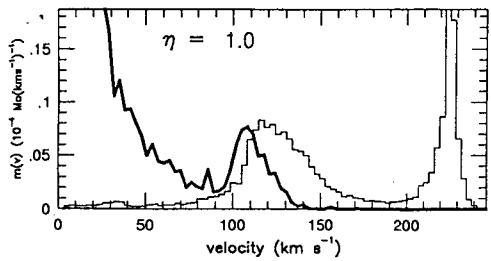

Figure 2. Mass spectrum of material near the head of the jet in a bow shock. The light line shows jet material and the heavy line shows ambient material. The feature near 120 km/s resembles a so-called "molecular bullet."

Outflow Statistics

The improved understanding of outflow properties has led to a new interpretation of outflow statistics. It has long been realized that most of the commonly quoted properties of outflows, such as mass and velocity, are ill-defined, as they depend strongly on the velocity range used for the integration (e.g. Lada 1985). Recently, Masson & Chernin (1994) have shown that only momentum can be calculated in a consistent way. If it is assumed that all of this momentum is supplied by a jet with a velocity of 300 kms^{-1}, it is possible to estimate the total mass ejected in the jet, integrated over the age of the flow. The lowest luminosity sources, such as VLA1623, have derived jet masses of $\sim 0.005 M_{\odot}$, while the most luminous have jet masses approaching 1 $M_{\odot}$. Since the mass range of the underlying stars is roughly 0.1 - 10 $M_{\odot}$, and the jet masses are slightly underestimated, we estimate that roughly 10% of the mass of a typical star is ejected in a jet during its formation.

References

Bachiller, R., Cernicharo, J., Martin-Pintado, J., Tafalla, M., & Lazareff, B. 1990, A&A, 231, 174

Chernin, L. M., Masson, C. R., Dal Pino, E., & Benz, W. 1994, ApJ, in press

De Young, D. S. 1986, ApJ, 307, 62

Lada, C. J. 1985, ARA&A, 23, 267

Masson, C. R. & Chernin, L. M. 1992, ApJ, 387, L47

Masson, C. R. & Chernin, L. M. 1993, ApJ, 414, 230

Masson, C. R. & Chernin, L. M. 1994, ApJ, submitted

Meyers-Rice, B. & Lada, C. J. 1991, ApJ, 368, 445

Mundt, R., Brugel, E. W., & Buhrke, E. 1987, ApJ, 319,275

Padman, R., 1994, these proceedings

Raga, A. C., & Cabrit, S. 1993, A&A, in press

Stahler, S., 1993, in *Astrophysical Jets*, eds. M. Livio, C. O'Dea, & D. Burgarella, Cambridge University Press

$C^{17}O$ and submillimetre continuum observations of M17SW

M.P. Hobson

Mullard Radio Astronomy Observatory, Cavendish Laboratory, Madingley Road, Cambridge CB3 0HE, England

Introduction

The M17SW molecular cloud core is adjacent to the M17 H^+ region, at a distance of 2.2 kpc, and appears to be an excellent example of triggered star-formation. A nearby cluster of OB stars, recently formed from the molecular cloud complex, is surrounded by a prominent H^+ region which is heating and compressing the molecular material, possibly initiating its collapse to form the next generation of stars. Using the JCMT, this region has been mapped in the $C^{17}O$ $J = 3 \rightarrow 2$ transition at 15-arcsec resolution, and in 450, 600, 800, 1100 and 1300 μm continuum emission, giving 8-arcsec resolution for the shortest wavelength (Hobson et al. 1993a,b)

$C^{17}O$ $J = 3 \rightarrow 2$ observations

The large scale structure of the maps agree well with previous observations with previous observations (e.g. Stutzki & Güsten 1990), and the clumpy nature of the cloud core is clearly revealed in this optically thin transition. Obvious features include the northern condensation, the well defined 'hole' in emission to the west of this region, and the bright ridge of emission running S–E along the H^+ region/molecular cloud interface (Fig. 1b). A more detailed comparison reveals a close agreement between individual peaks of emission, particularly in the prominent northern condensation (NC) region. In the NC region the emission is dominated by three main clumps, although it is possible that these clumps may themselves be comprised of smaller components.

We find that the NC coincides closely with the NH_3 clumps observed by Massi, Churchwell & Felli (1988), and is bounded to the N–E by a radio-continuum arc found by Felli, Churchwell & Massi (1984), which contains the ultra-compact H^+ region M17-UC1. The overall velocity structure of the NC suggests that it may be the front face of a shell of molecular material expanding at $\sim$ 1.5 km s^{-1} (SG90; Hobson 1992, Hobson et al. 1993a), possibly driven by the outflows of a few unobserved low to medium mass stars.

A Gaussian clump decomposition of the $C^{17}O$ data-set, similar to that used on the $C^{18}O$ emission by SG90, identifies 35 clumps. After deconvolving the beam, these clumps range in size from $\sim$ 0.05 to 0.5 pc, with characteristic linewidths of 1 - 2 km s^{-1}. Clump masses range from 10 to 10^3 $M_\odot$ and are consistent with a power-law mass-spectrum of the form $dN/dM \propto M^{-2.1}$. The clump volume filling factor is about 0.1 – 0.2. Molecular hydrogen densities range between 10^{11} – $10^{11.5}$ molecules m^{-3}, with a clump-interclump contrast of at least $\sim$ 20. Clumps are found to have velocity dispersions slightly less than required for virial equilibrium, suggesting that they may be unstable to gravitational collapse. Larson's $M \propto R^2$ relation is observed, but is severely affected by observational selection effects, while no correlation is found between size and linewidth.

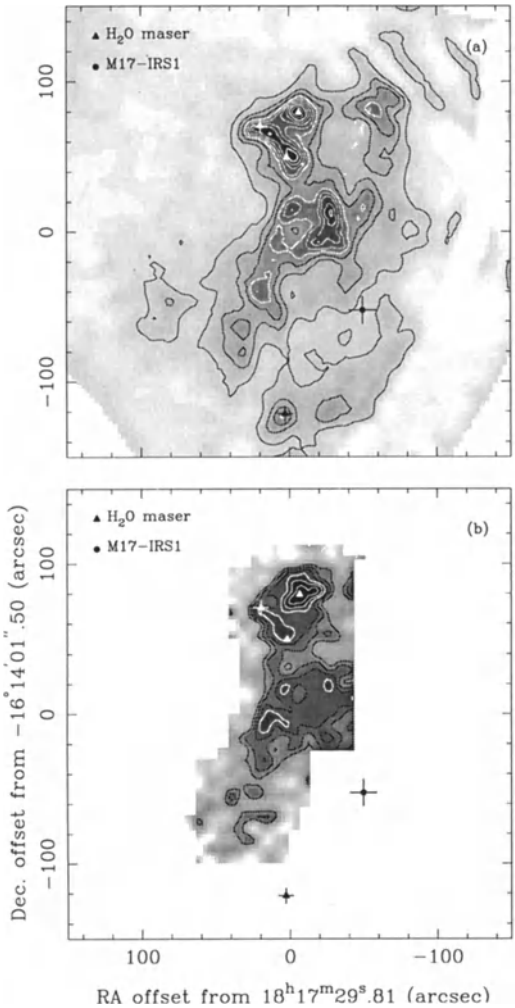

Figure 1: A comparison of (a) the 600-μm emission, and (b) the $C^{17}O$ $J = 3 \rightarrow 2$ integrated intensity in M17SW. Also shown are the positions of the four known H_2O masers in the region and of the infrared source M17-IRS1.

Continuum Observations

The continuum dust emission was found to be optically thin at all the observed wavelengths, and we therefore expect these observations to be good tracers of column density, albeit weighted by temperature. The 600 and 450 μm maps, in particular, show the dust emission to be highly clumped (Fig. 1a); these clumps may, in some cases, be identified with those observed in $C^{17}O$ line emission. A comparison of the 600 μm and $C^{17}O$ maps shows not only the same broad regions of emission, but that individual features across the two maps have relative positions which coincide to within 2–3 arcsec (Fig. 1). This close correlation suggests that the dust and molecular line emission are sampling the same volume of gas.

Fig. 1 also shows the four known H_2O masers in the M17SW region to be closely associated with peaks in the dust and molecular line emission. The flux from the NC is again dominated by three main component, which we label N–S as FIR1–FIR3, each of which lies within a few arcsec of an H_2O maser. These objects have masses in the range 300–450 $M_\odot$, with luminosities of 8000–12000 $L_\odot$, and appear to be gravitationally unstable. These values are consistent with them containing young stellar objects of mass $\sim$ 10 $M_\odot$. The positions of FIR1–FIR3 are consistent with them lying in the shell of material observed in $C^{17}O$, and suggests that the formation of these features may have been triggered by the compression of the gas from both sides.

Greybody fits to the mm and sub-mm fluxes suggest a characteristic dust temperature of 30 K and a dust index $\beta \approx 2$, and imply masses of 7600 and 1300 $M_\odot$ for the entire M17SW region and for the NC respectively. These masses are underestimates by about a factor of two as compared to those derived from the $C^{17}O$ data and the $C^{18}O$ observations by SG90. This discrepancy may be due to either calibration difficulties or to the presence of a lot of cold dust. Indeed, the continuous dust temperature analysis of Xie et al. (1993) suggests that there is a significant mass of dust at $\sim$ 20 K, resulting in a mass estimate closer to those derived from the molecular line emission.

References

Felli M., Churchwell E., Massi M., 1984, A&A, 136, 53
Güsten R., Fiebig D., 1988, A&A, 204, 253
Hobson M.P. 1992, MNRAS, 256, 457
Hobson M.P., Jenness T., Padman R., Scott P.F., 1993, MNRAS, in press
Hobson M.P., Padman R., Scott P.F., Prestage R.M., Ward-Thompson D., 1993, MNRAS, 264, 1025
Massi M., Churchwell E., Felli M., 1988, A&A, 194, 116
Stutzki J., Güsten R., 1990, ApJ, 356, 513 (SG90)
Xie T., Goldsmith P.F., Snell R.L., Zhou W., 1993, ApJ, 402, 216

Submillimetre Observations of the Mon R2 Cluster

H.E. Matthews[1], G.F. Mitchell[2], J. Giannakopoulou[2]

[1]Joint Astronomy Centre, University Park, Hilo, Hawaii 96720, U.S.A.
[2]Dept. of Astronomy, St. Mary's University, Halifax, Nova Scotia, Canada B3H 3C3

The Mon R2 molecular cloud contains a cluster of infrared sources (Aspin and Walther 1990), a compact HII region (Massi *et al.* 1985) and a large and complex bipolar CO outflow (Meyers-Rice and Lada 1991, and references therein). At a distance of 830 pc, the cloud extends for about 30 pc; the dense core is $\sim$0.5 pc in extent. From these and the many other observations it is clear that Mon R2 contains many of the signatures of star formation. Not so clear however is the *present* status of the Mon R2 core as a star-forming region. One of the brightest infrared sources (IRS 3 in the nomeclature of Hackwell *et al.* 1982) does appear to be a compact stellar cluster with a massive circumstellar disk (Koresko *et al.* 1993) and seems to be a site of present activity. Is this the source also of the extended outflow, or is it a separate, younger object; and is IRS 3 the last site of star formation in the Mon R2, or are some of the other infrared sources also at an early evolutionary state?

We have undertaken an extensive program of (mostly) submillimetre observations with the JCMT[2] on Mauna Kea to gain some insight into these questions. Fundamentally we are interested in obtaining the true density distribution and velocity field of the Mon R2 core.

We have made maps in the ^{12}CO(3$\rightarrow$2), HCN(4$\rightarrow$3) and $H_2CO(5_{15}\rightarrow4_{14})$ transitions, with supplementary measurements in the ^{13}CO(3$\rightarrow$2), CO(2$\rightarrow$1) transitions and two other H_2CO lines. The beamsize of the JCMT is about 21″ at the lower frequencies and 14″ for CO(3$\rightarrow$2). In addition we made continuum mapping observations using the facility bolometer over a comparable region of the Mon R2 core, at four wavelengths, 450, 800, 1100 and 1300μm. The beamsizes for the latter observations range from 14 to 25″. Below we comment on some of our conclusions, mostly from a morphological standpoint.

CO(3$\rightarrow$2) emission is detectable at all velocities from -10 to 30 kms^{-1}. A map of the total integrated emission shows three main concentrations, one in the north (blue-shifted overall), one in the southeast (red-shifted, and one coincident with IRS 3, surrounding an area of much lower integrated intensity in the centre, where the HII region and the core of the IR cluster are situated.

The CO velocity profiles are very complex. Nevertheless CO(3$\rightarrow$2) is not optically thick for most velocities, and we are confident that most of the gas has been detected. On the basis of an examination of the intensity distribution and velocity information in the CO data we identify 13 physically distinct density enhancements, or 'clumps'. Under standard assumptions the masses of these clumps range from less than 0.1 up to 2.7M$_\odot$, and the molecular hydrogen densities lie between about 10^3 and 10^5 cm^{-3}. One of the most dense and massive clumps is coincident with IRS 3. The CO emission at this point also shows strong velocity outflow wings with both red- and blue-shifted components (without any evidence of spatial bipolarity however), a feature shared by only four of the other clumps. These five clumps are also the most massive; all have masses in excess of 2M$_\odot$. Based on the derived masses and their respective velocity dispersions we find that the individual clumps are not gravitationally bound, by a considerable margin (by factors of 10 to 1000); the situation for the Mon R2 core as a whole is less clear. Velocity-channel maps also show no connnecting bridge between the IRS 3 outflow and the main bipolar flow of Mon R2; this suggests either that IRS 3 is not the source of the large-scale flow or that the outflow is episodic.

CO(3$\rightarrow$2) is self-absorbed at LSR velocities close to 11 kms^{-1}, and this obscures the morphology of the Mon R2 core at these velocities. NH_3(1,1) emission is seen (Torrelles *et al.* 1990) at this velocity in an arc curving around the IR cluster to the southwest. In the HCO^+(1$\rightarrow$0) data taken by Gonatas *et al.* (1992) there is a dip in the line profiles at this velocity and the distribution of emission is again quite different than that of CO(3$\rightarrow$2). It seems likely that

[2]The James Clerk Maxwell Telescope is operated by the Royal Observatory Edinburgh on behalf of the United Kingdom Science and Engineering Research Council, the National Research Council of Canada and the Nederlandse Organisatie voor Wetenschappelijk Onderzoek.

self-absorption severely modifies the apparent morphology of the Mon R2 core as seen in this and other low-excitation lines.

The spectral line profiles of H_2CO and HCN(4→3) are however quite simple and display only a small (about 1 kms^{-1}) velocity shift on the large scale across the region. Thus with these transitions it is possible to examine the distribution of dense material. For example, in Figure 1(a) we show the integrated emission from the ortho-$H_2CO(5_{15}\rightarrow4_{14})$ transition, which is at an excitation level of 63 K above ground. The distribution is similar to that of CO(3→2) in showing three major complexes of emission (one of which is coincident with IRS 3), a pronounced minimum at the position of IRS 2 and the HII region, and a clear gap to the north-west.

Compare the H_2CO distribution in Figure 1(a) with that of the 800-μm emission shown in Figure 1(b). The beamwidths are very similar. At 800μm essentially all the radiation is from dust. The detailed correspondence between these data and our 450-μm map, and the 1300-μm map made by Henning *et al.* (1992) with the 30-m IRAM telescope is good, although there are some differences. Chief amongst these is that emission in the neighbourhood of IRS 1 and IRS 2 at 1300μm is replaced by a relative hole in our maps at 800 and 450μm. At all wavelengths longward of about 1 mm, there is a continuum peak at IRS 1. Our data at both 800 and 450μm show that the peak emission has shifted from IRS 1 several arcseconds southward. This indicates that free-free emission from the central HII region is still significant at 1300μm.

We can identify 11 distinct features in our continuum maps. The correspondence between these and the CO clumps discussed above is not very good; perhaps 3 or 4 would seem to correspond. IRS 3 is once again the best instance, and for the others the tendency is for the higher-mass CO clumps to be associated with dust emission. Most of the other IR objects mentioned by Aspin and Walther (1990) cannot be definitively associated with submm continuum emission. One possible interesting object is their source 'd', 1′ to the west of IRS 3, which lies on the side of a submm continuum peak for which there is no molecular line emission.

The overall similarity of the H_2CO and dust emission distributions suggests that these both trace the gas column density quite closely. As we note above there appear to be strong optical depth effects in many of the published maps of line emission. IRS 3 is a particular case in point: it is a very strong submm line and continuum peak, while it is weak or non-existent in previous CS, NH_3 and HCO^+ maps. It is also quite difficult to find one-to-one correspondences between the CO(3→2) emission and other tracers. The weaker CO clumps we identify may well have dust and other molecules, but these would likely be below the limit of our sensitivity.

In our data we may also see the effects of the HII region on its environment. The 1.3-mm continuum peak close to IRS 1 is not a maximum for molecular emission, which instead has a ridge of emission several arcsec to the south. This suggests that either (a) the column density of molecules in this region is such that the emission is optically thick, or (b) the molecules are destroyed here by their proximity to the HII region. The latter seems more likely to us.

References

Aspin, C., Walther, D.M. 1990, *Astron. Astrophys.* **235**, 387
Gonatas, C.P., Palmer, P., Novak, G. 1992, Ap. J., , **398.**, **118**
Hackwell, J.A., Grasdalen, G.L., Gehrz, R.D. 1982, Ap. J., , 252., 250
Henning, Th., Chini, R., Pfau, W. 1992, *Astron. Astrophys.* **263, 285**
Koresko, C.D., Beckwith, S., Ghez, A.M., Matthews, K., Herbst, T.M., Smith, D.A. 1993, A. J., , 105., 1481
Massi, M., Felli, M., Simon, M. 1985, *Astron. Astrophys.* **152, 387**
Meyers-Rice, B.A., Lada, C.J. 1991, Ap. J., , 368., 445
Torelles, J.M., Ho, P.T.P., Rodríguez, L.F., Cantó, J. 1990, Ap. J., , 349., 529

Molecular Outflow in the Vela Molecular Ridge

Michael Olberg

Onsala Space Observatory, S-439 93 Onsala

The Vela Molecular Ridge (VMR) is a region of intense CO line emission extending over galactic longitude $l \approx 260°$–$273°$ and confined to within $\pm 2°$ of the galactic plane (Murphy & May, 1991). The ridge is composed of at least four giant molecular clouds (A–D) with masses exceeding $10^5\,M_\odot$. Except for cloud B these clouds are relatively nearby (700 ± 200 pc). The clouds appear to be situated at the inner edge of the local spiral arm which is seen tangentially in the direction of Vela.

Recently, the VMR has been studied at IRAS- and near-infrared wavelengths in order to identify the Lada & Wilking Class I sources among its IRAS sources and determine the current stage of star formation in this region (Liseau et al., 1992, Lorenzetti et al., 1993). According to this work the GMCs in Vela largely reflect initial conditions, prior to destructive O star formation, and are currently forming stars at a rate representative of the solar neighbourhood.

Given the results of Liseau, Lorenzetti et al. we observed a sample of 61 red IRAS sources in the VMR cloud D region at millimeter wavelengths in an attempt to identify the molecular outflow sources among them and to shed some light on the physical conditions of their molecular cloud environment.

The molecular line observations presented in this poster were carried out in February 1993 with the 15 m Swedish ESO submillimetre telescope (SEST). All 61 IRAS sources were observed in the ^{12}CO $J = 1 - 0$ transition in an attempt to detect high velocity wings, indicative of molecular outflow activity. The velocity interval used to associate the IRAS sources with VMR cloud D was $0 \leq V_{LSR} \leq 20.0$ km/s.

Out of 61 sources 8 show no or very little (≤ 0.7 K) ^{12}CO emission within this velocity interval. These 8 sources lie mainly along a line separating VMR cloud D from cloud C, in a region of generally low CO emission. They are marked with open circles in Fig. 1. The remaining sources were subsequently observed at 110 GHz (^{13}CO $J = 1 - 0$) and 89 GHz (HCO^+ $J = 1 - 0$).

Sources showing line wings or non-gaussian line shapes in ^{12}CO were observed in additional positions with $\pm 30''$ offsets in both R.A. and Dec resulting in five-point maps. In four cases these maps were extended to a total of 25 positions of a regular 5 by 5 point grid.

The ^{13}CO centre velocities fall between 0 and 16 km/s, with more than half the sources being concentrated at velocities 5, 8 and 11.5 km/s.

16 sources show ^{12}CO line widths at their base in excess of 10 km/s. These sources are all found near CO emission maxima. Sources belonging to this group and which, in addition, showed HCO^+ emission (indicative of densities $\geq 10^4\,cm^{-3}$) are marked with $\oplus$ in Fig. 1. The four sources which were mapped on 5 by 5 point grids all fall into this group. In all four cases there is indication of bipolar distribution of red- and blue-shifted CO emission.

The strongest correlation between our mm-line data and the IRAS data taken from the papers by Liseau and Lorenzetti is between the 100 μm flux (and to a lesser extent the 60 and 25 μm fluxes) and the ^{13}CO(and HCO^+) line intensity. Of the IRAS colours only the [25-12] data show a similar correlation.

If most stars are formed in giant molecular clouds, then one can hope that the study of these objects will tell us how the majority of stars in the Galaxy form. Due to their location in the galactic plane and its presently quiescent stage of star formation the relatively nearby giant molecular clouds in the Vela molecular ridge may well be of great importance to our understanding of star formation, not the least in a comparison with the excessively studied Orion clouds.

References

Murphy, D.C., May, J.: 1991, A&A 247, 202.
Liseau, R., Lorenzetti, D., Nisini, B., Spinoglio, L., Moneti, A.: 1992, A&A 265, 577.
Lorenzetti, D., Spinoglio, L., Liseau, R.: 1993, A&A 275, 489.

Prospects for Submillimeter Observations

T. G. Phillips
California Institute of Technology 320-47, Pasadena, CA 91125, USA

Abstract

A discussion is given of some current and future projects designed for submillimeter-wave astronomy, ranging from ground-based telescopes, through airborne and balloon to space-based. Emphasis is given to the space project to be flown at the start of the next century, FIRST, which is now known to be the Fourth Cornerstone of the ESA Horizon 2000 plan. Discussion is given concerning the role that NASA may play in that project.

Introduction

Although at the present time there is a general difficulty, worldwide, in funding new projects, the submillimeter is a field in which several new projects are currently under construction, with several more in the planning stage. This reflects the strong possibilities for new science opportunities, in terms of opening up new spectroscopic windows and pushing to large cosmological distances , with low resolution dust spectroscopy and high resolution molecular and atomic fine-structure spectroscopy.

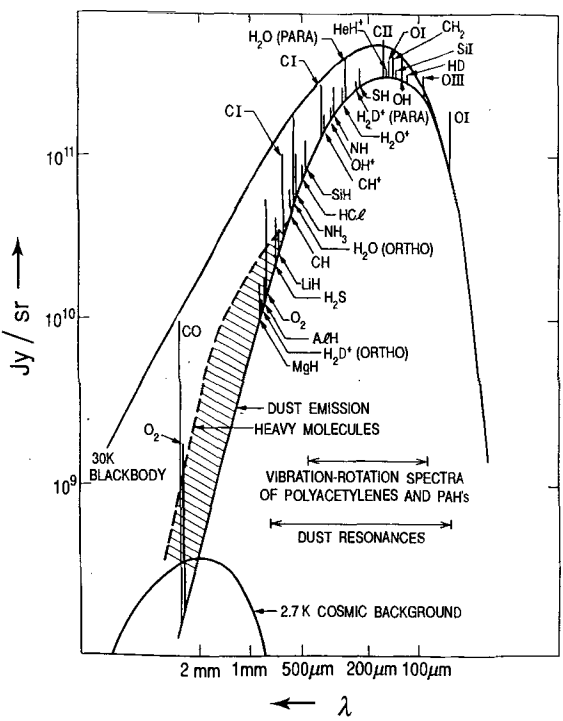

Figure 1. An indication of the spectrum of a dense interstellar cloud.

The range of prospective features in the submillimeter band is shown in figure 1, which displays a possible dust, molecular and atomic spectrum for a 30K dense interstellar cloud. The forest of molecular lines, seen at millimeter wavelengths (Blake et al, 1987) is now known to continue into the submillimeter band (Groesbeck et al, 1994) as shown in figure 2.

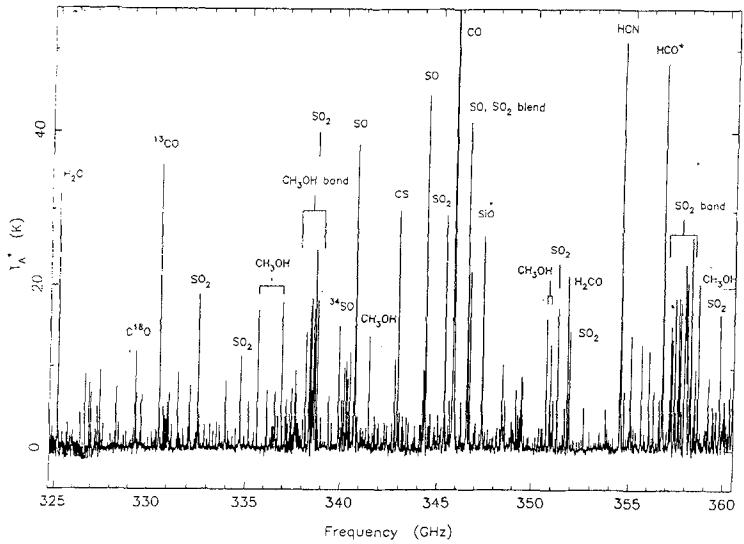

Figure 2. A portion of the heavy molecule submillimeter spectrum of OMC-1.

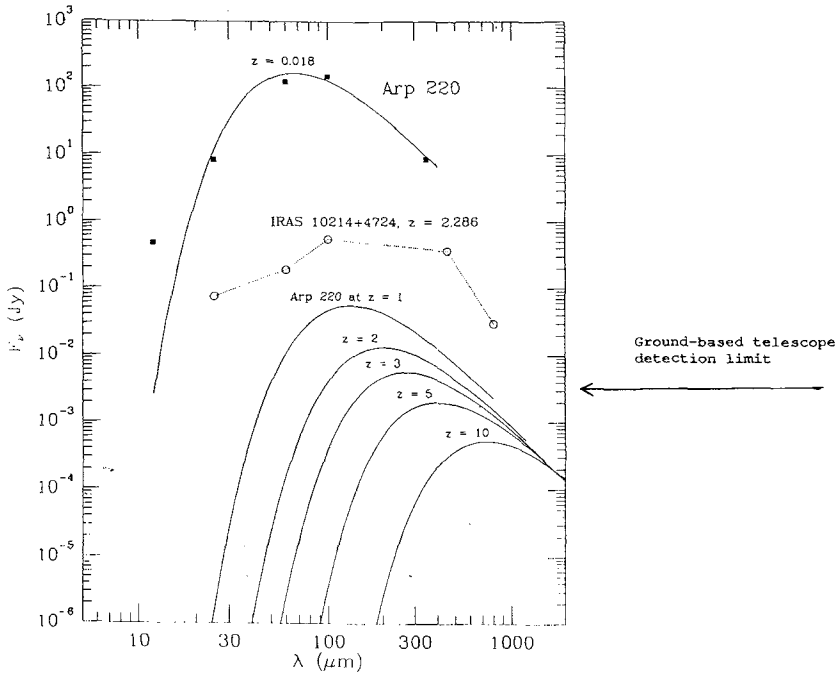

Figure 3. Redshifted dust spectra for luminous galaxies.

Some of the fundamental transitions of simple hydride molecules, predicted to be observable in the submillimeter, are already detected, e.g. HCl, NH_3, NH_2, H_2O, OH ... (see article by VanDishoeck, this publication). Atomic fine-structure lines such as CI, CII and OI can be observed from molecular clouds, circumstellar clouds etc.. (for discussion of the extensive observations of the 492 GHz CI line see the article by Keene, this publication) and COBE has obtained a low resolution, spatially averaged spectrum of the galaxy, pointing out the strong cooling lines of CO, CI, CII and NII (Wright et al, 1991). In the millimeter band highly redshifted lines of CO and H_2O have been observed from a galaxy at z=2.3 (see the article by Radford, this publication), which indicates the tremendous opportunities for observation of strong, highly redshifted fine-structure lines from such objects, when the full submillimeter band is available. Continuum detection of dust emission from such distant galaxies is possible with existing ground-based telescopes, as shown in figure 3.

Current and Future Facilities

The Earth's atmosphere severely restricts the spectral range available for ground-based telescopes. This is seen in figure 4, where the atmospheric transmission is plotted for a high, dry site, such as Mauna Kea, Hawaii (4,200m) and for the flight altitude of the NASA Kuiper Airborne Observatory (12km). From Mauna Kea the transparency is very good up to about 360 GHz, apart from some specific H_2O and O_2 frequencies, but then degrades rapidly and is characterized better by windows. The two highest frequency ones are at about 650 and 850 GHz. At higher frequencies yet, the mountain sites are essentially opaque. However, from airborne altitudes the transparency is clearly a lot better, but still not good enough for low background continuum work, wideband line surveys or complete redshift coverage of distant objects. For those important projects, the best platforms would clearly be in space. Balloons offer a compromise.

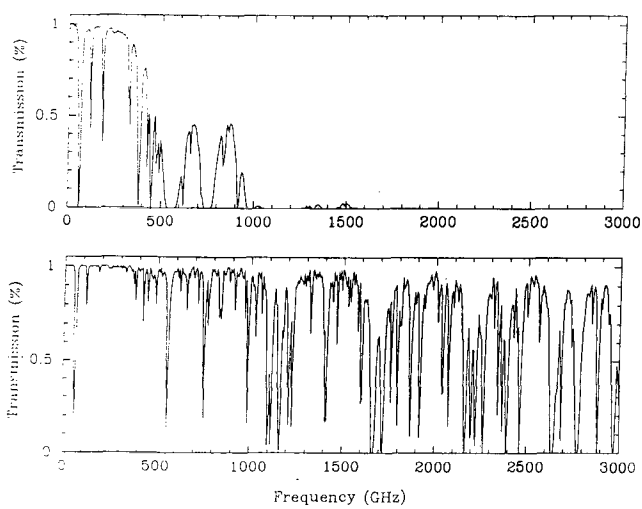

Figure 4. Atmospheric transmission for Mauna Kea (upper) and KAO (lower).

One site, which will be used more often in the future, is the South Pole. Due to the very cold, dry air, this is an excellent site, even though it is not the highest. Figure 5 shows a comparison of South Pole cumulative opacities with those at Mauna Kea. Clearly the South Pole has more low opacity time available, especially in the Astral winter. The value of 0.05 for the 225 GHz opacity corresponds to about 1mm of precipitable water, which is roughly where the submillimeter windows become extremely useful. The South Pole and Mauna Kea apparently have similar limiting low values of opacity, but the South Pole has about twice the available time at the best values, except in the Astral summer. Also it has the advantage of no storms.

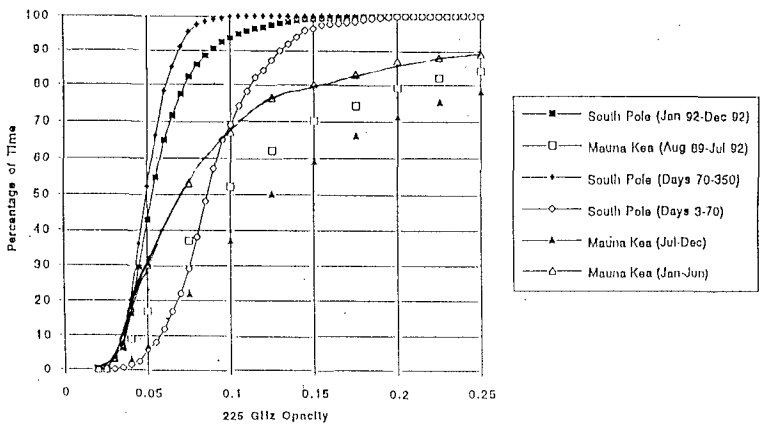

Figure 5. Cumulative opacities at 225 GHz for Mauna Kea and South Pole.

Table 1 shows a list of some existing and proposed submillimeter projects. The list is not exhaustive, but includes most major projects. The ground-based telescopes CSO, JCMT and KOSMA have been operating for several years and have been used to demonstrate and improve technology items such as SIS and bolometer detectors. The Max Planck/Arizona 10m telescope (SMT) on Mount Graham, the Smithsonian Submillimter Array (SMA) on Mauna Kea and the ASTRO South Pole telescope will add great capability. The SMA will be a major new facility, since it certain from the initial work with the CSO/JCMT two element interferometer link (see article by Hills, this publication), that many aspects of star-formation and galaxy nuclear studies will be very successful. In fact the combined collecting area of a possible Mauna Kea array including the SMA, CSO, JCMT, JNLT and the two Keck telescopes, operating at 800GHz would be equivalent, for some special experiments, to the order of 100 ten meter telescopes operating at 200GHz.

The only airborne facility operating at the moment is the NASA KAO. This 90cm telescope has been tremendously effective in starting submillimeter astronomy and is still available for new instruments and experiments. It is, however, now somewhat elderly and hopefully will be replaced soon by SOFIA, a 2.5m telescope in a converted Boeing 747 aircraft, to be a joint project of the USA and Germany. Budgets permitting, this project will start in 1995.

The spaceborne category represents an essential goal for the field, since there is no atmospheric interference and missions can provide several years of continuous observing, so permitting many new aspects, including deep surveys. The NASA SWAS project is a 0.6m telescope, a Small Explorer class mission (SMEX) using Schottky diode receivers and is on schedule for a 1995 launch. Its primary goals are detections and maps for water and oxygen lines in the 500 GHz band, plus a galactic survey of the 492 GHz CI line. ODIN, a 1m class telescope, is predominantly a Swedish project, again using Schottky diode receivers for various lines in the 119 to 575 GHz range. It is for joint astronomical and atmospheric research and should be launched towards the end of the century. The last two entries in this part of the table form the focus of the space effort in both Europe and the US. They have a long heritage, involving reincarnation (descoping) in various ways. SMIM (Phillips, 1990), the NASA version, is an "Intermediate" class mission, with a 2.5m telescope, developed from concepts used in the design program for LDR, a 1980 proposal for a very large mission. SMIM would have a liquid helium cooled focal plane and be launched by a Delta rocket. FIRST (Beckwith et al. 1993) is the ESA project, at 3m diameter, reduced in size from earlier versions, but nevertheless of immense capability. Both SMIM and FIRST would use SIS receivers in the range from about 500 GHz to 1200 GHz and bolometer detectors to frequencies possibly as high as 3 THz.

Table 1.
Submillimeter Projects (Existing and Proposed)

Ground-Based			
CSO	10m	4,000m	1987
JCMT	15m	4,000m	1987
KOSMA	3m	3,000m	1988
SMT	10m	3,000m	1994
ASTRO	1.7m	3,000m	1995
SMA	6 x 6m	4,000m	1997
Airborne			
KAO	0.9m	12,000m	1975
SOFIA	2.5m	12,000m	2000
Balloonborne			
PRONAOS	2m	40,000m	1995
Various smaller balloons			
Spaceborne			
SWAS	0.6m	600km	1995
ODIN	1.1m	600km	1998
SMIM#	2.5m	1,000 x 70,000km	2005
FIRST*	3.0m	1,000 x 70,000km	2005

Possibly to be combined with FIRST. *As 4th Cornerstone

The major news to be reported here is that FIRST has been assigned to the 4th Cornerstone of the Horizon 2000 plan and will definitely move forward as such, with a

launch date of 2005. A concerted attempt is being made by scientists in the US and Europe to combine SMIM and FIRST into one mission and progress in that will be detailed below.

To complete the description of future projects, balloons must be discussed. The major project here is PRONAOS, a 2m balloon telescope built by the French space agency, CNES. The atmospheric effects from balloon altitude are limited to quite narrow features around the major water and oxygen lines, so for only moderate velocity shifts, as are found in the galaxy, some searches can be made for water and oxygen themselves. The first flight for PRONAOS will be in 1995. A difficulty for balloon operation is to achieve an adequate flight frequency and flight duration of more than a few hours. The expectation for PRONAOS is for two flights per year.

The Relationship between FIRST and SMIM

Due to the complex history of both project and to the changing budgetary and planning situations in both Europe and the USA, it turns out that the projects are now very similar. Science goals range over studies of the physics, chemistry and dynamics of interstellar gas and dust for solar system, galactic, extragalactic and cosmological objects. Figures 6 and 7 show pictures of the missions as currently conceived and include resumes of the basic specifications. The data for FIRST given here (as of about May, 1993) is somewhat out of date already, as the project is in an active definition phase. The major differences in instrument features are the use of mechanical cryo-coolers by FIRST as compared to a liquid helium cryostat for SMIM, a bolometer continuum capability for FIRST, but none for SMIM and complete heterodyne spectral coverage for SMIM, but only specific bands for FIRST.

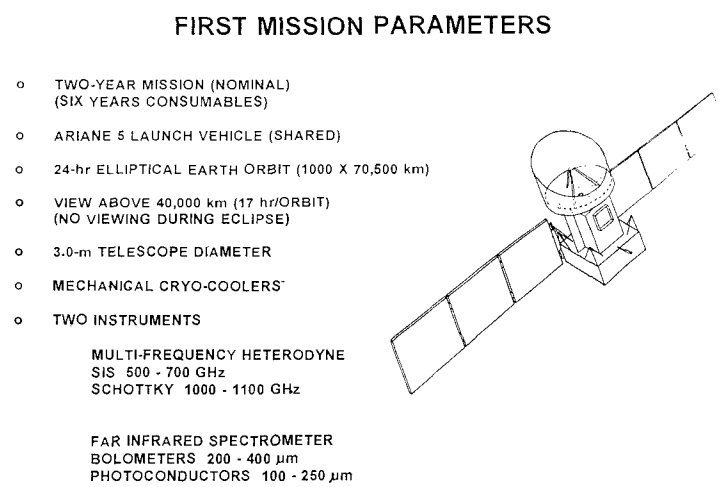

Figure 6. The FIRST project, as of about May, 1993.

As both missions became reduced in size to fit available or possible budget scenarios, during the 1980s, it became clear that the most effective project would be a combined

one. In 1990, at a conference in Liege, a discussion on this topic was held and susequently more than 200 scientists signed a statement pointing out the benefits of a joint approach. Of course, it is extremely difficult from a technical and management point of view to run a joint project. Nevertheless, both NASA and ESA have recognized the potential and are moving towards a joint position. The current discussions are based on the assumption that ESA will be the lead agency and NASA would provide technical, scientific and facility contributions, where suitable. Currently, both agencies have agreed to cross representation on science committees and to discussion of options.

SMIM MISSION PARAMETERS

- ONE-YEAR MISSION
- DELTA II LAUNCH VEHICLE
- 24-hr ELLIPTICAL EARTH ORBIT (1000 X 70,500 km)
- VIEW ABOVE 40,000 km (17 hr/ORBIT)
- 2.5-m TELESCOPE DIAMETER
- 1000-l CRYOSTAT
- TWO INSTRUMENTS
  - FAR IR SPECTROMETER 100 - 300 μm
  - SIS HETERODYNE 400 - 1200 GHz

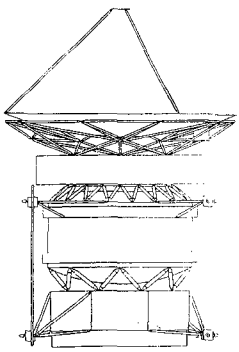

Figure 7. The SMIM project as of about September, 1990.

Table 2.

SUBMM MISSION COMPARISON

	SMIM	FIRST (ESA)	FIRST (NASA/ESA)
LAUNCH YEAR	2005/6	2002/3	2002/3
MISSION DURATION (yr)	1	2	3
ORBIT	GEOCENTRIC	GEOCENTRIC	HELIOCENTRIC
PERIOD	24 hr	24 hr	365 days
VIEWING TIME (hr/day)	17	17	24
TELESCOPE DIAMETER (m)	2.5	3.0	4.5
COOLING	SFH CRYOSTAT	MECHANICAL	SFH CRYOSTAT
INSTRUMENTS			
SPECTROSCOPY			
SIS HETERODYNE (GHz)	400 - 1200	500 - 700	820 - 1150
SCHOTTKY (GHz)	NONE	1000 - 1100	NONE
BOLOMETERS (um)	100 - 300	200 - 300	85 - 180
PHOTOCOND. (um)	NONE	100 - 250	POSSIBLE
PHOTOMETRY (um)	NONE	NONE	70 - 700

Table 2 provides a comparison of SMIM and FIRST and an option where NASA con-

tributes some key components. The table is based on a scenario developed for FIRST as a contender for the position of 3rd Cornerstone, but which was not included in the final plan, in part because NASA could not commit to the necessary expenditure in the required timeframe. A similar plan will now be considered as an option fro FIRST as the 4th Cornerstone, but with more time available to achieve a mutually acceptable result. The new launch date for FIRST is 2005/6.

The basic components of a NASA contribution to FIRST range over several possible elements. One goal would be to enhance the mission by making it possible to achieve a High-Earth, or heliocentric orbit, as opposed to the elliptical orbit. This would greatly improve the thermal situation and increase the observing time. Elements here are cryostat design and/or procurement and Deep Space Network groud support. A second goal would be to help restore the aperture to the full 4.5m allowed by the ARIANE shroud, by contributing lightweight, high accuracy telescope panel technology. Other areas would include contributions to instruments through SIS and bolometer detector technologies and to data products through the IPAC facility.

References

Beckwith, S. et al. 1993, ESA SCI(93)6
Blake, G., Sutton, E., Masson, C., Phillips, T. 1987, Ap.J. 315, 621
Groesbeck, T. et al. 1994, in preparation
Phillips, T. 1990, ESA SP-314, 221

THE SUBMILLIMETER WAVE ASTRONOMY SATELLITE: INSTRUMENT HARDWARE

V. Tolls[1], G. J. Melnick[1], N. Erickson[2], P. Goldsmith[3], M. Harwit[4], R. Schieder[5], R. Snell[2], J. Stauffer[1]

[1]Harvard-Smithsonian Center for Astrophysics, [2]University of Massachusetts, [3]Cornell University, [4]National Air and Space Museum, [5]University of Cologne

Introduction

The Submillimeter Wave Astronomy Satellite (SWAS) will study galactic star formation and interstellar chemistry through a survey of dense molecular clouds in five astrophysically important transitions of H_2O, $H_2{}^{18}O$, O_2, CI, and ^{13}CO. To carry out this mission the SWAS instrument and spacecraft are designed to embody all the elements of a ground-based radio telescope. The "instrument" portion of the satellite is comprised of: (1) the antenna, (2) two heterodyne receivers, (3) an acousto-optical spectrometer, (4) the thermal control system, (5) the instrument control electronics, (6) the star tracker, and (7) the instrument structure. The "spacecraft" portion of the satellite is comprised of: (1) the attitude control system (ACS), (2) the solar arrays and power regulating hardware, (3) the onboard command, data, and ACS computer, (4) the solid-state memory for data recording, and (5) all data uplink and downlink receivers and transmitters. This contribution will center only on the instrument hardware. Another paper in these proceedings summarizes the science goals of the SWAS mission.

Instrument Hardware

A block diagram of the signal detection subsystem, elements of which are described below, is shown in Fig. 1 and a summary of key instrument parameters is given in Table 1. The SWAS optical subsystem consists of a 54×68-cm diameter off-axis Cassegrain primary mirror, a secondary mirror, a secondary mirror chopping mechanism, a calibration load, and a calibration load flip mirror. Both the primary and secondary mirrors are made of aluminum and have been polished to a combined rms surface accuracy of 6.5 μm. This mirror surface accuracy along with a receiver feedhorn Gaussian edge taper of 11 dB results in an overall aperture efficiency of about 80% and a main beam efficiency of almost 90%. For sources that appear point-like within the approximately 3.5×4.5-arcminute SWAS beam, a chopping secondary mirror mechanism is available for beam switching 10 arcminutes on the sky along a fixed axis. The chopping rate is selectable among three options: 2 Hz, 1/4 Hz, and off. The 2 Hz rate is used in conjunction with the total power continuum detectors associated with each receiver channel and is synchronized with their readout. The 1/4 Hz rate is used in conjunction with spectroscopic observations and is synchronized with the readout rate of the acousto-optical spectrometer (AOS). When the chopping mechanism is off, the incoming beam is on-axis. This mode will be employed when the spacecraft is used to nod the telescope over spatial distances greater than 10 arcminutes, as will be required for extended sources. An $\sim$ 240 K blackbody radiator thermally connected to the instrument structure will be used in combination with blank sky measurements to periodically measure the system

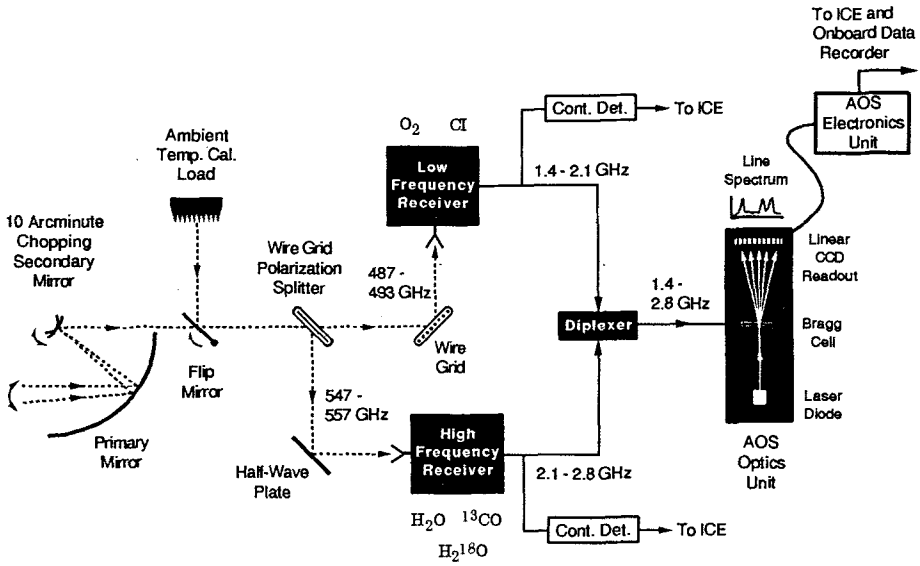

Fig. 1. Block diagram of the SWAS submillimeter signal detection system.

noise temperature. This calibration load is nominally out of the beam, but it can be viewed by engaging a flip mirror (see Fig. 1).

The detection system consists of two independent second harmonic Schottky diode mixers, operating in orthogonal linear polarizations, pumped by frequency-tripled InP Gunn oscillators. The oscillator frequencies are 81.5 GHz for the lower frequency receiver, which is used to observe O_2 and CI at 487 GHz and 492 GHz respectively, and 92.3 GHz for the higher frequency receiver, which is used to observe H_2O and ^{13}CO at 557 GHz and 551 GHz respectively. A fifth line, the ground state transition of ortho-$H_2{}^{18}O$ at 548 GHz, can be observed by tuning the higher frequency local oscillator slightly beyond its normal operating range resulting in about two times higher system noise temperature. (The $H_2{}^{18}O$ is deemed to be worth observing, in spite of the higher system noise temperature, since it can be used to obtain a better estimate of the water abundance than may be derived from the $H_2{}^{16}O$ line alone, which is likely to be highly optically thick.) The first IF stage, referred to as the cooled frontend (CoFE), consists of input optics, a mixer, a tripler, and a HEMT amplifier for each of the two receiver channels, all of which are passively cooled to $\sim$ 150 K. The measured noise temperature in each channel is approximately 1500 K (DSB) at this operating temperature. The output of each receiver is down converted and diplexed with a resulting bandwidth per channel of 700 MHz and an input band to the AOS of 1.4 to 2.8 GHz.

As mentioned above, SWAS will also carry two broadband (700 MHz) total power continuum detectors, one associated with each receiver. The continuum detectors will be used primarily when observing point-like sources, such as Jupiter, for purposes of: (1) verifying the co-alignment of the two submillimeter beams, (2) verifying the co-alignment of the submillimeter beams and the star tracker, and (3) establishing flux calibration.

Table 1. SWAS Instrument Summary

Telescope:	54 x 68 cm Diameter Off-Axis Cassegrain
Diffraction-Limited Field-of-View:	3.3 x 4.2 arcminutes @ 557 GHz 3.8 x 4.8 arcminutes @ 490 GHz
Mirror Surface Accuracy:	$< \lambda/80$ @ 557 GHz Total Error
Pointing Accuracy:	$\leq$ 19 arcseconds (1σ)
Receiver Type:	Schottky Barrier Diode Harmonic Mixers
Receiver Temperature:	140 - 150 K (Passively Cooled)
Receiver Noise Temperature:	$\sim$ 1500 K (Double Sideband)
Operating Frequencies:	Receiver 1: 557 GHz (H_2O); 551 GHz (^{13}CO); 548 GHz ($H_2{}^{18}O$) Receiver 2: 487 GHz (O_2); 492 GHz (CI)
Velocity Coverage:	1.4 GHz Bandwidth (840 kms^{-1}) AOS Backend
Velocity Resolution:	0.6 km s^{-1}
Instrument Power/Weight Budget:	60.7 Watt average (83.1 Watt peak)/92.9 kg
Orbit:	550 - 600 km; 65° Inclination
Mission Lifetime:	$\geq$ 3 years

The SWAS spectrometer is a single AOS with 1400 1-MHz channels (about 1700 kHz resolution bandwidth and about 2100 kHz equivalent noise bandwidth per channel). This yields a velocity channel spacing of approximately 0.6 km s^{-1} and a total bandwidth of 840 km s^{-1}, or about 200 km s^{-1} per line. The SWAS AOS is based on the design of other broadband AOSs built by the University of Cologne and incorporates redundant 780 nm laser diodes, a $LiNbO_3$ Bragg cell, and a 1728-pixel Thomson linear CCD. The digitized output of the CCD is co-averaged within the AOS electronics unit and forwarded, via the Instrument Control Electronics (ICE), to the onboard solid state memory within the spacecraft for later transmission to the ground. During normal operations, these data will be downlinked twice a day. On-orbit calibration of the AOS is achieved through the use of signal blanking switches in each receiver channel as well as an RF comb generator which can substitute for the receiver output into the AOS.

The thermal control subsystem consists of three Winston cone passive radiators, two equipment plate radiators (part of the outer shell structure), the instrument shell (part of which also serves as a sunshade), a Goretex cover over the telescope aperture, selected surface finishes on various parts and assemblies, and multi-layer insulation blankets to provide additional thermal isolation where required. The Winston cone passive radiators are intended to view only dark sky during the mission (i.e., avoiding Earth and Sun radiation), thus cooling a plate at the base of each cone, and ultimately the CoFE to which they thermally are connected, to $\sim$ 150 K. The equipment plate radiators

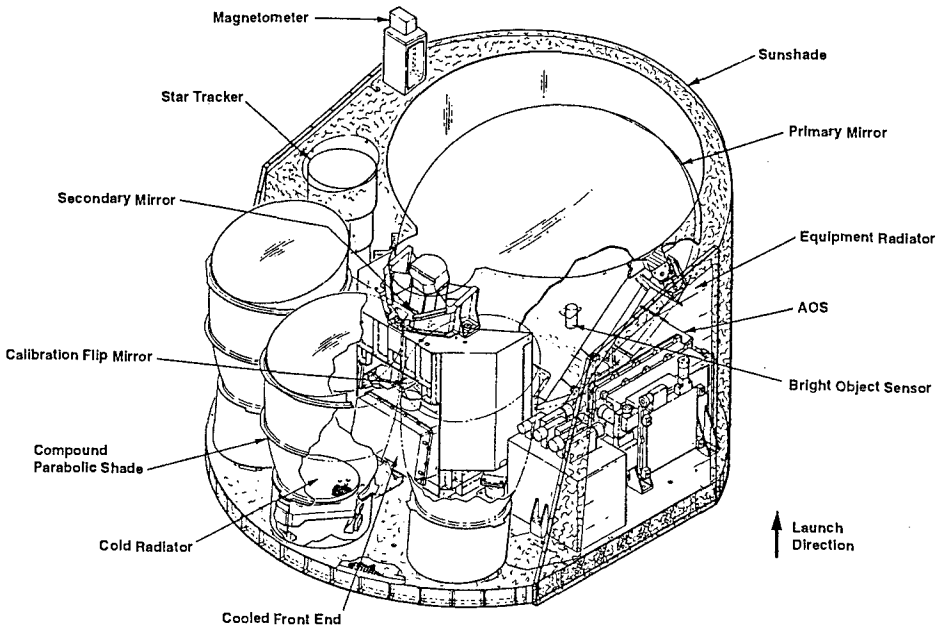

Fig. 2. Cutaway view of the SWAS instrument. In the foreground are the three Winston cone shades, inside of which are the passively cooling radiators. These radiators cool the mixers and first amplifier stages to a temperature of about 150 K. The cooled frontend and the structure which holds the secondary mirror are located behind the radiators. Most parts of the electronics and the AOS components are mounted onto the baseplate under the main mirror. The baseplate mounts to the top of the spacecraft.

maintain a nominal operating temperature environment for all electronic boxes mounted to the instrument baseplate. The Goretex cover protects the telescope and receivers in the event of the Sun's traversing the field-of-view during launch and early orbit operations or of anomalous spacecraft behavior during the mission. A cutaway view of the instrument is shown in Fig. 2.

The receivers are being built by Millitech Corporation; the AOS is being provided by the University of Cologne; and the optics, cooling radiators, star tracker, and instrument structure as well as the thermal design, systems integration, and testing are the responsibility of Ball Aerospace Systems Group. The spacecraft bus and its subsystems are being built by NASA Goddard Space Flight Center.

THE SUBMILLIMETER WAVE ASTRONOMY SATELLITE: MISSION SCIENCE OBJECTIVES

G. J. Melnick[1], A. Dalgarno[1], N. R. Erickson[2], G. G Fazio[1], P. F. Goldsmith[3] M. Harwit[4], D. J. Hollenbach[5], D. G. Koch[5], D. A. Neufeld[6], R. Schieder[7] R. L. Snell[2], J. R. Stauffer[1], P. Thaddeus[1], V. Tolls[1], G. F. Winnewisser[7]

[1]Harvard-Smithsonian Center for Astrophysics, [2]University of Massachusetts, Amherst, [3]Cornell University, [4]National Air & Space Museum, [5]NASA Ames Research Center, [6]Johns Hopkins University, [7]University of Cologne (Germany)

Abstract

The Submillimeter Wave Astronomy Satellite (SWAS) mission is dedicated to the study of star formation and interstellar chemistry. To carry out this mission, SWAS will survey dense ($n_{H_2} > 10^3$ cm^{-3}) molecular clouds within our galaxy in either the ground-state or a low-lying transition of five astrophysically important species: H_2O, $H_2^{18}O$, O_2, CI, and ^{13}CO. By observing these lines SWAS will: (1) test long-standing theories that predict that these species are the dominant coolants of molecular clouds during the early stages of their collapse to form stars and planets and (2) supply heretofore missing information about the abundance of key species central to the chemical models of dense interstellar gas. SWAS will employ two independent Schottky barrier diode mixers, passively cooled to $\sim$150 K, coupled to a 54 $\times$ 68-cm off-axis Cassegrain antenna with an aggregate surface error $\leq$11 μm rms. During its three-year mission, SWAS will observe giant and dark cloud cores with the goal of detecting or setting an upper limit on the water abundance of 3×10^{-6} (relative to H_2) and on the molecular oxygen abundance of 2×10^{-6} (relative to H_2). In addition, advantage will be taken of SWAS's relatively large beamsize of 3.2 $\times$ 4.0 arcminutes at 551 GHz and 3.6$\times$4.5 arcminutes at 492 GHz to obtain large-area ($\sim 1^\circ \times 1^\circ$) maps of giant and dark clouds in the ^{13}CO and CI lines. With the use of a 1.4 GHz bandwidth acousto-optical spectrometer, SWAS will have the ability to *simultaneously* observe the H_2O, O_2, CI, and ^{13}CO lines. All measurements will be conducted with a velocity resolution of less than 1 km s^{-1}.

Introduction

During their collapse to form stars and planets, heat is generated within interstellar clouds as gravitational potential energy is converted into kinetic energy. This heat *must* be efficiently removed from these clouds lest the internal gas pressure eventually exceed the binding gravitational force, halting the collapse. Moreover, this build-up of pressure is so rapid that cooling must be significant during the very earliest stages of collapse.

Much of the cooling within molecular clouds occurs through atomic and molecular collisions that populate excited states and which subsequently decay, producing photons which leave the cloud, carrying with them energy. By far the most abundant collision partners in these clouds are H, H_2, and He. Unfortunately, none of these species possesses excited states capable of being collisionally populated at the 10 – 30 K temperatures typical of these clouds. The next most abundant elements are oxygen and carbon. In addition to their

TABLE 1. Spectral Lines to be Observed by SWAS †

Species	Transition	Energy Above Ground State (E/k)	Frequency (GHz)	Critical Density (cm^{-3})
O_2	$(3,3-1,2)$	26 K	487.249	10^2
CI	$(^3P_1 - {}^3P_0)$	24 K	492.162	10^4
^{13}CO	$(J = 5-4)$	79 K	550.926	3×10^5
H_2O	$(1_{10} - 1_{01})$	27 K	556.936	10^9 ‡
$H_2{}^{18}O$	$(1_{10} - 1_{01})$	26 K	547.676	10^9 ‡

† SWAS will *simultaneously* observe the O_2, CI, ^{13}CO, and H_2O transitions.
‡ The critical density for H_2O will likely be less than this value by a factor of 10^3-10^4 due to significant radiation trapping in this line. The critical density for $H_2{}^{18}O$ could be reduced by a factor of $1.5-50$ due to the same effect.

atomic form, oxygen and carbon are present within a variety of molecules: some of these atoms and molecules have energy levels that are easily excited between 10 and 30 K (e.g., CO, CI, H_2O, and O_2) and others do not (e.g., OI). In this way, the chemistry within a cloud can directly affect the cooling which, in turn, can affect the cloud dynamics. In the sections below, the relevance of the SWAS-selected lines to these questions will be briefly discussed and the observing strategy will be summarized.

Science Objectives

The species selected for study by SWAS are important because:

(1) they are predicted to be major reservoirs of oxygen and carbon in dense interstellar clouds

(2) they should be valuable probes of the physical conditions in these regions

(3) they will provide important tests of chemical models in both well-shielded and photo-illuminated regions of molecular clouds

(4) they are predicted to play a major role in determining the temperature within interstellar clouds.

Oxygen and Carbon Reservoirs: Oxygen and carbon atoms and molecules, including their hydrated forms, are expected to be major constituents of molecular clouds – examples include OI, O_2, CI, CO, H_2O, OH, and CH. Radio observations have clearly demonstrated the significant presence of CO within molecular clouds; however estimates of the CO abundance in these clouds leave most of the oxygen and carbon unaccounted for. More recent observations of CI from both COBE and ground-based observatories and

of C^+ from the Kuiper Airborne Observatory imply abundances of carbon in these forms which go a long way toward bridging the gap between the carbon abundance derived from CO measurements and the solar abundance of carbon. The situation with oxygen remains quite different: the amount of oxygen locked up in CO is typically less than 10 percent of the solar abundance of oxygen, and other oxygen-bearing species measured to date, such as OI and OH, do not account for the difference. The low apparent oxygen abundance may be reconciled with its solar abundance in two ways. First, oxygen in the form of OI may be present in large amounts but, because its first excited state lies 228 K above the ground-state, OI emission is too weak to be detectable toward regions with $T \sim 10-30$ K. Second, a large fraction of the oxygen may be tied up in H_2O or O_2, neither of which have been observed due to strong atmospheric absorption. By observing both H_2O and O_2 SWAS will determine whether these species are significant reservoirs of interstellar oxygen. If SWAS does not detect H_2O or O_2, particulary toward warmer regions, and sensitive searches with facilities such as ISO fail to detect OI toward the same lines of sight, then it may be concluded that the oxygen abundance is unusually high in the solar neighborhood.

Probes of Physical Conditions: The conditions required to excite each of the SWAS lines are sufficiently different so as to make these transitions useful diagnostics of the densities and temperatures within molecular clouds. One measure of the relative sensitivity of the SWAS lines to density is given in Table 1 in which the critical density for collisional de-excitation, n_{cr}, is given for temperatures characteristic of molecular clouds ($10-30$ K). As an example of their diagnostic potential, the line strengths of O_2 and CI are largely temperature insensitive at densities greater than 10^4 cm^{-3}, varying by only a factor of 2 between 10 K and 35 K, whereas H_2O and ^{13}CO display variations in line strength greater than a factor of 10 over this same temperature range. Thus, H_2O and ^{13}CO make very effective probes of warm, dense gas. Similarly, limited observations of both CI and ^{13}CO ($J = 6 \rightarrow 5$) have demonstrated that these lines are good tracers of UV-illuminated photodissociation regions.

Molecular Cloud Chemistry: The distribution of oxygen and carbon in atomic and molecular form in the gas phase and on the surfaces of grains is a critical unknown in understanding the chemistry, the ionization structure, and the thermal balance of interstellar clouds, and hence in predicting their evolutionary course. The abundances of the more complex carbon-containing interstellar molecules are directly responsive to the fraction of the carbon that is available as neutral atoms and, because of the different reactivities of O, O_2, and H_2O, the overall molecular composition is sensitive to the oxygen distribution. The cooling rate depends on composition because OH and H_2O are efficient radiators whereas O_2, by virtue of its not possessing a dipole moment, is not. In this way, cloud evolution, dynamics, fragmentation, collapse, and star formation can all be directly affected by the chemistry. The main reactions governing the oxygen and carbon chemistry are outlined in Fig 1.

Molecular Cloud Cooling: Due primarily to their predicted abundance and their possession of easily excited, low-lying transitions, CO, H_2O, O_2, and CI are expected to be dominant coolants within molecular clouds for $10 \leq T \leq 40$ K, with H_2O, O_2, and CI becoming particularly effective at higher temperatures (c.f., Goldsmith and Langer, 1978).

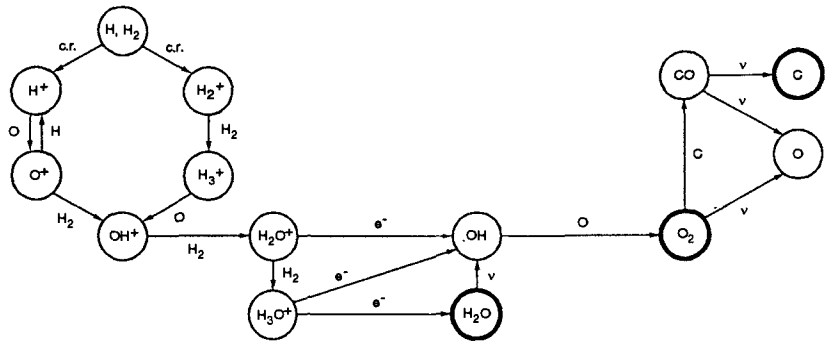

Fig. 1. Schematic of the major oxygen chemistry in dense interstellar clouds. SWAS-observed lines are indicated by bold circles.

By observing H_2O, O_2, and CI, SWAS will test this long-standing prediction.

Observing Strategy

The observing strategy for SWAS is twofold: (1) establish the presence of, or set a scientifically interesting abundance upper limit on H_2O and O_2, and (2) map the large-scale distribution of CI and ^{13}CO. A measured upper bound on the H_2O and O_2 abundance (relative to H_2) of 3×10^{-6} and 2×10^{-6}, respectively, has been adopted for the SWAS mission for several reasons. For H_2O, a non-detection at an abundance of 3×10^{-6} implies that the ion-molecule chemistry within interstellar clouds does *not* favor the production of H_2O, but instead may favor the production of OH (see Fig. 1). Further, a non-detection of H_2O at this abundance toward warmer regions would eliminate the class of models which predicts that large amounts of water will be injected into the interstellar medium when water-ice evaporates from the mantles of dust grains. A non-detection of O_2 at an abundance of 2×10^{-6} would eliminate all models of molecular cloud chemistry which start from the assumption that oxygen is more abundant than carbon (as in the solar region). If the H_2O and O_2 abundances are low and SWAS must integrate for the time required to set the above limits, then SWAS will be able to observe approximately 80 giant and 80 dark cloud cores during the half of the mission dedicated to this part of the science objective. Clearly, if H_2O and O_2 are detected then more regions will be observed.

Since the presence of CI and high-J ^{13}CO emission has been established, approximately half of the mission will be dedicated to conducting large-scale CI and ^{13}CO mapping of giant and dark clouds. Based on a combination of measured and predicted line strengths, it is expected that about 20 giant and 20 dark clouds can be mappped over $\sim 1^\circ \times 1^\circ$ with half-beam spacing.

References

Goldsmith, P. F., and Langer, W. D. 1978, *Ap. J.*, **222**, 881.

The James Clerk Maxwell Telescope. Developments into the 1990's.

E.I. Robson

660 N.A'ohoku Pl. University Park, Hilo, Hawaii, 96720, USA

Introduction

The JCMT is operated by the UK Science and Engineering Research Council on behalf of the National Research Council of Canada, the Netherlands Organisation for Scientific Research (ZWO) and the University of Hawaii. The 15m diameter mm- submm telescope is located on the 14,000 ft (4.24 km) summit of Mauna Kea Hawaii, which has a latitude of 20o allows excellent sky access. The site is acknowledged to be the best in the world for all-year round submillimetre observations.

The JCMT is alt-azimuthally mounted and is housed in a carousel with a transparent membrane to protect the dish from the Sun, wind and dust. The telescope surface accuracy is continually being improved through a well defined programme and is currently 26 microns large scale and 18 microns small scale (as determined from holography measurements and out of focus beam maps of Uranus). The JCMT has excellent absolute pointing, with RMS errors of 1.5 arcseconds or better in each axis under stable atmospheric conditions. A chopping secondary is employed, continuum observations are made at 7.8 Hz and chop throws up to about 150 arcseconds are possible.

The telescope operates two eight-hour shifts per night and is scheduled in two semesters a year. Time is available for observing requests from international astronomers. Observers are supported at the telescope by an operator and a support astronomer is available for assistance with instrumentation parameters or specific aspects of execution of the observing programme. Two Newsletters and an Annual Report are published each year.

Instrumentation

The facility is provided with common-user heterodyne and continuum receivers located at Cassegrain and Nasmyth foci. The current suite of instruments comprise: RxA2 - a single channel Pb SIS receiver covering 208-280 GHz with an IF bandwidth of 600 MHz and an EIP phase lock. Separate hot and cold loads provide calibration and Trec = 85-115 K (dsb) from 220-270 GHz and the main beam efficiency = 0.72. The HPBW = 20.8". RxB3i is a single channel Pb SIS receiver covering 298-380 GHz with an IF bandwidth of 750 MHz. It also has separate hot and cold loads and has Trec = 105K (dsb) at 310 GHz, 270K (dsb) at 330 GHz, 160K (dsb) at 345 GHz. The main beam efficiency = 0.53 and the HPBW = 14.3". RxC2 is a single channel Pb SIS receiver for the 450-504 GHz regions with an instantaneous IF bandwidth >1 GHz. The phase lock is by an EIP and it has a closed cycle cooler and internal cold load. The Trec = 220K (dsb) at 490 GHz and 180K (dsb) at 460 GHz. The main beam efficiency is 0.43 with a HPBW of 10.5".

A 600 - 800 GHz receiver owned by the MPE group in Garching is also available on a collaborative basis for specific observing campaigns. This is currently being upgraded from a Schottky to an SIS mixer which will allow observations in the 660-692 GHz region.

There are two backend spectrometers for the heterodyne receivers, an AOS and the DAS, a Digital Autocorrelation Spectrometer. This has 2048 delay channels with a maximum bandwidth of 920 MHz in each of two inputs. It can be configured to a wide range of inputs, providing spectral resolutions ranging from 0.14 to 1.5 MHz. The AOSC is an accousto-optical spectrometer with a resolution of around 330 kHz and a total bandwidth of 500 MHz with a single IF channel.

UKT14 is the single channel He3 bolometer supplied with a range of continuum broadband filters centred at 2.0, 1.3, 1.1, 0.85, 0.8, 0.75, 0.6, 0.45 and 0.35 mm. A variable aperture stop allows diffraction limited beams (18"- 8") for 1.1 mm and shorter wavelengths. The NEFD's range from 400 mJy Hz-0.5 at 1.1mm to 5 Jy Hz-0.5 at 0.45mm. The shorter wavelengths values are strongly weather dependent. Unlike the other instruments, UKT14 is mounted on the Nasmyth platform. It has a polarimeter available for 1.1 and 0.8 mm.

Developments

The JCMT has an aggressive programme of receiver development. As well as work which continues to upgrade the current receivers in terms of state-of-the-art performance, there are a number of exciting new receivers under construction or planning. The first of these is SCUBA, the Submillimetre Continuum Bolometer Array scheduled for delivery in the early summer of 1994. SCUBA contains two arrays, one covering the long-wavelength 850 mm, 750 mm or 600 mm regions, the other the short-wavelength 450 mm or 350 mm wavebands. The two wavebands required are selected by broadband filters; SCUBA then observes simultaneously using both long and short wavelength arrays. The bolometers are cooled by means of a dilution refrigerator to temperatures <100 mK, giving background limited performance. The target NEFD's (assuming excellent weather) are: 50 mJy Hz-0.5 at 850mm and 400 mJy Hz-0.5 at 450mm. The 450/350 mm array has 91 pixels while the 850/750/600 mm array has 37, giving diffraction limited performance at 850 and 450 mm. There are also single photometry pixels at 2.0, 1.4 and 1.1 mm, each with diffraction limited beams. The field of view of SCUBA covers 2.5 arcmin and calibration is provided by an internal calibration signal.

The 300-400 GHz window is regarded as the bread-and-butter wavelength range for the JCMT, observations being possible for most of the time. A new receiver for this band, RxB3 will be delivered in the summer of 1994. This has dual SIS mixers and covers the range 330 - 360 GHz. It will be provided with a single sideband filter, an IF bandwidth >1 GHz and should have a receiver temperature <200 K at 345 GHz. To improve operational efficiency it will be remotely tuneable. To provide the next generation of high frequency receivers, a dual channel 450 - 500 GHz (band C) and dual channel 660 - 690 GHz (band D) receiver will arrive at the JCMT at the end of 1994. This is receiver W and has single sideband filters and an IF bandwidth >1 GHz. Like RxB3 it will be remotely tuneable. The goals for the receiver temperature are <200 K at C and <500 K at D.

The jewel in the crown of the heterodyne instrumentation programme is the production of a B-Band array. This is described elsewhere in these proceedings (by Russell) and is anticipated to have between 25 and 35 pixels and adequate backend performance for extragalactic work. As well as instrumentation, facility developments include continued work on surface accuracy and pointing improvements along with a programme of maintenance and fault prevention, aimed at increased reliability and reduced fault downtime. This is currently running at well below 5% of available clear time. Further work includes provision of a sophisticated commercial database which can be used for monitoring system performance as well as data archiving.

Astronomical developments include the newly commissioned short baseline, twin element interferometry with the Caltech Submillimetre Observatory. This is reported in detail elsewhere in these proceedings by Hills. There is also the opportunity for VLBI - the Hilo-centric array. The first experiment failed to detect fringes, the next anticipated run is in late 1994. Collaboration with the SMA is another exciting possibility for future developments in submillimetre interferometry on Mauna Kea.

Operational Developments

It has been clear to all observers at submillimetre wavelengths that the standard mode of telescope scheduling - blocks of time assigned rigidly to specific programmes, is far from acceptable in terms of maximising the scientific return from the facility. However, the solution of fully flexible LST scheduling remains an elusive goal in terms of implementation mechanisms acceptable to the observing astronomical communities. In steps to move towards this essential goal, the use of SERVICE observing has been a very useful introduction. This might be anticipated to increase in the future, however it has a cost penalty in terms of staff resources. Hand-in-hand with SERVICE observing, the use of remote eavesdropping has proven successful, especially when a dedicated line was available from Hawaii to the UK. Due to cost considerations this has now lapsed and we have found that the current INTERNET is not adequate for effective communications from the remote location. Also, the niggling problem of voice communication over the networks was never solved, the usual resort was to pick up the telephone. Nevertheless, flexible scheduling will have to come about to ensure that the really dry times are reserved for those programmes which absolutely require them. I suspect that observing programmes will have to evolve towards the level of detail required for satellite programmes and then flexible scheduling will encompass a mix of modes, including SERVICE with remote eavesdropping when possible.

The Kuiper Widefield Infrared Camera (KWIC)

Gordon J. Stacey, Thomas L. Hayward, Harri Latvakoski, Liang Peng, and George E. Gull Department of Astronomy, Cornell University, Ithaca, NY 14853-6801, USA

We have constructed a new imaging spectrometer/spectrophotometer for use between 18 and 44 μm on the Kuiper Airborne Observatory (KAO). Our spectrometer, **KWIC** (**K**uiper **W**idefield **I**nfrared **C**amera) centers around a new, SIRTF funded, 128 x 128 pixel Si:Sb blocked impurity band (BIB) array. The array pixel scale (3″) was chosen as to over-sample the primary diffraction lobe from the KAO (8″ at 35 microns). Even with this over-sampling, KWIC has a *6.4 x 6.4 arc minute field of view.* KWIC spectrally scans in both its low ($\frac{\lambda}{\Delta\lambda} \sim 70$) and high ($R \sim 2000$) spectral resolution modes through the use of two Fabry-Perot interferometers (FPIs) in series. In the high resolution mode, the low order FPI (LOFPI) sorts orders for the resolution achieving high order FPI (HOFPI). In the low resolution mode, a mechanical stage withdraws the HOFPI from the optical path permitting high throughput, low spectral resolution imaging in the thermal dust continuum. The HOFPI withdrawal can be accomplished during a KAO flight. Considerable attention to the optical design ensures uniform spectral coverage and sensitivity over the entire field of view. At present, KWIC is in its final testing stages in anticipation of February, 1994 flights.

KWIC addresses several astrophysical problems. The fine-structure lines available to KWIC (e.g. [SiII], [SIII] and [NeIII]) are excellent probes of the density and ionization structure of interstellar gas clouds. The mid-IR continuum arises from warm ($T_{dust} \sim 85\ K$) dust heated by nearby starlight. We will use KWIC to (1) explore molecular cloud structure, probing the physical conditions of the gas near embedded sources and condensations (2) examine the relationship between the interstellar medium and star formation activity on galactic scales through complete imaging of nearby galaxies (3) examine the complex kinematics and density structure of the gas clouds associated with the center of the Galaxy and (4) conduct high spatial resolution, large scale imaging of young stellar objects in the dust continuum thereby probing the dusty disks predicted to accompany low mass star formation.

Instrument Description

Our optical design attempts to minimize the number of optical elements consistent with good image quality and spectral purity. The infrared beam from the KAO dicroic tertiary is transmitted directly into the KWIC dewar through its polyethelyne window. KWIC employs seven diamond turned aluminum cryogenic mirrors. The mirror pairs M1, M4 and M6, M7 are off-axis paraboloids set in Czerny-Turner configuration to minimize coma. M2, M3 and M5 are flats. Near-IR and optical radiation are rejected by a scatter filter near the entrance window. The collimated beam is sent through the HOFPI, located at the Lyot stop, and re-imaged on the LOFPI. M6 and M7 convert the image to the proper f-number (f/5.3) for imaging onto the array (3" per 70 μm pixel). Just in front of the detector is a MgO crystal who's reststrahlen bands reject unwanted mid-IR radiation. A detailed ray-trace shows that our optical design achieves good image quality over the entire field of view. We expect the mix of KAO seeing and telescope diffraction ($\lambda/D \sim 7.9''$ at 35 μm) to yield a point-spread function of about 8 to 9" for KWIC.

We have designed the LOFPI and HOFPI such that no mechanical access is required from outside the dewar. The LOFPI design centers around the flex-vane principle used successfully in the UCB/MPE **F**ar-infrared **I**maging **F**abry-Perot **I**nterferometer (**FIFI**) (Poglitsch et al. 1991). The device is constructed of machined aluminum with magnetic stainless mesh rings. Coarse adjustments of the plate separation (20 to 44 μm) are made before installation into the dewar via a fine adjustment screw. We use piezo-electric translators (PZTs) for both fine adjustment and scanning the FPI. These PZTs expand $\sim 24\ \mu m$ at 4 K — more than a free spectral range at our longest wavelength (44 μm) thereby ensuring access to all wavelengths of interest. Parallelism is adjusted at room temperature through 3 fine adjustment screws, and corrected at cryogenic temperatures with three short PZT stacks (2.5 μm displacement at 4 K). To minimize mechanical vibrations, we chose to operate the HOFPI in a fixed order (usually ~ 70), which makes the HOFPI identical in operation to the LOFPI. The HOFPI is moved in and out of the beam during flight by a mechanical feed through to a translation stage.

Our FPI etalons are constructed of free standing metal mesh, with typical transmissions of 50% when operating with a finesse of 50. The FPI plate spacing is measured with a capacitive bridge circuit, which compares the mesh-mesh capacitance to a reference capacitor. To permit their use as capacitors, the rings are electrically isolated from the LOFPI assembly with nylon plugs. The mesh rings are held in place with magnets.

128× Si:Sb BIB arrays were developed by Rockwell for the SIRTF Infrared Spectrometer team (Huffman et al. 1992). These arrays demonstrate very good performance characteristics (Van Cleve et al. 1993). The quantum efficiency is $\sim$ 30%, and the read noise is $\sim$ 500 e^-. Dark current is $\sim$ 10^5 electrons per second — much smaller than the photo current ($\sim$ 10^8 to 10^9 e/s) in the high KAO background. We anticipate system NEPs, including all loses and referred to the sky $\sim$ 6 to 12×10^{-15} $W\ Hz^{-1/2}$ in spectrometer mode, and $\sim$ 25 $Jy\ Hz^{-1/2}$ in photometry mode over the band.

Acknowledgement This work was supported by NASA grant NAG2-800.

References

Poglitsch, A., Beeman, J.W., Geis, N., Genzel, R., Haggerty, M., Haller, E.E., Jackson, J.M., Rumitz, M. Stacey G.J. and Townes, C.H. 1991, Internat. J. Infrared Millimeter Waves, 12, 859

Huffman, J.E., Crouse, A.G., Halleck, B.L., Downes, T.V., and Herter, T.L. 1992 preprint

Van Cleve, J.E., Herter, T., Pirger, B., Gull, G. Huffman, J., Seib, D. Halleck B.L., and Reynolds, D.B., in Proceedings of *IR Arrays: the Next Generation.*

Receiver A2 – A 210 to 280 GHz SIS Receiver for the James Clerk Maxwell Telescope

S.R. Davies[1], C.T. Cunningham[2], L.T. Little[1] and D.N. Matheson[3]

[1] Electronic Eng. Laboratory, Univ. of Kent, Canterbury, Kent CT2 7NT, U.K.

[2] Herzberg Inst. of Astrophys., 100 Sussex Drive, Ottawa, Ontario K1A OR6, Canada

[3] Rutherford Appleton Laboratory, Chilton, Didcot, Oxon OX11 0QX, U.K.

Introduction

In March 1992 a 210–280 GHz heterodyne receiver, using a Pb-alloy SIS junction as the mixing element, was commissioned on the James Clerk Maxwell Telescope, Hawaii. This receiver, designated Receiver A2, is based on a prototype version which was tested on the JCMT in May 1989, developed for use on the telescope as a facility instrument.

At the time of commissioning, the receiver utilised a comparatively lossy beamsplitter (50 μm thick mylar film) to couple in the LO power, and had best performance of T_R (DSB) = 110 K near 230 GHz (Davies et al, 1992), as shown in Fig. 1. Since commissioning, some improvements have been made to the receiver, the most important being the replacement of the LO beamsplitter with one having less loss (23 μm thick mylar film). Originally, the LO power was provided by a frequency multiplied Gunn oscillator having a wide range of operating frequency, but with low output power at some frequencies across its band. Replacement of the Gunn oscillator with one having a narrower frequency band, but a flatter power response permitted the use of a beamsplitter with a smaller reflection coefficient. The current performance of Receiver A2 is shown in Fig. 1, best performance being T_R (DSB) = 75 K at 232 GHz.

Receiver Configuration

The SIS devices consist of a Pb–Au–In alloy base electrode, an indium oxide tunnel barrier, and a Pb–Au counter–electrode (Davies et al., 1987). Junctions are formed having areas $\sim 0.5\ \mu m^2$, yielding ωCR products of $\sim 2-3$.

The mixer block consists of quarter–height rectangular waveguide, with an adjustable, non–contacting, choked backshort, operating in half–height waveguide. Radiation is coupled into the waveguide via a corrugated circular feed–horn.

An IF of 1.5 GHz is used, the IF signal from the mixer passing to a cooled (to 4 K) isolator, followed by a cooled (to 18 K) HEMT amplifier. An IF impedance matching circuit, fabricated in stripline, is situated between the SIS junction and the subsequent 50 Ω components of the IF chain.

The receiver is fitted with a superconducting magnet, to allow the suppression of Josephson currents through the junction. The magnetic field is necessary to permit stable operation and reliable calibration of the receiver (Davies et al., 1992).

Cryogenic receiver components are mounted in a hybrid liquid helium cryostat, the radiation shields being cooled by a two–stage refrigerator. The cryostat has a 10 day hold–time from a single fill ($\sim$ 3.5 litre) of liquid helium.

Receiver Performance

The receiver performance at the present time (September 1993) is shown in the central plot of Figure 1. The best performance was measured at 232 GHz, where the DSB receiver noise temperature is T_R (DSB) = 75 K. The receiver noise temperature appears to be less than 110 K (DSB) across the whole RF band. A main beam efficiency of $\eta_{mb} \simeq 0.72$, and telescope transmission $\eta_l \simeq 0.91$ were measured and found to be essentially constant across the RF band.

Measurements have also been made using an even lower loss beamsplitter (12 μm thick mylar film), the results being shown in Fig. 1. Best performance was measured at 232 GHz, where T_R (DSB) = 63 K. At some frequencies across the band, it was not possible to find sufficient LO power to drive the mixer. A more efficient LO source would permit the very low loss beamsplitter to be installed permanently.

The noise temperature for the complete receiver, T_R may be written as

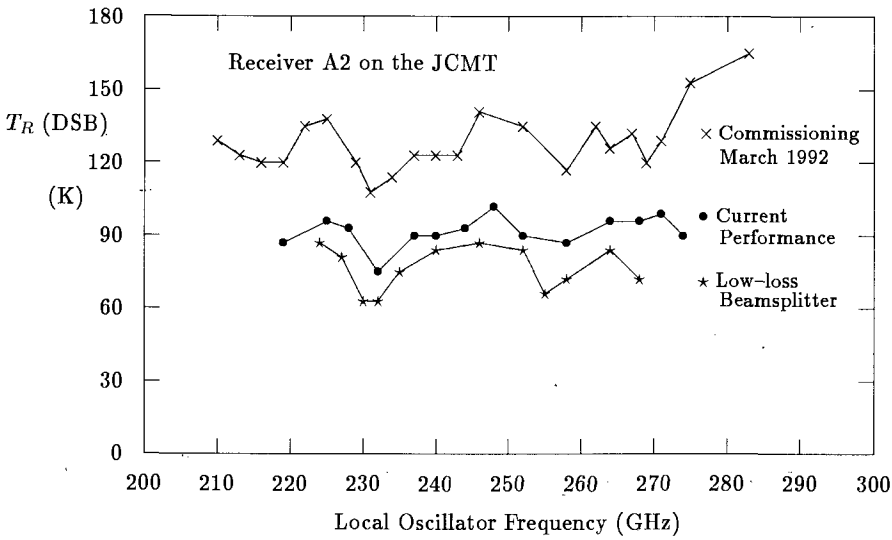

Figure 1. Performance of Receiver A2 on the JCMT (a) at the time of commissioning; (b) at the present time; (c) with a lower–loss beamsplitter

$$T_R \text{ (DSB)} = T_{in} + L_{in} T_M + L_{in} L_M T_{IF}$$

where L_{in} is the input loss arising from the quasioptical components in the beam, which also contribute noise T_{in}. T_M is the DSB mixer noise temperature, L_M the mixer conversion loss and T_{IF} the noise temperature of the IF amplification chain.

Measurements / estimates of the various components contributing to the loss of the complete receiver (Davies et al., 1994, in preparation) indicate that $T_{IF} \simeq 5$ K, with T_M (DSB) $\simeq$ 25 K, L_M (DSB) $\simeq 3.3$ dB, and $L_R = L_{in} L_M \simeq 4.9$ dB.

References

S.R. Davies, C.T. Cunningham, L.T. Little and D.N. Matheson : Int. J. of Infrared and Millimeter Waves **13**, 647–658 (1992).

The Arcetri 40 – 50 GHz Receiver for the Medicina Radiotelescope

G. Tofani[1], M. Catarzi[1], V. Natale[2]

[1] Osservatorio Astrofisico di Arcetri, L.go E. Fermi 5, 50125 Firenze, Italy

[2] CAISMI - CNR, Largo E. Fermi 5, 50125 Firenze, Italy

Introduction

Numerous spectral lines of relevant astronomical importance are available in the wavelength range between 20 and 70 GHz. In this band transitions of several molecules like SiO, CS, HNCO, CH_3OH, H_2CO plays a central role in the different phases of the interstellar medium. In order to extend the observations with the Medicina Radiotelescope of galactic masers, a cooled receiver operating in the range 40 - 50 GHz has been built for continuum and line observations. The system has been tested at the Cassegrain focus of the Medicina Radiotelescope on continuum and SiO maser sources.

The receiver

The receiver, whose schematic diagram is shown in fig. 1, is based on the use of a commercial Watkins-Johnson Schottky mixer, cooled to 20 K by means of a CTI closed cycle mechanical cryogenerator. The mixer is mounted at the end of a cooled corrugated feed horn followed by a tapered transition; the IF signal from the mixer is amplified by a three stages cooled HEMT amplifier that provides $\sim$ 25dBgain. A WR22 waveguide termination, also cooled at about 20 K is used as the reference cold load. Two waveguide windows, made of 50μ mylar, are inserted in the local oscillator and the cold reference load paths. The first local oscillator can be mechanically tuned in the range between 40.5 and 48.5 GHz. An electronic phase lock system provides the required locking to the reference synthesizer for spectroscopy and interferometric observations. The mean double sideband system noise has been measured to be 120 K over the 0.6 GHz IF band centered at 1.5 GHz, at a receiver frequency of 43 GHz.

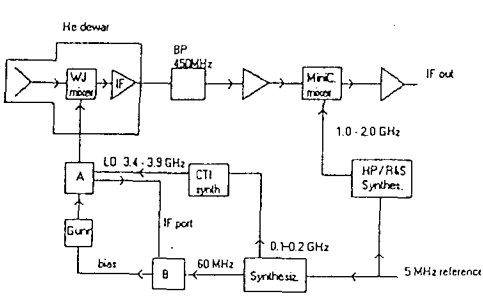

A : directional coupler,harmonic mixer and diplexer

B : XL phase lock electronics

Fig. 1 Schematic diagram of the receiver

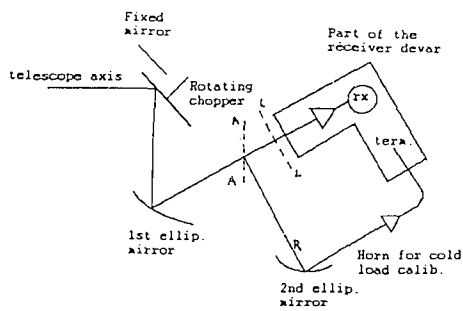

Fig. 2 Optical layout. R shows the cold calibration ray path.

Fig. 2 shows the layout of the optical coupling to the telescope and the calibration system. The beam coming from the telescope is refocussed on the input horn of the receiver by means of an elliptical mirror. A rotating chopper and a plane mirror allow focal plane chopping both for fast beam switching and continuum obervations. The calibration is obtained by alternatively inserting in front of the input horn an ambient temperature load made by a sheet of Eccosorb AN72 (L - L in fig.2) and a plane mirror (A - A in fig.2) which couples the signal coming from the cold reference through a standard horn and a second elliptical mirror. A serial line interface allows the remote control of the receiver.

Test Observations

The receiver has been tested at the Cassegrain focus of the 32 meter Medicina Radiotelescope by observing both planets in the continuum, for calibration purposes, and SiO maser emission from the evolved stellar objects at the rest frequency of 43.122 GHz. Fig. 3 shows a typical Jupiter transit while fig. 4a and 4b show spectra, obtained in the beam switch mode using the 1024 channels digital autocorrelator available at Medicina. The integration time is 300 sec per beam over a 50 MHz bandwidth, which corresponds to a velocity range of 350 kms^{-1}. The antenna efficiency at 43 GHz turns out to be 8% and the measured rms noise for each channel is 16 Jy (for 300 sec of integration time and 50 MHz bandwidth).

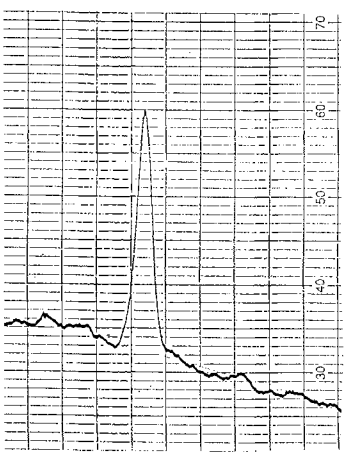

Fig. 3 Jupiter transit

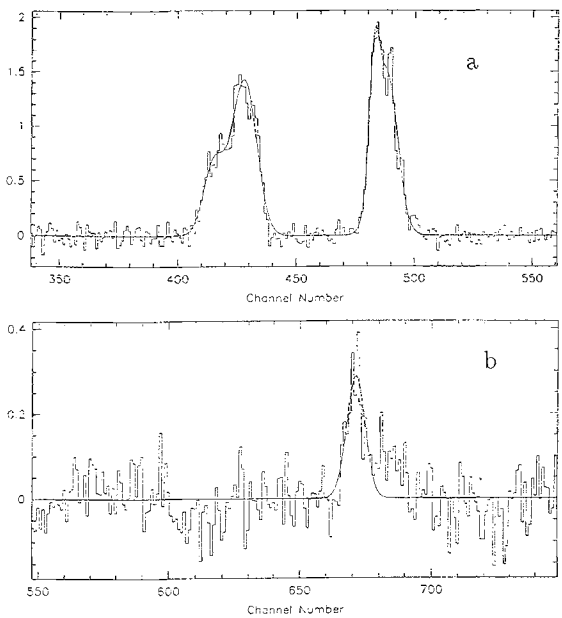

Fig. 4 SiO spectra of ORIIRC2 (a) and OCETI (b).

The Renewal of the POM_2 Radiotelescope

G.Duvert[1], A. Castets[1], L. Pagani[2], B. Fouilleux[1], P.Petmezakis[1]

1. Observatoire de Grenoble, BP 53X, F-38041 Grenoble CEDEX, France
2. DEMIRM, Observatoire de Meudon, F-92195 Meudon CEDEX, France

The POM_2 radiotelescope (Castets et al 1988) was until recently equipped with a Sckottky diode receiver of $Trec_{DSB}$ = 300K with a limited frequency coverage, due to a lack of local oscillator power. The best system temperatures obtained would seldom fall below 1500K. This in turn would force POM_2 to a simple observing strategy, namely the mapping of strong lines in giants molecular clouds. Even this simple task would take a large amount of time when one mapped the ^{13}CO and $C^{18}O$ $J = 2 \rightarrow 1$ lines in Orion A (Castets et al 1990, Dutrey et al 1992, 1993). On the software side, POM_2 was driven by a PDP-11 computer of limited storage and memory and several receiver functions were performed through a dedicated Z80 microprocessor with a very unhandy hexadecimal keyboard control.

POM_2 is now equipped with a state-of-the art SIS (Niobium) junction developped at IRAM by A. Karpov. The present junction has a $Trec_{DSB}$ = 80K all the way from 219 to 267 GHz. A cooled HEMT amplifier (4K noise temperature over a 500Mhz bandwidth centered at 1.5 Ghz) has been installed behind the mixer and preserves the SIS sensitivity. This amplifier was built at the Yebes Astronomical Observatory (Spain) under an European Community contract.The POM_2 frequency range is now limited only by its Local Oscillator (GUNN diode) range. The present values are 218–278 GHz.

The POM_2 SIS receiver is cooled to 1.5K by a 4-stage closed-loop cryogenerator designed by G. Maréchal (Maréchal 1985) and donated by the École Normale Supérieure (Paris). This cryogenerator can dissipate 200 mW at 1.9K; the main time between failures of the third prototype now in use in the "real world" of an observatory is of the order of five weeks. This cryogenerator can only work in upright position, and was too large to fit at the cassegrain focus. It is now installed at a Nasmyth focus, after some mechanical work that involved an extension of the altitude axis of the mount. To refocus the beam, a set of three mirrors, one of them elliptical, has been installed in the Cassegrain cabin. The losses are insignificant. The mixer horn was also changed and provides a better illumination of the secondary mirror, and the forward and beam efficiencies have improved. They are now 0.82 and 0.68 at 220 GHz. The rather low value of the forward efficiency is mainly due to the presence around the antenna, of a dome that protects it from the sometimes harsh weather at 2650m on the Plateau de Bure.

The motorized settings of the receiver have been extended to drive the SIS backshort and LO attenuator, the latter being a critical tuning since the SIS performances are extremely sensitive to the LO power. The obsolete dedicated microcomputer has been replaced by a new one that accomodate the numerous step motors and allows an RS-232 dialog with the VaX.

Thanks to its wide frequency range and its better sensitivity (the DSB system temperature being now of the order of 500K with 2 mm of precipitable water), the observing range of POM_2 is now greatly improved. faint sources, rare molecules and extragalactic objects are now within reach of POM_2.

References

Castets A., Lucas R., Lazareff B., Cernicharo J., Omont A., Duvert G., Fouilleux B., Forveille T., Pagani L., Beaudin G., Deschamps A., Encrenaz P., Lebourg S., Gheudin S., Pérault H., Ruffié G., Clavelier B., Lacroix J., Lauqué R., Montignac G., Baudry A. and Champion M., 1988: A&A 194, 340
Castets A., Duvert G., Dutrey A., Bally J., Langer W.D. and Wilson R.W., 1990: A&A 234, 469
Dutrey A., Langer W.D., Bally J., Duvert G., Castets A. and Wilson R.W., 1991: A&A (Letters) 247, L9
Dutrey A., Duvert G., Castets A., Bally J., Langer W.D. and Wilson R.W., 1993: A&A 270, 468
Kutner M.L. and Ulich B.L., 1981: Ap.J. 250, 341
Maréchal J.C., Pernot J.C., Encrenaz P.J., 1984: Intl. J. of Ir and Mm Waves 5, 7
Pagani L., Langer W., Castets A., 1993: A&A (Letters) 274, L13

ODIN — A Swedish Submillimetre Wave Satellite for Astronomy and Aeronomy

Åke Hjalmarson
Onsala Space Observatory, S–439 92 Onsala, Sweden

Main Scienticfic Themes. ODIN is a result of the shared desire of astronomers and aeronomers to observe molecular lines in unexplored bands of the electromagnetic spectrum around 0.5 and 2.5 mm, where ground–based observations are hindered by the atmospheric absorption due to H_2O and O_2. Observations of the very same molecules — missing links in our understanding of interstellar oxygen chemistry and the cooling of molecular clouds — form the basis of the astronomy side of the mission. The major aeronomy driving force is ozone chemistry. A limb scanning mode of the terrestial atmosphere will be used for studies of the distribution of H_2O, O_2, O_3, CO, $C\ell O$, and several other molecules as well as aerosols. Here complementary information will be obtained from spectral lines at ultraviolet and optical wavelengths.

Payload Overview. Our original idea was to investigate the feasibility of launching a small but very sensitive submillimetre wave satellite equipped with low noise SIS mixer(s). This also would have been a step towards "space qualification" of SIS mixers and of a 4 K closed cycle Stirling cooler for ESA's cornerstone satellite FIRST. However, it soon turned out that cooling to 4 K would be much too expensive in terms of power and weight (and hence funding).

In the present concept we still emphasize sensitivity. We use active cooling (although only to 80 K) and the antenna size is maximized (to fit to a Pegasus launcher). We have included a low noise 119 GHz O_2 channel to gain an order of magnitude in sensitivity compared to the submm line for nearby cold, lower density molecular clouds. ODIN will be equipped with:

- A 1.1 m size offset antenna (surface rms 10 μm)
  beamsize: 2′ at 0.5 mm, 9′ at 2.5 mm
  resolution: 2 km at 0.5 mm in aeronomy mode
- Tunable Schottky mixers (tuning range ±1.5 %) at
  572 GHz (O_3, $C\ell O$, CO, NH_3, H_2S)
  555 & 549 GHz (H_2O, $H_2^{18}O$, ^{13}CO, $C^{18}O$)
  495 GHz (H_2O, HDO, $C\ell O$, O_2, CI, CS)
- HEMT/Schottky mixer (no tuning) at 119 GHz (O_2)
- Stirling cycle cooling to 80 K
- Spectrometers:
  2 high/low resolution hybrid autocorrelators (150 kHz/ 1 MHz)
  Broad band AOS
- Optical grating spectrometer with 200–800 nm & 1270 nm bands

Astronomy Research. Emphasis will be on observations of interstellar H_2O (557 GHz), $H_2^{18}O$ (548 GHz) and O_2 (119 & 488 GHz), aiming at an improved understanding of oxygen chemistry and cooling processes governing molecular cloud evolution towards star formation. CO (576 GHz) and ^{13}CO (551 GHz) observations are foreseen as complements to the H_2O and O_2 surveys, especially in accounting for the PDR component of the molecular clouds. The NH_3 (572 GHz) ground state transition is an important high density probe, which may be useful for the interpretation of the H_2O data.

We also plan spectral line surveying, of bands not accessible from ground, towards a few selected molecular clouds and circumstellar envelopes. Studies of atmospheric chemistry in the giant planets and of H_2O outgassing in comets are being considered. Observations of H_2O and CO in some relatively nearby galaxies will also be attempted.

Project Status. The ODIN project is a joint venture between the space agencies in Canada, Finland, France, and Sweden. Launch is planned to take place in late 1997.

New Techniques for Submillimeter Precision Broadband Spectroscopy

M. Liedtke, Th. Klaus, R. Schieder, G. Winnewisser, K.M.T. Yamada[1]
V. Wagener, M Winnewisser[2]
O.P. Pavlovsky, G.M. Altshuller, O.K. Anikin, A.A. Uljanov[3]
S.P. Belov, E.N. Karyakin, A.F. Krupnov, A.P Shkaev, M. Yu. Tretyakov, N.F. Zobov[4]

[1]I. Physikalisches Institut, Universität zu Köln, D-50937 Köln, Germany
[2]Physikalisch-Chemisches Institut, Justus-Liebig-Universität, D-35392 Giessen, Germany
[3]Institute of Electronic Measurement, KVARZ, Nizhnii Novgorod, 603024 Russia
[4]Applied Physics Institute, Nizhnii Novgorod, 603024 Russia

We report precision broadband spectroscopic measurements in the spectral region up to 1.1 THz. Continuous frequency coverage is achieved by employing frequency and phase stabilized Backward Wave Oscillators (BWOs). This breakthrough in high-resolution scanning spectroscopy in the terahertz region with microwave accuracy and hitherto unparalled sensitivity became possible by the opening of the borders between East and West and essentially by the collaborative technical efforts between the University of Cologne and Giessen, Germany, and the Institute of Applied Physics, Nizhnii Novgorod, Russia.

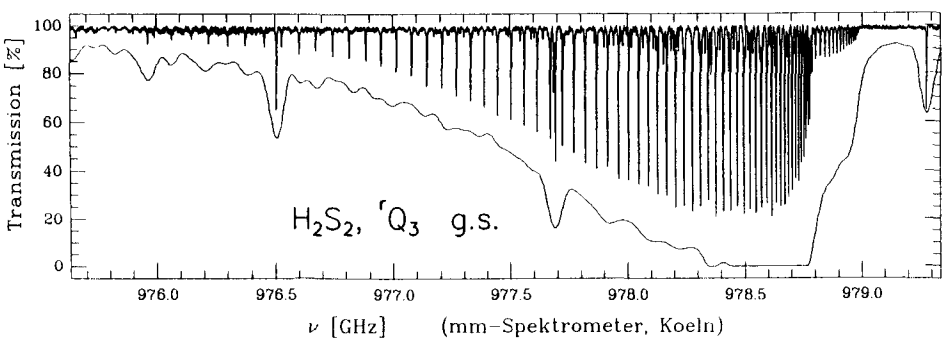

Figure 1: The $^rQ_3$ branch of HSSH near 1 THz in comparison with a Fourier transform recording (lower trace) obtained in the Giessen laboratory.

The essential components of the Cologne Terahertz spectrometer system consist of high-frequency, broadband tunable BWOs, supplied by the ISTOK Research and Production Company (Fryazino, Moscow region), a newly designed multiplier-mixer with a low noise HEMT amplifier circuitry, two precision tunable millimeter wave synthesizers covering the frequency region between 78 to 118 GHz and 118-178 GHz. They are commercially available from the Institute of Electronic Measurement, KVARZ (Nizhnii Novgorod). A He-cooled InSb-hot electron bolometer is used as a detector.

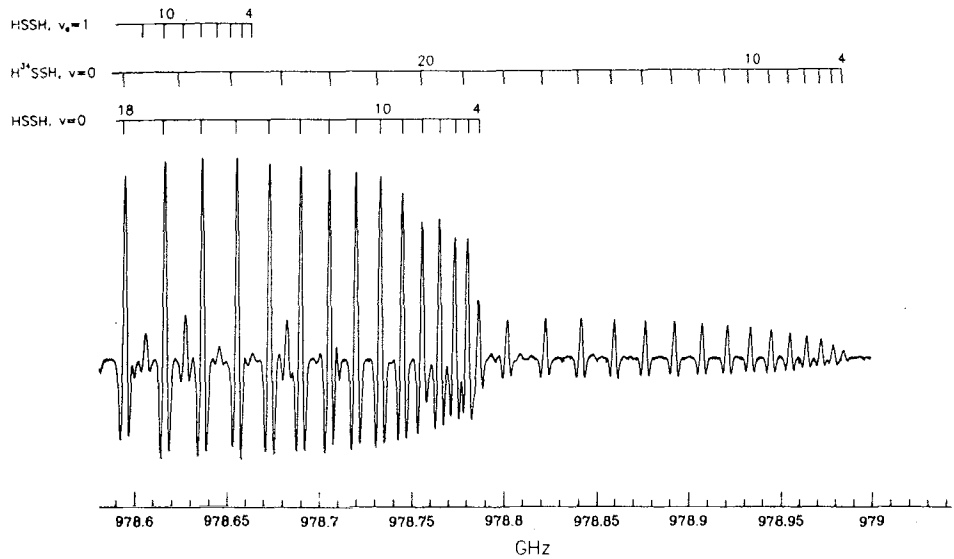

Figure 2: Band head of the ${}^rQ_3$ branch of HSSH recorded with a phase locked BWO.

Extensive measurements have been performed on HSSH, HOOH, on their various isotopomers, and on a large number of astrophysically relevant molecules, such as SO_2, H_2S, HCN, H_2CO, HNCS, HNCO, CH_3OH, and radicals SO, CN, NO, and CCH. The pure rotational spectra of simple chain molecules such as HSSH in the ground and various vibrationally excited states are particularly amenable to broadband high-resolution spectroscopy, both in the Doppler limited and in the sub-Doppler domain. The beauty of perpendicular spectra exhibited by near prolate tops and the wealth of information contained in the spectra is revealed impressively by this new technique. We have performed comprehensive measurements of the ${}^rQ_{Ka}$ branches for higher $K \geq 2$ values of HSSH and its various isotopomers. In Fig.1 we display the ${}^rQ_3$ branch of HSSH, recorded with a free-running THz BWO as radiation source. The trace underneath represents the best recording of this Q branch by high resolution Fourier transform spectroscopy. The band head of this $K_a = 3$ Q branch, registered with a frequency and phase stabilized BWO, demonstrates the high sensitivity of the spectrometer (estimated to be about 10^{-5} cm^{-1}). The appropriate J-assignments are given.

An essential part in the phase-lock-loop (PLL)-system of the Cologne Terahertz spectrometer are the new, continuously tunable frequency synthesizers, which employ a PLL-stabilized BWO, which can be locked to the output of an atomic clock. In the Giessen Microwave Laboratory, the 78 to 118 GHz unit has been employed to record the OCCCS spectrum continuously over the entire tuning range. These automated measurements yielded more than 4000 spectral lines, belonging to the ground and various vibrationally excited states, particularly the excited bending states, the lowest of which is ν_7 at 78 cm^{-1}. The extreme frequency stability of the KVARZ- frequency synthesizer allowed reference spectra to be taken hours later with the cell empty. Subtraction of the two scans yielded the OCCCS spectrum with greatly reduced baselines as shown in Fig 3. Fig. 4 presents a portion of the ${}^rQ_0$ branch of HSSH recorded in Cologne with the 118 to 178 GHz KVARZ svnthesizer. With the Cologne system saturation dip spectra have also been obtained.

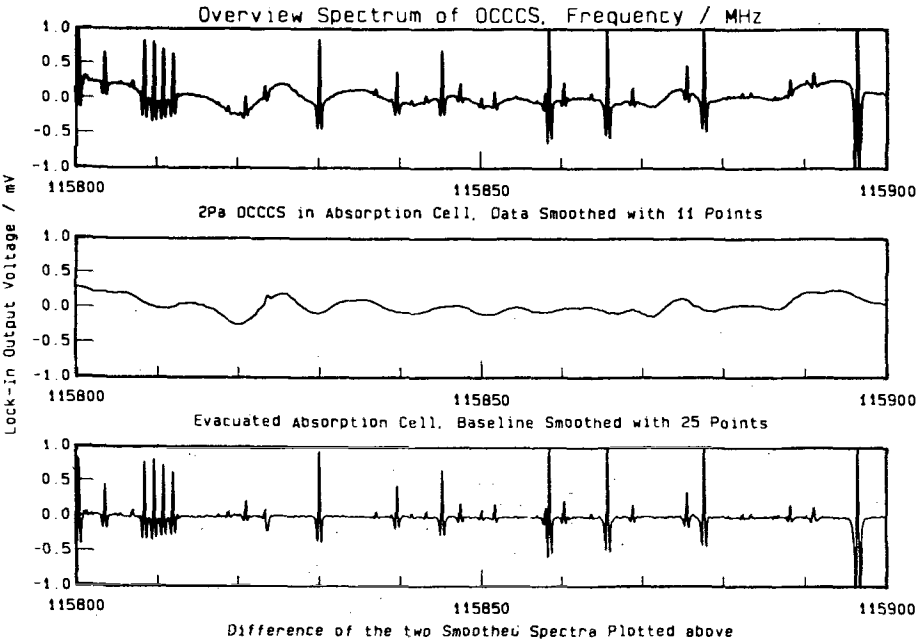

Figure 3: Small part of the frequency scan of OCCCS. Upper trace: filled cell; middle trace: reference spectrum taken with an empty cell; lower trace: difference (filled-evacuated) spectrum. The sensitivity is about 10^{-7} cm^{-1} with a time constant of 120 msec.

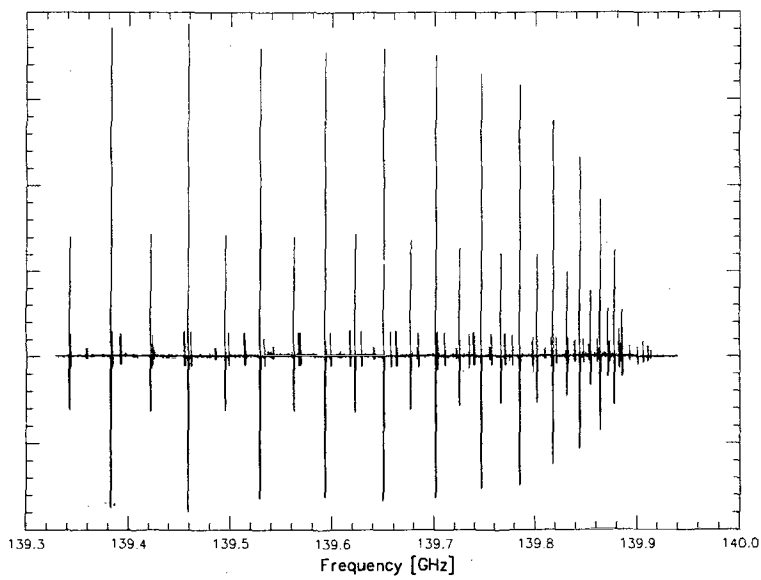

Figure 4: Band head of the $^rQ_0$ branch of HSSH, recorded with a KVARZ synthesizer. The 3:1 intensity alternation of adjacent J lines is clearly seen.

ARNICA, the NICMOS 3 Imaging Camera of TIRGO

Franco Lisi[1], **Carlo Baffa**[1], **Leslie Hunt**[2], **Ruggero Stanga**[3]
[1]Osservatorio Astrofisico di Arcetri
[2]CAISMI–CNR
[3] Università degli Studi di Firenze

Largo E. Fermi 5, Firenze (Italy)

ARNICA (ARcetri Near Infrared CAmera) is the imaging camera for the near infrared bands between 1.0 and 2.5 μm that Arcetri Observatory has designed and built as a general facility for the TIRGO telescope (1.5 m diameter, f/20) located at Gornergrat (Switzerland). The scale is 1″ per pixel, with sky coverage of more than 4 min $\times$ 4 min on the NICMOS 3 (256 $\times$ 256 pixels, 40 μm side) detector array. The camera is remotely controlled by a 486 PC, connected to the array control electronics via a fiber–optics link. A C–language package, running under MS–DOS on the 486 PC, acquires and stores the frames, and controls the timing of the array.

The camera is intended for imaging of large extra–galactic and galactic fields; a large effort has been dedicated to explore the possibility of achieving precise photometric measurements in the J, H, K astronomical bands, with very promising results.

The optics give good quality images in the whole spectral range, by providing also a partial correction for the off–axis aberrations of the telescope. The focal plane is placed inside the dewar in order to house the cold field stop (or the slit for spectroscopy in a near future) at cryogenic temperatures; this provide good shielding from off–axis sources of light without adding radiating flux from warm surfaces. The optical design provides also a cold, aberration–free image of the entrance pupil of the telescope. The latter helps to further screen out stray light, by simply inserting a cold stop. As a further benefit, it offers a suitable plane for inserting a grism into the optical beam, enabling the operation of the camera as a long slit spectrometer.

The filter wheel can hold a total of eight 1–inch filters in the current implementation; besides the standard set of astronomical filters for the J, H, K bands, presently mounted are four narrow–band filters for collecting images in selected spectral lines (FeII, HeI, H_2 and Brγ). However, due to the limited total physical volume of the commercial dewar we used to lodge the optics, the useful field for narrow–band imaging is reduced to a circle of about 2 min diameter.

The low level of dark current of the NICMOS 3 array necessitates a very low level of stray light inside the dewar. To this end, the mechanical design presents careful positioning of cold baffles and stops. In particular, the lenses are completely enclosed in a light–tight pipe, and the filter wheel is mounted inside a box; the inner surfaces of the pipes and of the filter box are sand–blasted and blackened. Cooling is provided by means of liquid nitrogen contained in two vessels.

For extended source observations, the typical observing procedure consists of a group of exposures on the source, interleaved by exposures on blank sky. The sky exposures are conveniently shifted relative to the source position, and typically are taken on different non–overlapping positions. For point–source observations, each telescope position is shifted by roughly 7–10 seeing–disk diameters relative to the preceding one, and there are no sky exposures as such. The sky frames are combined with a stack median filter and a clipping algorithm to remove most field stars; this provides a reference frame for flat fielding. The process of read–out using double–sampling obviates the need for explicit subtraction of a bias frame. Also, at present we do not subtract dark current frames; the dark current level is very low (of the order of 0.5 e s^{-1} at the working temperature of 76 K) and the associated fluctuations are negligible.

Table 1 lists the parameters that describe the performance of the camera ARNICA at TIRGO. Without exceptions, we read the array detector twice, first at the very beginning of the integration period, just after resetting the array, and then at the end of the integration time. The stored frame is the result of the subtraction of the former frame from the latter one. The read–out noise is about 40 electrons, so that the background noise sets the limiting sensitivity stated in Table 1 after a typical integration time of few seconds. While most of the entries are self–explanatory, we comment briefly on the definitions of limiting magnitude. The limiting magnitude per square arcsecond assumes that all the flux from the source falls on a single

Table 1: Typical performance of ARNICA at TIRGO.

	J	H	K
Efficiency (e/photons)	0.15	0.23	0.27
Background (mag arcsec^{-2})	15–15.5	12–13	12.5–13.5
Limiting magnitude (arcsec^{-2}, 3σ, 60 s)	20.5–21	19.3–19.6	19.1–19.6
Limiting magnitude ($5''$ apert., 3σ, 60 s)	18.8–19.3	17.6–17.9	17.4–17.9

pixel, as in the case of extended sources or the sky. The atmospheric turbulence has the effect of broadening the image of a point–like source, spreading the flux over a number of pixels. In this situation, the limiting magnitude is scaled to take into account the dimension of the aperture where most of the flux is collected. In Table 1 we chose an aperture of $5''$ as representative of the dimension of the artificial diaphragm which must be considered during the data reduction process to enclose all the flux coming from a point source after broadening by the atmospheric turbulence. Obviously, under this assumption, the sensitivity is strictly dependent on the seeing conditions at the moment of the observation.

References

Lisi, F., Baffa, C., Hunt, L. (1993) "ARNICA: the Arcetri Observatory NICMOS 3 imaging camera" in *Infrared Detectors and Instrumentation* (Albert M. Fowler, ed.) SPIE Proc. Vol. 1946, in press.

JCMT Receivers – Present and Future

A. P. G. Russell

Royal Observatory, Blackford Hill, Edinburgh EH9 3HJ, Scotland

Introduction The JCMT is a 15m diameter mm/sub-mm telescope operated by the UK Science and Engineering Research Council on behalf of the National Research Council of Canada, the Netherlands Organisation for Scientific Research (NWO) and the University of Hawaii.

Instruments under construction There are three major new instruments currently being developed for the JCMT. These are SCUBA, RxB3 and RxW. SCUBA is a Submillimetre Continuum Bolometer Array with two arrays operating simultaneously at 450 μm (91 pixels) and at 850 μm(37 pixels). SCUBA is described in more detail by Robson in these proceedings and in some depth by Gear & Cunningham (1990).

RxB3 and RxW are both heterodyne receivers — built by the Herzberg Institute of Astrophysics (HIA) and the Mullard Radio Astronomy Observatory (MRAO) respectively. These will both be second generation receivers for JCMT and will bring significant advances over previous instruments. They are both dual polarisation receivers employing Niobium SIS mixers and will have a very high degree of automation. RxB3 operates in the 345 GHz window, whilst RxW covers both the 460 GHz and the 660 GHz windows using a total of four mixers.

A major new feature for both these instruments is the use of quasi-optical single sideband filters. The SSB filter will play a dual role. Firstly of course it rejects lines in the image sidebands to avoid confusion. However their real utility comes from the fact that the image sideband will be terminated on a cold load (at approximately 10K). Such a termination can make a big difference to the overall system temperature, particularity at the higher frequencies. For example with a single channel instrument operating under typical 'good' sky conditions on Mauna Kea at 490 GHz with a DSB noise temperature of 150K, one would typically expect a single sideband system temperature of 2500K. A dual polarisation system with a cold terminated image sideband, would have an SSB system temperature of 1500K under the same conditions.

Future Work

We are presently planing the next generation of instruments for the JCMT. This centres around a 345 GHz (B-band) Facility Array. This project has now been approved to go into the first major design phase in early 1994. The proposal is to produce a 32 pixel array through a series of phases.

- Phase I – will be a 16 channel 345 GHz array using the existing DAS spectrometer. This will have a velocity coverage of about 100 kms^{-1} per pixel and will therefore be suitable for Galactic work.
- Phase II – will run in parallel with phase I and will be to develop a new 16 x 1 GHz spectrometer (MIDAS - Multi Input Digital Autocorrelation Spectrometer) and the associated IF system.
- Phase III – will add a further 16 pixels to the system.

The design goal is to make the front end upgradable to easily accommodate more pixels and ultimately arrays of higher frequency. The target number of 32 pixels has been chosen in order to gain a factor of ten speed improvement in mapping extended sources when compared to a state of the art dual channel instrument like RxB3. The number 32 comes from considering the increased losses associated with the optics of a focal plane array compared to an optimised single or dual channel receiver. In order to realise this gain, the array will also have its image sideband terminated on a cold load. An initial design study for an Array Front End has been carried out by SRON, Groningen. This study has produced an outline design for a 25 pixel array and has demonstrated a fixed tuned waveguide mixer design (employing a diagonal horn) which is suitable for close packing in an array.

References

Gear, W.K. & Cunningham, C.R. 1990. in *Proc. 29th Liège International Astrophysical Colloquium From Ground-Based to Space-Borne Sub-mm Astrononomy*, ESA SP-314, p353.

Submillimeter Bolometer Array for the CSO

Ning Wang, T. Hunter, D. Benford, T. G. Phillips

California Institute of Technology, M/S 320-47, Pasadena, CA 91125

We are building a bolometer array for use as a submillimeter continuum camera for the Caltech Submillimeter Observatory (CSO) located on Mauna Kea. This effort is a collaboration with Moseley *et al.* at Goddard Space Flight Center, who have developed the technique for fabricating monolithic bolometer arrays on Si wafers, as well as a sophisticated data taking system to use with these arrays (Moseley *et al.*, 1984). Our primary goal is to construct a camera with 1x24 bolometer pixels operating at 350 μm and 450 μm using a ^{3}He refrigerator.

The monolithic bolometer arrays are fabricated using the techniques of photolithography and micromachining. Each pixel of the array is suspended by four thin Si legs 2 mm long and 12x14 μm^2 in cross section. These thin legs, obtained by wet Si etching, provide the weak thermal link between the bolometer pixel and the heat sink. A thermistor is formed on each bolometer pixel by P implantation compensated with 50% B. The bolometer array to be used for the camera will have a pixel size of 1x2 mm^2, which is about half of the CSO beam size at a wavelength of 400 μm.

We plan to use mirrors to focus the beam onto the pixels instead of Winston cones. In order to eliminate background radiation from warm surroundings reaching the bolometers, cold baffles will be inserted along the beam passage. To increase the bolometer absorption to radiation, a thin metal film will be deposited on the back of each bolometer pixel. It has been demonstrated that a proper impedance match of the bolometer element can increase the bolometer absorption efficiency to about 50% (Clarke *et al.*, 1978). The use of baffle approach to illumination will make it easier for us to expand to more pixels in the future.

The first stage amplification will be performed with cold FETs, connected to each bolometer pixel. Signals from each bolometer will be digitized using a 16 bit A/D with differential inputs. The digitizing frequency will be up to 40 kHz, though 1 kHz should be sufficient for our application. The output from the A/D will be fed to a digital signal processing (DSP) board via fiber optic cables, which will minimize the RF interference to the bolometers.

To date, we have assembled a 1x24 bolometer array, and we are in the process of testing it. We are also designing and building cryogenic optics. The data acquisition hardware is nearly completed, as well as the electronics. Our goal is to get the instrument working after a new chopping secondary mirror is installed at the CSO in the summer of 1994.

References

Moseley, S.H., Mather, J.C., McCammon, D., J. Appl. Phys. Vol. 56(5) 1257-1262(1984).
Clarke, J., Hoffer, G.I., Richards, P.L., Yeh, N.-H., J. Appl. Phys. Vol. 48(12) 4865-4879(1977).

FTS Atmospheric Transmission Measurements and Observations of Planetary Atmospheres

E. Serabyn, E.W. Weisstein, and D.C. Lis
California Institute of Technology 320-47, Pasadena, CA 91125, USA

The shearing interferometer originally designed for CSO surface measurements (Serabyn, Masson & Phillips 1991) has been upgraded to operate as a moderate resolution Fourier Transform Spectrometer. With a maximim one-sided travel of 44 cm, the attainable unapodized spectral resolution is 170 MHz. Used with the CSO facility bolometric detector, the range of applicability of this FTS is 150-1000 GHz. This instrument has now been used for observations of the transmission of the Earth's atmosphere above Mauna Kea, as well as observations of planetary spectra in the millimeter/submillimeter wavelength ranges. We present a few preliminary results here.

Fig. 1 shows a set of atmospheric transmission curves measured at the CSO with the FTS. To generate these curves, the measured sky emission has been converted to absorption by comparison with an ambient temperature blackbody, and use of Kirchhoff's law. The instrumental gain is calibrated by looking at both hot (room temperature) and cold (77 K) blackbody emitters. The top panel shows the zenith transmission from 330 to 530 GHz on 9 July 1993. This plot actually concatenates the transmission data acquired with two of the CSO's standard filters (note the discontinuity near 447 GHz). The bottom curve shows the measured atmospheric transmission from 160 to 370 GHz on 12 Feb 1993. In order to highlight the weaker lines, the data for an airmass of 2 are plotted. In addition to the strong H_2O and O_2 lines present, two lines of $O^{18}O$, and numerous O_3 lines appear.

Both panels also include model curves for the atmospheric transmission, calculated with the aid of the numerical code AT (Grossman 1989). The code itself allows for a choice of pressure-broadened lineshape (e.g. Waters 1976), as well as the inclusion of an empirical "continuum" contribution to the opacity (due to the distant wings of FIR H_2O lines). It was found possible to fit the lower frequency spectrum (bottom panel) to equal accuracy with either a Zhevakin-Naumov/harmonic oscillator, or Van Vleck-Weisskopf line profile, although each requires a different continuum slope. Assuming a power law continuum opacity in this range, the required exponents are 1.1 for the Zhevakin-Naumov line profile, and 1.5 for Van Vleck-Weisskopf. The model curve compared to the high frequency data (top panel) is the result of extrapolating the derived Van Vleck-Weisskopf model to this frequency range.

The FTS has also been used for observations of the giant planets. Fig. 2 shows the measured brightness temperature spectrum of Saturn between 210 and 295 GHz. These observations were calibrated with respect to Venus, which subtended approximately the same solid angle as Saturn at the time of the observations. The very pressure broadened J = 1-0 rotational transition of PH_3 (phosphine) at 266.9 GHz has been detected, and shows a FWHM of 11.2 GHz. The continuum level agrees well with previous measurements, although the contribution of flux from Saturn's rings complicates the comparison. In particular, the slight rise in continuum level with frequency is most likely due to ring emission.

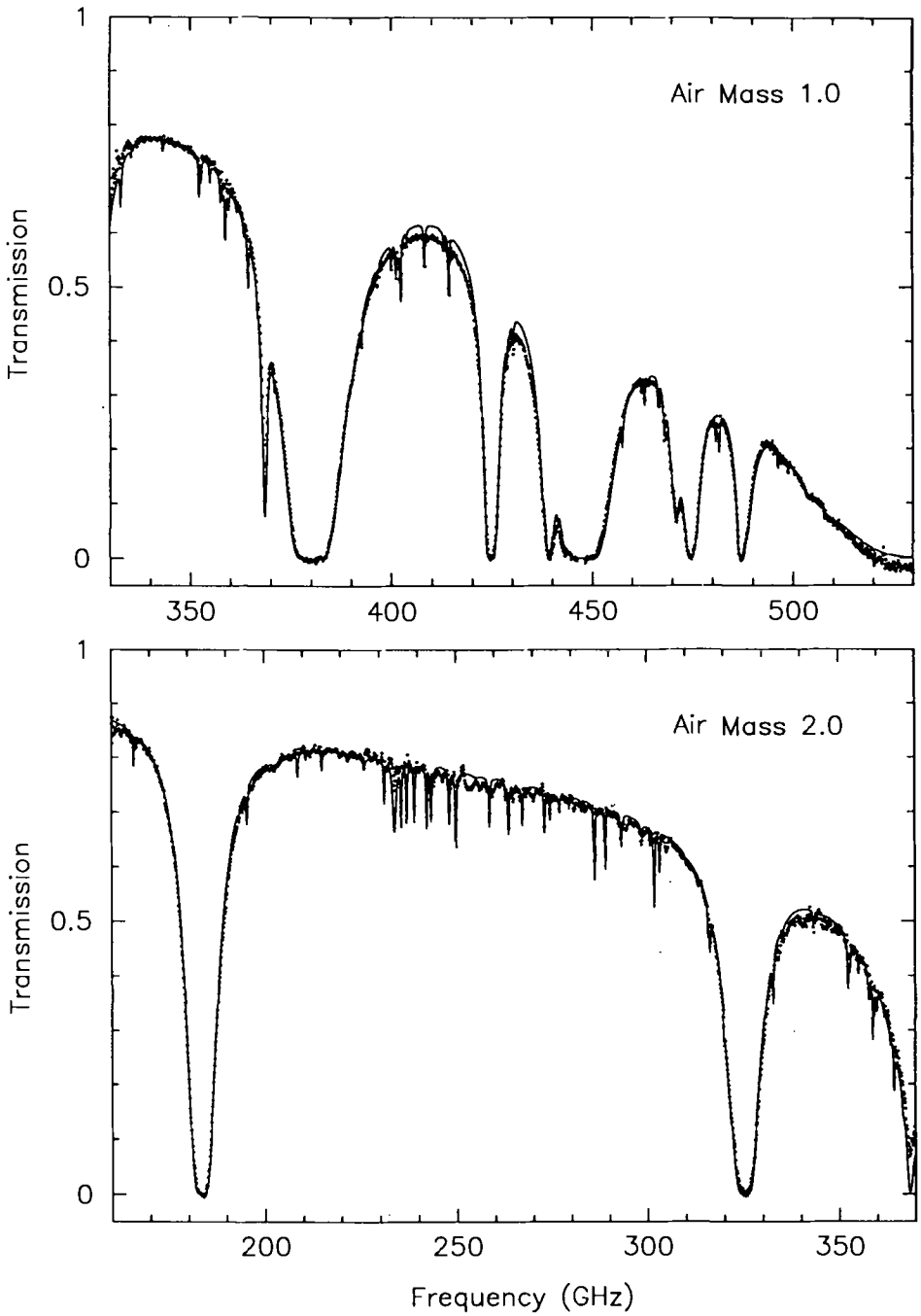

Fig. 1. Points: Atmospheric transmission at the CSO measured with the FTS. Solid lines: Models for same, as described in text.

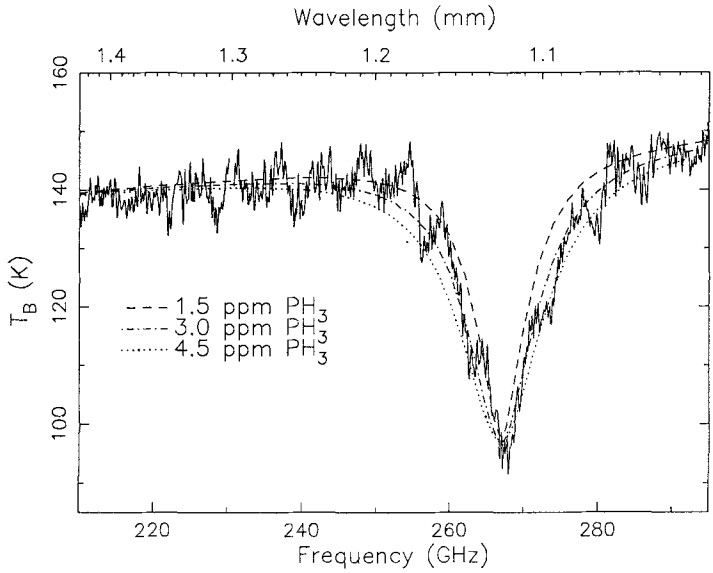

Fig. 2. Solid line: Measured Saturn brightness temperature spectrum. Dashed and dotted curves: Radiative transfer models with the indicated abundances of PH_3.

Radiative transfer modelling of Saturn's atmosphere and rings as in Grossman, Muhleman & Berge (1989) & Grossman (1990) allows us to derive the abundance of PH_3 in Saturn's atmosphere. The lack of a narrow stratospheric emission core, and the depth of the line both provide evidence for a lack of phosphine above Saturn's tropopause. With a cutoff level of about 100 mbar, the abundance of PH_3 in the troposphere below this altitude is then (see Fig. 2) $3.0 \pm 1.0 \times 10^{-6}$, much greater than the solar P abundance. These results compare favorably with a theoretical picture in which PH_3 originates deep in Saturn's troposphere, is carried upward by convection, and is then destroyed in the stratosphere by UV photolysis (e.g. Prinn *et al.* 1984).

The results presented here represent only our first steps into the field of Fourier transform spectroscopy of planetary atmospheres at submillimeter wavelengths. Higher frequencies, other molecules, and the rest of the planets await our attention.

This work was supported by NSF grant AST90-15755 and NASA grant NAGW-3303.

References

Grossman, A.W. 1990, Ph.D. thesis, Caltech

Grossman, A.W., Muhleman, D.O., & Berge, G.L. 1989, Science, 245,1211

Grossman, E. 1989, Airhead Software, Boulder, CO

Prinn, R.G., Larson, H.P., Caldwell, J.J., & Gautier, D. 1984, in Saturn, Univ. Arizona Press, eds. T. Gehrels & M.S. Matthews, 88

Serabyn, E., Masson, C., Phillips, T.G. 1991, Applied Optics, 30, 1227

Waters, J.W. 1976, in Meth. Exp. Phys., Vol. 12B, 142

A Theorist's View of Interstellar Chemistry

A. Dalgarno

Harvard-Smithsonian Center for Astrophysics, 60 Garden Street,
Cambridge, Massachusetts 02138 USA

Abstract. Some comments are made about interstellar chemistry. They are not to be taken seriously. They were made in an after-dinner address given during the conference banquet.

It is with considerable reluctance and some discomfort that I arise to speak. Perhaps I should take my shoes off.[‡] To follow Gerhard Herzberg is burden enough but to follow me there waits Bill Klemperer. I spoke once before on the same occasion as Bill and I promised myself I would never do so again. After it, no one present except me remembered my having spoken. Somehow I allowed Gisbert to inveigle me into agreeing to speaking this evening despite Bill's expected presence.

I have put together a few disconnected and disjointed remarks made from the point of view of a theorist looking dispassionately at interstellar chemistry. I do so with humility, noting that Gisbert in his introductory remarks took the trouble to assert that no progress is possible without more observations.

Ever since the formation of the first neutral molecule H_2 in the recombination era of the Early Universe 100,000 years or so after the beginning, chemistry has been an integral part of astronomy though recognition that it is so has been slow in coming and it has been a struggle to achieve respectability. I have here a recent review, published in the August 1993 issue of the Journal, The Observatory, of an IAU symposium on the Astrochemistry of Cosmic Phenomena which took place in Brazil in 1991. I will read to you the first three sentences. "Ten years ago astrochemists had something of a credibility problem. Their models of star-forming clouds included hundreds of reactions and yet failed to give the observed abundances for some very simple molecules. Few at the time could have predicted the great progress that was about to be made." After this meeting, I have news for that reviewer.[§]

Serious theoretical interstellar chemistry began with papers by Swings and Kramers and Ter Haar, but what many regard as the foundation is a paper by Bates and Spitzer which appeared in 1954. They constructed a specific set of chemical reactions and equated the production and destruction rates of the chemical species involved. They were attempting to explain the observed abundances of CH and CH^+ that had been found in absorption in the 1930's and 1940's. (Gerhard Herzberg it was who identified the absorption lines of CH^+.) In their paper, Bates and Spitzer set an example for all to follow and the same structural approach is used still. They also set an example by failing to explain the observed abundance of CH^+, just as we, with some elaboration, continue to do today. Bates and Spitzer attempted to deal with the problem, again much as we do now, by manipulating the rate coefficients of the various reactions they had selected as important. It did not work. It was much more promising, and it may even teach us some astronomy, to invoke instead some special astronomical event. Bates and Spitzer postulated a scenario in which a star passing through a cloud sublimes methane off the grains and photodissociation and photoionization rapidly reduce CH_4 to CH^+. More recently, shocks have been invoked, following a paper by Elitzur and Watson in 1978. At this point we encounter one of the two major hazards encountered by theorists—the hazard consists of observers unwilling to let well alone—instead they make more observations to test the model. The newly acquired data show no velocity differences between CH^+ and neutral molecules, effectively ruling out shocks as a general explanation. Theorists are now forced to turn to the current last refuge of the desperate and are invoking turbulence. (It might even work!)

[‡]Gisbert Winnewisser had earlier regaled the audience with the story of a buffet dinner which he attended wearing no shoes. After directing him to a table located in an obscure corner of the room, the waiter insisted on serving him personally so that his state of shoelessness could not be observed by the other guests.

[§]The review was written by Jim Cohen. It is an authoritative, informed account of the subject and its broad connections in astronomy.

Interstellar chemistry remained a minor preoccupation until the radio region of the spectrum was opened by the discovery there of the hydroxyl radical in interstellar space, followed soon by the detection of a polyatomic species, ammonia. But it was the identification of Xogen as the molecular ion HCO^+ by Bill Klemperer that is primarily to blame for the explosion of theoretical papers on interstellar chemistry that have apeared in the past twenty years. A molecular ion HCO^+ in a dense cloud had to mean cosmic ray ionization. An elaborate and glorious theoretical edifice has been built on the assumption that cosmic ray driven ion-molecule chemistry is resopnsible for the hundred or so molecules that have been found in interstellar clouds. The chemistry is entertainingly exotic, involving systems at very low temperatures with level populations far from thermal equilibrium in a diverse range of radiation environments. From the beginning, the models had to struggle to make enough of the complex organic molecules, and always looming as an ominous perhaps fatal threat were the dust grains which, whilst shielding the molecules from the external radiation field, provided surfaces on to which all the interstellar gas atoms and molecules would condense given 10^5 years to do so.

The theorists also had to confront the second of their major hazards. It is that laboratory chemists would become interested and do measurements in the relevant range of physical conditions with the appropriate atomic and molecular species. We heard from Eric Herbst yesterday that indeed the laboratory chemists have done so with the consequence that if the laboratory measurements are correct, the more or less accepted early time explanation of the molecular abundances, that edifice of which I spoke, has collapsed. Theorists clearly have work to do. We should bear in mind that the only enduring theories are those that rely on laboratory data that are impossible to obtain and that predict consequences that are impossible to verify, so we should not be disappointed when theories fail. It means they made testable predictions that stimulated new astronomical or chemical measurements. (You may think that testable predictions are a requirement of all theoretical research. If you do, I urge you to look at recent theories in elementary particle physics.)

Perhaps our theoretical models have become too complicated and we need to learn from the observers.

Dan Jaffe made the trenchant comment that we all have to make simplifying assumptions. As he explained, "That's life". Sometimes, though, I think observers take it to extremes. One example is the relationship between the integrated ^{13}CO emission and the column density of H_2. In the beginning, the observers made no pretence that they knew the relationship. They introduced a parameter and they called it X, making clear it was an unknown. But then they measured it a few directions in the Galaxy and after some highly circular arguments, they announced that X is 2 not only where it had been measured but everywhere in our galaxy and by extension all galaxies. In a subject where one is often taken to be identical to ten, they then indulged in passionate arguments as to whether X is really one rather than two. Dr. Johanssen told us in his presentation that for the LMC it is 1.5. It will not be long before they argue about the second decimal place. They blithely disregard theoretical models of diffuse and translucent molecular clouds, of clumpy dense clouds, of extended photon dominated regions and of dissociative shocks, which we theorists predict to have values of X differing from unity by orders of magnitude. What is truly galling about their X hypothesis is that they may be right. When you take global averages, errors tend to cancel out and it may all fall into place, as some calculations reported by Dave Hollenbach suggested.

However, I assure you that theory is alive and well. The recent discovery by the French group, Le Bourlot et al., that the chemical equations have two solutions—if two, why not many?—offers new regimes of exploration and despite the impression I may have given, I believe new observations driven in part by new instrumentation will carry theory forward to meet new challenges. Progress is there to be made. We seem to be at a stage where we are learning about chemistry by studying astronomy. I think the next decade will see a change where we use chemistry to understand and predict astronomical events.

Gisbert asked me several times to speak tonight, either directly or indirectly through Jürgen Stutzki and Eric Herbst. I applied one of those sophisticated filtering techniques of the kind Bill Langer described to those various messages and I detected an inverse correlation between the length of the talk I was being asked to give and Gisbert's confidence that Bill Klemperer would arrive. Bill is in fact here, so I think I should stop now before Gisbert communicates with me again.

Index

Θ^1C Ori, 167
γ Cas, 203
ρ Oph, 79, 158
ρ Oph B1, 160
ρ Ophiuchi, 214
ρ Ophiuchi, 300
ζOri, 178
30 Dor, 56
0212+735, 120
0355+508, 120
2200+420, 120

continuum
  dust emission , 337
  submillimeter , 337

abundance, 122, 130, 175, 248, 255, 258, 268, 269
AFGL 961, 128
ARNICA, 373
Arp 220, 61
atmosphere
  earth, 377
  saturn, 378
Azelfafage, 58

B1, 79
B164, 58
B216-217, 83
B335, 136
BL Lac, 120
bolometer, 376
bow
  shock, 276
BWO, 371

$C^{34}S$, 50
Cas A, 79
Cas-Tau OB association, 118
cb145, 207
cb155-2, 207
cb17, 207
cb205, 207
cb224, 207
cb230, 207
cb232, 207
cb243, 207
cb244, 207
cb246, 207
cb3, 207
cb34, 207
cb52, 207
cb54, 207
cb58-2, 207
cb6, 207
cb68, 207
center
  galactic, 41, 154, 322
CepA, 212
Cepheus OB3, 320
CH_3CN, 259
Chamaeleon, 300
Chameleon, 113
Chemistry, 380
chemistry, 164, 218, 240, 247, 259, 269
  grain, 218
circumstellar
  disk, 206, 249
  material, 306
cirrus
  cloud, 237
cloud, 118
  cirrus, 237
  high latitude, 237
  high latitude molecular, 271
  model, 130, 138, 152, 175, 199
  structure, 271
  translucent, 54
Cloud Structure, 132
clumping, 150
clumps, 130, 132, 134, 136, 144, 168, 178, 182, 197, 199, 312, 326, 337
COBE, 92
Cocoon Nebula, 265
collapse, 274
collosion
  two-cloud, 274
continuum, 56, 92, 158, 206, 249, 259, 285, 341, 376
  emission, 64, 289, 300
cooling, 165, 180, 278
cores, 50, 52, 265, 266, 294, 310, 314, 326
Corona Australis, 300
could
  model, 123

disk
  circumstellar, 206, 249
DL Tau, 249
DR21, 316
dust, 56, 64, 92, 158, 164, 289, 304, 339, 341
  continuum emission, 292
dynamics, 115

earth
  atmosphere, 377
edge
  galaxy, 13
EL29, 315
emission

continuum, 64, 289, 300
evolution, 118

field
magnetic, 76, 82, 123
formation, 118
star, 14, 30, 50, 76, 160, 169, 265, 276, 298, 310, 320, 322
region, 274

G0.15-0.05, 322
G0.18-0.04, 322
G10.6-0.4, 281
G228-29, 238
G29.96+0.19, 282
G29.96-0.02, 245, 279
G310-45, 238
G34.3+0.15, 291
G34.3+0.2, 288
G5.89-0.39, 280
G9.62+0.19, 246
galactic center, 41, 154, 322
galaxies, 60
galaxy, 56, 90, 243
edge, 13, 30
gas-phase, 218
GG Tau, 249
GG Tau N, 249
globules, 206
cometary, 208
Gould's Belt, 118
grain
chemistry, 218
G 35.2–0.74, 294

H II region, 14, 144, 156, 201, 208, 210, 245, 254, 258, 265, 274, 276, 296, 316, 320, 326, 337, 341
ultracompact, 291
H II regions, 285
HD147889, 214
HD206672, 58
HD29647, 54
HD5005, 326
HD62542, 54
heating, 16, 164, 165, 180, 278
Herbig-Haro object, 318
HH object, 318
HH34, 142
high latitude molecular cloud, 271

IC1805,, 208
IC1848, 92
IC5146, 265
IC63, 203
Infrared Band, 156
Infrared Camera, 362
IRAS, 342
00494+5617, 327
04365+2535, 315
04368+2557, 315
05155+0707, 315
05332-0637, 315
05335-0645, 315
05338-0624, 247, 249
05338-0647, 315
05342-0639, 315
05345-0643, 315
05367-0712, 315
05375-0731, 249
05381-0921, 315
05389-0756, 315
05445+0016, 315
06058+2138, 308
06061+2151, 308
06314+0427, 128
08282-4545, 14
10214+4724, 60, 243
10215-5916, 304
16293-2422, 248
16342-3814, 304
17150-3224, 304
19500-1709, 304
21046+5110, 315
21106+4712, 315
21526+5728, 315
22451+6154, 315
22512+6201, 315
22517+6215, 315
point source, 128, 266
source, 206, 249, 308, 332
IRAS 1, 315
IRc2, 269
IRS37, 315
IRS43, 315
IRS54, 315

JCMT, 360, 375
jet, 332

KAO, 362
Kuiper Airborne Observatory, 362

L1204, 133, 210
L1262, 331
L134N, 221, 329
L1448, 335
L1457, 133
L1495, 15
L1498, 136
L1521B, 136
L1544, 136
L1641, 300, 314
L1755, 83
L1778, 146
L1780, 146
L183, 268
L204, 116
Lac OB1, 118
LDN1010-55, 265
line shapes, 86, 140
Lk Hα 101, 265
Lupus, 300

M16, 180
M17, 164, 180
M17 SW, 133
M17SW, 85, 150, 337
M82, 181
Maddalena molecular cloud, 312

magnetic field, 82, 123
magnetic fields, 76
maser, 296
  H_2O, 308
  OH, 296
mass spectraum, 133
mass spectrum, 18, 134, 144, 312, 337
material
  circumstellar, 306
MBM16, 140
MBM32, 15
MCLD126.6+24.5, 271
medium
  turbulent, 86
MLY22, 315
MLY25, 315
model
  cloud, 123, 138, 152, 175, 199
  could, 130
molecular
  outflow, 280, 314, 318, 334
momentum-driven, 334
Mon R2, 340
Mrk 231,, 61

Near Infrared
  camera, 373
Near Infrared Imaging, 41
NGC 7538, 144
NGC1333, 300, 314
NGC1333 IRAS 4A, 249
NGC1333 IRAS 4B, 249
NGC1499, 133
NGC1579, 265
NGC2023, 134
NGC2024, 134, 178, 180, 212
NGC2024), 252
NGC281A, 326
NGC6946, 90
NGC7023, 164, 265
NGC7538, 133, 329
NGC891, 90
North Polar Cirrus, 113
NRAO150, 120

object
  Herbig-Haro, 318
  HH, 318
  protostellar, 314
  young stallar, 331
ODIN, 369
OMC-1, 258, 269
OMC-2, 50
OMC-3, 50
Ori OB1, 118
Orion, 164, 269, 300
Orion A, 79, 134, 180, 252
Orion B, 79, 133, 134, 252
Orion Bar, 201
Orion-KL, 248
Orion-S, 248
outflow, 51, 206, 300, 308, 316, 331, 342
  molecular, 280, 314, 318, 334

PDR, 90, 164, 175, 178, 195, 201, 203, 210, 212, 237, 316
  model, 197
Per OB2, 118
Perseus, 300
photodissociation, 138, 178, 203, 214, 237
pistol-sickle, 322
point source
  IRAS, 266
polarization, 77, 82
POM_2, 368
Post–AGB stars, 304
pressure-driven, 334
protostellar
  object, 314

receiver, 360, 366, 375
  SIS, 364, 368
region
  H II, 14, 144, 156, 201, 208, 210, 245, 254, 258, 265, 274, 276, 285, 296, 316, 320, 326, 337, 341
    ultracompact, 291
  star formation, 160, 274
RNO 43,, 332
Rosette molecular cloud, 156
rosette molecular cloud, 128, 312
rotation
  temperature, 254
RY Tau, 249

S106, 79
S125, 265
S140, 133, 210, 212, 265, 294
S152, 294
S153, 294
S155, 320
S159, 294
S184, 294, 326
S199, 294
S255, 294
S68, 294
S68 FIRS1, 249
S76E, 294
S88B, 79, 294
Satellite
  ODIN, 369
  SWAS, 352, 356
saturn
  atmosphere, 378
Sco-Cen, 118
self–shielding, 203
Self-gravity, 115
self-shielding, 170
Serpens NW, 248
Sgr A, 41
Sgr A*, 322
Sgr B2, 85, 268
Sgr C, 154
shock
  bow, 276, 318
SIS
  receiver, 364, 368
spectroscopy
  submillimetre, 370
spectrum
  mass, 18, 337

star
formation, 14, 30, 50, 76, 160, 169, 265, 276, 298, 310, 320, 322
region, 274
structure
cloud, 271
Submillimetre Wave Satellite, 369

T Tau, 306
Taurus, 300
telescope, 366, 373
temperature, 262, 291
rotation, 254
TIRGO, 373
TMC-1, 136, 221, 248
TMC1, 268
translucent
clouds, 54
transmission, 377
trapezium stars, 201
turbulence, 76, 318
turbulent
medium, 86

Vela Molecular Ridge, 342
visual extinction, 146
VLA1623, 336

W22, 79
W3, 79, 85, 212, 254
W3(OH), 296
W43, 180
W49, 268
W49A, 274
W49B, 79
W51, 85, 285
WB283, 15
WL12, 315
WL16, 315
WL22, 315

young stellar objects, 331
YS, 206
YSO, 248, 249, 331

Zeeman effect, 77

Index

^{12}CO, 14, 54, 58, 120, 144, 146, 152, 154, 195, 197, 203, 237, 265, 271, 326, 340, 342
^{13}C II, 196
^{13}CN, 252
^{13}CO, 14, 54, 112, 120, 128, 138, 146, 152, 154, 178, 195, 197, 203, 212, 237, 258, 265, 273, 289, 306, 316, 326, 340, 342
$^{16}O^{18}O$, 329

Ammonia, 142, 240, 245, 259, 268, 273, 282, 288, 308, 327

C, 54, 139, 220
C I, 128, 164, 182, 195, 197, 210, 212, 289, 316
C II, 90, 93, 128, 134, 164, 175, 178, 180, 195, 197, 214, 259
C^+, 54, 139, 175
$C^{15}N$, 252
$C^{17}O$, 150, 210, 337
$C^{18}O$, 50, 54, 138, 144, 201, 212, 247, 263, 265, 271, 289, 306
$C^{32}S$, 50
$C^{34}S$, 261, 285, 294
C_2, 54
C_2H, 54, 259
C_2H_2, 221
C_3H, 221
C_3H_2, 54, 263
C_4H, 221
CCH, 120
CCS, 136
CH, 54, 175, 220, 379
CH^+, 175
CH^+, 379
CH_2, 175, 220
CH_3, 240
CH_3CCH, 259
CH_3OCH_3, 254
CH_3OH, 247, 254, 258
CH_3C_2H, 291
CH_3CN, 291
CH_3OH, 269
CH_4, 379
ClO, 369
CN, 54, 120, 175, 221, 252, 254, 259, 269
CNH_2^+, 240
CO, 60, 87, 90, 92, 128, 134, 138, 164–166, 178, 220, 240, 247, 255, 258, 274, 298, 314, 331, 369
CO^+, 175
CS, 52, 54, 142, 158, 176, 201, 203, 247, 258, 265, 269, 294, 306, 314

DCN, 247
DCO^+, 265

Fe, 276

H, 14, 240, 278
H I, 58, 246
H II, 92
$H^{13}CN$, 247, 263
$H^{13}CO^+$, 263, 265, 288
H_2, 138, 164, 166, 201, 220, 316
H_2CO, 160, 201, 254, 340
H_2O, 243, 255, 298, 369, 377
H_2S, 176, 268
H_2CS, 269
HC_3N, 221, 259, 265
HC_5N, 221
HC_3N, 269
HCN, 60, 120, 142, 150, 240, 247, 258, 294, 340
$HCN_,$, 54
$HCNH^+$, 240
HCO^+, 54, 120, 142, 150, 201, 220, 254, 259, 265, 288, 306, 342
HCO^+, 380
HCOOH, 269
HCS^+, 259
He I, 322
$HN^{13}C$, 261
HNC, 120, 240, 258
HSSH, 370

N, 175
N II, 93
N_2H^+, 122, 259
Ne III, 362
NH, 240
NH_3, 142, 240, 245, 259, 268, 273, 282, 288, 308, 327
NH_3, 292, 294
NO, 175

O, 175, 220
O I, 164, 197
O III, 322
$O^{18}O$, 377
O_2, 175, 369, 377
O_3, 369, 377
OCS, 176, 269
OH, 79, 175, 296

PAH, 164
PAHs, 156
PH_3, 378

S II, 176
S III, 362
S^+, 175
Si II, 362
Si^+, 175
SiO, 247, 259, 269
SiO^+, 175
SO, 247, 259, 268, 269
SO^+, 175
SO_2, 254
SO_2, 269

List of Participants

Abt	Bernd	Dornier GmbH	Germany
Adams	Fred C.	Physics Department, University of Michigan fadams@umiphys.bitnet	USA
Allen	Ronald J.	Space Telescope Science Institute rjallen@stsci.edu	USA
André	Philippe	CEA - Service d'Astrophysique andre@sapvxg.saclay.cea.fr	France
Bally	John	University of Colorado bally@janos.colorado.edu	USA
Barnes	Peter	CfA peterb@cfacx2.harvard.edu	USA
Bischoff	Uwe	I. Physikalisches Institut Universität zu Köln bischoff@ph1.uni-koeln.de	Germany
Bloemhof	Eric E.	CfA bloemhof@cfa.harvard.edu	USA
Boissé	Patrick	Ecole Normale Superieure boisse@ensapa.span.cnes.fr	France
Booth	Roy S.	Onsala Space Observatory roy@oso.chalmers.se	Sweden
Bors	Ingo	I. Physikalisches Institut Universität zu Köln bors@ph1.uni-koeln.de	Germany
Brancati	Aldo	Universita 2 TOR Vergata	Italy
Brand	Jan	Instituto di Radioastronomia, CNR brand@astbo1.bo.cnr.it	Italy
Burton	W.B.	Leiden Observatory burton@strw.leidenuniv.nl	NL
Casali	Mark	Royal Observatory Edinburgh mmc@star.roe.ac.uk	UK
Castets	Alain	Observatoire de Grenoble castets@gag.observ-gr.fr	France
Catarzi	Marco	OSS. Arcetri catarzi@arcetri.astro.it	Italy
Cernicharo	Jose	Centro Astrónomic cerni@cay.es	Spain
Churchwell	Ed	University of Wisconsin, Astronomy Dept. churchwell@madraf.astro.wisc.edu	USA
Clark	Frank O.	PL-GPOB fclark@plh.af.mil	USA
Corneliussen	Uwe	I. Physikalisches Institut Universität zu Köln corneli@ph1.uni-koeln.de	Germany
Crutcher	Richard	University of Illinois crutcher@uiuc.edu	USA
Dalgarno	Alex	Harvard College Observatory dalgarno@cfa.bitnet	USA
Dame	Thomas M.	CfA dame@cfa.harvard.edu	USA
Davies	Steven R.	University of Kent srd@starlink.ukc.ac.uk	UK
Davis	Christopher J.	MPI für Astronomie davis@mpia-hd.mpg.de	Germany
Dishoeck	Ewine, van	Leiden Observatory ewine@strwchem.leidenuniv.nl	NL
Dolgner	Alexandra	I. Physikalisches Institut Universität zu Köln	Germany
Duvert	Gilles	Observatoire de Grenoble duvert@gag.observ-gr.fr	France
Eckard	Andreas	MPI für Extraterrestrische Physik eckart@mpe.mpe-garching.mpg.de	Germany
Engargiola	Gregory	University of Illinois, Dept. of Astronomy	USA

		greg@sirius.astro.uioc.edu	
Falgarone	Edith	Ecole Normal Superieure Lab. de Physique falgarone@ensapa.ens.fr	France
Felli	Marco	Arcetri Astrophysical Observatory felli@arcetri.astro.it	Italy
Fiegle	Klaus	I. Physikalisches Institut Universität zu Köln fiegle@ph1.uni-koeln.de	Germany
Frerick	Johannes	I. Physikalisches Institut Universität zu Köln frerick@ph1.uni-koeln.de	Germany
Genzel	Reinhard	MPI für Extraterrestrische Physik genzel@dgampe5d.bitnet	Germany
Gerin	Maryvonne	Laboratoire de Physique de l'ENS gerin@ensapa.ens.fr	France
Geus	Eugene, de	Caltech edg@phobos.caltech.edu	USA
Götting	Bernd	I. Physikalisches Institut Universität zu Köln goetting@ph1.uni-koeln.de	Germany
Goodman	Alyssa	CfA agoodman@cfa.harvard.edu	USA
Gredel	Roland	European Southern Observatory rgredel@eso.org	Chile
Haas	Sybille	I. Physikalisches Institut Universität zu Köln haas@ph1.uni-koeln.de	Germany
Haikala	Lauri K.	University of Helsinki Observatory haikala@hylk.helsinki.fi	SF
Harris	Andrew I.	MPI für Extraterrestrische Physik harris@mpe.mpe-garching.mpg.de	Germany
Harrison	Andrew	Department of Astronomy, Royal Observatory aph@starlink.roe.ac.uk	UK
Hauschildt	Harald	MPIfR p591hau@mpifr-bonn.mpg.de	Germany
Hayashi	Masahiro	Dept. of Astronomy Faculty of Science hayashi@apsun1.astron.s.u-tokyo.ac.jp	Japan
Heithausen	Andreas.	I. Physikalisches Institut Universität zu Köln heithausen@ph1.uni-koeln.de	Germany
Helmich	Frank	Leiden Observatory fph@strwchem.leidenuniv.nl	NL
Henning	Thomas	MPG-WG: Dust in star-forming regions mail@fred.astro.uni-jena.de	Germany
Hepp	Martin	I. Physikalisches Institut Universität zu Köln hepp@ph1.uni-koeln.de	Germany
Herbst	Eric	Ohio State University, Department of Physics herbst@ohstpy.mps.ohio-state.edu	USA
Hertenstein	Thomas	Institut für Theor. Physik Universität Frankfurt hertenstein@astrophysik.physik.uni-frankfurt.dbp	Germany
Herzberg	Gerhard	National Reserach Council djg@nrcvm01.bitnet	Canada
Hills	Richard	Mullard Radio Astronomy Observatory richard@mrao.cam.ac.uk	UK
Hjalmarson	Åke	Onsala Space Observatory hjalmar@oso.chalmers.se	Sweden
Ho	Paul T.P.	CfA ho@cfa.harvard.edu	USA
Hobson	Michael P.	MRAO, University of Cambridge mph@phy-ravx.cam.ac.uk	UK
Hofner	Peter	University of Wisconsin, Astronomy Department hofner@madraf.astro.wisc.edu	USA
Hogerheijde	Michiel	Leiden Observatory michiel@strwchem.leidenuniv.nl	NL
Hollenbach	David	NASA/AMES Research Center hollenbach@gal.arc.nasa.gov	USA
Horn	Jochen	I. Physikalisches Institut Universität zu Köln horn@ph1.uni-koeln.de	Germany
Howe	John E.	University of Maryland, Dept. of Astronomy jhowe@astro.umd.edu	USA
Irvine	William M.	FCRAO-Univ. Massachusetts irvine@fcrao.umass.edu	USA
Jacobs	Karl	I. Physikalisches Institut Universität zu Köln jacobs@ph1.uni-koeln.de	Germany
Jaffe	Daniel T.	MPI für extrateristrische Physik jaffe%mpei3@mpe.mpe-garching.mpg.de	Germany
Janness	Timothy	Mullard Radio Astronomy Obs. Cavendish Laboratory tj105@mrao.cam.ac.uk	UK
Jansen	David	Sterrewacht Leiden jansen@strw.leidenuniv.nl	NL

Johannson	Lars E.B.	Onsala Space Observatory leb@oso.chalmers.se	Sweden
Kärcher	Hans J.	MAN GHH	Germany
Keene	Jocelyn	Caltech jbk@tacos.caltech.edu	USA
Kegel	Wilhelm H.	Institut für Theor. Physik Universität Frankfurt kegel@astrophysik.physik.uni-frankfurt.dbp.de	Germany
Klaus	Thomas	I. Physikalisches Institut Universität zu Köln klaus@ph1.uni-koeln.dc	Germany
Koch	Timothy C.	University of California tim@cfi.ucsb.edu	USA
Kömpe	Carsten	Universitäts Sternwarte Jena koempe@mathematik.uni-jena.dbp.de	Germany
Köster	Benedikt	I. Physikalisches Institut Universität zu Köln koester@ph1.uni-koeln.dc	Germany
Krabbe	Alfred	MPI für Extraterrestrische Physik krabbe_3%mpei3@mpens.mpe-garching.mpg.dc	Germany
Kramer	Carsten	I. Physikalisches Institut Universität zu Köln kramer@ph1.uni-koeln.de	Germany
Krause	Dirk	I. Physikalisches Institut Universität zu Köln krause@ph1.uni-koeln.dc	Germany
Krenz	Thomas	MPI für Extraterrestrische Physik krenz%mpei2@mpens.mpe-garching.mpg.de	Germany
Krupnov	Andrei	Institut of Applied Physics kru@appl.nnov.su	Russia
Küfer	Sabine	I. Physikalisches Institut Universität zu Köln	Germany
Lada	Elizabeth	CfA lada@cfa.harvard.edu	USA
Langer	William D.	Jet Propulsion Lab. langer@langer.jpl.nasa.gov	USA
Langevelde	Huib, van	Sterrewacht Leiden vlangeve@strwchem.leidenuniv.nl	NL
Launhardt	Ralf	MPG-WG, Dust in Star Forming Regions launh@sol.astro.uni-jena.de	Germany
Lefloch	Bertrand	Observatoire de Grenoble lefloch@gag.observ-gr.fr	France
Leisawitz	David	NASA Goddard Space Flight Center leisawitz@stars.gsfc.nasa.gov	USA
Lequeux	James	Observatoire de Paris-Meudon aanda@mesiob.obspm.circe.fr	France
Liseau	René	IFSI-CNR erina@hp.ifsi.fra.cnr.it	Italy
Lisi	Franco	Arcetri Astrophysical Observatory lisi@arcetri.astro.it	Italy
Little	Leslie T.	Electronics Engineering Lab. ltl@ukc.ac.uk	UK
Lork	Rainer	I. Physikalisches Institut Universität zu Köln	Germany
Lucas	Robert	IRAM lucas@iram.grenet.fr	France
Luhman	Michael L.	University of Texas at Austin luhman@astro.as.utexas.edu	USA
Lyken	Klaus	I. Physikalisches Institut Universität zu Köln lyken@ph1.uni-koeln.de	Germany
Macdonald	Geoffrey H.	University of Kent, Electronic Engineering Lab. ghm@star.ukc.ac.uk	UK
Mao	Ruiging	Qinghai Radio Astronomy	China
Martin	Katharina	MPG, AG: Staub in Sternentstehungsgebieten martin@mathematik.uni-jena.dbp.de	Germany
Martinez	Andrea	Instituto Astrofisica Spaziale	Italy
Masson	Colin	CfA crm@cfa.harvard.edu	USA
Matthews	Henry E.	Joint Astronomy Centre hem@jach.hawaii.edu	USA
McMullin	Joseph P.	University of Maryland joe@astro.umd.edu	USA
Mebold	Ulrich	Radioastronomisches Institut der Universit"at Bonn mebold@astro.uni-bonn.de	Germany
Melnick	Gary	CfA melnick@cfa.harvard.edu	USA
Merluzzi	Paola	Universita di Napoli merluzzi@40060.span	Italy
Miller	Martin	I. Physikalisches Institut Universität zu Köln	Germany

		miller@ph1.uni-koeln.de	
Minchin	Nigel	Physics Department, Queen Mary and Westfield College nrm@starlink.qmw.ac.uk	U.K.
Mochizuki	Kenji	The Institut of Space and Astronautical Science mochi@astro.isas.ac.jp	Japan
Mundy	Lee G.	University of Maryland lgm@astro.umd.edu	USA
Nakagawa	Takao	Institut of Space and Astronautical Science nakagawa@astro.isas.ac.jp	Japan
Natale	Vincenzo	CAISMI-CNR natale@arcetri.astro.it	Italy
Nitsch	Ralf	I. Physikalisches Institut Universität zu Köln	Germany
Nummelin	Albert	Onsala Space Observatory albert@oso.chalmers.se	Sweden
Okuda	Haruyuki	Institut of Space and Astronautical Science okuda@astro.isas.ac.jp	Japan
Olberg	Michael	Onsala Space Observatory olberg@oso.chalmers.se	Sweden
Oliver	Richard J.	Bristol University, Astrophysics Group, Physics Dept. oliver@cfa.harvard.edu	UK
Olofsson	Göran	Stockholm Observatory olofsson@astro.su.se	Sweden
Padman	Rachael	MRAO, University of Cambridge, Cavendish Laboratory rachael@phy-ravx.cam.ac.uk	UK
Pagani	Laurent	DEMIRM, Observatoire de Meudon pagani@mesioa.obspm.circl.fr	France
Pelz	Guido C.	I. Physikalisches Institut Universität zu Köln pelz@ph1.uni-koeln.de	Germany
Phillips	Thomas G.	Caltech phillips@tacos.caltech.edu	USA
Piehler	Georg	Institut für Theor. Physik Universität Frankfurt piehler@astrophysik.physik.uni-frankfurt.dbp.de	Germany
Plumé	René	University of Texas plume@astro.as.utexas.edu	USA
Radford	Simon	Institut de Radioastronomie Millimétrique radford@iram.grenet.fr	France
Rausch	Elke	Institut für Theor. Physik Universität Frankfurt rausch@astrophysik.physik.uni-frankfurt.dbp.de	Germany
Robson	Ian	JCMT eir@jach.hawaii.edu	USA
Russell	Adrian P.G.	ROE (JCMT) apgr@star.roe.ac.uk	UK
Saraceno	Paolo	IFSI-CNR erina@hp.ifsi.fra.cnr.it	Italy
Schieder	Rudolf	I. Physikalisches Institut Universität zu Köln swas@ph1.uni-koeln.de	Germany
Schneider	Nicola	I. Physikalisches Institut Universität zu Köln schneider@ph1.uni-koeln.de	Germany
Schwenk	Ute	I. Physikalisches Institut Universität zu Köeln schwenk@ph1.uni-koeln.de	Germany
Scott	Paul	MRAO, Cavendish Laboratory paul@mrao.cam.ac.uk	UK
Serabyn	Gene	Caltech 320-47 serabyn@tacos.caltech.edu	USA
Simon	Robert	I. Physikalisches Institut Universität zu Köln simon@ph1.uni-koeln.de	Germany
Smith	Michael D.	Max-Plank-Institut für Astronomie smith@mpia-hd.mpg.de	Germany
Spaans	Marco	Steerewacht Leiden spaans@deuterium.leidenuniv.nl	NL
Spinoglio	Luigi	IFSI-CNR erina@hp.ifsi.fra.cnr.it	Italy
Stacey	Gordon J.	Cornell University stacey@astosun.tn.cornell.edu	USA
Staguhn	Johannes	I. Physikalisches Institut Universität zu Köln staguhn@ph1.uni-koeln.de	Germany
Stark	Ronald	Leiden University stark@rulhl1.leidenuniv.nl	NL
Sternberg	Amiel	School of Physics and Astronomy amiel@wise4.tau.ac.il	Israel
Störzer	Herbert	I. Physikalisches Institut Universität zu Köln stoerzer@ph1.uni-koeln.de	Germany
Stutzki	Jürgen	I. Physikalisches Institut Universität zu Köln stutzki@pk1.uni-koeln.de	Germany

Surdin	Vladimir		Russia
Sutton	Edmund C.	University of Illinois sutton@submm.astro.uiuc.edu	USA
Tacconi	Linda	MPI Garching linda@mpe-garching.mpg.de	Germany
Talbi	Dahbia	Lab. Radioastronomie talbi@vega.ens.fr	France
Thaddeus	Patrick	CfA thaddeus@cfa.harvard.edu	USA
Thoraval	Sophie	Radioastronomie, ENS thoroval@ensapa.ens.fr	France
Tigges	Alexander	I. Physikalisches Institut Universität zu Köln tigges@ph1.uni-koeln.de	Germany
Tofani	Gianni	Arcetri Astrophysical Observatory gtofani@arcetri.astro.it	Italy
Tolls	Volker	CfA tolls@cfa.harvard.edu	USA
Troland	Thomas H.	Physics Department phy132@ukcc.uky.edu	USA
Uchida	Keven	MPIfR uchida@29553.span	Germany
Ungerechts	Hans	FCRAO - Univ. of Mass. hans@phast.umass.edu	USA
Velusamy	Thangasamy	Jet Propulsion Laboratory MS 169-506 velu@kuiper.jpl.nasa.gov	USA
Vowinkel	Bernd	I. Physikalisches Institut Universität zu Köln	Germany
Walker	Robin N.F.	Univ. of Bristol, H.H. Will Physics Lab. rnfw@19716.span	UK
Walmsley	Malcolm	MPI Bonn walmsley@mpifr-bonn.mpg.de	Germany
Wang	Tung-Yang	I. Physikalisches Institut Universität zu Köln wang@ph1.uni-koeln.de	Germany
Wang	Ning	California Institute of Technology nwang@tacos.caltech.edu	USA
Ward-Thompson	Derek	Royal Observatory Edinburgh dwt@star.roe.ac.uk	UK
Warin	Sophie	Laboratoire d'Astrophysique warin@gag.observ-gr.fr	France
Welch	Jack	Univ. of California welch@bkyast.berkeley.edu	USA
Wiedner	Martina C.	 wiedner@vampi.mpi-hd.mpg.de	Germany
Williams	Jonathan	University of California williams@ucbast.berkeley.edu	USA
Wilson	Robert W.	AT & T Bell Laboratories rww@hoh-2.att.com	USA
Winnewisser	Gisbert	I. Physikalisches Institut Universität zu Köln winnewisser@ph1.uni-koeln.de	Germany
Wiseman	Jennifer J.	CfA jwiseman@cfa.harvard.edu	USA
Wouterloot	Jan	I. Physikalisches Institut Universität zu Köln wouterloot@ph1.uni-koeln.de	Germany
Yue	Zeng-Yuan	I. Physikalisches Institut Universität zu Köln yue@ph1.uni-koeln.de	Germany
Yui	Yukari Y.	The Institut of Sapce and Astronautical Science yui@astro.isas.ac.jp	Japan
Zimmermann	Thomas	I. Physikalisches Institut Universität zu Köln zimmermann@ph1.uni-koeln.de	Germany
Zinchenko	Igor	Institut of Applied Physics zin@appl.nnov.su	Russia
Zylka	Robert	MPI für Radioastronomie zylka%mpir2.dnet@dec15.mpifr-bonn.mpg.de	Germany

Springer-Verlag and the Environment

We at Springer-Verlag firmly believe that an international science publisher has a special obligation to the environment, and our corporate policies consistently reflect this conviction.

We also expect our business partners – paper mills, printers, packaging manufacturers, etc. – to commit themselves to using environmentally friendly materials and production processes.

The paper in this book is made from low- or no-chlorine pulp and is acid free, in conformance with international standards for paper permanency..

Lecture Notes in Physics

For information about Vols. 1–429
please contact your bookseller or Springer-Verlag

Vol. 430: V. G. Gurzadyan, D. Pfenniger (Eds.), Ergodic Concepts in Stellar Dynamics. Proceedings, 1993. XVI, 302 pages. 1994.

Vol. 431: T. P. Ray, S. Beckwith (Eds.), Star Formation and Techniques in Infrared and mm-Wave Astronomy. Proceedings, 1992. XIV, 314 pages. 1994.

Vol. 432: G. Belvedere, M. Rodonò, G. M. Simnett (Eds.), Advances in Solar Physics. Proceedings, 1993. XVII, 335 pages. 1994.

Vol. 433: G. Contopoulos, N. Spyrou, L. Vlahos (Eds.), Galactic Dynamics and N-Body Simulations. Proceedings, 1993. XIV, 417 pages. 1994.

Vol. 434: J. Ehlers, H. Friedrich (Eds.), Canonical Gravity: From Classical to Quantum. Proceedings, 1993. X, 267 pages. 1994.

Vol. 435: E. Maruyama, H. Watanabe (Eds.), Physics and Industry. Proceedings, 1993. VII, 108 pages. 1994.

Vol. 436: A. Alekseev, A. Hietamäki, K. Huitu, A. Morozov, A. Niemi (Eds.), Integrable Models and Strings. Proceedings, 1993. VII, 280 pages. 1994.

Vol. 437: K. K. Bardhan, B. K. Chakrabarti, A. Hansen (Eds.), Non-Linearity and Breakdown in Soft Condensed Matter. Proceedings, 1993. XI, 340 pages. 1994.

Vol. 438: A. Pękalski (Ed.), Diffusion Processes: Experiment, Theory, Simulations. Proceedings, 1994. VIII, 312 pages. 1994.

Vol. 439: T. L. Wilson, K. J. Johnston (Eds.), The Structure and Content of Molecular Clouds. 25 Years of Molecular Radioastronomy. Proceedings, 1993. XIII, 308 pages. 1994.

Vol. 440: H. Latal, W. Schweiger (Eds.), Matter Under Extreme Conditions. Proceedings, 1994. IX, 243 pages. 1994.

Vol. 441: J. M. Arias, M. I. Gallardo, M. Lozano (Eds.), Response of the Nuclear System to External Forces. Proceedings, 1994, VIII. 293 pages. 1995.

Vol. 442: P. A. Bois, E. Dériat, R. Gatignol, A. Rigolot (Eds.), Asymptotic Modelling in Fluid Mechanics. Proceedings, 1994. XII, 307 pages. 1995.

Vol. 443: D. Koester, K. Werner (Eds.), White Dwarfs. Proceedings, 1994. XII, 348 pages. 1995.

Vol. 444: A. O. Benz, A. Krüger (Eds.), Coronal Magnetic Energy Releases. Proceedings, 1994. X, 293 pages. 1995.

Vol. 445: J. Brey, J. Marro, J. M. Rubí, M. San Miguel (Eds.), 25 Years of Non-Equilibrium Statistical Mechanics. Proceedings, 1994. XVII, 387 pages. 1995.

Vol. 446: V. Rivasseau (Ed.), Constructive Physics. Results in Field Theory, Statistical Mechanics and Condensed Matter Physics. Proceedings, 1994. X, 337 pages. 1995.

Vol. 447: G. Aktaş, C. Saçlıoğlu, M. Serdaroğlu (Eds.), Strings and Symmetries. Proceedings, 1994. XIV, 389 pages. 1995.

Vol. 448: P. L. Garrido, J. Marro (Eds.), Third Granada Lectures in Computational Physics. Proceedings, 1994. XIV, 346 pages. 1995.

Vol. 449: J. Buckmaster, T. Takeno (Eds.), Modeling in Combustion Science. Proceedings, 1994. X, 369 pages. 1995.

Vol. 450: M. F. Shlesinger, G. M. Zaslavsky, U. Frisch (Eds.), Lévy Flights and Related Topics in Physics. Proceedigs, 1994. XIV, 347 pages. 1995.

Vol. 451: P. Krée, W. Wedig (Eds.), Probabilistic Methods in Applied Physics. IX, 393 pages. 1995.

Vol. 452: A. M. Bernstein, B. R. Holstein (Eds.), Chiral Dynamics: Theory and Experiment. Proceedings, 1994. VIII, 351 pages. 1995.

Vol. 453: S. M. Deshpande, S. S. Desai, R. Narasimha (Eds.), Fourteenth International Conference on Numerical Methods in Fluid Dynamics. Proceedings, 1994. XIII, 589 pages. 1995.

Vol. 454: J. Greiner, H. W. Duerbeck, R. E. Gershberg (Eds.), Flares and Flashes, Germany 1994. XXII, 477 pages. 1995.

Vol. 455: F. Occhionero (Ed.), Birth of the Universe and Fundamental Physics. Proceedings, 1994. XV, 387 pages. 1995.

Vol. 456: H. B. Geyer (Ed.), Field Theory, Topology and Condensed Matter Physics. Proceedings, 1994. XII, 206 pages. 1995.

Vol. 457: P. Garbaczewski, M. Wolf, A. Weron (Eds.), Chaos – The Interplay Between Stochastic and Deterministic Behaviour. Proceedings, 1995. XII, 573 pages. 1995.

Vol. 458: I. W. Roxburgh, J.-L. Masnou (Eds.), Physical Processes in Astrophysics. Proceedings, 1993. XII, 249 pages. 1995.

Vol. 459: G. Winnewisser, G. C. Pelz (Eds.), The Physics and Chemistry of Interstellar Molecular Clouds. Proceedings, 1993. XV, 393 pages. 1995.

Vol. 461: R. López-Peña, R. Capovilla, R. García-Pelayo, H. Waelbroeck, F. Zertuche, (Eds.), Complex Systems and Binary Networks. Lectures, México 1995. X, 223 pages. 1995.

Vol. 462: M. Meneguzzi, A. Pouquet, P.-L. Sulem (Eds.), Small-Scale Structures in Three-Dimensional Hydrodynamic and Magnetohydrodynamic Turbulence. Proceedings, 1995. IX, 421 pages. 1995.

Vol. 463: H. Hippelein, K. Meisenheimer, H.-J. Röser (Eds.), Galaxies in the Young Universe. Proceedings, 1994. XV, 314 pages. 1995.

New Series m: Monographs

Vol. m 1: H. Hora, Plasmas at High Temperature and Density. VIII, 442 pages. 1991.

Vol. m 2: P. Busch, P. J. Lahti, P. Mittelstaedt, The Quantum Theory of Measurement. XIII, 165 pages. 1991.

Vol. m 3: A. Heck, J. M. Perdang (Eds.), Applying Fractals in Astronomy. IX, 210 pages. 1991.

Vol. m 4: R. K. Zeytounian, Mécanique des fluides fondamentale. XV, 615 pages, 1991.

Vol. m 5: R. K. Zeytounian, Meteorological Fluid Dynamics. XI, 346 pages. 1991.

Vol. m 6: N. M. J. Woodhouse, Special Relativity. VIII, 86 pages. 1992.

Vol. m 7: G. Morandi, The Role of Topology in Classical and Quantum Physics. XIII, 239 pages. 1992.

Vol. m 8: D. Funaro, Polynomial Approximation of Differential Equations. X, 305 pages. 1992.

Vol. m 9: M. Namiki, Stochastic Quantization. X, 217 pages. 1992.

Vol. m 10: J. Hoppe, Lectures on Integrable Systems. VII, 111 pages. 1992.

Vol. m 11: A. D. Yaghjian, Relativistic Dynamics of a Charged Sphere. XII, 115 pages. 1992.

Vol. m 12: G. Esposito, Quantum Gravity, Quantum Cosmology and Lorentzian Geometries. Second Corrected and Enlarged Edition. XVIII, 349 pages. 1994.

Vol. m 13: M. Klein, A. Knauf, Classical Planar Scattering by Coulombic Potentials. V, 142 pages. 1992.

Vol. m 14: A. Lerda, Anyons. XI, 138 pages. 1992.

Vol. m 15: N. Peters, B. Rogg (Eds.), Reduced Kinetic Mechanisms for Applications in Combustion Systems. X, 360 pages. 1993.

Vol. m 16: P. Christe, M. Henkel, Introduction to Conformal Invariance and Its Applications to Critical Phenomena. XV, 260 pages. 1993.

Vol. m 17: M. Schoen, Computer Simulation of Condensed Phases in Complex Geometries. X, 136 pages. 1993.

Vol. m 18: H. Carmichael, An Open Systems Approach to Quantum Optics. X, 179 pages. 1993.

Vol. m 19: S. D. Bogan, M. K. Hinders, Interface Effects in Elastic Wave Scattering. XII, 182 pages. 1994.

Vol. m 20: E. Abdalla, M. C. B. Abdalla, D. Dalmazi, A. Zadra, 2D-Gravity in Non-Critical Strings. IX, 319 pages. 1994.

Vol. m 21: G. P. Berman, E. N. Bulgakov, D. D. Holm, Crossover-Time in Quantum Boson and Spin Systems. XI, 268 pages. 1994.

Vol. m 22: M.-O. Hongler, Chaotic and Stochastic Behaviour in Automatic Production Lines. V, 85 pages. 1994.

Vol. m 23: V. S. Viswanath, G. Müller, The Recursion Method. X, 259 pages. 1994.

Vol. m 24: A. Ern, V. Giovangigli, Multicomponent Transport Algorithms. XIV, 427 pages. 1994.

Vol. m 25: A. V. Bogdanov, G. V. Dubrovskiy, M. P. Krutikov, D. V. Kulginov, V. M. Strelchenya, Interaction of Gases with Surfaces. XIV, 132 pages. 1995.

Vol. m 26: M. Dineykhan, G. V. Efimov, G. Ganbold, S. N. Nedelko, Oscillator Representation in Quantum Physics. IX, 279 pages. 1995.

Vol. m 27: J. T. Ottesen, Infinite Dimensional Groups and Algebras in Quantum Physics. IX, 218 pages. 1995.

Vol. m 28: O. Piguet, S. P. Sorella, Algebraic Renormalization. IX, 134 pages. 1995.

Vol. m 29: C. Bendjaballah, Introduction to Photon Communication. VII, 193 pages. 1995.

Vol. m 30: A. J. Greer, W. J. Kossler, Low Magnetic Fields in Anisotropic Superconductors. VII, 161 pages. 1995.

Vol. m 31: P. Busch, M. Grabowski, P. J. Lahti, Operational Quantum Physics. XI, 230 pages. 1995.

Vol. m 32: L. de Broglie, Diverses questions de mécanique et de thermodynamique classiques et relativistes. XII, 198 pages. 1995.

Vol. m 33: R. Alkofer, H. Reinhardt, Chiral Quark Dynamics. VIII, 115 pages. 1995.

Vol. m 34: R. Jost, Das Märchen vom Elfenbeinernen Turm. VIII, 286 pages. 1995.

Vol. m 35: E. Elizalde, Ten Physical Applications of Spectral Zeta Functions. XIV, 228 pages. 1995.

Vol. m 36: G. Dunne, Self-Dual Chern-Simons Theories. X, 217 pages. 1995.

Vol. m 37: S. Childress, A.D. Gilbert, Stretch, Twist, Fold: The Fast Dynamo. XI, 410 pages. 1995.